ATLAS OF
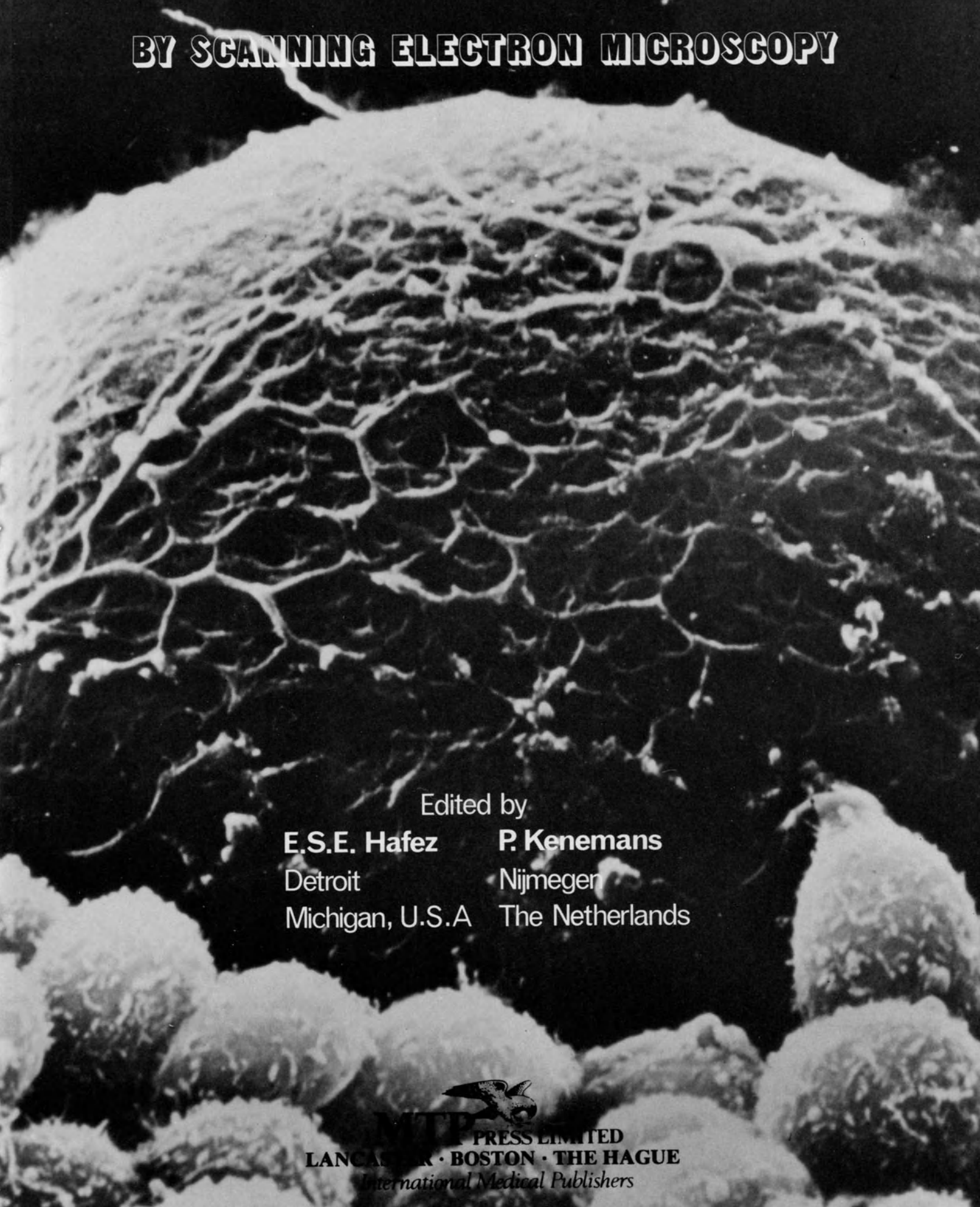# HUMAN REPRODUCTION

ATLAS OF
HUMAN REPRODUCTION
BY SCANNING ELECTRON MICROSCOPY

Edited by

E.S.E. Hafez   **P. Kenemans**
Detroit   Nijmegen
Michigan, U.S.A   The Netherlands

CONTENTS

II. ANDROLOGY

III. CONCEPTUS

IV. SPECIAL TECHNIQUES

V. EPILOGUE

Contributors

Abe, J.
Department of Anatomy,
Kurume University School of Medicine,
Kurume,
Japan

Baccetti, B.
Universita di Siena,
Istituto de Zoologia,
Via Mattioli 4,
53100 Siena,
Italy

Berger, R. E.
Department of Biological Structure,
Urology and Obstetrics/Gynecology,
University of Washington,
School of Medicine,
Seattle,
Washington 98195,
USA

Boeckx, W.
The Unit for the Study of Human Reproduction,
Catholic University,
Leuven,
Belgium

Boyde, A.
Anatomy Department,
University College of London,
Gower Street,
London WC1E 6BT,
United Kingdom

Brophy, O.
Departments of Anatomy and Urology,
State University of New York,
Upstate Medical Center,
Syracuse,
New York 13210,
USA

Brosens, I. A.
The Unit for Study of Human Reproduction,
Catholic University,
Leuven,
Belgium

Brunk, U.
Institute of Pathology,
University of Linkoping,
Linkoping,
Sweden

Brueschke, E. E.
Department of Family Practice,
Rush Medical School,
Chicago,
Illinois,
USA

Bush, M.
Department of Anatomy and Urology,
State University of New York,
Upstate Medical Center,
Syracuse,
New York 13210,
USA

Castellucci, M.
Abt. Elektronenmikroskopie,
der Medizinischen Hochschule,
Karl-Wiechert-Allee 9,
3000 Hannover 61,
West Germany

Chrétien, F. C.
Travaux Pratiques de Biologie Animale du PCEM,
12, rue Cuvier,
75005,
Paris,
France

Collins, V. P.
Institute of Tumor Pathology,
Karolinska Institute,
Stockholm,
Sweden

Daunter, B.
Department of Obstetrics/Gynecology,
University of Queensland,
Clinical Sciences Building,
Royal Brisbane Hospital,
Q 4029,
Australia

Davina, H.
Institute for Submicroscopic Morphology,
University of Nijmegen Medical School,
6525 GA Nijmegen,
The Netherlands

El-Badrawi, H. H.
24 Falah St,
Madinet El-Mohandsin,
Giza, Cairo,
Egypt

Eskes, T. K. A. B.
Department of Gynecology/Obstetrics,
University of Nijmegen,
PO Box 9101,
6500 HB Nijmegen,
The Netherlands

Flowers, C. E. Jr
Department of Obstetrics/Gynecology,
University of Alabama,
Birmingham,
Alabama 36688,
USA

van Geijn, H. P.
Department of Obstetrics/Gynecology,
University of Amsterdam,
Free University,
Amsterdam,
The Netherlands

Gordts, S.
The Unit for the Study of Human Reproduction,
Catholic University,
Leuven,
Belgium

Gould, K. G.
Division of Reproductive Biology,
Yerkes Regional Primate Research Center,
Emory University,
Atlanta,
Georgia 30322,
USA

Haan, R. W. de
Department of Obstetrics/Gynecology,
University of Nijmegen,
Nijmegen,
The Netherlands

Hafez, E. S. E.
Department of Gynecology/Obstetrics,
School of Medicine,
Wayne State University,
550 East Canfield,
Detroit,
Michigan 48201,
USA

Hamasaki, M.
Department of Anatomy,
Kurume University School of Medicine,
Kurume,
Japan

Hodde, K. C.
Laboratory for Surgical Research,
Wilhelmina Gasthuis University of Amsterdam,
Amsterdam,
The Netherlands

Hodges, G. M.
Imperial Cancer Research Fund,
PO Box 123,
Lincolns Inn Field,
London WC2A 3PX,
United Kingdom

Hyde, B. M.
Department of Anatomy,
University of South Alabama,
Mobile,
Alabama 36608,
USA

Ida, K.
Department of Obstetrics/Gynecology,
Shiga University of Medical Sciences,
Shiga,
Japan

Ishiwata, I.
Department of Obstetrics/Gynecology,
School of Medicine,
Keio University,
35 Shinanomachi,
Shinjukuru,
Tokyo 160,
Japan

Iwaki, A.
Department of Obstetrics/Gynecology,
Toho University,
School of Medicine,
Tokyo 143,
Japan

Karp, L. E.
Department of Biological Structure,
Urology and Obstetrics/Gynecology,
University of Washington,
School of Medicine,
Seattle,
Washington 98195,
USA

Kaufmann, P.
Department of Anatomy,
University of Hamburg,
School of Medicine,
Hamburg,
West Germany

Kauppila, A.
Department of Obstetrics/Gynecology,
University of Oulu,
Kajaanintie 52 D,
SF-90220 Oulu 22,
Finland

Kenemans, P.
Department of Gynecology/Obstetrics,
University of Nijmegen,
PO Box 9101,
6500 BH Nijmegen,
The Netherlands

Koehler, J. K.
Department of Biological Structure,
University of Washington School of Medicine,
Seattle,
Washington 98195,
USA

Kurihara, S.
Department of Obstetrics/Gynecology,
School of Medicine,
Keio University,
35, Shinanomachi,
Shinjukuru,
Tokyo 160,
Japan

Lutjen, P. J.
Department of Obstetrics/Gynecology,
University of Queensland,
Clinical Sciences Building,
Royal Brisbane Hospital,
Herston 4029,
Queensland,
Australia

Makabe, S.
Department of Obstetrics/Gynecology,
Toho University School of Medicine,
11-1 Omoriniski 6 Chome,
IKA-TU,
Tokyo 143,
Japan

Molday, R. S.
Department of Biochemistry,
University of British Columbia,
2075 Westbrook Mall,
Vancouver,
British Columbia,
Canada V6T 1W5

Motta, P. M.
Instituto di Anatomia Umana Normale,
Universita di Roma,
Viale Regina Elena,
289–00161, Rome,
Italy

Murakami, M.
Department of Anatomy,
Kurume University School of Medicine,
Kurume,
Japan

Nilsson, B. O.
Reproduction Research Unit,
Biomedical Center,
PO Box 571,
751 23 Uppsala,
Sweden

Nishida, T.
Department of Anatomy,
Kurume University School of Medicine,
Kurume,
Japan

Nozawa, S.
Department of Obstetrics/Gynecology,
School of Medicine,
Keio University,
35 Shinanomachi,
Shinjukuru,
Tokyo 160,
Japan

Numann, P. J.
Department of Anatomy and Urology,
State University of New York,
Upstate Medical Center,
766 Irving Avenue,
Syracuse,
New York 13210,
USA

Okamura, H.
Department of Virology and Rickettsiology,
National Institute of Health,
Kamiosaki,
Shinagawaku,
Tokyo 141,
Japan

Omura, G.
Department of Obstetrics/Gynecology,
Tokyo University School of Medicine,
Tokyo 143,
Japan 606

Oshima, M.
Department of Obstetrics/Gynecology,
Shiga University of Medical Sciences,
Tuskinowa-Cho-Seta,
Otsu-City,
Shiga-Pref.,
Japan 520-521

Roomans, G. M.
Wenner-Gren Institute,
University of Stockholm,
Norrtullsgatan 16,
S-11345 Stockholm,
Sweden

Rubio, C. A.
Department of Pathology,
Karolinska Sjukhuset,
S-10401, Stockholm 60,
Sweden

Smith, D.
Departments of Biological Structure,
   and Obstetrics/Gynecology,
University of Washington School of Medicine,
Seattle,
Washington 98195,
USA

Spornitz, U. M.
Anatomisches Institut
   der Universität Basel,
Pestalozzistrasse 20,
CH 4056 Basel,
Switzerland

Spring-Mills, E.
Departments of Anatomy and Urology,
State University of New York,
Upstate Medical Center,
766 Irving Avenue,
Syracuse,
New York 13210,
USA

Stenback, F.
Department of Pathology,
University of Oulu,
Kajaaintie 52D SF 90220,
Oulu 22,
Finland

Sugita, A.
Department of Anatomy,
Kurume University School of Medicine,
Kurume,
Japan

Sundström, P.
Department of Obstetrics/Gynecology,
Malmo Allmanna Sjukhus,
S-214 01 Malmo,
Sweden

Taguchi, S.
Department of Obstetrics/Gynecology,
School of Medicine,
Keio University,
Tokyo 160,
Japan

Tauber, P. F.
Department of Obstetrics/Gynecology,
University of Essen,
Essen,
West Germany

Tsukahara, S.
Department of Obstetrics/Gynecology,
School of Medicine,
Keio University,
Tokyo 160,
Japan

Tyden, O.
Department of Obstetrics/Gynecology and Anatomy,
University of Uppsala,
50750 14 Uppsala,
Sweden

Vasquez, G.
The Unit for the Study of Human Reproduction,
Catholic University,
Leuven,
Belgium

Vooys, G. P.
Department of Pathology,
University of Nijmegen,
6525 GA,
Nijmegen,
The Netherlands

Waterman, R. E.
Department of Anatomy,
School of Medicine,
University of New Mexico,
Albuquerque,
New Mexico 87131,
USA

Wilborn, W. H.
Department of Anatomy,
University of South Alabama,
Mobile,
Alabama 36688,
USA

Willemsen, W. N. P.
Department of Gynecology/Obstetrics,
University Hospital,
Sint Radboud,
PO Box 9101,
6500 BH Nijmegen,
The Netherlands

Winston, R. L. M.
Hammersmith Hospital,
London,
England

Zaneveld, L. J. D.
Department of Physiology, Biophysics and Obstetrics/
   Gynecology,
College of Medicine,
University of Illinois At the Medical Center,
Chicago,
Illinois 60680,
USA

Foreword

The suggestion of Max Knoll that an electron microscope could be developed using a fine scanning beam of electrons on a specimen surface and recording the emitted current as a function of the position of the beam was launched in 1935. Since then several investigators and clinicians have used this concept to develop techniques now known as scanning electron microscopy (SEM) and scanning transmission electron microscopy (STEM). The choice to study the female reproductive organs was a logical one because cells and tissue samples can be sampled relatively easily; furthermore, these cells and organs are influenced continuously by the cyclic production of hormones.

This atlas demonstrates the state of the art in 1983. Having such predecessors as *Mammalian Reproduction* and *The Human Female Reproductive Tract* one can judge the progress made in techniques and their application. The basis for this research was laid during an international SEM Symposium, 'Human Reproduction in Three Dimensions', held in Nijmegen, The Netherlands, in September 1981. As one of the organizers, and especially not a morphologist, I was fascinated by the numerous SEM photographs, the wealth of information and the enthusiasm of the researchers covering a variety of disciplines. All aspects of the female and male genital tract have been covered, culminating in the prizewinning award showing the *in vitro* fertilized human egg.

In clinical diagnostics SEM also proved to be a valuable complementary technique, shedding new light on oncology, the pathogenesis of tubal disease and the maturation process of the placenta. Future research has still to be accomplished; e.g. quantification of SEM photographs for meaningful and sound biological, scientific and statistical evaluation in diagnostic gynecology, obstetrics, andrology and oncology.

If this atlas does encourage the investigators in the field and their offspring to take up this challenge, the numerous people who used their 'electrons' to make the Nijmegen SEM Symposium so successful, and this atlas possible, will be completely satisfied.

Nijmegen, October 1982   TOM ESKES

Preface

Within only two decades of its commercial innovation, SEM has become an indispensable morphological tool, not only in basic research but also in clinical application in gynecology, andrology, oncology and pathology. This atlas represents an international symposium on 'Human Reproduction in Three Dimensions' held in Nijmegen, the Netherlands, 13–16 September 1981, under the presidency of Prof. T. K. A. B. Eskes and Prof. G. P. Vooys. A major objective of this symposium was to describe the state of the art of scanning electron microscopy in the field of human reproduction. Several investigators in the field of human reproduction who work with SEM (alone or in combination with other techniques) were brought together on this occasion for the first time. The clinical significance of scanning electron microscopy was evaluated, and advanced techniques and future developments were discussed.

The symposium was co-sponsored by the C. S. Mott Center for Human Growth and Development, Wayne State University School of Medicine, Detroit, Michigan, USA; Department of Obstetrics/Gynecology, Faculty of Medicine, Catholic University, Nijmegen, The Netherlands; Cilag Chemie, Philips Nederland B.V., Organon Nederland B.V., Upjohn International and the Sint Radboud Hospital, University of Nijmegen, The Netherlands.

Thanks are specially due to the Dutch program committee: Prof Dr A. M. Stadhouders, Prof. D. J. L. Mastboom, Dr H. P. van Geijn, Mr H. M. Noorbergen, Prof. Dr N. F. Th. Arts, Dr W. A. A. van Os and Prof. Dr J. G. Stolk.

The critical remarks of the following advisory committee are gratefully acknowledged: John A. Chandler, Francois Ch. Chretien, B. Daunter, Kenneth G. Gould, Kees C. Hodde, Gisela M. Hodges, James K. Koehler, Ove Nilsson, Janice Nowell, Hitoshi Okamura, Eva Patek, Godfried M. Roomans, Lourens J. D. Zaneveld. Thanks are also due to Ms. Monica Klessens, Ms. Jackie Mucci and Ms. Judy Butcher for their editorial skills. The fine co-operation of Mr David Bloomer and Mr P. Johnstone of MTP Press is gratefully appreciated.

13 April 1982   E.S.E.H.
                                                       P.K.

Selected General References

Ferenczy, A. (1980). The female reproductive system. In Hodges, G. M. and Hallowes, R. C. (eds). *Biomedical Research Applications of Scanning Electron Microscopy.* Vol. 2, pp. 127–65. (London: Academic Press)

Ferenczy, A. and Richart, R. M. (1974). *Female Reproductive System. Dynamics of scan and transmission electron microscopy.* (New York: Wiley)

Fujita, T. (1981). *SEM Atlas of Cells and Tissues.* (Tokyo: Igaku-Shoin)

Glauert, A. M. (1975). Fixation, dehydration and embedding of biological specimens. In Glauert, A. M. (ed.). *Practical Methods in Electron Microscopy.* Vol. 3, Part I. (Amsterdam: Elsevier/North Holland Biomedical Press)

Hafez, E. S. E. *et al.* (1975). SEM of human reproductive physiology. *Obstet. Gynecol. Scand.,* Suppl. 40, 1

Hafez, E. S. E. (ed.) (1978). *Scanning Electron Microscopy of Human Reproduction.* (Ann Arbor: Ann Arbor Science Publishers)

Hyat, M. A. (1978). *Introduction to Biological Scanning Electron Microscopy.* (Baltimore: University Park Press)

Hyat, M. A. (ed.) (1980). *X-Ray Microanalysis in Biology.* (Baltimore: University Park Press)

Johari, O. (ed.). SEM/ITT Research Institute, Chicago Proceedings 1968–1977*

Johari, O. (ed.). SEM Symposium, SEM Inc., Chicago Proceedings 1978 onward*

Kessel, R. G. and Kardon, R. H. (1979). *Tissues and Organs: a text-atlas of scanning electron microscopy.* (San Francisco: W. H. Freeman)

Ludwig, H. and Metzger, H. (1976). *The Human Female Reproductive Tract. A scanning electron microscopical atlas,* (New York: Springer Verlag)

Suzuki, S. (1973). *Atlas of Mammalian Ova.* (Tokyo: Igaku-Shoin)

Van Blerkom, J. and Motta, P. M. (1979) *The Cellular Basis of Mammalian Reproduction.* (Baltimore, Munich: Urban & Schwarzenberg)

Wells, O. C. (1974). *Scanning Electron Microscopy.* (New York: McGraw-Hill)

*Note:

REFERENCES
The Proceedings of the Annual Scanning Electron Microscope Symposium sponsored by IIT Research Institute, Chicago between 1968 and 1977, are abbreviated to SEM/IITRI: the subsequent Proceedings, from 1978 onwards, are abbreviated to SEM Symposium. Each annual number is considered as a volume number. This applies in the References throughout this volume.

1

Specimen preparation techniques

P. KENEMANS*, V. P. COLLINS† and U. BRUNK‡

* Division of Gynecological Oncology, University Hospital, Nijmegen, The Netherlands
† Institute of Tumor Pathology, Karolinska Institute, Stockholm, Sweden
‡ Institute of Pathology, University of Linköping, Uppsala, Sweden

Scanning electron microscopy (SEM) provides a highly appropriate and effective method for studying the shape and surface morphology of cells and tissues. Objects studied with SEM must be non-volatile, mechanically stable, and conductive. However, seldom do biological specimens fulfill any of these demands naturally. Therefore, various methods must be used to transform the material into a proper state for examination by SEM. Paradoxically, however, while the primary objective of such methods is to preserve the structure of the surfaces of the specimens with minimal change in spatial arrangement these obligatory techniques can, and often will, modify the cell morphology considerably (Table 1). Since spatial changes, or artifacts, do occur in specimen preparation, a thorough knowledge of their location and extent is a prerequisite for an adequate interpretation of the findings. Various preparation techniques, and problems related to these methods, are hereby described. Special attention is given to fundamental aspects of fixation which were studied using in vitro cultivated cells as a model system.

GENERAL ASPECTS OF SPECIMEN PREPARATION

All preparative techniques of vertebrate tissues for SEM (de Harven et al., 1975; Bell and Revel, 1980; Boyde, 1976) have in common that cells stop living during the procedures. It is here that SEM loses the temporal dimension of organization. It is essential that cell death is instantaneous, otherwise the process of cell dying is

Table 1 Specimen preparation

Technique	Main goal	Main problems
Preparation	observation with high magnification; preservation of in vivo cell shape and surface	deformation; miniaturization (shrinkage); loss of time aspect
Sampling	attainment of the tissue, or population of cells wanted	selectivity; contamination
Cleaning	removal of extracellular material, such as mucus, lymph, serum	obscuration of cell surface; osmotic or biochemical effects
Mounting	attachment of specimen to solid support	contamination; selective cell loss; crowding of cells
Fixation	stabilization of cell morphology	osmotic artifacts
Dehydration and drying	removal of cell water; removal of cell fluid leaving the solids in their original location	lipid extraction; shrinkage; distructions
Coating	attainment of electrical conductivity	charging; heating; melting

depicted rather than processes of cell life. Cells, either alive or having been just killed, must be treated with utmost care until all structural elements (relevant for SEM) are suitably stabilized. This stabilization should be able to sustain crude conditions such as vacuum, irradiation, heating and charging. As cells from various organ systems are different in nature, there cannot be a single procedure which is optimal for all cell populations. Little is known about extracellular environment and intercellular fluid conditions. Thus, individual experimentation and experience is necessary to discover the optimal procedures to be used. In order to determine which procedure will be best suited, an overall strategy for preparing samples routinely should include the use of at least two different procedures.

METHODS OF SPECIMEN COLLECTION, CLEANING AND MOUNTING

Small blocks of specimen tissue obtained by surgery and pinned into a cork plate with the surface of interest upwards are suitable for processing. Isolated cells are generally best collected as suspensions. The suspensions are either natural (e.g. ascites cells; amniotic cells) or artificial in nature (e.g. cervical cells suspended in buffer or buffered fixative) obtained after aspiration, or by gentle scraping from the tissue of origin.

Extracellular material, such as mucus, lymph, or serum proteins, is removed before fixation, as it might obscure the surface architecture when fixed. This is mostly done by rinsing with an iso-osmotic warm buffer solution. Mucolytic enzymes and agents can also be used. As the specimens must be cleaned prior to structural stabilization by fixation, the maintenance of the cell surface integrity has to be explicitly guaranteed during this phase. Cells in suspensions can be attached to a support prior to or after fixation, which also results in some differences.

Living cells, when not yet fixed, show a reactive alteration in their surface features when placed onto the surface of a substratum (de Harven et al., 1975; Westbrook et al., 1975).

Cells can either be centrifuged onto glass slides (Thornthwaite et al., 1975) or allowed to sediment onto coverslips, which are preferably coated with a polycationic substance e.g. poly-L-lysine (Mazia et al., 1974). Cells can also be collected by gentle filtration onto commercial filter discs of 1–3 μm pore size, such as the millipore and nucleopore filter (Westbrook et al., 1975) or the Flotronic silver membrane (de Harven et al., 1975). Metal substrates are more suitable for freeze-drying.

Nucleopore filters, which may be made transparent, and glass supports (with a location grid), allow the relocation and re-examination of the same cells in SEM, once they have been classified by light microscopy (LM). In many studies it is essential to have correlative LM/SEM observations performed consecutively on the same material. This allows proper identification by conventional cytological criteria as a basis for SEM characterization (Wetzel et al., 1973; Noonan and Riddle, 1977; Kenemans et al., 1981).

Cells adhering to a substratum may be lost during further processing. Cell loss need not be at random, but instead may be selective.

FIXATION

The plasma membrane of cells is semipermeable and as long as it retains this property, it is quite sensitive to changes in osmolality. Glutaraldehyde (as opposed to OsO_4) does not completely destroy membrane semipermeability (Jard et al., 1966). Therefore, all cells are sensitive to variations in osmolality until the OsO_4 fixation (Bone and Ryan, 1972).

The glutaraldehyde molecule is readily transported across cell membranes (Arborgh et al., 1976). Therefore, it is not the total osmotic pressure of the fixative solution which must equal the osmolality of the natural cell environment, but rather the osmolality of the fixative vehicle, consisting of buffer and other additives (Figure 1). Even high concentrations of glutaraldehyde add little or nothing to the effective osmotic pressure of the fixative. The effective osmotic pressure is produced by molecules which are not capable of transversing the membrane.

Morphological changes are caused by primary glutaraldehyde fixation when hypotonic vehicles are used. Comparatively slight deviations in the osmotic pressure of the fixative vehicle may even give rise to fixation artifacts. Thus, the commonly utilized fixative, 2% glutaraldehyde in 0.1 mol/l Cac (total osmotic pressure 410 mOsmol; vehicle osmotic pressure 200 mOsmol) causes detectable swelling of glial cells cultured at 200 mOsmol (Figures 2, 3). A 2% glutaraldehyde in 0.1 mol/l Na-cacodylate-HCl buffer with 0.1 mol/l sucrose (pH 7.2; total osmolality 510 mOsmol; vehicle osmolality 300 mOsmol) produces no detectable artifacts on human cells grown in commonly used complete media which have a total osmolality of around 280–290 mOsmol (Arborgh et al., 1976; Collins et al., 1977). This fixative is suitable for initial fixation for all morphological, and many cytochemical studies (Figure 1a). Ruffles and microvilli appear to be the surface structures most sensitive to osmotic effects (see the swollen ruffles and microvilli in Figures 2 and 3).

The changes made by fixatives with only slightly hypotonic vehicles require high resolution and magnification for detection; but are, under such conditions, conspicuous.

The primary fixative solution should have a temperature equal to that of the site of origin of the tissues or cells used. After approximately 15 min at 37 °C, the specimen is then transferred to 4 °C until further processing. A minimal glutaraldehyde fixation time of 1 h is required. All buffer washes following glutaraldehyde fixation, up to and including the secondary fixation in OsO_4, must have the same osmolality as the vehicle of the primary fixative and the natural cell environments.

When studying cells in the low and middle magnification ranges, glutaraldehyde fixation alone may be used. This fixation should, however, be greatly prolonged for several days (Boyde, 1972; Vesely and

Boyde, 1973). If high magnifications are required, or if time is limited, a secondary OsO_4 fixation is recommended. Figures 4 and 5 demonstrate the surfaces of cells fixed in glutaraldehyde for 24 h at a proper osmotic pressure with and without ensuing osmium post-fixation.

Without osmium postfixation (Figure 5), the morphology of the plasma membrane is irregular and defective. The glutaraldehyde fixation alone does not adequately stabilize the lipid-rich plasma membrane and it therefore cannot withstand the stresses of the subsequent preparative procedures which result in multiple small tears. Even a prolonged fixation in glutaraldehyde cannot compensate for osmium post-fixation (Figure 6).

Secondary fixation is performed with 1% OsO_4 in 0.15 mol/l Cac buffer at room temperature for 90 min, following a rinse with 0.15 mol/l Cac buffer only.

DRYING OF THE SPECIMEN

Dehydration (removal of cell water) and drying (removal of intracellular fluid), while the solids remain in their original location, can be performed in one of three ways, each having its advantages and disadvantages (Table 2). While adequate fixation does not cause significant dimensional change, severe preparative shrinkage with drying is to some extent unavoidable (Boyde et al., 1977).

With air-drying from the liquid phase, the solvent/vapor phase boundary is crossed and surface tension is high, depending on the solvent used. Shrinkage to less than 30% of the original volume is common.

In critical point drying (CPD), the CO_2 (or Freon 13) liquid phase passes into a CO_2 (or Freon 13) gas state without changes in volume, since the transition takes place at or above the critical point (Anderson, 1951). However, shrinkage is also common with this method, even when accidental air-drying is avoided. Shrinkage (20% volume) occurring within the bomb (during substitution, heating and depressurization) adds to the shrinkage caused by dehydration in a graded ethanol (30%) volume), which is obligatory with CPD. The result is a total specimen shrinkage of some 40–50% in volume. Freeze-drying avoids the problem of the surface forces at the liquid/gas phase boundary by

changing from a liquid phase to a solid state by quenching (i.e. rapid freezing; e.g. in liquefied and cooled Freon 22, or in a liquid-nitrogen slush). Subsequently, this allows the specimen to pass the solid/gas phase boundary by way of sublimation in a high vacuum system at a low temperature.

Freeze-drying of fixed material from water is fast and allows minimal shrinkage (10–15% volume) as dehydration can be omitted. However, ice crystal damage can occur if temperatures do not remain low for a prolonged period of time.

COATING

Evaporation, or more superior and more popular sputter coating using a special apparatus, allows uniform deposition of a metal (gold or gold-palladium) layer onto the cells and the substratum (Echlin, 1974; 1975). Alternatively to metal coating, metal impregnation techniques, e.g. Oto technique (Murakami, 1974), have been successfully employed for rendering specimens conductive.

CONCLUDING REMARKS

Specimen preparation methods that are necessary to obtain a technically acceptable image of the specimen studied in the SEM, at the same time unavoidably introduce specimen deformations, or artifacts. This is because all SEM preparative methods have two ideal objectives, that, in practice, are partly conflicting, viz.:

(1) attainment of a stable and conductive specimen; and

(2) preservation of surface structure of the specimen.

There are two groups of artifacts: avoidable ones, that must be prevented, and unavoidable ones, that must be known in order to be recognized as such. Processing artifacts vary both with the method used and the type of specimen under study. Therefore, although some general rules for specimen processing can be given, especially as to fixation and dehydration, each student using SEM has to find and establish the optimal method for his problem.

Table 2 Drying techniques

	Advantages	Disadvantages
Air-drying	no special instrument; simple and fast; displays subcellular structures	enormous shrinkages; enormous distortion
Critical point drying	good morphology	special instrument; considerable shrinkages; dehydration needed; accidental air-drying; health and safety hazards
Freeze-drying	good morphology; no hydration; little shrinkage; freeze cleaving possible	special instrumentation; ice crystal damage; thermal stress damage
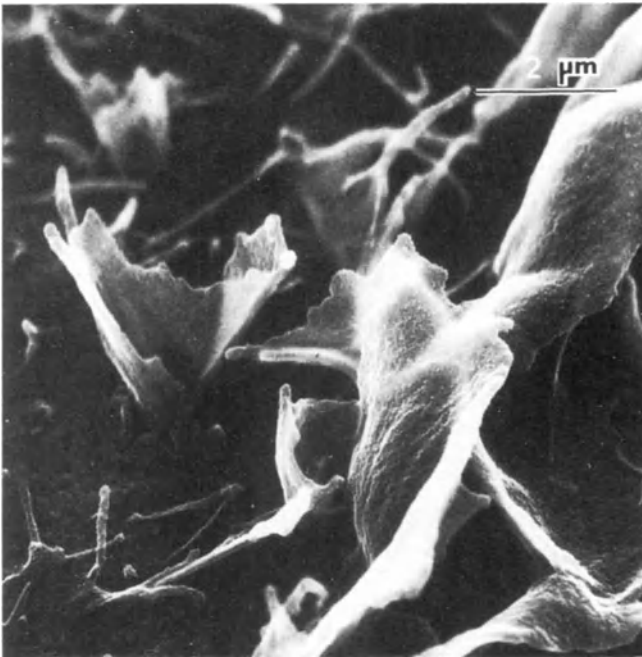
Figures 1 and 2 High magnification of ruffling areas of cultured human glial cells following fixation in 2% glutaraldehyde (GA) in vehicles of 300 and 200 mOsmol, respectively. The membranes are well preserved in Figure 1 but show obvious swelling artifacts in the form of small bubbles in Fig. 2. Postfixation in OsO_4, critical-point dried (CPD)
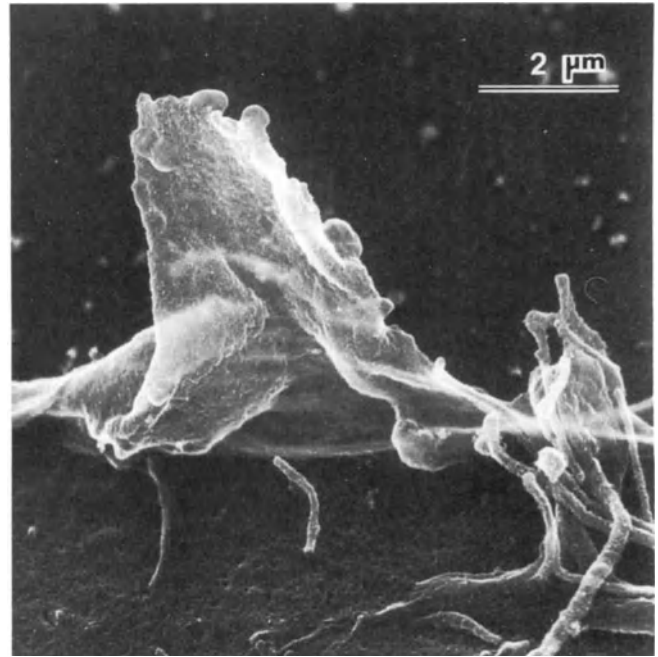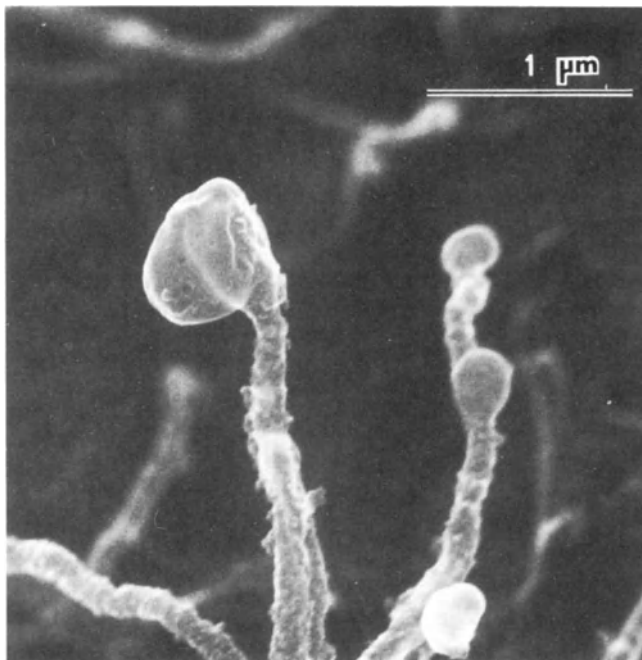
Figure 3 Details of distal, artifactually swollen ends of microvilli following initial GA fixation with a vehicle of 200 mOsmol.
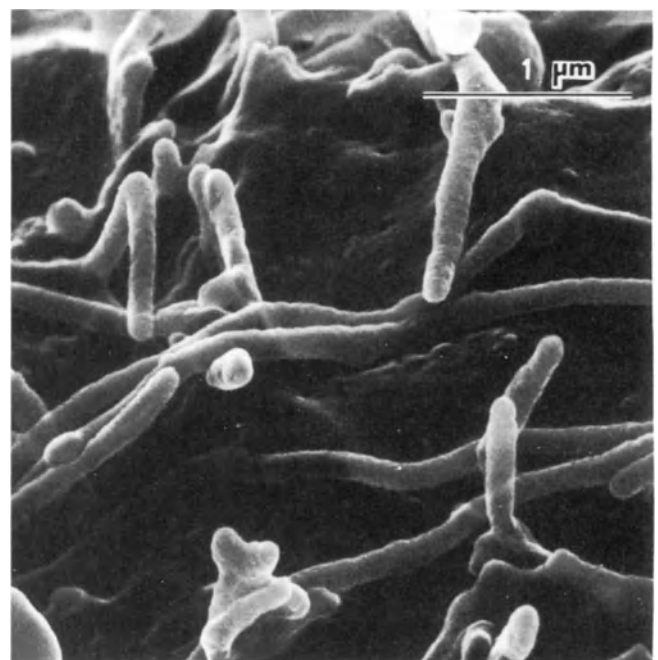
Figures 4 and 5 Microvilli-covered cell surfaces after fixation in GA in a 300 mOsmol vehicle for 24 h with (Figure 4) and without (Figure 5) postfixation in OsO_4. Note pronounced artifactual alterations in the plasma membrane in the form of small holes and irregular rifts when osmium postfixation was omitted. CPD.
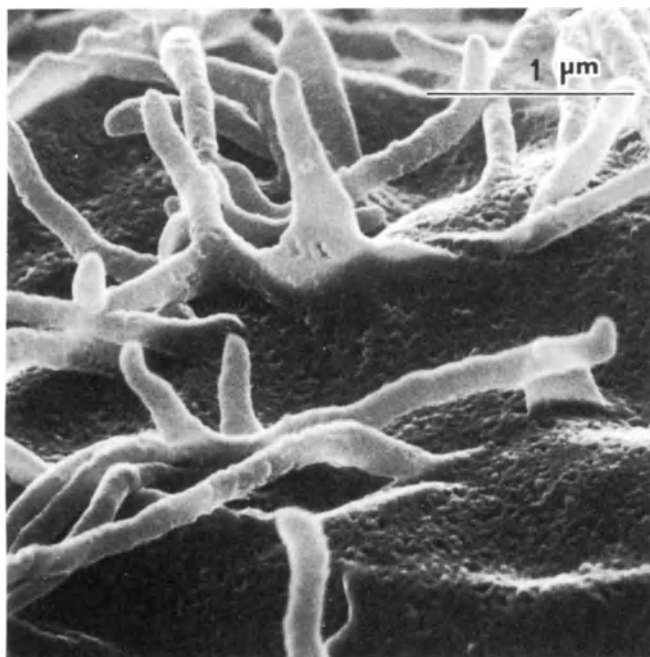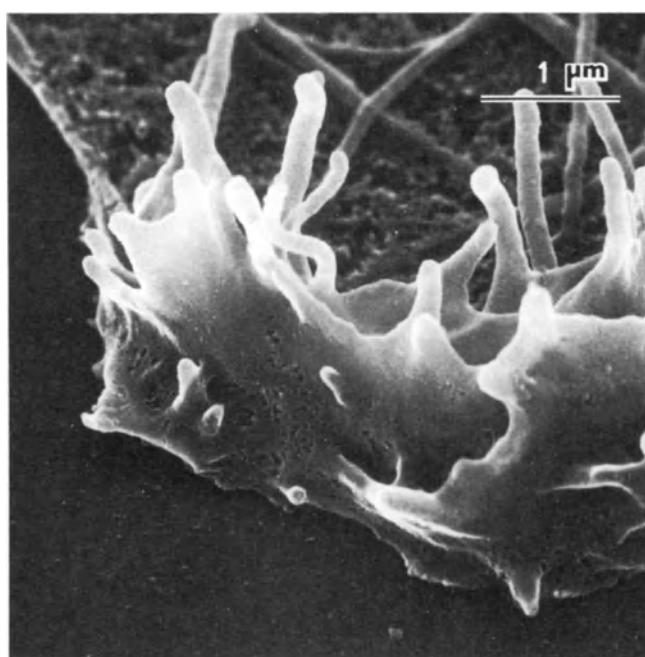
Figure 5 (see legend to Figure 4)

Figure 6 High magnification of a ruffling area of a cell fixed in GA in a 300 mOsmol vehicle for 14 days. No postfixation in osmium. Note same type of artifacts as are shown in Figure 5. CPD.

References

Anderson, T. F. (1951). Techniques for the preservation of three-dimensional structure in preparing specimens for the electron microscope. *Trans. N.Y. Acad. Sci. Ser. II,* **13,** 130

Arborgh, B., Bell, P., Brunk, U. and Collins, V. P. (1976). The osmotic effect of glutaraldehyde during fixation. A transmission electron microscopy, scanning electron microscopy and cytochemical study. *J. Ultrastruct. Res.,* **56,** 339

Bell, P. B. and Revel, J.-P. (1980). Scanning electron microscope application to cells and tissues in culture. In Hodges, G. M. and Hallowes, R. C. (eds), *Biomedical Research Applications of Scanning Electron Microscopy.* Vol. 2, pp. 1–63. (London: Academic Press)

Bone, Q. and Ryan, K. P. (1972). Osmolarity of osmium tetroxide and glutaraldehyde fixatives. *Histochem. J.,* **4,** 331.

Boyde, A. (1972). Biological specimen preparation for the scanning electron microscope. An overview. *SEM/IITRI,* **5,** 257

Boyde, A. (1970). Do's and don't's in biological specimen preparation for the SEM. *SEM/IITRI,* **9** (I), 683

Boyde, A., Bailey, E., Jones, S. J. and Tamarin, A. (1977). Dimensional changes during specimen preparation for scanning electron microscopy. *SEM/IITRI,* **10** (I), 507

Collins, V. P., Arborgh, B. and Brunk, U. (1977). A comparison of the effects of three widely used glutaraldehyde fixatives on cellular volume and structure. *Acta Pathol. Microbiol. Scand. Sect. A,* **85,** 157

Echlin, P. (1974). Coating techniques for scanning electron microscopy. *SEM/IITRI,* **7,** 1019

Echlin, P. (1975). Sputter coating techniques for scanning electron microscopy. *SEM/IITRI,* **8,** 217

de Harven, E., Lampen, N., Polliack, A., Warfel, A. and Fogh, J. (1975). New observations on methods for preparing cell suspensions for scanning electron microscopy. *SEM/IITRI,* **8,** 361

Jard, S., Bourguet, V., Carasso, N. and Favard, P. (1966). Action de divers fixateurs sur la perméabilité et l'ultra-structure de la vessie de grenouille. *J. Microscopie,* **5,** 31

Kenemans, P., Davina, J. H. M., de Haan, R. W., van der Zanden, P., Stolk, J. G. and Stadhouders, A. M. (1981). Cell surface morphology in epithelial malignancy and its precursor lesions. *SEM/IITRI,* **14** (III), 23

Mazia, D., Sale, W. S. and Schatten, G. (1974). Polylysine as an adhesive for electron microscopy. *J. Cell Biol.,* **63,** 212a

Murakami, T. (1974). A revised tannin osmium method for non-coated scanning electron microscope specimens. *Arch. Hist. Jpn,* **36,** 187

Noonan, S. M. and Riddle, J. M. (1977). Dynamic surface activities of exudative leucocytes. *SEM/IITRI,* **10** (II), 53

Thornthwaite, J. T., Thornthwaite, B. N., Cayer, M. L., Hart, M. A. and Lief, R. C. (1975). A new method for preparing cells for critical point drying. *SEM/IITRI,* **8,** 387

Vesely, P. and Boyde, A. (1973). The significance of SEM evaluation of the cell surface for tumour cell biology. *SEM/IITRI,* **6,** 689

Westbrook, E., Wetzel, B., Canon, G. B. and Berard, D. (1975). The impact of culture conditions on the surface morphology of cells *in vitro. SEM/IITRI,* **8,** 351

Wetzel, B., Erickson, B. W. and Lewis, W. R. (1973). The need for positive identification of leukocytes examined by SEM. *SEM/IITRI,* **6,** 535

2

Tissue organization and human reproduction

E. S. E. HAFEZ* and P. KENEMANS†

* Department of Gynecology/Obstetrics, Wayne State University School of Medicine, Detroit, Michigan 48201, USA
† Department of Gynecology/Obstetrics, University Hospital, Nijmegen, The Netherlands

The basic morphological pattern of the genital tract is that of a tubular system lined with epithelial cells showing a variety of luminal surface ultrastructures.

There are remarkable differences in the pattern of tissue organization of mucosa of different segments of the female and male reproductive organs. In most organs the cells are uniform in size, and closely packed, resembling 'cobblestones'. In some instances the surfaces of the cells are ill-defined and with short microvilli, or covered with residual mucus. The lining of oviduct, endometrium and endocervix consists basically of two types of cells: (a) ciliated cells and (b) non-ciliated secretory cells.

The ovaries have superficial epithelium with numerous microvilli and occasional blebs, ruffles, cytoplasmic projections and solitary, non-functional cilia.

The vagina and portio vaginalis of the cervix show large flat cells with microridges at the luminal cell surface.

In the fallopian tube the percentage of ciliated cells is highest near the fimbriae of the oviduct, declines with the approach to the uterus where the non-ciliated cells are abundant (Hafez et al., 1977). Variations in the percentage of ciliated and secretory cells along the length of the tube have some functional significance. Ciliated cells are most abundant where the egg is picked up from the ovarian surface, whereas secretory cells are more abundant where luminal fluids are needed as a medium for the interactions of eggs and spermatozoa. Although the ciliated cells in the ampulla appear to arise from crypt-like crevices because of the apical protrusion of the non-ciliated cells, the ciliary tips have free access of movement into the lumen. The longitudinal mucosal folds with underlying musculature are characteristic of the ampullary junction. The folds are involved in the rotation of the egg and its subsequent transport. In estrogen-deprived postmenopausal women the tubal epithelium is characterized by deciliation and loss of secretory activity. These changes occur in all segments of the tube and only rarely are there clusters of cilia, which appear short, scant and often degenerating.

The endometrium is characterized by the presence of numerous openings of the endometrial glands. Ciliated cells are less abundant in the endometrium than the tubal epithelium. A few ciliated cells may persist from one menstrual cycle to the next. Large cytoplasmic projections are noted at the apical membrane of the non-cilliated cells (Johannisson and Nilsson, 1972; Patek and Nilsson, 1973; Hafez et al., 1975). The abundance, length and shape, and interbranching, of these apical microvilli vary throughout the cycle. Development of luminal microvilli, synthesis, storage, release of endometrial secretory granules, and ciliogenesis are hormone-dependent. Degenerated cells are found at random at different stages of the menstrual cycle. Following the release of secretory material from the protruding cell membrane the cell collapses and becomes wrinkled and devoid of microvilli.

The vagina and ectocervix are lined by a stratified epithelium, containing some twenty to thirty pseudo-layers of cells, depending on estrogen levels. There is a maturation process in progress in which small round proliferating basal cells gradually develop into mature large flat squames. These latter, more superficially situated cells, show a microridge pattern at their luminally directed side, but a microvillus-like pattern on their basally directed cell side (Figure 1) (Davina et al., 1981; Kenemans et al., 1981, 1982).

CILIOGENESIS AND CILIARY ACTIVITY

Ciliated cells are found singly, or in groups, arranged in rows or a mosaic pattern. In the fimbriae the ciliated cells are so closely packed that it is impossible to distinguish between their boundaries. The non-ciliated cells are of uniform diameter.

Cilia first grow at the periphery of the cell and then fill in the central area. Cilia appear first as stubby, short
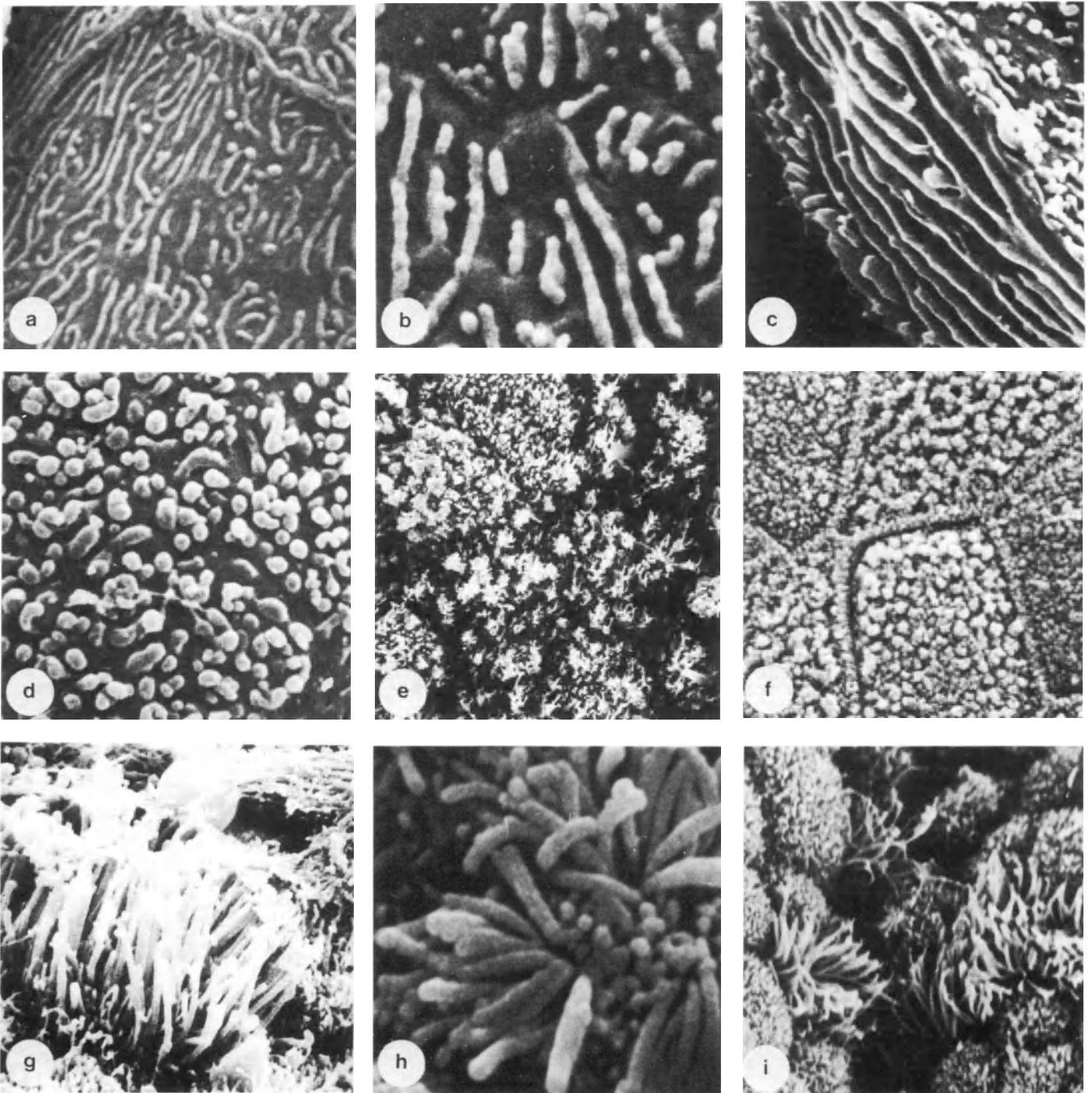
Figure 1   Scanning electron micrographs showing variability in cell surface ultrastructure within the female reproductive tract

a: microridge pattern on vaginal epithelium;
b: microridge pattern on ectocervical epithelium;
c: microridge pattern on lateral cell side of dysplastic ectocervical cell;
d: microvillous pattern on basal side of ectocervical cell;
e: microvillous pattern of endocervical cells;
f: microvillous pattern on metaplastic cervical cells;
g: ciliated cell of endocervix;
h: ciliated cell of endometrium;
i: ciliated cells of fallopian tube

Figure 2 Scanning electron micrographs giving sample of structures and surface architecture, which can be studied in low, and high magnification with the SEM (SEM photographs by Flechon, Hafez, Kanagawa *et al.*)

a: granulosa cells;
b: zona pellucida;
c: glans penis;
d: sperm cells;
e: two blastomeres;
f: placental villi;
g: fetal membrane;
h: umbilical cord

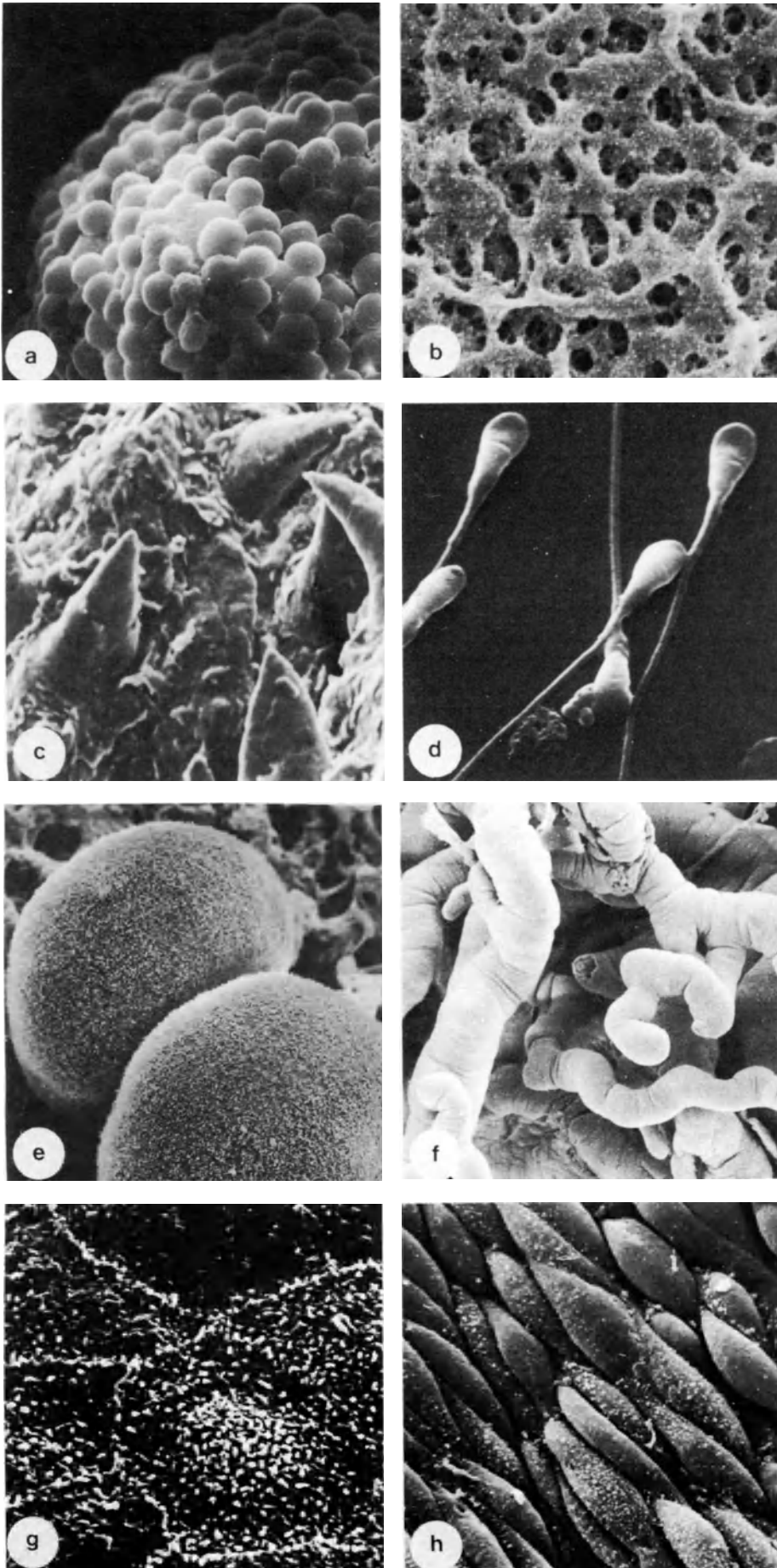cylinders on those cells which have large numbers of microvilli on their surfaces. Ciliary growth occurs randomly over the mucosal surface, and unevenly over each individual cell. Development of centrioles, which give rise to the necessary number of basal bodies for the induction of ciliary growth, is also asynchronous throughout the epithelium as well as within a single cell. There are, however, cells which at a given age are so undifferentiated that it is not possible to predict their final outcome. As cilia increase in length they become able to bend.

In the female reproductive tracts, kinocilia play an important role in the transport of particles and in directing the flow of luminal fluids. Two types of ciliary motility have been recognized: an effective stroke and a recovery stroke (Hafez and Kanagawa, 1972a,b, 1973), which is a slightly wavy motion. In the recovery stroke the cilia bend near the basal body and the degree of bending proceeds as a slow wave towards the tip. The recovery stroke carries the cilia back to the effective stroke position. Cilia beat approximately 1200 times/min. The kinocilia in the female reproductive tract beat rhythmically toward the vagina, creating a directional flow of luminal fluids.

Ciliary activity is responsible for the movement of ova into the ostium of the fimbriated tip and through the upper ampulla. Concomitant with this there is, at the time of ovulation and during preliminary migration through the tube, a sharp increase in the intensity of muscular contractions. Cilia of ampullary cells usually point toward the uterus. Ciliary currents in the tube and uterus sweep particles placed on the mucosal surfaces. The cilia covering the tubal and uterine epithelium seem to play a major role in the release of secretory material from the adjacent secretory cells, and in the distribution of the secretions within the lumen. Thus the function of the ciliated cells is generally believed to be the transport of eggs, zygotes and secretory material. Notwithstanding this common assumption, it was found that women suffering from a recently discovered syndrome, characterized by congenital immotility of the cilia (Kartagener's syndrome), are usually fertile (Afzelius et al., 1978), thus proving that ciliary motility is not essential for female fertility.

SECRETORY ACTIVITY AND LUMINAL FLUIDS

The tubal and uterine fluid plays a major role in the transport and maturation of the gametes. There is a close similarity between the tubal fluid and serum contents (immunoglobulins, electrolytes, glucose and enzymes) (cf. Hafez et al., 1975; Hafez, 1975).

The functional significance of the morphology of the secretory surface is well established. Using histochemical techniques, several types of secretory cells were noted in the cervical mucosa of macaques and rabbits (Hafez and Kanagawa, 1972a,b). It is not known whether these types are distinct cell types or different stages of one cell type. In the bonnet macaque (M. radiata) the cervix exhibits a complex glandular structure and exceptional secretory activity (Ovadia et al., 1971).

The rheological properties of cervical mucus are responsible for the retention and slow progression of spermatozoa through the cervix. Ciliated cells in the cervix may facilitate the orientation and flow of cervical mucus from the epithelium to the anterior vagina. This arrangement creates an alignment of micelles of mucus, thus providing pathways for the progression of spermatozoa to the uterus.

PROTECTING EPITHELIA

Normal cervical squamous epithelium shows an orderly tissue organization with a superficial layer consisting of large (30–50 μm in diameter), flat polygonal cells. These superficial cells overlap one another, while many cells are in the process of exfoliation. Therefore the superficial cells do not form a real continuous layer. Cells may exfoliate singly or in clusters. The latter are most probably cells still interconnected by desmosomes.

The cell surface micromorphology of the free luminal side of the normal, mature superficial cells shows, characteristically, three distinct features, viz.: (a) microridges; (b) terminal bars, the interconnected and elevated cell boundaries of two laterally adjacent cells; and (c) linear bars.

These latter cell surface elevations are morphologically similar to the terminal bars. They are not situated at the cell border, but on the cell surface. The bars may join each other. Most probably these linear bars are present at those locations on the cell surface where two (or more) initially more superficially positioned adjacent cells (which have been desquamated already) had their cell borders joining each other. Light microscopically these linear bars give the well-known dark lines within the cytoplasm, which were sometimes held to be 'artifacts or cell-wrinkles'.

The surface micromorphology of the non-luminal cell side, the side originally directed to the basement membrane (i.e., the so-called 'basal cell side') of normal, mature superficial and intermediate ecto-cervical cells show different characteristics, viz.: (a) globular microvilli and (b) so-called linear grooves, which are most probably 'complementary' to the protruding terminal bars on the luminal cell sides of the subadjacent cells (Kenemans et al., 1980, 1981, 1982; Davina et al., 1980, 1981).

The normal squamous epithelium of the lower vagina is smooth, with very little undulation of the surface architecture. At a higher power, the cells appeared to be flat, polygon-shaped, with demonstrable but thin-edged interdigitating borders. The cells lie multilayered, overlying each other irregularly, much like haphazardly laid shingles on a roof. The edges of these cells roll back giving the characteristic picture of exfoliation as they lift up from their borders. The surfaces of these cells for the most part have a pattern of delicate interlacing microridges similar to fingerprints. The exfoliated cells appear wrinkled as if dried up, with a loss of, or obscured, surface microridges.

The vulva, made up of the labia majora and minora, the clitoris and vaginal introitus, is covered by stratified

squamous epithelium similar to all other skin areas; with some follicles, and sebaceous and sweat glands. The surfaces of the cells show the usual interlacing microridges. The edges of these cells are thin in contrast to the slightly raised terminal bars on the squamous cells of the upper vagina and ectocervix.

In the female genital tract the stratified epithelium plays an important role in the protection of the organism against external influences. At the same time the structural organization permits metabolic interchange with, and by way of, the intercellular space. The more superficial cells have intermeshing cell surface projections, resulting in an increase in surface adhesiveness, and especially in an increased resistance to sideways movements.

References

Afzelius, B. A., Camner, P. and Mossberg, B. (1978). On the function of cilia in the female reproductive tract. *Fertil. Steril.*, **29**, 72

Davina, J. H. M., Stadhouders, A. M., Kenemans, P. and van Haelst, U. J. G. M. (1980). A stripping technique for scanning electron microscopical study of adjoining cell surfaces in stratified squamous epithelium of the uterine ectocervix. *Beitr. Electronenmikroskop. Direktabb. Oberfl.* **13**, 253

Davina, J. H. M., Stadhouders, A. M., Lamers, G. E. M., van Haelst, U. J. G. M. and Kenemans, P. (1981). Surface pattern differentiation of the epithelial cells of the human uterine ectocervix. *SEM Symposium*, **14**, (III), 37

Hafez, E. S. E. and Kanagawa, H. (1972a). Ciliated epithelium in the uterine cervix of the macaque and rabbit. *J. Reprod. Fertil.*, **28**, 91

Hafez, E. S. E. and Kanagawa, H. (1972b). Histomorphology of ciliated cells in oviduct and cervix uteri of macaques. *Prod. 3rd Conf. Exp. Med. Surg. Prim. Lyon, Med. Primat,* part 1, 233

Hafez, E. S. E. and Kanagawa, H. (1973). Scanning electron microscopy of human monkey and rabbit spermatozoa. *Fertil. Steril.*, **24**, 776

Hafez, E. S. E., Barnhart, M. I., Ludwig, H., Lusher, J., Joelsson, I., Daniel, J. L., Sherman, A. I., Jordan, J. A., Wolf, H., Stewart, W. C. and Chrétien, F. C. (1975). Scanning electron microscopy of human reproductive physiology. *Acta Obstet. Gynecol. Scand.,* Suppl. 40, 1

Hafez, E. S. E., Fadel, H. E., Noonan, S. M. P., Oshima, M., Ilamura, H., Watson, J. H. L., Zaneveld, L. J. D. and Steger, R. W. (1977). Scanning Electron Microscopy of Human Female Reproductive tract and Amniotic Fluid Cells. *Int. J. Fertil.* **22**, 193

Johannisson, E. and Nilsson, L. (1972). Scanning electron microscopic study of the human endometrium. *Fertil. Steril.*, **23**, 613

Kenemans, P., van der Zanden, P. H. T., Stolk, J. G., Vooys, G. P. and Stadhouders, A. M. (1980). Cell surface ultrastructure in neoplasia of the uterine cervix. In Letnansky, K. (ed.) *Biology of the Cancer Cell,* pp. 307–18. (Amsterdam: Kugler)

Kenemans, P., Davina, J. H. M., de Haan, R. W., van der Zanden, P., Vooys, G. P., Stolk, J. G. and Stadhouders, A. M. (1981). Cell surface morphology in epithelial malignancy and its precursor lesions. *SEM Symposium,* **14** (III), 23

Kenemans, P., Davina, J. H. M., de Haan, R. W., van der Zanden, P., Vooys, G. P., Stolk, J. G. and Stadhouders, A. M. (1982). Surface ultrastructure of the uterine cervix and early detection of irreversible neoplasia. In Hafez, E. S. E. and Smith, J. P. (eds). *Carcinoma of the Cervix: biology, etiology and diagnosis,* pp. 91–9 (The Hague: Martinus Nijhoff)

Ovadia, J., McArthur, J. S., Kopito, L. and Ulefelder, H. (1971). The cervical mucus secretion of the bonnet monkey *(M. radiata):* anatomical basis and physiological regulation. *Biol. Reprod.,* **5,** 127

Patek, E. and Nilsson, L. (1973). Scanning electron microscopic observations on the ciliogenesis of the infundibulum of the human fetal and adult fallopian tube epithelium. *Fertil. Steril.,* **24,** 819

I GYNECOLOGY

3

The vagina (normal)

E. S. E. HAFEZ* and P. KENEMANS†

* Department of Gynecology/Obstetrics, School of Medicine, Wayne State University, Michigan 48201, USA
† Department of Gynecology/Obstetrics, University of Nijmegen, Nijmegen, The Netherlands

The vagina is a sensitive indicator of age-related alterations in the endocrine milieu, but also exhibits age-associated changes that may not be under direct endocrine control (Hafez, 1975, 1977; Hafez et al., 1975; Hafez and Evans, 1978; Jaszczak and Hafez, 1980).

VAGINAL EPITHELIUM

Vaginal rugae

The reddish grey vaginal surface (incorrectly termed mucosa since it does not secrete mucus) is corrugated by the development of numerous transverse folds or rugae (Figure 1). At the anterior and posterior vaginal wall there are two ridges of folds: the anterior and posterior columnae rugarum. Because of the ridges the cross-section of the vagina has an H-shape. The anterior ridge of the folds is caused by longitudinal muscular tracts which lie underneath; the posterior one is caused by venous plexuses embedded in the layer of connective tissue of the mucosa (Platzer et al., 1978). The vaginal rugae are most prominent in nulliparous women and following repeated deliveries, gradually diminish, resulting in the smooth epithelial surface noted in highly parous women (Kistner, 1978). The vaginal rugae appear in the pubescent female as a result of estrogen stimulation and disappear in postmenopausal women with the decline of estrogen levels.

Cellular layers

The vaginal epithelium is made up of five different layers of cells: (a) basal cells made of a single layer of cuboidal cells overlying the basement membrane; (b) a parabasal layer made of several layers of polyhedral cells with distinct nuclei: (c) an intermediate layer composed of larger flatter cells with nuclei; (d) a transitional layer; and (e) a superficial zone composed of several layers of large flat cells with pyknotic nuclei (Table 1). Each layer has ill-defined limits and shows a gradual change in structure. Under adequate estrogen stimulation the squamous cells proliferate into 30 or 40 layers. The basal and parabasal layers are the most active proliferative compartments or germinal beds of the epithelium (Averette et al., 1970).

The epithelial layer of the vagina consists of an epithelial lamina and a lamina propria (Figures 2 and 3). The epithelium is a non-cornified, stratified squamous epithelium. Being very high in the neonate, it flattens within 3 weeks due to the decline in the maternal estrogen level. The squamous epithelium is 150–200 μm thick. The vaginal epithelium is made of flat, polygon-shaped cells with demonstrable but thin edged interdigitating borders (Ferenczy and Richart, 1974). The cells lie multilayered, overlying each other irregularly, much like haphazardly laid shingles on a roof. The edges of these cells roll back giving the characteristic picture of exfoliation as they lift up from their borders. The cell surface is made of delicate interlacing microridges whose appearance resembles the pattern of fingerprints (Figures 4 and 5).

The highly flattened outer cells in the stratified squamous epithelium are continuously shed by the process of desquamation and are replaced by division of generative cells in the basal layer of the epithelium. In the process of exfoliation, the cells show slightly elevated and detached cell borders, exposing similar-appearing layers of cells beneath them. Upon degeneration and desquamation, the exfoliated cells accumulate in the vagina. These are mixed with normally present Doderlein bacilli, vaginal transudate and cervical mucus to form a small amount of acid, whitish material resembling curdled milk.

Ultrastructural characteristics

Cellular microridges

The surface of the vaginal epithelial cell is made up of numerous microridges that run longitudinally or in circles. In this multilayered stratified epithelium the cells are wedged one upon the other by interlocking
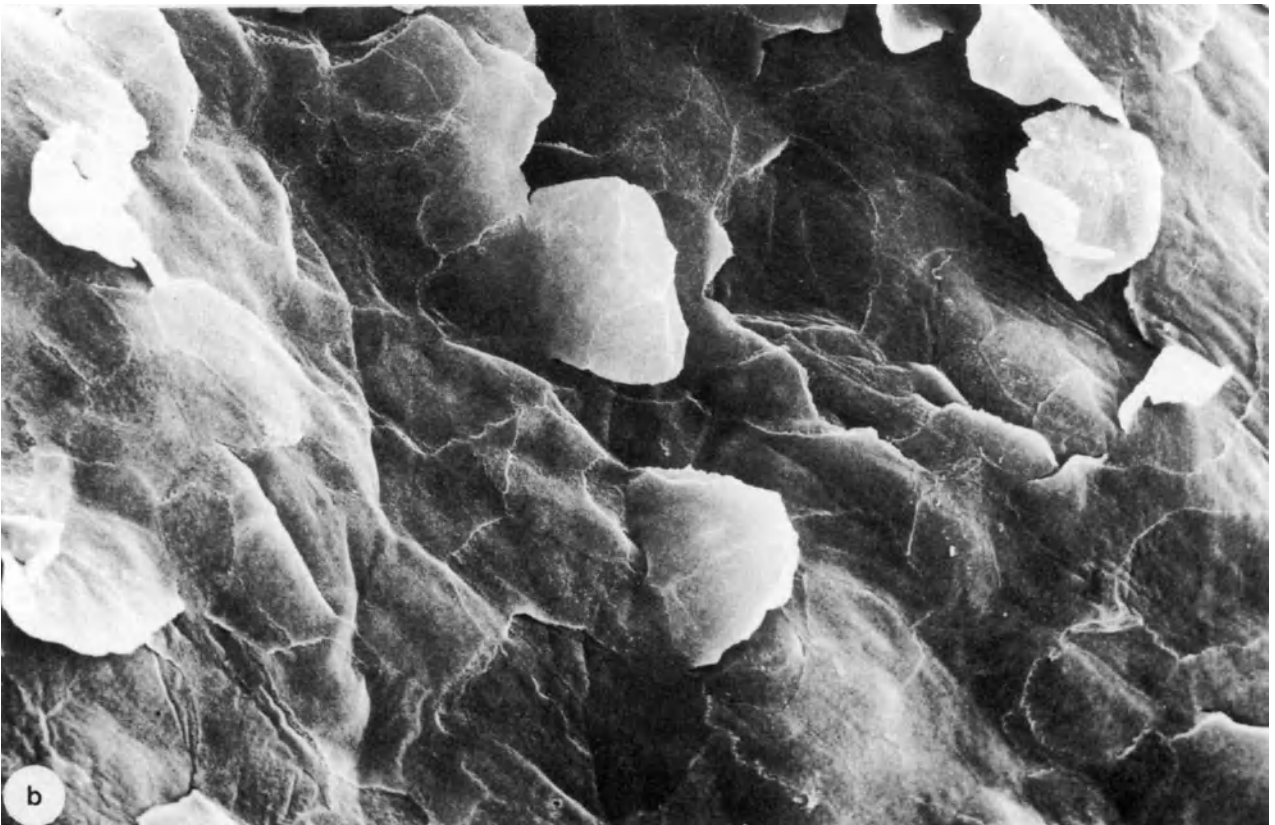
Figure 1

Top: Vaginal rugae at a low magnification: note the   Bottom: Exfoliation of cells from the vaginal superficial
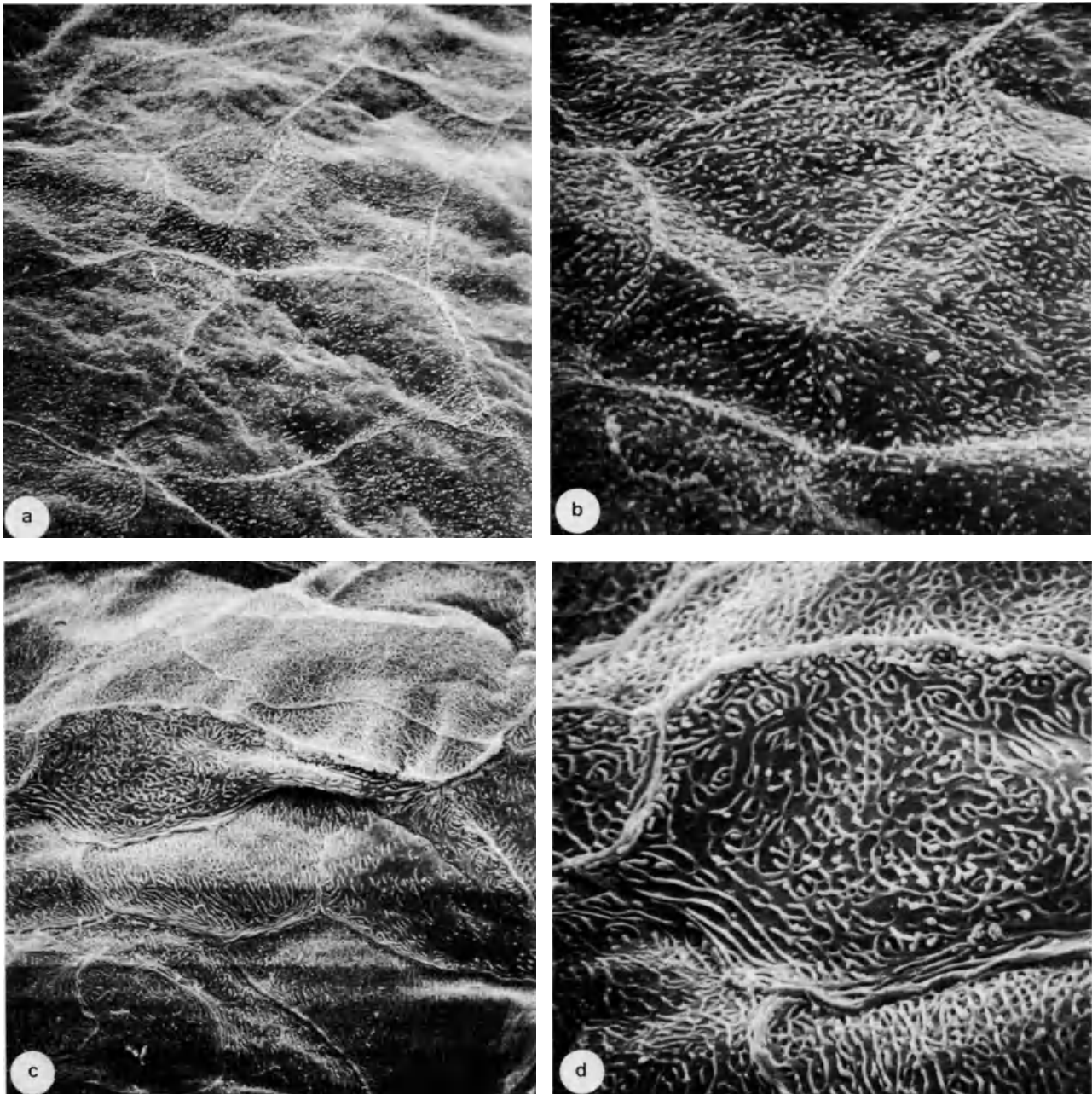   transverse folds   layers

Figure 2

a and b: Vaginal surface during high proliferation (preovulatory phase)

a: Homogeneous surface pattern with large polygonal superficial cells (×1070)

b: Cornified surface ultrastructure of superficial cells with short and coarse rudiments of microridges (×2678)

c and d: Vaginal surface during pregnancy

c: Effects of extension within the vaginal surface and within the individual cells during pregnancy (×1070)

d: Distended intercellular microridges, tender cellular borders because of enlarged elasticity (×2678)
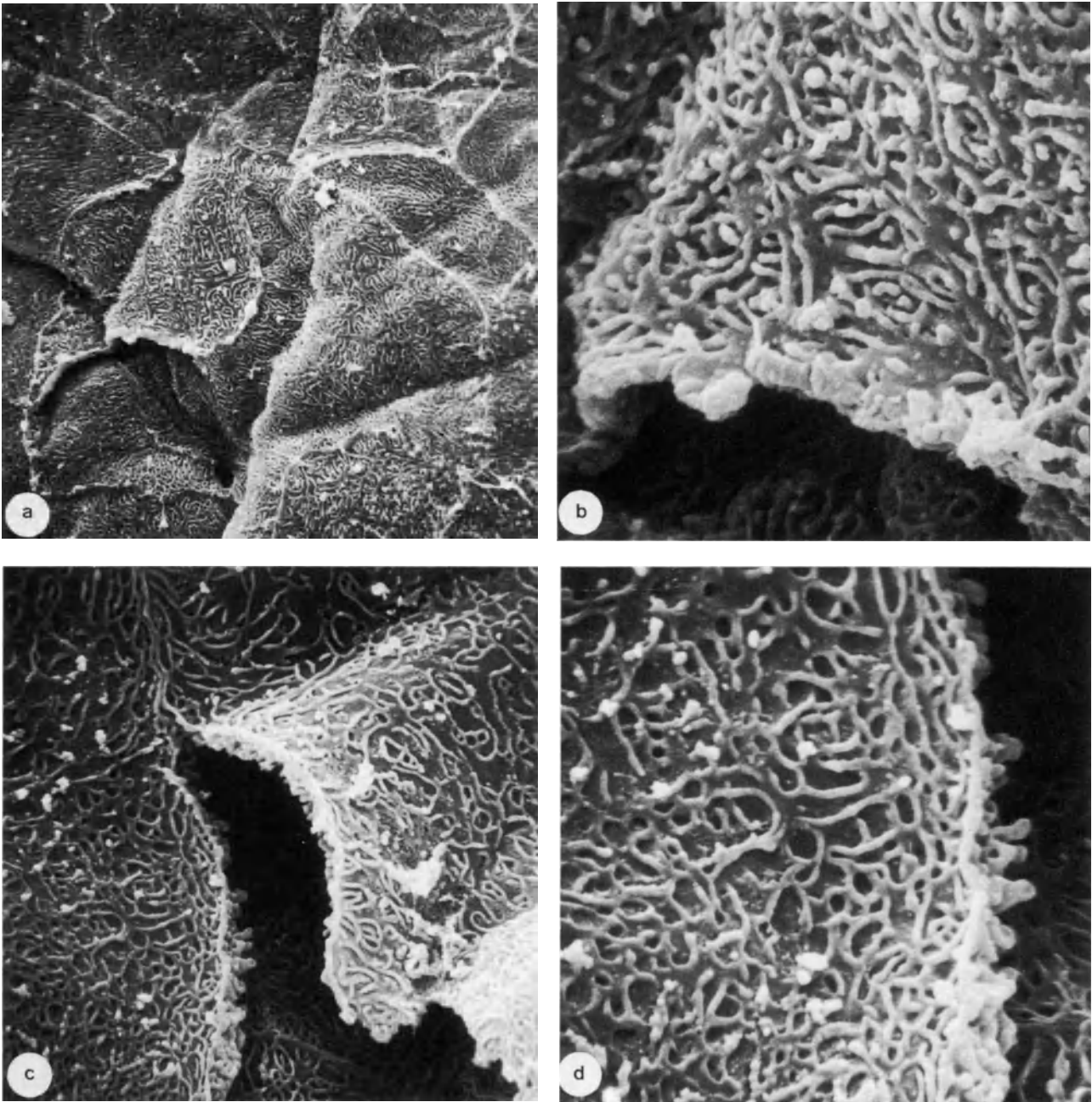
(Walz et al., 1978)

Figure 3   Vaginal epithelium in desquamation during luteal phase

a: Loss of intact ultrastructural surface pattern – contamination with physiological coatings of non-structural substances because of cytolysis (×1070)

b: Intercellular microridges open-ended on desquamating cells (×6300)

c: Zipper-like intercellular connection (×2678)

d: Sharply defined polygonal flattening of open-ended microridges, i.e. the position of intercellular desmosomes (×5355)
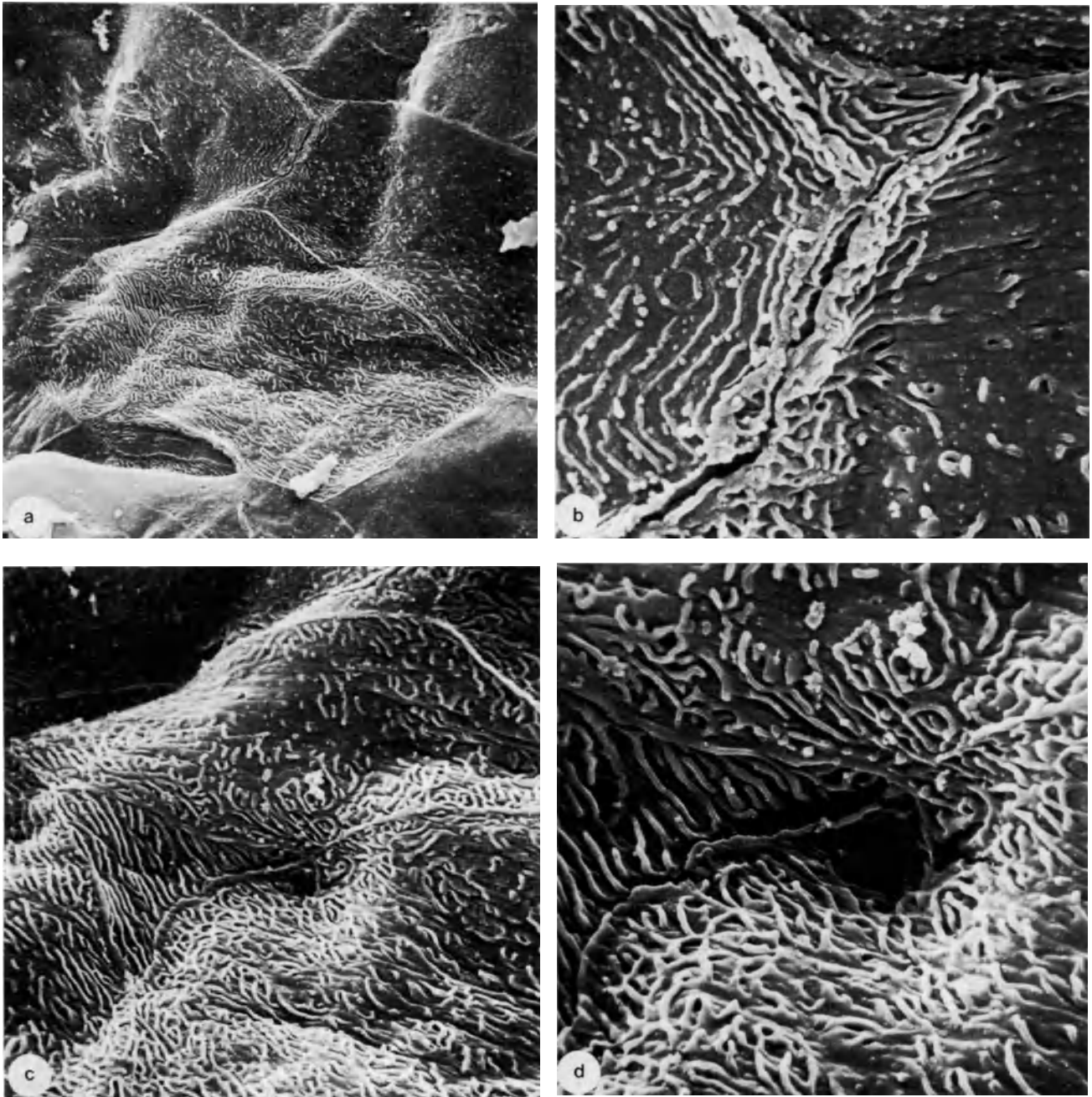
(Walz et al., 1978)

Figure 4   Vaginal surface during desquamation phase
a and b: Desquamation of surface epithelium cells preceded by loosening of intercellular grooves (×1070 **a** and ×5355 **b**)

c and d: Pore-like widening of intercellular crevices for intense contact between the space system and the vaginal surface (intercellular porosity). (×2678 **c** and ×5355 **d**) (Walz *et al.*, 1978)
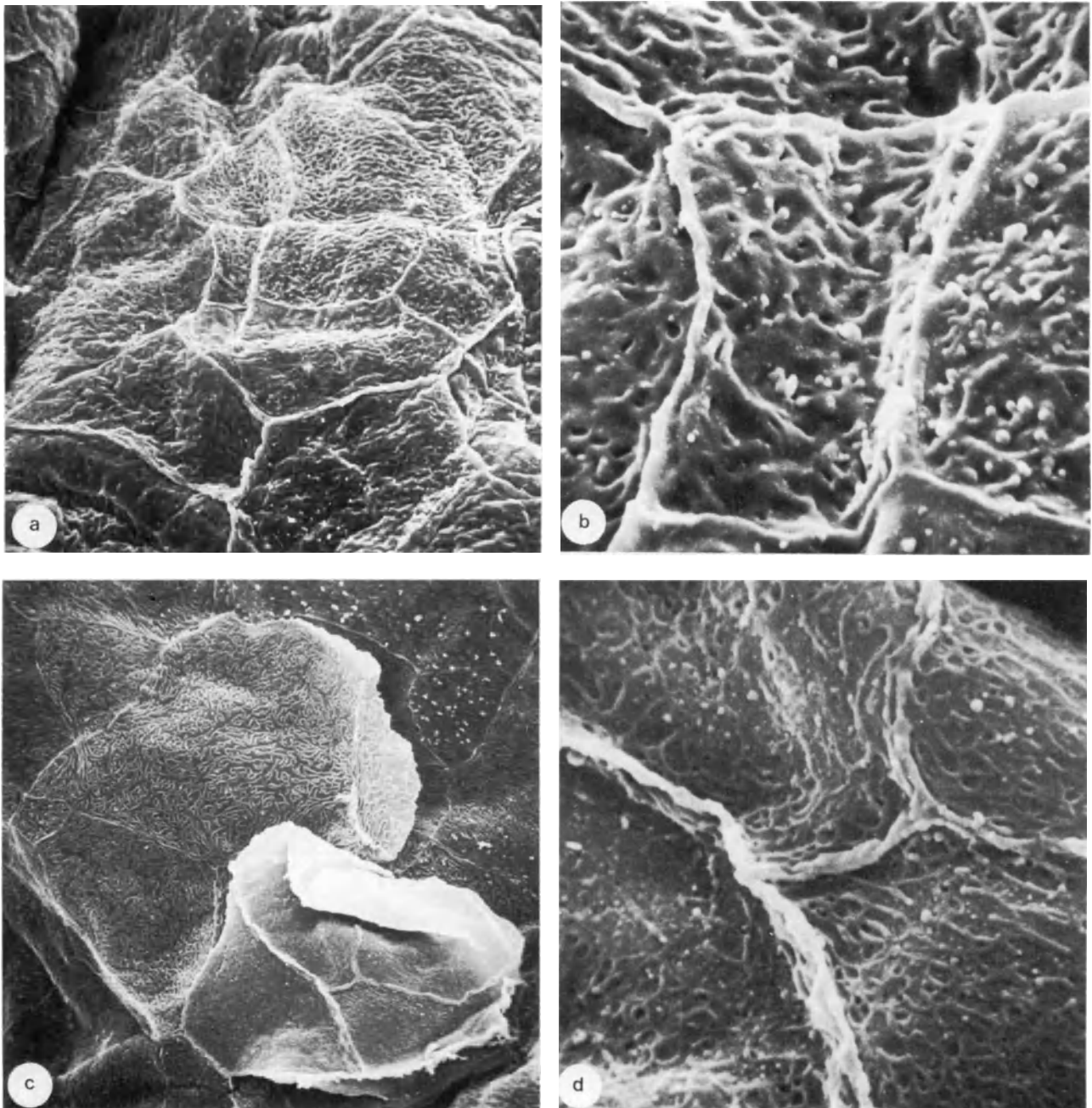
Figure 5 Vaginal surface during prepuberty and during senescence

a: Proliferation of vaginal epithelium during pre-puberty – dense ultrastructure of intercellular grooves (×1070)

b: Signs of superficial cornification – predisposed pore-like widening within the intercellular grooves (×5355)

c: Further flattening of the vaginal surface pattern during senescence, i.e., state of atrophy with keratinization; desquamation and fragmentation of keratinized cell platelets (×1070)

d: Intercellular grooves locked together (×5355) (Walz et al., 1978)

Table 1 Some histological and ultrastructural characteristics of cell types in the human vagina

Cell type	Histological characteristics	Ultrastructural characteristics	Nucleocytoplasmin ratio
Basal			
	Single row of low columnar cells closely opposed to basement membrane, thickness of layer 10 μm	Membrane shows projections of microvilli which interdigitate at lateral and apical borders with those of neighbor cells; pinocytic vesicles and occasionally larger caveolae between microvilli and at the basal border. Desmosomes are absent at sides and more numerous at apical border. Basal junctions or hemidesmosomes are found as in other stratified epithelia. Nucleus is irregular with numerous indentations with chromatin as a condensed ribbon at the periphery and dispersed in the rest of the nucleus. One or two prominent nucleoli with well-developed granular components, fibrillar portions and clusters of small (20–25 nm) and large (40–45 nm) particles. Cytoplasm has organelles, differentiations and inclusions. Mitochondria in moderated amount of small size, with few cristae, clear matrices. Endoplasmic reticulum is poorly developed at the follicular stage with few cisternae of rough endoplasmic reticulum. Organelles appear to be more developed at the ovulatory and luteinizing stages. At beginning of follicular phase free ribosomes predominate, but at the end of this phase they form clusters of polysomes. Few cytoplasmic filaments which are clustered and anchored to basal junctions and desmosomes at beginning of follicular phase.	1:1
Parabasal			
	Two rows of polygonal or polymorphic shape; thickness layer is 14 μm	Similar in size and fine structure to basal type. Surface shows a higher development of cell membrane projections consisting of microvilli and clusters of interdigitations. Number of desmosomes, twice the number in basal cells, are distributed around cell periphery. Nucleus is irregular with frequent indentations; nucleolus cells prominent but less dense than in basal cells. During follicular phase the cytoplasm shows free ribosomes and fascicles of filaments in similar proportions to the basal cells. During luteal phase polysomes and profiles of rough endoplasmic reticulum are in the cytoplasm close to the nucleus or between mitochondria. Mitochondria located at peripheral cytoplasm; Golgi complex is more prominent during luteal phase; Centrioles in some cells appear related to a short cytoplasmic projection which resembles a cilium.	
Intermediate			
	10 rows of round or irregular cells with a prickle contour; cells have largest volume; toward ovulation cell volume increases to become the thickest layer of epithelium	Periphery of cell studded with desmosomes and microvilli. Nucleus is a more regular ovoid with some indentations. Nucleoli are prominent. The chromatin is dispersed with some peripheral conglomerates, numerous small dense particles or interchromatin granules and large dense particles or perichromatin granules. Cytoplasm is more elaborate and heterogeneous than in the other cell types. Fibrillogenesis evident during follicular phase; clusters of polysomes and mitochondria surrounded by a network of filaments 100 Å. Synthesis of glycogen appears as a juxtanuclear crescent of particles which are molecules of glycogen of beta-particle type. In vacuolized cells the nucleus adopts a crescent shape around a large vacuole or becomes slightly depressed at the pole contacting the vacuole.	1:40
Transitional			
	Changes gradually from an oval elongated type into a squamous type; has 10 layers with maximal	Signs of involution surfaces have gradually lost most of microvilli; desmosomes become less prominent. As involution progresses, the irregular contour and density of nuclei increase and peripheral conglomeration of condensed chromatin as well as dark clumps in the nucleoplasm appear. Typical pyknotic nuclei appear in outer layers and nucleoli are no longer recognized. Ribosomes and endoplasmic reticulum disappear. Stages of mitochondrial swelling and involution and mitochondrial ghosts are in marginal cytoplasm.	1:20

Table 1 cont.

Cell type	Histological characteristics	Ultrastructural characteristics	Nucleocytoplasmin ratio
	thickness ovulation (80 μm)	Lysosomes are recognized. Filaments are clustered in fascicles at the cell margin; accumulation of dark granules surrounded by a single membrane vacuole at marginal cytoplasm. Cell becomes superficial during the luteal phase due to the loss of the desquamating layer.	
Superficial	10 rows of squamous cells; layers reach maximum thickness at ovulation	Cells are flat scales with an irregular serrated contour or a smooth linear surface; serrated border appears as a series of wedge-shaped prominences in the marginal zone of scales which correspond to elongated bars or microridges. Great variation of patterns in cell surface. Irregular and pyknotic nuclei, flattened following the long axis of the cell, show ill-defined contour; dark particles of large size appear set apart from the main clump of chromatin. Fascicles of filaments are concentrated at marginal cytoplasm; a few large vacuoles in cytoplasm. No organelles are recognized and there are also some dark and irregular clumps of material.	1:50

Data from Burgos and Vargas-Linares, 1970, 1978; Dembitzer *et al.*, 1976; Hinglais-Guillaud, 1959; Richter, 1971

Table 2   Cytological characteristics of human vaginal epithelium during the follicular and luteal phase

Parameters	Follicular phase	Luteal phase
Cytological characteristics	Increased mitosis in basal and parabasal layers with increase in epithelial thickness and number of layers. Increased number of intercellular junctions and more cohesion. Increased number of desmosomes and cytoplasmic filaments (tonofibrils). Increased accumulation of glycogen in intermediate transitional and superficial layers. Lipid droplets appear during late follicular phase.	Desquamation of cells before complete differentiation. Nuclear chromatin forms dense clumps concentrated at nuclear envelope. Nucleus shrinks, becomes irregular in shape, and pyknotic. Nucleoli lose granular component. Most organelles lose definition upon reaching desquamating layer. Glycogen is degraded intercellularly by lysosomal enzymes, leaving empty spaces. Loss of adhesive properties of desmosomes, inert scales are shed in lumen.
Number of cell layers	22 layers on day 10. 46 layers on day 12–14. 32 layers on day 19.	23 layers on day 24.

Data from Averette *et al.*, 1970; Burgos and Vargas-Linares, 1978; unpublished data

Figure 6 (opposite)

Top: Luteal phase. Cell processes of the adjacent cells (intermediate layers) showing numerous desmosomes. Arrow marks a gap or nexus. Note the orientation of the tono-filaments (F) and their interrelationship with the desmosome. Asterisk points out the opened intercellular channel (×42 000)

Bottom: Follicular phase. A stromal macrophase showing a Golgi complex (G), mitochondrion (M) and lysosomes (L). A portion of a small lymphocyte appears partially covered by a dense material resembling a basal lamina (arrow) (×15 400) (Burgos and Roig de Vargas-Linares, 1978)
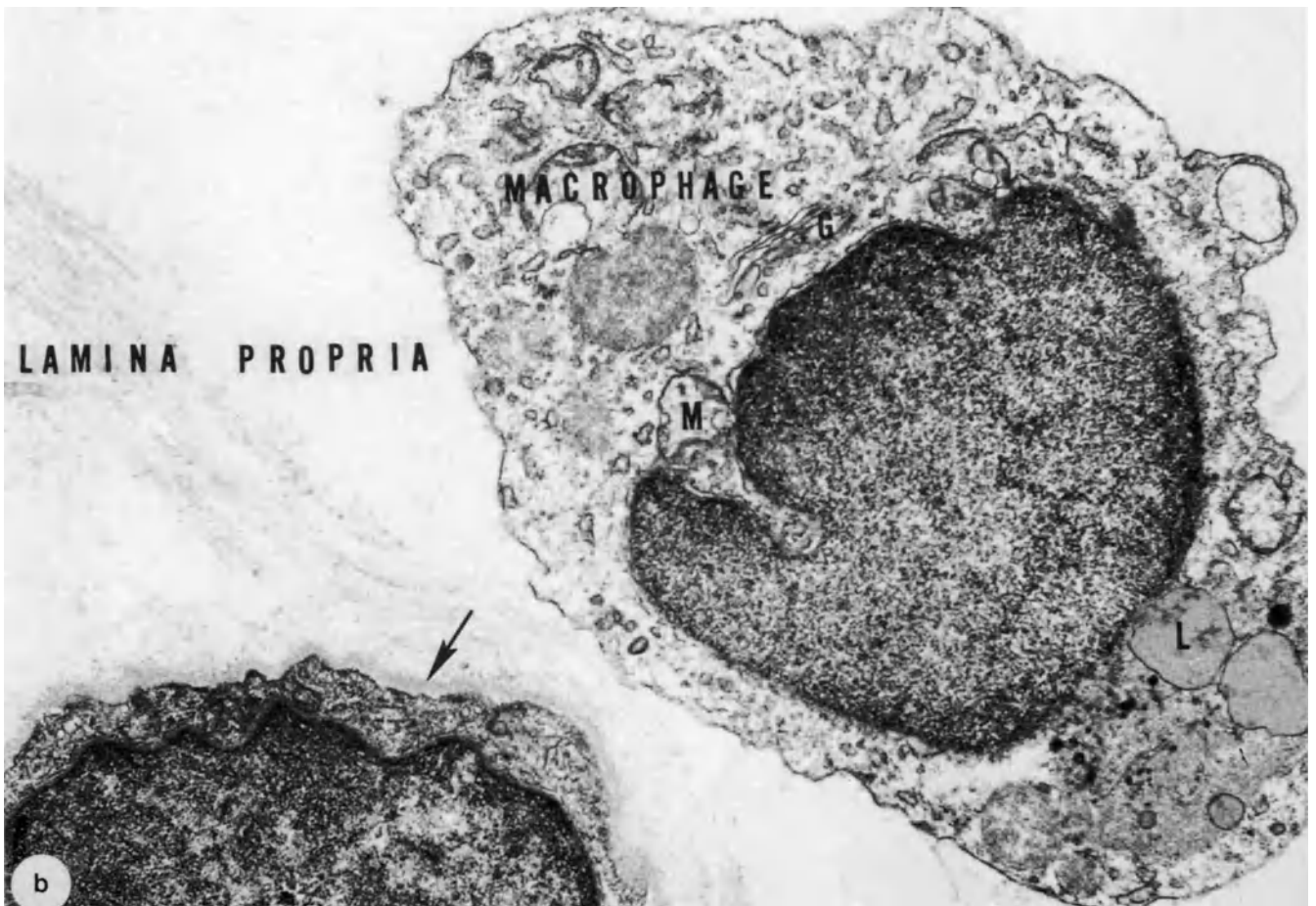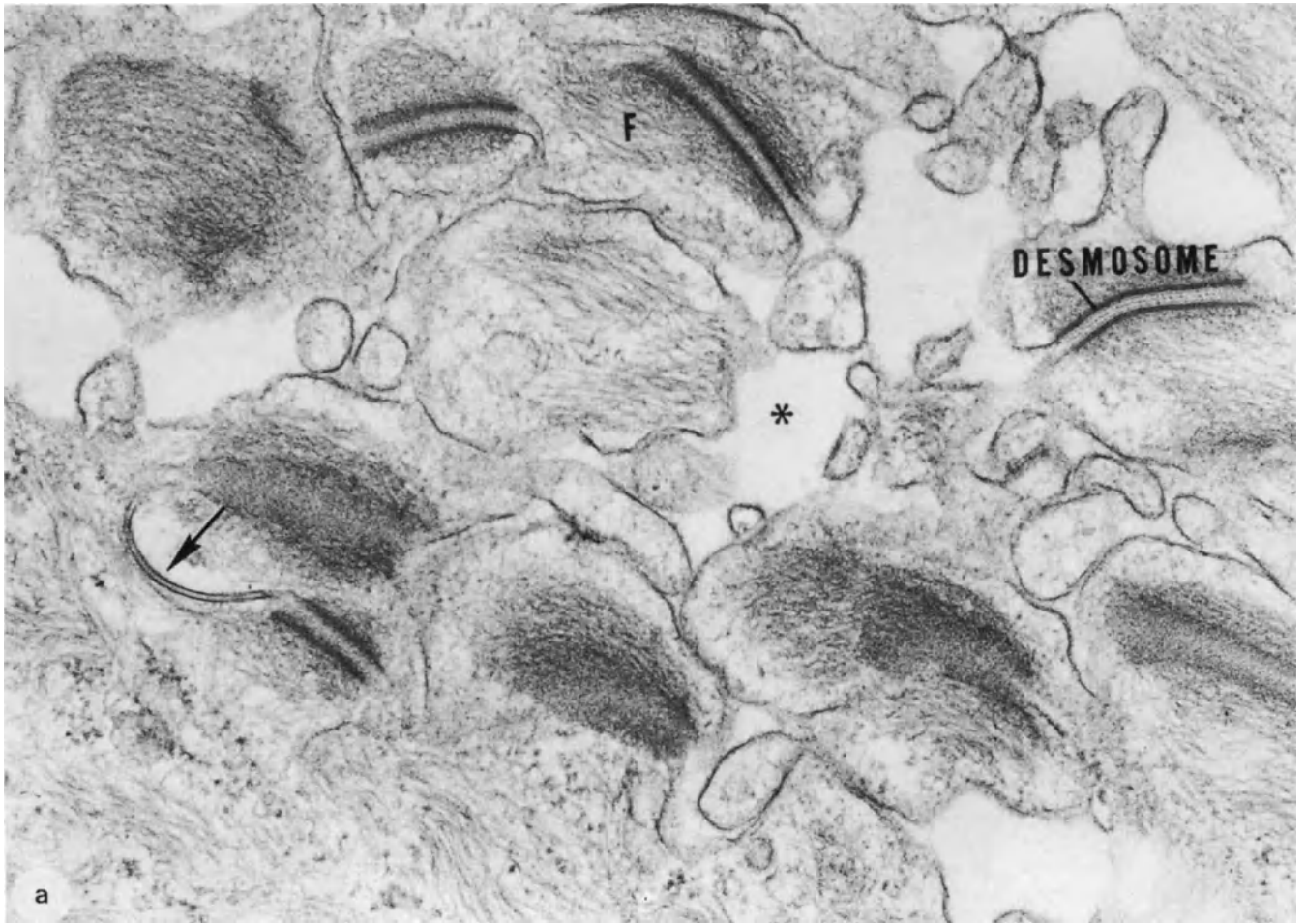
Figure 6

Table 3 Structural changes in the human vagina during the reproductive cycle and menopause

Phase	Cytology	Histology	Histochemistry	Surface ultrastructure
Proliferative	Progressive increase in superficial cells. Rise in karyopyknotic index. Decrease in leukocytes and bacteria.	Well-defined epithelial layer consisting of four distinct cell layers (basal, parabasal, intermediate and superficial).	Glycogen accumulates to a maximum just prior to ovulation.	Numerous exfoliating cells, especially just prior to menstruation. Well-defined microridges and cell borders.
Secretory	Dominated by intermediate cells often found in clusters. Individual cells folded or have curled edges. Low karyopyknotic index.	Similar to proliferative phase with possible reduction in superficial cell layer.	Glycogen decreases without depletion in intermediate layer.	Decreased numbers of exfoliating cells. Microridges still well developed
Menopausal	Variable from highly proliferative to atrophic with mixed patterns of superficial and parabasal cells.	Epithelial thickness variable, but generally thinner.	Glycogen is variable, generally low, increased collagen deposition in lamina propria.	Decreased number of microridges on some cells.

Microridges oriented in one direction only. |
| Postmenopausal | Variable, occasionally completely atrophic with a predominance of parabasal cells. Abundant intermediate cells with occasional superficial and parabasal cells. Low karyopyknotic index. | Epithelium becomes markedly thinner, often invaded with leukocytes. Areas completely denuded of an epithelial covering. | Glycogen is very low or completely absent, restored by estrogen administration. Collagen replaces many of elastic fibers in lamina propria. Lipofuscin granules in muscle cells. | Decrease in numbers of exfoliating cells. Surface microridges absent or markedly reduced. Cell borders less distinct and nuclear bulges occasionally observed |

Data from Steger and Hafez, 1978.

Figure 7 (opposite)
Top: Luteal phase. A stromal mast cell in close vicinity with a small lymphocyte. Asterisk marks the particulate material in a specific granule which shows the lamellar component at the periphery. Arrow points out the epithelial basal lamina ($\times 12\ 600$)
Bottom: Luteal phase. Portion of the cytoplasm of a plasma cell showing a material of moderate electron density in the cisternae of the cell surface. Arrow marks a prominent nucleolus in the nucleus of a lymphocyte. Ground substance (star) ($\times 75\ 600$) (Burgos and Roig de Vargas-Linares, 1978)
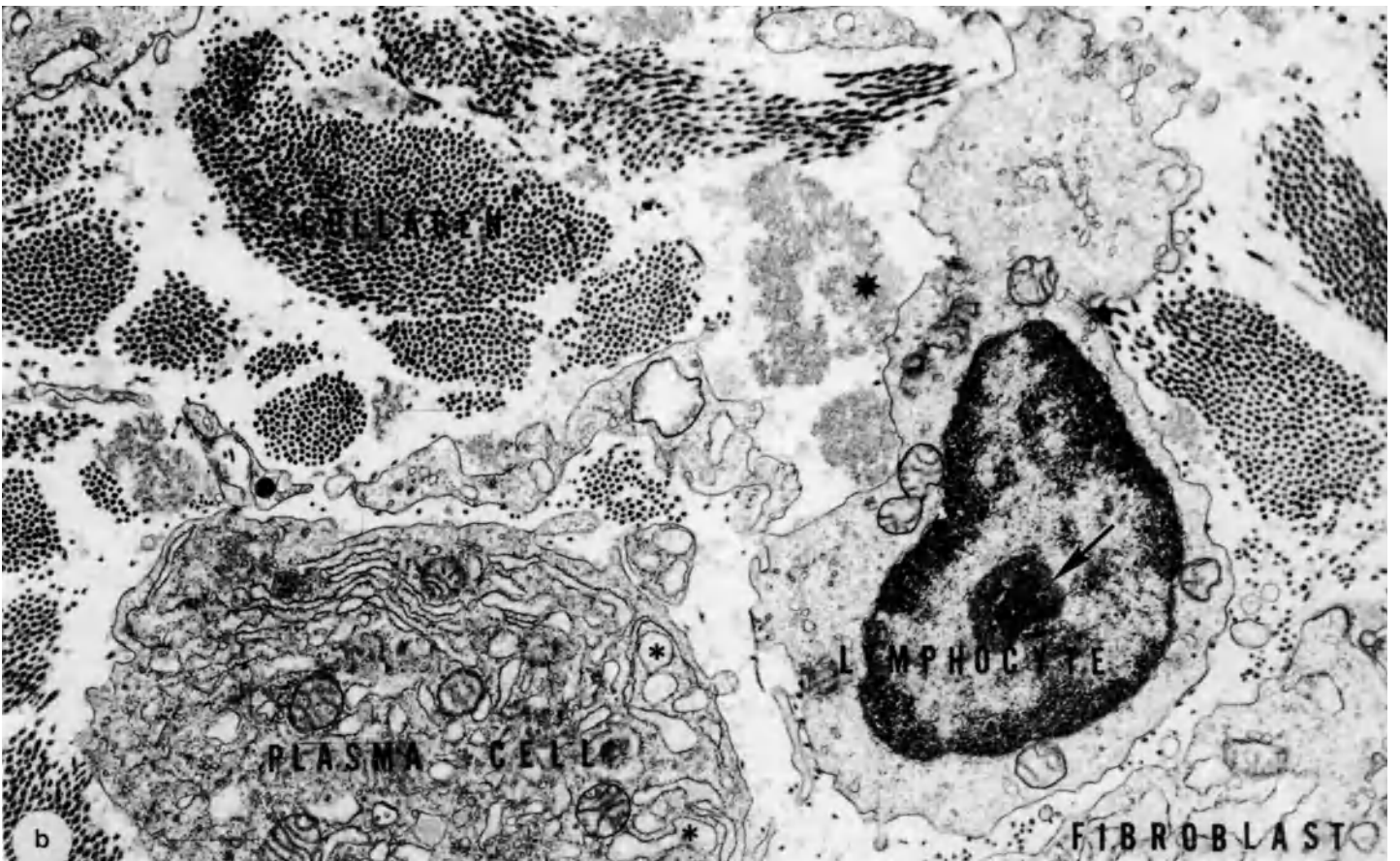
Figure 7

opposed microridges, thus forming a firm surface.

The morphology and pattern of these microridges, which affect the firmness of the epithelium, vary throughout the reproductive cycle. The microridges may be important for holding and distributing secretory products (Parakkal, 1974): and/or may serve to interlock or hold the epithelial cell layers together (Ludwig and Metzger, 1976).

Intercellular junctions

Intercellular junctions are present in the human vaginal epithelium during the entire cycle (Figures 6 and 7). Three types of junctions are recognized: desmosomes (macula adhaerens), the tight junction (zonula occludens) and the intermediate junction (zonula adhaerens). A fourth type of junction is found at the basement membrane: the basal junction or hemidesmosome (Burgos and Roig de Vargas-Linares, 1970, 1978).

The epithelial cells have elaborate intercellular channels which attain maximal development during the ovulatory and luteal phases upon reaching the time of ovulation, the intercellular channels become wider in the basal, parabasal and intermediate layers, but the thickness of the channels apparently does not change in the transitional and superficial layers throughout the entire follicular phase. During the luteal phase the intercellular channels appear wider than those during the follicular phase.

The cyclic desquamation of surface epithelium cells is preceded by the widening of intercellular grooves. Upon the cell surfaces there is a densely convoluted arrangement of microridges. Microridges which normally connect cells operating on a zip-fastener principle are exposed to the vaginal surface defining the cell layer. This porosity ensures a better contact between the intercellular space system of vaginal epithelium and the vaginal surface. These intercellular pores allow for passage of vaginal lubricating fluid.

STRUCTURAL CHANGES IN THE VAGINA

Cyclical changes

A few weeks after birth the vaginal epithelium diminishes in thickness and after a few months it is quite thin. This condition is maintained until puberty with the result that the natural barriers to disease during this time are minimal and gonorrheal and non-specific vaginitis are common.

The vaginal epithelium is under the endocrine control of estrogens and progesterone (Tables 2 and 3). Estrogens stimulate cellular proliferation and differentiation in both epithelium and lamina propria. Progesterone reinforces estrogens in glycogen synthesis, opens the intercellular channels and mobilizes through them the migrating lymphocytes from the lamina propria.

The cyclical changes of the vaginal epithelium are less pronounced than those of the endometrium. Differential cytology of the vaginal epithelium can be used to identify the stages of the cycle. The epithelium is highest in the proliferative stage and reaches the highest glycogen content during ovulation. During the secretory phase the thickness of the epithelium again decreases due to the shedding of cells (Platzer et al., 1978). The vaginal surface loses its intact structure once the luteinization starts. After desquamation on the surface of isolated vaginal epithelium cells the contamination with physiological coatings can occasionally be observed too, as well as non-structural substances, resulting from bacterial cytolysis.

Effects of oral contraceptives

The combined estrogen–progestin oral contraceptives produce histological changes and if the amount of estrogen is low, e.g. 3–50 μg per tablet, the effects of the progestin predominate causing drying of vaginal epithelium and dyspareunia. The over-all effect of oral contraceptives depends on the ratio and cumulative amounts of progestin and estrogen in each tablet. For example Enovid-E is more estrogenic than Enovid-5 since the estrogen content in the former increases from 75 to 100 μg and the progestin is decreased from 5 to 2.5 mg. The progestin in Enovid-5 and Enovid-E is norethynodrel, a more 'estrogenic' progestin than other compounds.

Effect of pregnancy

During pregnancy the remarkable extension of vaginal surface is associated with hyperemia of the vaginal wall. The intercellular microridges seem to be less per cell, because formerly they reveal a more dense convolution. Cellular borders are compressed, but are still clearly apparent. Along the cell borders the intercellular microridges form an extended course because of their elasticity (Walz et al., 1978). The vaginal epithelium reaches a maximal thickness with concomitant increase in glycogen content. The thickness of the epithelium increases to a great extent during the first half and then diminishes greatly.

Effect of menopause

Menopause is associated with remarkable structural changes in the vagina, e.g. decrease in the depth and caliper of the vagina due to loss of elasticity, pelvic relaxation, uterine descensus and/or disuse atrophy, regression of rugae, loss of expansive ability, color changes due to loss of vascularity or chronic inflammation and ulceration of the posterior vaginal wall due to abrasion by the cervix (Lang and Aponte, 1967).

In postmenopausal women the vaginal epithelium becomes extremely thin and is often invaded with leukocytes. This is associated with a decline in the frequency of mitosis in the basal and parabasal layers. In certain women the epithelium is completely lost exposing the subepithelial connective tissue (Table 3).

The surface ultrastructure of senile vaginal epithelium is flattened coinciding with the decline of ovarian function. The onset of atrophy causes a superficial keratinization resulting in further flattening of the vaginal surface as well as in fragmentation within single cells and rudiments of microridges (Walz et al., 1978).

In postmenopausal women, low levels of estrogens, produced by the ovaries and the adrenals, or from the peripheral conversion of ovarian androgens into estrogens, often maintain some proliferative activity in the vagina (Watchel, 1975). Thus, completely atrophic smears are not common; instead most postmenopausal women have a pattern of intermediate proliferation, being composed mainly of intermediate cells but also occasionally showing superficial and parabasal cells. Due to the influence of androgen hormones during senescence the surface pattern occasionally shows signs of some proliferation. The surface pattern of this androgen type of proliferation (Wied and Christiansen, 1953) is characterized by small intermediate cells and extreme cytolysis.

It appears that without continuous exposure to estrogen, the vaginal epithelium becomes somewhat refractive to exogenous estrogen therapy. Menopausal women with hypotrophic cornification curves or slightly atrophic vaginal epithelium respond faster and respond to lower doses of estrogen than do women with advanced atrophy of the vaginal epithelium (DeAllende and Orias, 1950).

Estrogen originating from ovarian tumors or from topical or oral exogenous replacement not only restores the thickness and glycogen content of the vaginal epithelium but partially restores the surface ultrastructural appearance. However, the pattern of microridge distribution is somewhat different from that seen in the premenopausal women and not all cells are completely covered with microridges. The functional significance of these changes is unknown.

Acknowledgment

References

Averette, H. E., Weinstein, G. D. and Frost, P. (1970). Autoradiographic analysis of cell proliferation kinetics in human genital tissues. I. Normal cervix and vagina. *Am. J. Obstet. Gynecol.*, **108**, 8

Burgos, M. H. and Roig de Vargas-Linares, C. E. (1970). Cell junctions in the human vaginal epithelium. *Am. J. Obstet. Gynecol.*, **108**, 565

Burgos, M. H. and Roig de Vargas-Linares, C. E. (1978). Ultrastructure of the vaginal mucosa. In Hafez, E. S. E. and Evans, T. N. (eds), *The Human Vagina*. (Amsterdam: Elsevier/North-Holland)

DeAllende, I. L. C. and Orias, O. (1950). In *Cytology of the Human Vagina*. (New York; Paul B. Hoeber, Inc.)

Dembitzer, H. M., Herz, F., Schreiber, K., Wolley, R. C. and Koss, L. G. (1976). The fine structure of exfoliated cervical and vaginal cells. *Acta Cytol. Philadelphia*, **20**, 243

Ferenczy, A. and Richart, T. M. (1974). Female reproductive system. In: *Dynamics of Scanning and Transmission Electron Microscopy*, p. 213. (New York: Wiley)

Hafez, E. S. E. (1975) In *Scanning Electron Microscopic Atlas on Mammalian Reproduction*. (Tokyo: Igaku Shoin)

Hafez, E. S. E., Barnhart, M. E., Ludwig, H., Lusher, J., Joelsson, I., Daniel, J. L., Sherman, A. I., Jordan, J. A., Wolf, H., Stewart, W. C. and Chretien, F. C. (1975). Scanning electron microscopy of human reproductive physiology. *Acta Obstet. Gynecol. Scand.*, Suppl. 40

Hafez, E. S. E. (1977). The vagina and human reproduction. *Am. J. Obstet. Gynecol.*, **129**, 573

Hafez, E. S. E. and Evans, T. N. (eds) (1978). *The Human Vagina*. (Amsterdam: Elsevier/North Holland

Hinglais-Guillaud, N. L. (1959). Ultrastructure de l'exocol normal de la femme. *Bull. Cancer*, **46**, 212

Jaszczak, S. and Hafez, E. S. E. (1980). The vagina and reproductive processes. In Hafez, E. S. E. (ed.), *Human Reproduction: Conception and Contraception*. (New York: Harper & Row)

Kistner, R. W. (1978). Physiology of the vagina. In Hafez, E. S. E. and Evans, T. N. (eds), *The Human Vagina*. (Amsterdam: Elsevier/North-Holland

Lang, W. R. and Aponte, G. E. (1967). Gross and microscopic anatomy of the aged female reproductive organs. *Clin. Obstet. Gynecol.*, **10**, 454

Ludwig, H. and Metzger, H. (1976). *The Human Female Reproductive Tract: A Scanning Electron Microscopic Atlas* (Berlin: Springer-Verlag)

Parakkal, P. F. (1974). Cyclic changes in the vaginal epithelium of the rat seen by scanning electron microscopy. *Anat. Rec.*, **178**, 529

Platzer, W., Poisel, S. and Hafez, E. S. E. (1978). Functional anatomy of the human vagina. In Hafez, E. S. E. and Evans, T. N. (eds), *The Human Vagina*. (Amsterdam: Elsevier/North Holland)

Richter, K. (1971). Erkrankungen der Vagina. In Schualm, and Doderlein, G. (eds), *Klinik der Frauenheilkunde*. Vol. 8, p. 433. (Munich: Urban und Schwarzenberg)

Steger, R. W. and Hafez, E. S. E. (1978). Age associated changes in the vagina. In Hafez, E. S. E. and Evans, T. N. (eds), *The Human Vagina*. (Amsterdam: Elsevier/North Holland)

Walz, K. A., Metzger, H. and Ludwig, H. (1978). Surface ultrastructure of the vagina. In Hafez, E. S. E. and Evans, T. N. (eds), *The Human Vagina*. (Amsterdam: Elsevier/North Holland)

Watchel, E. G. (1975). Vaginal cytology after the menopause. In van Keep, P. A. and Lauritzer, C. (eds), *Estrogen in the Postmenopause*. (Basel: Karger)

Wied, G. L. and Christiansen, W. (1953). Die Ztolyse von Epithelien des Vaginalsekretes. *Geburtsch. u. Frauenheilk*, **13**, 986

4

The vagina (pathology)

R. W. de HAAN*, W. N. P. WILLEMSEN*, G. P. VOOYS†, E. S. E. HAFEZ‡ and P. KENEMANS*

* Department of Obstetrics/Gynecology, University of Nijmegen, Nijmegen, The Netherlands
† Department of Pathology, University of Nijmegen, Nijmegen, The Netherlands
‡ Department of Gynecology/Obstetrics, Wayne State University School of Medicine, Detroit, Michigan 48201, USA

INTRODUCTION

The embryologic development of the vagina normally leads to the formation of a mucosal lining of non-keratinizing stratified squamous epithelium. When keratinization does occur, it is usually in cases of a prolapsed vagina or a vitamin A deficiency (Kistner, 1978). Due to its location, the vagina is exposed to various infections and is subjected to growths of tumors which affect the vulva. Some pathologies of the cervix also develop within the vagina. The lower portion of the vagina is derived from the urogenital sinus. The upper part is of Müllerian origin (Koff, 1933). The mucosa of both parts reacts strongly to hormonal changes during the reproductive cycle and the menopausal period. Disturbance of the pH-dependent vaginal environment creates various pathological conditions (Kistner, 1978).

Inflammatory lesions

The vaginal pathology most frequently encountered by gynecologists is of an infectious origin. Most vaginal infections are sexually transmitted and therefore, frequently occur in the reproductive period. The main symptoms are vaginal discharge and dyspareunia. The most frequent pathogenic infections are:

(1) Candida albicans (Figure 1a)
(2) Trichomonas vaginalis
(3) Haemophilus vaginalis (Figure 1b)
(4) Neisseria gonococcus
(5) Herpes virus
(6) Papilloma virus.

Vaginal infections can also be detected by additional characteristics to which the degree of severity is influenced. For instance, Döderlein bacteria (Figures 1c and 1d) are responsible for the maintenance of a low pH level (Kistner, 1978). Vaginitis is accompanied by a pronounced inflammation of the vasculature and is marked by pain and purulent discharge. In a Trichomonas vaginalis infection, dilatation of blood vessels occurs which causes an irregular surface of the vaginal mucosa. Viral infections usually cause clearly distinguishable warts (Figures 1e, 1g, 1h) with an irregular elevated hyperkeratotic surface or flat lesions (Figure 1f). It is sometimes difficult to differentiate colposcopically these infections from dysplasias. Viral infections may even be the cause of some dysplasias (Laverty, 1978). Inflammatory lesions do not generally affect the degree of all surface maturation of the superficial layers; consequently, well-formed micro-ridges and terminal bars can be observed.

Adenosis

Ordinarily, the ectocervix is lined with stratified squamous epithelium. In the case of adenosis, glandular cells may cover the ectocervix and parts of the vagina. Microscopically, elements of glandular structures are found in 40% of women. The usual squamous epithelial lining is replaced by columnar cells of endocervical type; whereas in the underlying stroma, glandular structures of endocervical and endometrial type may occur.

In the majority of cases, adenosis is associated with maternal ingestion of synthetic estrogens such as diethylstilbestrol (DES). When administered during early pregnancy, adenosis may become evident when the exposed child reaches puberty (Vooys et al., 1973; Stafl et al., 1974; Stafl and Mattingly, 1974). The fine structural organization of these ectopic mucin-producing glandular cells resembles that of endocervical columnar cells (Figure 2a) (Fenoglio et al., 1976).

The gross appearance of the cervix and vagina is usually characteristic, consisting of a cervical hood, or praeputium, or a 'cock's-comb' surface of the ectocervix (Figure 2b). The large surfaces of glandular epithelium are subject to a process of squamous metaplasia similar to that of the endocervix. This process starts at the tips of the rugae and micropolyps. Glandular cells with abundant microvilli gradually change into flat polygonal cells with terminal bars and microridges. The colposcopic appearance of metaplastic tissue in the adenosis patient (Figure 2c) may be very misleading by mimicking the appearance of more serious lesions presenting with large fields of a mosaic structure and punctation (Fenoglio et al., 1976). During this process, if the DNA content of the stem cells is transformed, metaplasia dedifferentiates into dysplasia (Stafl and Mattingly, 1974).

The progressive lack of differentiation could eventually lead to the formation of carcinoma in situ, with possible subsequent invasion resulting in overt squamous cell-type cancer. During this process, surface differentiation gradually disappears.

Although it has been reported only twice, adenosis may also transform into a clear cell carcinoma. Even though this has been known to happen, adenosis more frequently leads to the development of epidermoid tumors. The reported incidence of squamous carcinoma is 1 per 1000 DES-exposed girls (Robboy et al., 1979; Bibbo et al., 1978).

Clear cell carcinoma of the vagina

Clear cell carcinoma of the vagina is an extremely rare condition in young women. One out of each 10 000 DES-exposed girls will ultimately develop a clear cell carcinoma (Robboy et al., 1979; Herbst, 1971; Anderson et al., 1979). This is referred to as 'clear' because of the abundant amount of optically clear cytoplasm usually without vacuoles. Mucus production usually results in the formation of vacuoles such as seen in columnar cells of endocervical type. The gross appearance (Figure 2e) is that of a friable polypoid tumor which bleeds easily (Silverberg et al., 1972).

Large fields of tumor cells grown in papillary, tubular or solid arrangement can be seen in LM (Figure 2f). Cells are cuboidal to columnar with PAS-positive, optically clear cytoplasm. TEM shows large cytoplasmic accumulations of glycogen, tight junctional complexes, and well-developed microvilli (Ferenczy and Richart, 1974). SEM demonstrates the cobblestone appearance with scarcely defined terminal bars and junctions. Cells without any regional differences are covered with closely packed microvilli (Figure 2g). Characteristic 'hobnail cells' were found with a consecutive LM/SEM method (Figure 2h; de Haan et al., 1981).

Squamous cell carcinoma of the vagina

This tumor is much more frequently seen than adenocarcinoma. Its occurrence however is still rare, being less than 1% of all genital malignancies. Squamous cell carcinoma generally occurs between the ages of 50 and 70. It is usually located in the upper third part of the vagina on the anterior and lateral walls. TEM shows pleiomorphic cells with tonofibrils and intracellular bridges (Ferenczy and Richart, 1974). SEM demonstrates the usual lack of tissue organization and differentiation. Only in well-differentiated epidermoid tumors can microridges be seen (Ferenczy and Richart, 1974).

Other tumors such as melanoma, sarcoma, and metastatic tumors are rare occurrences in the vagina.

Congenital aplasia in the vagina

The construction of a neovagina, in a case of congenital aplasia of the vagina, can be accomplished in several ways. The Davydov technique (Davydov and Zhvitiashvili, 1974) consists of mobilizing the Douglas peritoneum and transposing it through a dissected canal between the bladder and rectum. The existing vaginal epithelium gradually covers the whole neovagina and is hardly distinguishable from a normal vagina. The epithelialization may take place from the existing rudimentary vagina. However, squamous metaplastic changes in glandular cells, lying under the surgical dressing, may play an equally important role in the epithelialization process (Herman et al., 1982). Epithelialization of the neovagina is usually completed within 1 year (mean: 8.6 months; Willemsen and Mastboom, 1981).

LM investigation of cells and biopsies in the neovagina reveal a close similarity to the usual patterns. SEM studies, however, show less maturation of all mucosal cell-surface structures, as in hypoestrogenic states (Figures 3g and 3h).

CONCLUDING REMARKS

The vagina displays a number of highly interesting pathological conditions (Hafez, 1977). Depending on hormonal status and sexual activity, the vaginal flora can be disturbed by an overgrowth of specific and aspecific agents. Infection usually does not disturb the process of cell surface maturation, except in Trichomonas. Herpes and papilloma viruses seem to be related to some dysplasias. Adenosis and clear cell adenocarcinoma are related to maternal ingestion of synthetic estrogens. Ultrastructural analysis shows a rough similarity of adenosis with endocervical cells and

Figure 1 (opposite)
a: Candida albicans colony in SEM
b: Cells covered with closely packed Haemophilus vaginalis ('clue cells')
c: Ectocervical cell with Doderlein bacteria
d: Detail of colposcopy showing cytolysis by the Doderlein bacteria
e: Colposcopy of elevated Herpes virus infection
f: Surface of keratinizing cells of the same lesions
g: Detail showing the pronounced cell surface structure
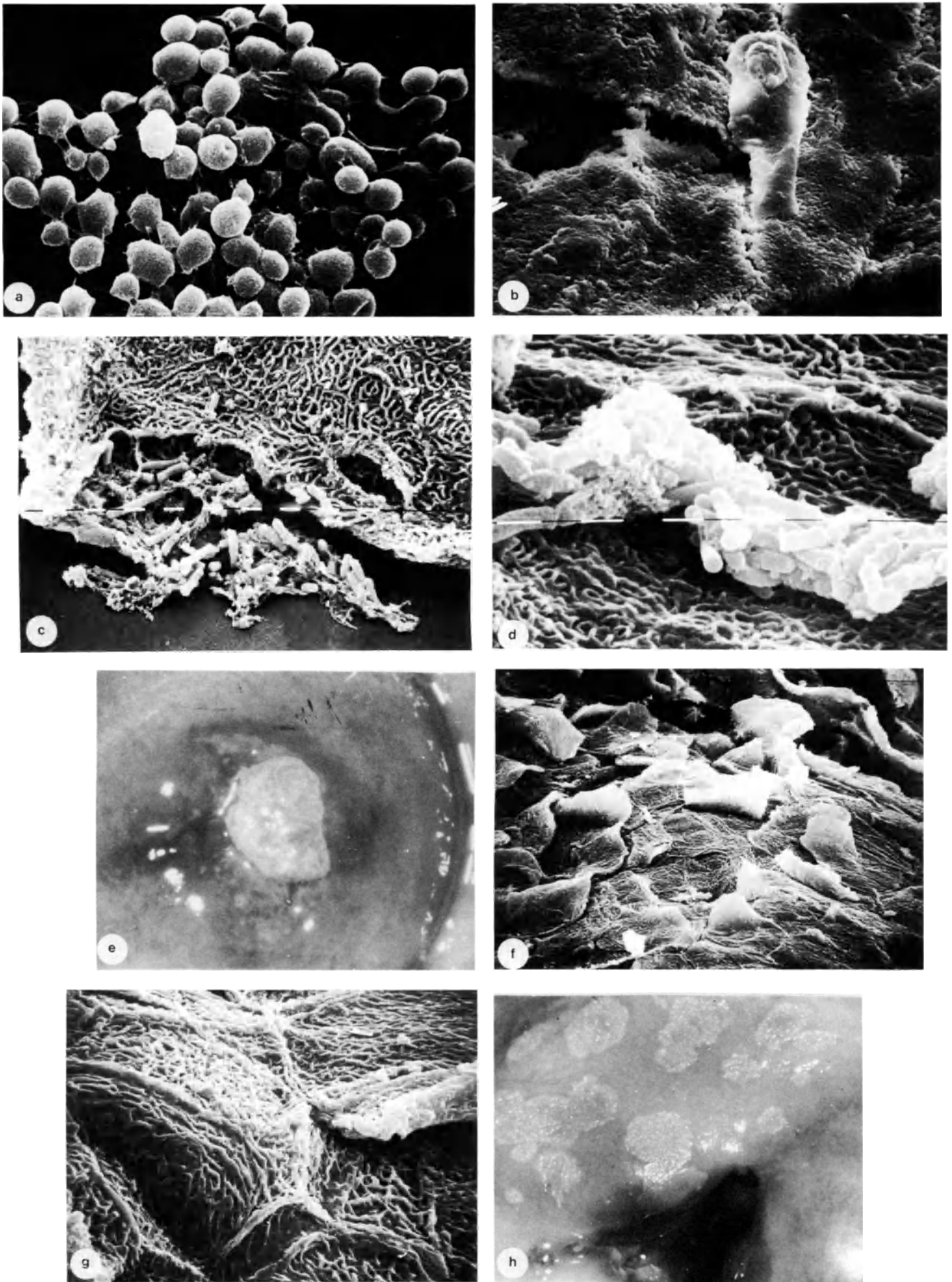h: Colposcopy of flat condylomata in a patient with a Herpes virus infection

Figure 1

Summarizing Table   Characteristics of various vaginal pathologies

	LM	SEM
Candidiasis	septate hyphae conidia (spores)	chains of oval hyphae with chlamydospores
Trichomoniasis	vascular dilatation, unicellular protozoa with flagella	less differentiation
Haemophilus vaginalis	clue cells, Gram-variable bacillus	closely packed micro-organisms covering the whole cell surface
Viral warts (herpes and papilloma)	hyperkeratotic exophytic tumor	highly differentiated, cornified cell surfaces
Flat papilloma	koilocytosis, dysplasia	dedifferentiation
Adenosis	mucin-rich columnar cells	endocervical-type cells
Clear cell adenocarcinoma	glycogen-rich clear, cells, 'hobnail' cells	cobblestone appearance, closely packed microvilli, endometrial-type cells
Squamous cell carcinoma	stromal invasion of epidermoid sheets	tissue disorganized microvilli (rarely microridge in well-differentiated carcinoma)
Neovagina	not distinguishable from a normal vagina, navicular cells	hypoestrogenic status showing less differentiation

of clear cell adenocarcinoma with endometrial cells. Squamous cell carcinoma demonstrates the usual lack of tissue organization and surface differentiation. The neovagina reveals a cell pattern, after epithelialization is completed, which is almost indistinguishable from the normal vagina.

References

Anderson, B., Watring, W. G., Edinger, D. D., Small, E. C. and Metland, A. T. (1979). Development of DES-associated clear cell carcinoma: the importance of regular screening. *Obstet. Gynecol.*, 53, 293

Bibbo, M., Haenstel, W. M., Wied, G. L., Herbst, M. H. and Herbst, A. L. (1978). A twenty-five-year follow-up study of women exposed to diethylstilbestrol during pregnancy. *N. Engl. J. Med.*, 298, 763

Davydov, S. N. and Zhvitiashvili, O. D. (1974). Formation of the vagina (colpopoiesis) from peritoneum of Douglas pouch. *Acta Clin. Plast.* (Prague), 16, 35

Fenoglio, C. M., Ferenczy, A., Richart, R. M. and Townsend, D. (1976). Scanning and transmission electron microscopic studies of vaginal adenosis and the cervical transformation zone in progeny exposed in utero to diethylstilbestrol. *Am. J. Obstet. Gynecol.*, 126, 170

Ferenczy, A. and Richart, R. M. (1974). *Female Reproductive System: Dynamics of Scan and Transmission Electron Microscopy.* (New York: Wiley)

Haan, R. W. de, Davina, H., Zanden, P. H. T. van der and Kenemans, P. (1981). Clear cell adenocarcinoma of the vagina and cervix. Human Reproduction in Three Dimensions SEM Symposium, Nijmegen, The Netherlands. Abstract no. 56.

Hafez, E. S. E. (1977). The vagina and human reproduction. *Am. J. Obstet. Gynecol.*, 129, 573

Herbst, A. (1971). Adenocarcinoma of the vagina. *N. Engl. J. Med.*, 284, 878

Herman, C. J., Erp, A. van, Willemsen, W. N. P., Mastboom, J. L. and Vooys, G. P. (1982). Epithelium of artificial vaginas: relationship to vaginal adenosis. *Human Pathology.* (Submitted for publication)

Kistner, R. W. (1978). Physiology of the vagina. In Hafez, E. S. E. and Evans, T. N. (eds), *The Human Vagina.* (New York: Elsevier/North-Holland)

Koff, A. K. (1933). Development of the vagina in human fetus. *Contr. Embryol. Carneg. Inst.*, 140, 59

Laverty, E. (1978). The significance of non-condylomatous wart-virus infection of the cervical transformation zone. A review with discussion of two illustrative cases. *Acta Cytologica*, 22, 195

Robboy, S., Kaufman, R. H., Prat, J., Welch, W. R., Gaffey, T., Scully, R. E., Richart, R., Fenoglio, C. M., Kirata, R. and Filley, B. C. (1979). Pathologic findings in young women enrolled in the national cooperative diethylstilbestrol adenosis project (DESAD). *Obstet. Gynecol.*, 53, 309

Silverberg, S. G. and De Giorgi, L. S. (1972). Clear cell carcinoma of the vagina. A clinical, pathologic and electron microscopic study. *Cancer*, 29, 1680

Stafl, A., Mattingly, R. F., Foley, D. V. and Tetherston, W. C. (1974). Clinical diagnosis of vaginal adenosis. *Obstet. Gynecol.*, 43, 118

Stafl, A. and Mattingly, R. F. (1974). Vaginal adenosis: a precancerous lesion? *Am. J. Obstet. Gynecol.*, 120, 666

Vooys, G. P., Ng, A. B. P. and Wentz, W. B. (1973). The detection of vaginal adenosis and clear cell carcinoma. *Acta Cytologica*, 17, 59

Willemsen, W. N. P. and Mastboom, J. L. (1981). Treatment of vaginal aplasia in the syndrome of Mayer–Rokitansky–Küster. *Surg. Forum*, 32, 459

Figure 2 (opposite)
a: Adenosis vaginalis in LM
b: Colposcopy of a cervical praeputium in adenosis vaginalis
c: Colposcopy of large metaplastic surfaces in adenosis vaginalis with no proof of dysplasia in the biopsies
d: Adenosis vaginalis in SEM
e: Colposcopy of a clear cell adenocarcinoma of the vagina and ectocervix
f: LM section of the same lesion
g: Cell surface structure of a clear cell adenocarcinoma in SEM
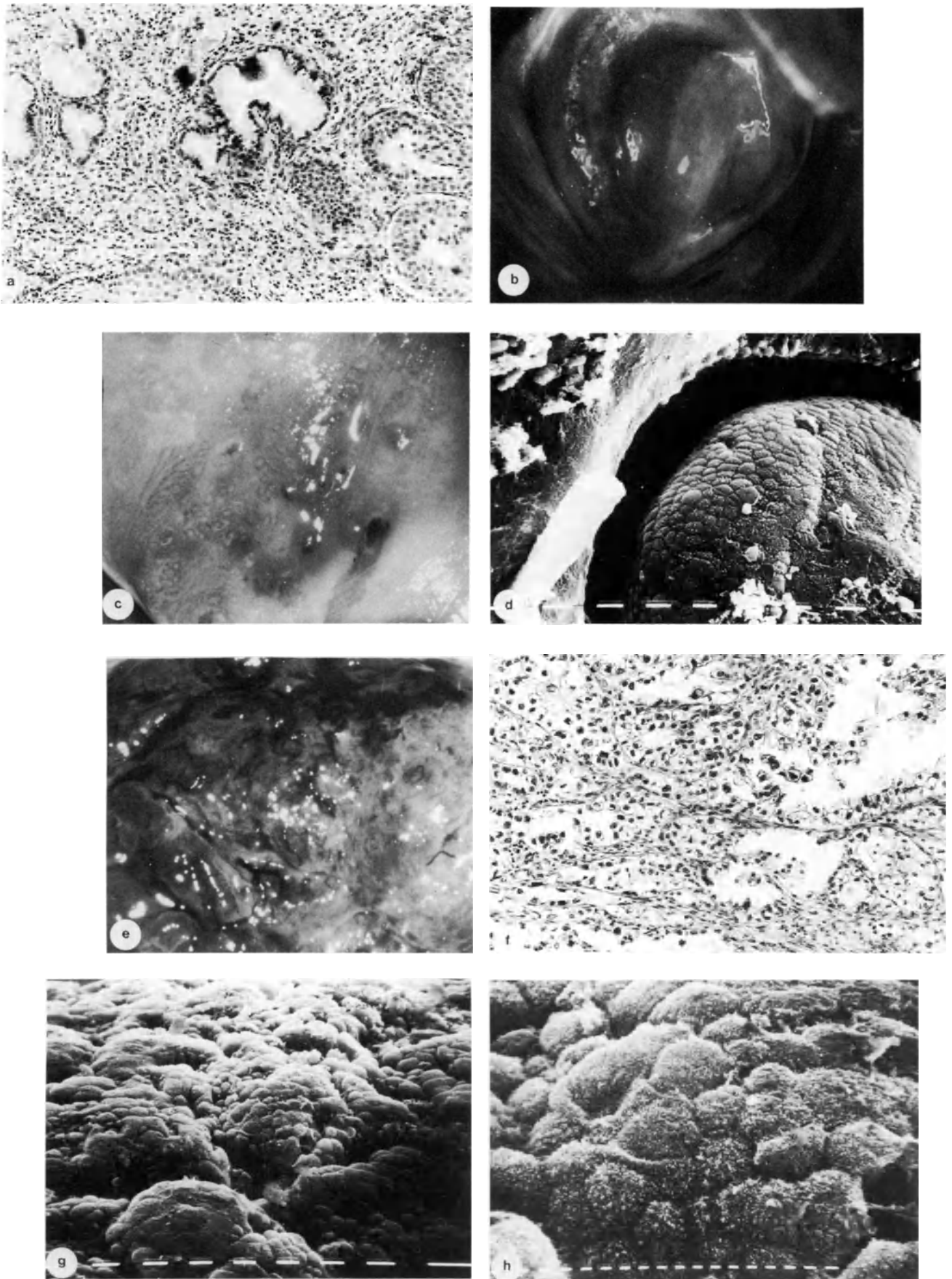h: Detail of the clear cell adenocarcinoma

Figure 2

Figure 3 (opposite)
a: Group of cells of a clear cell adenocarcinoma with some hobnail cells
b: A single hobnail cell in SEM
c: Detail of another hobnail cell
d: Group of clear cells
e: Colposcopy of a neovagina with the demarcation of neovaginal epithelium and peritoneum
f: LM of neovaginal cells
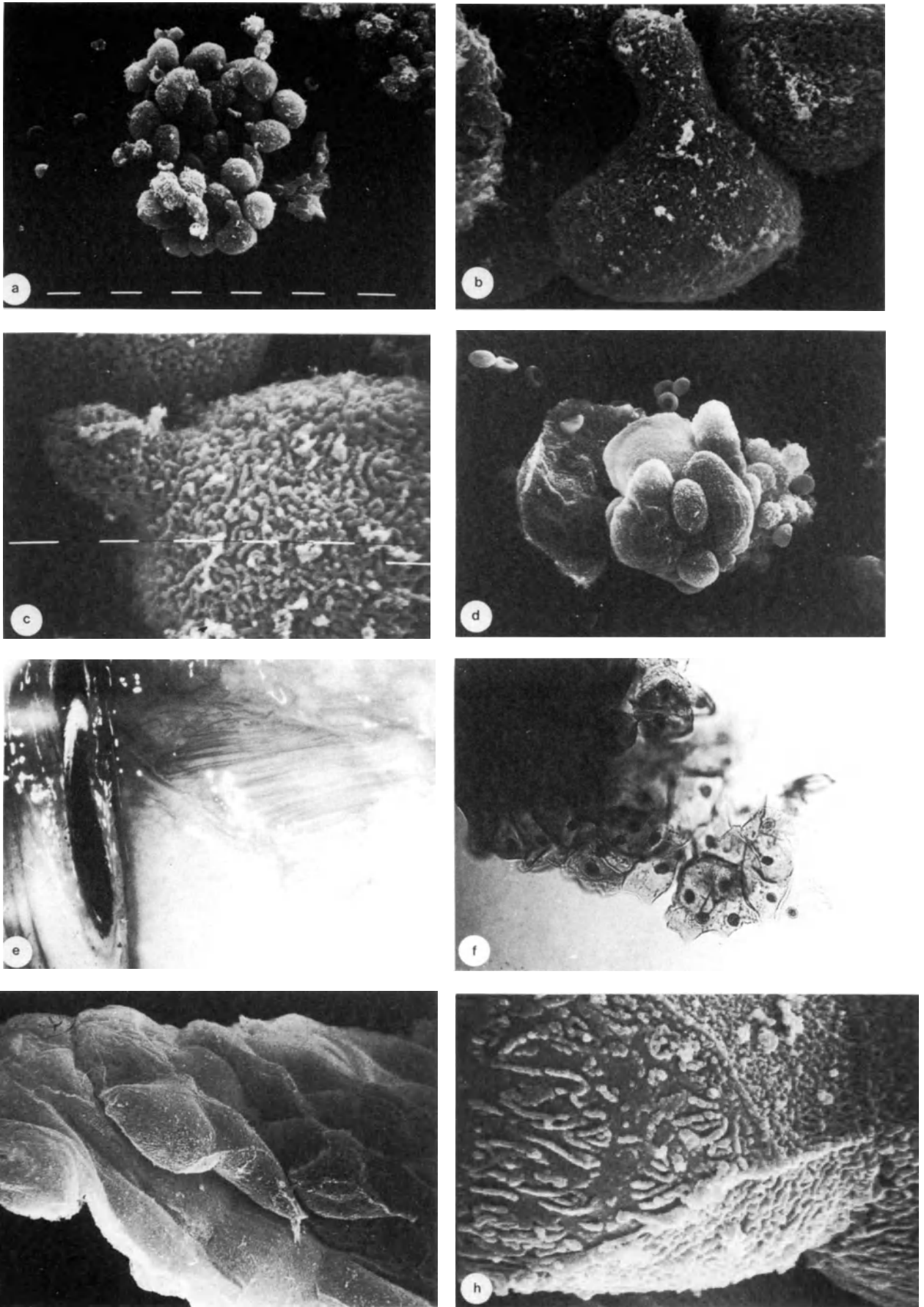g: Sheet of neovaginal cells in SEM
h: Detail of the same group of cells

Figure 3

5

The Bartholin gland

M. MURAKAMI, J. ABE and T. NISHIDA

* Department of Anatomy, Kurume University School of Medicine, Kurume, Japan

The Bartholin gland is analogous to the Cowper bulbourethral gland in the male and discharges lubricating mucus in response to sexual stimulation.

In the past, this organ was studied mainly by German histologists in some mammals, including humans, by means of light microscopy and histochemical technique (Schröder, 1930; Ehrenbrand and Strasser, 1965; Horstmann and Stenger, 1966; Friess, 1972).

There is much controversy as to the presence or absence of myoepithelial cells around the secretory end-piece and as to tubular or acinar type in glandular classification.

In comparison with a number of light microscopic and histochemical studies, surprisingly little has been done to investigate the fine structure of the Bartholin gland with the electron microscope.

In the present study all kinds of surfaces such as luminal, cut and basal, were visualized in the human Bartholin gland by SEM. Special attention was given to the configuration of the basal surface of this gland.

Tissue mass containing the Bartholin gland was isolated from a woman aged 31, and with aseptic, unilateral Bartholin gland duct cysts.

The specimens were microdissected and immersed in buffered paraformaldehyde–glutaraldehyde mixture. They were postfixed in cold buffered OsO_4, dehydrated in an ascending acetone series and dried from liquid CO_2 by the critical point method, briefly sputter-coated with gold/palladium. In order to visualize the basal surface of the gland the specimens were prepared by HCl–collagenase procedure according to Evan et al. (1976).

For transmission electron microscopy some specimens postfixed in the buffered OsO_4 were processed routinely for TEM.

For routine light microscopy the tissues were fixed in Bouin solution, and embedded with paraffin. Sections were stained with HE and PAS.

LIGHT MICROSCOPY

The human Bartholin glands are divided into lobules by the septa which contain smooth and striated muscle fibers in addition to numerous collagen and elastic fibers. The lumen of the secretory end-pieces is lined by a single row of columnar epithelial cells with spherical nuclei at their base. In routine HE preparations the cytoplasm of the epithelial cells is stained pale and has a foamy appearance, but the histochemical finding that the cells contain PAS-positive and alcian-blue-positive secretory granules has already been described in human Bartholin glands (Ehrenbrand and Strasser, 1965; Rorat et al., 1975) (Figure 1a). These epithelial cells are regarded as typical mucous cells. The epithelium lining the excretory ductule is composed of pseudostratified cuboidal cells, some of these being stained positively with PAS just as secretory cells of the end-pieces.

ULTRASTRUCTURE

The epithelium of the end-piece is composed of the tall prismatic cell showing a wide base and a narrow apex. Most epithelial cells have cytoplasm which is crowded with spherical, membrane-bound secretory granules of varying sizes. These findings are characteristic of mucus-producing cells as found elsewhere (Figure 1b). The epithelium lining the excretory ductules consists of one- to four-cell-thick, low columnar or cuboidal cells with abundant free ribosomes, mitochondria, and filamentous structure presumably as tonofilaments. In the initial portion of the ductule there are many epithelial cells rich in mucous granules which can be easily seen in the secretory end-piece (Figure 1c). The elongated cells are frequently observed in the location between the base of epithelial cells and the basement lamina in both secretory end-pieces and excretory ductules. They are characterized by a large amount of

filamentous material akin to smooth muscle cells, and hence may be designated myoepithelial cells. The existence of myoepithelial cells in the Bartholin gland was recently reported in the Japanese monkey using TEM (Nishida, 1979), and this experiment has revealed that the myoepithelial cells are present also in the human Bartholin gland.

SURFACE ULTRASTRUCTURE

The lumen within secretory end-pieces, or of excretory ductules, is tubular or saccular.

The apices of the cells of the secretory end-pieces protrude slightly into the lumen, and the luminal surface is covered by stubby microvilli (Figure 1d) whereas the boundary surface is constructed by close interdigtation by microvilli of adjacent cells. On the epithelial surface spherical masses of varying sizes and small round pits can be frequently seen (Figure 2a,b). The former may represent the aggregates of discharged mucous granules, and the latter may have resulted from mucus secretion. Morphological evidence indicating the type of apocrine secretion as described by Rorat et al. (1975) was not detected in the present study.

The apical surface of the epithelial cells of the excretory ductule is rather flattened (Figure 2c,d) and provides occasional single cilia in addition to short microvilli. The microvilli are most prominent in the peripheral region of one cell and thereby outline the cell boundary (Figure 3a). Such outline makes the surface of the epithelium polygonal. The apical surfaces also have spherical particles, presumably discharged mucin, but there is no cytoplasmic protrusion suggesting apocrine secretion.

Removal of extracellular tissue material by HCl and collagenase resulted in exposure of the basal surface of the Bartholin gland. The Bartholin gland is constructed by branching and twisted tubules with blind ends which are often bifurcated and more or less enlarged (Figure 3b). The basal surface of secretory end-piece or excretory ductule is surrounded by a complete single layer of myoepithelial cells (Figure 3b,c). Individual myoepithelial cells are long, fusiform cells with tapering ends, being 30–60 μm in length and 3–6 μm in width. From the cell body short fern-leaf-like processes extend to interdigitate with those from adjacent cells (Figure 3d). The myoepithelial cells run in parallel with each other and they are oriented longitudinally or spirally to the long axis of the gland. A similar parallel arrangement of myoepithelial cells has also been demonstrated by SEM in apocrine sweat glands which

are thought to be a typical tubular gland (Kawabata and Kurosumi, 1976; Ohmagari et al., 1980). The basal surface configuration of the human Bartholin glands is quite similar to that of the monkey Cowper's glands observed by SEM (Murakami et al., 1981).

There is disagreement about the histological classification of the Bartholin glands; some authors have referred to them as a tubular type; others have sorted them into a tubuloalveolar type (see the review of Schröder, 1930). The human Bartholin gland should be classified into a tubular type rather than a tubuloalveolar type. The shape and arrangement of the associated myoepithelial cells also may support our hypothesis.

References

Ehrenbrand, F. and Strasser, F. (1965). Beiträge für Morphologie und Histochemie der menschlichen Glandulae vestibulares majores. Anat. Anz., 117, 69

Evan, A. P., Dail, W. G., Dammrose, D. and Palmer, C. (1976). Scanning electron microscopy of cell surfaces following removal of extracellular material. Anat. Rec., 185, 433

Friess, A. E. (1972). Histochemische Untersuchungen an den Glandulae vestibulares majores (Bartholini) des Rindes. Acta Histochem., 44, 62

Horstmann, E. and Stenger, H.-E. (1966). Die äusseren Geschlechtsorgane. In: Möllendorff's Handbuch der mikroskopischen Anatomie des Menschen. VII/4, pp. 150–62. (Berlin, Heidelberg, New York: Springer)

Kawabata, I. and Kurosumi, K. (1976). Transmission and scanning electron microscopic study of the human ceruminous apocrine gland. 11. Myoepithelial cells. Arch. Histol. Jap., 39, 231

Murakami, M., Sugita, A., Abe, J., Hamasaki, M. and Shimada, T. (1981). SEM observation of some exocrine glands, with special reference to configuration of the associated myoepithelial cells. Biomed. Res., 2 (suppl.), 99

Nishida, T. (1979). Transmission and scanning electron microscopic observation of the major vestibular glands of the Japanese monkey (In Japanese). J. Kurume Med. Assoc., 42, 933

Ohmagari, N., Ogawa, K. and Miyoshi, M. (1980). Myoepithelial cells in canine apocrine sweat gland (In Japanese). Acta Anat. Nippon., 55, 162

Rorat, E., Ferenczy, A. and Richart, R. M. (1975). Human Bartholin gland, duct, and duct cyst. Histochemical and ultrastructural study. Arch. Pathol., 367

Schröder, R. (1930). Die weibliche Geschlechtsorgane. In: Möllendorff's Handbuch der mikroskopischen Anatomie des Menschen. VII/1, pp. 329–535. (Berlin: Springer)

Figure 1 (opposite)
a: Section of the Bartholin gland taken from a 31-year-old woman. The epithelial cells are typically mucous secretory in nature and characterized by pale cytoplasm and nuclei locating at the base. HE stain. (Inset: section stained by PAS procedure)
b: Transmission electron micrograph reveals epithelial cells in the secretory end-piece. The cytoplasmic space of the epithelial cells is filled with secretory granules. Note a myoepithelial cell existing in close association with epithelial cells (×8000)
c: Transmission electron micrograph of an initial segment

of the excretory ductule. In this portion the epithelium is pseudostratified low columnar cell epithelium and consists of secretory and non-secretory cells. Myoepithelial cells are also seen locating basal to epithelial cells (×6400)
d: SEM view of the luminal surface of the secretory end-piece. The luminal surface of the epithelial cells protrudes more or less into the lumen and gives the feature of cobblestone. The honeycomb appearance of the cytoplasm of the fractured epithelial cell may be caused by traces from which secretory granules have been released during fracture (×3000)
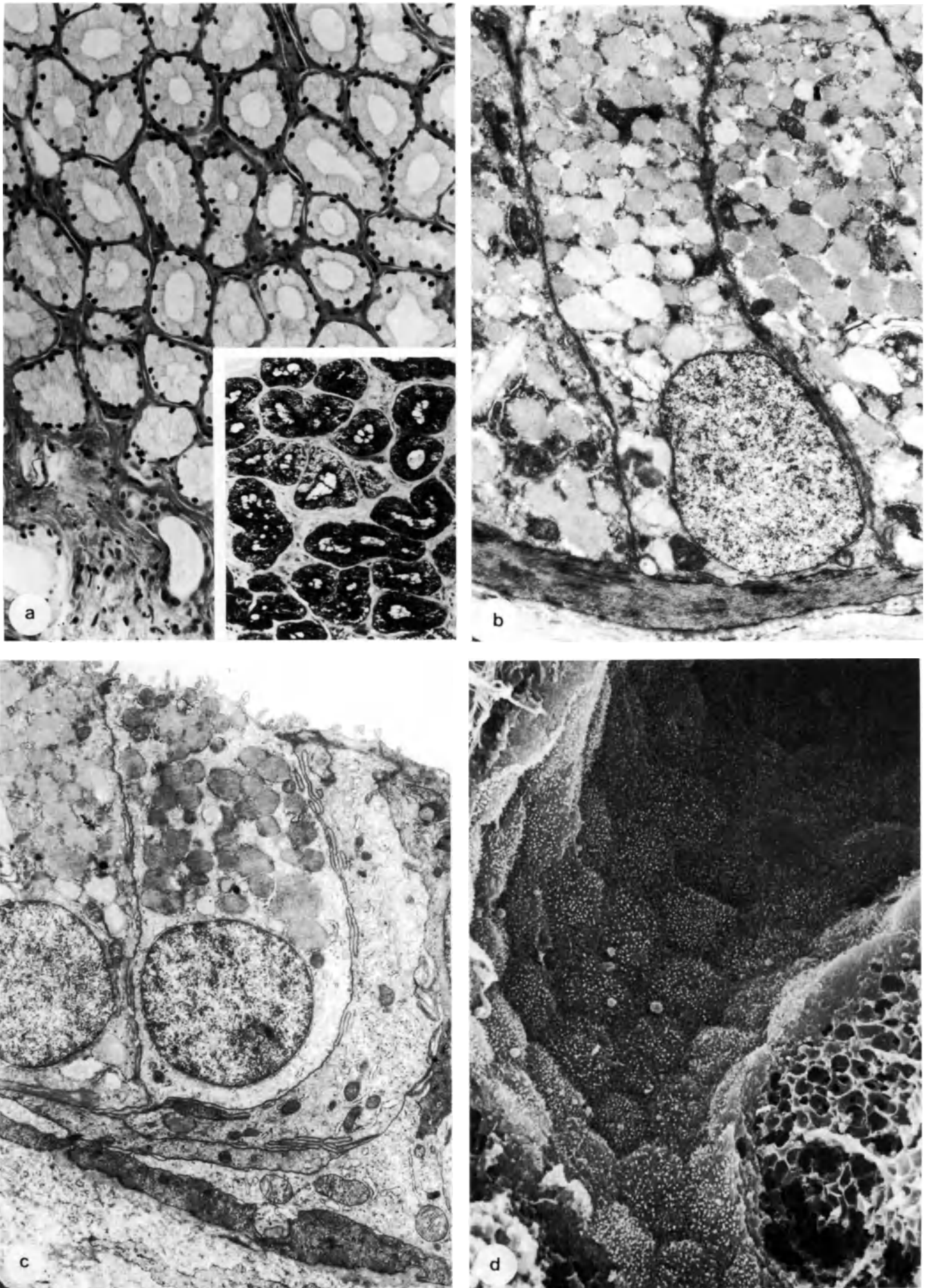
Figure 1

Figure 2 (opposite)
a: Higher magnification view of an area in Figure 1d. Individual epithelial cells are covered by stubby microvilli. Occasional small pits on the epithelial surface may result from release of secretory granules ($\times$7500)

b: Enlarged detail of the epithelial surface in Figure 2. At the cell periphery the microvilli closely interdigitate with those of the adjacent cells. Spherical masses on the cell surface may be aggregation of secretory granules released ($\times$23 500)

c: SEM view of an excretory ductule at low magnification. Surface of the epithelial cells lining the lumen is flattened and gives a tile pattern ($\times$470)

d: Mid-range magnification view of the luminal surface of an excretory ductule. The epithelial cells lining the lumen are polygonal and have distinct cell boundaries. Rod-shaped objects on the luminal surface may be aggregates of secretory granules discharged ($\times$1300)
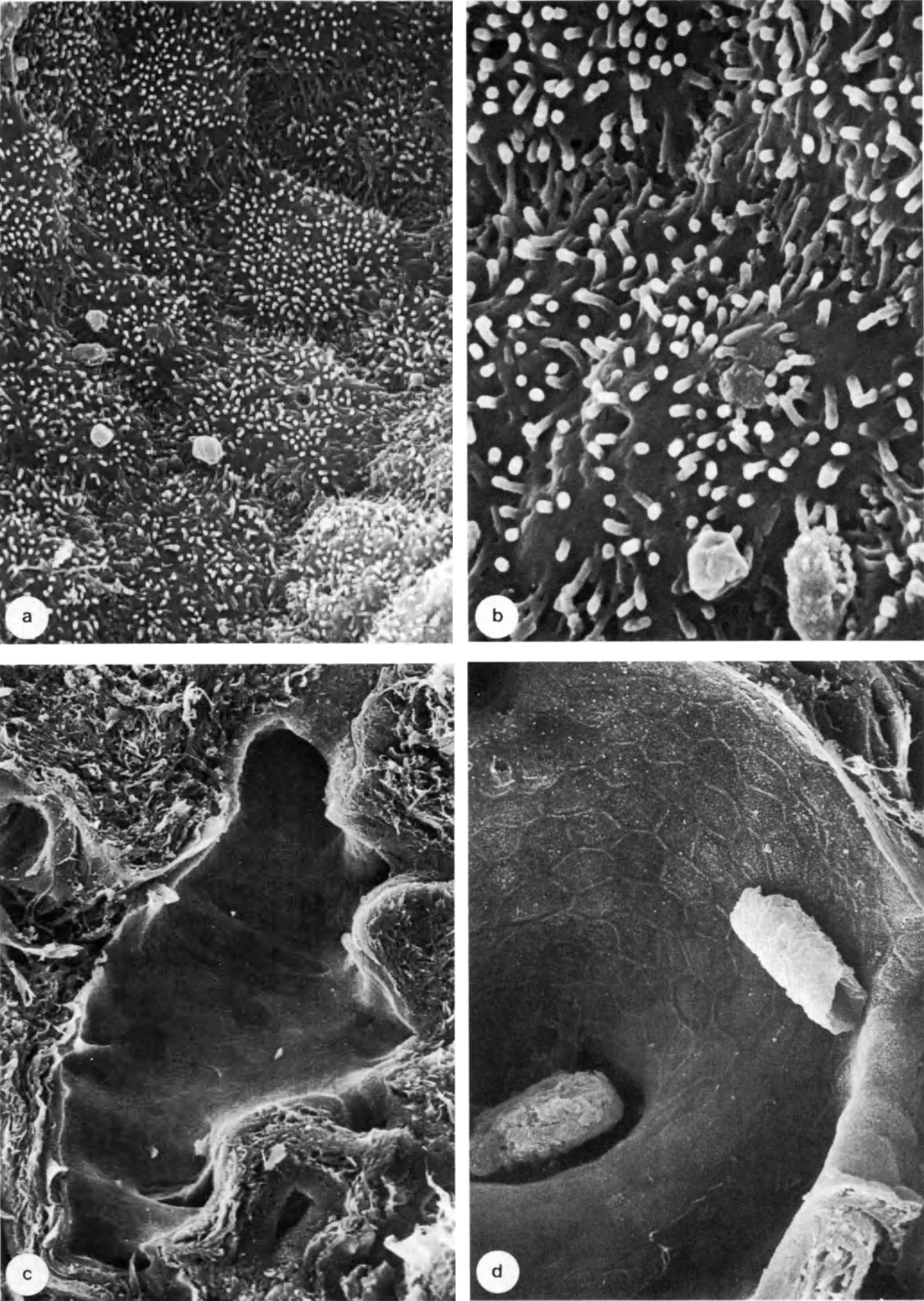
Figure 2

Figure 3 (opposite)

a: High magnification view of the epithelial cell surface of an excretory ductule showing short microvilli evenly distributed and occasional single cilium. Small droplets attached to the epithelial surface may be secretory granules released (×5600)

b: Survey micrograph of the stromal surface of the Bartholin glands after treatment with HCl and collagenase. In surface configuration the glands are coiled or twisted tubules (×400)

c: Higher magnification view of an area in Figure 3b. Secretory end-pieces often tend to bifurcate and more or less enlarge at terminal. Note prominent myoepithelial cells surrounding the end-piece. They are oriented parallel to the long axis of the gland (×1300)

d: High magnification view of the stromal surface of the Bartholin gland. In this figure myoepithelial cells are oriented spirally to the long axis of the gland (×2900)
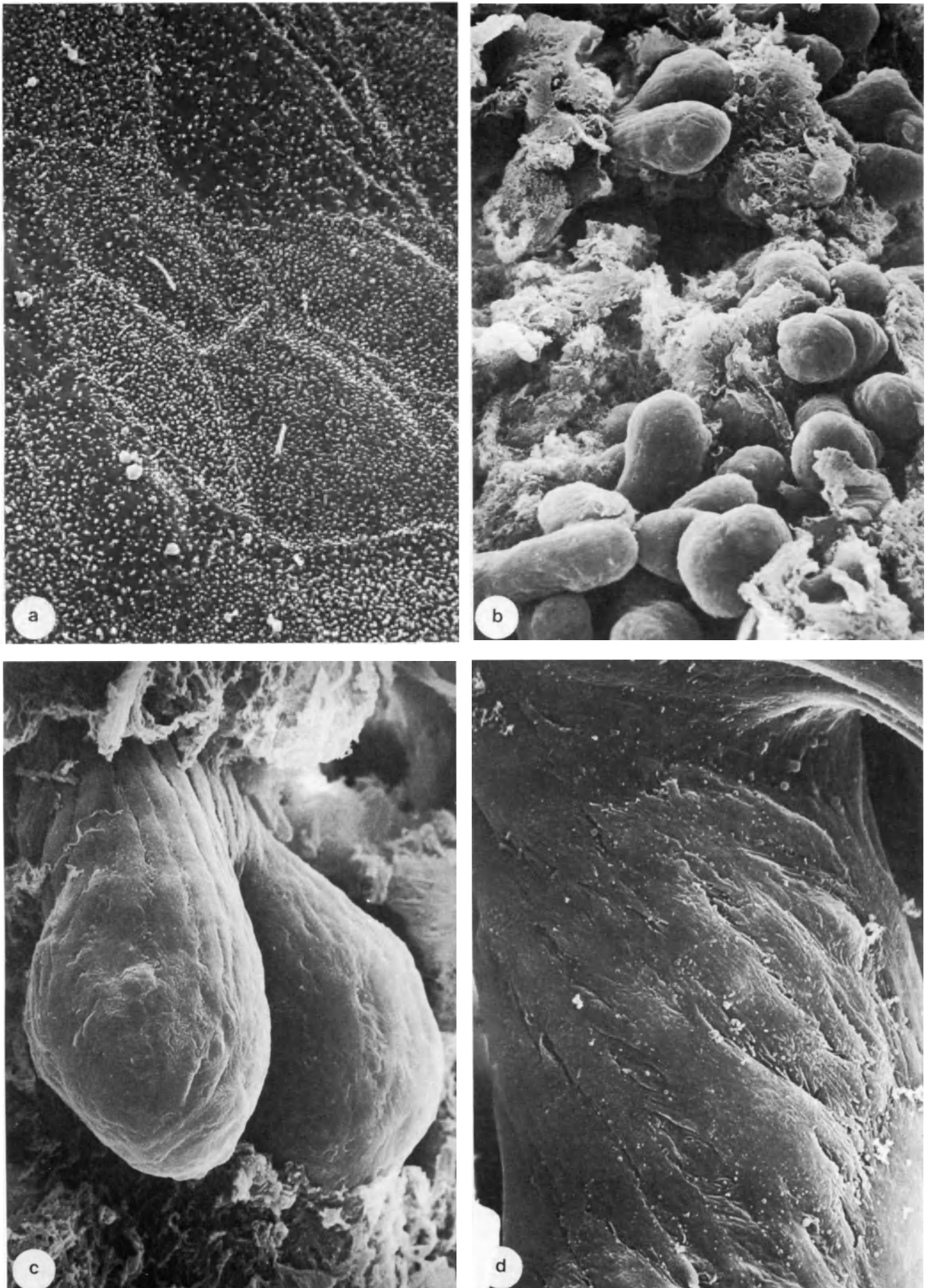
Figure 3

6

The cervix

P. KENEMANS*, J. H. M. DAVINA†, R. W. de HAAN* and E. S. E. HAFEZ‡

* Division of Gynecological Oncology; Department of Obstetrics and Gynecology, University of Nijmegen, The Netherlands
† Department of Submicroscopic Morphology, University of Nijmegen, The Netherlands
‡ Department of Gynecology/Obstetrics; Wayne State University School of Medicine, Detroit, Michigan 48201, USA

The uterine cervix, the fibrous narrow neck of the uterus, is without any sharp demarcation continuous with the more muscular body of the uterus. The central cavity of the cervix, the endocervical canal, is lined with a single layer of columnar cells which, in the isthmic region, changes fairly abruptly into the endometrial cell lining of the cavum of the uterine corpus. At the side of the portio vaginalis, the part of the cervix projecting into the cavity of the vagina, the endocervical glandular epithelium meets the ectocervical stratified squamous epithelium, which is similar to and continuous with the vaginal epithelium. This squamocolumnar junction site can be a sharp line or, and more often, a more extensive transitional zone, varying in its position and extent under diverse physiological, hormonal and environmental conditions. As metaplasia of the columnar epithelium takes place in this zone resulting in transformation of ('ectopic') columnar cells into squamous epithelium, this zone is mostly referred to as the transformation zone.

Thus, the lining of the cervix uteri is usually composed of three types of normal epithelium (Figure 1):

(1) the stratified squamous epithelium of the ectocervix;
(2) the one-cell layer thick glandular lining of the endocervix;
(3) the metaplastic epithelium of the transformation zone.

SEM studies of human cervical epithelium have been reported previously by Hafez et al. (1975); Ludwig and Metzger (1976); Jordan (1976); Ferenczy (1980) and Davina et al. (1981). Various other studies have been done on normal and preneoplastic material with the intention of finding out whether or not SEM can be useful for establishing an early marker of irreversible neoplastic transformation (Kenemans et al., 1981, 1982), for the study of which the human cervix offers an unique opportunity (Wilbanks, 1976).

THE ORIGINAL ECTOCERVICAL SQUAMOUS EPITHELIUM

In the stratified epithelium of the ectocervix, four zones can be distinguished (Figure 2):

(1) the basal zone with cuboid to cylindrical cells;
(2) the parabasal zone with polyhedral cells;
(3) the intermediate zone with large cells;
(4) the superficial zone with layers of flattened cells.

The intercellular space in the intermediate and superficial zones is less wide than that in the basal and parabasal zones. Going from the basement membrane to the free luminal surface of the epithelium functional changes (increased maturation and decreased potential for proliferation) coincide with gradual morphological alterations (flattening of cells, decreased nucleocytoplasmatic ratio, and increased polarity of the cell surface ultrastructure). The number of pseudolayers of epithelial cells is determined by the hormonal state. Estrogens cause the epithelium to thicken, whereas progesterone causes a thinning. The relation between the cell surface pattern and the cyclical activity has not been investigated systematically.

The lumen bordering superficial cells have been extensively studied by SEM (Jordan and Williams, 1971; Williams et al., 1973a,b; Nasr et al., 1973; Ferenczy and Richart, 1973; Bonilla-Musoles et al., 1974; Ferenczy and Richart, 1974; Ludwig and Metzger, 1976; Rubio and Kranz, 1976; Rubio and Einhorn, 1977; Sherman, 1977; Ferenczy and Gelfand, 1979). Fully differentiated cells on the top of the ectocervical epithelium are large, flat, polygonal cells

arranged in an irregular pavement-like pattern. The partially overlying cells seem loosely attached to one another, demonstrating various stages of exfoliation (Figure 2). The surface of exfoliating cells (Figure 2) possesses the same microridge pattern as is present on the surface of normal superficial exfoliated cells in smears (Murphy et al., 1973; Llanes et al., 1973; Murphy et al., 1974; 1975; Leif et al., 1975; Kjaergaard and Poulsen, 1977). These microridges are 1–4 μm long, about 0.15 μm in width as well as in height, and are separated from each other by a distance of about 0.25 μm. As a rule no particular orientation of the microridges is observable in the central part of the cell. At the periphery some orientation parallel to the cell boundary is occasionally seen. In addition to the microridge pattern, the cell surfaces show well-defined structural elevations (crests or bars) separating cell surface areas. These elevations have frequently been interpreted as cell borders (Jordan and Williams, 1971; Williams et al., 1973a,b; Bonilla-Musoles et al., 1974; Rubio and Kranz, 1976; Sherman, 1977; Lamb et al., 1978; Steger and Hafez, 1978). However, in addition to these terminal bars, which are interconnected elevated cell boundaries of two laterally adjacent cells, so-called linear bars have been described (Kenemans et al., 1981). These cell surface elevations are morphologically similar to the terminal bars; they are not situated at the cell border, but on the cell surface. Most probably these linear bars are present at those locations on the cell surface where two (or more) initially more superficially positioned adjacent cells (which have been desquamated already) had their cell borders joining each other. Light microscopically these linear bars give the well-known dark lines within the cytoplasm, which were sometimes held to be 'artefacts or cell-wrinkles'.

The view which has previously existed was that microridges cover both the upper and lower surface of superficial cells (Ferenczy, 1980). However the surface micromorphology of the basal cell side, the side originally directed to the basement membrane, of normal, mature superficial cells shows different characteristics, a fact only recently recognized (Kenemans et al., 1980). The basal cell side shows globular microvilli and so-called linear grooves, which intermesh with the microridges and with the protruding crest bars on the luminal cell sides of the subadjacent cells (Figure 2). Thus, bars (or crests) and grooves (or furrows) are not only cell border structures, but are also cell surface structures related to borders of cells which have lain above or below (Murphy et al., 1975; Bahr et al., 1976; Ludwig and Metzger, 1976). The regions outlined by crests and furrows show some variation in microridge and microvillous pattern, which implies that the cell possesses 'regional' differences (Davina et al., 1981).

The surface pattern of the non-lumen bordering superficial cells has been investigated using a stripping technique (Davina et al., 1980, 1981). Stripping of flattened cells clearly demonstrates the surface pattern differences of the luminal and basal side of adjoining cells (Figure 2). Moreover, it shows that the structures are complementary and interlocking. The surface pattern varies with the location of the cell in the superficial zone. During cell migration the crests and

furrows become more prominent, whereas the degree of branching and anastomosing of the microridges, as well as the width of the microridges and the top diameter of the microvilli, increases.

Cells of the deeper zones bear many villus-like projections which possess desmosomes at the top. In this way cell-to-cell contacts are formed within a large interlacing intercellular space. The number of intact desmosomes and gap junctions is large, whereas they are hardly present, or are absent in the superficial zone (McNutt et al., 1971; Wiernik et al., 1973; Ferenczy and Gelfand, 1979). A freeze-fracturing method has been used for the SEM study of cells in the intermediate, parabasal and basal zones (Davina et al., 1981). In these zones fracture planes occur inter- and intracellularly, in contrast to the superficial zone with only intracellular fracture planes. The character of the fracture planes may depend on the size of the intercellular space and whether the cellular projections interlock strongly. The cell surface pattern of intermediate cells consists of filiform projections and some globular microvilli. The parabasal and basal cell surface possesses more or less foliate projections which are longer than the projections of the intermediate cells (Figure 3).

THE ORIGINAL ENDOCERVICAL EPITHELIUM

The original columnar epithelium lines the endocervical canal and occasionally extends onto the ectocervix. It consists of tall, slender and elongated columnar cells uniformly arranged in one layer and closely packed in a 'cobblestone' pattern (Figure 4). Compound tubular racemose branching and mucine-secreting endocervical glands, do not exist. Fluhmann (1961) showed the endocervical pattern to be formed by oblique, transverse and longitudinal directed crypts and clefts occasionally branching but never crossing each other. Endocervical clefts crypts, folds, villi and micropolyps are highly similar in lining, all showing columnar cells, some of which are ciliated (Williams et al., 1973b). The nuclei are round or oval, and basal in position. The plasma may show irregular vacuolation. Underneath this single cell row of mucus-secreting or ciliated columnar cells the subcolumnar basal cell may be present. There is evidence that daughter cells of these basal cells can differentiate into either mucus-secreting or ciliated columnar cells (Gould et al., 1979).

Figure 1 (opposite)   The human uterine cervix
a,b: Colposcopic view of the anterior cervical lip, showing the two basic types of original cervical epithelium: the squamous epithelium (1) shows a distinct border (2) the squamocolumnar junction with the columnar epithelium (3) of the endocervical canal (4)
c,d: Colposcopic picture of the anterior cervical lip, showing a physiological transformation zone. The original squamocolumnar junction (2) between the original squamous epithelium of the ectocervix (1) and the original columnar epithelium (3) of the endocervix (4) is less evident. Due to the process of active squamous metaplasia (5) a neo-squamo-columnar junction (6) is now being formed
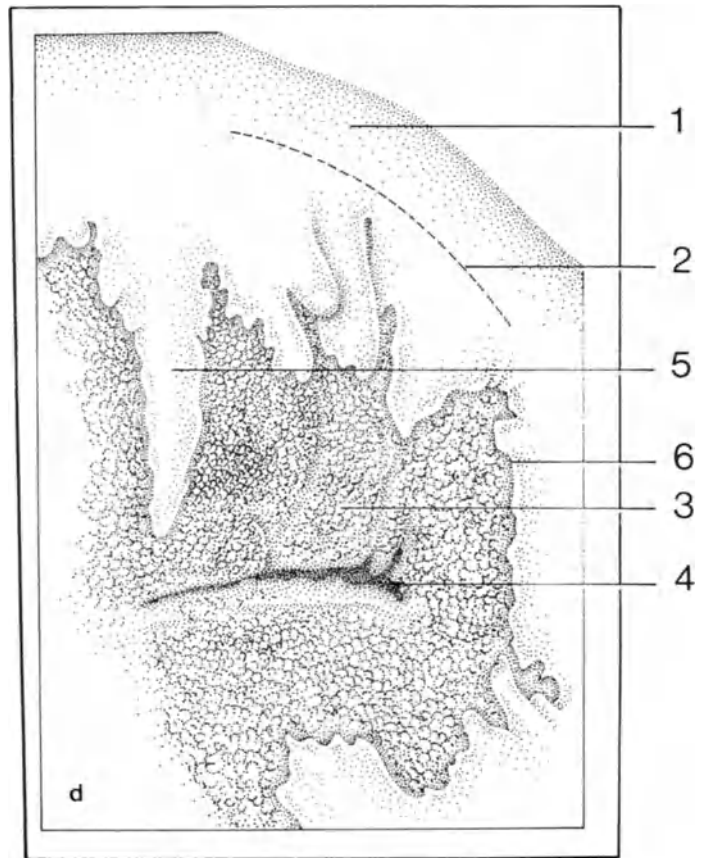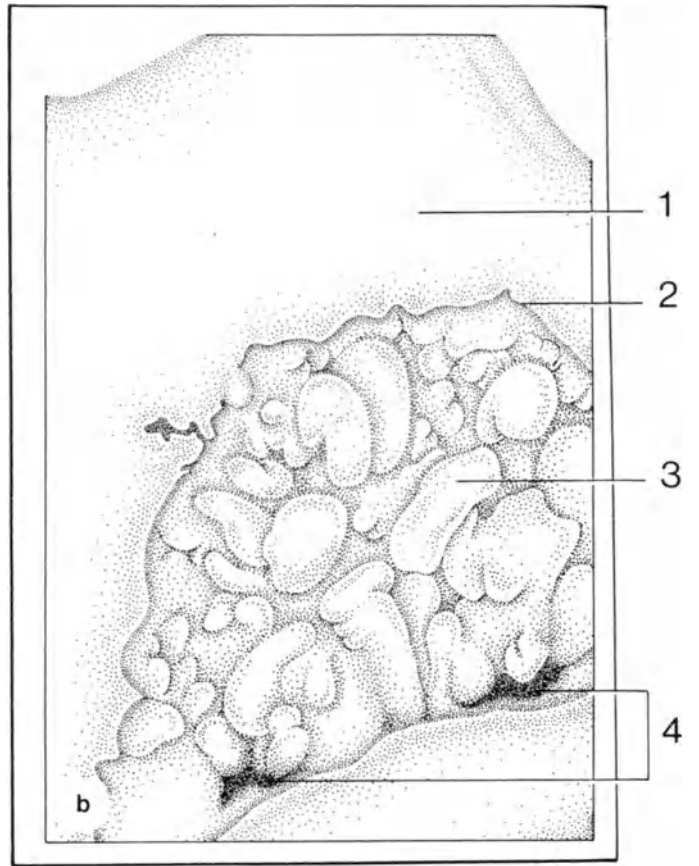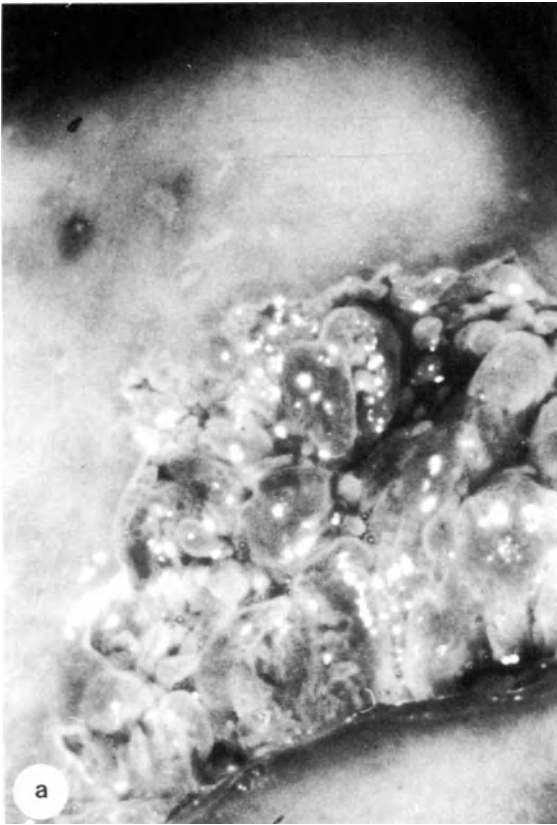
Figure 1

Ciliated cells have a distinctive round nucleus. The luminal surface exhibits cilia similar to those in the endometrium and oviduct. Ciliated cells also have surface microvilli interspersed amongst the kinocilia. The function of the ciliated cells is not clear, although it is assumed that they are involved in the mucociliary clearance of secretory macromolecules from the adjacent secretory cells. The kinocilia beat rhythmically towards the cervical canal and the vagina. Ciliated cells are more frequent in the endocervical columnar epithelium, particularly at the cervico-endometrial junction but rarely on ectocervical columnar epithelium.

The majority of the small cylindrical cells have numerous microvilli on their free apical dome-shaped surfaces. These are the mucus-secreting cells. In the presecretion situation apical mucinous secretions bulge from the cell surface, which is then devoid of microvilli.

The secretory activity of the cervical epithelium involves both apocrine and merocrine mechanisms (Nilsson and Westman, 1961). There are approximately 100 mucus-secreting gland-like units or crypts in the cervical canal (Odeblad, 1966), producing midcycle up to 700 mg mucus per day (Pommerenke, 1946). The cyclical variation in epithelial morphology in the endocervix is less noticeable than those of vaginal or endometrial epithelium.

THE METAPLASTIC EPITHELIUM OF THE TRANSFORMATION ZONE

The junctional interface between the squamous ectocervical and the columnar endocervical epithelium varies in its topographical location and its extent throughout reproductive life. This squamocolumnar junction lies within the endocervical canal during childhood, on the ectocervix in reproductive years and within the endocervical canal postmenopausally.

Especially during adolescence and pregnancy dynamic events proximal to the original squamocolumnar junction can lead to formation of an extensive transformation zone between the one-cell-layer thick original endocervical lining and the stratified ectocervical epithelium. In this zone the very interesting process of squamous metaplasia of cylindrical cells takes place. In most adult women the original columnar epithelium has been replaced by metaplastic epithelium at its most distal portion. Underneath, remnants of crypts lined with cylindrical epithelium can be found. The original squamocolumnar junction, now delineating two types of squamous epithelium – original and metaplastic (Coppleson et al., 1976) – is situated at the last glandular 'duct', which can be identified with the colposcope. The 'new' squamocolumnar junction refers to the line of demarcation separating the metaplastic squamous epithelium from the original columnar epithelium.

Physiological squamous metaplasia often occurs as a patchy process in which, starting at the tips of the endocervical columnar villi and rugae, the endocervical columnar cells (bearing microvilli) become converted to large, flat, new squamous epithelial cells with a

microridge surface pattern on their luminal cell sides. The process may become arrested at any stage. Closely located immature metaplastic cells may show different degrees of maturation and, therefore, may differ as to cell shape, cell volume and cell surface microvillous pattern (Williams et al., 1973b; Ferenczy and Richart, 1973; Sherman, 1977). Early metaplastic cells resemble more the endocervical glandular cell type, in that they are smaller in diameter, rounder, and with a slightly raised and bulging cell surface, covered with microvilli. More advanced metaplastic cells become larger, irregularly polygonal and more flattened, with typical cell borders (Figure 3). It is only in the final stage of late metaplasia that the large flattened cells acquire an elaborate microridge cell surface pattern, and then become indistinguishable from native squamous cells. Atypical squamous metaplasia may play an important role in cervical carcinogenesis and the transformation zone 'precisely defines the field of neoplastic potential' (Coppleson et al., 1976).

NEOPLASIA OF THE CERVIX EPITHELIUM

The human uterine cervix offers a unique opportunity to study early lesions of squamous cell carcinoma (Wilbanks, 1976). The light microscopy (LM) method of diagnostic cytology, using the Papanicolaou subclassification system, is well known and of established value. However, light macroscopy allows neither pretreatment staging nor prognostication of individual lesions (Patten, 1978). SEM, by revealing cell surface ultrastructure with high resolution and greath depth of field while surveying large areas of interest with a wide range of magnification, – offers a potentially powerful approach to diagnostic cytopathology.

Figure 2 (opposite The original ectocervical squamous epithelium
a,b: Adjoining cell surfaces of normal ectocervical cells within the tissue are observable in SEM after intercellular cleavage of the stratified tissue using a special stripping technique (see text). Scanning electron micrographs (a and b) depict parts of the surfaces of two adjoining superficial cells after stripping, showing the luminal side of a cell with microridges and crests (b) and the basal side of the adjoining cell with globular microvilli and furrows (a). The complementary aspect of the surface structures and the different patterns of microridges and microvilli in the regions outlined by crests and furrows respectively (regional differences) are noticeable (×9000)
c,d: Light microscopical morphology (c) and highly schematic diagram (d) illustrating the various zones that can be distinguished in the stratified epithelium of the ectocervix.
Abbr.: gm, globular microvilli; v, vacuole; f, furrow; fi, filiform processes; mr, microridges; d, desmosome; c, crest; m, mitochondria; pn, pycnotic nucleus; fo, foliate processes; cs, cytoskeleton; n, nucleus with nucleolus; bl, basal lamina
e: Exfoliating flat polygonal cells at the free, luminal side of the ectocervical epithelium (×180)
f: Cuboid to cylindrical cells of the basal and parabasal zones. Typical intercellular contacts are visible within the rather wide intercellular space (×1125)
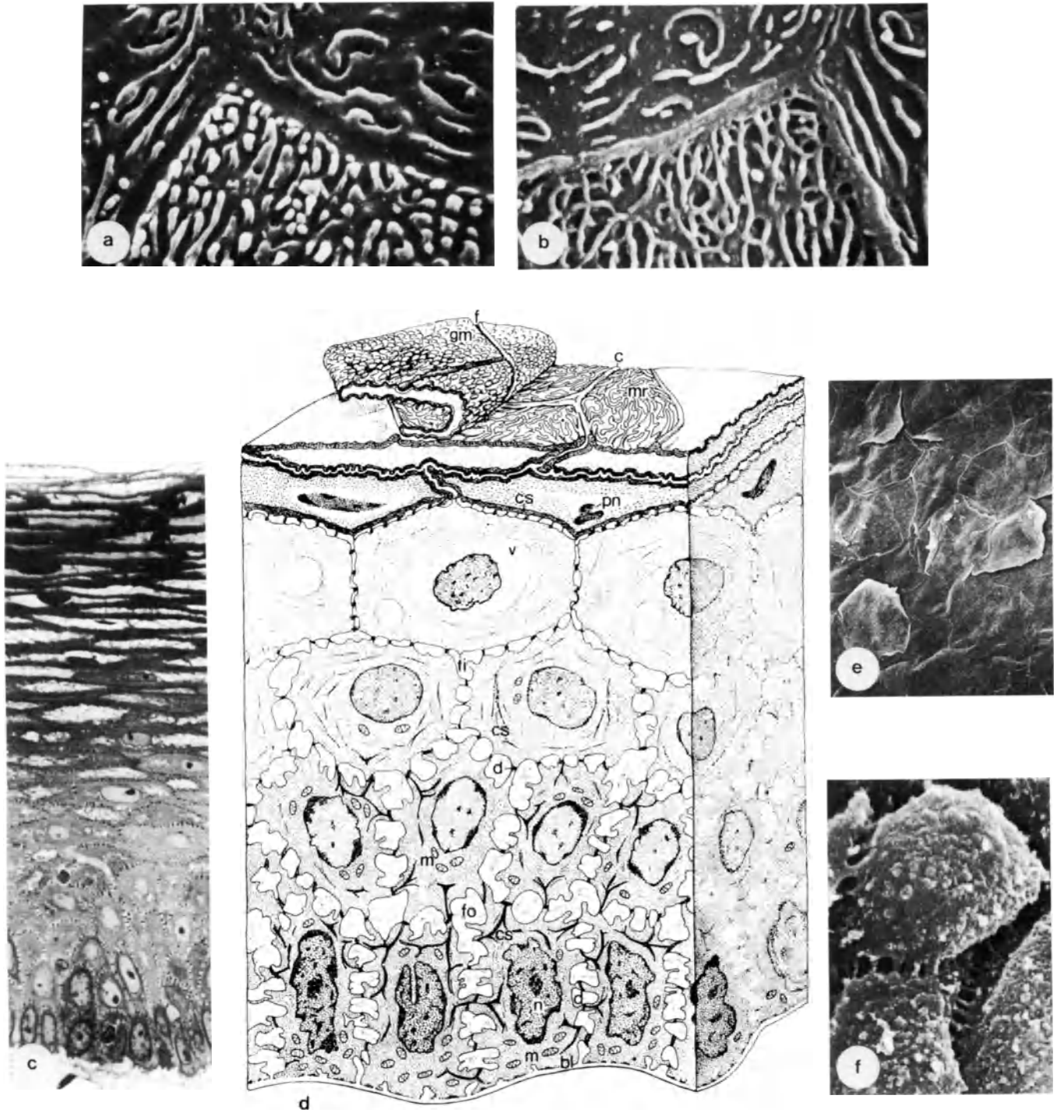
Figure 2

Theoretically, the cell surface organization on cancer cells is of paramount importance, as it may not only permit (early) diagnosis, but it may also harbour markers for refined prognosis and targets for selective cancer therapy.

Transmission electron microscopy (TEM) and freeze-etch studies (McNutt and Weinstein, 1969; McNutt et al., 1971; Shingleton and Wilbanks, 1974) have shown that differences in surface architecture exist between normal and abnormal ectocervical cells. These studies indicate that there is an increased number of microvilli on the surface of neoplastic cells together with a decreased number of desmosomes, which may explain the decrease in cohesiveness of malignant cells.

SEM studies (Murphy et al., 1973, 1974, 1975; Allen et al., 1976) also reveal obvious differences in the surface morphology between normal and abnormal cervical epithelia. Using SEM, desmosomes are not seen at all. A distinct feature of normal superficial or intermediate squamous cells is the presence of microridges, covering the cell surface of these flat cells. In TEM studies, the microridges were not recognized as such but, because of their appearance when transversely cut, were described as microvilli (Williams and Smith, 1978; Allen and Jordan, 1978; Kenemans et al., 1980).

A microvilli-dominated pattern was found on the surface of exfoliated abnormal cells. Pleomorphic microvilli have also been demonstrated by SEM on free (luminal) surfaces of malignant cells in situ, while a gradual transformation of cell surface morphology was found in the premalignant range of human ectocervical epithelium (Allen et al., 1976; Murphy et al., 1974; Jordan et al., 1975; Rubio and Kranz, 1976; Sherman, 1977; Rubio and Einhorn, 1977; Ferenczy and Gelfand, 1979; Kenemans et al., 1980).

Cell shape, which can still be polygonal and flat (but with obvious nuclear enlargement) in some types of dysplasia is, as in metaplasia, globular and pleomorphic in the smaller CIS cells. The characteristic luminal cell surface organization of normal superficial cells, which is generally considered to represent an end-stage of squamous cell differentiation or maturation, is progressively impaired: from an increasingly stunted microvillous pattern in dysplasia, with intermediate forms consisting of surfaces with both microridges and microvilli, to the well-known tightly packed long microvilli on the bulging surfaces of CIS cells. Linear bars and terminal bars disappear, intercellular junctions become ill-defined in CIS, while sometimes in dysplasia lateral cell side specializations in the form of a particular microridge system on still rather flat cells, are noted. We have the impression that the basal sides of the cells also show modification of their cell surface pattern in comparison with normal mature squamous cells. The microvilli look more stunted in dysplasia, and more abundant in CIS.

Thus, the precancerous lesions show a continuous spectrum of modifications. The description we have given is not at great variance with that of other researchers (Allen et al., 1976; Murphy et al., 1974; Jordan et al., 1975; Rubio and Kranz, 1976; Sherman, 1977; Rubio and Einhorn, 1977; Ferenczy and Gelfand, 1979).

These unanimous reports have also provoked a tendency to reverse the relationship by hypothesizing that cell surface microridges indicate normality, while cell surface microvilli imply abnormality. The SEM approach would be of paramount importance if any of the ultrastructural cell surface parameters could be considered as an early marker of irreversible neoplastic transformation, as suggested by some authors (Allen et al., 1976; Wilbanks, 1976).

However, the awareness of a 'basal'/'luminal' cell side difference will lead to a different interpretation of cell surfaces described, especially when studying exfoliated cells.

'Microvilli' as such (without more detailed description) cannot be considered to be indicative of abnormality, as these cell surface structures are also found on non-malignant cells, viz. normal (para)basal cells, metaplastic cells and on normal more superficial squamous cells, on their 'basal' side.

The question of whether or not the appearance of long, pleomorphic microvilli reflects an irreversible alteration of the epithelium, and thus provides an early marker of irreversible neoplastic transformation, has to be answered yet.

Although SEM has contributed significantly to the description of oncogenesis, up to now it has no early diagnostic, prognostic or therapeutic significance.

CONCLUDING REMARKS

Cell surface topography is a dynamic concept. It is not solely an expression of genetic cell properties but it is also related to several other factors and circumstances (e.g. preparation techniques, hormonal stimuli, and cell maturation). Microvilli are found on endocervical cells, normal immature ectocervical cells (parabasal cells, metaplastic cells) and on normal, more superficial, squamous cells, on their 'basal' side. Microvilli can also be found on neoplastic cells where they have been considered not to be tumor-specific, but merely a consequence of rapid epithelial turnover in the neoplastic epithelium which brings immature, deeper-lying cells too quickly to the surface.

Figure 3 (opposite) Cell topography and cell surface ultrastructure in ectocervical and metaplastic epithelium

a: Flat, polygonal lumen bordering cells of the ectocervical epithelium, one of which is desquamating. Cell surface ultrastructure of the free, luminal side of the superficial cells showing microridges and linear bars (×1500)

b: Luminal side of a superficial ectocervical cell showing branching and anastomosing microridges (×10 000)

c: Intercellular fracture plane through intermediate cells after freeze-fracturing showing globular microvilli and filiform processes (×10 000)

d: Intercellular fracture plane through parabasal cells after freeze-fracturing showing filiform to foliate processes (×10 000)

e: Transformation zone with immature metaplastic cells that show different degrees of maturation, and therefore differ as to cell shape, cell volume and cell surface microvillous pattern (×1000)

f: Small early metaplastic cells together with more advanced metaplastic cells, which are larger, irregularly polygonal and more flattened, with typical cell borders (×2000)
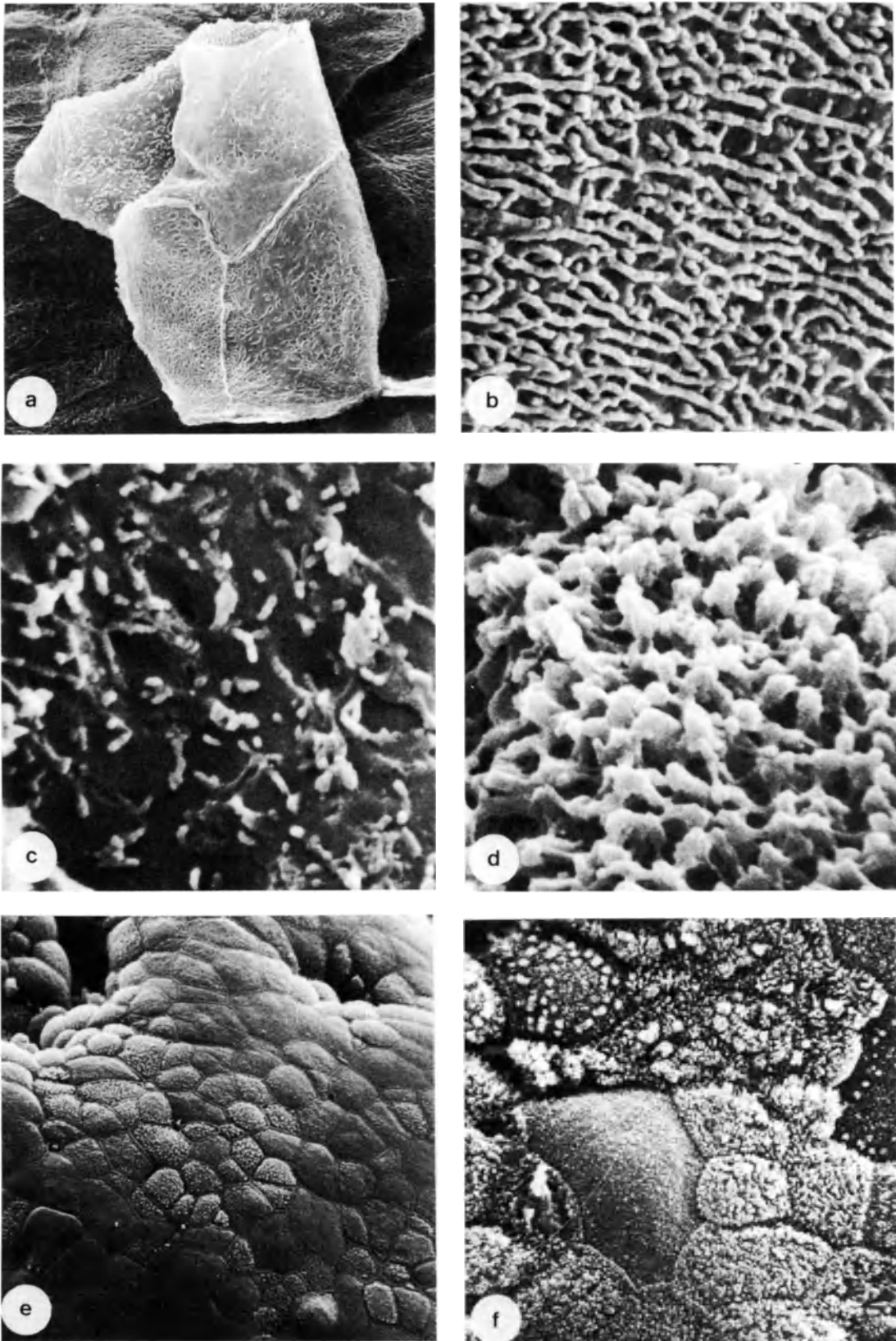
Figure 3

Microridges are found on the luminal sides of normal superficial squamous cells, and also on mature (late) metaplastic cells. They constitute an interlacing cell surface system, with several degrees of complexity which relate to the degree of maturation. These cytoplasmic ridges were also described on superficial invasive well-differentiated squamous cells, whereas in poorly differentiated carcinoma a microvillous pattern is observed (Ferenczy, 1980). The microridges and crests on the luminal cell side intermesh with globular microvilli and furrows present on the basal side of the overlying cell respectively. Crests and furrows delineate regions on the cell surface in which variable microridge and microvillus patterns appear. Because crests and furrows are not only present on the cell margins but also more centrally on the surface, the cell surface shows 'regional' differences.

The functional significance of the cell surface structure may be inferred from these facts. Endocervical cells are clearly either mucine-secreting glandular, or mucine-transporting ciliated, cells. The surface processes of the basal and parabasal ectocervical cells presumably are engaged in the enhancement of intercellular contact and must permit metabolic interchange with the intercellular space. The intermeshing projections of superficial cells probably result in an increase of the surface adhesiveness and, in particular, in an increased resistance to sideways movements (Williams et al., 1973a,b; Ferenczy and Richart, 1973).

Malignant cells show modifications in their cell surface organization, which theoretically may be relevant to cancer diagnosis, prognosis and therapy. Several of these surface properties can be studied with SEM techniques (e.g., using surface-labeling techniques). It is probably not the most promising approach to the problem, when out of all these cell surface parameters the surface topography is chosen as the object of study in the search for an early marker of irreversible neoplastic transformation.

References

Allen, J. M., Murphy, J. F., Jordan, J. A. and Williams, A. E. (1976). The use of scanning electron microscopy in cervical cytology: results from the examination of 218 patients. SEM Symposium, 9, 315

Allen, J. M. and Jordan, J. A. (1978). The cervix uteri. In Hafez, E. S. E. (ed.). Scanning Electron Microscopy of Human Reproduction, pp. 147–57. (Ann Arbor: Ann Arbor Science)

Bahr, G. F., Bibbo, M., Mikel, U., Engler, W., Rao, C. and Wied, G. L. (1976). Correlation of light and scanning electron microscopy: a new method for exfoliative cytology. Acta Cytol., 20, 239

Bonilla-Musoles, F., Hernandez-Yago, J. and Torres, J. V. (1974). Scanning electron microscopy of the cervix uteri. Arch. Gynäkol., 216, 91

Coppleson, M., Pixley, E. and Reid, B. (1976). Colposcopy, a Scientific and Practical Approach to the Cervix in Health and Disease. (Springfield, Ill.: Thomas)

Davina, J. H. M., Stadhouders, A. M., Kenemans, P. and van Haelst, U. J. G. M. (1980). A stripping technique for scanning electron microscopical study of adjoining cell surfaces in stratified squamous epithelium of the uterine

ectocervix. Beitr. Elektronenmikroskop. Direktabb. Oberfl., 13, 253

Davina, J. H. M., Stadhouders, A. M., Lamers, G. E. M., van Haelst, U. J. G. M. and Kenemans, P. (1981). Surface pattern differentiation of the epithelial cells of the human uterine ectocervix. SEM Symposium, 14 (III), 37

Ferenczy, A. (1980). The female reproductive system. In Hodges, G. M. and Hallowes, R. C. (eds). Biomedical Research Applications of Scanning Electron Microscopy. Vol. 2, pp. 127–65. (London: Academic Press)

Ferenczy, A. and Gelfand, M. M. (1979). The cytodynamics of normal and neoplastic cervical epithelium. Obstet. Gynecol. Surv., 34, 808

Ferenczy, A. and Richart, R. M. (1973). Scanning electron microscopy of the cervical transformation zone. Am. J. Obstet. Gynecol., 115, 151

Ferenczy, A. and Richart, R. M. (1974). Female Reproductive System: dynamics of scan and transmission electron microscopy, pp. 61–100. (New York: Wiley)

Fluhmann, C. F. (1961). The Cervix Uteri and its Diseases, pp. 30–102. (Philadelphia: Saunders)

Gould, P. R., Barter, R. A. and Papadimitriou, J. M. (1979). An ultrastructural, cytochemical and autoradiographic study of the mucous membrane of the human cervical canal with reference to subcolumnar basal cells. Am. J. Pathol., 95, 1

Hafez, E. S. E., Barnhart, M. I., Ludwig, H., Lusher, J., Joelsson, I., Daniel, J. L., Sherman, A. I., Jordan, J. A., Wolf, H., Stewart, W. C. and Chretien, F. C. (1975). Scanning electron microscopy of human reproductive physiology. Acta Obstet. Gynecol. Scand. (Suppl. 40), 7

Jordan, J. A. (1976). Scanning electron microscopy of the physiological epithelium. In Jordan, J. A. and Singer, A. (ed.). The Cervix, pp. 44–50. (London: Saunders)

Jordan, J. A., Murphy, J. F., Allen, J. M. and Williams, A. E. (1975). The neoplastic cervix. In Hafez, E. S. E. (ed.). Atlas of Mammalian Reproduction, pp. 250–7. (Stuttgart: Georg Thieme)

Jordan, J. A. and Williams, A. E. (1971). Scanning electron microscopy in the study of cervical neoplasia. J. Obstet. Gynaecol. Br. Commonw., 78, 940

Kenemans, P., van der Zanden, P. H. T., Stolk, J. G., Vooys, G. P. and Stadhouders, A. M. (1980). Cell surface ultrastructure in neoplasia of the uterine cervix. In Letnansky, K. (ed.). Biology of the Cancer Cell, pp. 307–15. (Amsterdam: Kugler)

Kenemans, P., Davina, J. H. M., de Haan, R. W., van der Zanden, P., Vooys, G. P., Stolk, J. G. and Stadhouders, A. M. (1981). Cell surface morphology in epithelial malignancy and its precursor lesions. SEM Symposium, 14 (III), 23

Figure 4 (opposite)   The original endocervical epithelium
a: The original columnar epithelium lining the endocervical canal consists of tall, slender and elongated columnar cells uniformly arranged in one layer and closely packed in a 'cobblestone' pattern (×750)
b: Endocervical clefts, crypts, folds, villi and micropolyps are highly similar in lining, all showing columnar cells, some of which are ciliated (×10 000)
c: Two small cylindrical cells having numerous microvilli on their free apical dome-shaped surfaces. These are emptied mucus-secreting cells (×5000)
d: Endocervical columnar cells in the presecretion situation. Apical mucinous secretions bulge from the cell surface, which is partly devoid of microvilli (TEM, ×10 000)
e: Diagram showing endocervical columnar glandular cells during mucus secretion (left), and in the emptied, post-secretion situation (right)
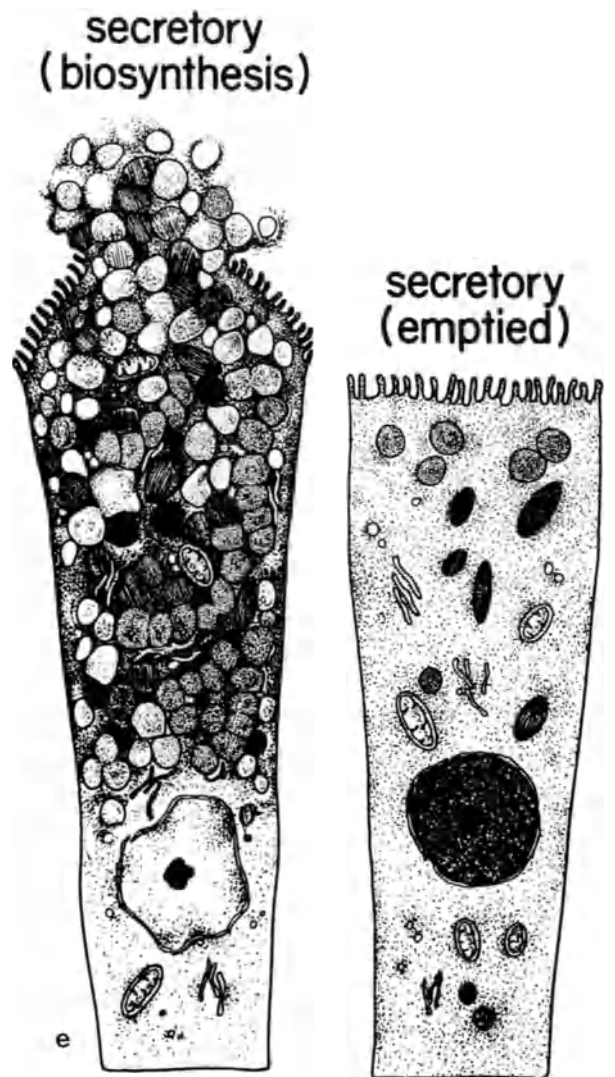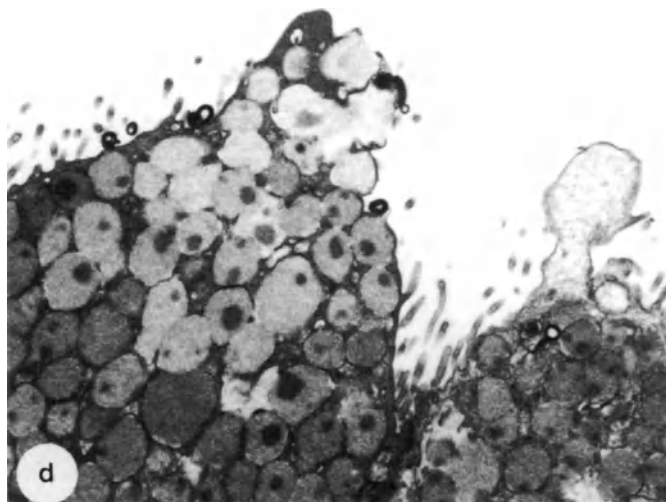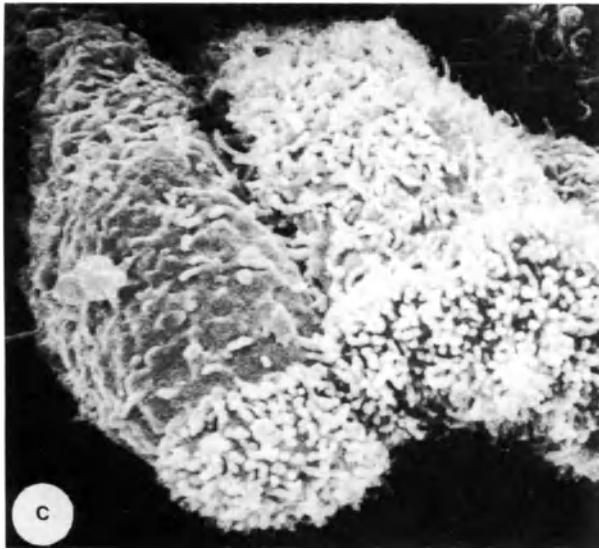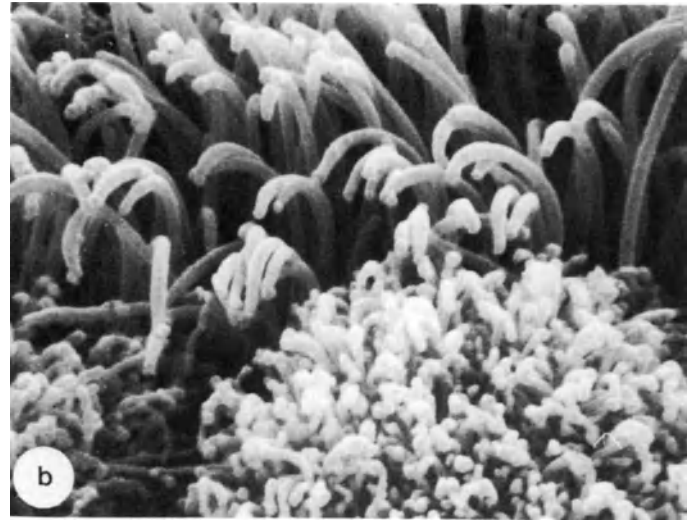
secretory
(biosynthesis)

secretory
(emptied)

Figure 4

Kenemans, P., Davina, J. H. M., de Haan, R. W., van der Zanden, P. H. T., Vooys, G. P. and Stadhouders, A. M. (1982). Surface ultrastructure of the uterine cervix and early detection of irreversible neoplasia. In Hafez, E. S. E. and Smith, J. P. (eds). *Carcinoma of the Cervix: Biology, Etiology and Diagnosis*, pp. 91–9. (The Hague: Martinus Nijhoff)

Kjaergaard, J. and Poulsen, E. F. (1977). Scanning electron microscopy of cotton swab smears from ectocervix: a methodological study. *Acta Cytol.*, **21**, 68

Lamb, J. C., Newbold, R. R., Strumpf, W. B. and McLachlan, J. A. (1978). Transitional changes in the surface epithelium of the cycling mouse vagina, cervix and uterus: scanning electron microscopic studies. *Biol. Reprod.*, **19**, 701

Leif, R. C., Gall, S., Dunlap, L. A., Railey, C., Zucker, R. M. and Leif, S. B. (1975). Centrifugal cytology. IV: The preparation of fixed stained dispersions of gynecological cells. *Acta Cytol.*, **19**, 159

Llanes, A. T., Farre, C. B., Ferenczy, A. and Richart, R. M. (1973). Scanning electron microscopy of normal exfoliated squamous cervical cells. *Acta Cytol.*, **17**, 507

Ludwig, H. and Metzger, H. (1976). *The Human Female Reproductive Tract; a Scanning Electron Microscopic Atlas*, pp. 8–29, 116–25, 159. (Berlin: Springer-Verlag)

McNutt, N. S., Hershberg, R. A. and Weinstein, R. S. (1971). Further observations on the occurrence of nexuses in benign and malignant human cervical epithelium. *J. Cell Biol.*, **51**, 805

McNutt, N. S. and Weinstein, R. S. (1969). Carcinoma of the cervix – deficiency of nexus intercellular junctions. *Science*, **165**, 597

Murphy, J. F., Allen, J. M., Jordan, J. A. and Williams, A. E. (1973). Examination of exfoliated cervical cells by the scanning electron microscope. *SEM/IITRI*, **6**, 605

Murphy, J. F., Jordan, J. A., Allen, J. M. and Wiliams, A. E. (1974). Correlation of scanning electron microscopy, colposcopy and histology in 50 patients presenting with abnormal cervical cytology. *J. Obstet. Gynaecol. Br. Commonw.*, **81**, 236

Murphy, J. F., Allen, J. M., Jordan, J. A. and Williams, A. E. (1975). Scanning electron microscopy of normal and abnormal exfoliated cervical squamous cells. *Br. J. Obstet. Gynaecol.*, **82**, 44

Nasr, M. F., Lagasse, L. D., Chang, N. and Moore, J. G. (1973). Scanning electron microscopy of the human cervix: description of a new method to study the surface anatomy. *Acta Cytol.*, **17**, 141

Nilsson, O. and Westman, A. (1961). The ultrastructure of the epithelial cells of the endocervix during the menstrual cycle. *Acta Obstet. Gynecol. Scand.*, **40**, 223

Odeblad, E. (1966). Micro-NMR in high permanent magnetic fields. *Acta Obstet. Gynecol. Scand.*, **45**, 127

Patten, S. F., Jr. (1978). *Diagnostic Cytology of the Uterine Cervix*. (Baltimore: Williams & Wilkins)

Pommerenke, W. T. (1946). Cyclic changes in the physical and chemical properties of cervical mucus. *Am. J. Obstet. Gynecol.*, **52**, 1023

Rubio, C. A. and Kranz, I. (1976). The exfoliating cervical epithelial surface in dysplasia, carcinoma in situ and invasive squamous carcinoma, I. Scanning electron microscopic study. *Acta Cytol.*, **20**, 144

Rubio, C.. A. and Einhorn, N. (1977). The exfoliating epithelial surface of the uterine cervix. IV: Scanning electron microscopical study in invasive squamous carcinoma of human subjects. *Beitr. Pathol.*, **161**, 72

Sherman, A. I. (1977). Comparison of cancer cell surfaces of the lower reproductive tract by scanning electron microscopy. *Am. J. Obstet. Gynecol.*, **129**, 893

Shingleton, H. M. and Wilbanks, G. D. (1974). Fine structure of human cervical intraepithelial neoplasia in vivo and in vitro. *Cancer*, **33**, 981

Steger, R. W. and Hafez, E. S. E. (1978). Age-associated changes in the vagina. In Hafez, E. S. E. and Evans, T. N. (eds). *The Human Vagina*, pp. 95–106. (Amsterdam: North Holland)

Wiernik, G., Bradbury, S., Plant, M., Cowdell, R. H. and Williams, E. A. (1973). A quantitative comparison between normal and carcinomatous squamous epithelia of the uterine cervix. *Br. J. Cancer*, **28**, 488

Wilbanks, G. D. (1976). In vivo and in vitro 'markers' of human cervical intraepithelial neoplasia. *Cancer Res.*, **36**, 2485

Williams, A. E., Jordan, J. A., Murphy, J. F. and Allen, J. M. (1973a). The surface ultrastructure of normal and abnormal cervical epithelia. *SEM/IITRI*, **6**, 597

Williams, A. E., Jordan, J. A., Allen, J. M. and Murphy, J. F. (1973b). The surface ultrastructure of normal and metaplastic cervical epithelia and of carcinoma in situ. *Cancer Res.*, **33**, 504

Williams, A. E. and Smith, A. N. (1978). A scanning electron microscope study of normal and pathological human gall-bladder. *SEM Symposium*, **11**, (II), 713

7

Cervical mucus

B. DAUNTER and P. LUTJEN

Department of Obstetrics & Gynaecology, University of Queensland, Clinical Sciences Building, Royal Brisbane Hospital, Herston, Queensland, Australia

The uterine cervix and its secretions are under hormonal control and spermatozoa can only gain entry, in large numbers, into the cervical canal at or near the time of ovulation (midcycle). The midcycle secretions of the uterine cervix not only enhance the passage of 'normal' spermatozoa, but also appear to filter out most morphologically abnormal spermatozoa, preventing them from gaining access to the uterus (Fredericsson and Bjlorke, 1977; Perry *et al.*, 1977). At other times in the menstrual cycle the passage of spermatozoa into the cervical canal is impeded, and should spermatozoa gain entry they may become immobilized by the cervical secretions. It is these secretions, cervical mucus, which mainly determine the fate of spermatozoa in the female genital tract. Midcycle mucus possesses an increased Spinnbarkeit, which is a rheological property of the mucus which allows it to be pulled out into a thin strand, up to 8 cm, depending on the volume of mucus used (Figure 1). At other times in the menstrual cycle the Spinnbarkeit is greatly reduced.

INSOLUBLE PHASE (MUCIN)

Cervical mucus consists of an aqueous phase dispersed in an insoluble phase or mucin matrix. Under the influence of the hormonal milieu, the cervical mucin matrix undergoes structural changes throughout the menstrual cycle. At midcycle the structure of the mucin enhances the passage of spermatozoa and at other times in the menstrual cycle impedes their entry. The rheological properties of this mucin have been described in detail (Wolf *et al.*, 1977a,b,c).

Mucins, including cervical mucin, are glycoproteins characterized by their high proportion of carbohydrate, more than 40% distributed along the peptide core in the form of numerous side-chains (Gottschalk, 1972). The oligosaccharide side-chains of the glycoproteins that make up the mucin may terminate with either L-fucose or sialic acid(s) (Gottschalk, 1972). In general, there is an inverse relationship between the content of fucose and sialic acid(s) in epithelial mucins (Dische,

1973), as in the case of cervical mucin. The glycoproteins of cervical mucin also bind water, mainly by hydrogen bonding (Odeblad, 1976) and form a hydrogel. The rheological properties of this hydrogel suggest that the glycoproteins are random-coiled molecules (Lee *et al.*, 1977). Such molecules can interact to form a molecular network and in extreme cases these molecules may become so closely associated that individual molecular identity is lost (Gibbons, 1972). Glycoprotein molecules associated in this manner show rheological properties of viscoelastic 'solutions' (Lodge, 1964; Berry and Fox, 1968), as does cervical mucin. Therefore the idea that the glycoprotein molecules of cervical mucin may be cross-linked by another protein to form the mucin (Masson, 1973) may not be tenable. In addition, the suggestion that the mucin may be formed by subunits of glycoproteins associated by disulfide bonds (Elstein, 1976), as in the case of pig gastric mucin (Allen *et al.*, 1976), may not be possible when we consider the low concentration of disulfide and sulfhydryl groups in cervical mucin (Daunter *et al.*, 1977, 1978). Therefore the disulfide bonds present in cervical mucin may be intramolecular rather than intermolecular.

Cervical mucin may be formed by the association of glycoproteins via hydrogen bonding. However, the presence of highly charged negative groups on the oligosaccharide side-chains of the glycoprotein molecules, such as the terminal sialic acid(s), would prevent hydrogen bonding unless they were first 'neutralized'. Since 90% of the copper present in the cervical mucus is associated with the mucin (Daunter *et al.*, 1977), the carboxylic acid groups of the sialic acid(s) moieties of the glycoproteins may chelate this copper. Therefore this process may link individual glycoproteins to each other via the carboxylic acid groups of the sialic acid(s) to form 'fibers', which then associate by hydrogen bonding to form the mucin *per se* (Figure 2). In addition, the sialic content of cervical mucin is increased at midcycle (Kesseru and Westphal, 1975; Daunter, 1978) as is the sialyltransferase activity (Chantler and Debruyne, 1977). This suggests that

early pre-ovulatory   mid-cycle   post-ovulatory
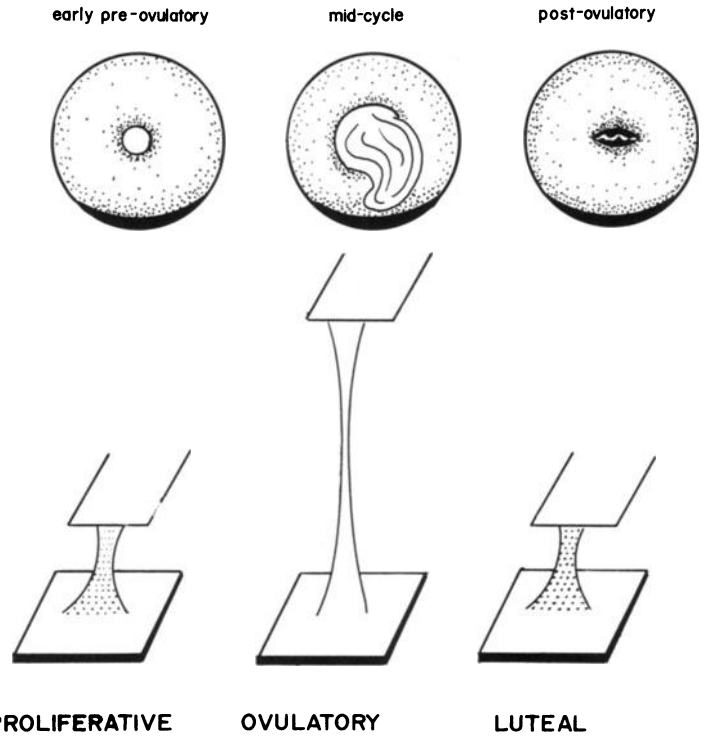
Figure 1

Top: Changes in the diameter of the external cervical os and mucus production throughout the menstrual cycle

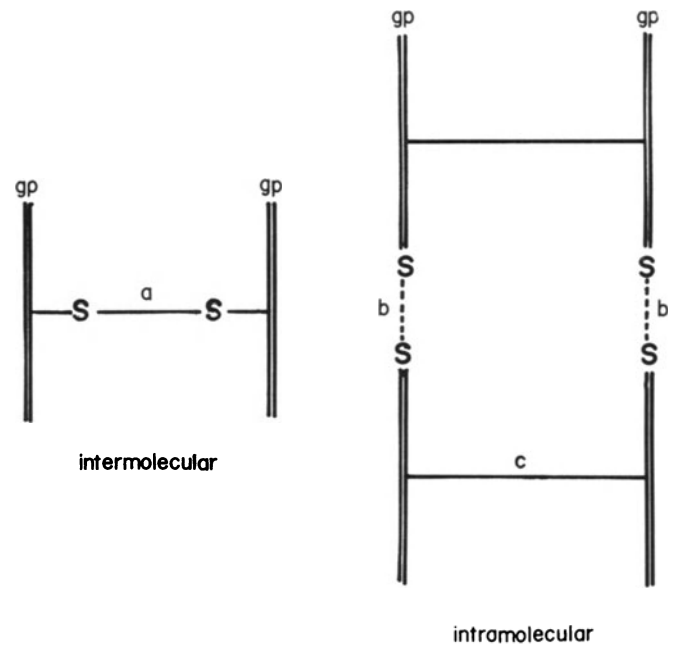**Bottom:** Changes in the Spinnbarkeit of cervical mucus during the menstrual cycle

PROLIFERATIVE   OVULATORY   LUTEAL

Figure 2

Top: Diagrammatic representation of intermolecular disulfide bonds (a) and intermolecular disulfide bond (b) existing between the glycoprotein (gp) chains of cervical mucus. The intramolecular bonds designated (c) have yet to be positively identified

Bottom: Diagrammatic representation of the copper-sialic acid complex postulated to link individual glycoproteins

intermolecular

intramolecular

COO⁻ ⁺Cu⁻ ⁺OOC

COO⁻ ⁺Cu⁺ ⁻OOC
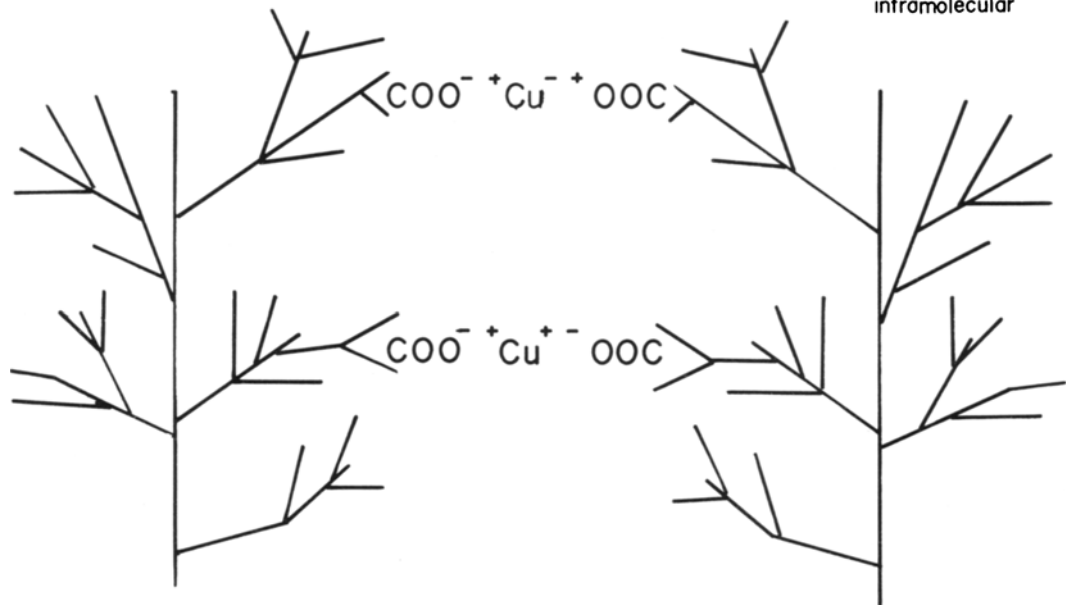
sialic acid is important to the structural integrity of cervical mucin.

SEM OF CERVICAL MUCIN

Daunter et al. (1976) employed mild fixation techniques for cervical mucus. The mucus was fixed in 0.6% glutaraldehyde in 0.2 mol/l Sørensen phosphate buffer pH 7.4, which preserved the Spinnbarkeit of the mucus while preventing the action of endogenous enzymes. The mucus was then immersed in liquid nitrogen and freeze-dried at 1.0 Torr for 10 h. The serial results showed the mucin to consist of a honeycomb-like structure with interconnecting channels separated by thin 'membranous' walls. The diameter of the channels in the early proliferative phase was 2–6 μm and at midcycle 30–35 μm, in which spermatozoa were found, and 4–6 μm in the luteal phase (Figure 3a-c). In the first trimester of pregnancy a compact dense form of the mucin structure was observed (Figure 3d).

HOSTILE CERVICAL MUCUS

In some cases of unexplained infertility spermatozoa may become immobilized in midcycle cervical mucus (Beer and Neaves, 1978) even though both components of this system appear normal. In such cases the spermatozoal penetration of the mucus is impeded; they may lose progressive motility, vibrate or become agglutinated, eventually resulting in complete immobilization. Immunological explanations have been given for this, such as the presence of cytotoxic and agglutinating antibodies (Wong, 1978), and the same explanation has been given for similar observations in seminal plasma (Friberg and Friberg, 1976). Considering that both cervical mucus and seminal plasma lack most of the components of the complement system (Beer and Neaves, 1978), it appears unlikely that immunoimmobilization of the spermatozoa could occur. An alternative explanation may involve some structural change of the cervical mucus and biochemical reactions between the cervical mucus and spermatozoa.

When midcycle mucus samples were analyzed for the uptake of radioactive sialic acid from CMP-sialic acid, it was found that the 'hostile' mucus had significantly more receptor sites for sialic acid, 4.24 ± 1.47 μmol/l for each 100 mg dry mucin (n ± 9) relative to normal mucin 1.47 ± 0.40 μmol/l for each 100 mg dry mucin (n ± 9). In addition, SEM revealed that the honeycomb pore-like structure was greatly diminished in the samples of hostile mucus (Figure 4a) which may account for the lack of spermatozoal penetration in such mucus. That such gross changes in cervical mucin structure can be attributed to the absence of small amounts of sialic acid is difficult to comprehend, thus 'hostile' mucus may also be deficient in, and/or contain an excess of, other components. However, modulation of small amounts of cervical mucin sialic acid may well induce large structural changes in the mucin, because one molecule of sialic acid will associate with five molecules of water (Apffel, 1970).

The immobilization of the spermatozoa in hostile mucus may result from the transfer of spermatozoal sialic acid to the increased number of sialic acid receptor sites of the mucin. The transfer of spermatozoal sialic acid to the mucin is possible because spermatozoa carry sialyltransferase and CMP sialic acid synthetase (Daunter and Newlands, 1981). Spermatozoal sialic acid is normally transferred to the zona pellucida, as in the murine system (Durr et al., 1977) as a prelude to fertilization. The transfer of spermatozoal sialic acid to the 'hostile' cervical mucin may result in the loss of spermatozoal motility, although this has yet to be demonstrated. The desialylated spermatozoa may then be agglutinated by naturally occurring antibodies to desialylated cells (Tisserand-Jochem, 1974).

INTRAUTERINE DEVICES (IUDs)

There does not appear to be any major observable effect of the Copper Seven IUD (Cu7 IUD) on the structure of midcycle mucus, apart from a few globular appendages on the membranous walls of the channels (Figure 4b). However, in the luteal phase the structure is more compact (Figure 4c) compared to that of mucus from a non-contraceptive cycle. The copper levels in the luteal phase mucin from women using Cu7 IUDs is greatly increased (Daunter et al., 1977). This suggests an association of the copper with the mucin resulting in structural modification of the mucin.

ORAL CONTRACEPTIVES

350 μg norethisterone daily do not appear to affect the trace metal balance of the cervical mucus, but the sulfhydryl group content is increased (Daunter et al., 1978). This suggests that the amino acid sequence of the peptide core, involving cysteine of the cervical mucin glycoprotein, may be under gestagenic control and possibly cystine under oestrogenic control. This may explain to some degree the rheological properties of cervical mucin, the disulfide groups imparting a particular structural stability to the cervical mucin at or around the time of ovulation. The ultrastructure of the mucin at midcycle appears as a honeycomb pore-like structure covered with a fine meshwork (Figure 4d). Thus, there appear to be two types of mucin being produced, possibly representing a balance between the effects of the exogenous progestagen and endogenous estrogen.

References

Allen, A., Pain, R. H. and Robson, T. R. (1976). Model for the structure of the gastric mucosal gel. Nature (London), 264, 88

Apffel, C. H. (1970). Regulation of antigenic expression. J. Theoret. Biol., 26, 47

Beer, A. and Neaves, W. B. (1978). Antigenic status of semen from the view points of the female and male. Fertil. Steril., 29, 3

Berry, G. C. and Fox, T. G. (1968). The viscosity of polymers and their concentrated solution. Adv. Polymer. Sci., 5, 261

Chantler, E. N. and Debruyne, E. (1977). The relationship between the cervical glycosyltransferase and mucus
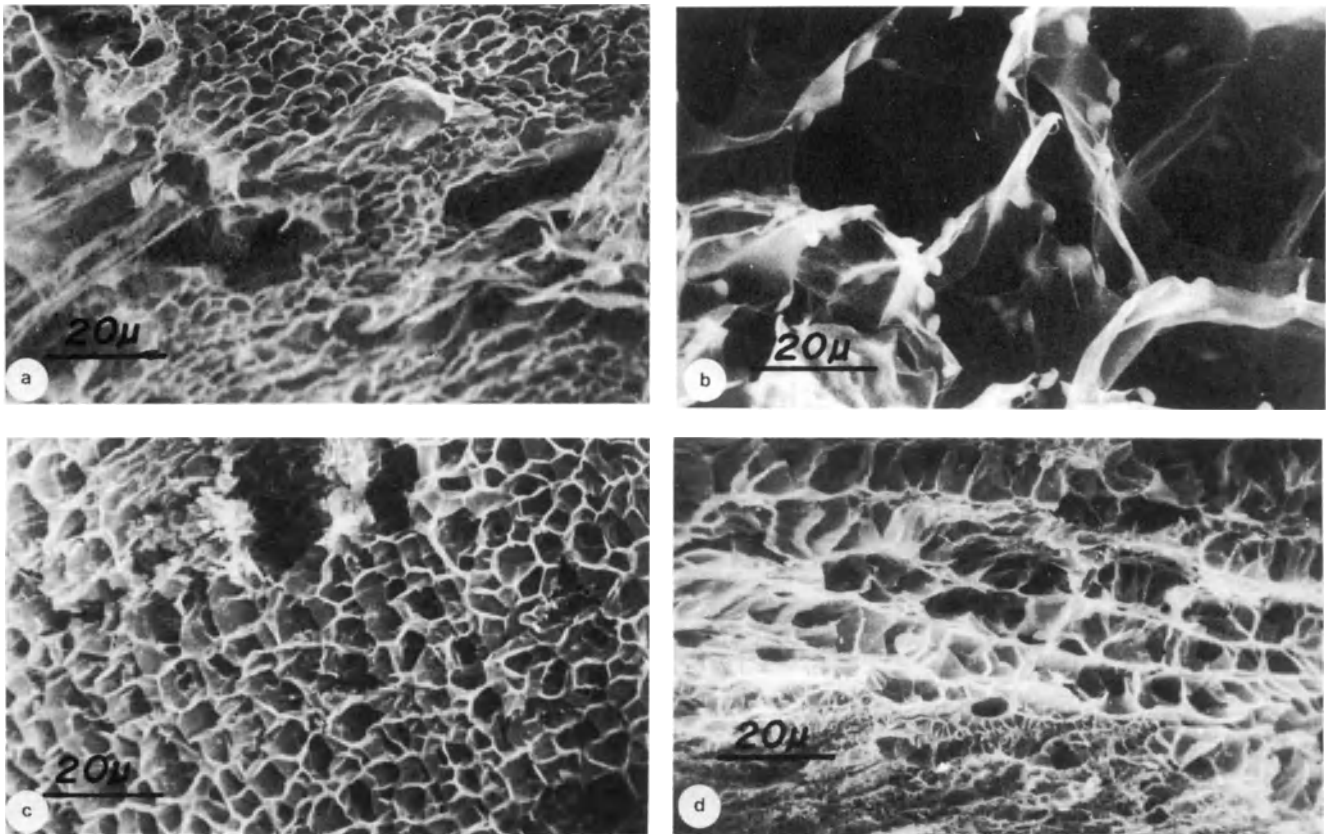
Figure 3
a: SEM of normal preovulatory cervical mucin, Day 10
b: SEM of normal midcycle cervical mucin, Day 19

c: SEM of normal postovulatory cervical mucin, Day 24
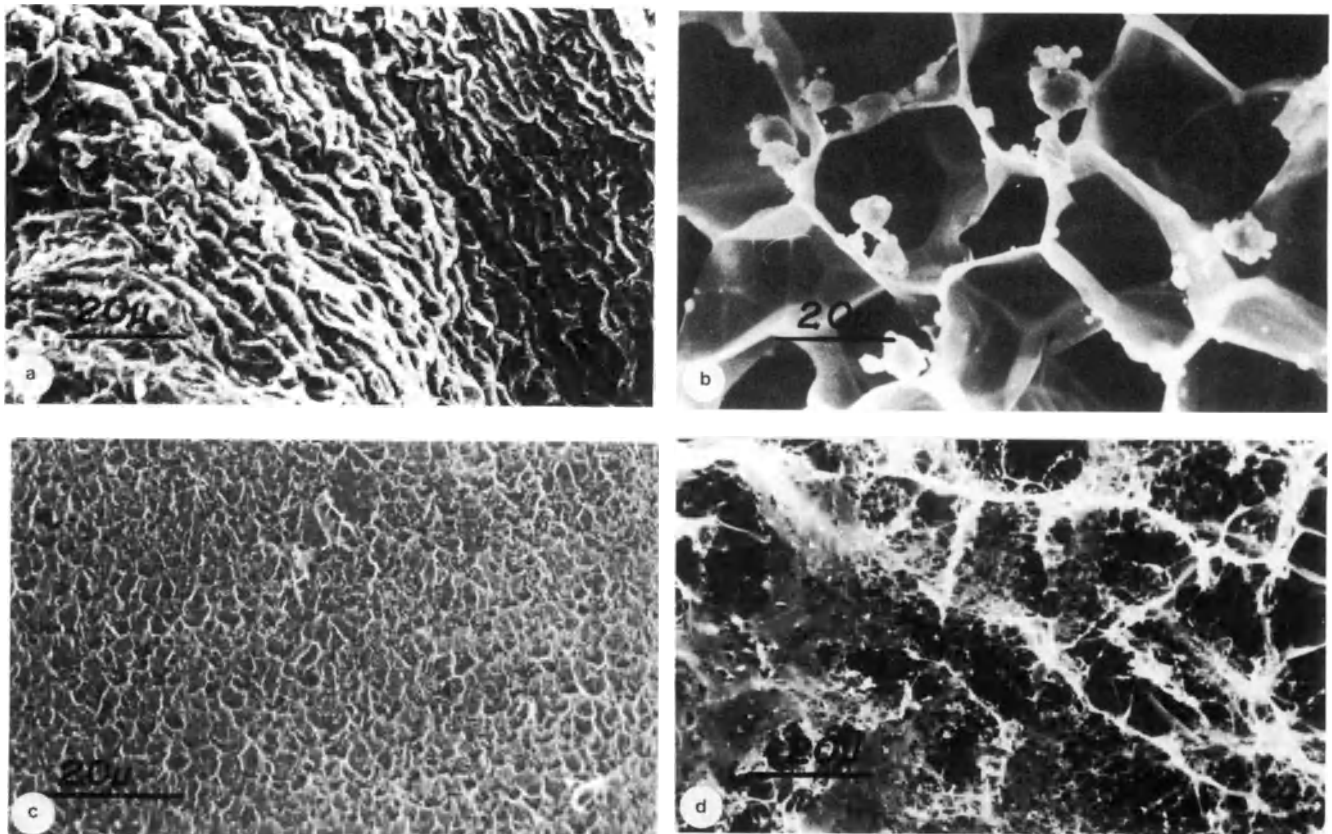d: SEM of cervical mucin in pregnancy, 11 weeks' gestation

Figure 4
a: SEM of hostile midcycle cervical mucin
b: SEM of midcycle cervical mucin, effect of a Copper Seven intrauterine device

c: SEM of postovulatory cervical mucin, effect of a Copper Seven intrauterine device
d: SEM of midcycle cervical mucin, effect of orethisterone

rheology. In Insler, V. and Bettendorf, G. (eds.). *The Uterine Cervix in Reproduction*, pp. 77–83. (Stuttgart: Georg Thieme)

Daunter, B. (1978). Sialic acid levels and scanning electron-microscopy of cervical mucus. *Contraception*, 17, 27

Daunter, B., Chantler, E. N. and Elstein, M. (1976). The scanning electronmicroscopy of human cervical mucus in the non-pregnant and pregnant states. *Br. J. Obstet. Gynaecol.*, 83, 738

Daunter, B., Chantler, E. N. and Elstein, M. (1977). Trace metals (Cu, Mn, Zn, Fe), sulphydryl and disulphide groups of cervical mucus. *Contraception*, 15, 543

Daunter, B., Chantler, E. N. and Elstein, M. (1978). The effect of a low dose progestagen on the trace metal content and disulphide and sulphydryl groups in cervical mucus. *Contraception*, 17, 35

Daunter, B. and Newlands, J. (1980). Seminal plasma and spermatozoal sialyltransferase and CMP sialic acid synthetase activities. *Andrologia*. 13, 215

Dische, Z. (1973). Reciprocal relation between fucose and sialic acid in mammalian glycoproteins. *Ann. N.Y. Acad. Sci.*, 106, 259

Durr, K., Shur, B. and Roth, S. (1977). Sperm associated sialyltransferase activity. *Nature, (London)*, 265, 547

Elstein, M. (1976). Biochemistry of cervical mucus. In Jordan, J. A. and Singer, A. (eds.) *The Cervix*, pp. 147–54. (London: Saunders)

Fredericsson, B. and Bjlorke, G. (1977). Morphology of postcoital spermatozoa in the cervical secretion and its clinical significance. *Fertil. Steril.*, 28, 841

Friberg, J. and Friberg, I. T. (1976). Antibodies in human seminal fluid. In Hafez, E. S. E. (ed.). *Human Semen and Fertility Regulation in Men*, Chapter 23, pp. 258–64. (St Louis: C. V. Mosby)

Gibbons, R. A. (1972). Physico-chemical methods for the determination of the parity, molecular size and shape of glycoproteins. In Gottschalk, A. (ed.). *Glycoproteins*, Part A, pp. 131–40. (London: Elsevier)

Gottschalk, A. (1972). Definition of glycoproteins and their delineation from other carbohydrate-protein complexes. *Glycoproteins, their Composition, Structure and Function*, Part A, pp. 24–30. (London: Elsevier)

Kesseru, W. and Westphal, N. (1975). Variation of the sialic acid–protein ratio in the human cervical mucus. *Reproduction*, 2, 131

Lee, W. I., Verdugo, P., Blandau, R. J. and Gaddum-Rosse, P. (1977). Molecular arrangement of cervical mucus: a re-evaluation based on laser light scattering spectroscopy. *Gynecol. Invest.*, 8, 254

Lodge, A. S. (1964). *Elastic Liquids*, p. 223. (New York: Academic Press)

Masson, P. L. (1973). In Elstein, M. and Moghissi, K. S. (eds.). *Cervical Mucus in Human Reproduction*. W.H.O. Colloquium, September 1972. (Chicago: University of Chicago Press)

Odebald, E. (1976). The biophysical aspects of cervical mucus. In Jordan, J. A. and Singer, A. (eds.). *The Cervix*. pp. 155–63. (London: Saunders)

Perry, G., Glezerman, M. and Insler, V. (1977). Selective filtration of abnormal spermatozoa by the cervical mucus *in vitro*. In Insler, V. and Bettendorf, G. (eds.). *The Uterine Cervix in Reproduction*, pp. 118–28. (Stuttgart: Georg Thieme)

Tisserand-Jochem, E. M. (1974). Natural auto antibodies against neuraminidase-treated cells in normal sera and seminal plasma. *Behring Inst. Mitt.*, 55, 197

Wolf, D. P., Blasco, L., Khan, M. A. and Litt, M. (1977a). Human cervical mucus. I. Rheological characteristics. *Fertil. Steril.*, 28, 41

Wolf, D. P., Blasco, L., Khan, M. A. and Litt, M. (1977b). Human cervical mucus. II. Changes in viscoelasticity during the ovulatory menstrual cycle. *Fertil. Steril.*, 28, 47

Wolf, D. P., Blasco, L., Khan, M. A. and Litt, M. (1977c). Human cervical mucus. III. Isolation and characterization of rheologically active mucins. *Fertil. Steril.*, 28, 53

Wong, W. P. (1978). Sperm antibodies in the cervical mucus and sera and postcoital tests in infertile women. *Eur. J. Obstet. Gynecol. Reprod. Biol.*, 8, 363

8

Postovulatory endometrium

P. SUNDSTRÖM* and B. Ove NILSSON†

* Department of Obstetrics and Gynecology, Allmänna Sjukhuset, S-214 01 Malmö
† Reproduction Research Unit, Biomedical Centre, Box 571, S-751 23 Uppsala, Sweden

Dating of endometrial biopsy specimens by light microscopy is a well-known procedure (Noyes et al., 1950). Transmission electron microscopy also reveals certain intracellular changes in the uterine epithelium, especially between the proliferative and secretory phase (Ferenczy and Richart, 1973; Nilsson, 1962a,b). Cyclic changes have also been found in the scanning electron microscope, but it has not yet been settled how consistent they are in the secretory phase, and whether the appearance of the luminal surface is specific at the time of implantation (Baraggino et al., 1980; Ferenczy, 1977; Ferenczy and Richart, 1973; Hafez et al., 1977; Johannisson and Nilsson, 1972; Martel et al., 1981; Nathan et al., 1978; Nilsson, 1980; Nilsson and Nygren, 1972).

This chapter concerns the types of surface changes demonstrable in endometrial biopsy specimens obtained in the early or late postovulatory phase in women with and without previous stimulation of the ovaries by exogenous hormones to yield several oocytes. Ovarian stimulation is often used for obtaining one or more preovulatory oocytes in association with in vitro fertilization and embryo transfer.

Three features were studied in detail for detecting any cyclic changes of the endometrium, namely frequency and structure of ciliated cells, of non-ciliated cells, and of apical protrusions.

Ciliated cells with their bristling cilia were intermingled with the more numerous non-ciliated cells (Figure 1). The proportion of ciliated cells varied within different areas of a specimen and between different specimens of the same biopsy specimen. Therefore, reliable quantification of ciliated cells was not possible. The cilia seemed to be of equal length and number in both early and late biopsy specimens. Thus, both in unstimulated and stimulated cycles neither the frequency nor the surface structure of the ciliated cells

showed any clear regular changes from the early luteal phase to the time for implantation.

Non-ciliated cells showed a surface area which varied in size, and microvilli which varied in number and length (Figures 2a, 4a,b). Thus, the appearance of the non-ciliated cells differed widely between and within specimens, whether the biopsy specimens were obtained early or late after ovulation, and whether the ovaries had been stimulated or not.

Apical protrusions of the non-ciliated cells, though fairly few, were more common in endometrial folds. Sometimes a border was clearly visible between areas of non-ciliated cells with and without protrusions (Figure 2b,c). The apical protrusions varied in shape (Figure 3a–c). Some were rather smooth and low, situated in the center of non-ciliated cells, and in seemingly different stages of development (Figure 3c). Other protrusions were morel-like, either large or small, and emerging from a part of a non-ciliated cell (Figure 3a,c). Apical protrusions were seen in both early and late biopsy specimens and showed no cyclic change in frequency or appearance, nor were they influenced by an ovarian stimulation.

In conclusion, no consistent ultrastructural changes of the endometrial surface can be detected in biopsy specimens obtained early or late in unstimulated or stimulated cycles. The lack of consistent, cyclic postovulatory changes in the surface structure might indicate that the properties of the luminal cell membrane of the surface epithelium are not continuously differentiating to reach a specific state at the expected time for implantation. The surface may perhaps be ready to accept the embryo (natural or in vitro fertilized) at any time within a certain range of days, and the crucial point of time for implantation may be governed by other changes in the endometrium or by the developmental stage of the embryo.

Acknowledgement

References

Baraggino, E., Dalla Pria, S., Cuberli, C. and Bortolotti, S. (1980). Scanning electron microscopy of the human normal endometrium. *Clin. Exp. Obstet. Gynecol.*, 7, 66

Ferenczy, A. (1977). Surface ultrastructural response of the human uterine lining epithelium to hormonal environment. A scanning electron microscopic study. *Acta Cytol.*, 21, 566

Ferenczy, A. and Richart, R. M. (1973). Scanning and transmission electron microscopy of the human endometrial surface epithelium. *J. Clin. Endocrinol. Metab.*, 36, 999

Hafez, E. S. E., Fadel, H. E., Noonan, S. M., Oshima, M., Okumara, H., Watson, J. H. L. and Zaneveld, L. J. D. (1977). Scanning electron microscopy of human female reproductive tract and amniotic fluid cells. *Int. J. Fertil.*, 22, 193

Johannisson, E. and Nilsson, L. (1972). Scanning electron microscopic study of the human endometrium. *Fertil. Steril.*, 23, 613

Martel, D., Malet, C., Gautray, J. P. and Psychoyos, A. (1981). Surface changes of the luminal uterine epithelium during the human menstrual cycle: a scanning electron microscopic study. In de Brux, J., Mortel, R. and Gautray, J. P. (eds.). *The Endometrium. Hormonal Impacts*, pp. 15–29. (New York and London: Plenum)

Nathan, E., Knoth, M. and Nilsson, B. O. (1978). Scanning electron microscopy of the effect of short-term hormonal therapy on postmenopausal endometrium. *Uppsala J. Med. Sci.*, 83, 175

Nilsson, O. (1962a). Electron microscopy of the glandular epithelium in the human uterus. I. Follicular phase. *J. Ultrastruct. Res.*, 6, 413

Nilsson, O. (1962b). Electron microscopy of the glandular epithelium in the human uterus. II. Early and late luteal phase. *J. Ultrastruct. Res.*, 6, 422

Nilsson, O. (1980). Scanning electron microscopic responses by the endometrial surface to various estrogens and gestagens. In Dallenbach-Hellweg, G. (ed.). *Functional Morphologic Changes in Female Sex Organs Induced by Exogenous Hormones*, pp. 137–45. (Berlin: Springer)

Nilsson, O. and Nygren, K. G. (1972). Scanning electron microscopy of human endometrium. *Uppsala J. Med. Sci.*, 77, 3

Noyes, R. W., Hertig, A. T. and Peck, J. (1950). Dating the endometrial biopsy. *Fertil. Steril.*, 1, 3

Figure 1 (opposite)

a: Survey view of luminal surface of stimulated endometrium, day 7 after ovulation. The mucosa is irregular and folding (×350)

b: Luminal surface of unstimulated endometrium, day 7 after ovulation. Two cell types, ciliated and non-ciliated (secretory) cells, form the surface epithelium. The ciliated cells can be recognized by the presence of kinocilia. The openings of two endometrial glands are observed in the upper part of the picture (×1000)

c: Ciliated and non-ciliated cells of stimulated epithelium, day 7 after ovulation. The ciliated cells carry kinocilia and the non-ciliated cells possess microvilli and sometimes mushroom-like, apical protrusions (×8000)
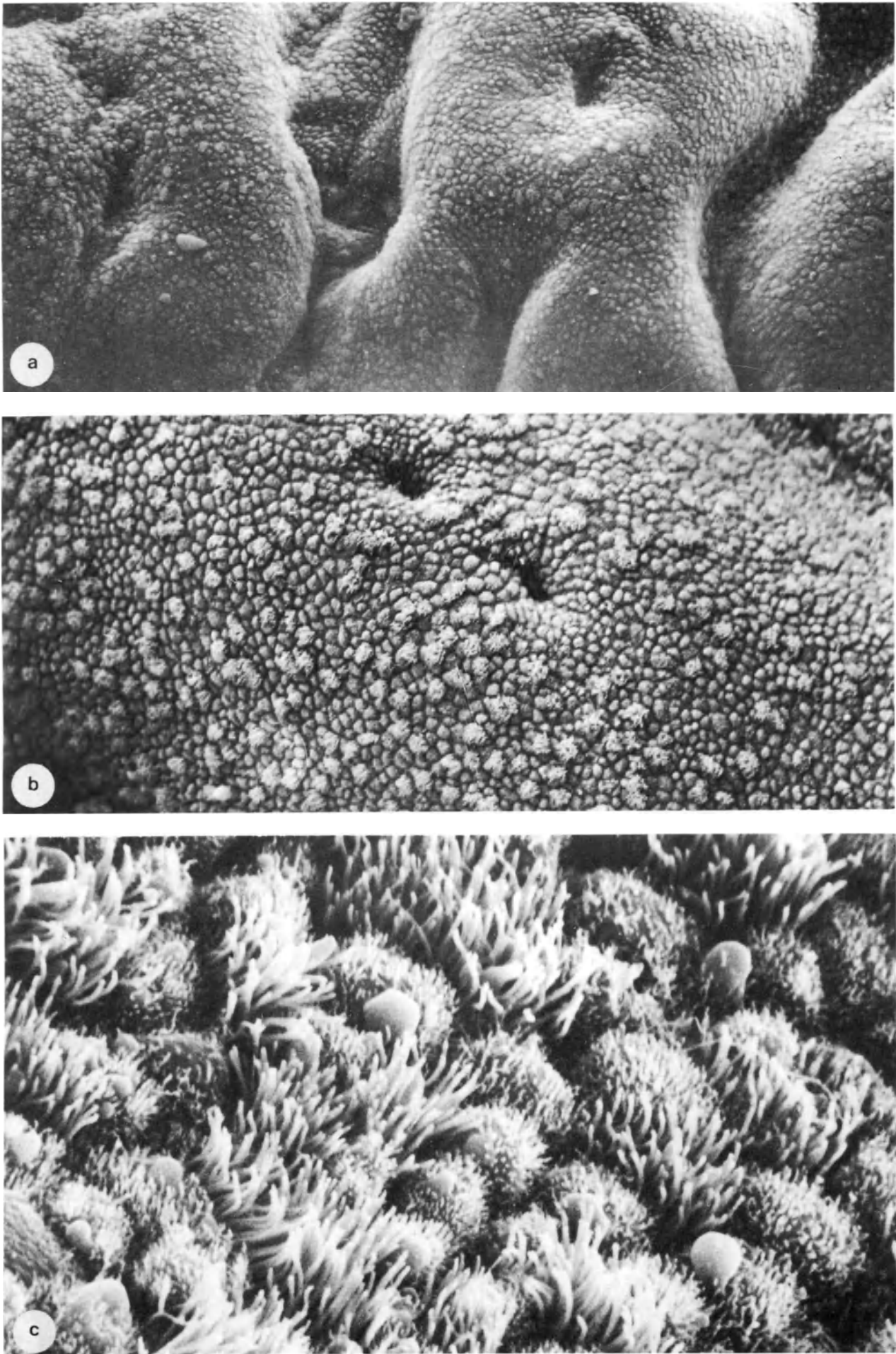
Figure 1

Figure 2 (opposite)

a: Luminal surface of stimulated endometrium, day 2 after ovulation. The differences in surface area among the non-ciliated cells are demonstrated. A few ciliated cells are observed ($\times 4000$)

b: Luminal surface of unstimulated endometrium, day 7 after ovulation. Several ciliated cells are noticed among the non-ciliated cells. No apical protrusions are present on the non-ciliated cells ($\times 3000$)

c: Luminal surface of unstimulated endometrium, day 7 after ovulation (same specimen as in Figure 2b). Few ciliated cells are observed in this area of the biopsy. Further, a clear borderline is noticed between non-ciliated cells without apical protrusions (right) and non-ciliated cells with apical protrusions (left) ($\times 3000$)
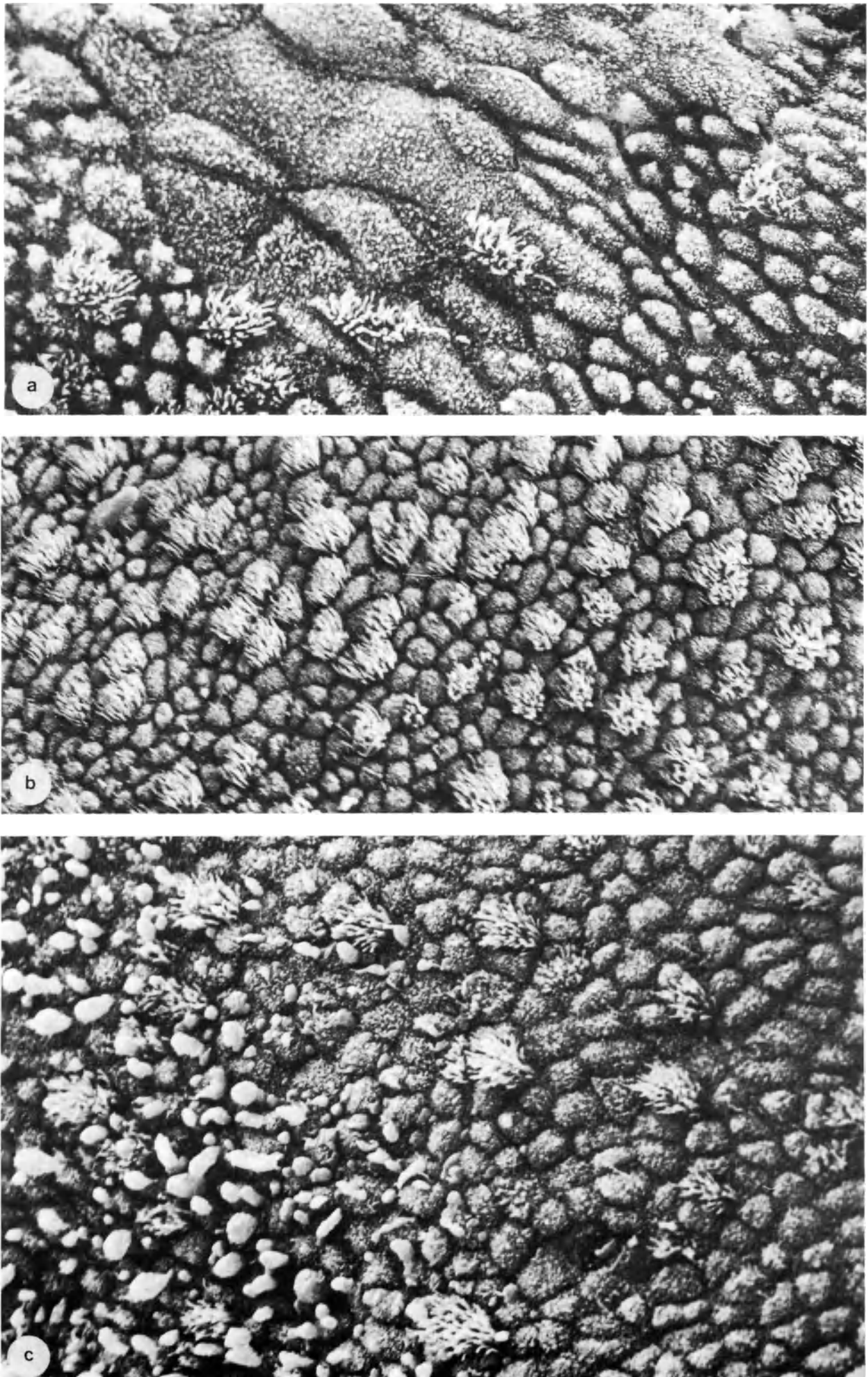
Figure 2

Figure 3 (opposite)

a: Apical protrusions of unstimulated endometrium, day 7 after ovulation (same specimen as in Figures 2b and c). The protrusions have a smooth or slightly wrinkled surface (×9000)

b: Apical protrusion of unstimulated endometrium, day 1 after ovulation. The protrusion has a granulated, wrinkled surface (×17 000)

c: Apical protrusions of unstimulated endometrium, day 6 after ovulation. Rather small protrusions are located in the middle of the cells (×30 000)
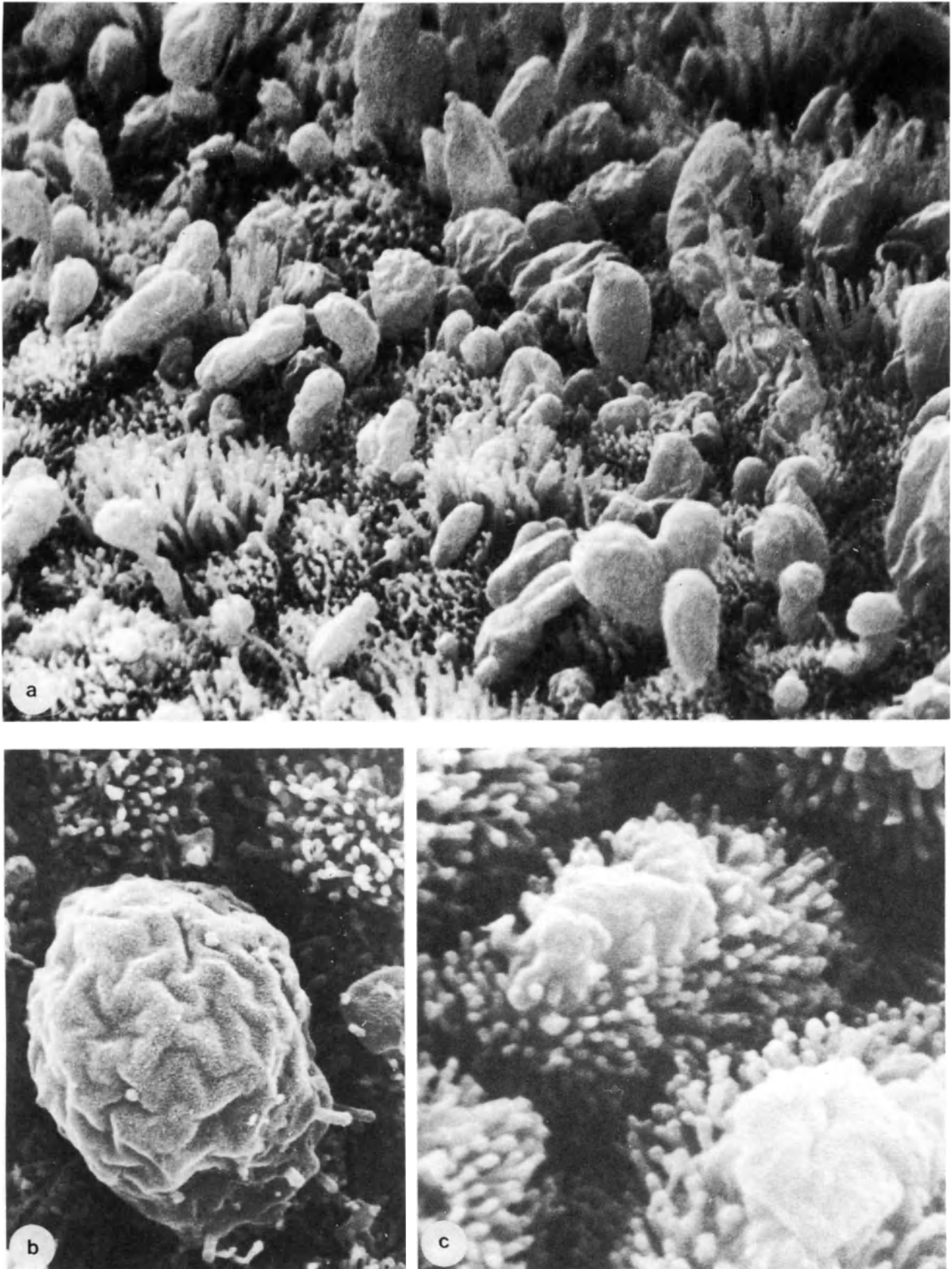
Figure 3

Figure 4 (opposite)
a: Non-ciliated cells of stimulated endometrium, day 7 after ovulation. The microvilli are short (×30 000)
b: Non-ciliated cells of stimulated endometrium, day 7 after ovulation (same specimen as in Figure 4a). The microvilli are long (×30 000)
c: Artifactual structure of kinocilia. The cilia are clumped together and not lying freely. This is probably caused by a slight drying of the specimen during the dehydration (×8000)
d: Artifactual structure of microvilli. The tips of the microvilli are swollen due to fixation in a hypotonic solution (×20 000)
e: Artifactual structure of the ends of the cilia and microvilli which have a brush-like appearance. The cause of this change is unknown (×30 000)
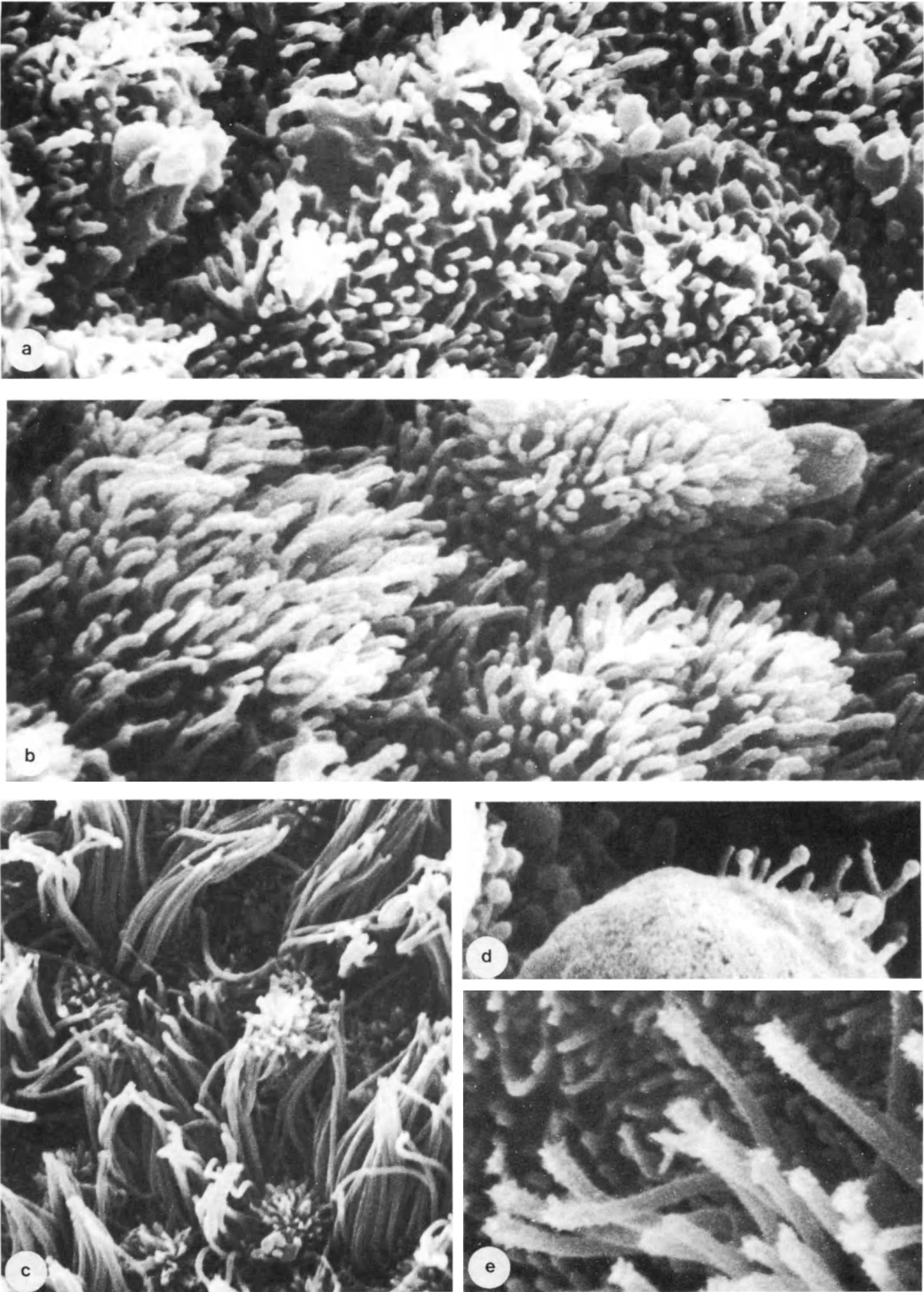
Figure 4

9

Endometrial tumors

F. STENBÄCK*, M. OSHIMA†, K. IDA†, H. OKAMURA‡ and A. KAUPPILA§

* Department of Pathology, University of Oulu Medical School, Oulu, Finland
† Department of Obstetrics and Gynecology, Shiga University of Medical Sciences, Shiga, Japan
‡ Department of Obstetrics and Gynecology, Kyoto University Medical School, Kyoto, Japan
§ Department of Obstetrics and Gynecology, University of Oulu Medical School, Oulu, Finland

SEM analysis of the endometrial surface shows relatively constant cyclical morphological features similar to those demonstrated by conventional histopathological methods and transmission electron microscopy (Nilsson, 1962; Wynn and Harris, 1967; Wynn and Woolley, 1967; Blaustein, 1977). The surface epithelium, however, differs morphologically from its glandular counterpart as the uterine lining has a different sensitivity to cyclic hormonal stimuli than does the glandular epithelium (Hafez et al., 1975, 1978; Ferenczy, 1976a, 1976b). These changes bear a close resemblance to the changes noted in tubal epithelium (Ludvig et al., 1972; Ferenczy, 1974) and are most likely related to similar cellular functions, such as mobilization and reception of the sperm and the blastocyst.

The endometrial lining is not only sensitive to hormonal stimuli, it also reflects stromal alterations, polyps and leiomyomas, as well as inflammatory changes and necrosis. Malignant transformation of the epithelial lining is also reflected in alterations in cell size and structure as well as number and size of specialized surface structures (Ferenczy, 1974; Stenbäck et al., 1980). The different types of lesions are summarized in Table 1.

NORMAL ENDOMETRIUM

Endometrial surface cells (Figure 1a) are cuboidal or columnar ciliated or microvillous cells as well as secretory cells. The basalis-type or proliferative cell has a high nucleus-to-cytoplasm ratio, a scanty cytoplasm and prominent surface microvilli in the proliferative phase compared to the low epithelium in senile atrophy (Figures 2a,b). The number of microvilli varies in relation to normal cycle (Figures 3a-c). The ciliated cells are variants of the proliferative cell, more prominent near the isthmus region (Figures 3d,e). These cells have a distinctive round nucleus with fine chromatine and prominent surface cilia.

Initially the terminal surface of the cell is concave but during continued development it becomes convex, and ultimately the cilia may pinch off. Secretory cells are of three types: vacuolated and non-vacuolated, as well as tubal. The vacuolated secretory cell contains a clear round vacuole in either a subnuclear or a supranuclear position. The non-vacuolated secretory cell has a uniform eosinophilic cytoplasm and often a frayed luminal border. The third type resembles the secretory cell of the fallopian tube and is more common on the surface than in the glandular portion. This cell has a elongate nucleus, moderate eosinophilic cytoplasm and a rounded luminal bleb. The structure and degree of development is associated with cell location, external or glandular surface, hormonal status of the patient; premenarche or postmenopause, stage of hormonal cycle, as well as abnormal conditions, whether hormonal unbalance, inflammation, degenerative or neoplastic conditions.

Table 1 Types of endometrial changes observable by SEM

1. Normal endometrium
     cell types

2. Cyclic endometrium
     proliferative phase
     secretory phase

3. Abnormal hormonal patterns
     atrophy
     hyperplasia
     iatrogenic effects

4. Inflammation, necrosis

5. Benign tumors and tumor-like lesions
     endometrial polyps
     uterine leiomyoma

6. Malignant tumors, adenocarcinoma
     tumor types
     tumor differentiation
     effect of treatment
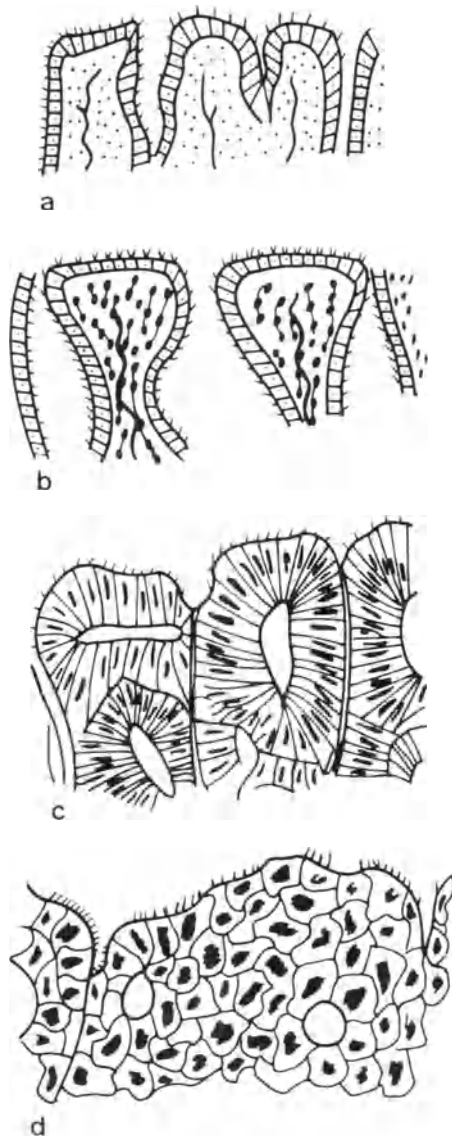
Figure 1 Line drawing of human endometrium: low magnification
a: Normal proliferative stage
b: Hyperplastic endometrium
c: Adenomatous hyperplasia
d: Endometrial adenocarcinoma
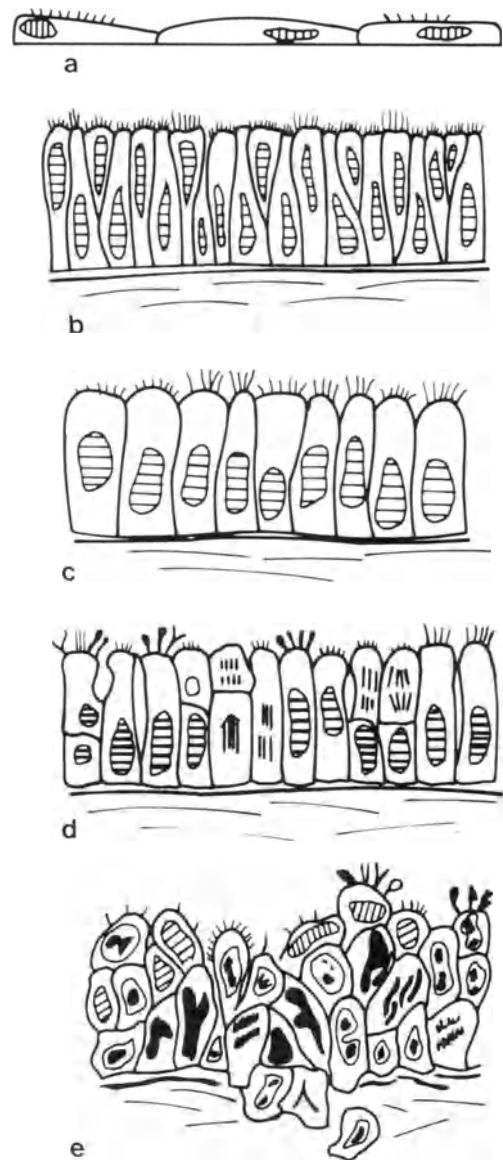
Figure 2 Line drawing of human endometrium: high magnification
a: Atrophy
b: Proliferative stage
c: Adenomatous hyperplasia
d: Atypical adenomatous hyperplasia
e: Adenocarcinoma with invasion

Figure 3 (opposite) Cyclical changes in human endometrium
a: Early proliferative phase: cells are semispherically protruded with fine and short microvilli (×10 000)
b: Late proliferative phase: cells are fully expanded with overcrowded microvilli (×10 000)
c: Late proliferative phase: microvilli are variable length and may resemble drumsticks (×20 000)
d: Apocrine secretion of the mid-secretory phase with prominent ciliated cells (d ×4500; e ×9000)
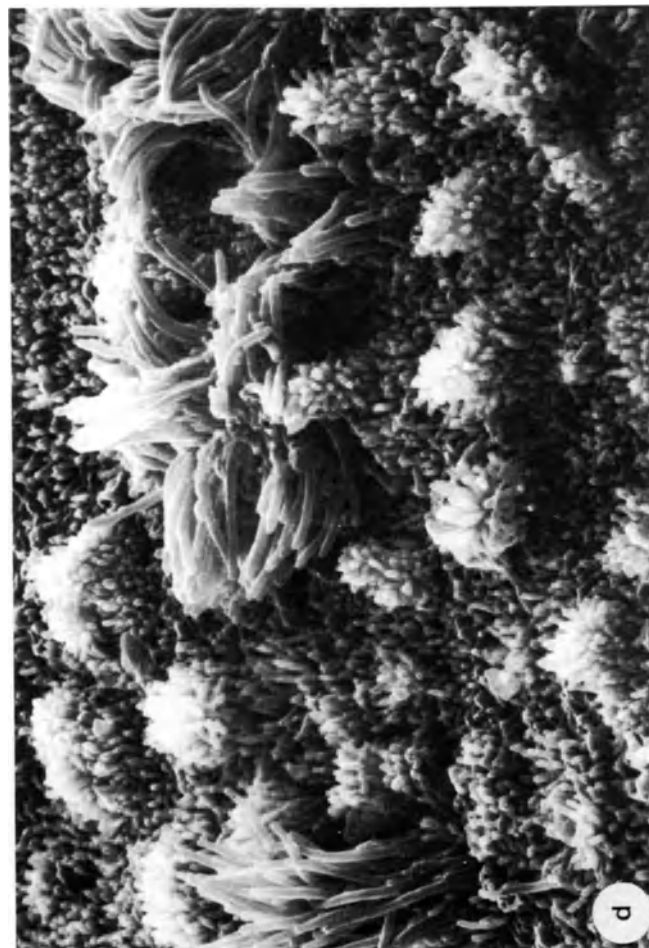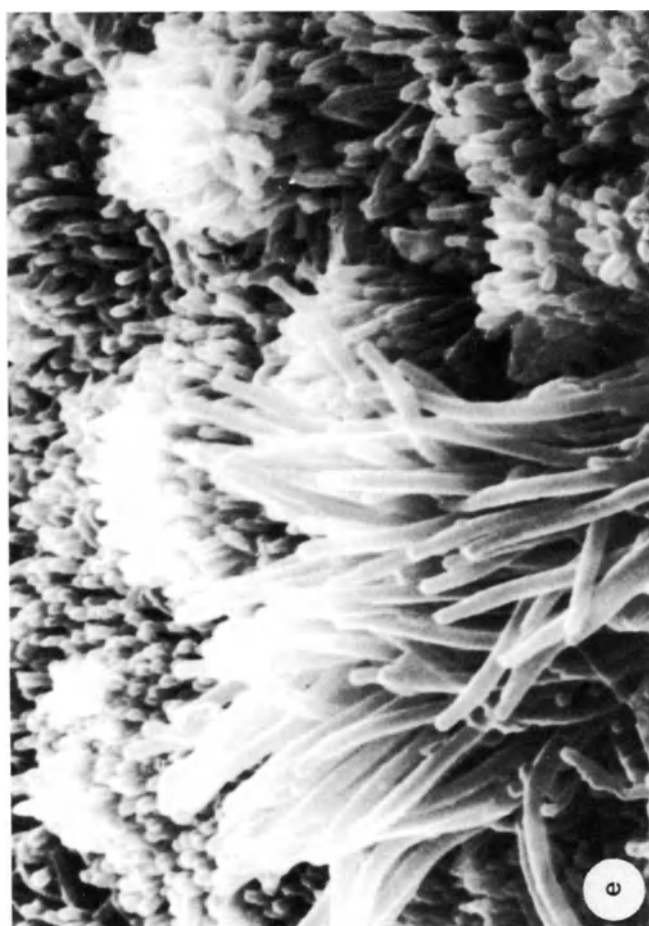
Figure 3

CYCLIC CHANGES

Morphological analysis of surface structures developing during the normal hormonal cycle is affected by cell location the changes being less prominent in the isthmus region.

The early proliferative phase (Figure 3a) is characterized by straight glands covered by microvillous cells. In high magnification SEM analysis of early proliferative endometrium shows evenly distributed cuboidal or columnar cells with small microvilli (Figure 3a). Ciliated cells are found primarily around glandular openings. During continued estrogen stimulation the cells gradually expand, the microvilli increasing in number and length (Figure 3b). In the mid-proliferative phase single ciliated cells are seen on the interglandular surface with the dome-shaped ciliated cells covered by abundant microvillous projections. In the late proliferative phase numerous microvilli, some resembling drumsticks, are seen. The cilia vary in size and shape, representing various stages of ciliary differentiation (Figure 3c).

During the secretory phase, the number and the size of microvillous cells is greater than in the early mid-proliferative phases, most of the increase apparently having taken place during the late proliferative phase (Figure 3d). The increase also occurs in both number and size of ciliated cells (Figures 3d,e). In addition to cells with well-developed cilia, large randomly distributed groups of well-preserved non-ciliated cells with umbilical apical plasma membranes and short microvilli, were seen (Figure 4a). The type of secretion, apocrine and microapocrine is also shown (Figures 4b-e). The surface structure is summarized in Figures 5b,c.

The normal hormonal cycle which depends on estrogenic and progesteronic influences is associated with surface ciliogenesis and growth of microvilli, since a marked decrease in or absence of hormonal activity leads to loss of cellular specialization (Johannissen and Nilsson, 1972; Ferenczy and Richart, 1973; Ferenczy, 1977a, 1977b). The reactivity of the surface structures to estrogens, notably 17β-estradiol, is further emphasized by the decrease in number and size of cilia and microvilli in atrophic endometrium. Higher levels of 17β-estradiol binding and uptake have been shown to coincide with endometrial hyperplasia (Evans et al., 1974). This is reflected in ciliary proliferation and formation of microvilli, indicating a direct correlation between hormone level and surface structures. Also hormonal activity is reflected by the concentration of ciliated cells wound the gland orifices, the comparative decrease in the length of the microvilli and peak of secretory activity is seen in the mid-luteal phase (Ferenczy et al., 1972; Hafez, 1972; Nilsson and Nygren, 1972; Ludvig et al., 1976; Ludvig and Metzger, 1976).

Non-cyclical and abnormal hormonal patterns

Surface cells are sensitive indicators of hormonal activity, showing lack of stimulation as atrophy and excessive hormonal production as hyperplasia. The surface structure as summarized in Figure 5 depends upon physiological conditions of the endometrium as well as on diseased states i.e. inflammation and regeneration. In senile endometrium the cell population is arranged in a cobblestone pattern and the gland openings are wide (Figure 6b). The cells are small (Figure 6b) and slightly irregular outlines (Figure 6c). The cilia are nonexistent, the microvilli are short and thin (Figures 6d, 7c,d), and slightly irregular in structure (Figure 6e). Surface structure in necrosis (Figure 7a) is sometimes similar with lack of microvilli; the lesions are, however, irregular, varying from one area to another.

In endometrial hyperplasia (Figures 1b, 5e and 7b), when compared to atrophy (Figures 7c,d) and to hormone-dependent cells previously described, the difference in size, as well as number, of cilia and microvilli is obvious. Specimens with cystic hyperplasia possess a considerable number of ciliated cells covering large fields. The average size of microvillous cells is increased, as well as the number and size of microvilli; the cilia are also prominent. The endometrial surface appears flattened, occasionally undulating with numerous gland openings.

Endometrial hyperplasia as studied by histopathological methods (Welch and Scully, 1977), encompasses a wide variety of patterns of epithelial and stromal proliferation characterized by a varying biological behavior and an increased incidence of malignant transformation (Vellios, 1972). The significance of the morphological alterations usually associated with adenomatous hyperplasia, and the relationship to subsequent carcinoma, have been disputed (Welsh and Scully, 1977). As shown by SEM studies (Stenbäck et al., 1980), adenomatous hyperplasia differs considerably in surface structure from its cystic, less proliferating, histologically benign counterpart only when associated with histologically detectable atypical features. Microvillous projections generally are numerous and large; an increase was also seen in ciliar size and in number of cilia per cell. The results indicated a close association with a gradual transition from one stage to another between cystic hyperplasia and adenomatous hyperplasia (Vellios, 1972).

INFLAMMATION

Normal menstrual endometrium and focal regions of the decidua of pregnancy normally exhibit acute necrosis and inflammation (Ludwig and Metzger, 1976). Endometritis denotes pathological endometrial infiltration by inflammatory cells (Hendrickson and Kempson, 1980). In addition to bacteria, ascending organisms – from the fallopian tube or hematogenously and established foreign bodies (i.e. IUDs)may cause inflammatory surface changes (Ludwig et al., 1976). In

Figure 4 (opposite)   Human endometrium during secretory phase
a: Apocrine and micro-apocrine secretion (×10 000)
b: Apocrine secretion (×20 000)
c: Micro-apocrine secretion: arbor-like microvilli (×10 000)
d: Apocrine secretion (×10 000)
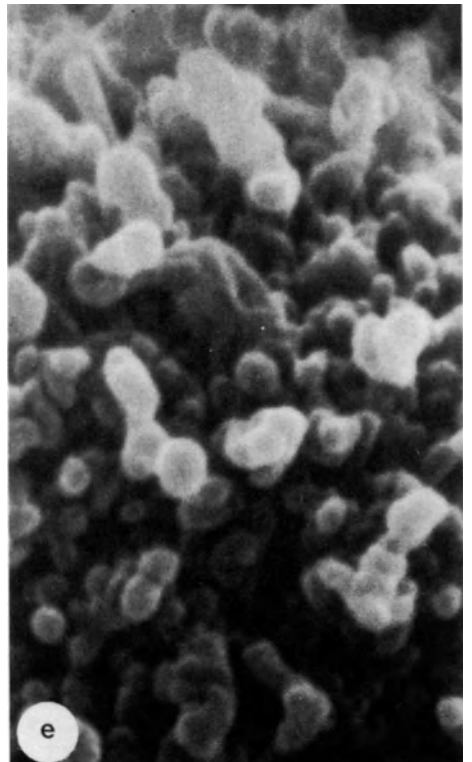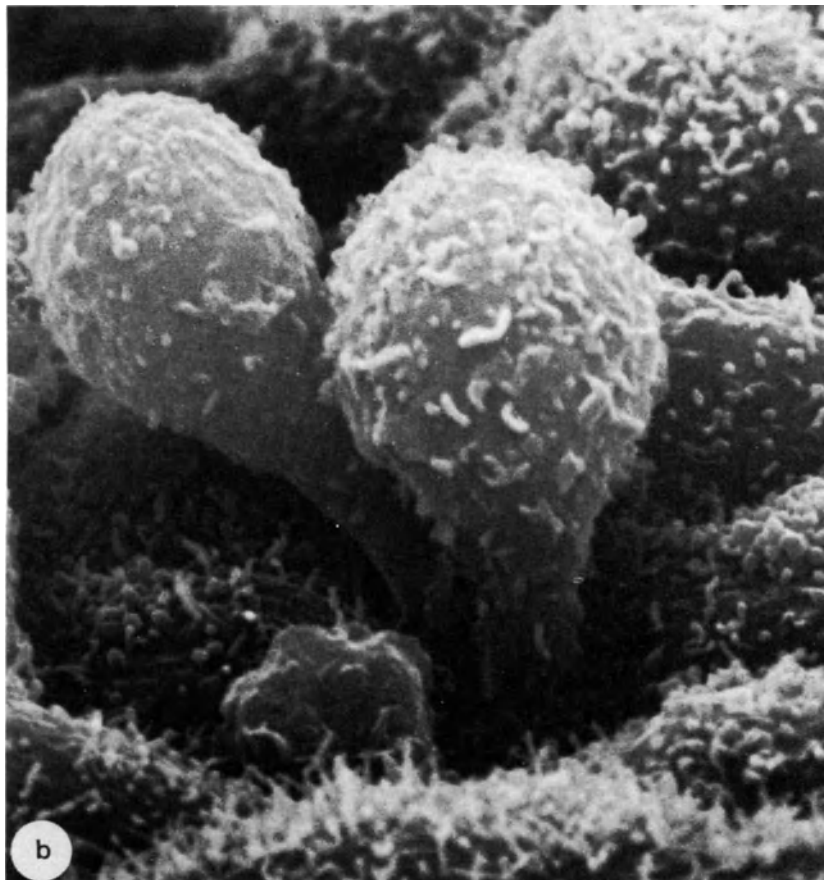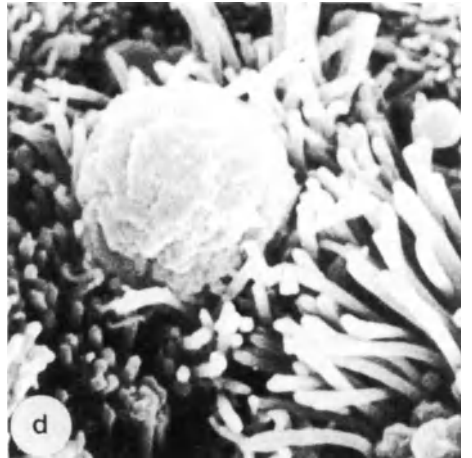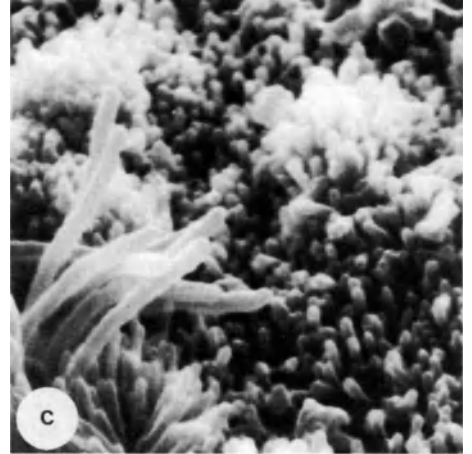e: Micro-apocrine secretion (×30 000)

Figure 4

SEM the surface cells are mostly well developed and uniform with prominent surface structures (Figures 5d and 8a), slightly protruding (Figures 8b,c). The microvilli are uniform and prominent (Figure 8d).

BENIGN TUMORS

In addition to endometrial epithelial lesions, mixed glandular and stromal lesions such as polyps, and stromal tumors such as myomas, also reveal surface abnormalities (Richart and Ferenczy, 1974). Endometrial polyps are the result of focal endometrial and stromal overgrowth, their neoplastic nature is questionable (Hendrickson and Kempson, 1980). Leiomyomas are benign smooth muscle tumors and the most frequent neoplasm to develop in the uterus. The surface abnormalities associated with this condition are occasionally similar to polyps (Figures 9a,b). Lack of development of specialized surface structures is common in myomas, particularly when in the submucous position (Figure 9c). Polyps commonly have prominent surface cells (Figure 9d), swollen intercellular parts (Figure 9e) and pinhead-like microvilli (Figure 9f).

The interrelationship of submucus myomas and polyps is depicted in Figure 10. Myoma knots are of three types. Slightly-protruded myoma knots (Figure 10a) have cellular surfaces slightly smaller than those of the normal endometrium. Their central protrusions are surrounded by flat peripheral portions of free cellular surface. Semi-spherically protruded myoma knots (Figure 10b) have an endometrial surface with severe atrophic changes. The cellular arrangement is irregular. Polyp-like myoma knots (Figure 10c) show the most severe atrophy. Free surfaces protrude slightly in the shape of triangular or hexangular prisms. Microvilli are pinhead-like and cilia needle-like. Their numbers are reduced. When compared to uterine smooth muscle leiomyomas endometrial polyps show smooth free cell surfaces quite wide, and they have a polygonal shape defined by the swollen intercellular parts which seem to be terminal bars. Microvilli are similar to pinheads.

MALIGNANT ENDOMETRIAL TUMORS

Precursors of endometrial carcinomas are morphologically indistinct, though clinically significant. Surface analysis of atypical adenomatous hyperplasia (Figure 1c) shows an undulating surface with irregular development of specialized structures (Figure 2d, compared to simple adenomatous hyperplasia (Figure 2c). Some areas have short microvilli and cilia. The average, however, is that of an exaggerated number of large microvilli and cilia. Histological analysis reveals a correlation to morphology with atypical glandular arrangements in denuded areas and hyperplastic glands in areas with well-developed cilia and microvilli (Figure 11a).

Surface analysis of well-differentiated adenocarcinoma (grade I) (Figures 1d and 2e), under low power, shows cells of variable form and size (Figure 11b), considerably smaller than those previously described (Figure 2). The surface is irregularly undulating with cellular projections of varying appearance. The cilia are also affected; the microvilli size and number are virtually unchanged. The structural alterations as revealed by TEM consisted of branching, club formation, ballooning and different degrees of destruction.

With decreasing histological differentiation of endometrial adenocarcinomas (grade II), the alterations in surface structure, including the size and shape of microvilli and cilia, become more evident (Figure 1k). Surface plasma membranes are often wrinkled or ruptured and microvilli were short and disorganized. Occasionally areas completely devoid of surface structures, either microvilli or cilia, occur and microvilli vary greatly in size and shape, not only from cell to cell but also within an individual cell. Some cells show denuded areas partly devoid of surface structures (Figure 11d). Some appear stubby or clubbed; others branched.

In well-differentiated adenocarcinomas the surface structures, cilia and microvilli, are frequently well preserved when compared to normal endometrium (White and Buchsbaum, 1973, 1974). Morphological alterations, club-shaped and branched microvilli, are seen, as noted in normal endometrium (Hando et al., 1978), contrary to reports by Ferenczy (1977b). The well-differentiated cancers deviate occasionally and only minimally from normal cells of origin, whereas cells or poorly differentiated lesions have correspondingly greater differences from normal endometrium.

Tumor types

In addition to degree of differentiation, endometrial adenocarcinomas can be divided into three main types depending upon gross growth pattern (Figure 12), namely tubular, adenomatous and papillary types.

The tubular type (Figure 13) shows infundibular recesses, transformed into deep pits. Cancer cells, much larger than those found in hyperplasia, are distended into spindle, semi-oval or cylindrical shapes. The overall cellular arrangement is quite irregular. Surface structures are undeveloped with sparse and small microvilli (Figures 13c,d). In the papillary type (Figure 13) glandular openings are inconspicuous (Figure 14a). At gland openings arborescent masses of cells protrude into the uterine cavity (Figures 14b,c). Microvilli on free surfaces are sparse and spot-like. In most cases rough and irregular tissue is observed among necrotic tissue when the covering endometrium has fallen off. In the adenomatous type (Figure 13) the gland openings are densely distributed (Figure 14d). The gland openings are elevated like a bank, surrounded by 6–10 cells (Figure 14e). Atrophy inflammation and/or

---

Figure 5 (opposite) Line drawing of human endometrial cells
a: Regeneration
b: Late proliferative phase
c: Mid-secretory phase
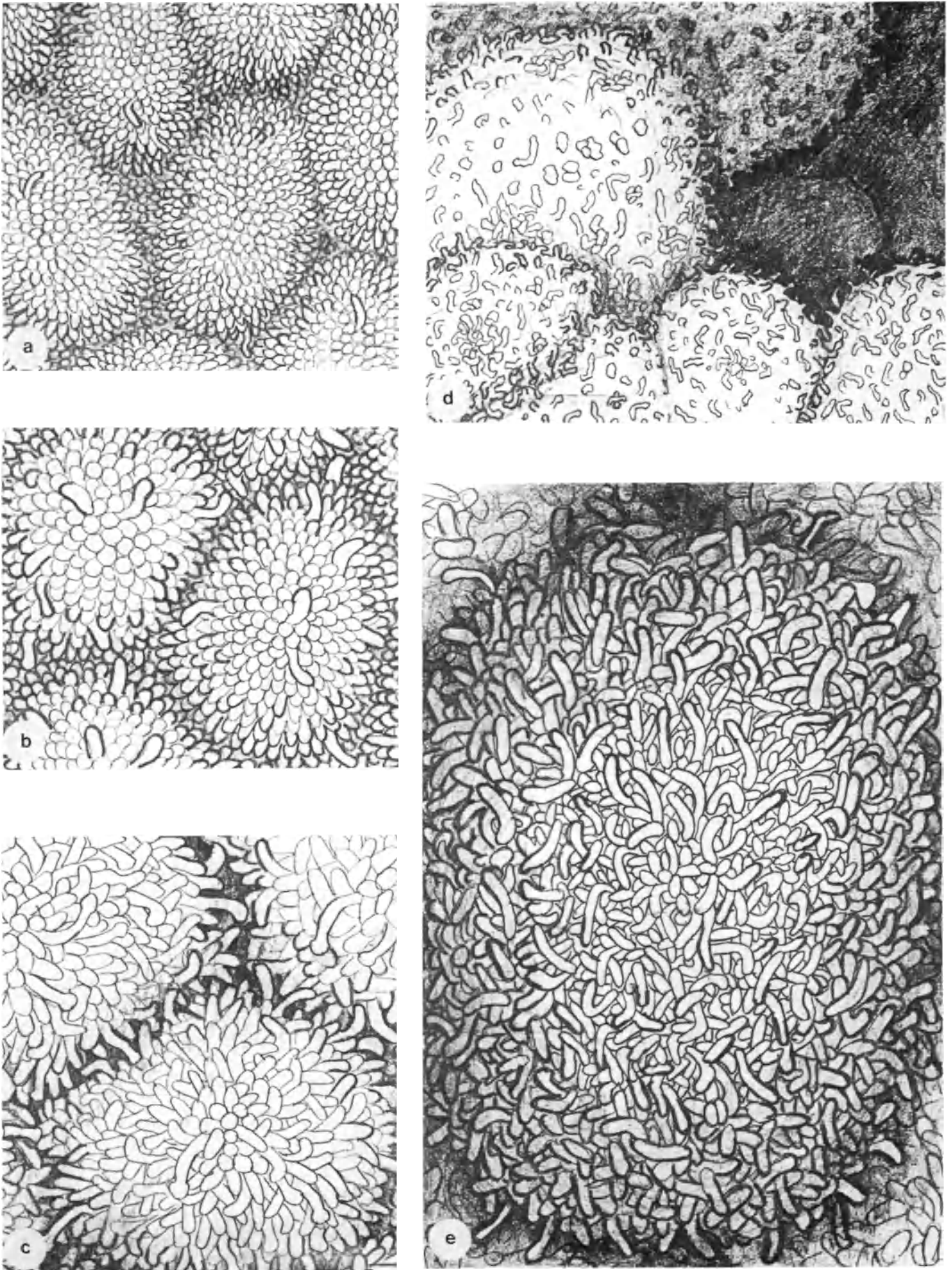d: Inflammation
e: Hyperplasia; cells doubled in size

Figure 5

necrosis is also observed in mixed forms with varying intensities on cancer cell surfaces.

The relationship between tumor type as shown have and clinical behavior is not yet settled. Clinical differential diagnosis from benign polyps occasionally poses problems, and the differences are distinct in SEM. Fewer than 1% of adenocarcinomas derive from polyps (Blaustein, 1977). Papillary tumors frequently resemble serous cystadenocarcinoma of the ovary (Blaustein, 1977). The relationship to atypical hyperplasia is most obvious again in the adenomatous type.

Effect of treatment

The use of cytostatic and hormonally active agents, as well as X-irradiation therapy, is extensive, in addition to surgery, in treatment of endometrial adeno-carcinomas (Kauppila and Kiviniitty, 1980; Kauppila et al., 1980). Irradiation of adenocarcinoma causes the appearance of large areas devoid of specific structural features (Figure 15). The average number and size of microvilli is considerably lower than in untreated ones, though varying from one area to another. The remaining microvilli are small stub-like or single structures (Figure 15). Gestational agents, i.e. medroxyprogesterone, cause some differentiation of surface structures reminiscent of normal endometrium.

Thus SEM studies enable us to verify the extent as well as degree of intensity of action of hormonal and cytostatic agents. Surface analysis shows the conversion of normal cells induced by estrogens and gestagens (Nilsson, 1980; Nilsson et al., 1980; Herbst and Multier-Lajous, 1980) visible also in neoplastic endometria, due to the heterogeneous cellular population varying in sensitivity (Ferenczy, 1980).

Morphological classifications of endometrial alterations, lesions and tumors including adeno-carcinomas are frequently disputed. The problems are partly due to limitations in size of the sample available for conventional histopathological analysis. This influences the analysis of the biological character as different parts of the lesions have different behavior. The morphological appearance, differentiation and maturation has to be taken into account in treatment planning (Dallenbach-Hellenweg, 1975). Studies of the effect of treatment on the extermination of malignancy are also hampered by the difficulties in obtaining samples large enough to reflect the general pattern in a representative fashion, which is easily overcome by SEM analysis. Surface structure studies are also useful in studies on histogenesis and classifi-cation of tumors (Stenbäck and Kauppila, 1980) to further our understanding of the biological behavior of neoplasms.

Ferenczy, A. (1974). The surface ultrastructure of the human Fallopian tube. A comparative morphophysiologic study. In Johari, O. (ed.) Scanning Electron Microscopy on Advances in Biomedical Applications of the SEM, pp. 613–622. (Chicago: IIT Research Institute)

Ferenczy, A. (1976a). Studies on the cytodynamics of human endometrial regeneration. I. Scanning electron microscopy. Am. J. Obstet. Gynecol., 124, 64

Ferenczy, A. (1976b). Studies on the cytodynamics of human endometrial regeneration. II. Transmission electron microscopy and histochemistry. Am. J. Obstet. Gynecol., 124, 582

Ferenczy, A. (1977a). Surface ultrastructural response of the human uterine lining epithelium to hormonal environ-ment. A scanning electron microscopic study. Acta Cytol., 21, 566

Ferenczy, A. (1977b). Ultrastructural pathology of the uterus. in Wynn, R. M. (ed.) Biology of the Uterus, pp. 545–85. (New York: Plenum)

Ferenczy, A. (1980). Morphological effects of- exogenous gestagens on abnormal human endometrium. In Dallenbach-Hellenweg, G. (ed.). Functional Morpho-logical Changes in Female Sex Organs Induced by Exogenous Hormones, pp. 101–110. (New York: Springer)

Ferenczy, A. and Richart, R. M. (1973). Scanning and transmission electron microscopy of the human endometrial surface epithelium. J. Clin. Endocrinol. Metab., 36, 999

Ferenczy, A. and Richart, R. M. (1974). The Female Reproductive System: dynamics of scanning and transmission electron microscopy. (New York: John Wiley & Sons)

Ferenczy, A., Richart, R. M., Agate, F. J. Jr, Purkerson, M. L. and Dempsey, E. W. (1972). Scanning electron microscopy of the human endometrial surface epithelium. Fertil. Steril., 23, 515

Hafez, S. E. (1972). Scanning electron microscopy of female reproductive tract. J. Reprod. Med., 9, 119

Hafez, E. S. E., Barhnart, M. I., Ludwig, H., Lusher, J., Joelson, I., Daniel, J. L., Sherman, A. I., Jordan, J. A., Wolf, H., Stewart, W. C. and Chretien, F. C. (1975). Scanning electron microscopy of human reproductive physiology. Acta Obstet. Gynecol. Scand., Suppl., 40, 1

Hafez, E. S. E., Fadel, H. E., Noonan, S. M., Oshima. M., Okamura, H., Watson, J. H. L., Zaneveld, L. J. D. and Steger, R. W. (1977). Scanning electron microscopy of human female reproductive tract and amniotic fluid cells. Int. J. Fertil., 22, 193

Hafez, E. S. E., Ludwig, H. and Metzger, H. (1975). Human endometrial fluid kinetics as observed by scanning electron microscopy. Am. J. Obstet. Gynecol., 122, 929

Hando, T., Okada, D. M. and Zamboni, L. (1968). Atypical cilia in human endometrium. J. Cell Biol., 39, 475

Hendrickson, M. R. and Kempson, R. L. (1980). Surgical Pathology of the Uterine Corpus. (Philadelphia: W. B. Saunders)

References

Blaustein, A. (1977). Pathology of the Female Genital Tract. (New York: Springer)

Dallenbach-Hellweg, G. (1975). Histopathology of the Endometrium, 2nd edn. (New York: Springer)

Evans, L. H., Martin, J. D. and Hahnel, R. (1974). Estrogen receptor concentration in normal and pathological human uterine tissues. J. Clin. Endocrinol. Metab., 38, 23

Figure 6 (opposite) Senile human endometrium
a: Gland openings (×500)
b: Cells are small and irregular, with little surface protrusions (×6000)
c: Cells show irregular contour (×2800)
d: Sparsely distributed cells with short slender microvilli (×8000)
e: High magnification of irregular surface structures (×28 000)

Figure 6

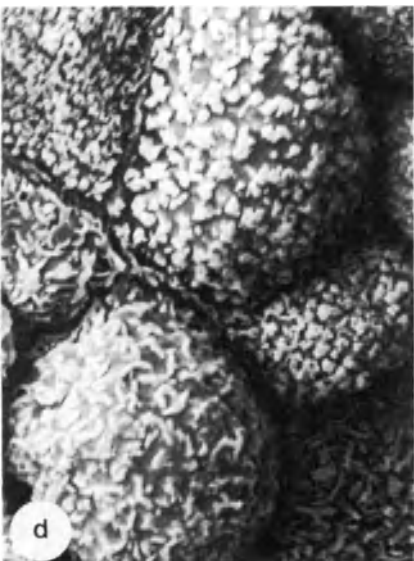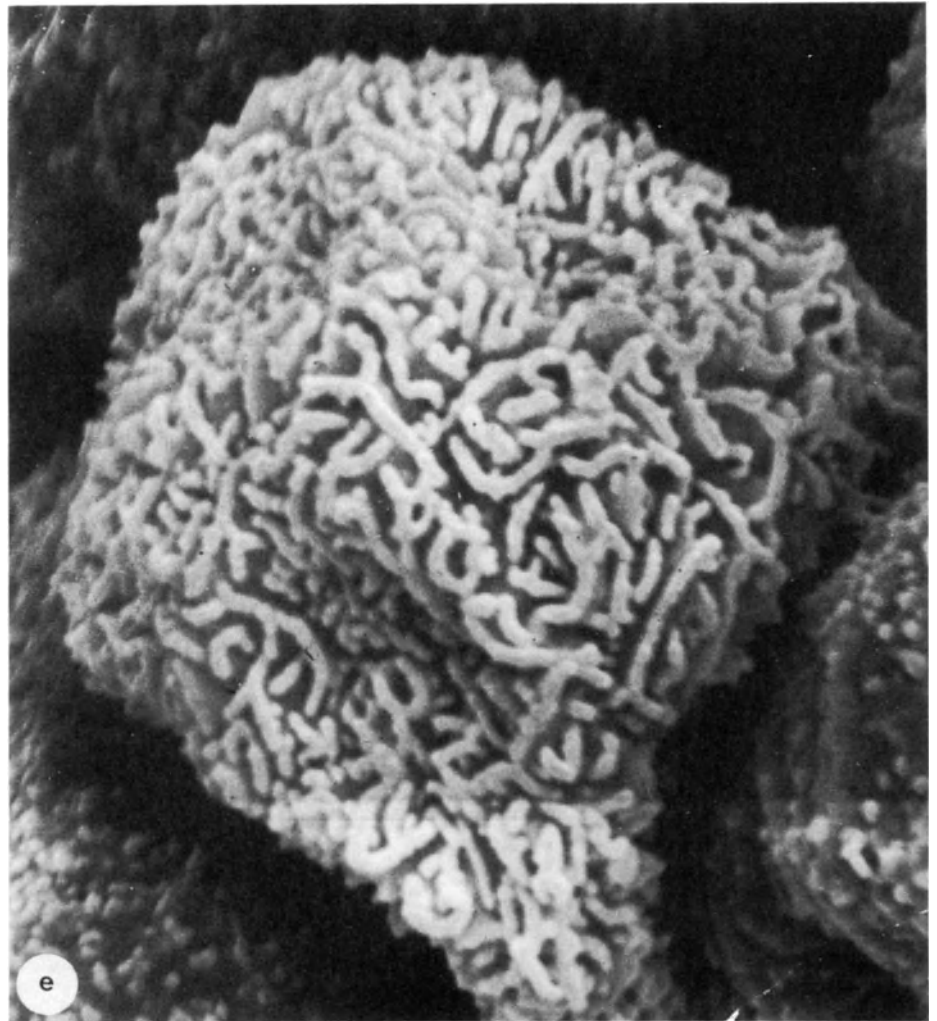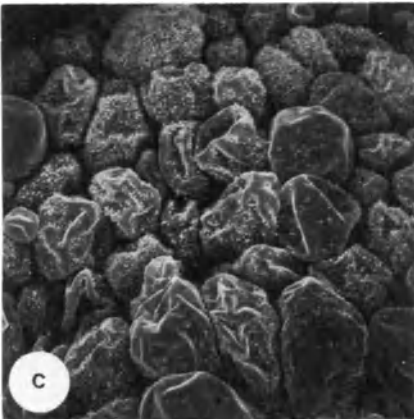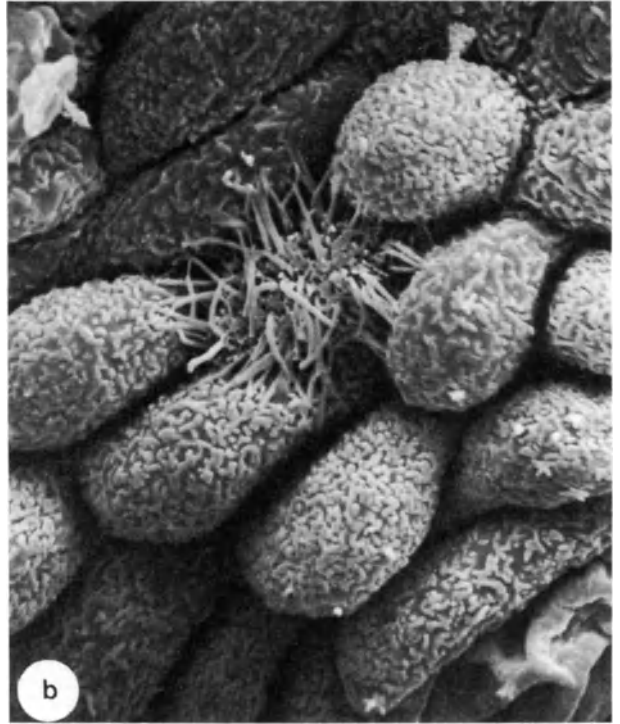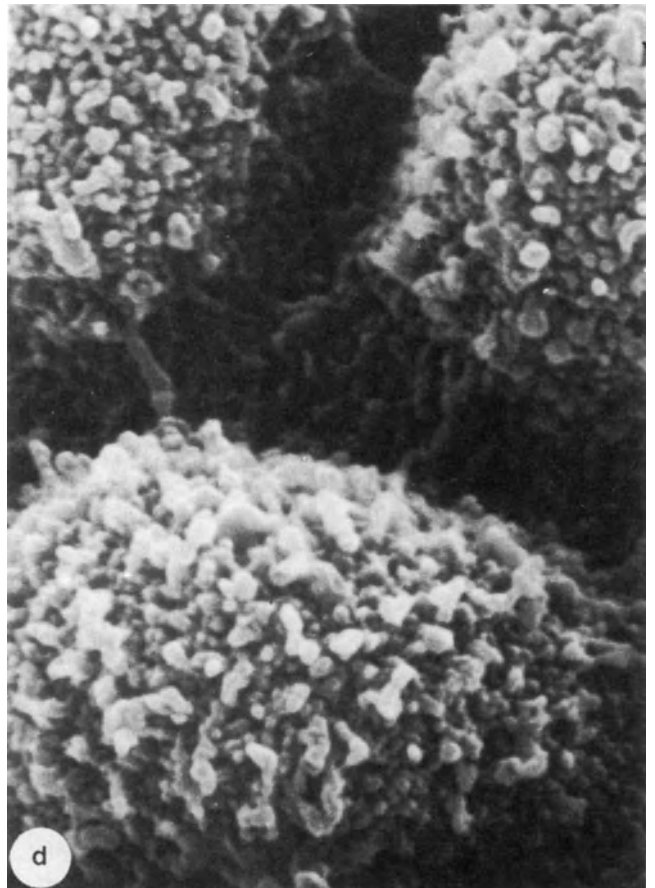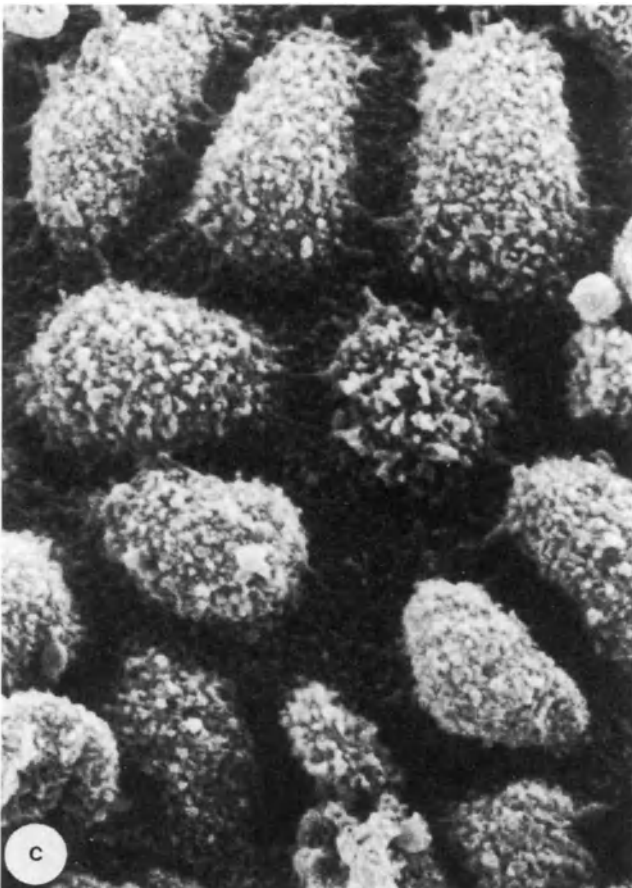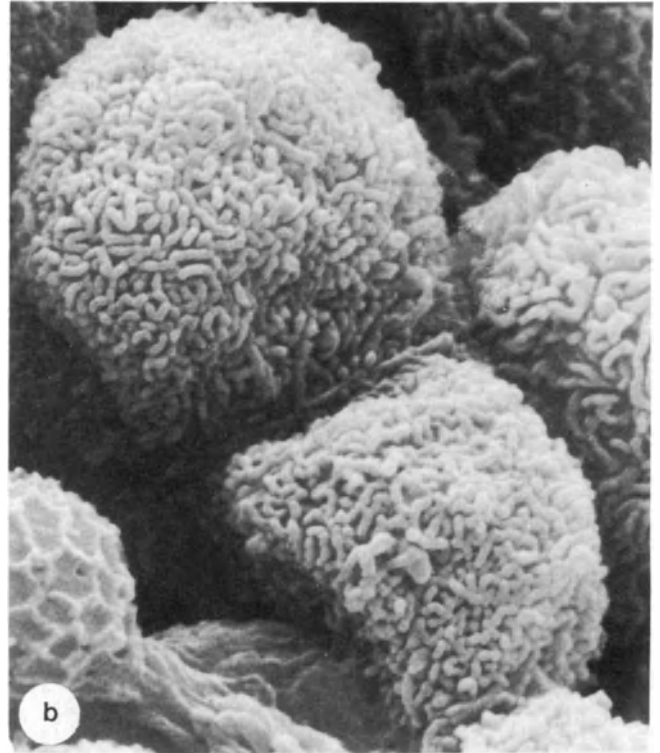**Figure 7**   Human endometrial cells

a: Necrotic cells. Note irregular contour and sparsely short microvilli, sometimes microvilli are absent, cell border is unclear (×6000)

b: Hyperplasia. Size of cells is variable and degree of protrusion is 1.4 times as much as those at proliferative phase. Microvilli are rather slender and densely-packed (×10 000)

c: Atrophic cells. Cells are small but irregular, with few surface protrusions (×7000)

d: Atrophic cells. Microvilli are short, slender and irregular (×20 000)
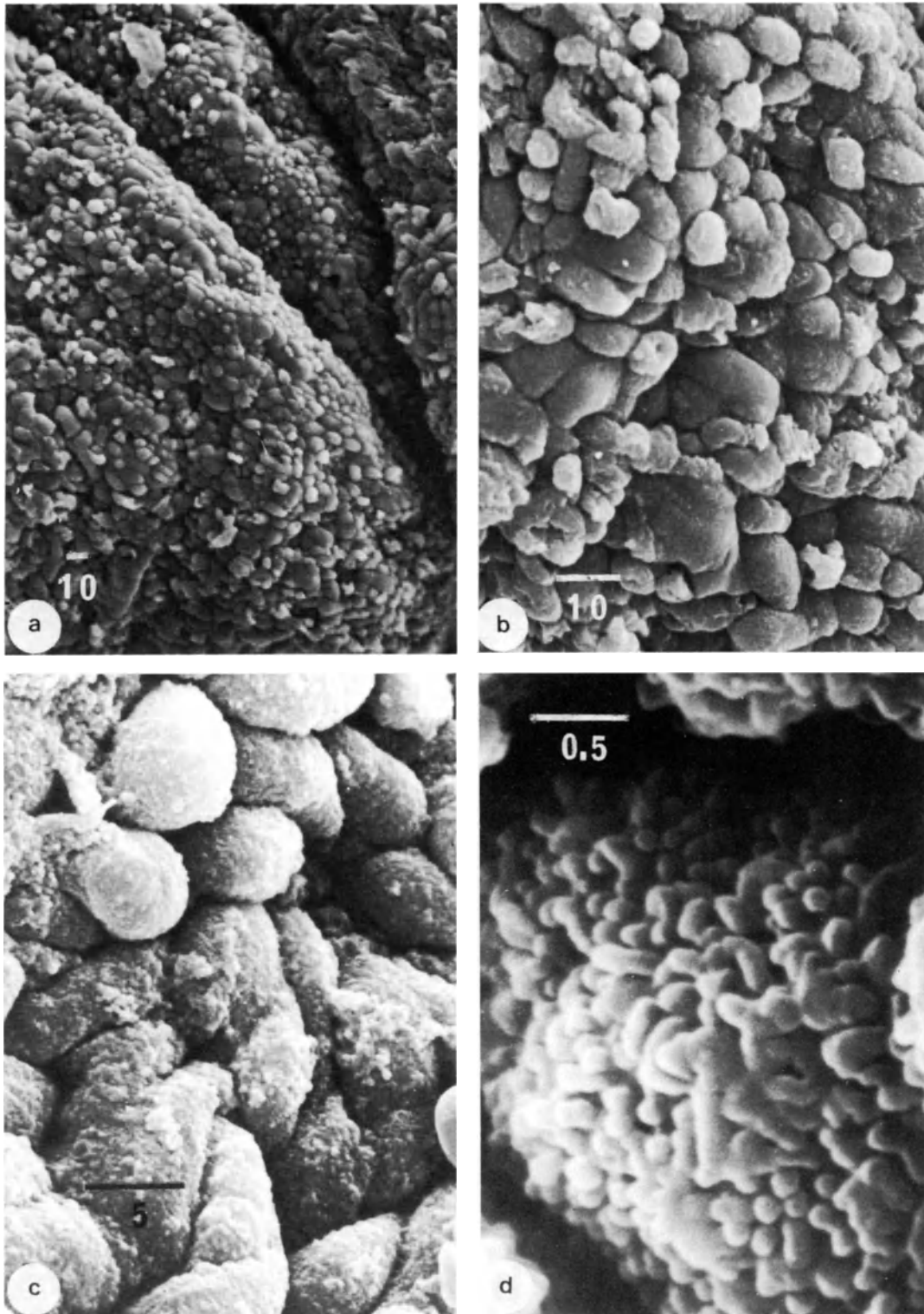
Figure 8 Inflammatory cells in human endometrium. Large, uniform, and fully expanded cells are noted mostly semioval or cylindrical in shape. (a ×1000; b ×2000; c ×5000). Microvilli are uniform and edematous (d ×8000)

Herbst, R. and Multier-Lajous, A.-M. (1980). Effects of hormones on surface structure of human endometrium. In: Dallenbach-Hellenweg, G. (ed.). *Functional Morphological Changes in Female Sex Organs Induced by Exogenous Hormones*, pp. 45–50. (New York: Springer)

Johannisson, E. and Nilsson, L. (1972). Scanning electron microscopic study of the human endometrium. *Fertil. Steril.*, **23**, 613

Kauppila, A., Jänne, O., Kujansuu, E. and Vihko, R. (1980). Treatment of advanced endometrial adenocarcinoma with a combined cytotoxic therapy. Predictive value of cytosol estrogen and progestin receptor levels. *Cancer*, **46**, 2162

Kauppila, A. and Kiviniitty, K. (1980). High dose-rate intracavity irradiation in the treatment of cervical and endometrial carcinomas. Preliminary observations. *Br. J. Radiol.*, Serial Report N17, pp. 59–64

Ludwig, H. and Metzger, H. (1976). The re-epithelialization of endometrium after menstrual desquamation. *Arch. Gynäk*, **221**, 51

Ludwig, H., Metzger, H. and Gallies, R. (1976). The tissue surface of the human endometrium after the insertion of intrauterine contraceptive device (IUD). *SEM Symposium*, **2**, 343

Ludwig, H., Wolf, H. and Metzger, H. (1972). Zur Ultrastruktur der Tubeninnenfläche im Rasterelektronenmikroskop. *Arch. Gynäkol.*, **212**, 380

Nilsson, O. (1962). Electron microscopy of the human endometrial carcinoma. *Cancer Res.*, **22**, 492

Nilsson, B. O. (1980). Scanning electron microscopic responses by the endometrial surface to various estrogens and gestagens. In Dallenbach-Hellenweg, G. (ed.). *Functional Morphological Changes in Female Sex Organs Induced by Exogenous Hormones*, pp. 137–45. (New York: Springer)

Nilsson, O., Englund, D., Weiner, E. and Victor, A. (1980). Endometrial effects of levonorgestrel and estradiol: a scanning electron microscopic study of the luminal epithelium. *Contraception*, **22**, 71

Nilsson, O. and Nygren, K. G. (1972). Scanning electron microscopy of human endometrium. *Uppsala J. Med. Sci.*, **77**, 3

Richart, R. M. and Ferenczy, A. (1974). Endometrial morphologic response to hormonal environment. *Gynecol. Oncol.*, **2**, 180

Stenbäck, F. and Kauppila, A. (1980). Endometrioid ovarian tumors: Morphology and relation to other endometrial conditions. *Gynecol. Obstet. Invest.* **12**, 80

Stenbäck, F., Väänänen, R. and Kauppila, A. (1980). Surface ultrastructure of human endometrium. Effect of hormonal status and neoplastic progression. *Eur. J. Obstet. Gynecol. Reprod. Biol.*, **11**, 69

Vellios, F. (1972). Endometrial hyperplasias, precursors of endometrial carcinoma. In Sommers, S. C. (ed.). *Pathology Annual*, pp. 201–29. (New York: Appleton-Century-Crofts)

Welch, W. R. and Scully, R. E. (1977). Precancerous lesions of the endometrium. *Human Pathol.*, **8**, 503

White, A. J. and Buchsbaum, H. J. (1973). Scanning electron microscopy of the human endometrium. I. Normal. *Gynecol. Oncol.*, **1**, 330

White, A. J. and Buchsbaum, H. J. (1974). Scanning electron microscopy of the human endometrium. II. Hyperplasia and adenocarcinoma. *Gynecol. Oncol.*, **2**, 1

Wynn, R. M. and Harris, J. A. (1967). Ultrastructural cyclic changes in the human endometrium. I. Normal pre-ovulatory phase. *Fertil. Steril.*, **18**, 632

Wynn, R. M. and Woolley, R. S. (1967). Ultrastructural cyclic changes in the human endometrium. II. Normal postovulatory phase. *Fertil. Steril.*, **18**, 721

Figure 9 Human endometrial polyps

a: Polyp-like myoma knot with atrophic appearance. Slightly elevated cell surface with angular cells in a cobblestone arrangement (×2000)

b: Polyp-like myoma knot with microvilli resembling pinheads and reduced number of microvilli (×1000)

c: Semispherically protruded myoma knots. Cells are flat and large, and show severe atrophic changes (×10 000)

d–f: Endometrial polyp. Cells are quite wide and smooth, having polygonal shape defined by swollen intercellular parts which may represent terminal bars. Microvilli are similar to pinheads (d ×300; e ×1000; f ×10 000)
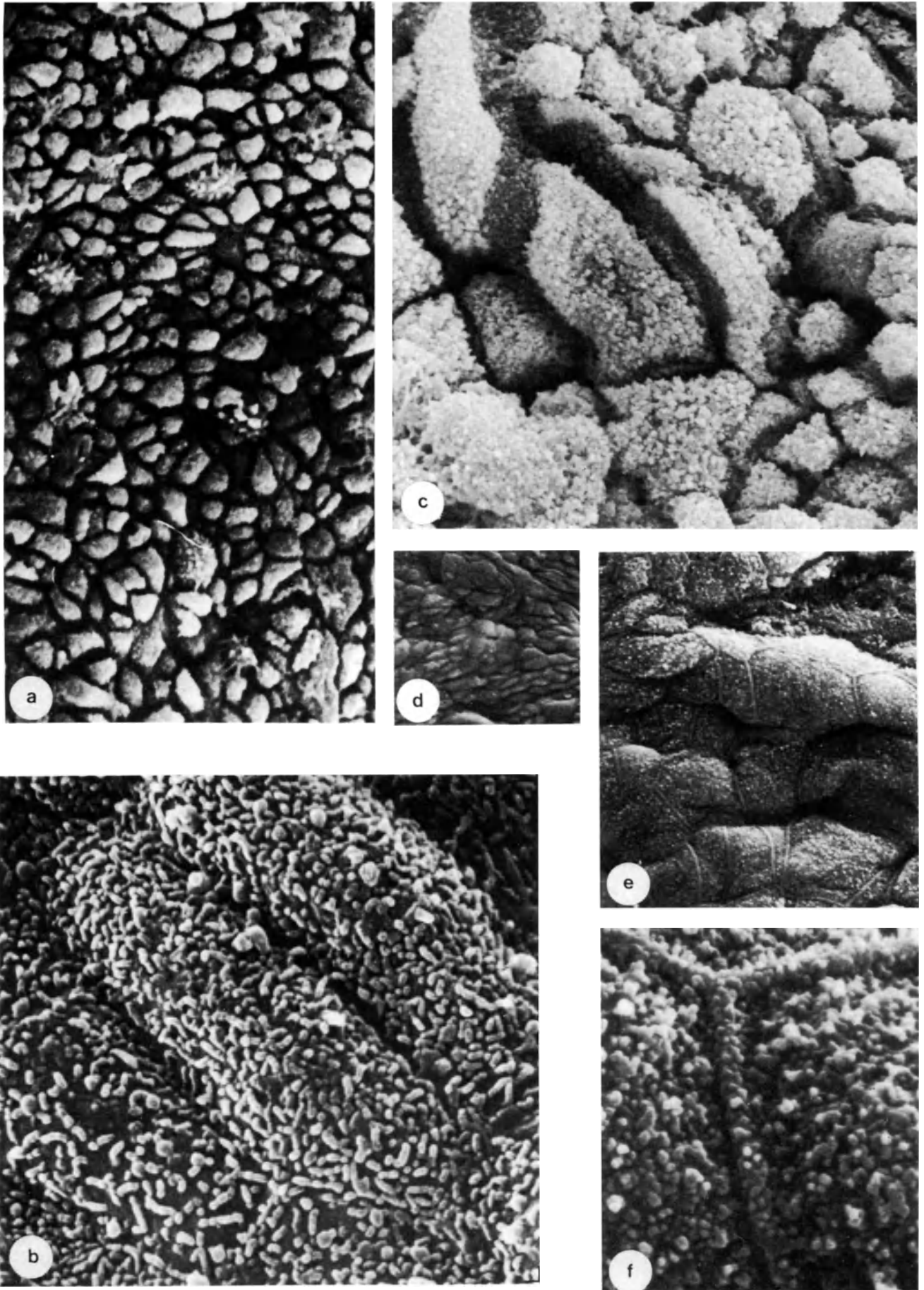
Figure 9

Figure 10 (opposite) Line drawing showing submucous myomata in human endometrium

a: Slightly protruding myoma knots. Cellular surfaces are slightly smaller than those of the normal endometrium. The central protrusions are surrounded by flat peripheral portions of free cellular surface

b: Semispherically protruding myoma knots. Note severe atrophic changes, and irregular cellular arrangement

c: Polyp-like myoma knots showing extreme atrophy. Free surfaces protrude slightly in triangular or hexangular prisms. Microvilli resemble pinheads. Cilia reduced in number

d: Endometrial polyps. Note polygonal shape defined by the swollen intercellular connections which resemble terminal bar. Microvilli resemble pinheads
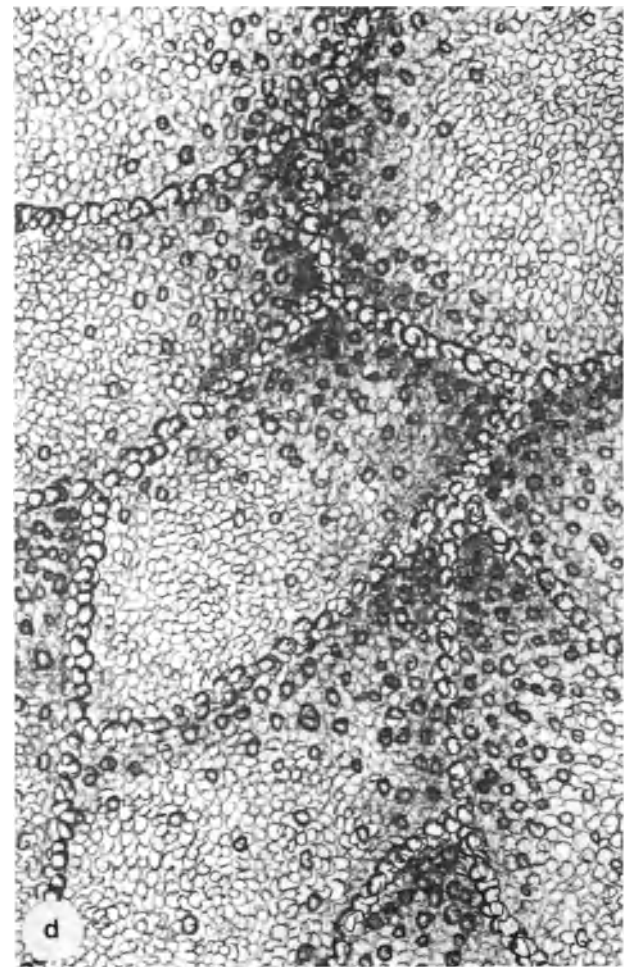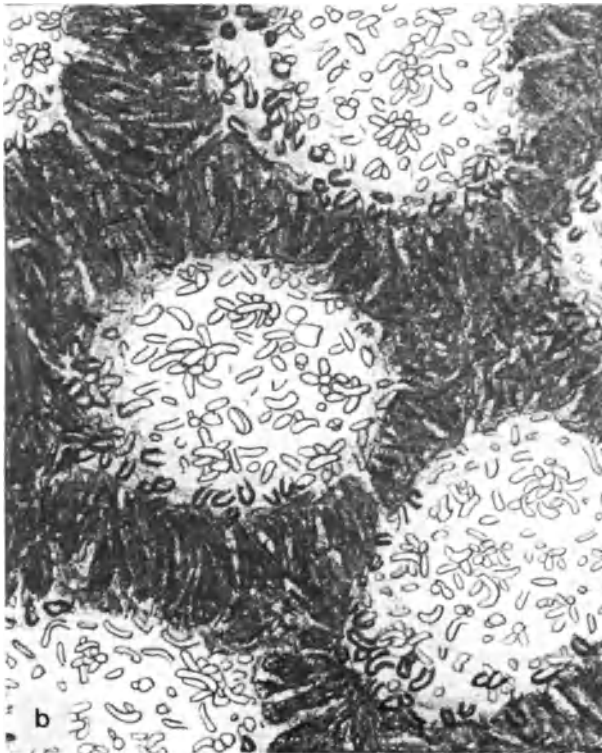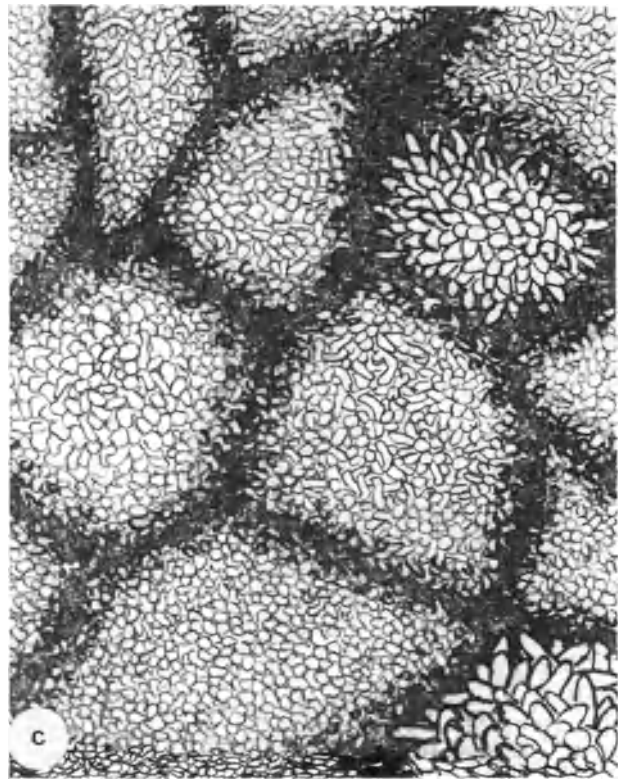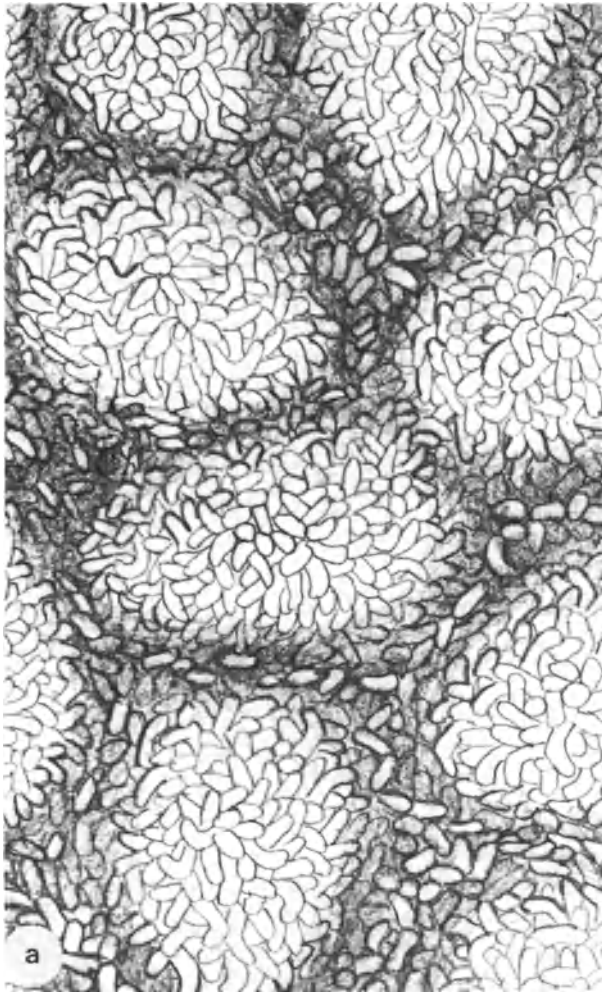
Figure 10

Figure 11 (opposite)

a: Endometrium, atypical adenomatous hyperplasia, showing protruding cells varying in size and shape (×2000)

b: Well-differentiated endometrial adenocarcinoma (grade I) showing similar, though more distinct, variations in size and shape; no microvillous cells (×2000)

c: Endometrial adenocarcinoma, moderately differentiated (grade II), showing polymorphic surface cells with small microvilli (×2000)

d: High magnification of surface of moderately well-differentiated adenocarcinoma (grade II) showing tiny and sparse microvilli (×10 000)
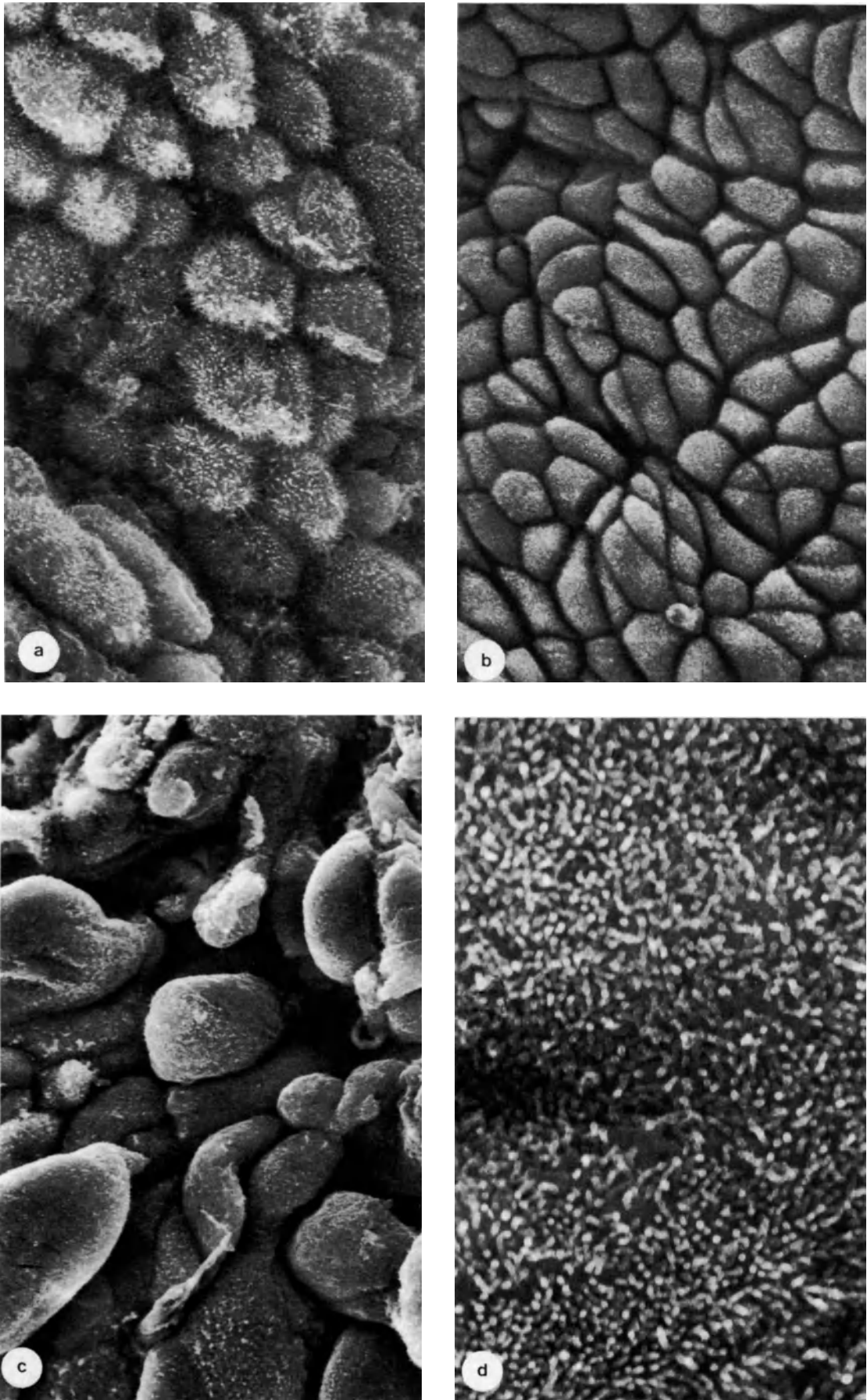
Figure 11

Tubular type
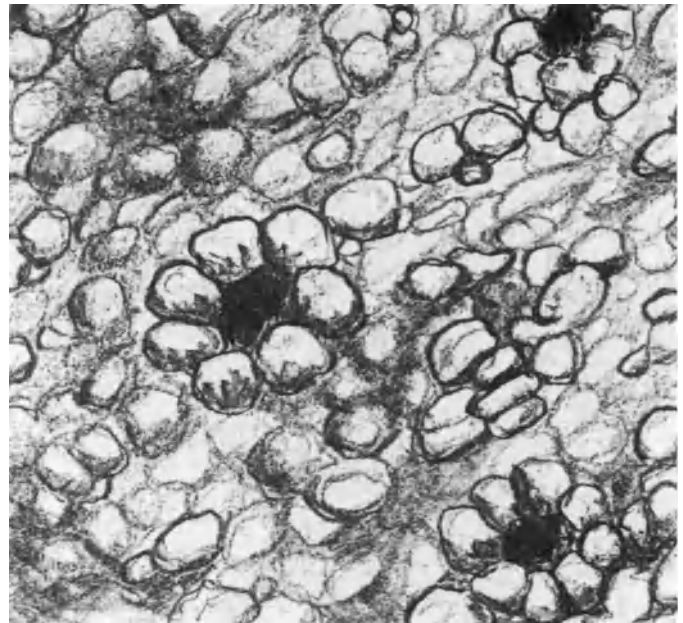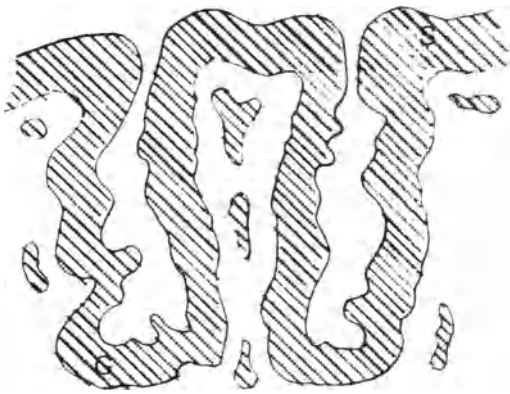
Adenomatous type
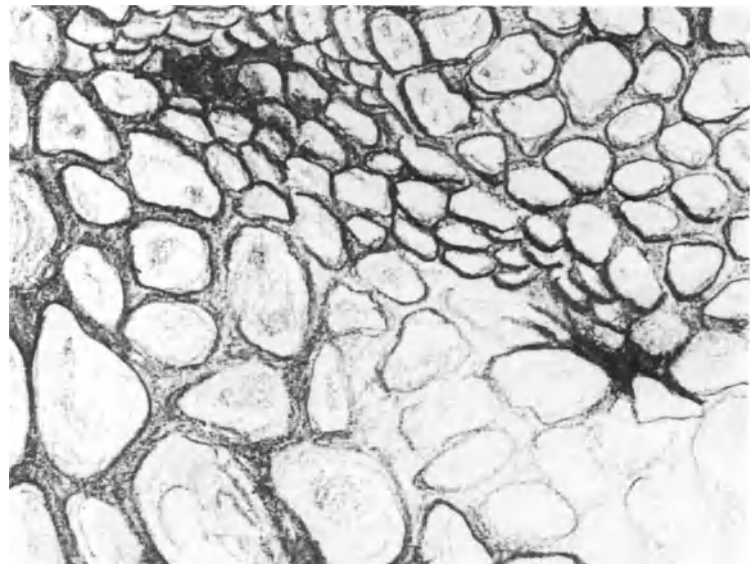
Papillary type
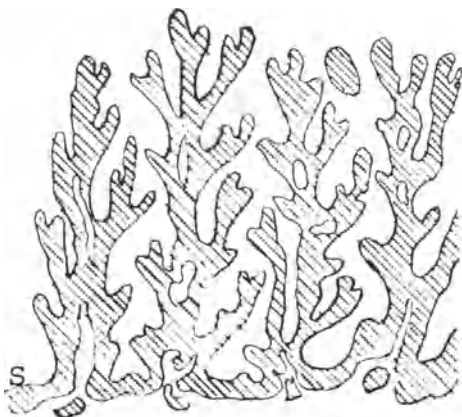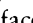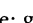
Figure 12 Line drawing of human endometrial cancer (S. surface; g, Gland; ⚏, normal; ▨, cancer)
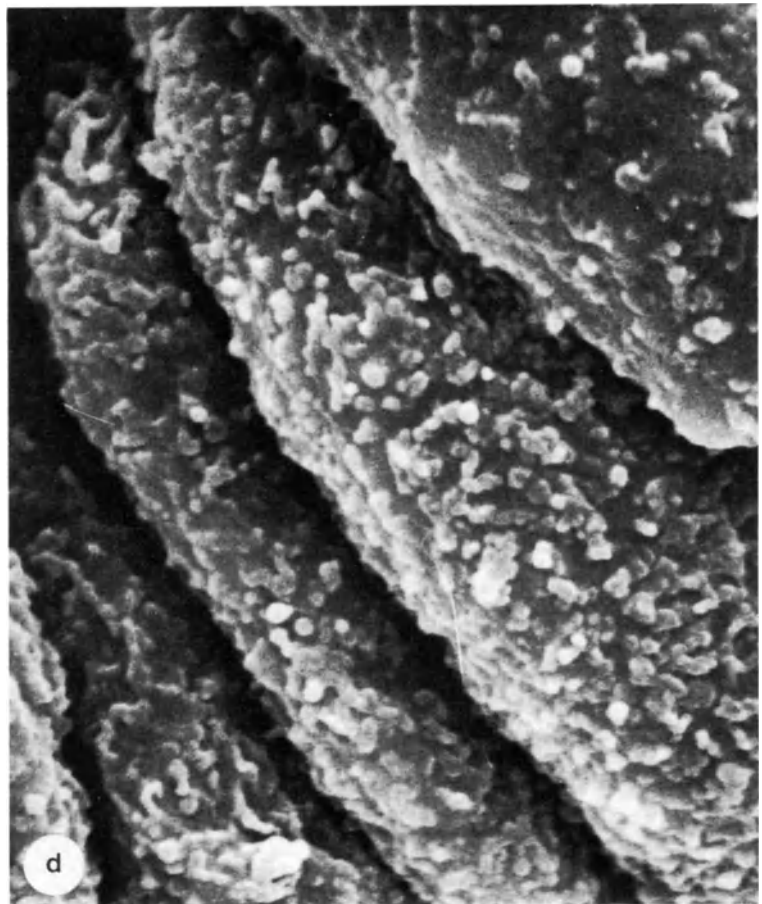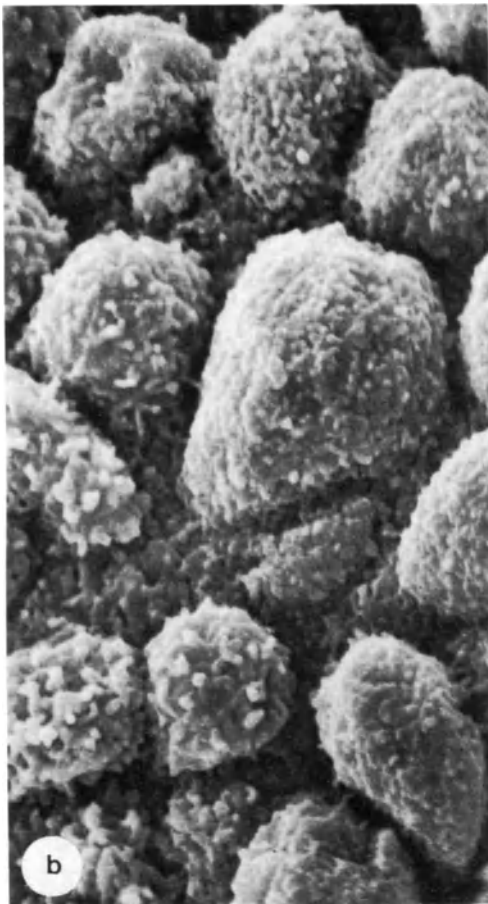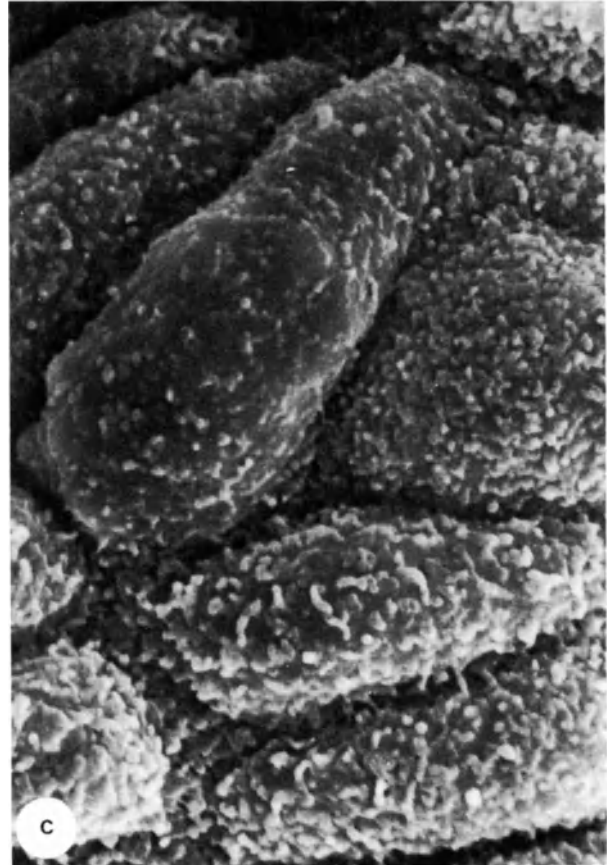
Figure 13 Tubular type of human endometrial cancer. The glandular openings show the infundibular recesses which have been transformed into a deep pit. Cells are quite large and distributed into spindle, semi-oval, or cylindrical. Cellular arrangement is quite irregular. Microvilli are sparse, rough and spot-like. Note gland openings (a), and irregular cell shape (c) (a ×1000; b×2000; c ×5000; d ×10 000)

Figure 14 (opposite) Types of human endometrial cancer
a–c: Papillary type of endometrial cancer. Papillae and syncytial formations project into gland lumina (a ×500; b ×1000; c ×1000)
d,e: Adenomatous type of endometrial cancer. The gland openings are surrounded by six to ten cells which are elevated; gland openings are densely distributed (d ×500; e ×3000)
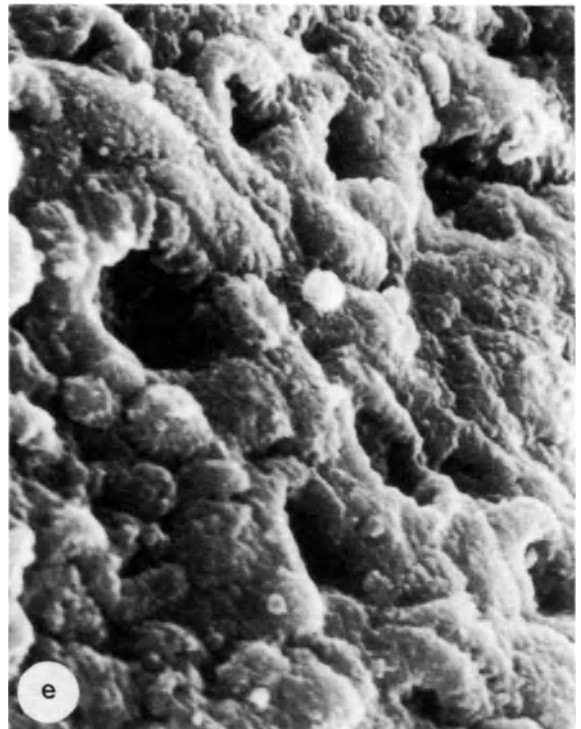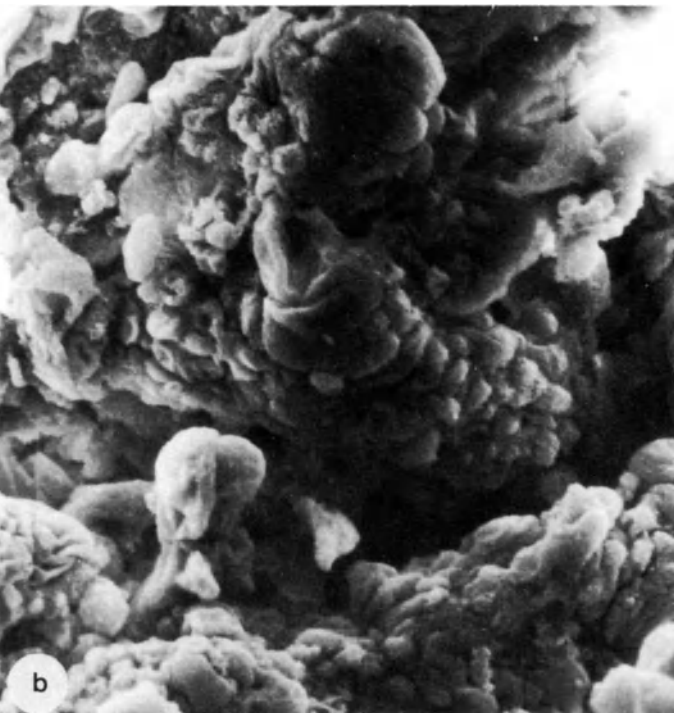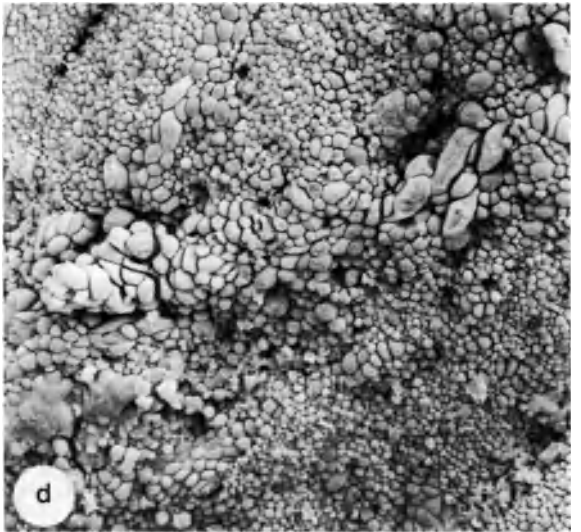
Figure 14

Figure 15 (opposite)
a: Irradiated endometrial adenocarcinoma showing enlarged, elongated cells, partly denuded (×2000)
b: High magnification of surface of endometrial adenocarcinoma with microvilli varying in size and shape. X-irradiation and medroxyprogesterone treatment (×2000)
c: Pleomorphic microvilli on surface of endometrial adenocarcinoma treated with irradiation and medroxyprogesterone (×10 000)
d: Surface of endometrial adenocarcinoma treated with X-irradiation and low doses of medroxygesterone, showing abnormal, partly destructed microvilli (×6000)
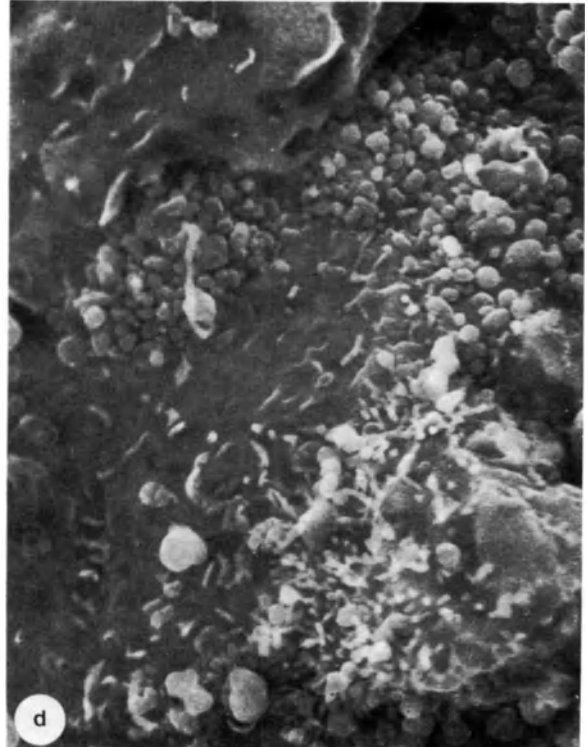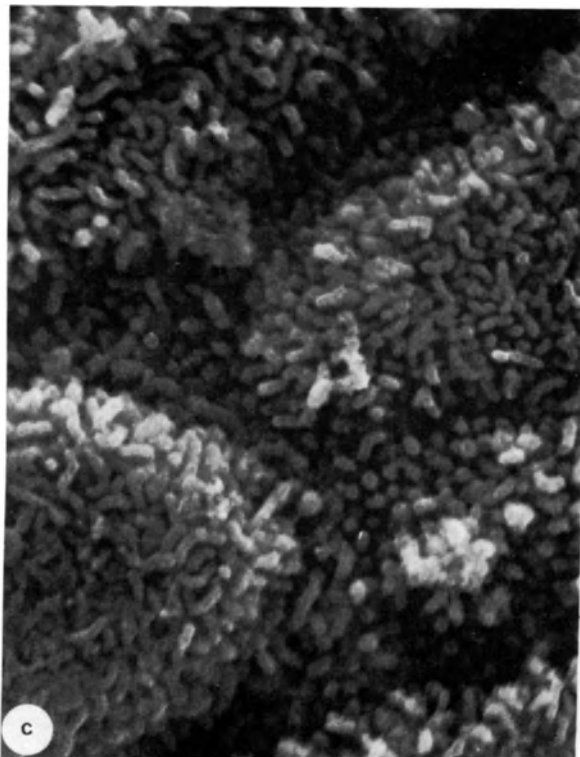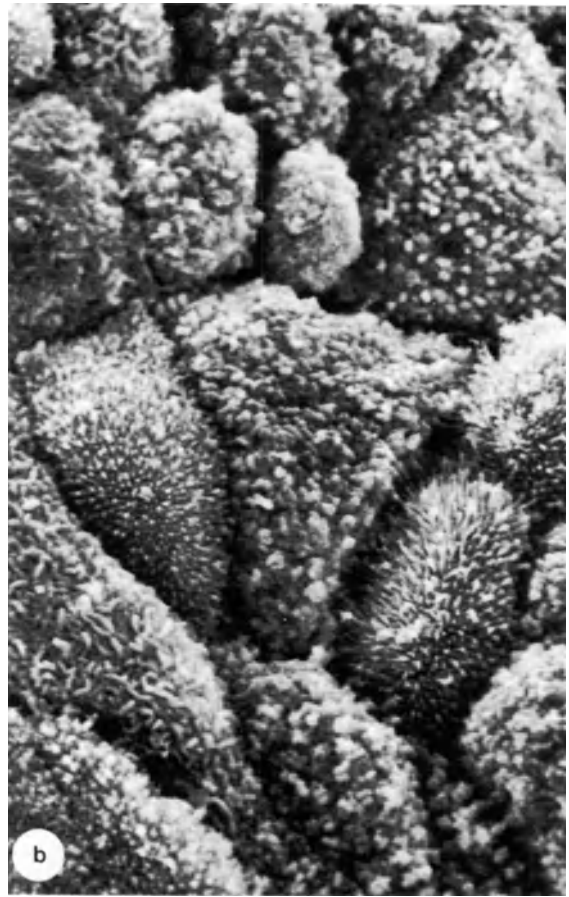
10

Response of postmenopausal endometrium to hormonal therapy

W. H. WILBORN*, C. E. FLOWERS, JR† and B. M. HYDE†

* Electron Microscopy Center and Department of Anatomy, College of Medicine, University of South Alabama, Mobile, Alabama
† Department of Obstetrics and Gynecology, School of Medicine, University of Alabama in Birmingham, Birmingham, Alabama

SEM has revealed that remarkable surface changes occur in the uterine epithelium during the estrogenic and progestational phases of the normal menstrual cycle (Ludwig and Metzger, 1976). The purpose of the present SEM study is to show that the uterine epithelium of postmenopausal patients likewise undergoes dramatic surface changes upon treatment with an estrogen and a progestin for control of climacteric disturbances.

METHODOLOGY

Twelve postmenopausal patients, as determined by clinical symptoms, endometrial biopsies, and radioimmunoassays, were carefully selected for this study. Endometrial biopsies were taken from these patients before and during therapy for a period of 4 years. One group of biopsies was obtained before the initiation of therapy; a second, during treatment with Premarin (estrone sulfate; Ayerst Laboratories, New York, NY 10017) alone; a third, during treatment with Premarin and Provera (medroxyprogesterone acetate; Upjohn Co., Kalamazoo, Mich. 49001). The drugs were taken orally in the conventional manner (Premarin, 1.25 mg/day on days 21–27 of the calendar month); Provera, 10.0 mg/day on days 21–27 of the calendar month). All specimens were handled according to standard, previously described methods (Wilborn and Flowers, 1979).

PRIOR TO TREATMENT

Untreated postmenopausal endometrium varied in appearance within the same biopsy (Figures 1 and 2). The glands and uterine cavity were lined by a low, regressed epithelium. Cell surfaces lacked prominent protrusions and were demarcated by distinct boundaries. Many cells had short microvilli, a few had 'dwarfed' cilia, and an occasional cell had a single,

long cilium. Gaps marked sites where columns of cells had separated, and holes indicated where cells had degenerated. Glands were sparse in the quiescent endometrium. Most glands were atrophic and a few were dilated.

ESTROGEN TREATMENT ONLY

The response of endometrium to Premarin only was striking. During the first calendar month of treatment the low epithelial cells transformed into two types of tall columnar cells, ciliated and secretory. On the 20th day of treatment the endometrium resembled that of the normal, mature proliferative phase (Figure 2A). Secretory cells synthesized some secretory products which escaped from their bulging apices.

Treatment with Premarin only for 2 or more calendar months was associated with excessive ciliation, breakthrough bleeding, and inconsistency in the amount of endometrium that was shed during withdrawal bleeding when the medication was discontinued at the end of the calendar month (Figures 2b and 2c). Reduction of the dose level of Premarin to 0.625 mg/day maintained a proliferative endometrium, but it did not completely alleviate these afore-mentioned conditions associated with un-opposed estrogen therapy.

ESTROGEN–PROGESTIN TREATMENT

Addition of Provera to the regimen on days 21–27 of the calendar month rapidly changed the Premarin-stimulated, late proliferative endometrium to a progestational endometrium. After 5 days of Provera (calendar day 25), secretory cells resembled those on day 19 of the normal cycle in that the cells contained lakes of glycogen, hypertrophic Golgi membranes, much rough endoplasmic reticulum, and long
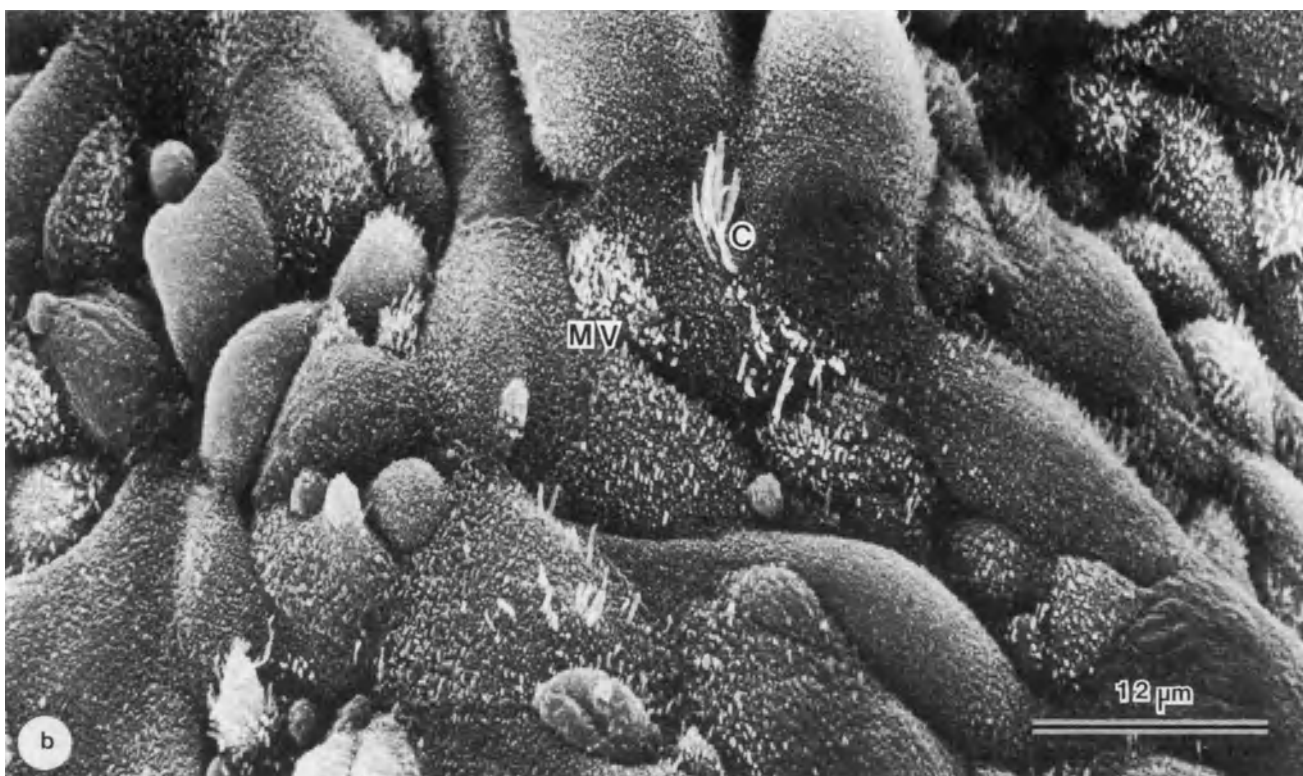
Figure 1   Untreated postmenopausal endometrium.

a: Surface epithelial cells are regressed and have distinct cell boundaries (arrows). Note edge of gland (GD) and gaps (g) where cells have separated

b: Luminal epithelial cells differ appreciably, but many have elongated, slightly bulging apices and microvilli (MV). 'Stunted' cilia (C) are occasionally present and randomly distributed, either singly or as small clusters with each cluster emerging from a small portion of the cell apex
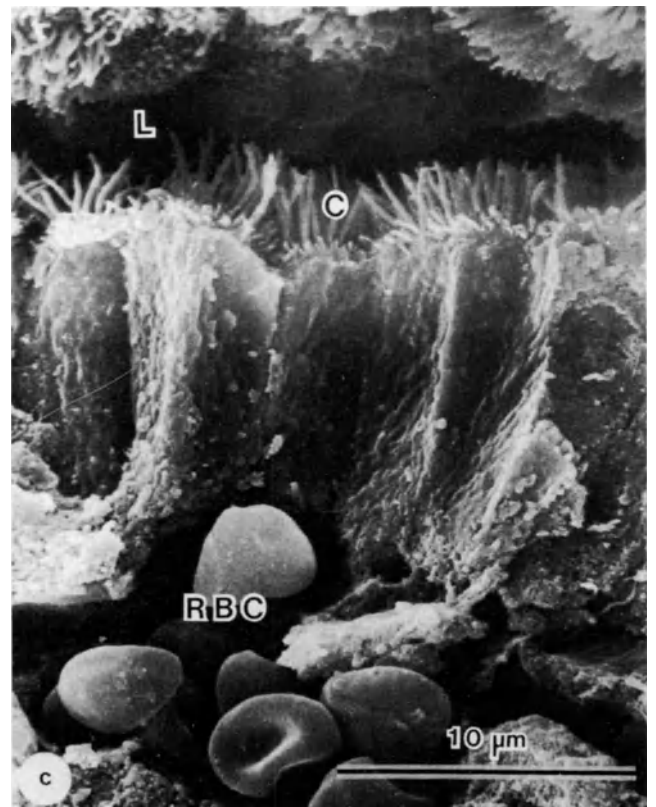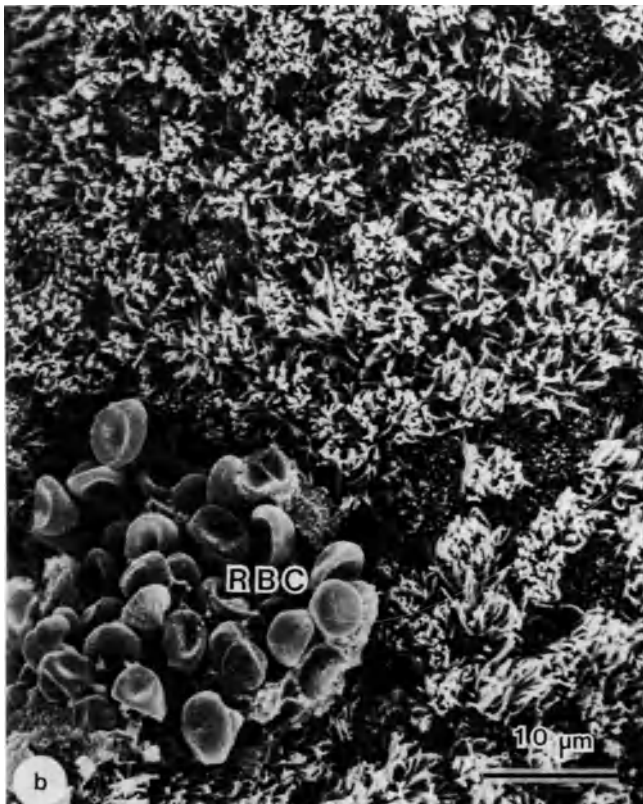
Figure 2 Estrogen treatment only

a: Response of surface epithelium to Premarin only on calendar day 20 during first month of treatment. Ciliated cells (C) are interspersed among secretory cells (S) which have protruding apices. Premarin only elicits production and expulsion of some secretory products, as illustrated by secretory cells whose apices 'inflate' as secretory products accumulate and 'deflate' as secretory products (SP) escape. The latter process results in holes (arrows) in the cell apices

b: Surface epithelium on calendar day 25 after treatment with Premarin only for 2 months. Sites of excessive ciliation and breakthrough bleeding (RBC) result from unopposed estrogen therapy for 2 or more months

c: Gland epithelium on calendar day 25 after treatment with Premarin only for 2 months. Extravascular red blood cells (RBC) in the stroma are passing through a break in the epithelium to enter the gland lumen (L) that is lined by an excessive number of cilia (C)
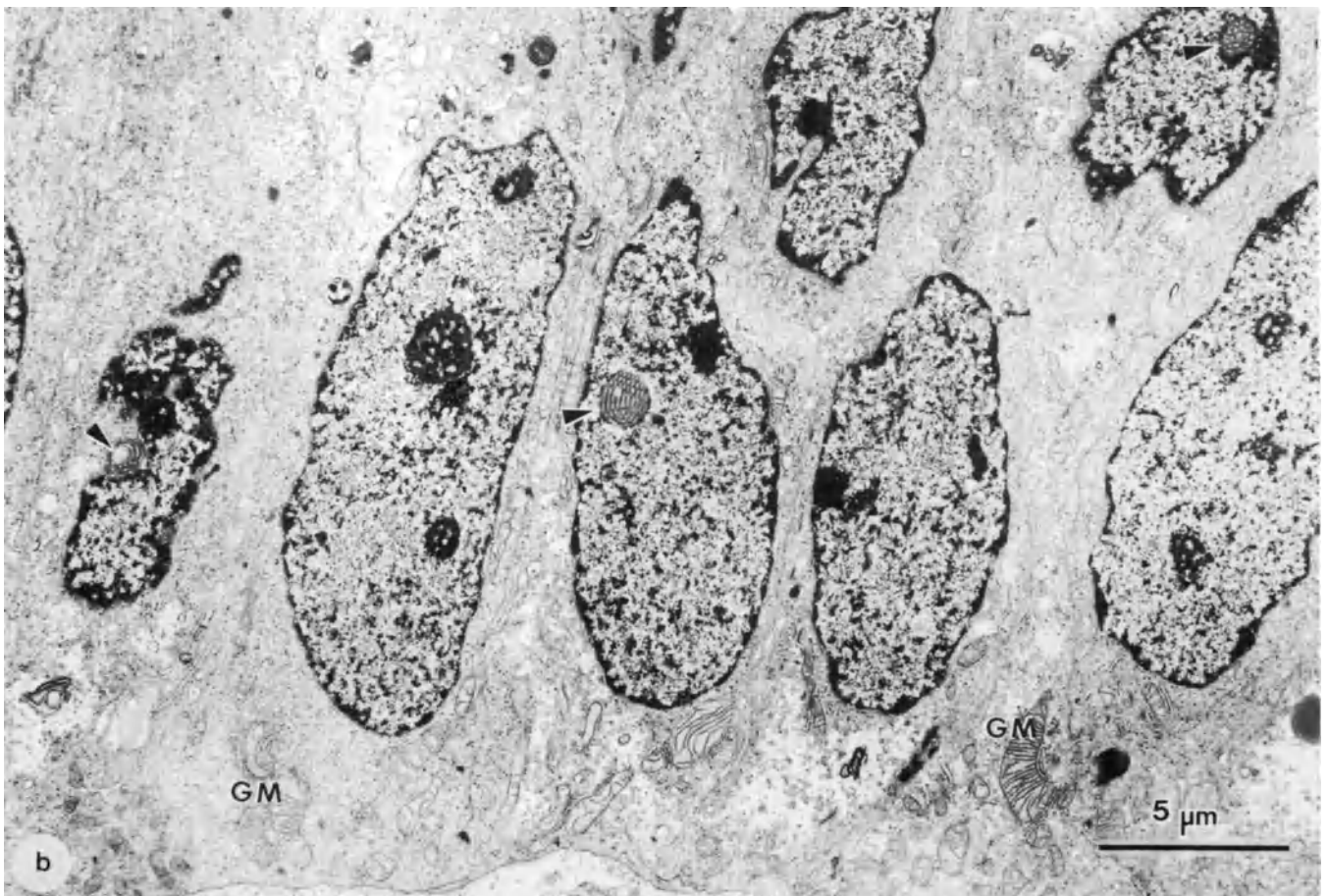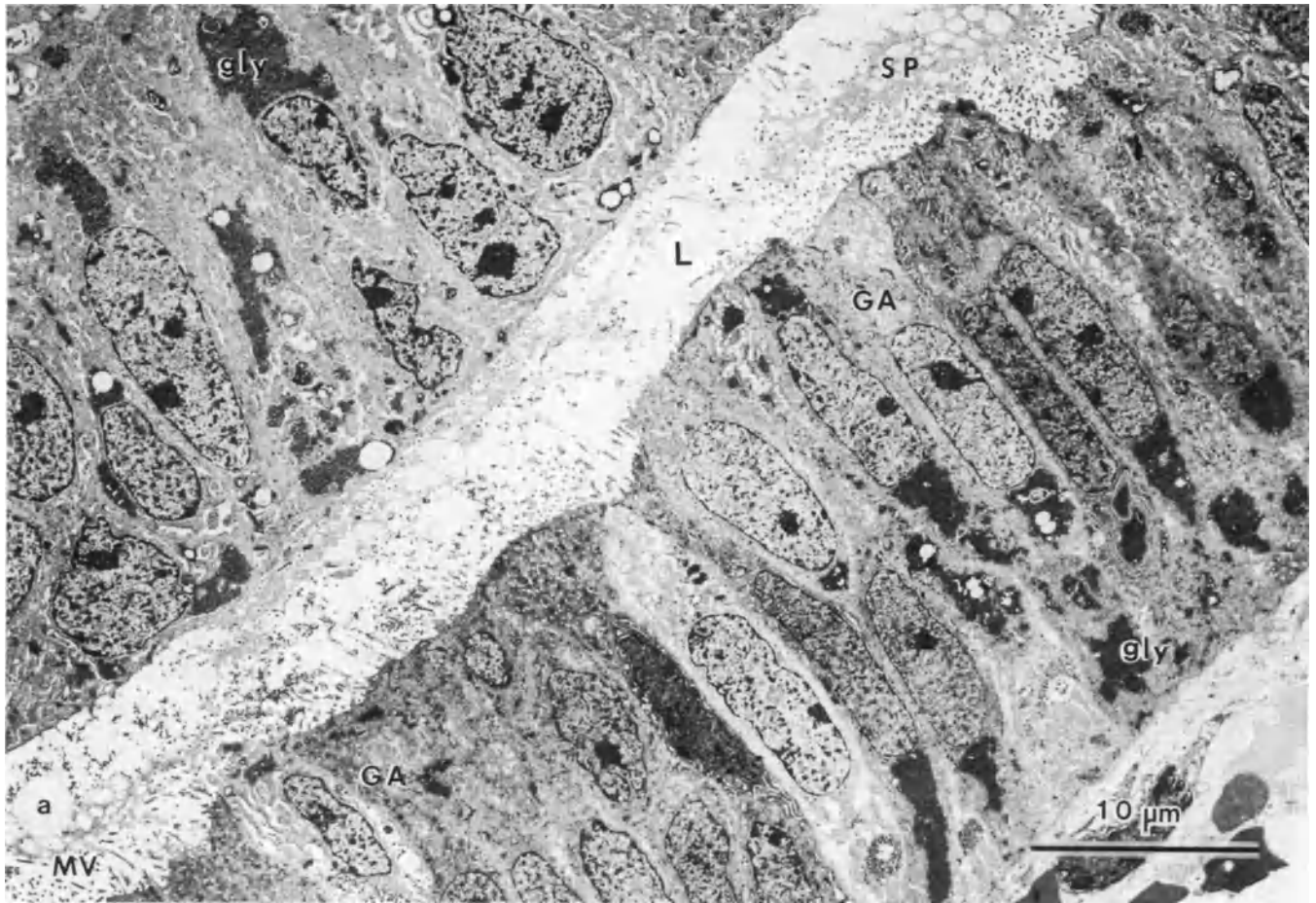
Figure 3
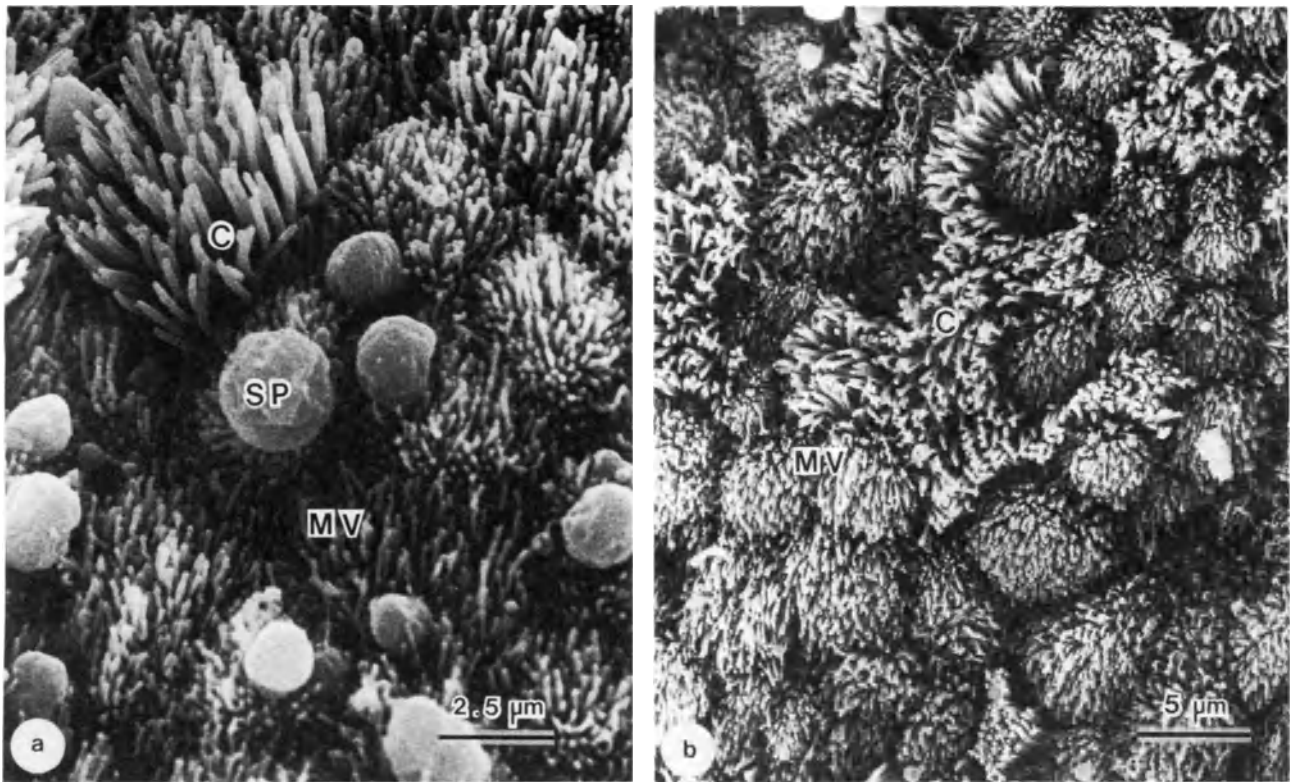
Figure 4 Estrogen–progestin treatment

a: Endometrial surface during first month of treatment with Premarin–Provera, calendar day 27. Cell apices have luteal phase characteristics that typify the endometrium at the time of implantation. Secretory products (SP) are abundant. Microvilli (MV) are long, slender, and especially dense. Fewer ciliated cells (C) are present than during treatment with Premarin only or prior to Provera administration in the estrogen–progestin regimen

b: Endometrial surface during sixth month of treatment with Premarin–Provera, calendar day 29. Expulsion of secretory products (SP) has subsided with the discontinuation of Provera on calendar day 27. Microvilli (MV) cover the apices of secretory cells, and some are almost as long as the cilia (C) of ciliated cells

Figure 3 Estrogen–progestin treatment, calendar day 25: (a) 18 months, and (b) 6 months

a: TEM illustrates the surge in synthetic activity in the glandular epithelium that follows Provera administration for 5 days. Gland cells resemble those in normal endometrium on day 19 of the secretory phase. The 'typical' secretory cell contains a large lake of glycogen (gly), an hypertrophic Golgi apparatus (GA), and long microvilli (MV). Some secretory products (SP) are in the

lumen (L), but maximal extrusion does not occur until calendar day 27

b: Gland cells after 5 days of Provera stimulation contain nucleolar channel systems (arrows) and giant mitochondria (GM). Serial sections show that the nucleolar channel system is characteristically located at the periphery of the nucleus adjacent to the nuclear envelope

microvilli (Figure 3a). Giant mitochondria and nucleolar channel systems were also present (Figure 3b). It was previously thought that nucleolar channel systems did not develop when artificial progestins were used.

On calendar day 27 the endometrium resembled that on day 21 of the normal cycle. Copious amounts of secretory products were being released by the microapocrine method (Figure 4a). Fewer ciliated cells were present during Promarin–Provera treatment on calendar days 21–27 than during treatment with Premarin only. TEM showed that Provera caused deciliation and transformation of many ciliated cells into secretory cells.

In normal endometrium the nucleolar channel system is present on day 19 and implantation usually occurs on day 21. The temporal difference between normal endometrium and progestin-treated postmenopausal endometrium can be explained by the fact that calendar days 25–27 represent days 5–7 of progestin therapy and correspond to days 19–21 of the normal menstrual cycle.

Expulsion of secretory products subsided when Provera was discontinued on calendar day 27, but microvilli remained long and numerous (Figure 4b). Regression and withdrawal bleeding occurred at the end of the calendar month in a manner that was similar to normal menstruation (Flowers and Wilborn, 1978).

CONCLUDING REMARKS

Atrophic postmenopausal endometrium responds to an estrogen and a progestin by developing proliferative, secretory, and bleeding phases similar to those of the normal menstrual cycle. These phases could not be simulated in postmenopausal endometrium treated with estrogen alone. It is concluded that estrogen–progestin therapy is the treatment of choice for the postmenopausal patient.

References

Flowers, C. E., Jr and Wilborn, W. H. (1978). New observations on the physiology of menstruation. *Obstet. Gynecol.*, 51, 16.

Ludwig, H. and Metzger, H. (1976). *The Human Female Reproductive Tract: A Scanning Electron Microscopic Atlas*, pp. 31–49. (New York: Springer).

Wilborn, W. H. and Flowers, C. E., Jr. (1979). Histoenzymology of human endometrium during the proliferative and secretory phases. In Beller, F. K. and Schumacher, G. F. B. (eds.). *Biology of the Fluids of the Female Genital Tract*, pp. 202–33. (New York: Elsevier North Holland).

11

Effect of IUDs on the endometrium

H. H. EL-BADRAWI* and E. S. E. HAFEZ†

* Department of Obstetrics/Gynecology, Faculty of Medicine, Cairo, Egypt
† Reproductive Physiology Laboratory, The C. S. Mott Center for Human Growth and Development, Wayne
State University School of Medicine, Detroit, Michigan 48201, USA.

IUD development has evolved with device design changes, the addition of pharmacologic agents, improved and safer insertion techniques and attention to consumer needs and concerns. In order to continue IUD development, still more fundamental knowledge of uterine and cervical physiology is needed (Sciarra and Zatuchni, 1980). The increasing worldwide utilization of IUDs has been associated with intensive investigation into the physiological mechanisms of their action. The constituents of IUDs play a major role in their function, as most studies have indicated that medicated IUDs have different and often better efficiency than non-medicated ones. The medicated IUDs were developed in an attempt to alleviate the side-effects while still maintaining a high antifertility effect.

The endometrial changes observed with copper devices, using light microscopy, do not differ from those seen with non-medicated devices except for an increase of the number of neutrophils and the foreign-body reaction (Moyer and Mishell, 1971).

ULTRASTRUCTURE OF ENDOMETRIUM WITH NON-MEDICATED IUDs (Lippes loop)

At the site of IUD impression

The surface epithelium shows few areas of superficial loss of cells and exposure of the basement membrane. Some of the erosive areas may contact each other. The basement membrane is destroyed only in few cases exposing the endometrial stroma. The disrupted areas are unevenly distributed throughout the entire contact zone with the IUD. Endometrial gland openings could be seen in a normal pattern and number (Figure 1).

There are great variations in the size of the non-ciliated cells with a decrease in the number of microvilli. Microvilli appear shorter than normal and more diffuse over the cell surface than in the areas not in contact with the IUD. The normal secretory pattern with non-medicated IUD appears to be altered. There is no secretion within the gland lumina at the area of IUD contact. The apical cytoplasmic protrusions of the secretory cells are hardly noted despite the abundant glycogen within the cytoplasm of endometrial cells as detected by TEM. Ciliated cells are markedly reduced in number at the contact zone. If present, they are flattened, compressed and short. However, they are occasionally found as healthy as in normal endometrium.

Changes away from the site of IUD impression

The surface ultrastructure of the endometrium away from the site of the Lippes loop impression has almost the normal characteristics of the endometrium at an equivalent phase of the menstrual cycle. There are some focal defects in surface epithelium close to gland openings (Figures 2 and 3).

The only marked morphologic difference between the epithelial cells away from the site of IUD impression and the normal endometrium is the extreme balloon distension of the upper portions of the non-ciliated cells within the glands as well as around them. The membranes of the ballooned tops are parous, with no signs of deflation. The distended structures appear within the microvilli, having their bases connected to the surface of the cell, which gives an impression of being a distended microvillus.

The gland openings show the usual architecture and distribution. Ciliated cells around openings correspond with the micromorphology of the normal endometrium at the luteal phase of the cycle. Intraglandular luminal secretions are comparable to the normal control group with detected macroapocrine secretory activities.

ULTRASTRUCTURE OF THE ENDOMETRIUM WITH COPPER IUDs

Changes at the site of impression of copper IUD

There is much more destruction of the cellular architecture at the site of copper–endometrium contact zone than that noticed with non-medicated IUDs.
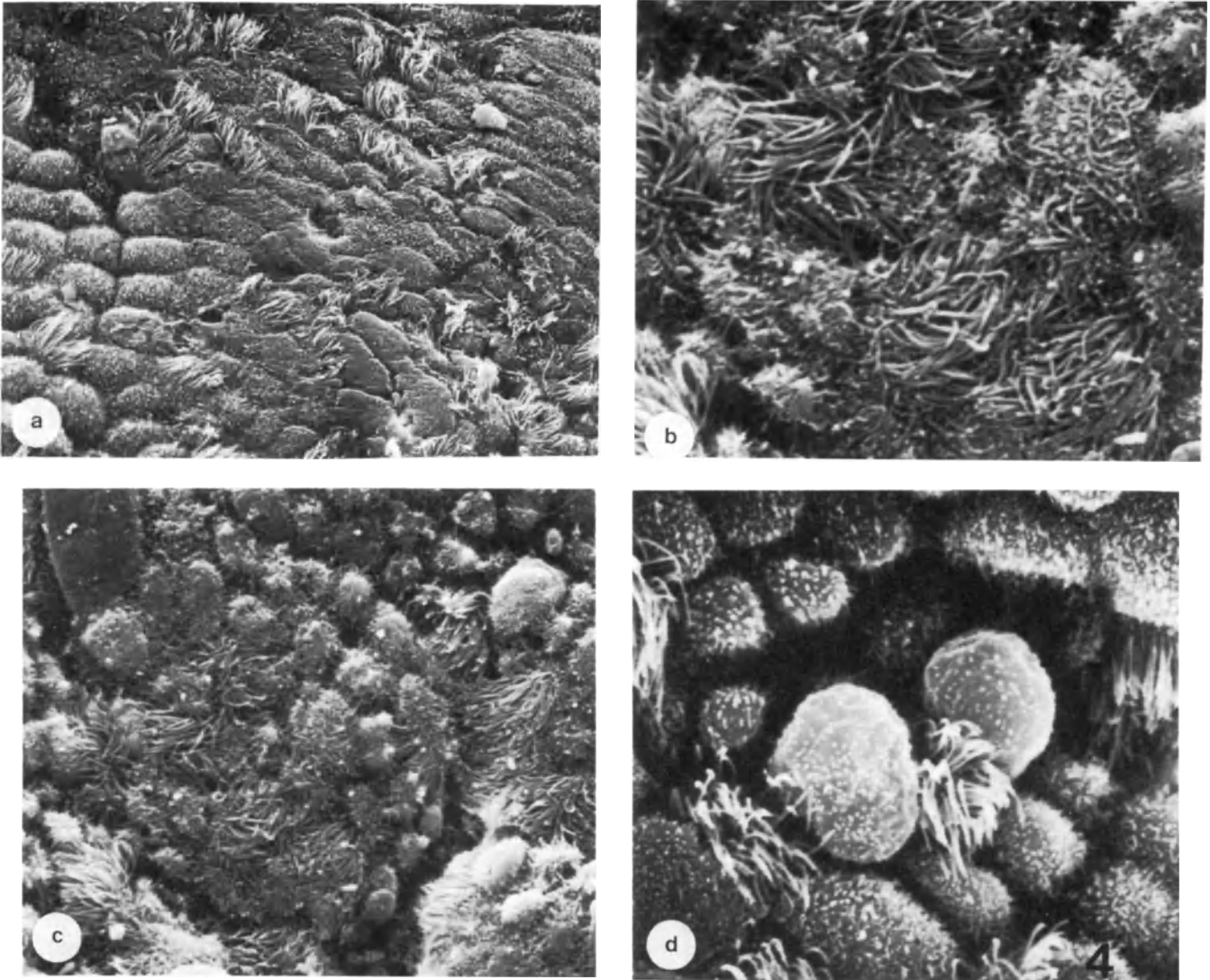
Figure 1 SEM of human endometrium at site of impression of Lippes loop

a: Note the loss of superficial cellular components, and absence of secretory activity (×1296)

b,c: Ciliated cells are compressed, not erect with indistinct intracellular boundaries in some areas of the impression site. (b, ×2880; c, ×1800)

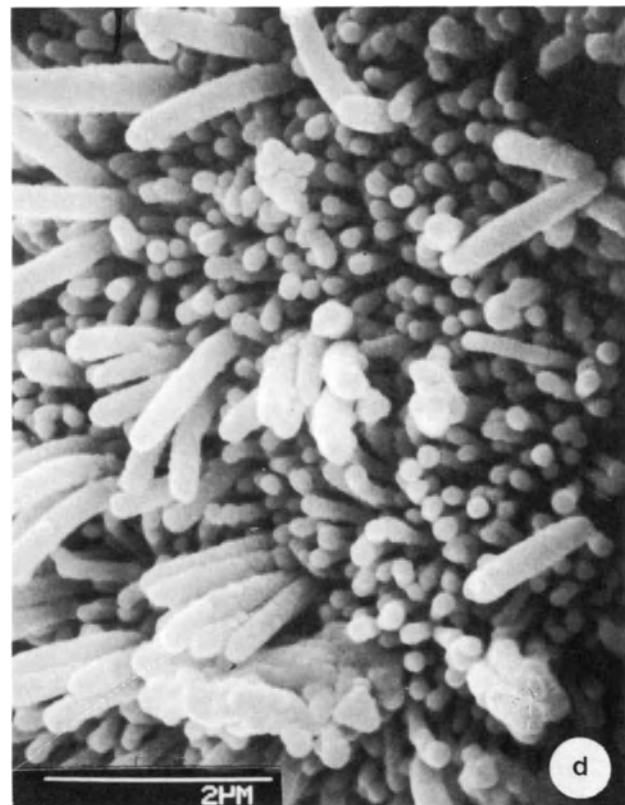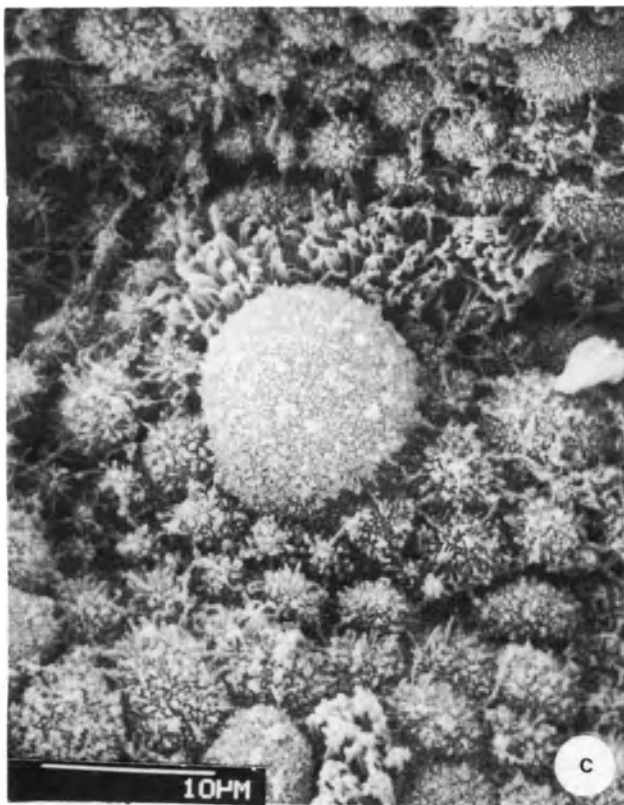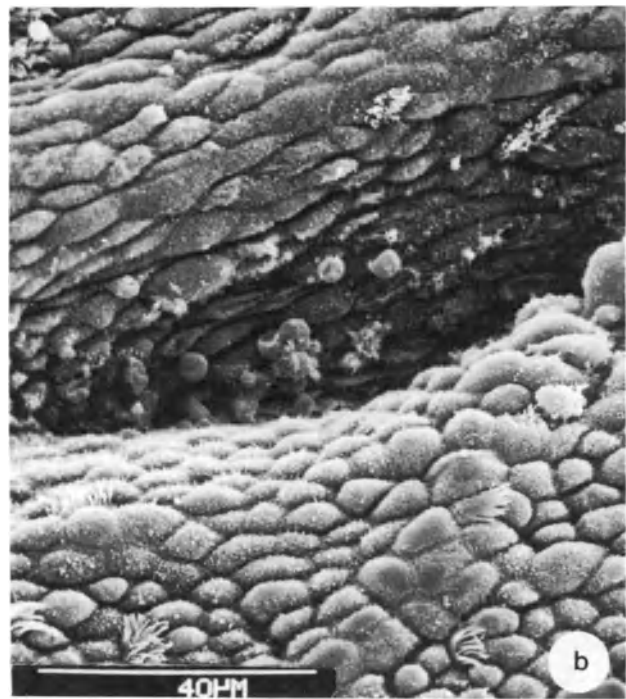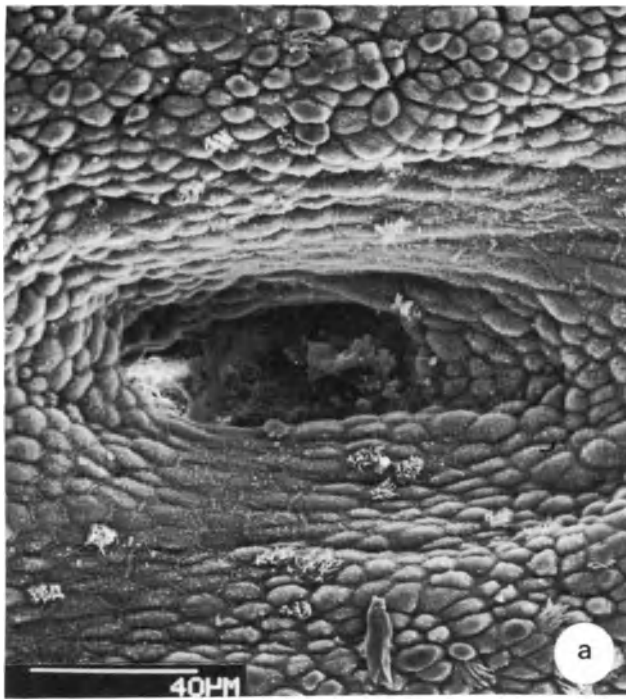d: Non-ciliated cells are variable in size with wide intercellular spaces (×4500)

Figure 2 SEM of human endometrium away from the site of Lippes loop impression (day 17)
a,b: Endometrial gland openings with exudate (a, ×600; b, ×1000)

c: Distended secretory cell among normal sized non-ciliated cells. Note the well-developed microvillous pattern and intercellular connections (×8600)
d: Normal ciliogenesis away from the IUD impression (×16 300)

There is an increase in the extent of cellular morphologic alteration with the increase of the amount of copper incorporated with the device. Epithelial cells appear abnormal in shape and distribution. Microvilli are either absent, short or very few per cell. Some of the cells show rupture of their apical membranes. There are flat erosions under the copper wire and in many cases they are covered by fibrin, cellular debris, macrophages, lymphocytes and RCSs. The surface epithelium is seen to be thinned out together with marked stromal edema and wide interstitial spaces between desmosomes, which have a normal number and appearance. With the exception of few cases, basal lamina is intact even in areas where superficial loss of epithelial cells is detected (Figures 4 and 5).

The epithelial cells are forced to the side and sometimes are overlapped. Even in the proliferative phase the apices of cells are flattened by the contact with the copper part of the device, so that the surface appears nearly structureless. Some cells retain their columnar shapes with stubby and depressed microvilli in contact with Cu T 200, but they show great individual variation, even with complete absence of microvilli with ML Cu 250 and 375. Ciliated cells are infrequently seen in areas of contact with copper. Cilia, if seen, are crushed and lie flush with the surface rather than projecting up into the uterine cavity.

There is complete absence of gland openings at the site of impression of ML Cu 250 and 375 in all phases of the menstrual cycle. Even with less copper incorporation (Cu T 200 devices) no gland openings appear at the IUD site in the proliferative or in the secretory phases. The surface epithelium discloses no secretion to the lumen of the uterus with complete absence of secretory blebs or granules.

Changes away from the copper IUD

The lining epithelium away from the copper wire is characterized by loss of microvilli, wide intercellular clefts, and absence of secretory cytoplasmic protrusions. Ciliated cells are decreased in number. Endometrial glands disclose some macroapocrine secretory activity but this is less than expected at this period of menstrual cycle (Figures 6 and 7).

Changes of the endometrium underlying plastic part of the copper device

The surface alterations of the non-medicated parts of the device are subjected to the influence of copper ions released (Figure 5). There is a mechanical impression on the endometrium which is comparable to that originating from non-medicated IUDs. The ultrastructural changes at the non-medicated part of the device include flattening of the surface epithelial cells, variability in cell shapes and loss of normal microvillous pattern. Ciliated cells are sparse with a smaller number of cilia. The gland openings decrease in number. The modification of the lining epithelium at these areas almost reaches the gland openings, although the epithelium inside the gland is not compressed by the device. The endometrial glands

show some activity with very few secretory blebs and intraluminal secretions.

ULTRASTRUCTURE OF THE ENDOMETRIUM OF WOMEN WITH IUD-INDUCED INTER-MENSTRUAL BLEEDING

SEM of the endometrial samples obtained from patients complaining of intermenstrual bleeding shows no specific surface ultrastructure characteristic that could be attributed to this clinical complication. The morphology of the surface epithelium with its endometrial gland openings, ciliated and non-ciliated cells, followed the same pattern obtained from endometrial samples with no bleeding except for the marked variability of the size of the cells. The large cells appear unevenly distributed along the surface, especially at the very near vicinity of the IUD impression. Endometrial gland opening distribution, and the growth pattern of microvilli, were the same as described before with the corresponding IUD.

CLINICAL IMPLICATION

Endometrial cells have several mechanisms of transport across the plasma membrane (Hafez et al., 1975). These processes regulate cellular volume, nutrition, excretion, and communication along the surface of the cell and inside them. During the active secretory phase of the menstrual cycle the normal uterine epithelial cells, both luminal and glandular, exhibit several apical protrusions containing glycogen and other secretory products. The apical protrusions, as observed by SEM, represent the mechanism by which the cells release their macroapocrine secretion (Nilsson et al., 1974).

Parr and Parr (1974) have investigated the irregular protrusions from the apical surfaces of the luminal epithelium at the secretory phase and they confirmed their existence but found no evidence that they are pinched off to form apocrine secretion. Bulges from the apical surfaces of luminal or glandular epithelial cells in the luteal phase of the human endometrium were also noted by Borell et al. (1959); Wessel (1960); Wynn and Woolley (1967); Colville (1968) and Armstrong et al. (1973). It was suggested that the protrusions, after being pinched off, degenerate to form nutritive material for the embryo before implantation.

Gonzalez-Angulo et al. (1973) indicated complete absence of these cytoplasmic protrusions in the endometrium with inert IUDs. In the present study the secretory activity of the surface endometrium is only noted away from the site of impression of non-medicated devices, sometimes with failure to separate from the secretory cells, and was completely absent with all copper IUDs. Glandular epithelium kept part of their secretory activity away from the copper IUD. It is concluded that there are different cellular reactions to the presence of IUD at the ultrastructural level of the glandular and surface epithelium. The copper ions seem to influence the entire endometrial surface more than the glandular cells.
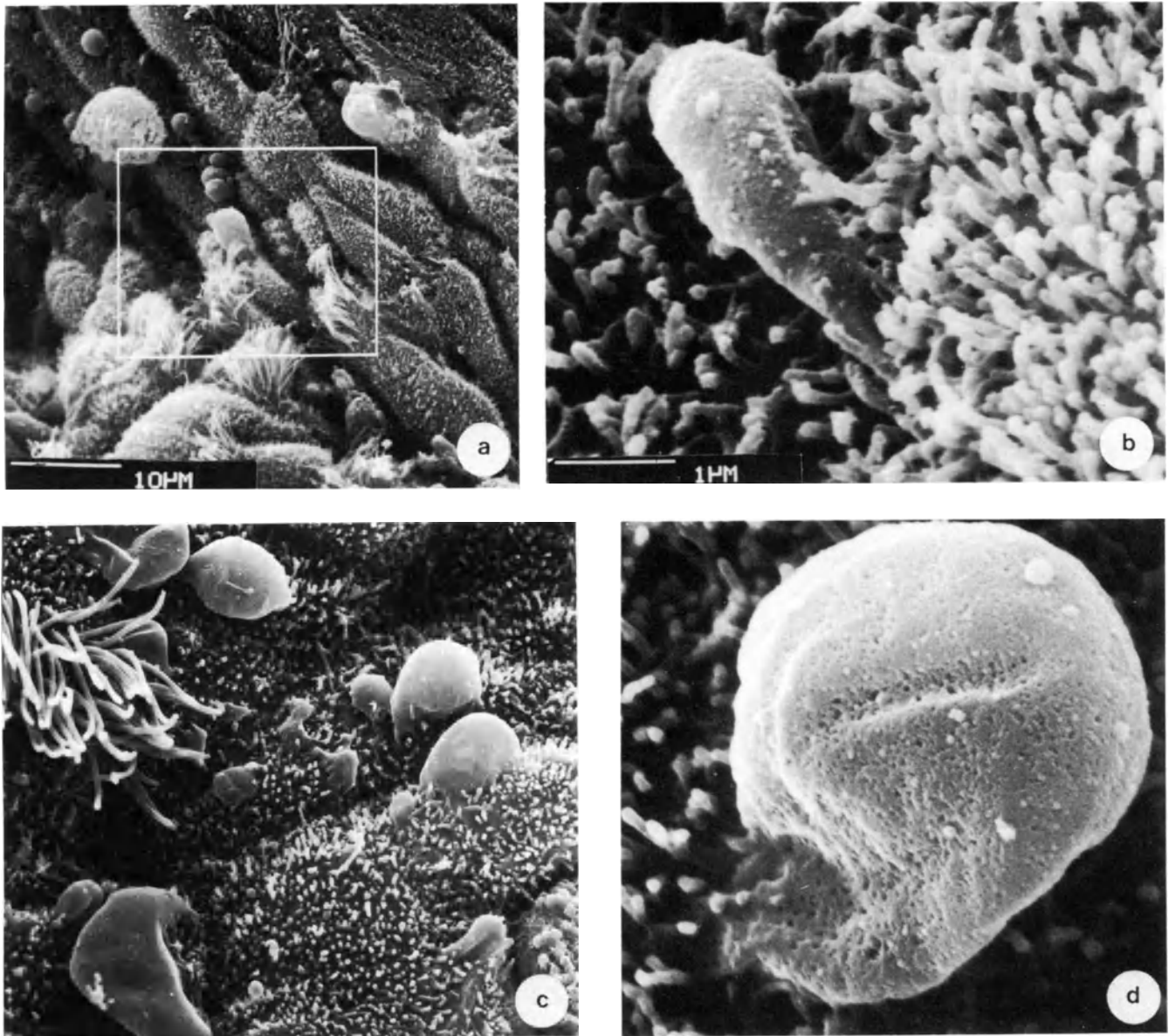
The absence of cytoplasmic macroapocrine

Figure 3 SEM of human endometrium away from site of impression of Lippes loop. Note the characteristic extruded distended structures commonly seen with Lippes loop. Note their connection with the surface of cell and their spongy irregular surface. They may indicate metabolic disturbance of secretory cells with defective secretory activities (a, ×1800; b, ×10 000; c, ×4800; d, ×17 200)

secretory granules with copper devices, and their defective separation with non-medicated IUDs, supports the theory that the IUD interferes with carbohydrate metabolism (Gonzalez-Angulo et al., 1973; Nilsson et al., 1974; and Ludwig Metzger, 1976). The light areas of glycogen granules are smaller and less frequent in glandular epithelium, leading to the theory that copper interferes with glycogen degradation, perhaps by enzyme inhibition. However, the IUD influences the endometrial cells on two levels: the metabolism of carbohydrate inside the cell, and the process of secretion.

The disturbed glycogen metabolism and secretory function of the endometrium, in both surface and glandular epithelium as detected by SEM and TEM, gives further support to the view that the mode of action of IUD, especially copper devices, might be through the interference with the blastocyst–endometrial interaction and blastocyst survival. The change in the intrauterine environment due to the absence of normal secretion may also affect the sperm capacitation process and/or the acrosomal reaction with subsequent failure of fertilization.

A variety of clinical and laboratory studies of Cu T IUDs indicated an absence of local copper accumulation, presumably because the endometrium is cast off monthly with menstruation. No toxic side-effects result from elevated levels of intrauterine copper, and several studies have failed to demonstrate increased levels of copper in general circulation. However, a greater concentration of copper in the endometrial cells, and to a lesser degree in the
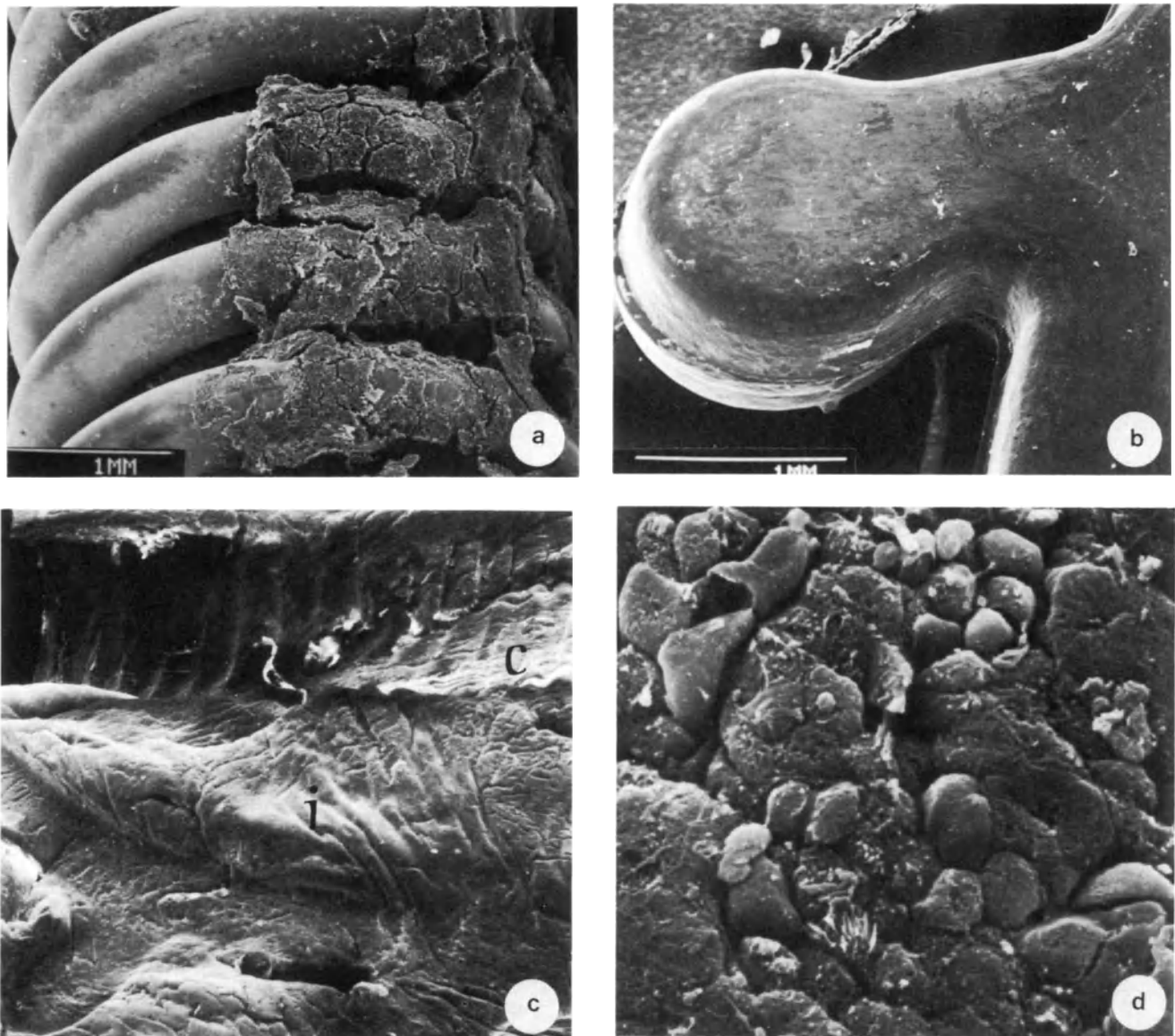
Figure 4 SEM of the endometrium with ML Cu 250 (day 18)

a: The copper wire of ML Cu 250. Note attachment of endometrial tissue ($\times$28)

b: The non-medicated wing of the ML Cu 250 ($\times$28)

c: The impression of the ML Cu 250 of the endometrial surface. The 'arrow' points to the non-medicated part of the device ($\times$20)

d: The endometrial surface at the site of impression of the copper wire. Note the variability of the size of the cells, the absence of ciliated cells and endometrial gland openings and the defective microvillous pattern ($\times$1600)
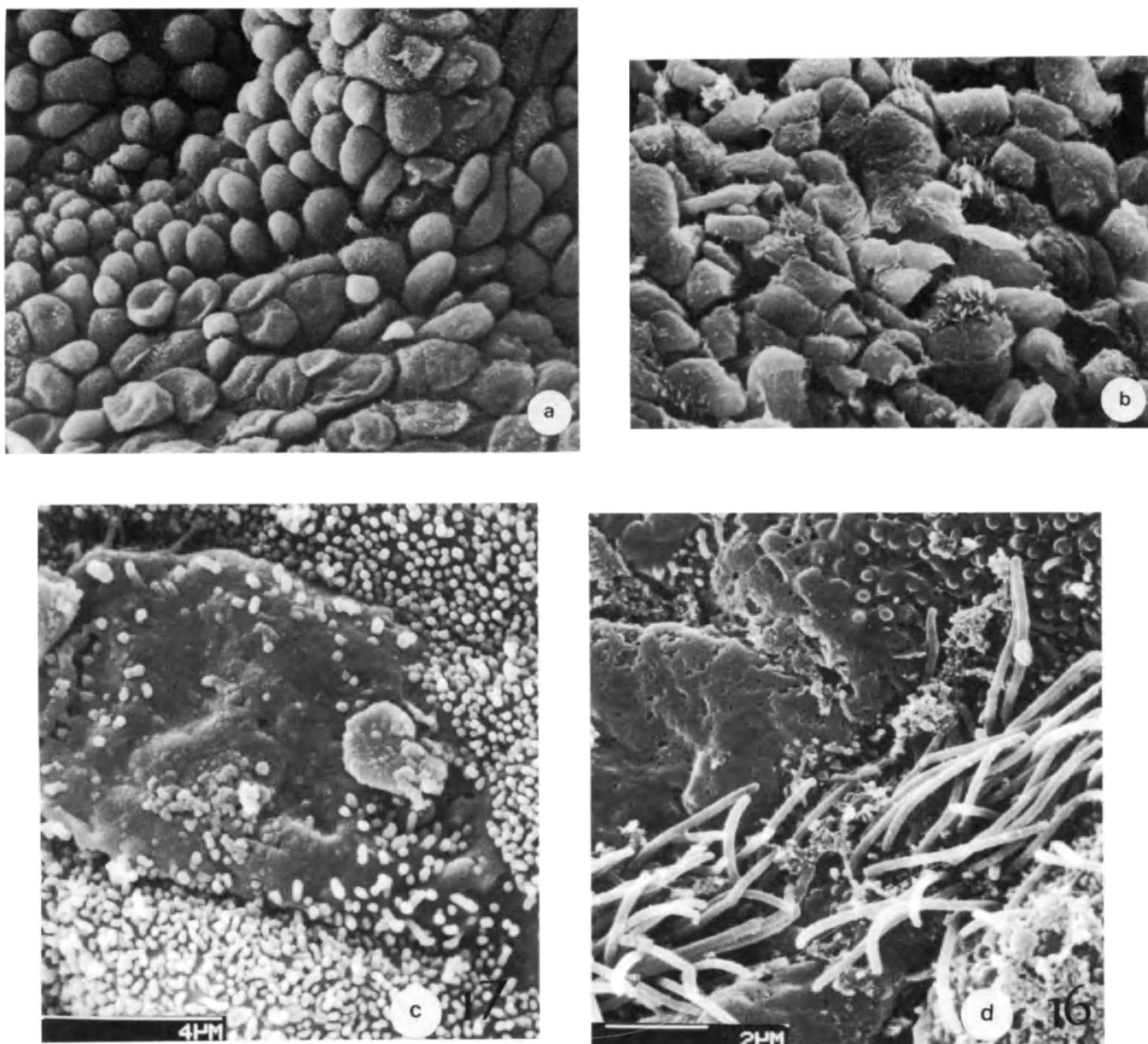
Figure 5   SEM of human endometrium at the site of copper IUD (Cu T 200)

a,b: At the site of copper wire impression, note the variability of the size of cells, the absence of any secretory projections, the reduced number of ciliated

cells and endometrial gland openings (a, ×1530; b, ×1870)

c,d: At the site of impression of the plastic (non-medicated) part. Note the abnormality in ciliary and microvillous growth (c, ×10 000; d, ×9500)

leukocytes, has been reported, but with no progressive increase in intrauterine copper levels (Hagenfeldt *et al.*, 1970; Ranney *et al.*, 1975).

In a spectrographic study of the late secretory phase, endometrial biopsies from women using Lippes loop and copper IUDs (Hefnawi *et al.*, 1974) found an elevation of endometrial copper levels in both groups as compared with controls. Of greatest significance was their observation that the degree of elevation in long-term Lippes loop wearers was as high as that found in women wearing the copper IUDs.

In agreement with Ludwig and Metzger (1976), it is suggested that the effect of copper IUDs is not localized at its site of the impression and it covers a larger area of the surface epithelium. However, other investigators   believe   that   the   ultrastructure

morphologic changes of copper devices, as well as inert ones, are localized at the site of IUD impression (Daniel *et al.*, 1975; Hsu *et al.*, 1976).

The variability of the changes in the ciliated cells and non-ciliated cells at the contact zone of the non-medicated devices may be due to the fact that the device does not touch the endometrium in all areas. This may also explain the more extensive effect of IUDs on the cilia, their tips being in contact with the device at all the contact zones. The complete absence of cilia at the site of contact of non-medicated IUD as reported by Ludwig and Metzger (1976) is not confirmed in the present study. However, the higher the copper content of the IUD, the more influenced are the ciliated cells.

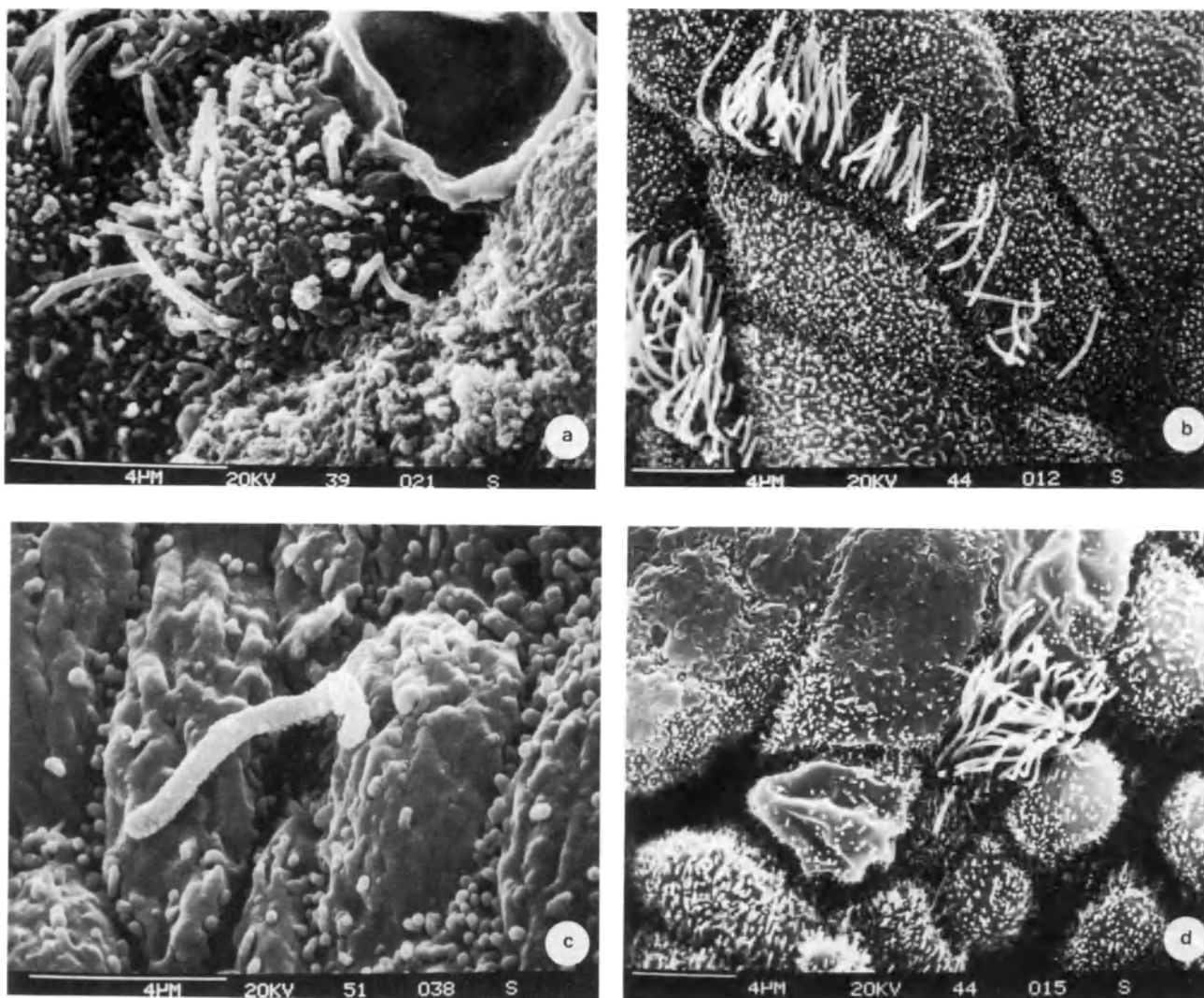The cilia of the endometrium are typical kinocilia

Figure 6 SEM of endometrium away from the ML Cu 375
a: Note the abnormality in cell topography, ruptured apical cellular membrane of one cell, delayed microvillous growth and decreased number of cilia per cell (×11 856)
b: Note the short microvilli pattern and defective ciliation (×4368)

c: Note the presence of solitary cilia and defective microvillous growth (×14 820)
d: Note the variability in the size of cells, the deflated secretory cell and wide intercellular spaces. One ciliated cell in the micrograph appears normal (×2340)

(motile) with nine peripheral and two central filaments. The development and maintenance of ciliated cells in both surface and glandular epithelium seems to be under estrogenic control since an absence of estrogen causes deciliation and cessation of secretory activity (Ferenczy and Richart, 1973; Schueller, 1968).

Divergent results have been presented from studies on the effect of the IUD on ovarian function in women. Sammour et al. (1967) and Faucher et al. (1969) have reported that ovulation and steroid production are influenced by the presence of IUDs, but Polidoro and Black (1970); Moyer and Mishell (1971); Nygren and Johannsson (1973); and Abdalla et al. (1979) have presented data of essentially normal steroid production.

As cilia, principally estrogen-dependent, are so much affected by the presence of IUD, especially on the surface epithelium, it can be concluded that the presence of IUD, especially with copper incorporation, might influence the estrogen receptors on the endometrium leading to defective ciliation in the presence of normal estrogen levels. This is in agreement with the studies of Dada and Adedevoh (1976) and Lovgren et al. (1978), which support the hypothesis that the estrogen receptor complex is influenced by copper IUDs.

The role of ciliated cells in supporting the process of implantation and the significance of their presence is not completely understood. However, several hypotheses were proposed by Schueller (1968), Ferenczy and Richart (1973), and Hafez et al. (1975).
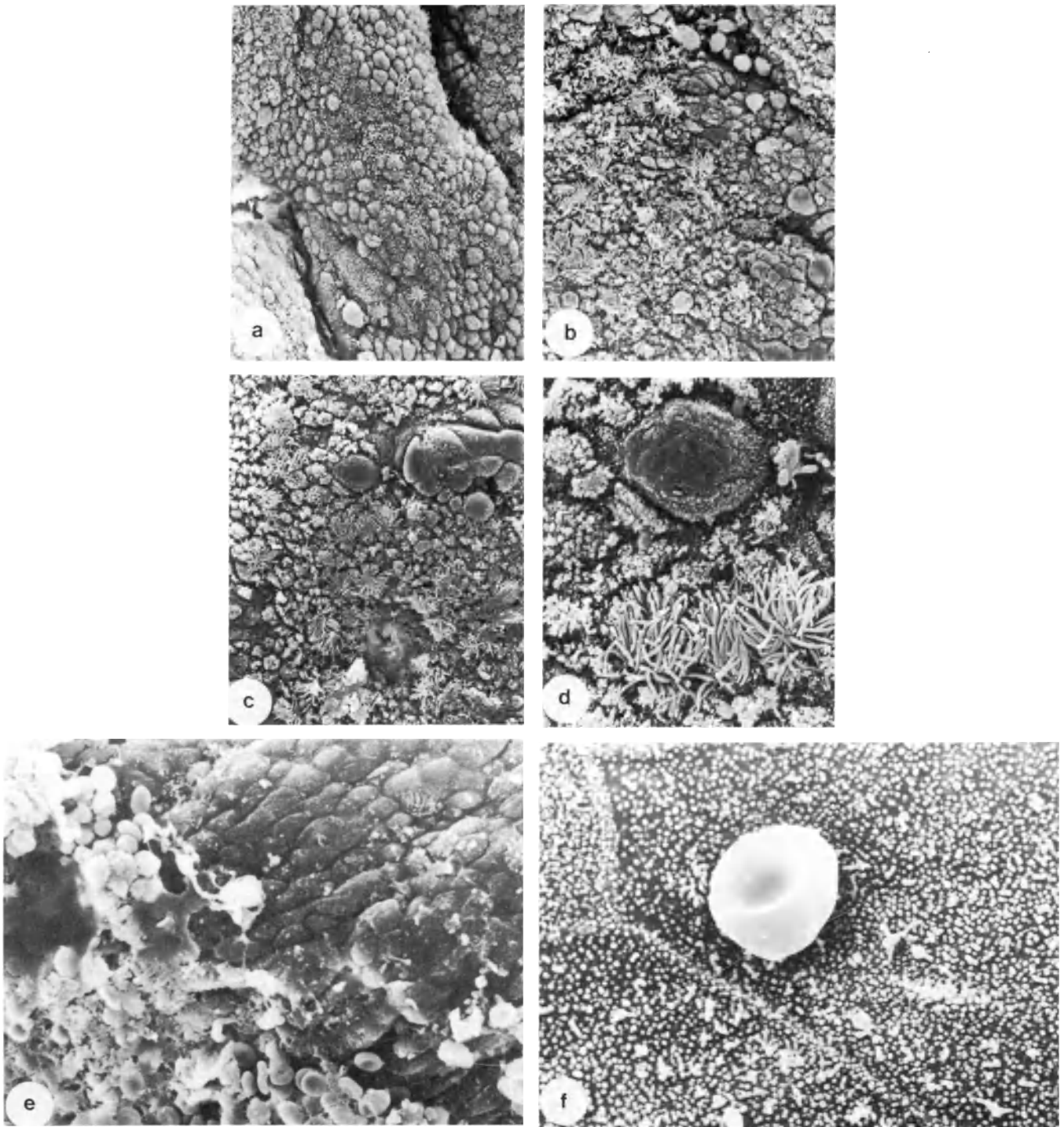
Figure 7 SEM of the endometrium with Lippes loop in patients with irregular uterine bleeding. Note the variability in the size of the cells. Some non-ciliated cells are distended.

There are no apparent large erosive areas (a,b,c, ×1000; d,e, ×3000)

f: Note the blood cells covering the surface epithelium which have few ciliated cells (×16 000)

Ciliary movement may promote fluid circulation, distribute glandular secretions, and/or sperm and egg transport. Ciliated cells, mechanically, may have a role in supporting the implanting blastocysts during the process of implantation, preventing their loss from the uterine cavity. Their disappearance or distortion in the presence of an IUD may have a significant influence on the process of implantation, thereby pointing out an important possible mechanism of action.

CONCLUDING REMARKS

IUDs have variable ultrastructural effects on the endometrial cells, depending on the presence or absence of copper and the amount of copper incorporated in the device. With few exceptions these ultrastructural characteristics cannot be related to a certain period of the cycle. The endometrial surface appears without structural integrity in some specimens underlying the ML Cu 375 IUD. The lining of the epithelium appears to lack function away from the copper wire. This can be detected morphologically by the loss of microvilli, the wide intercellular clefts and the absence of any secretory cytoplasmic protrusions.

References

Abdalla, M. I., Ibrahim, I. I., Makhlouf, A. M. and Abdoul Dahab, T. (1979). Effect of Lippes loop and Copper T-200 on pituitary–ovarian function. In Hafez, E. S. E. and van Os, W. A. A. (eds). *Proceedings, Medical IUDs and Polymetric Delivery Systems*, p. 26 (Amsterdam)

Armstrong, E. M., More, I. A. R., McSeveney, D. and Chatfield, W. A. (1973). Reappraisal of the ultrastructure of the human endometrial glandular cell. *J. Obstet. Gynaecol. Br. Commonw.*, 88, 446

Borell, U., Nilsson, O. and Westman, A. (1959). The cyclical changes occurring in the epithelium lining the endometrial glands: an electron-microscopical study in the human being. *Acta Obstet. Gynecol. Scand.*, 38, 364

Colville, E. A. (1968). The ultrastructure of the human endometrium. *J. Obstet. Gynaecol. Br. Commonw.*, 75, 342

Dada, O. A. and Adadevoh, B. K. (1976). The effect of intrauterine contraceptive devices on the estrogen-induced incorporation of (^{3}H-5) uridine into RNA by the rat uterus. *Acta Endocrinol.*, 81, 165

Daniel, J. L., Gibor, Y. and Riches, W. G. (1975). The human endometrium and effects of intrauterine devices. In Hafez, E. S. E. (ed.). *SEM Atlas of Mammalian Reproduction*. (Tokyo: Igaku Shoin)

Faucher, G. L., Ellegood, J. O., Mahes, V. B. and Greenblatt, R. B. (1969). Urinary estrogens and pregnandiol before and after insertion of intrauterine contraceptive device. *Am. J. Obstet. Gynecol.*, 104, 502

Ferenczy, A. and Richart, R. M. (1973). Scanning and transmission electron microscopy of the human endometrial surface epithelium. *J. Clin. Endocrinol. Metab.*, 36, 999

Gonzalez-Angulo, A., Aznar-Ramos, R. and Feria-Velasco, A. (1973). Ultrastructural changes found in endometrium of women using Lippes Intrauterine Device. *J. Reprod. Med.*, 10, 44

Hafez, E. S. E., Barnhart, M. I., Ludwig, H., Lusher, J., Joelsson, I., Daniel, J. L., Sherman, A. I., Jordan, J. A., Wolf, H., Stewart, W. C. and Chretien, F. C. (1975). Scanning electron microscopy of human reproductive physiology. *Acta Obstet. Gynecol. Scand.* (suppl), 40, 1

Hagenfeldt, K., Platin, L. and Diczfulusy, E. (1970). Trace elements in the human endometrium. I. Zinc, copper, manganese, sodium and potassium concentrations at various phases of the normal menstrual cycle. *Acta Endocrinol.*, 65, 541

Hefnawi, F., Kandil, O., Askalani, H., Zaki, K., Nasr, F. and Mousa, M. (1974). Copper levels in women using intrauterine devices or oral contraceptives. *Fertil. Steril.*, 25, 556

Hsu, C., Ferenczy, A., Richart, R. M. and Darabi, L. (1976). Endometrial morphology with copper-bearing intrauterine devices. *Contraception*, 14, 243

Lovgren, T., Pettersson, K., Lundberg, B. and Punnonen, R. (1978). Effect of Cu++ ions on the binding of estrogen to the human myometrial estrogen binding protein. *Contraception*, 18, 2181

Ludwig, H. and Metzger, H. (1976). *The Human Female Reproductive Tract, A Scanning Electron Microscopic Atlas*, p. 58. (Berlin: Springer-Verlag)

Moyer, D. L. and Mishell, D. R. (1971). Reaction of human endometrium to the intrauterine foreign body. II: Long term effects on the endometrial history and cytology. *Am. J. Obstet. Gynecol.*, 11, 66

Nilsson, O., Hagenfeldt, L. and Johannisson, E. (1974). Ultrastructural signs of an interference in the carbohydrate metabolism of the human endometrium produced by the intrauterine copper T. device. *Acta. Obstet. Gynecol. Scand.*, 53, 139

Nygren, K. G. and Johansson, E. D. B. (1973). Premature onset of menstrual bleeding during ovulatory cycles in women with an intrauterine contraceptive device. *Am. J. Obstet. Gynecol.*, 117, 971

Parr, M. B. and Parr, E. L. (1974). Uterine luminal epithelium; protrusions mediate endocytosis, not apocrine secretion, in the rat. *Biol. Reprod.*, 11, 220

Polidoro, J. P. and Black, D. L. (1970). The failure of the copper IUD to inhibit fertilization in the rabbit. *J. Reprod. Fertil.*, 23, 151

Ranney, R., Nutting, E. and Hackett, R. (1975). Uterine copper distribution in monkeys implanted with copper-carrying intrauterine device. *Fertil. Steril.*, 26, 80

Sammour, M. B., Iskander, S. G. and Rifai, S. F. (1967). Combined histologic and cytologic studies of intrauterine contraception. *Am. J. Obstet. Gynecol.*, 98, 946

Schueller, E. F. (1968). Ciliated epithelia of the human uterine mucosa. *Obstet., Gynecol.*, 31, 215

Sciarra, J. J. and Zatuchni, G. I. (1980). Research and new developments in intrauterine contraception. Proceedings, IUD Technology, International Symposium, Bordeaux, France. *Contracept. Deliv. Syst.*, 1, 257

Wessel, W. (1960). The electron microscopic picture of human endometrial glandular cells during the menstrual cycle. *Z. Zellforsch.*, 51, 633

Wynn, R. M. and Wooley, R. S. (1967). Ultrastructural cyclic changes in the human endometrium. I. Normal postovulatory phase. *Fertil. Steril.*, 18, 721

12

Uterine cervical and endometrial cells *in vitro:* Can reserve cells grow *in vitro?*

S. NOZAWA*, I. ISHIWATA*, S. TAGUCHI*, S. TSUKAHARA*, S. KURIHARA*, and H. OKUMURA†

* Department of Obstetrics and Gynecology, School of Medicine, Keio University, Tokyo 160, Japan
† Department of Virology and Rickettsiology, National Institute of Health, Kamiosaki, Shinagawaku, Tokyo 141, Japan

CHARACTERISTICS OF RESERVE CELLS

Reserve cells, located beneath the columnar cells under the squamo-columnar junction of the uterine cervix, are thought to be the original cells of most uterine cervical cancers. There is consensus that these cells can either differentiate into cervical glandular cells or into squamous epithelial cells via the process of 'squamous metaplasia' (Fink *et al.*, 1973).

We have shown that, although reserve cells are normal diploid cells, they contain the 'Regan-like isoenzyme' (Nozawa *et al.*, 1975, 1980, 1981), a heat-stable, L-phenylalanine-sensitive alkaline phosphatase (ALP). This isoenzyme is one of the oncotrophoblastic proteins and has been thought to exist only in the placenta and in some cancer cells (Fishman *et al.*, 1968).

To study the biological characteristics of reserve cells, and to obtain materials for carcinogenic experiments, their culture is necessary. However, while uterine cervical cells have been successfully cultured by others (Shingleton *et al.*, 1970; Wilbank *et al.*, 1972; Vesterinen *et al.*, 1980) we have failed in our attempts to grow reserve cells in culture. For these cultures, endocervical tissues were used but we found it difficult to differentiate cultured reserve cells from simultaneously present and proliferating squamous epithelial cells and endocervical or endometrial glandular cells.

Therefore, we used ectocervical-, endometrial- and endocervical explant cultures and subjected them to scanning electronmicroscopic (SEM), transmission electronmicroscopic (TEM), ALP staining, and chromosome studies, to determine whether reserve cells can proliferate *in vitro*.

METHODOLOGY (Table 1)

Ectocervical and endometrial tissue fragments were obtained from the portio vaginalis of the uterine cervix, as far distant as possible from the squamo-columnar junction, and the uterine fundus, respectively. They were used to ascertain the characteristics of squamous and glandular cells, respectively. Endocervical tissue fragments, which may contain reserve cells, were obtained from the area close to the internal os. All tissues were sampled under aseptic conditions, which were from hysterectomy specimens of women in the reproductive age (30–45 years).

Each sample was cut into 2 mm^3 fragments, placed on glass coverslips and cultured for 1–4 weeks at 37 °C in 5% CO_2 in Petri dishes in the presence of Ham's F-12 culture medium (Gibco, Grand Island, NY)

Table 1   Can reserve cells grow *in vitro?*

Materials:
1. Endometrial cells (EM)
2. Cervical squamous cells (SQ)
3. Endocervical cells (EC)

Method:
   Grow explant cultures in Petri dishes (1–4 weeks) in the presence of Ham's F-12 medium containing 20% FCS.

Identification:
1. Light microscopy
2. Transmission electron microscopy
3. Scanning electron microscopy
4. Histochemical staining of alkaline phosphatase
5. Chromosomal analysis

containing 20% new-born calf serum, 100 U penicillin and 100 µg streptomycin per ml. For SEM observations, we used double-fixation with 2.5% glutaraldehyde and 1% OsO_4, CO_2 critical-point drying, and the gold-ion sputter method. For TEM, we cut thin sections parallel to the culture glass.

ALP was stained by the azo dye method; the substrate was naphthol AS-MX phosphate (Nozawa *et al.*, 1980). Heat-stability was determined at 65 °C (30 min), as described by Jensen *et al.* (1968).

CHARACTERISTICS OF THE CULTURED CELLS (Table 2)

Counting colonies where the growth of only epithelial cells was taken as indicative of successful culture, 782 of 1052 (74%) colonies were successful in the ectocervical, 568 of 1047 (54%) in the endometrial, and 408 of 799 (51%) in the endocervical tissue fragment culture. In explant cultures of each fragment, after 3 days of lag phase, epithelial cells grew from all sides of the explant edges and formed enlarging circles of actively growing cells. After the 4th week of culture, growth almost completely stopped and many of the colonies degenerated.

The growth of cells from the ectocervical tissue fragments was most rapid; those of endocervical and endometrial tissues grew more slowly.

Cultured squamous cells from ectocervical tissue fragments

LM (Figure 1a): Near the center of the colony the cells were rather small, polygonal and grew in pavement fashion. Near the periphery of the outgrowth, large squamous polygonal cells with a low nucleocytoplasmic ratio were present, some of these cells were found to be eosinophilic by Papanicolaou staining. These findings indicate that the cells had retained the squamous differentiation ability that is observed *in vivo* from the deep toward the superficial layers of the squamous epithelium.

Table 2 Characteristics of uterine epithelial cells grown *in vitro*?

	Endometrium	Ectocervix	Endocervix
LM	spindle cells eccentric nuclei	polygonal cells pyknotic nuclei	spindle cells polygonal cells (squamous meta-plasia)
SEM	microgranules cilia-like structures	microvilli microridges	microgranules microvilli, microridges
TEM (Tonofilament)	little	much	little or much
Histochemistry (Heat-stable ALP)	(−)	(−)	(+)
Chromosome	diploid	diploid	diploid

SEM (Figures 2a–d): The cells overlapped and they were so flat and thin that raised areas appeared to be the nuclear and nucleolar structures of the underlying cells. The surface of most cells was covered by numerous microridges or microvilli; borders between adjacent cells were clearly defined. The cell surfaces of the uppermost cell layers were irregularly wrinkled or smooth, suggesting that these superficial cells were in the process of degeneration, physiological maturation or keratinization.

Where cells grew slightly apart from each other they were sometimes connected by fine cytoplasmic processes reminiscent of the intercellular bridges seen in squamous epithelium *in vivo*.

TEM (Fig. 2e): Microvilli on the cell surface and many desmosome-like complexes at the borders between adjacent cells were often observed. Some nuclei were round or oval with finely distributed nuclear chromatin; other nuclei showed indentations with coarsely distributed chromatin clumps. One or more nucleoli were often present. The cytoplasm was rich in free ribosomes, mitochondria, lysosomes and lipid droplets and often contained a large amount of tonofilament, indicating that the cultured squamous cells retained the *in vivo* characteristics of squamous epithelium.

Cultured glandular cells from endometrial tissue fragments

LM (Figure 1b): Around the center of the colony, there was dense proliferation of small, oval or polygonal cells; near the periphery, short spindle-shaped cells with eccentric nuclei grew in a whorled fashion. The nuclear chromatin pattern was generally finely granular; a conspicuous nucleolus was frequently present. In some of the peripheral cells, vacuoles were observed. These findings suggest that the cultured glandular cells retained their *in vivo* morphological properties.

SEM (Figures 3a–d): Most of the cultured glandular cells grew in single layers, the cells were relatively thick, so that raised nuclear areas were less conspicuous than in cultured squamous cells. The cell surface was covered by numerous short globular microvilli, these tended to be more dense around the central part of the cells; there were many anastomosing long microvilli. The cultured cells appeared to adhere tightly and they manifested clear cell borders. Some cultured glandular cells revealed cilia-like structures which were much longer than the microvilli.

TEM (Figure 3e): Desmosome-like complexes and many microvilli were present on the cell surface. Most of the nuclei were eccentric and showed slight indentation with coarsely distributed chromatin, there usually were one or two nucleoli and nuclear bodies were sometimes detected. Free ribosomes, rough endoplasmic reticulum, lysosomes, lipid droplets, and mitochondria were numerous in the abundant cytoplasm and some Golgi apparati were seen. Tonofilament bundles were less conspicuous in
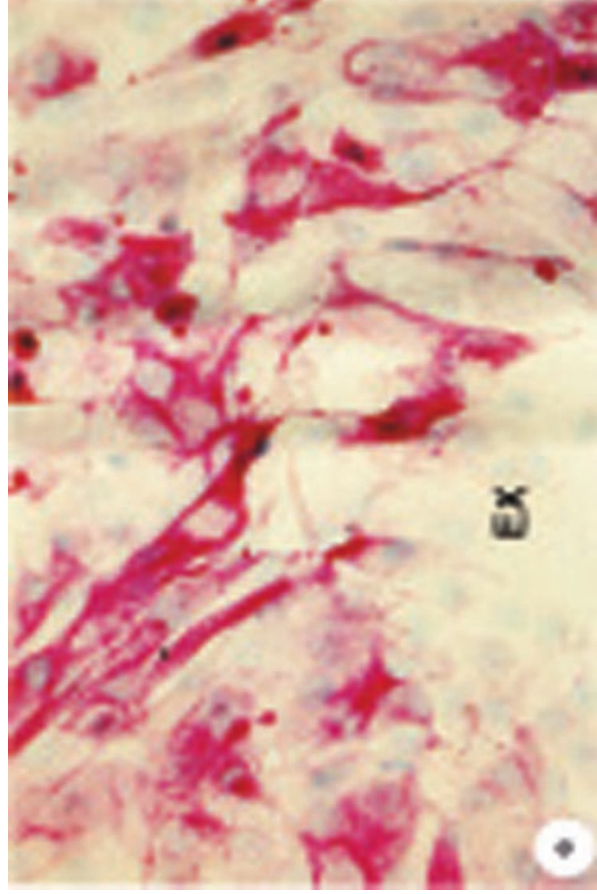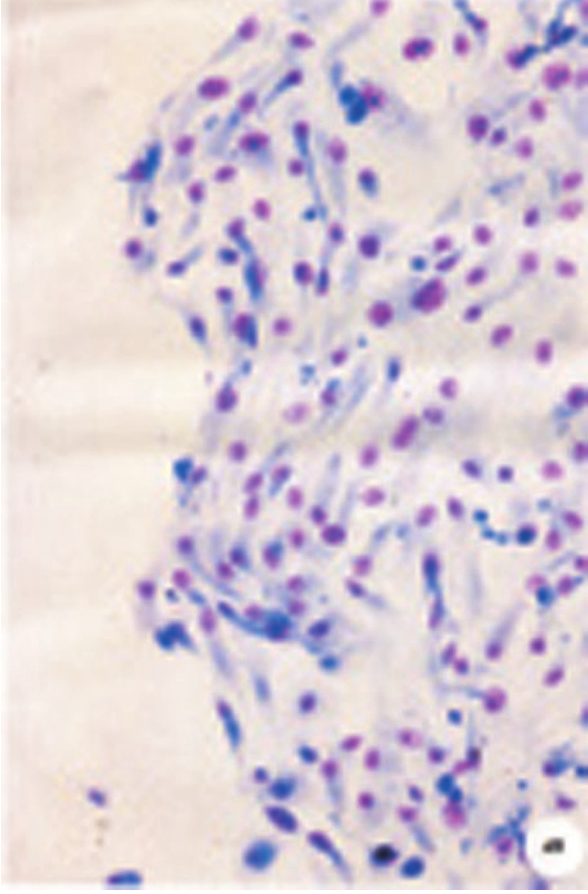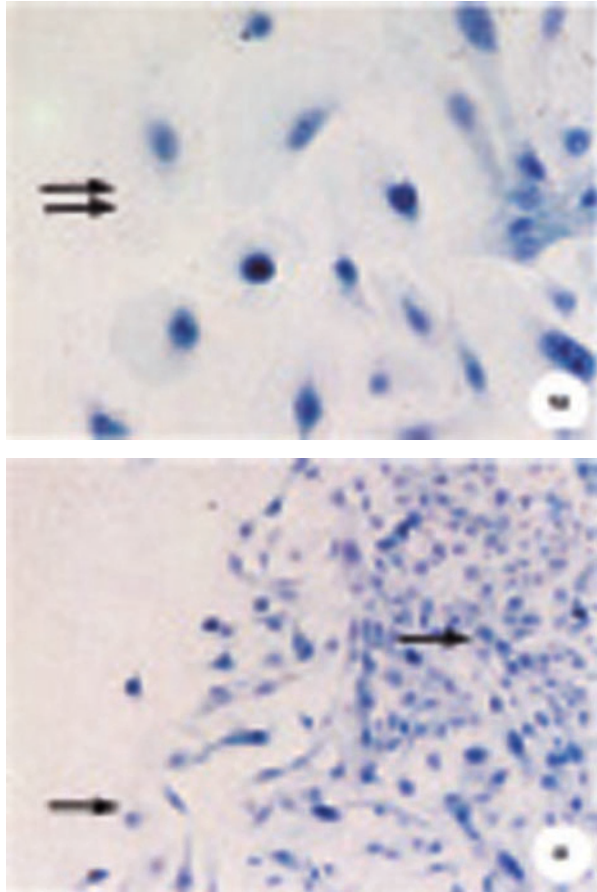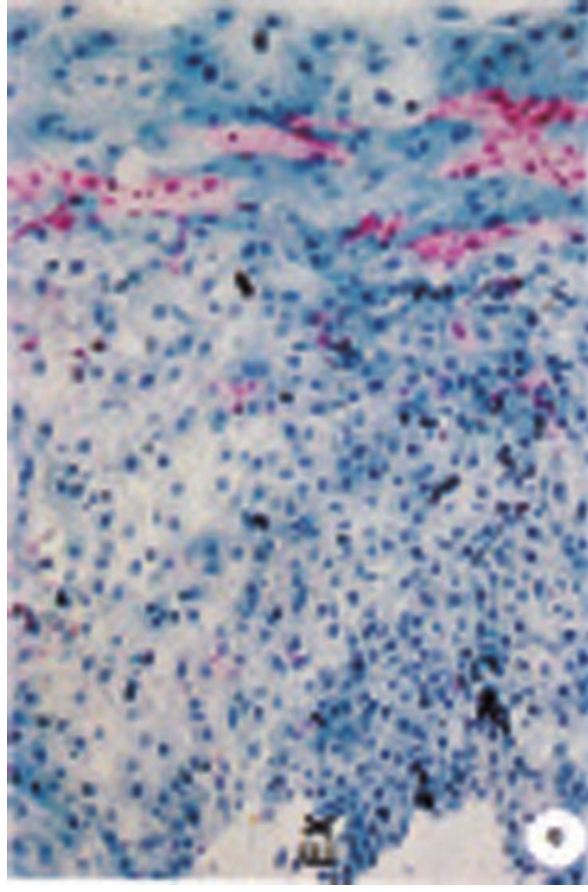
Figure 1

a: (Light micrograph, Papanicolaou stain). Cultured squamous cells from ectocervical tissue fragments. Around the center (EX) of the colony, rather small, polygonal cells grew in pavement fashion; near the periphery of the colony there are large, squamous polygonal cells with a low nucleocytoplasmic ratio; some of these cells were found to be eosinophilic

b: (Light micrograph, Giemsa stain). Cultured glandular cells from endometrial tissue fragments. Around the center of the colony, oval or polygonal small cells grew densely; near the periphery of the colony spindle-shaped cells with eccentric nuclei grew in a whorled fashion

c: (Light micrograph, Papanicolaou stain). Cultured cells from endocervical tissue fragments.

Near the center of the colony, oval or spindle-shaped small cells (↓) resembling cultured glandular cells were in the majority. At the extreme periphery of the colony, large polygonal cells (↓ ↓) resembling cultured squamous cells were observed. Many cells were in a transition stage from glandular-like to squamous cells ('squamous metaplasia' *in vitro*)

d: (Light micrograph, Papanicolaou stain). Higher magnification of Figure 1c. The transition from the glandular-like (↓) to squamous cells (↓ ↓) is obvious

e: (Light micrograph, alkaline phosphatase stain). ALP activity was observed on the plasma membrane of many cultured cells from endocervical tissue fragments. The activity was confirmed to be heat-stable by heat-treatment at 65 °C for 30 min
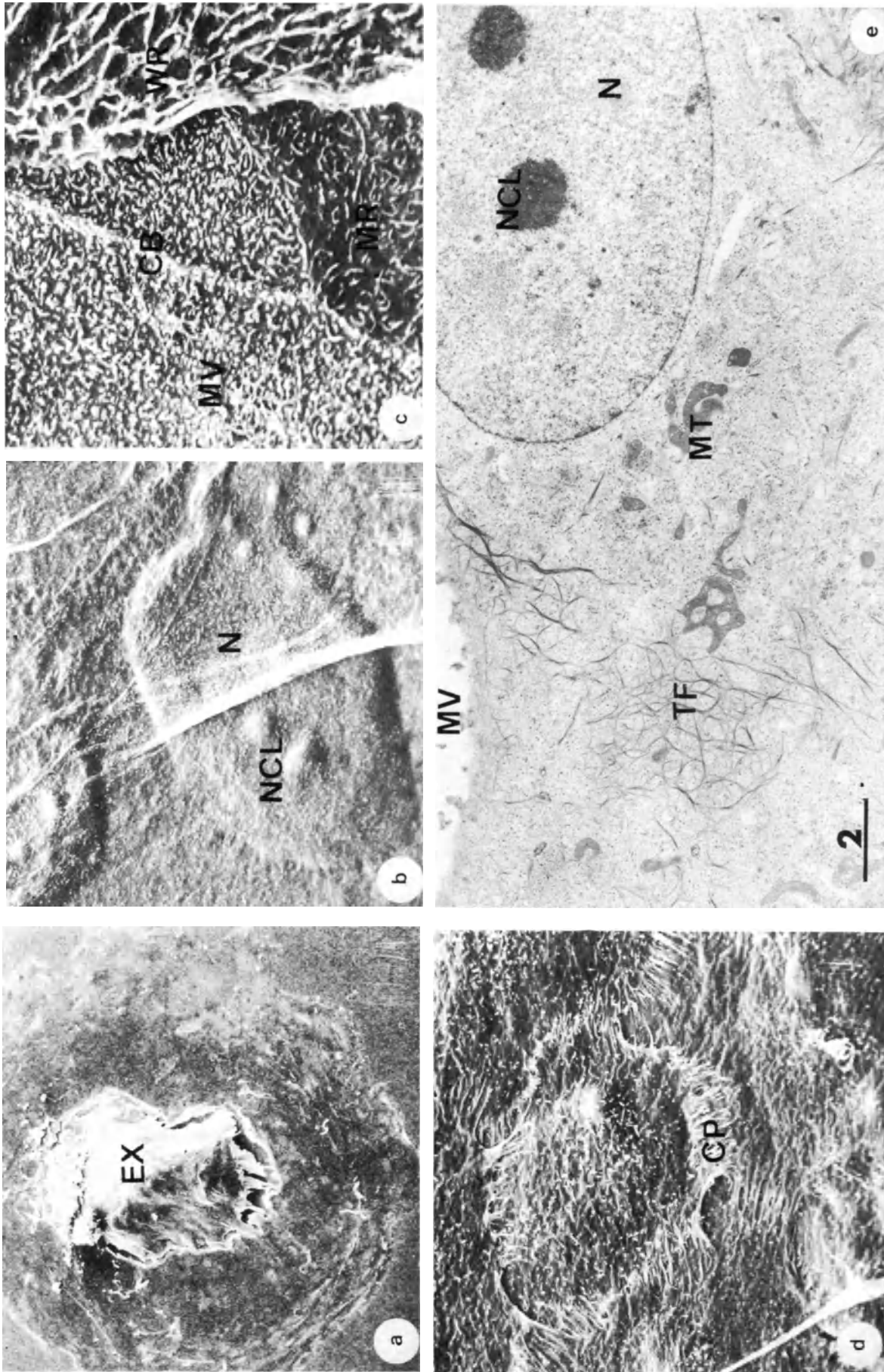
Figure 2

a: (SEM ×200). A colony from ectocervical tissue fragments. In the explant culture, after 3 days of lag phase, epithelial cells grew from all sides of the explant (Ex) edges and formed enlarging circles of actively growing cells

b: (SEM ×2000). Cultured squamous cells from ectocervical tissue fragments. Many of the cells over-lapped; they were so flat and thin that the raised areas suggested nuclear (N) and nucleolar structures (NCL) of underlying cells

c: (SEM ×3000). Cultured squamous cells from ectocervical tissue fragments. The surface of most cultured squamous cells was covered by numerous microridges (MR) or microvilli (MV); there were clear cell borders (CB)

between adjacent cells. The cell surface of the uppermost cell layers showed irregular wrinkles (WR)

d: (SEM ×1000). Cultured squamous cells from ectocervical tissue fragments. The cultured squamous cells were sometimes connected by fine cytoplasmic processes (CP) reminiscent of the inter-cellular bridges seen *in vivo* in squamous epithelium

e: (TEM). Cultured squamous cells from ectocervical tissue fragments. Many microvilli (MV) on the cell surface were present. Some nuclei (N) were oval with finely distributed nuclear chromatin; one or more nucleoli (NCL) were often detected. The cytoplasm was rich in free ribosomes, mitochondria (MT), and often contained a large amount of tonofilament (TF)
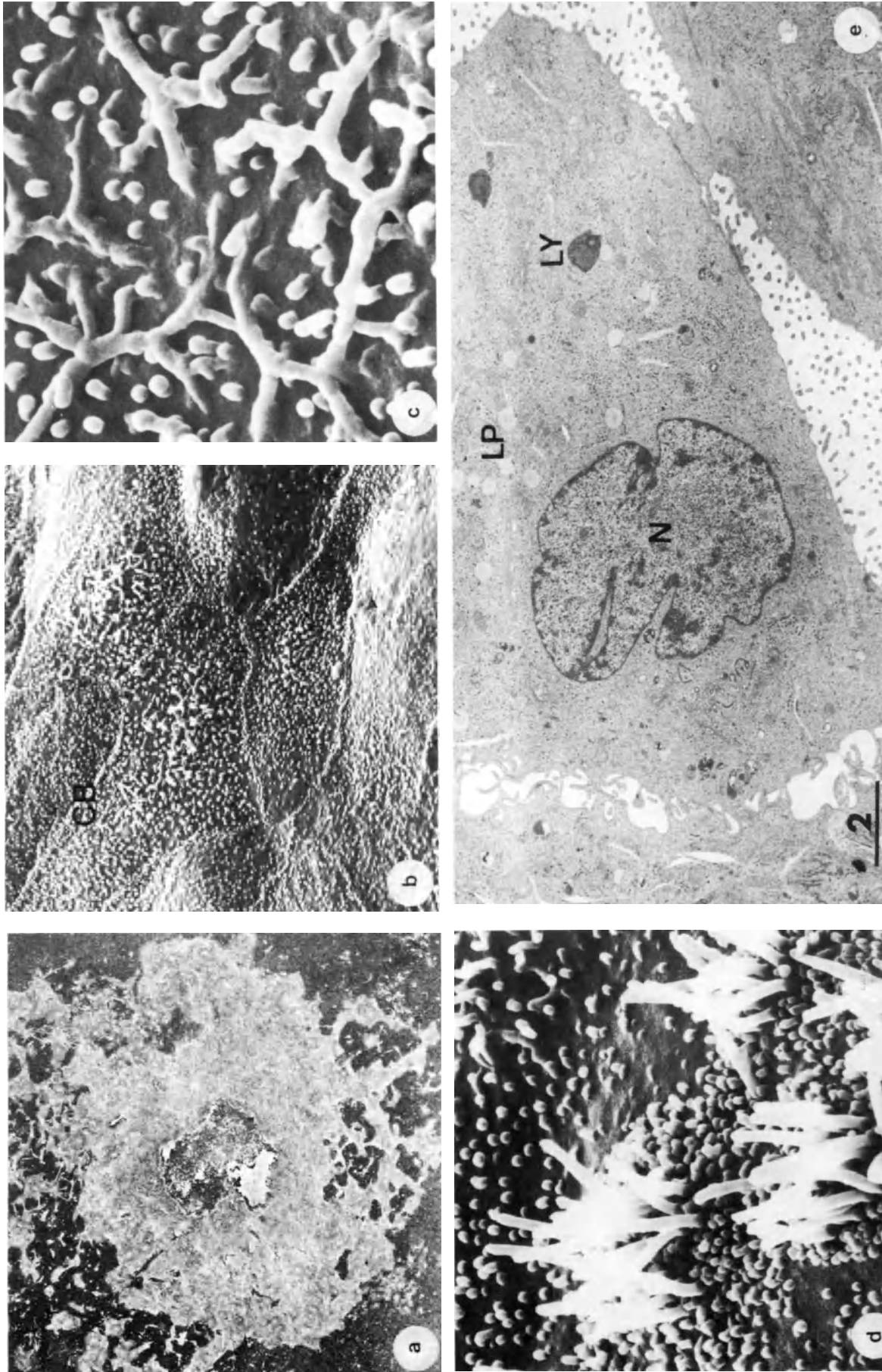
Figure 3

a: (SEM ×200). A colony from endometrial tissue fragments

b: (SEM ×2000). Cultured glandular cells from endometrial tissue fragments. The cultured endometrial glandular cells appeared to adhere tightly, there were clear cell borders (CB) between the cells. Most of the cells grew in a single layer; the cells were relatively thick, so that the raised nuclear areas were less conspicuous than in the cultured squamous cells

c: (SEM ×30 000). Cultured glandular cells from endometrial tissue fragments. The surface was covered by numerous short globular microvilli and anastomosing longer microvilli

d: (SEM ×10 000). Cultured glandular cells from endometrial tissue fragments. Some cilia-like structures, which were much longer than microvilli, were observed. Short globular microvilli tended to be more dense around the center of the cells

e: (TEM). Cultured glandular cells from endometrial tissue fragments. Most of the nuclei (N) were eccentric and showed slight indentation with coarsely distributed chromatin. Free ribosomes, rough endoplasmic reticulum, lysosomes (LY), lipid droplets (LD) and mitochondria were numerous in the abundant cytoplasm
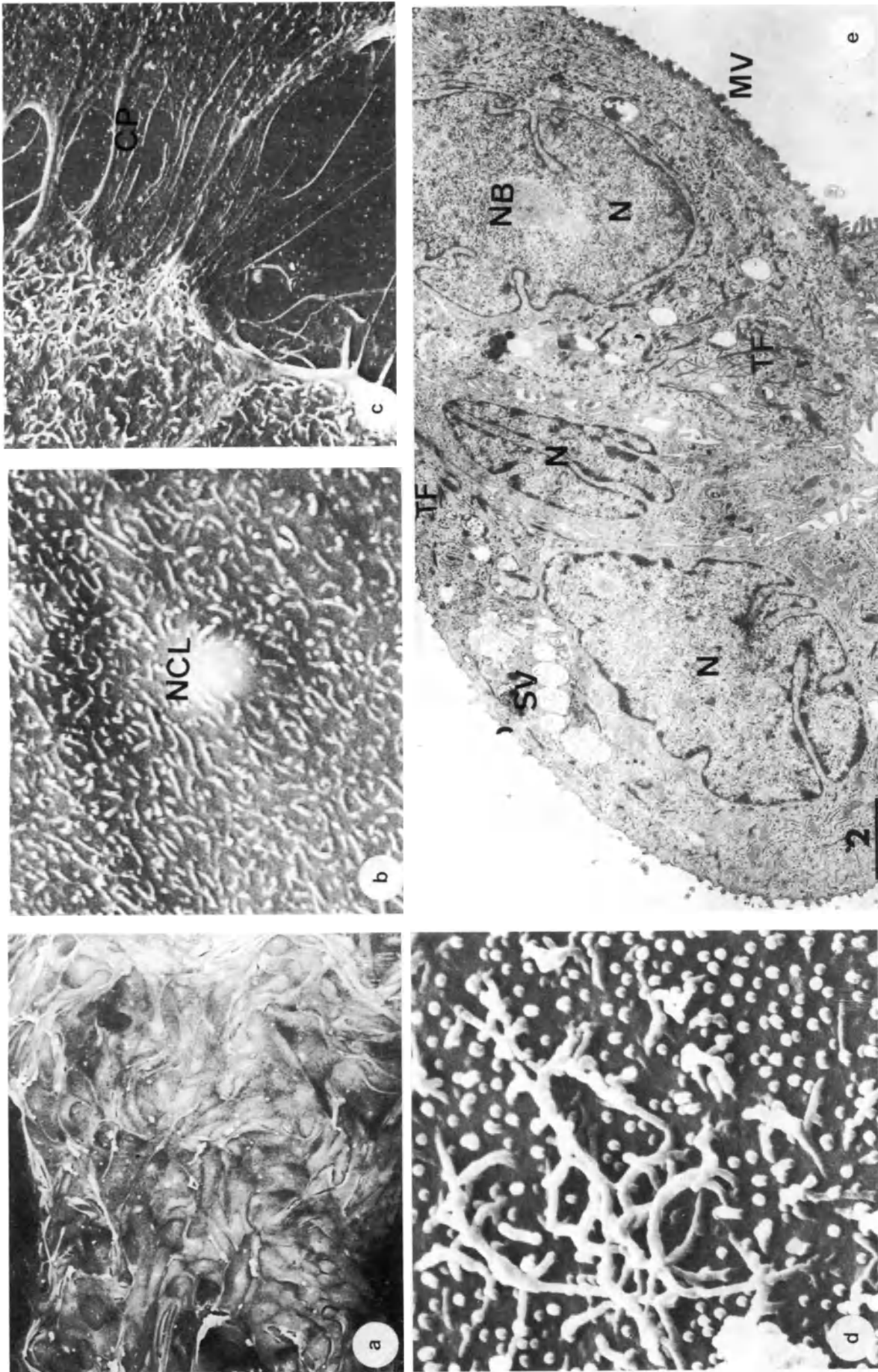
Figure 4

a: (SEM ×300). A colony from endocervical tissue fragments. Cultured cells grew in a whorled fashion

b: (SEM ×3000). Cultured cells from endocervical tissue fragments. SEM revealed two types of cell; one type consisted of large, polygonal thin cells covered with many microridges or microvilli; these closely resembled the cultured squamous cells from the ectocervix. NCL = nucleolus

c: (SEM ×3000). Cultured cells from endocervical tissue fragments. Cells which closely resembled squamous cells were often connected by fine cytoplasmic processes (CP)

d: (SEM ×10 000). Cultured cells from endocervical tissue fragments. The other type of cells consisted of small short spindle-shaped thick cells covered with many short globular microvilli and anastomosing longer microvilli; these closely resembled cultured glandular cells

e: (TEM). Cultured cells from endocervical tissue fragments. TEM also revealed two kinds of cells; glandular-like and squamous cells. Some cells with secretory vacuoles (SV) (observed in only cultured glandular cells) and tonofilament (TF) bundles (a characteristic of squamous cells) were detected around the periphery of the colonies. Some nuclear bodies (NB) were visualized

cultured glandular cells than in cultured squamous cells.

Cultured cells from endocervical tissue fragments

LM (Figures 1c–d): Most of the cells grew in whorled fashion. Around the center of most colonies, oval or short spindle-shaped small cells which resembled cultured glandular cells were in the majority. The nuclear chromatin was finely granular and nucleoli were generally conspicuous. At the extreme periphery of the colonies, polygonal cells with a low nucleocytoplasmic ratio were often observed. Papanicolaou staining revealed that some of these cells with pyknotic nuclei were eosinophilic, suggesting that these large polygonal cells at the extreme periphery had the characteristics of squamous epithelial cells *in vivo* and *in vitro*.

Near the colony periphery, many cells in a transitional stage from small short spindle cells to large squamous cells were observed, indicating that *in vivo* 'squamous metaplasia' could also occur *in vitro*.

SEM (Figures 4a–d): Two types of cells in colonies from endocervical tissues were seen. One type consisted of large, polygonal, thin cells covered with many microridges or microvilli; the cells were often interconnected by fine cytoplasmic processes. These cells closely resembled cultured squamous cells from the ectocervix. The other type consisted of small, short spindle-shaped, thick cells covered with many short globular microvilli and anastomosing longer microvilli.

TEM (Figure 4e): TEM also revealed the presence of two kinds of cells. One type consisted of squamous cells manifesting abundant cytoplasm with a large amount of tonofilament, located around the extreme periphery of the colony. The other type consisted of the short spindle-shaped cells with eccentric nuclei and conspicuous nucleoli, these cells were located around the center of colonies.

Cells with secretory vacuoles (a finding made only in cultured glandular cells) and a large amount of tonofilament (observed in cultured squamous cells) were sometimes detected around the periphery of the colonies.

ALP activity in the colonies (Figure 1E)

When colonies exhibiting non-specific ALP activity in the cell plasma membrane were designated as ALP-positive, 1 of 9 colonies (11%) from ectocervical fragments, 6 of 12 (50%) from endometrial fragments, and 11 of 15 (73%) from endocervical fragments were ALP-positive.

Upon preheating samples at 65 °C for 30 min, colonies from ectocervix and endometrium were ALP-negative, while 5 of 14 (36%) from endocervix were heat-stable ALP-positive. These data suggest that heat-stable ALP in the columnar cells or reserve cells of the uterine cervix was retained also *in vitro*.

Chromosomal analysis revealed that almost all of the cultured cells were normal in chromosome number and karyotype, indicating that they were normal diploid cells.

CAN RESERVE CELLS PROLIFERATE *IN VITRO*?

Our LM, SEM and TEM results showed that squamous and glandular cells derived from ectocervical and endometrial tissue fragments, respectively, proliferated *in vitro*. Furthermore, glandular-like and squamous cells coexisted in the cultures and cells in transition from the former to the latter type of cell ('squamous metaplasia' *in vitro*) were also detected in colonies derived from endocervical tissue fragments. The possibility that these glandular-like cells were contaminating endometrial cells could be ruled out, because the former cells in endocervical colonies manifested heat-stable ALP, which was not found in any endometrial colonies.

Based on these findings, we suggest that reserve cells are present among the endocervical glandular-like cells which retained the ability of 'squamous metaplasia' and manifested heat-stable ALP, representing characteristics of cervical reserve cells.

References

Fink, C. G., Thomas, G. H. and Allen, J. M. (1973). Metaplasia in endocervical tissue maintained in organ culture – an experimental model. *J. Obstet. Gynaecol. Br. Commonw.*, **80**, 169

Flishman, W. H., Inglis, N. R., Stolbach, L. L. and Krant, M. J. (1968). A serum alkaline phosphatase isoenzyme of human neoplastic cell origin. *Cancer Res.*, **28**, 150

Jensen, H., Lyngbye, J. and Davidson S. (1968). Histochemical investigation of the thermostable alkaline phosphatase in the normal full-term placenta. *Acta Obstet. Gynecol. Scand.*, **47**, 436

Nozawa, S., Izumi, S., Ohta, H., Shinozuka, T., Tsutsui, F., Kurihara, S. and Watanabe, K. (1975). Histochemical studies on alkaline phosphatase in uterine cervical reserve cells, precancerous and cancerous lesions. *Proc. 2nd Asian Cancer Conference*, p. 324

Nozawa, S., Ohta, H., Izumi, S., Hayashi, S., Tsutsui, F., Kurihara, S. and Watanabe, K. (1980). Heat-stable alkaline phosphatase in normal female genital organ – with special reference to the histochemical heat-stability and L-phenylalanine inhibition test. *Acta Histochem. Cytochem.*, **13**, 521

Nozawa, S., Ohta, H., Izumi, S., Hayashi, S., Tsutsui, F., Kurhara, S. and Watanabe, K. (1981). Heat-stable alkaline phosphatase in uterine cancer. *Histochem. J.*, **13**, 941

Shingleton, H. M. and Wilbanks, G. D. (1970). Fine structure of normal human cervical squamous epithelium in vitro. *Am. J. Obstet. Gynecol.*, **108**, 28

Vesterinen, E. H., Carson, J., Walton, L. A., Collier, A. M., Keski-Oja, J., Nedrud, J. G. and Pagono, J. S. (1980). Human ectocervical and endocervical epithelial cells in

culture: a comparative ultrastructural study. *Am. J. Obstet. Gynecol.*, **137**, 681

Wilbank, G. D. and Campbell, J. A. (1972). Effect of herpes virus hominis type 2 on human cervical epithelium. Scanning electron microscopic observations. *Am. J. Obstet. Gynecol.*, **112**, 924

13

The fallopian tube in infertility

G. VASQUEZ*, I. A. BROSENS*, S. GORDTS*, W. BOECKX*, and R. M. L. WINSTON†

* The Unit for the Study of Human Reproduction, Katholieke Universiteit, Leuven, Belgium
† Hammersmith Hospital, London, England

Tubal disease is responsible for at least 30% of female infertility (Case and Zuspan, 1969). Inflammatory lesions of the fallopian tubes, mainly the conditions related to specific and non-specific forms of chronic salpingitis lead to a partial or a complete occlusion of the fallopian tubes, and hence to infertility (Dougherty, 1968). Salpingitis may mainly affect the distal portions of the tube (ampulla and fimbriae), causing fimbrial phymosis, hydrosalpinx, pyosalpinx or chronic interstitial salpingitis. When confined to the proximal tube (intramural and isthmic portions) it may lead to cornual or isthmic blockages, luminal obliterations, diverticulosis, including the controversial 'salpingitis isthmica nodosa'. It may also affect the whole tube causing proximally blocked tubes with distal hydrosalpinges.

METHODOLOGY

Biopsies were removed from infertile patients undergoing microsurgical repair of their fallopian tubes in an attempt to restore fertility, and from salpingectomy specimens obtained from unoperable fallopian tubes (ruptured tubal pregnancy) or from total hysterectomies. All biopsy specimens have been studied with a Cambridge Mark II electron microscope, after fixation in 5% buffered glutaraldehyde, dehydration, critical point drying and gold sputtering (Andersen, 1951). The ultrastructural observations have been complemented with post-scanning 1 μm sections in many specimens (Goyens, 1978). The percentages of ciliated surface have been calculated by planimetrical counts on ×500–×1000 magnified scanning electron micrographs (SEM).

FIMBRIAL ADHESION AND PHYMOSIS

As sequelae of pelvic inflammation or in coexistence with ovarian or pelvic endometriosis, the fimbriated folds of the fallopian tube can be agglutinated, show partial adhesions, or may be completely hidden by adhesions, giving rise to a phymosis or a stenotic peritoneal ostium. When fimbrioplasty is performed the removal of adhesions usually reveals a basically normal infundibulum with its concentric folds leading to the ostium. The folds are densely ciliated, more than 50% of the surface being ciliated, which compares favorably with the mean values of 63.5 SD ± 5.9 obtained from normal fimbriae (Brosens and Vasquez, 1976; Vasquez et al., 1980). The individual ciliated cells have long numerous cilia, and non-ciliated cells have a rounded microvillous surface, no different from the normal.

Occasional cells with long microvilli suggesting the 'villous cell' described as a precursor of the ciliated cell (Oberti and Gomez-Rogers, 1972; Oberti et al., 1979) are found on biopsies taken during the follicular phase of the menstrual cycle. In a few biopsies, localized cell hyperplasia in the form of finger-like projections arise from the folds (Figure 1).

HYDROSALPINX

Hydrosalpinx, classically described as a dilated fallopian tube containing clear fluid, is generally accepted to be the end result of a pyosalpinx (Woodruff and Pauerstein, 1969), although it is considered as a dystrophic lesion by others (Park, 1978). Generally bilateral, it always means distally blocked tubes, lacking fimbriae. When cutting the tubal wall to perform a salpingostomy two different situations are met: either thin-walled tubes containing abundant fluid, or thick-walled tubes containing little fluid.

Thin-walled fallopian tubes

These show a marked attenuation, discontinuity, or total absence of the ampullary folds. The mucosal surface is frequently interrupted by areas where epithelial cells are missing, corresponding to the desquamation of individual cells or larger extensions of the mucosal surface.
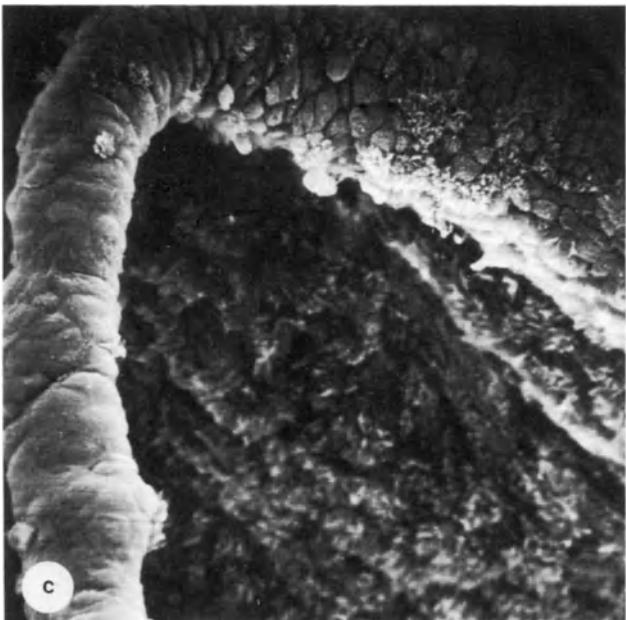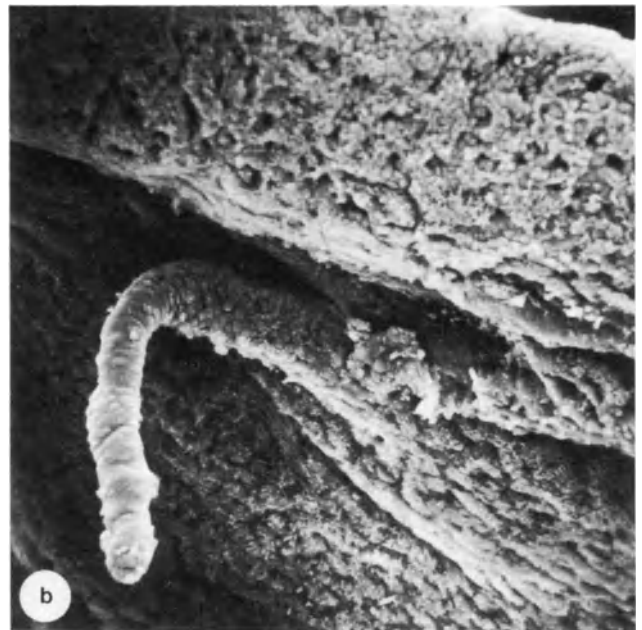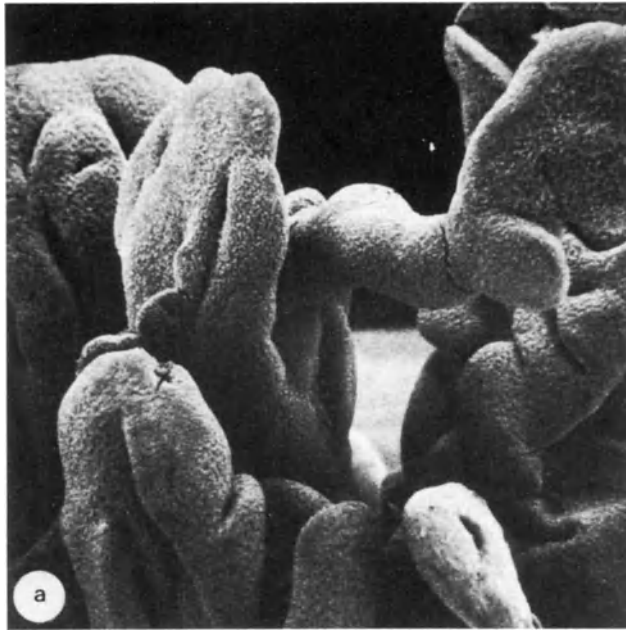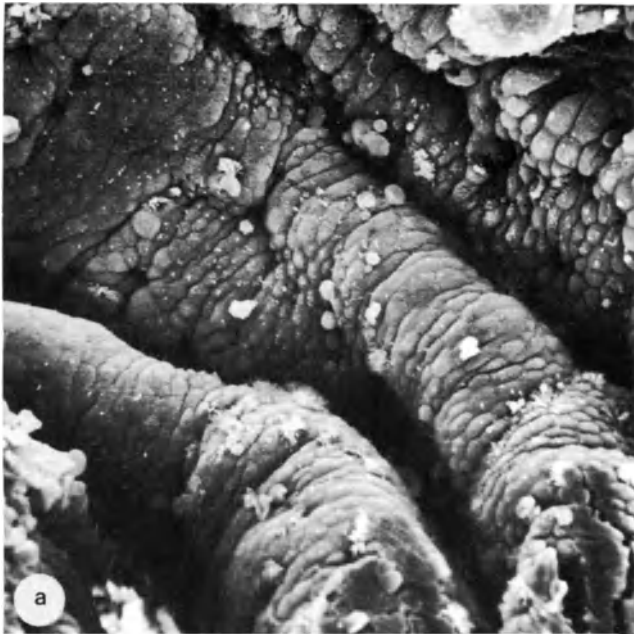
Figure 1
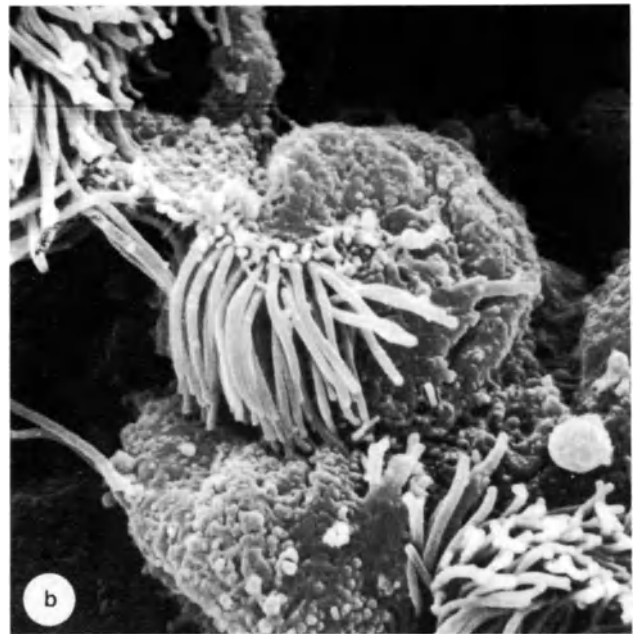
Figure 2 Thin-walled hydrosalpinx
a: Desquamating ciliated cell, with few cilia left on its surface (×4200)

b: Ampullary folds, though attenuated, are present, but their surface is mainly non-ciliated. Ciliated cells are isolated (×436)
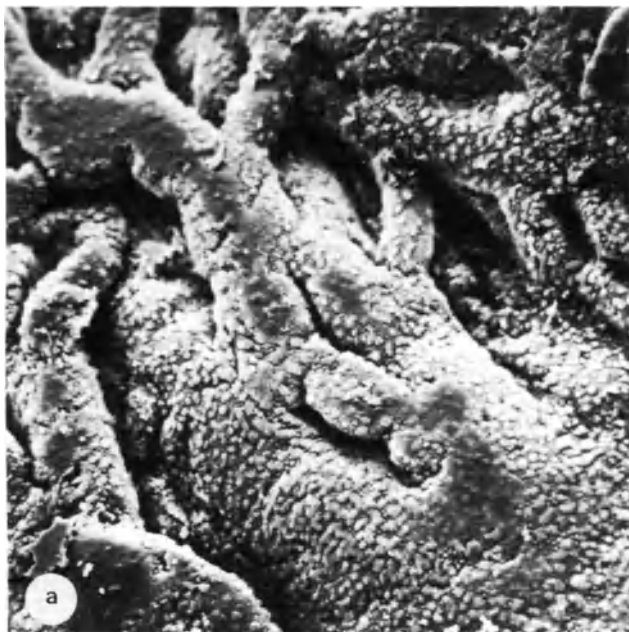

Figure 3 Thick-walled hydrosalpinx
a: Flattened ampullary folds adherent with each other forming bridges and pseudoglandular spaces (×109)

b: Enlargement shows ciliated cells, regularly distributed in small groups or linear pathways among cupoloid non-ciliated cells (×218)

Figure 1 (opposite)
a: Fimbrial biopsy from patient undergoing fimbrioplasty. Pattern of folds is typical of the fimbria (×35)
b: Fimbrial biopsy from another patient undergoing fimbrioplasty. Side of a fold shows a uniform well-ciliated surface, except for the finger-like epithelial projection, where ciliated cells are present only at its base (×184)
c: The finger-like projection shows ciliated and non-ciliated cells, with clear cell boundaries at its base, but the remaining surface is mainly non-ciliated (×462)
d: Circular surfaces of non-ciliated cells with fine microvilli;

long, densely packed cilia cover the surface of ciliated cells. Contaminating red blood cell at the upper left (×882)
e: Cells bearing short rounded microvilli, and others bearing mainly fine elongated microvilli. Few ciliae arise from some of these cells. Three more numerous ciliary bunches are partially seen among these cells (×4620)
f: One 'villous cell' with short cilia, contrasting with the neighbouring long cilia of mature ciliated cells. The microvillous surface at the bottom corresponds to non-ciliated cells (×8820)
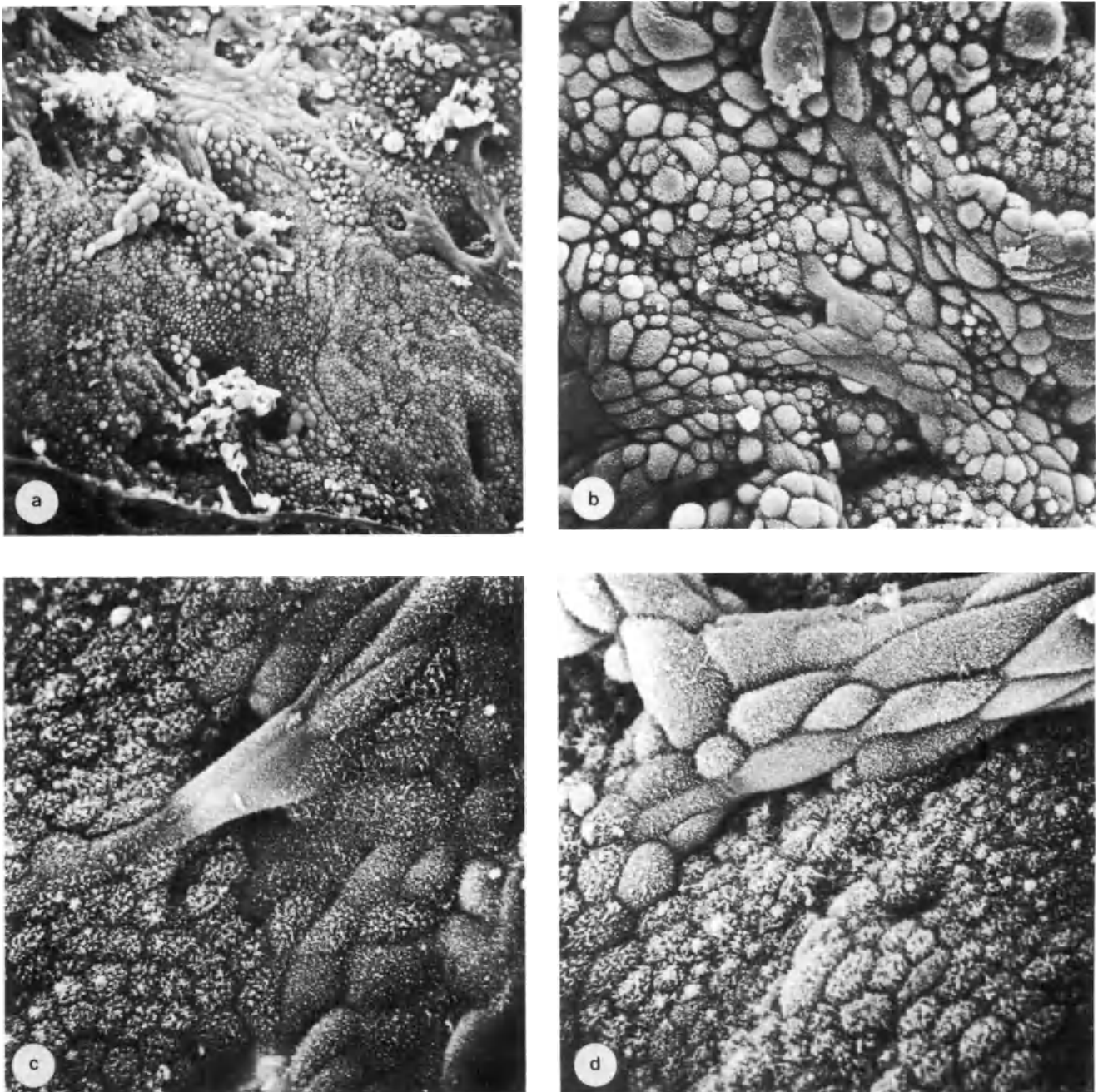
Figure 4

a: Mucosal surface showing numerous small pseudo-glandular spaces (×193)

b: The cells are all non-ciliated with great pleomorphism, small rounded, polygonal, stretched and giant forms (×462)

c: Hyperplastic, stretched cells form a bridge with more rounded cells. Note the difference in microvilli (×1008)

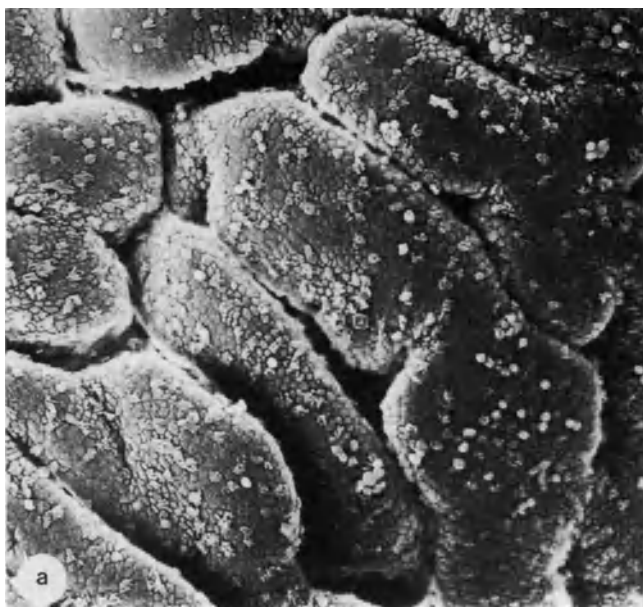d: A cord of hyperplastic cells. In this micrograph, as in the whole biopsy, none of the cells is ciliated (×1008)

Figure 5 Area adjacent to the implantation site (mid-ampulla) of an 8-week pregnancy
a: Folds are attenuated and flattened (×210)

b: Sprouts of trophoblast are seen on the surface of the endosalpinx (×235)

The epithelium shows a decreased population of ciliated cells (mean 32.7%) with additional loss of ciliae from individual cells. In general ciliated cells are more numerous on folded areas. Cells with a single cilium are common. Non-ciliated cells vary greatly: circular, polygonal, or markedly stretched, including giant forms with unclear cell boundaries. Fine microvilli cover most of the non-ciliated cell surfaces, but areas with cells devoid of microvilli or with decreased density of microvilli are frequent (Figure 2).

Thick-walled fallopian tubes

These fallopian tubes, with little or no distension, show higher ampullary folds, though frequently adherent, forming bridges or pseudoglandular spaces.

The mucosal surface is moderately deciliated in most biopsies (mean 45% of ciliated surface). Ciliated cells with a decreased number of ciliae are frequent. Non-ciliated cells usually show a great pleomorphism, with a microvillous surface and occasional blebs of secretion. Desquamation of cells, although present, is less marked than in thin-walled hydrosalpinges (Figure 3). The occasional finding of completely deciliated biopsies, with hyperplastic, adenomatoid cells, most probably corresponds to tuberculous salpingitis (although no tubercles were found on light microscopical sections) (Figure 4).

Tubal pregnancy

The fallopian tube is by far the most frequent localization of an ectopic pregnancy (Pauerstein, 1974), the ampullary portion being the commonest site of implantation (Breen, 1970).

Only a small proportion of tubal pregnancies have a clear anatomic–histologic cause (diverticula, accessory ostia, fistules) and, as first cited by Novak and

Woodruff, 1969, 'we are impressed with the fact that often pregnancy occurs in tubes which otherwise seem normal' (Novak and Woodruff, 1969). The fold pattern in fallopian tubes containing a gestation is normal, except for the separation and flattening of the folds at the area dilated by the gestational sac. Moderate to pronounced deciliation of the fimbriae and ampulla is characteristic and generalized, although more marked in the immediate vicinity of the gestational sac.

Non-ciliated cells are circular with different density of fine microvilli. Groups of cells showing blebs or protrusions on their surfaces, which probably represent secretion, and smaller blebs which may indicate endocytosis (Parr and Parr, 1974; Motta and Andrews, 1976) can be seen in the whole length of the tube, but are more frequent and numerous near the implantation area. Groups of large cells, with flat microvillous surfaces, resembling the squamous transformation of the endometrium during intrauterine pregnancy (Birch and Collins, 1961), are common.

An occasional finding is the focal epithelial hyperplasia, in the form of finger-like projections. Desquamation of individual cells and groups of cells, although generalized, is more common near the implantation site (Figures 5 and 6).

Sterilization

Tubal sterilization means a mechanical or thermic interruption of the fallopian tubes. In the last few years, interest has grown in the degree of integrity of the fallopian tubes after sterilization due to the increasing demand of reversal of sterilization. New sterilization techniques have been developed to meet the demands of simplicity, high safety and minimal tissue loss for potential reversibility (Brosens and Winston, 1978). Post-sterilization mucosal changes are
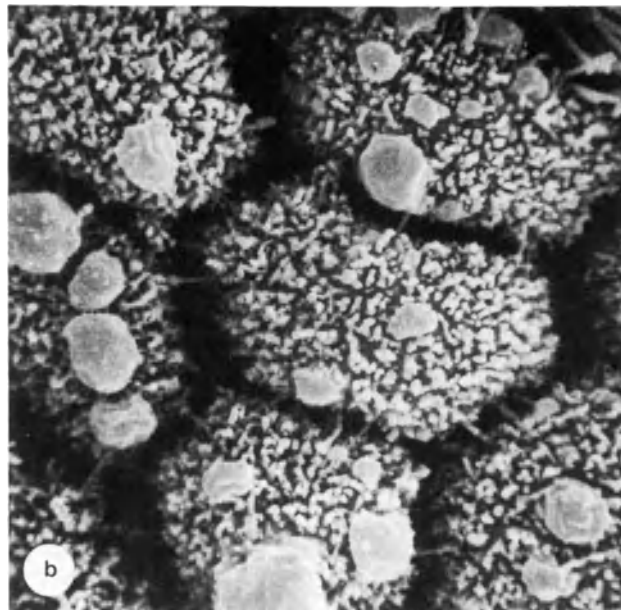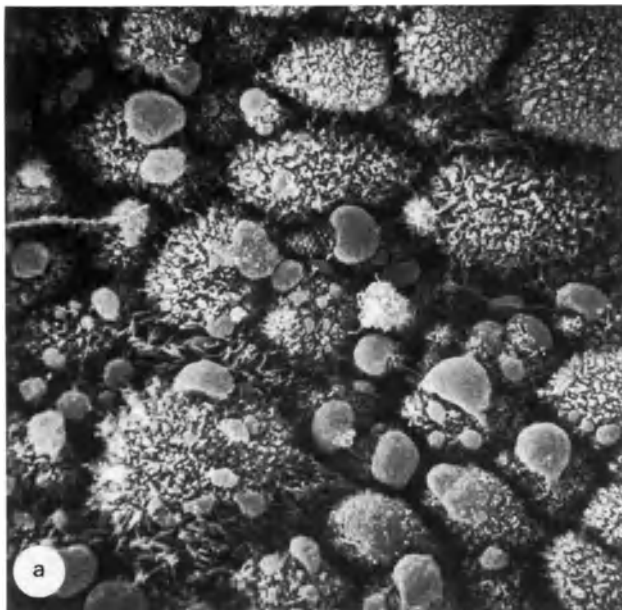
Figure 6 Ampullary biopsy of a 7-week ampullary pregnancy implanted at the ampullary isthmic junction
a: Area adjacent to the implantation site shows cells with apical protrusions, which probably represent endocytosis (×1512)

b: Enlargement of the previous area shows the relationship of the protrusions with the cell surface (×3780)

specially confined to the segment between the sterilization site and the uterus (Vasquez *et al.*, 1980) This segment, usually isthmic, may develop separation, attenuation or complete flattening of the mucosal folds. The epithelium may show well-outlined areas of deciliation which are not larger than 180×150 μm. Rounded or finger-like polypoid formations are a feature in many of these segments. They can be unique or multiple and measure 40–600 μm in height and 25–300 μm in width. They are lined by columnar ciliated and non-ciliated cells with underlying connective tissue but no glandular structures. Flattening of folds, deciliation and polyposis are more common in patients sterilized for more than 5 years. The segment of tube distal to the sterilization site is essentially normal with no alterations of the fold pattern, no polyps and normal ratios of ciliated cells (Figure 7).

In most of the above-described tubes catgut ligature or electrocoagulation had been used as sterilization technique. Preliminary studies suggest that mechanical methods of sterilization (rings, clips) are more frequently associated with normal endosalpinx up to the immediate vicinity of the occlusion (Figure 8), which is in agreement with a good prognosis post-reversal (Boeckx *et al.*, 1977; Winston, 1980).

Isthmic and cornual blocks

The most common feature of blocked segments of isthmus or cornua has been the presence of diverticulae. Many of them show a connection with the tubal lumen and a variable degree of muscular hyperplasia and hypertrophy, fulfilling the microsopical characteristics of salpingitis isthmica nodosa, the typical macroscopic nodular form being a rarer finding (Kistner, 1979).

Other blocked cornua show small multiple, mucosal

polyps, lined by ciliated and non-ciliated cells. These polyps measure 25–100 μm in length and 10–40 μm in width. They may be a hyperplastic response to inflammation, but they may also be secondary to the blockage, as similar structures have been found in sterilized tubes (Vasquez *et al.*, 1980) (Figure 9).

The presence of endometrial stroma, suggesting endometrial colonization, has been a less frequent finding, although it has been claimed as the most frequent underlying pathology of cornual blockages by other authors (Salat-Baroux *et al.*, 1980).

Intramural polyps

Intramural polyps, measuring 0.5–2 cm in length, are a possible cause of infertility when they are bilateral (Bret and Grepinet, 1967). They are orientated longitudinally along the length of the intramural portion of the tube, with their tips toward the distal lumen and a usually large implantation area toward the uterine end. Their epithelial surfaces have typical ciliated and secretory cells. The presence of gland-openings reveals their endometrial origin, which is confirmed by the stroma and glandular structures when sectioned. Mitoses and re-epithelialization, starting from the glandular collars, suggest their active condition (Figure 10).

CONCLUDING REMARKS

SEM has permitted a better understanding of the different surfaces which come in contact and interact with the ovum, the spermatozoa and the fertilized egg during their passage through the fallopian tube. Inflammation, and its sequelae, alter the complex structure of the oviduct, the surgical correction is not
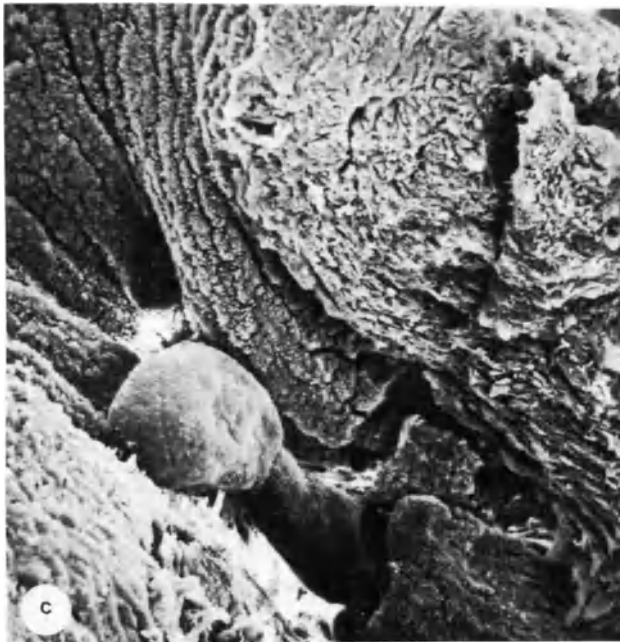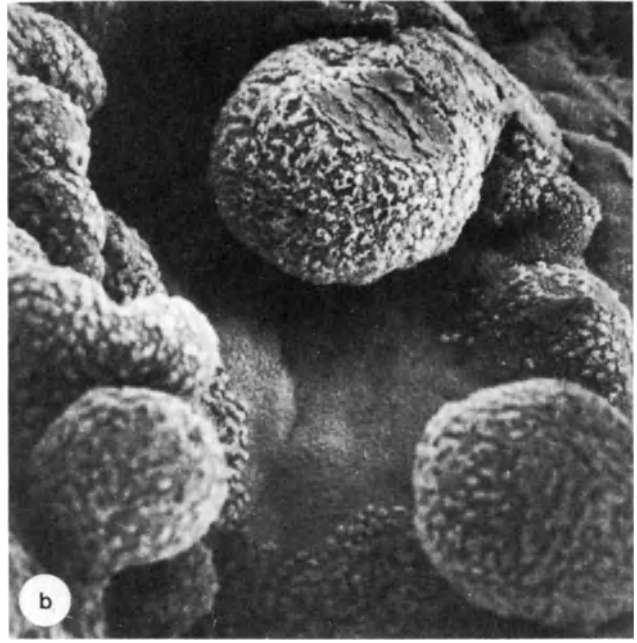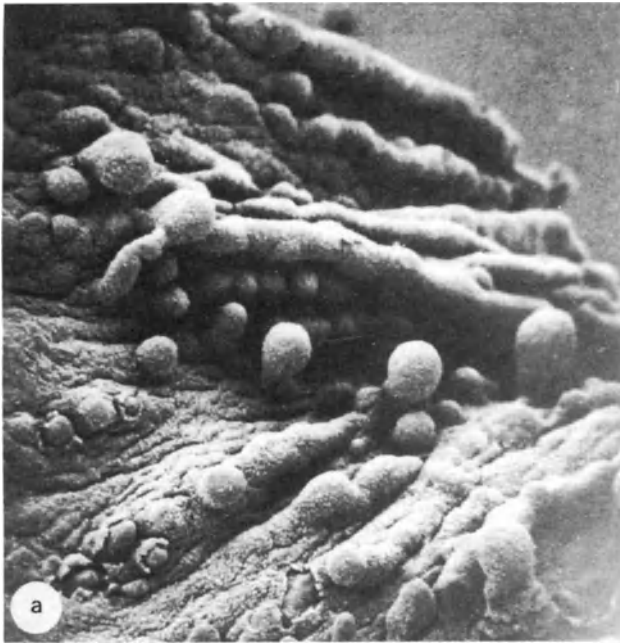
Figure 7

a: Proximal segment, isthmus close to the ampullary isthmic junction. Patient had a catgut ligature 5 years before. Numerous rounded polyps arise from the folds or on flattened areas (×44)

b: Higher-power view of the proximal segment of the opposite oviduct, shows three polyps with ciliated and non-ciliated surface. Note that the polyps are surrounding a completely deciliated area (×160)

c: Polyp at proximal segment, 5 years after Pomeroy sterilization. Folds have disappeared on this segment (×84)

d: Polyp at proximal segment 7 years after tubal ligature (×97)
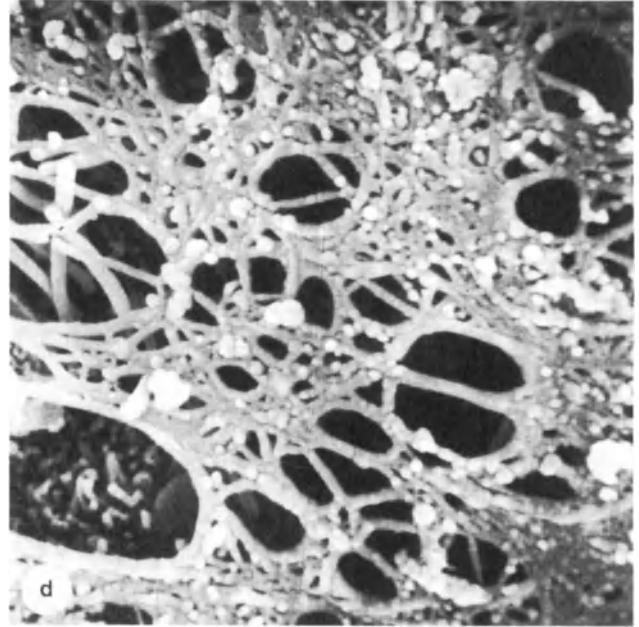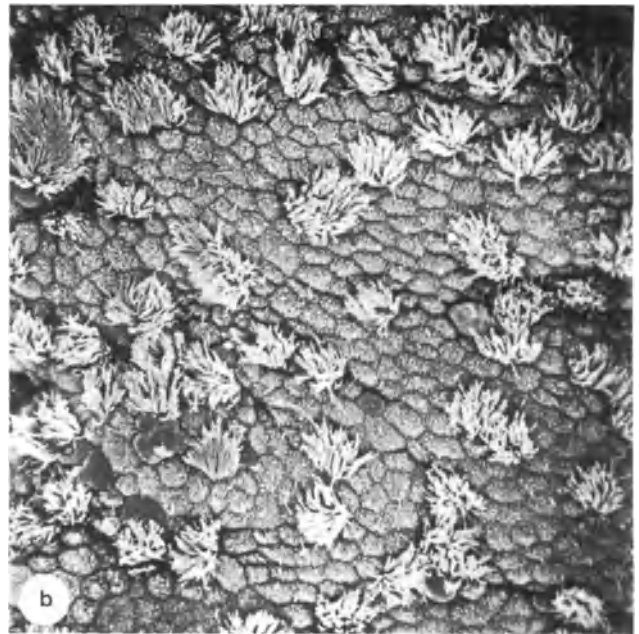
Figure 8 Segment of fallopian tube, proximal to a Falope-ring, 3 years after sterilization

a: Falope-ring on the isthmic segment ($\times 17$)

b: The distribution of cells is normal for the isthmus, with ciliated cells and more numerous non-ciliated cells ($\times 756$)

c: Cilia are well-developed. Non-ciliated cells show microvilli. Microvilli are scarce in three cells ($\times 4030$)

d: Mucus forming a network covers this area, ciliary tips come through mucus openings at the left, and microvilli from a non-ciliated cell are visible at the lower left ($\times 7560$)

Figure 9 Cornual biopsy from patient with bilateral cornual blocks
a: Two of the three polyps found at the cornua (×168)
b: Enlargement shows surface of the polyps with ciliated and

non-ciliated cells, and the walls of the intramural lumen of the oviduct with characteristic pattern of cells (non-ciliated with apical secretion, and few ciliated cells) (×403)

Figure 10 Intramural polyp
a: Low magnification (×17)

b: Enlargement of one glandular collar, with its opening, permitting a view of its epithelial lining, mainly non-ciliated (×378)

always followed by a resumption of normal function. The loss of mucosal folds and ciliated surface from the fimbriae and ampulla may decrease the efficiency of ovum transport, and explain the discrepancy between patency rate and pregnancy rate, after reconstructive tubal surgery (Winston, 1980). The possibility of assessing minute intratubal damage such as deciliation, micropolyposis or alterations of fold relationship may help to understand an unexplained infertility in association with a macroscopically 'normal' fallopian tube, or furthermore explain the pathogenesis of a tubal gestation.

References

Andersen, T. F. (1951). Techniques for the preservation of three-dimensional structures in preparing specimens for the electron microscope. *Trans. NY Acad. Sci.*, Ser-II, **13**, 130

Birch, H. W. and Collins, C. G. (1961). Atypical changes of genital epithelium associated with ectopic pregnancy. *Am. J. Obstet. Gynecol.*, **81**, 1198

Boeckx, W., Vasquez, G. and Brosens, I. (1977). Reversibility of tubal ring sterilization. *Contraception*, **5**, 505

Breen, J. L. (1970). A 21 year survey of 654 ectopic pregnancies. *Am. J. Obstet. Gynecol.*, **106**, 1004

Bret, A. J. and Grepinet J. (1967). Polypes endométriaux de la portion intramurale de la trompe. Leur rapport avec la stérilité et l'endométriose. *Sem. Hôp. Paris*, **43**, 183

Brosens, I. A. and Vasquez, G. (1976). Fimbrial microbiopsy. *J. Reprod. Med.*, **16**, 171

Brosens, I. A. and Winston, R. M. L. (1978). *Reversibility of Female Sterilization*. (London: Academic Press)

Case, A. L. and Zuspan, F. P. (1969). Infertility. *Surg. Clin. N. Am.*, **49**, 121

Dougherty, C. M. (1968). Diseases of the fallopian tube. In Dougherty, C. M. (ed.) *Surgical Pathology of Gynecologic Disease*, p. 425. (New York: Harper & Row)

Goyens, K. (1978). Post-scanning. *T. Belg. Veren. Laboratoriumtechn.*, **5**, 141

Kistner, R. W. (1979). The oviduct. In Kistner, R. W. (ed.) *Gynecology Principles and Practice*, 3rd edn, p. 312. (Chicago: Year Book Medical Publishers)

Motta, P. and Andrews, P. M. (1976). Scanning electron microscopy of the endometrium during the secretory phase. *J. Anat. (London)*, **122**, 315

Novak, E. R. and Woodruff, J. D. (1969). Ectopic pregnancy. In Novak, E. R. and Woodruff, J. D. (eds). *Novak's Gynecologic and Obstetric Pathology*, 6th edn, p. 432. (Philadelphia: W. B. Saunders)

Oberti, C. and Gomez-Rogers, C. (1972). De novo ciliogenesis in the human oviduct during the menstrual cycle. In Velardo, J. T. and Kasprow, E. A. (eds). *Biological Reports: Basic and Clinical Studies*, p. 241. Pan American Congress of Anatomy III, New Orleans

Oberti, C., Zanartu, J., Vasquez, G., Brosens, I. and Robertson, W. B. Ultrastructural changes in the human oviduct epithelium during the puerperium and lactation. In Beller, F. K. and Schumacher, G. F. B. (eds). *Biology of the Fluids of the Genital Tract*, p. 361. (North Holland, New York: Elsevièr)

Park, W. W. (1978). Lesions of the uterine tube. In Brosens, I. A. and Winston, R. M. L. (eds), *Reversibility of Female Sterilization*, p. 21. (London: Academic Press)

Parr, M. B. and Parr, E. L. (1974). Uterine luminal epithelium; protrusions mediate endocytosis, not apocrine secretion, in the rat. *Biol. Reprod.*, **11**, 220

Pauerstein, C. J. (1974). Tubal pregnancy. In Zuspan, F. P. (ed.), *The Fallopian Tube: a Reappraisal*, p. 92. (Philadelphia: Lea & Febiger)

Salat-Baroux, J., Cornier, E. and Coutourier, J. Y. (1980). Obstruction pathologique de la portion initiale de l'isthme tubaire. Analyse de 50 interventions microchirurgicales. *J. Gynecol. Obstet. Biol. Reprod.*, **9**, 579

Vasquez, G., Winston, R. M. L., Boeckx, W. and Brosens, I. (1980). Tubal lesions subsequent to sterilization and their relation to fertility after attempts at reversal. *Am. J. Obstet. Gynecol.*, **138**, 86

Vasquez, G., Winston, R. M. L., Boeckx, W. and Brosens, I. A. (1981). The epithelium of human hydrosalpinges: a light optical and scanning electron microscopic study. (In press)

Winston, R. M. L. (1980). Microsurgery of the fallopian tube. From fantasy to reality. *Fertil. Steril.*, **34**, 521

Woodruff, J. D. and Pauerstein, C. J. (1969). Non granulomatous salpingitis. In Woodruff, J. D. and Pauerstein, C. J. (eds), *The Fallopian Tube, Structure, Function, Pathology and Management*, p. 117. (Baltimore: Williams & Wilkins)

14

Fetal ovary

S. MAKABE* and P. M. MOTTA†

* Department of Obstetrics/Gynecology, Toho University School of Medicine, Tokyo, Japan
† Department of Anatomy, Faculty of Medicine, University of Rome, Italy

Superficial epithelium of the ovary undergoes morphodynamic changes which are related to the cyclic functions of the gonads, such as ovulation, transport of fluids and proliferation (Motta et al., 1971; Nilsson and Munshi, 1973; Motta and Van Blerkom, 1975, 1979; Cajander, 1976; Hafez et al., 1980).

Research carried out on the role of the superficial epithelium during ovarian differentiation indicates that it may give origin to 'germinal cords' (sex cords), and thus contribute to the formation of somatic cells such as follicular cells (Mossman and Duke, 1973; Guraya, 1977; Byskov, 1980) and interstitial cells (Mori and Matsumoto, 1970; Motta, 1974; Guraya, 1977; Guraya and Motta, 1980).

OVARIES BETWEEN 12 AND 16 WEEKS OF GESTATION

In these stages of development the sex cords appear in the cortical areas of the human ovary as irregular masses and are composed of both germ (germblasts) and somatic (somatoblasts) cells. A delicate basal lamina with scanty collagen fibrils separates the cords from the intercellular stroma of the ovarian tissue. The surface of the ovary exhibits invaginations highly variable in number and size (crypts). The apical surface of the ovarian epithelium displays various numbers of short microvilli, blebs, ruffles and long solitary cilia (Hafez et al., 1980; Makabe, 1981).

Closely associated to the crypts large solitary cells were observed. They have a rounded shape and a relatively smooth surface showing only a few short microvilli. As shown by correlating scanning electron microscopy (SEM) with transmission electron microscopic (TEM) results, these cells correspond to germ cells intermingled with somatic cells and contained in the subsurface areas of the superficial epithelium.

OVARIES BETWEEN 16 AND 24 WEEKS OF GESTATION

At this time of development the surface epithelium is often composed of several layers of cells. A basal lamina covers the epithelium and in some areas the nascent tunica albuginea apparently marks the separation between the surface epithelium and the cortical tips of the subjacent sex cords. Furthermore in several zones the sex cords contained in the cortex of the ovary are clearly continuous with the ingrowths of the proliferating surface epithelium and here both structures (cords and surface epithelium) are covered by a continuous and delicate basal lamina. The surface epithelium is irregularly shaped due to the superficial cells forming small projections (papillae) or infoldings (crypts), both of which are proliferative expressions of numerous mitoses occurring in the multilayered epithelium.

Germ cells exhibiting a large rounded shape are clearly distinguishable not only in the sex cords but also in the subsurface areas of the ovary within the surface epithelium. In both cases germ cells show ameboid evaginations and are closely associated to the somatic cells. These morphological dynamic features of surface and cords of the developing ovary in human are most likely an expression of a high process of proliferation and migration of germ as well as somatic cells. These proliferative and migrative phenomena apparently occur in two opposite directions, i.e.: from the cortex of the ovary to its exposed surface and from here to the subjacent cortical areas.

OVARIES BETWEEN 24 AND 38 WEEKS OF GESTATION

The ovary appears elongated and irregularly infolded in sulci and plicae, thus assuming a characteristic lobular
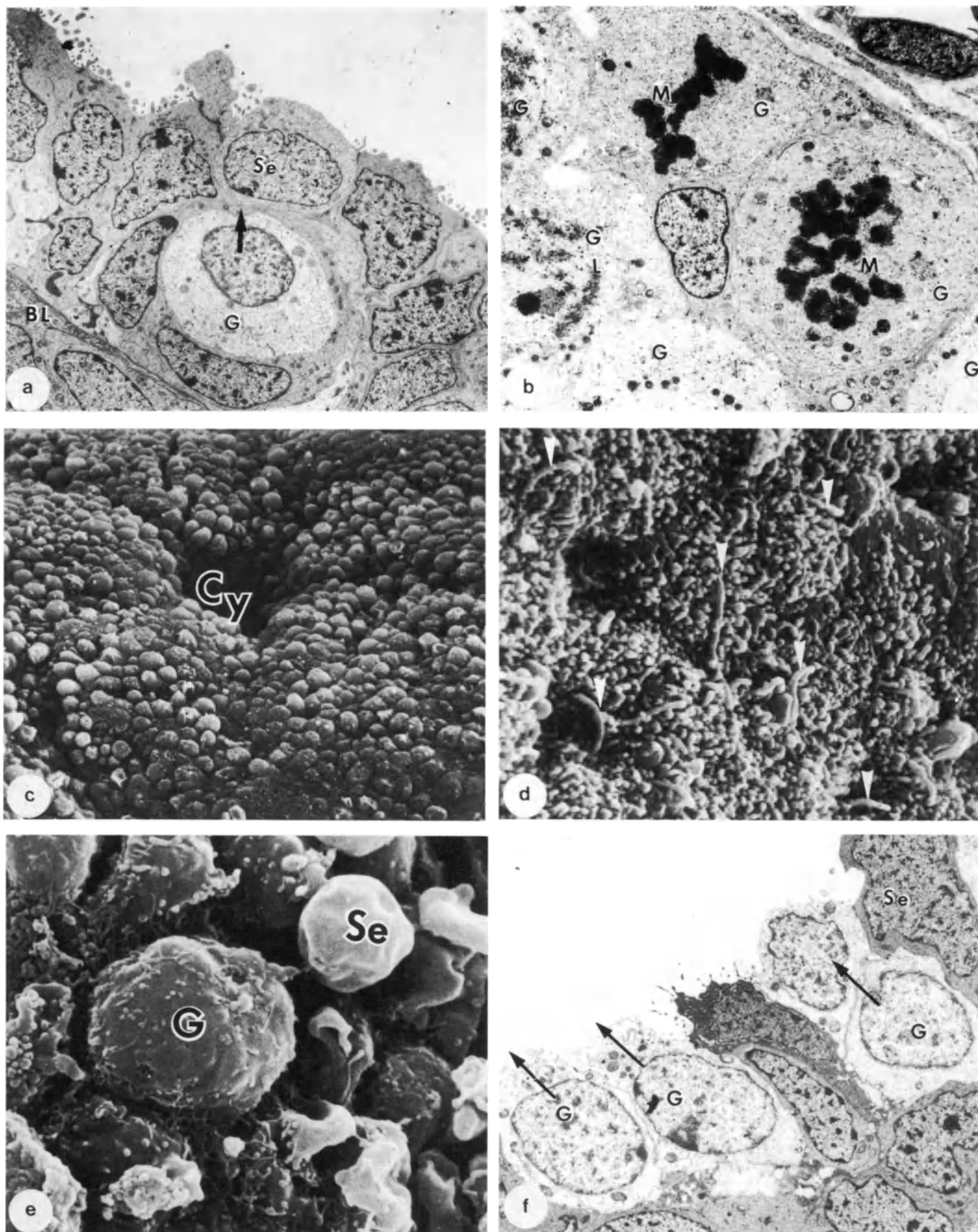
Figure 1 Human ovaries between 12 and 16 weeks of gestation

a: Proliferation of superficial epithelial cells (Se) continuous with cords by interposition of a delicate basal lamina (BL). The germ cells (G plus arrow) are intermingling with somatic cells and are located within the surface epithelium (TEM×1500)

b: Germ cells (G) in mitosis (M) (TEM×3000)

c: The surface of the ovary exhibits invaginations (crypts) of various size (Cy) (SEM×500)

d: The apical surface of the ovarian epithelium is displaying various short microvilli and long solitary cilia (arrows) (SEM×3000)

e: A large rounded cell having a relatively smooth surface is associated with a number of small superficial cells (Se). This corresponds to a migrating germ cell (G) (SEM×4000)

f: Desquamating and migrating germ cells (G) emerging (arrows) onto the ovarian surface (Se) (TEM×3000)
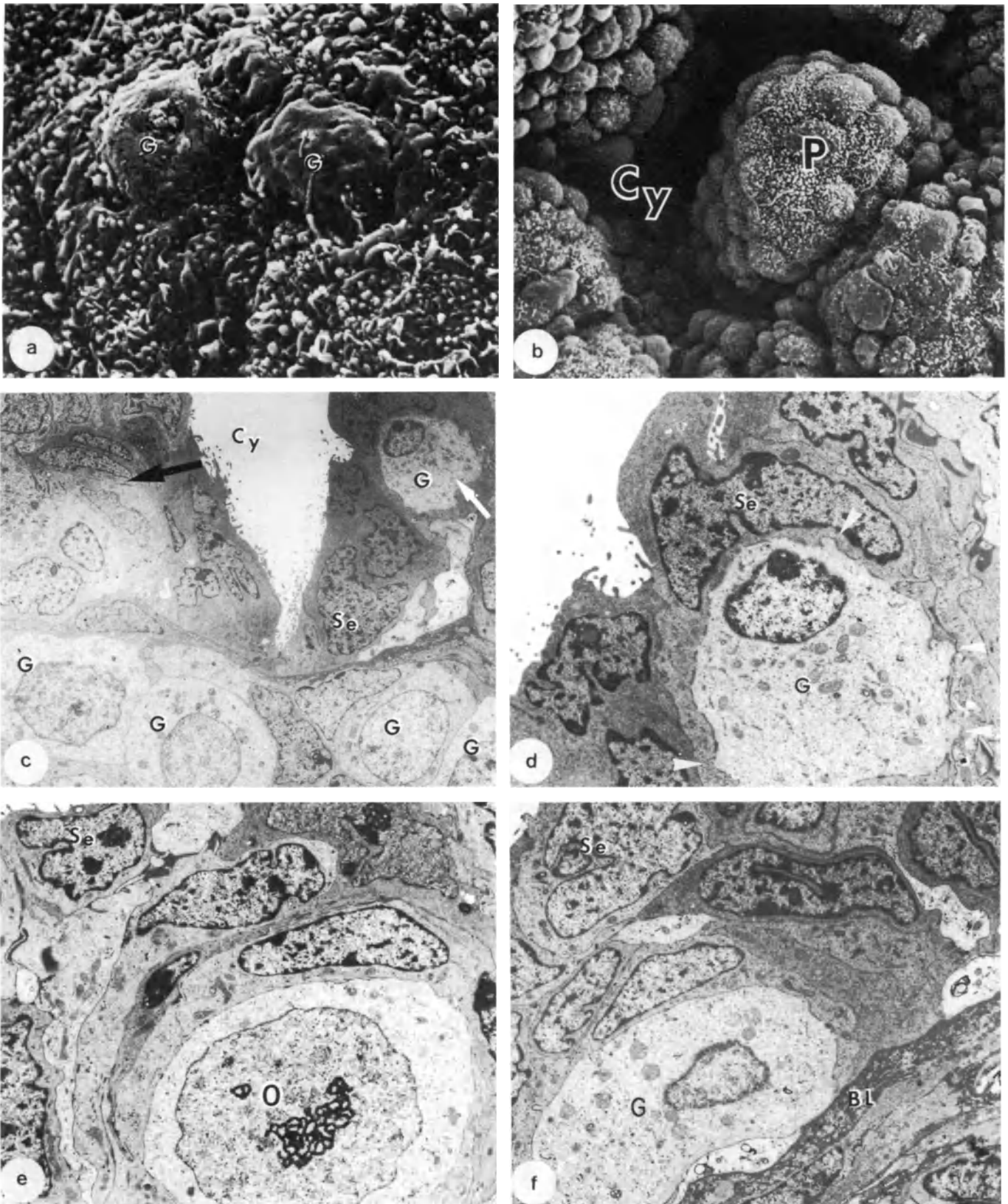
Figure 2 Human ovaries between 16 and 24 weeks of gestation

a: Germ cells (G) which have migrated to the surface of the ovary (SEM×4000)

b: Surface of the ovary exposing papillae (P) and crypts (Cy). See also Figure 2c for TEM correlation (SEM×1000)

c: The surface epithelium (Se) is composed of several layers of cells which have proliferated to form crypts (Cy). Germ cells (G) are intermingled with somatic cells of the crypts (arrows) (TEM×1500)

d: Higher magnification of the white arrow area in Figure 2d. Note the ameboidal appearance of the germ cell (G, plus arrows) in the superficial layer (Se) and the eccentric location of the nucleus of the germ cell (TEM×4800)

e: A clearly distinguishable oogonium (O) surrounded by developing granulosa cells is located within the surface epithelium (Se) (TEM×3600)

f: Area similar to that shown in Figure 2d. Note the well-developed basal lamina (BL) underlying the surface epithelium (Se); G = germ cell (TEM×3600)
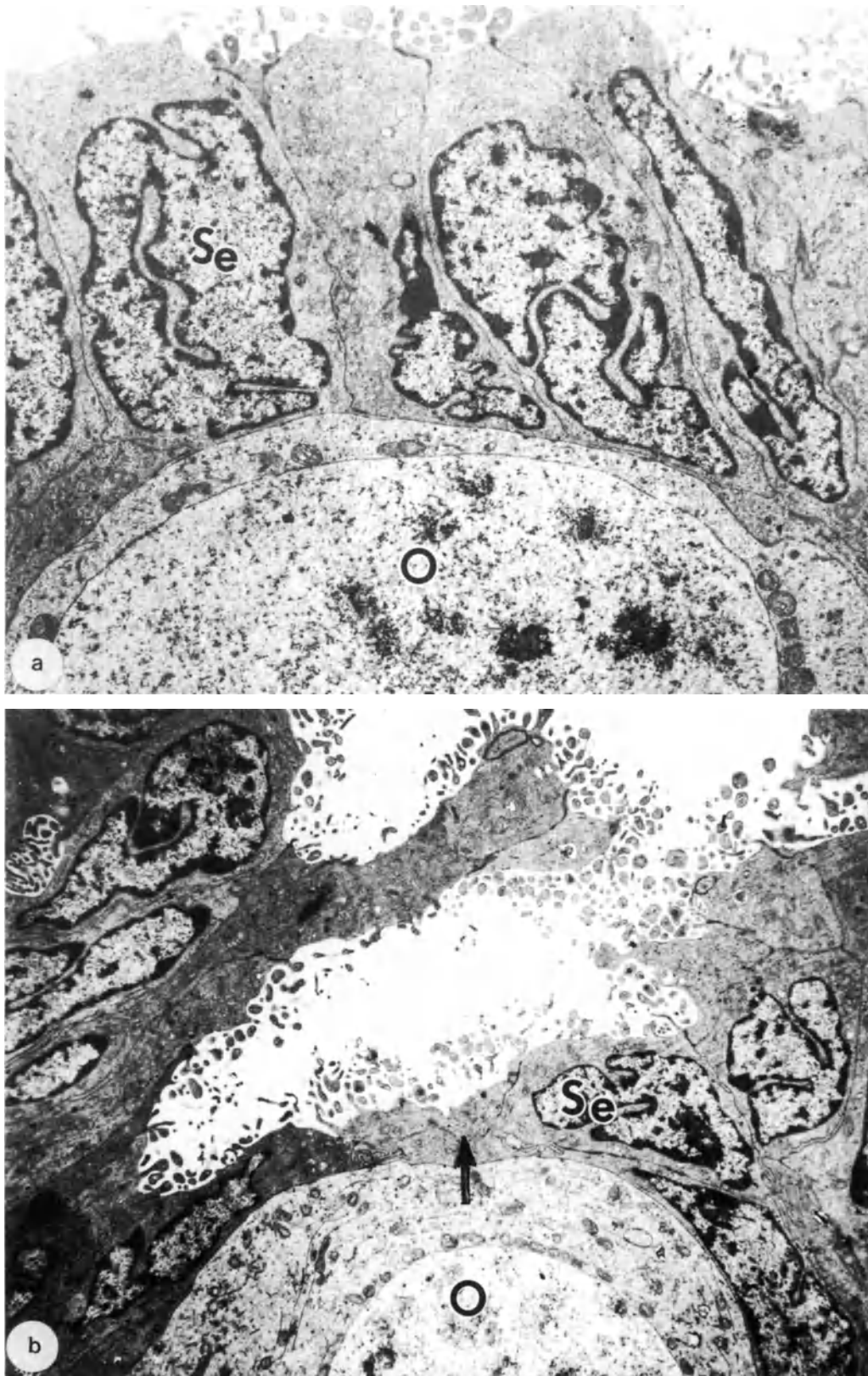
Figure 3 Human ovaries between 24 and 38 weeks old

a: The superficial epithelium (Se) is reduced to one layer displaying irregular microvilli and blebs. Oogonia (O) among the surface epithelial cells are also a common feature during this period (TEM×7200)

b: Area similar to that shown in Figure 3a. Note the oogonium (O) in close proximity to the ovarian surface (arrow). The superficial cells have here unusual elongated cytoplasmic extensions rich in microvilli and blebs (Se) (TEM×7200)

aspect. The superficial epithelium is mainly reduced to one layer with a few exceptions where it shows a stratified appearance. Microvilli, blebs, ruffles and solitary cilia are common on the apical surface of the epithelial cells. The tunica albuginea, now well developed, is thick and composed of numerous bundles of collagen fibers and elongated fibroblasts and fibrocytes. The germ cells (primitive germblasts) are rare at these stages. The oogonia and oocytes occur frequently among the cells of the cords which now detach themselves to form isolated follicles. Oogonia and oocytes are also a common feature within the superficial epithelial cells. The sex cords contain a large number of oocytes and some of these are surrounded by a single layer of flattened cells which correspond to pregranulosa cells of primordial and primary developing follicles.

CONCLUDING REMARKS

The cells populating the surface of the ovary (i.e. the so-called 'germinal epithelium' of the ovary) contribute during the fetal development to provide somatic cells, some of which will become transformed into granulosa cells (Gondos, 1975; Quattropani, 1975; Merchant-Larios, 1979; Van Blerkom and Motta, 1979; Guraya and Motta, 1980). Further it appears that the epithelial-like cells of the 'rete ovarii' (Byskov, 1980), which apparently correspond to mesonephritic tubules (Zamboni et al., 1979), contribute somatic cells to the ovary. Proliferation of both surface epithelial cells towards the cortex of the ovary and cord cells (mesonephritic elements) towards the surface of the ovary are confluent in many areas and thus both contribute to the population of the definitive granulosa cells.

Germ cells have the capability to actively migrate from the extra-ovarian territories to the gonadal primordium. Here they appear to have a special tropism towards cells having an epithelial-like arrangement such as those of the surface epithelium and mesonephritic tubes. Once the ovary is almost fully differentiated and the tunica albuginea established, germ cells (often developing in oogonia and/or oocytes) may remain contained within the surface epithelium where they early migrated.

From these areas they might only be able to move to the ovarian surface and, by being eliminated, might indirectly contribute to the reduction of gonocytes at birth in parallel with the atretic process. This phenomenon is clearly observed in small mammalian species (Jones and Krohn, 1961; Byskov and Rasmussen, 1973; Hiura and Fujita, 1977). The other possibility is that germ cells, retained within the surface epithelium, or better sequestered within closed cortical cords continuous with the surface epithelium, give rise to some abnormal proliferations such as teratomas.

Finally at birth when the ovary is well differentiated some germ cells might still retain their migratory ability within the gonad, as documented by their ameboid aspect, and by not being attached by junctional complexes to any other somatic cells of the ovary. But that such unusual germ cells are capable of

undergoing further maturative processes has not been demonstrated.

References

Byskov, A. G. (1980). Sexual differentiation of the mammalian ovary. In Motta, P. M. and Hafez, E. S. E. (eds). *Biology of the Ovary*, pp. 3-15. (The Hague, Boston, London: Martinus Nijhoff)

Byskov, A. G. and Rasmussen, G. (1973). Ultrastructural studies of the developing follicle. In Peters, H. (ed.) *The Development and Maturation of the Ovary and its Function*, pp. 55-62. (Amsterdam: Excerpta Medica)

Cajander, S. (1976). Structural analysis of rabbit ovarian follicles after mating, with special reference to the overlying surface epithelium. *Cell Tiss. Res.*, **173**, 437

Gondos, B. (1975). Surface epithelium of the developing ovary. Possible correlation with ovarian neoplasia. *Am. J. Pathol.*, **81**, 303

Guraya, S. S. (1977). Recent advances in the morphology, histochemistry and biochemistry of the developing mammalian ovary. *Int. Rev. Cytol.*, **51**, 49

Guraya, S. S. and Motta, P. M. (1980). Interstitial cells and related structures. In Motta, P. M. and Hafez, E. S. E. (eds), *Biology of the Ovary*, pp. 68-85. (The Hague, Boston, London: Martinus Nijhoff)

Hafez, E. S. E., Makabe, S. and Motta, P. M. (1980). Surface ultrastructure of functional and nonfunctional human ovaries. *Int. J. Fertil.*, **25**, 94

Hiura, M. and Fujita, H. (1977). Electron microscopic observations on the elimination of the oocytes through the peritoneal epithelium in the neonatal mouse ovary. *Cell Tiss. Res.*, **182**, 73

Jones, E. C. and Krohn, P. L. (1961). The relationship between ages, number of oocytes and fertility in virgin and multiparous mice. *J. Endocrinol.*, **21**, 469

Makabe, S. (1981). Scanning electron microscopy of normal and anovulatory human ovaries. In Allen, D. J., Motta, P. M. and Di Dio, L. J. A. (eds) *Three-dimensional Microanatomy of Cells and Tissue Surfaces*, pp. 245–66. (New York: Elsevier North Holland)

Merchant-Larios, H. (1975). Rat gonadal ovarian organogenesis with and without germ cells. An ultrastructural study. *Dev. Biol.*, **44**, 1

Mori, H. and Matsumoto, K. (1970). On the histogenesis of the ovarian interstitial gland in rabbits. I. Primary interstitial gland. *Amer. J. Anat.*, **129**, 289

Mossman, H. W. and Duke, K. L. (1973). *Comparative Morphology of the Mammalian Ovary*. (Madison, Wisconsin: University of Wisconsin Press)

Motta, P. M. (1974). Superficial epithelium and surface invaginations in the cortex of mature rabbit ovaries. A note on the histogenesis of the interstitial cells. *Fertil. Steril.*, **25**, 336

Motta, P. M., Cherney, D. D. and Di Dio, L. J. A. (1971). Scanning and transmission electron microscopy of the ovarian surface in mammals with special reference to ovulation. *J. Submicr. Cytol.*, **3**, 85

Motta, P. M. and Van Blerkom, J. (1975). A scanning electron microscopic study of the luteo-follicular complex. II. Events leading to ovulation. *Am. J. Anat.*, **143**, 241

Motta, P. M. and Van Blerkom, J. (1979). Morphodynamic aspects of the ovarian superficial epithelium as revealed by transmission, scanning and high voltage electron microscopy. *Ann. Biol. Anim. Biochem. Biophys.*, **19**, 1259

Nilsson, O. and Munshi, S. F. (1973). Scanning electron microscopy of mouse follicles at ovulation. *J. Submicr. Cytol.*, 5, 1

Quattropani, S. L. (1975). Microscopy of ovarian cords and mesothelium in the fetal monkey (*macaca arctoides*) and fetal human. *Anat Rec..*, 181, 454a

Van Blerkom, J. and Motta, P. M. (1979). *The Cellular Basis of Mammalian Reproduction.* (Baltimore, Munich: Urban & Schwarenberg)

Zamboni, L., Bezard, J. and Mauleon, P. (1979). The role of the mesonephros in the development of the sheep fetal ovary. *Ann. Biol. Anim. Biophys.*, 19, 1153

15

The ovary and ovulation

S. MAKABE*, E. S. E. HAFEZ† and P. MOTTA‡

* Department of Obstetrics/Gynecology, Toho University School of Medicine, Tokyo, Japan
† Department of Gynecology/Obstetrics, School of Medicine, Wayne University, Detroit, Michigan 40241, USA
‡ Department of Anatomy, Faculty of Medicine, University of Rome, Italy

Ovarian papillae are frequently evaginated into a series of villous-like projections which, depending upon the species, may vary widely in number, size and distribution over the ovarian surface (Harrison and Matthews, 1951). In human ovaries papillae are small and few in number under normal physiological conditions (Dabelow, 1939; Jensen and Norris, 1972; Sternberg, 1963). The superficial epithelium may be invaginated into adjacent cortical layers. These invaginations are well-defined and form simple or ramified clefts, crypts and cords (Harrison and Matthews, 1951; Makabe, 1981; Motta and Van Blerkom, 1974; Motta et al., 1977).

Morphological modifications of the surface fine structures of the superficial epithelium, e.g. blebs, ruffles, lamellipodia and branching evaginations may be related to different phases of the cell cycle or to cyclic changes reflecting metabolic and molecular events occurring within the ovary (Andrews and Porter, 1973).

SUPERFICIAL EPITHELIUM

The superficial epithelium is composed of a single layer of polyhedral (columnar or flattened) cells tenuously attached to the tunica albuginea. A characteristic feature of the ovarian epithelium is the high degree of variability in the density of the superficial cells (Figure 1). The superficial epithelium does not form a complete covering except in the perifollicular region of the Graafian follicle, the crypts and inside the pits.

At the apex of the preovulatory follicle, the superficial epithelium is flattened and irregular in shape and size with slender, rare microvilli. The proliferative activity of the epithelium is evidenced by the filopodia which appear in the mitotic stage. Furthermore, numerous prominent apical protrusions and ruffles may reflect secretory activity and endocytosis. Changes in surface morphology have been described by Porter et al. (1973).

Hormone receptors

Follicular development and luteinization involve a biphasic increase in the number of receptors in granulosa cells. The first increase is associated with maturation of these cells and the second with luteinization. In corpora lutea, receptor concentration is maximal on day 17 of the cycle then remains fairly constant until menstruation.

Follicular atresia

Once primordial follicles begin to grow and reach the primary follicle stage, many of them undergo atresia, which continues throughout the reproductive years until menopause. Only one of the developing secondary follicles is selected to continue its differentiation into a Graafian follicle for ovulation at midcycle. The rest of the follicles undergo follicular atresia.

Muscular apparatus

Smooth muscle cells in the theca externa are concentrated in the perifollicular stroma of the developing follicle, as well as in different ovarian regions. In growing antral follicles of several mammals, smooth muscle cells form a conspicuous investment ('capsule') of concentric layers of stretched and elongated elements located in the zones of the theca externa (Motta and Van Blerkom, 1979). However, in antral follicles reaching approximately the same growing phase but with clear signs of atresia, the contractile capsule of the follicles has an irregular outline due to an apparent dislocation and shortening of smooth muscle cells (Figure 3). In atretic follicles the majority of the cells forming this 'capsule' have the cytological characteristics of smooth muscle cells fixed in contraction. The occurrence of compressed, smooth muscle cells in the wall of atretic follicles suggests that some relationship exists between follicle contraction
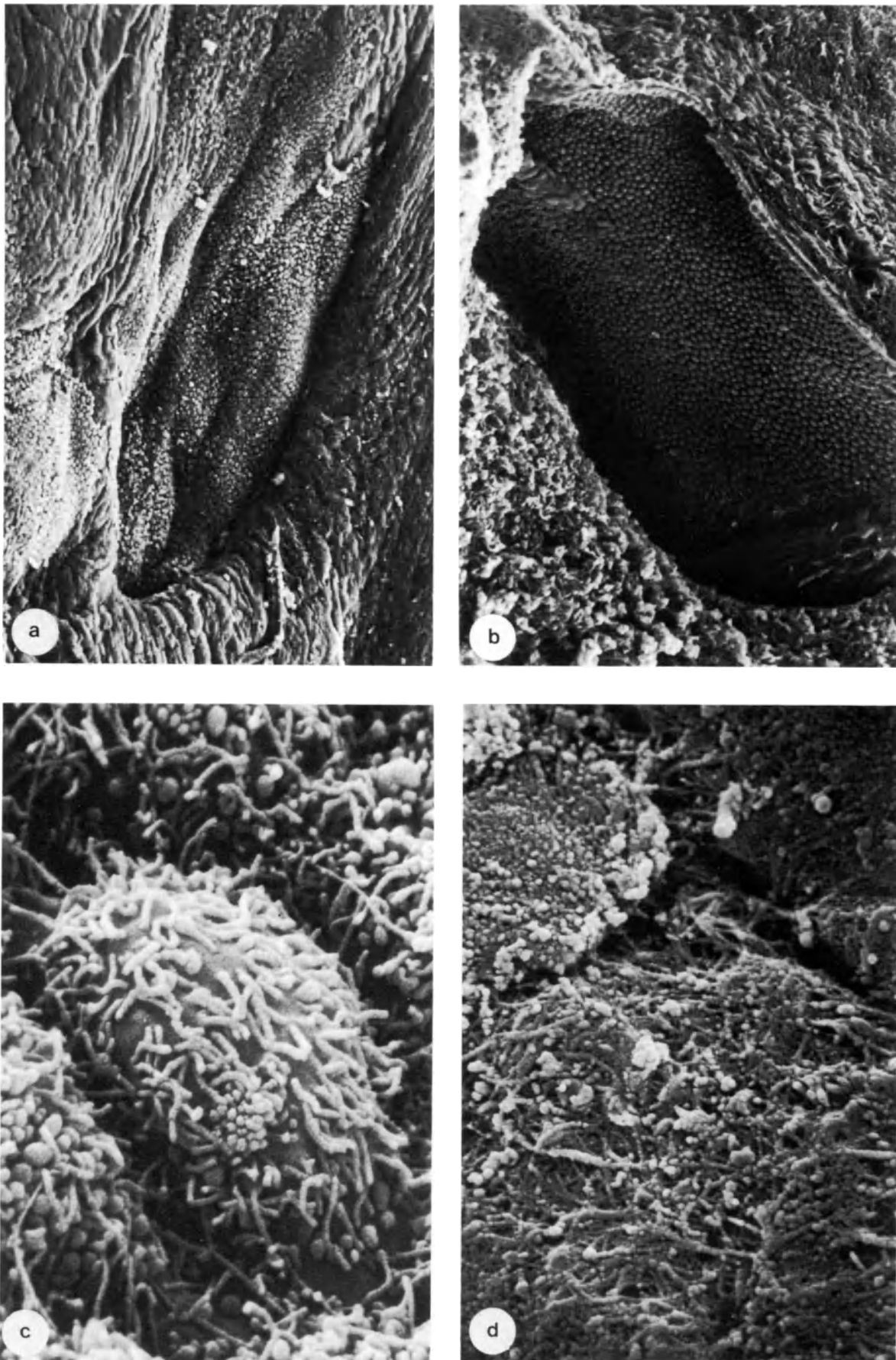
Figure 1 SEM of superficial epithelium of the human ovary

a: Note extensive proliferation of superficial epithelium in hollow area. Note the tunica albuginea (basement lamina) which is nearly exposed in the lower right-hand corner. Normally a single uniform superficial layer could be expected, but the superficial epithelial cells have begun to slough off in ovulating middle-aged ovaries (×100)

b: Cross-section of the ovarian correx. The inside of the crypt is covered by dense superficial epithelium (×200)

c: Higher magnification of Figure 1b. Note abundance of blebs and microvilli (×10 000)

d: Apex of preovulatory follicle. Note absence of superficial epithelium. Coarse collagenous fibers are evident (×5000)
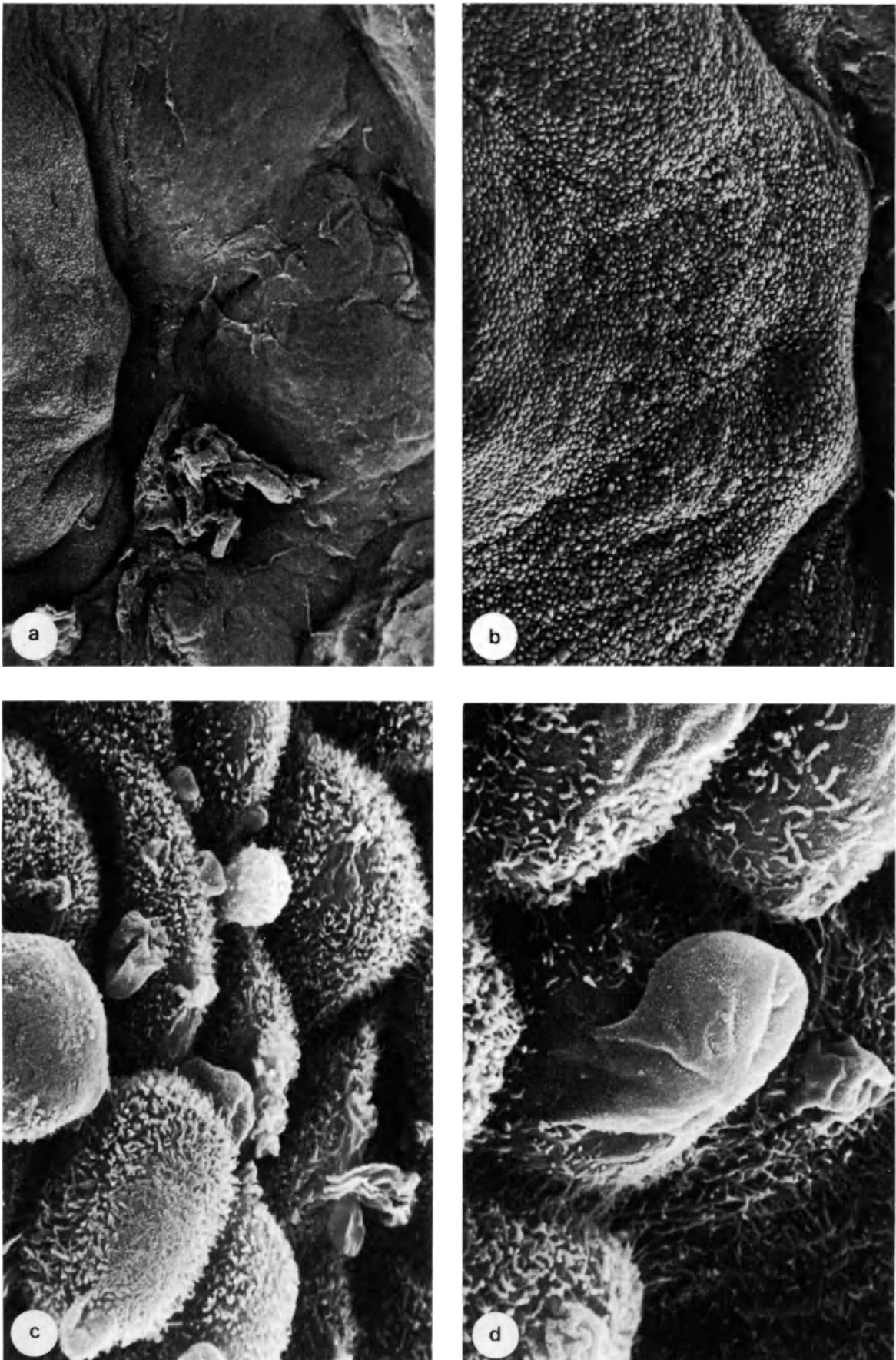
Figure 2 SEM of the ruptured site of a stigma in the human ovarian follicle

a: Stigma, approximately 20 hours following ovulation (×30)

b–d: Higher magnification of figure (2a) showing the superficial epithelium at the basal area of the postovulatory follicle. The superficial cells are flattened and irregular in size and shape. Note the apical cellular protrusions, ruffles and rare microvilli. Within a short time, flattened and elongated superficial cells migrate from adjacent areas in an attempt to cover the ruptured stigma and repair that site (b) ×200; (c) ×3000; (d) ×5000

Table 1 Some structural changes in the growth and differentiation of the follicle in the human ovary

Type of follicle and structural characteristics	Diameter of follicle	Diameter of oocytes (mirrors)	Hormone receptor in granulosa cells
Primordial			
During each menstrual cycle, several primordial follicles are selected and stimulated to grow; there is an increase in size of both follicle and embedded primary oocyte; granulosa cells increase from a single layer to several layers; theca interna cells appear outside the basement membrane	50 μm	17	nil
Primary			
Follicle, with 2 or 3 layers of cuboidal granulosa cells, fully developed primary oocyte, a base membrane and theca interna cells; in response to FSH stimulation, FSH receptors appear in granulosa cells; number of FSH receptors per granulosa cell remains relatively constant during follicular growth	130μm	100	FSH estradiol
As the total number of FSH receptors increases, an increasing number of FSH receptors permits the growing follicles to become more responsive to FSH stimulation			testosterone
Estradiol and testosterone receptors appear in the granulosa cells			
Secondary			
Follicles under control of gonadotropin stimulation increase in number of granulosa cells; antrum formation increases in number of theca interna cells; induction of LH receptors and an aromatase enzyme system in granulosa cells; LH receptors develop in theca interna cells	1–2 cm	150	FSH estradiol testoterone prostaglandin prolactin
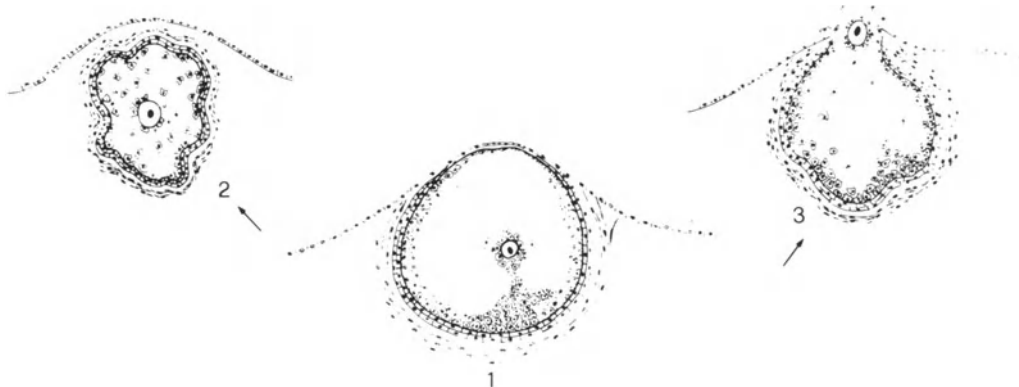
Figure 3 Diagrammatic illustration of the mature ovarian follicle. Motta and Familiari suggest the possible role of smooth muscle cells of the theca externa of the follicle at the time of atresia (2) or ovulation (3). In both cases, the contraction of this layer may favor collapse and subsequent alteration of the follicular complex. Growing follicle with smooth muscle cells in concentric layers of stretched elements (1). Similar follicles, during atresia (2) and ovulation (3) showing shortened and contracted smooth muscle cells

and atretic process (Motta and Familiari, 1981). Such perifollicular contractile tissue may favor the collapse of the follicle and subsequent involution during atresia.

DEVELOPMENT OF OVARIAN FOLLICLES

The ovarian follicles undergo sequential development and differentiation, whereas oogonia progress from primary oocytes to mature oocytes. The primordial follicle consists of a primary oocyte, one single layer of granulosa cells, and a basement membrane (Table 1). Primordial follicles undergo sequential development and differentiation into primary follicles, secondary follicles and Graafian follicles. The ovarian follicles undergo remarkable changes in morphological and ultrastructural characteristics throughout the menstrual cycle. These changes correspond to functional demands and changes in the endocrine profile (Channing and Tsafriri, 1977; Erickson, 1978; Ross and Vande Wiele, 1974).

OVULATION

One day before ovulation the superficial epithelium covers the areas of the ovary where follicles are evident. The apex of the cells is convex and completely covered with thin microvilli. Prior to ovulation the follicles become flaccid. Near the stigma of the follicle
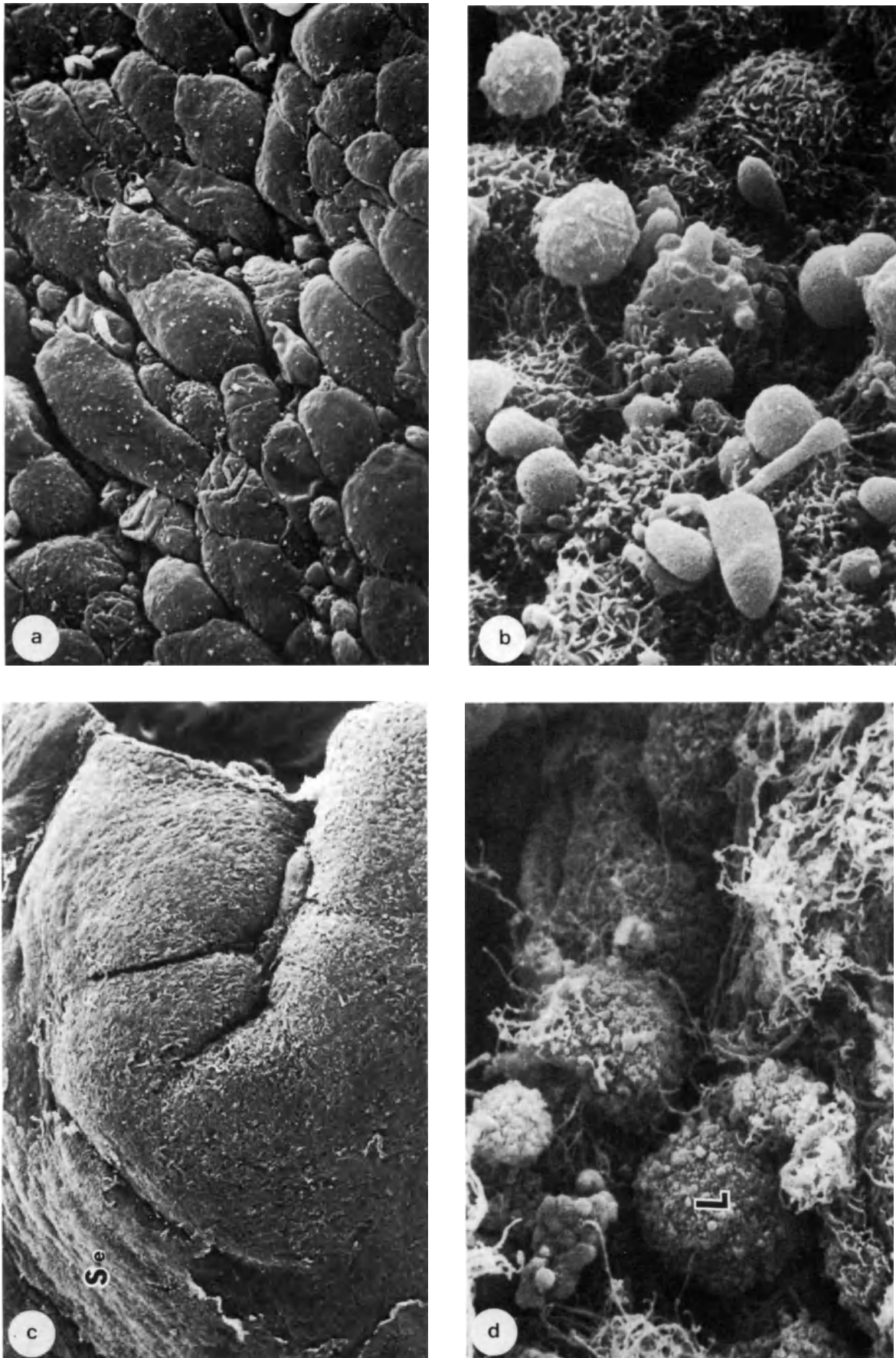
Figure 4 SEM of granulosa and granulosa-luteal cells of human ovarian follicle

a: Preovulatory follicles (×2000). Note enlarged cells.

b: Area surrounding 3rd day of postovulatory follicle in superficial epithelium. Note the irregularly shaped secretions; secretory material (×3000).

c: 6th day of postovulatory follicle. Superficial epithelium (Se) has not yet covered the postovulatory area (×40).

d: Higher magnification of Figure 4c. Note some luteal cells (L) are exposed on ovarian surface (×2000)
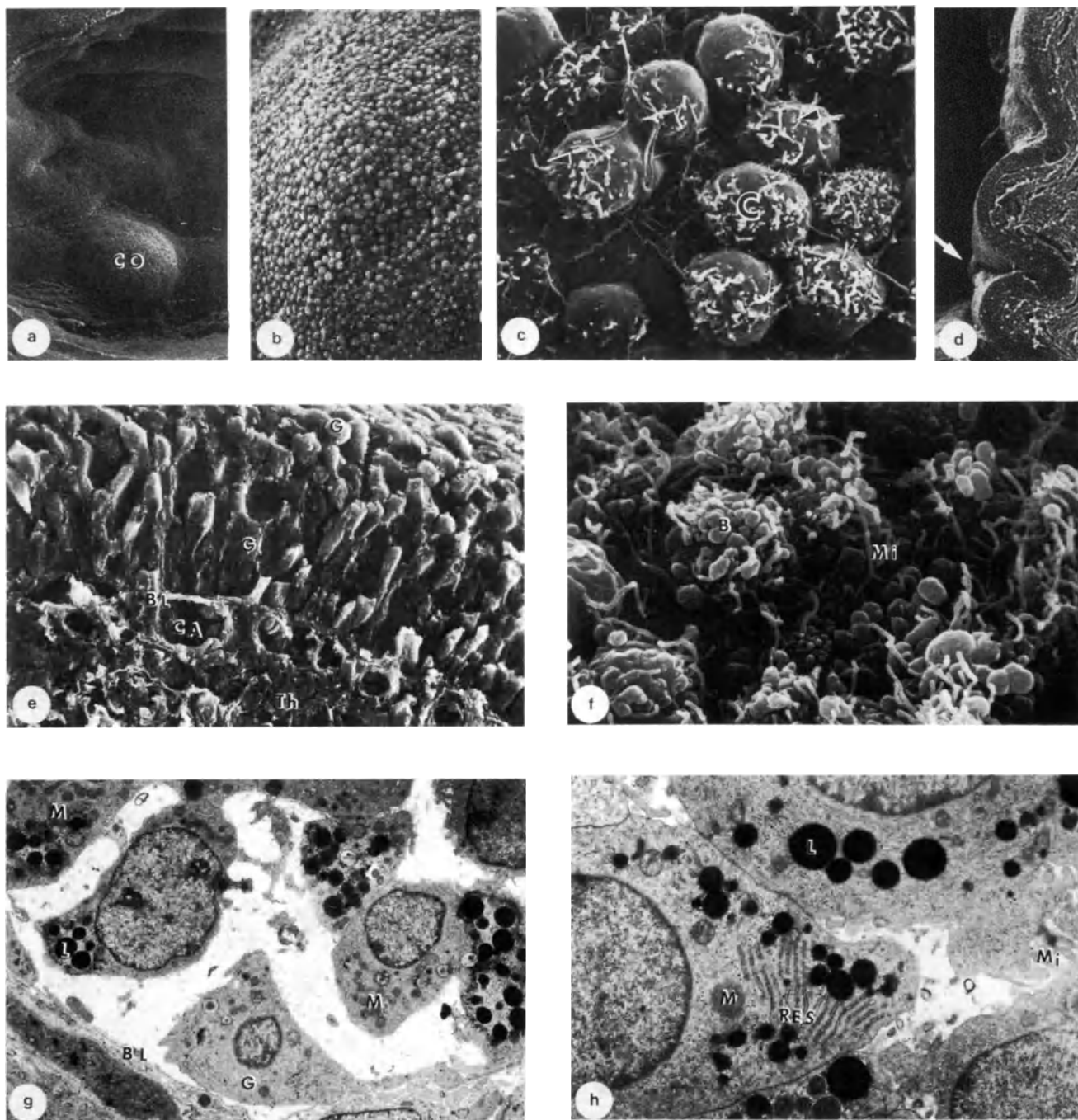
Figure 5

a–c: Medium-sized follicles
a: Note cumulus oophorus (CO) (×30)
b: Note cellular arrangement (×150)
c: Note distorted microvilli (arrow) of cumulus cells (C) ×1500)

d–g: Large preovulatory follicles
d: Note unfolding of follicular wall (arrow) (×30)
e: Granulosa cell layer. Note the granulosa cells (G), basal lamina (BL), capillary atreria (CA), and theca cell (T) (×450)
f: Higher magnification of apical feature of the granulosa cells of an area similar to that shown in Figure 5e. Note the slender microvilli (M) and blebs (B) (×3000)

g: TEM of granulosa cells adjacent to the basal lamina (BL). Note dissociated granulosa cells (g) with irregular ameboidal shape.
h: TEM of part of three adjacent granulosa cells in an area similar to that shown in Figure 4a. Note the microvilli (M) and blebs (B), the lipid drops (L), mitochondria which is in part lamelliform and in part-tubular-cristae (M) and stacks of rough endoplasmic reticulum (RES). These cellular organelles suggest that the initial luteinization occurs before ovulation.
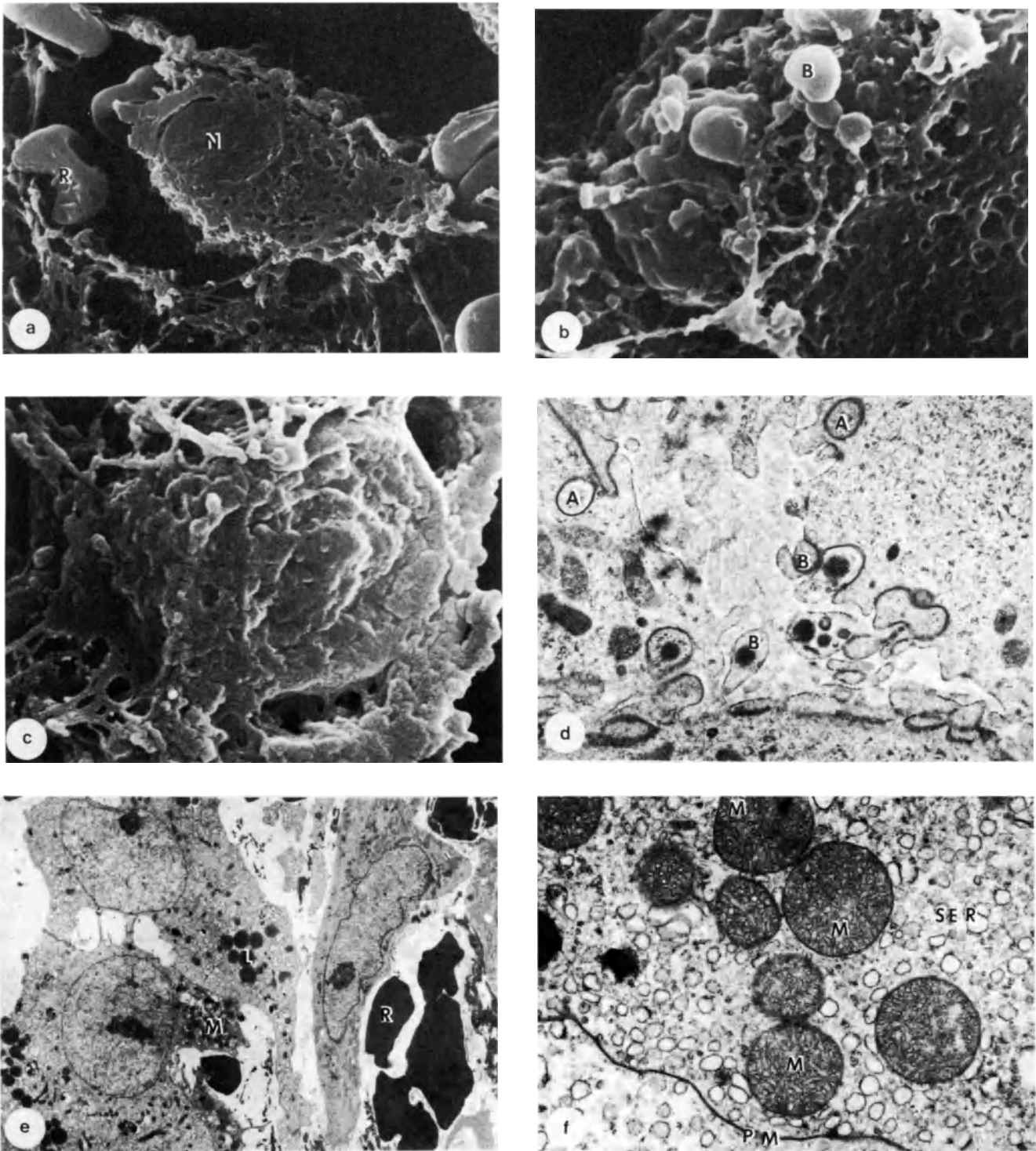
Figure 6 SEM and TEM of granulosa–lutein cell

a: Sectional surface of a granulosa–lutein cell on the 3rd day of the luteal phase ($\times 2550$)

b: Part of the apical surface of a granulosa–lutein cell on 3rd day of luteal phase. Note the prominent blebbing activity (B) ($\times 8500$)

c: Mature granulosa–lutein cells. Note ameboidal cytoplasmic projections, loss of microvilli and blebs ($\times 4250$)

d: Part of three adjacent granulosa–lutein cells on the 3rd day of the luteal phase. Note several blebs (B), and annular nexus (A). The mitrochondria have tubular-cristae ($\times 7650$)

e: Mature granulosa–lutein cells taken from 7th day of the luteal phase. The cells have become larger, with ameboidal cytoplasmic extensions and prominent organelles. Note many large mitochondria with villiform cristae (M), lipid droplets (L) and smooth endoplasmic reticulum ($\times 2550$)

f: TEM, higher magnification of area shown in Figure 6e. Note larger villiform cristae (M), smooth endoplasmic recticulum (SER) and plasma membrane (PM) ($\times 10\ 200$)
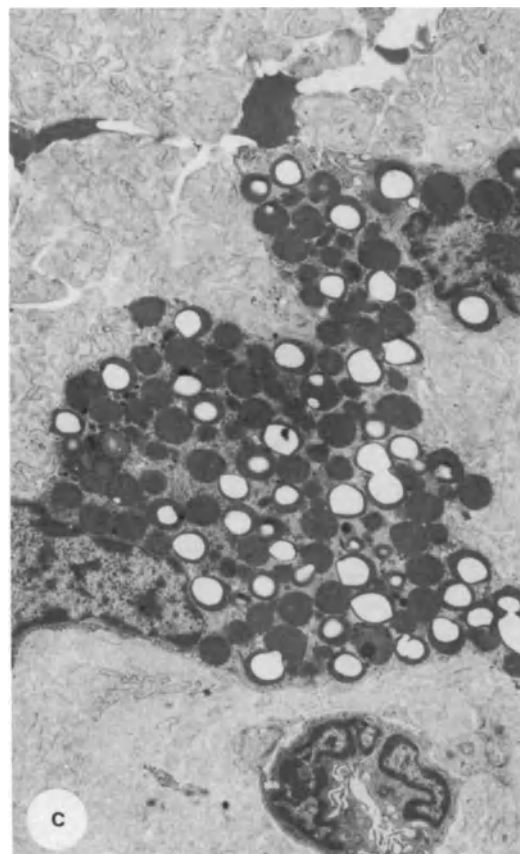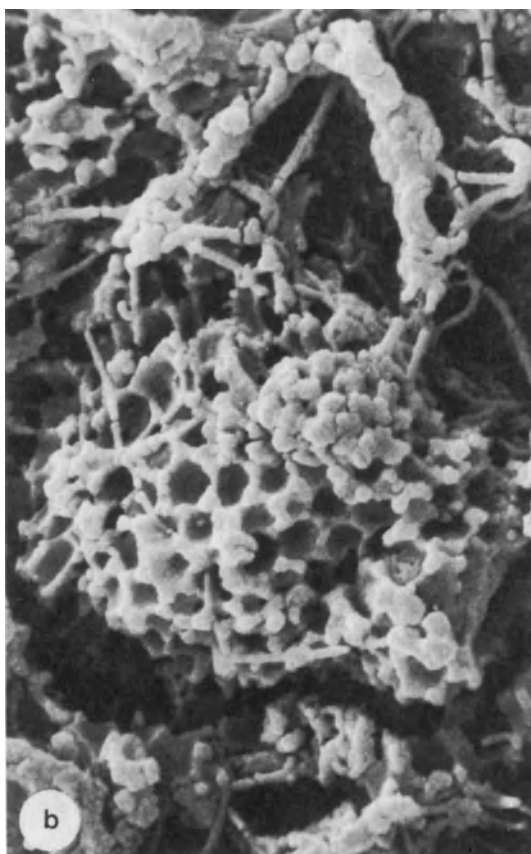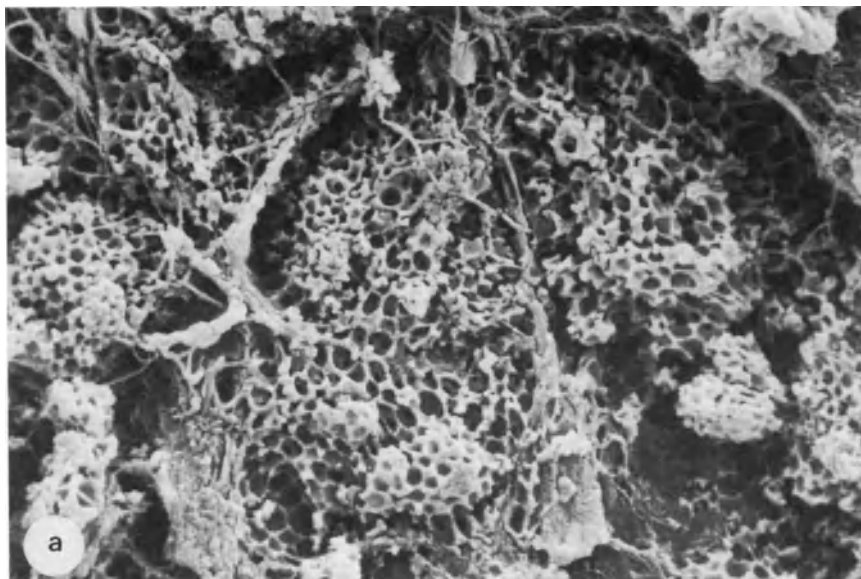
Figure 7 SEM and TEM of regressing luteal cells
a: Note honeycomb cells and the connective tissue enclosing
    the cells (×2000)
b: Note spheroidal blebs which correspond to lipid droplets,
    and residual invaginations following dissolution of the
    solid blebs (×5000)

c: TEM of an area similar to that shown in Figures 7a and b.
    The cytoplasm of the regressing luteal cells is filled with a
    large number of lipid droplets and autophagic vacuoles
    (×3000)

the epithelial cells are more flattened and their apex is rather smooth. Microvilli are distributed mainly on the cell borders. At the time of ovulation the epithelium degenerates, except at the base of the follicle where the cells have a convex apex and numerous microvilli The ovulation area first appears as a desquamated region where the basal membrane is lost. During the preovulatory stage the superficial surface epithelium of the follicle becomes very fragile. Desquamation occurs in several locations above the hemorrhage in the follicular walls.

Before ovulation there is localized tissue disintegration in the stigma and a general dissolution of the entire follicular wall. When the membrane granulosa cells in the area of stigma degenerate, the follicle basement membrane bulges from the stigma. When this membrane ruptures the mature oocyte–cumulus complex is expelled. Proteolytic enzymes may be responsible for the follicular dissolution at the time of ovulation.

LUTEINIZATION OF GRANULOSA CELLS

After ovulation, the granulosa cells of the ruptured follicle undergo luteinization as influenced by gonadotropins. Factors in the follicular fluid prevent luteinization of granulosa cells prior to ovulation. Luteinized granulosa cells, plus the surrounding theca cells, capillaries and blood vessels, intermingle to form a corpus luteum.

Functional lifespan of the corpus luteum is about 14 days, when it regresses and is replaced by an avascular scar and corpus albicans, unless pregnancy occurs.

The ultrastructure of human granulosa cells differentiating in lutein cells has been studied in an attempt to correlate morphological features with functional events. Little is known about the relationship between fine surface structure and interior cytoplasmic organelles.

The granulosa–lutein cells were obtained from corpus hemorrhagicum and corpus luteum at daily intervals to study their continuous transformation under the influence of gonadotropins. The role of cytoplasmic organelles in relation to the granulosa–lutein cell function has been evaluated. Mitochondria with tubulovesicular cristae are characteristic of steroid-secreting cells and contain the enzymes necessary for cholesterol side-chain cleavage. During the early stages of lutein cell differentiation, endoplasmic reticulum increases in total amount, concomitant with a shift from rough morphology to a predominantly smooth reticulum during luteinization. Lipid droplets represent the storage site for cholesterol and for other steroid precursors or final secretory products (Nicosia, 1980). The immature granulosa–lutein cells exhibit numerous microvilli which gradually disappear, while blebbing activity becomes prominent. Inside these cells mitochondria, with both lamelliform and tubular cristae, rough and smooth endoplasmic reticulum and dense lipid droplets, become evident (Figures 4a, 5g,h). However, mature granulosa–lutein cells show a few microvillous projections and some blebs and many ameboid cytoplasmic extensions. Mitochondria with

tubular and/or villiform cristae, prominent smooth endoplasmic reticulum and lipid droplets are characteristic of these cells (Figure 6a–f). The luteal cell surface in the regression stage has a mulberry like appearance. The cytoplasm of the luteal cell is filled with numerous lipid droplets, polymorphic lysosomes and autophagic vacuoles. A sectional surface of the luteal cells having the appearance of a honeycomb is also observed. Many connective tissues surround these luteal cells (Figure 7a–c).

ANOVULATORY FOLLICLES

In polycystic ovaries, along the basement membrane of the follicle, granulosa cells cluster unevenly, featuring numerous blebs and networks of cytoplasmic projections. The granulosa layer is disrupted in some of these follicles, with blood cells and macrophages invading the antrum. Thus, some areas along the anterior wall of the follicle are devoid of granulosa cells, which either appear scattered or in patches; at an advanced stage, they become smooth-surfaced, flattened, and irregular in size and shape. However, some residual granulosa cells produce long, slender microvilli, as well as blebs, filopodia, and ameboid evaginations. These surface features may suggest that some granulosa cells in atretric follicles can still undergo luteinization.

References

Andrews, P. M. and Porter, K. R. (1973). The ultrastructural morphology and possible functional significance of mesothelia microvilli. *Anat. Rec.*, **177**, 409

Channing, C. P. and Tsafriri, A. (1977). Mechanism of action of luteinizing hormone and follicle-stimulating hormone on the ovary *in vitro*. *Metabolism*, **26**, 413

Dabelow, A. (1939). Das Gefabnetz des Ovars und sein Verhalten wahrend der zykischen Verandergugen. *Anat. Anz.*, **88**, 173

Erickson, G. F. (1978). Normal ovarian function. *Clin. Obstet. Gynecol.*, **21**, 31.

Harrison, R. J. and Matthews, L. H. (1951). Subsurface crypts in the cortex of the mammalian ovary. *Proc. Zool. Soc.*, **120**, 699

Jenson, R. D. and Norris, H. T. (1972). Epithelial tumors of the ovary. *Arch. Pathol.*, **94**, 29

Makabe, S. (1981). Scanning electron microscopy of normal and anovulatory human ovaries. In DiDio, L. J. A. Motta, P. and Allen, D. J. (eds). *Three-dimensional Micro-anatomy of Cells and Tissue Surfaces*, pp. 245–66. (Amsterdam and New York: Elsevier, North Holland)

Motta, P., Andrews, P. M. and Porter, K. R. (1977). Micro-anatomy of cells and tissue surfaces. In *Atlas of Scanning Electron Microscopy*. (Philadelphia: Lea & Febiger)

Motta, P. and Van Blerkom, J. (1974). A scanning electron microscopic study of the luteo-follicular complex. II. Events leading to ovulation. *Am. J. Anat.*, **143**, 241

Motta, P. M. and Van Blerkom, J. (1979). Structure and ultrastructure of ovarian follicles. In Hafez, E. S. E. (ed.) *Human Ovulation*, pp. 17–53. (Amsterdam: Elsevier, North Holland)

Motta, P. M. and Familiari, G. (1982). On the occurrence of a contractile tissue in the theca externa of atretic follicles in the mouse ovary. *Acta Anatomica, Basel* (In press)

Nicosia, S. V. (1980). In Tozzin, R. I., Reeves, G. and Pineda, R. L. (eds). *Endocrine Physiopathology of the*

Ovary, pp. 101–19. (Amsterdam: Elsevier, North-Holland)

Porter, K. R., Prescott, D. and Frye, J. (1973). Changes in the surface morphology. *J. Cell Biol.*, 57, 815

Ross, G. T. and VandeWiele, R. L. (1974). The ovaries. In

Williams, R. H. (ed.) *Textbook of Endocrinology*, pp. 368–418. (Philadelphia: W. B. Saunders)

Sternberg, W. H. (1963). Non-functioning ovarian neoplasm. In Grady, H. S. and Smith, D. E. (eds). *The Ovary*. (Baltimore: Williams & Wilkins)

16

Ovarian tumors

F. STENBACK*, S. MAKABE†, G. OMURA†, A. IWAKI† and E. S. E. HAFEZ‡

* Department of Pathology, University of Oulu, Oulu 22, Finland
† Department of Obstetrics/Gynecology, Toho University School of Medicine, Tokyo 143, Japan
‡ Department of Gynecology/Obstetrics, School of Medicine, Wayne State University, Detroit, Michigan 40241, USA

There have been several classifications of ovarian tumors based on embryological, morphological, functional and clinical parameters (Janovski and Paramanandhan, 1973; Novak et al., 1975; Scully, 1953, 1970a,b; Taylor et al., 1978; Teilum, 1976; Melis and Carpino, 1980; Wilson et al., 1975; Zuckerman and Weir, 1977). The classification of Melis and Carpino (1980) is summarized in Table 1; the morphological characteristics are illustrated diagrammatically in Figures 1–3.

CORTICAL INCLUSION CYSTS

These cysts are probably due to an ingrowth of the paramesonephric celomic (Mullerian) epithelium. They develop from the surface into the cortex, forming a cystic structure which may detach. Histologically, these cystic structures are lined by cuboidal to tall-columnar epithelium, similar to the tubal epithelium. Clear serous fluid fills the cyst (Figure 4).

SURFACE EPITHELIAL TUMORS: MUCINOUS CYSTADENOMAS

Tumors of celomic epithelial cells are mainly subdivided into five different groups: mucinous, serous, endometrioid, mesonephrioid and Brenner tumors, depending upon direction of differentiation of surface epithelium (Figure 5). Histological examination of mucinous tumors has shown epithelial elements to contain cells resembling those of endocervical or gastrointestinal tract mucosa (Langley et al., 1972; Gondos, 1975). Numerous ultrastructural differences between ovarian epithelial mucinous cells, those of the endocervical canal, goblet cells of small intestine (Freeman, 1966), and intestinal metaplasia of the stomach have been described (Nevalainen and Järvi, 1977; Klemi and Nevalainen, 1978). Fenoglio et al.

(1975) reported that the benign areas of borderline mucinous cystadenomas were of mixed endocervical intestinal type (Kaye et al., 1973; Ferenczy and Richart, 1974), while malignant tumors were composed of intestinal cells (Fenoglio et al., 1975, 1976). Endocervical type cells normally have a low malignant potential, as malignant endocervical tumors are comparatively infrequent.

Morphologically the cystadenomas are divided into benign tumors innocent in behavior, and highly aggressive cystadenocarcinomas as well as ovarian epithelial tumors which are intermediate in their histologic appearance. These tumors have been designated potentially or possibly malignant, borderline tumor, semimalignant or hyperplastic tumors or proliferative tumors (Fox and Langley, 1976; Katzenstein et al., 1978).

Morphological analysis of benign mucinous cystadenomas showed the main cell types to be the columnar mucinous epithelial cells and goblet cells. Scanning electron microscopy of the tumor surface revealed wave-like arrangements of regular cells, with grooves and slits but no papillary structures (Figures 5a, 8c, 8d). Most cells were covered by microvillous projections, the number, size and distribution varying from cell to cell. Other cells showed numerous cilia as well as microvilli with rounded or slightly club-like ends. The ciliated cell type showed a mixed arrangement of centrally located cilia of different lengths and densities surrounded by varying amounts of microvilli. Holes in the surface epithelium caused by mucous secretion occurred unevenly.

Study of surface ultrastructure of borderline cystadenomas revealed undulating arrangements of slightly irregular cells. Higher magnification showed the surface to be lined by pentagonal or elongated cells with microvilli varying in size and number, the ciliated cells were few.

Table 1   Summary of primary ovarian tumors (classification
by Melis and Carpino, 1980)

Origin of ovarian tumor	Classification
Tumors of celomic cells	cystadenoma (a) mucinous (b) serous (c) mixed (seromucinous) cystadenocarcinoma (a) mucinous (b) serous (c) mixed (seromucinous) surface papilloma cystadenofibroma (adenofibroma) Brenner tumor carcinoma of ovary (a) adenocarcinoma (b) clear cell carcinoma (c) solid carcinoma
Tumors of non-specialized mesenchymal–mesodermal tissue	benign tumors of fibrous, muscular, vascular and nervous differentiation (a) fibroma (b) other types (myxoma, etc.) malignant tumors of fibrous, muscular vascular and nervous differentiation
Tumors of specialized ovarian stroma with potentially hormonal secretion	(1) granulosa cell tumor (2) theca cell tumor (thecoma) (3) granulosa-theca cell tumor (4) granulosa cell tumors and theca cell tumor with luteinized cells (luteoma/stromal luteoma) (5) hilus cell tumor (6) gynandroblastoma
Tumors of germ cell origin	(1) dysgerminoma (2) gonadoblastoma (3) teratomas (a) cystic teratoma (b) solid teratomas reproducing embryonic structures (c) solid teratomas reproducing embryonic structures solid benign teratoma; malignant teratoma; struma ovarii; carcinoid tumor; teilum tumor; primary chorioncarcinoma
Tumors from mesonephric nests	(1) mesonephric adenoma (2) mesonephric cystadenofibroma (3) mesonephroma
Tumors from heterotopic tissue	(1) heterotopic adrenal cell nest tumor (2) carcinoma arising in endometriosis (3) stromatosis ovarii (4) pheochromocytoma

The epithelial surface of cells lining the cystic cavities of malignant mucinous cystadenomas showed cleft-like arrangements of irregular cells varying in size and shape. These surface cells were covered by small irregular microvilli, few in number.

Surface ultrastructural findings are indicative though not diagnostic in the differential diagnosis between benign, borderline and malignant cystadenomas. Extensive sampling, especially critical with mucinous lesions, may be avoided by scanning electron microscopy, since a decrease in specialized surface structures is associated with advancing malignant behavior.

The origin of mucinous ovarian tumors is also in doubt. It is generally believed that the majority of these tumors are derived by metaplasia from celomic epithelial inclusion cysts supported by SEM studies (Stenbäck, 1980; Stenbäck and Kauppila, 1981a), though some authors favor a theory of germ cell origin and consider mucinous tumors to represent monophyletic teratomas (Langley et al., 1972). The occurrence of fully mature intestinal type cells and
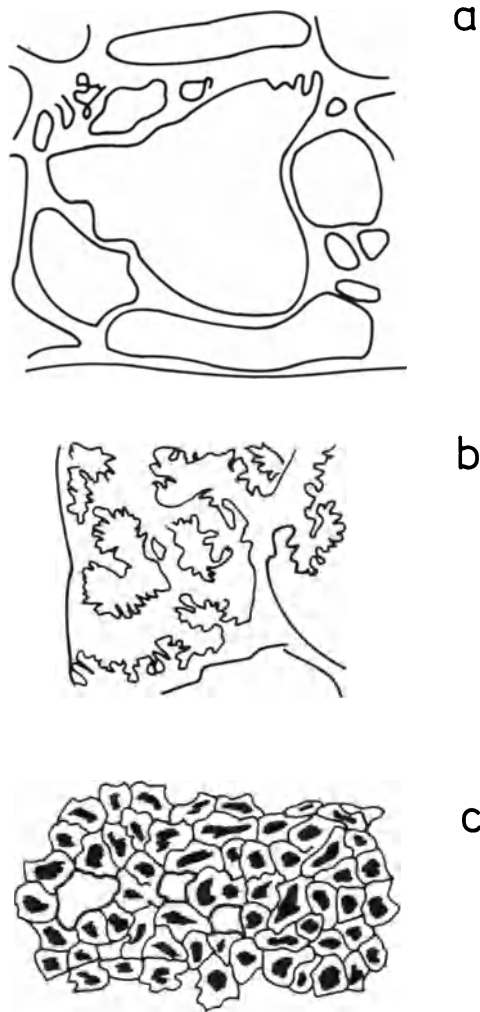
Figure 1 Ovarian surface epithelial tumors
a: Benign serous cystadenoma
b: Papillary serous cystadenoma, borderline type
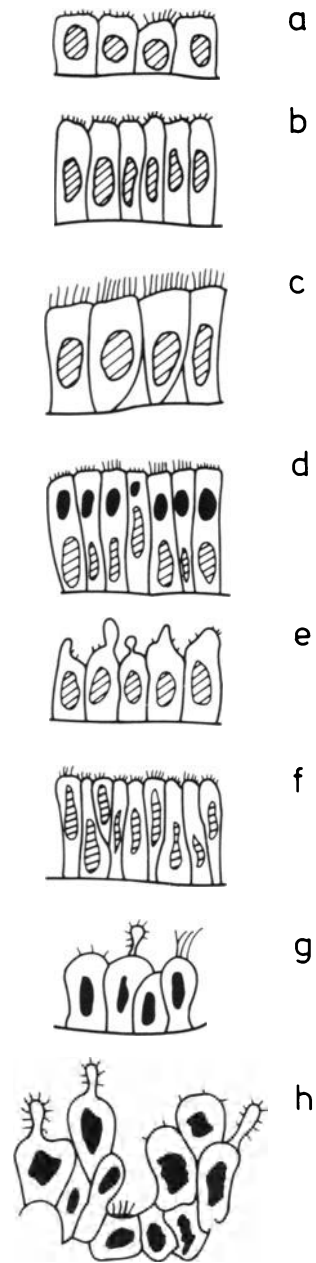c: Serous cystadenocarcinoma

Figure 2 Ovarian epithelial cell types
a: Cuboidal epithelium
b: Cylindrical microvillous cells
c: Ciliated cylindrical cells
d: Mucin-secreting cells
e: Hobnail cells
f: Hyperplastic epithelium
g: Atypical premalignant epithelium
h: Carcinomatous epithelium

argentaffine cells has been cited as evidence for the teratomatous origin of these tumors (Fox *et al.*, 1964), Langley *et al.*, 1972). Additional evidence that sustains the Müllerian rather than the germ cell derivation of ovarian mucinous cystadenomas is their frequent association with serous, endometrioid and Brenner tumors (Anderson, 1972).

SEROUS CYSTADENOMAS

The epithelium (Figures 1 and 2) of serous ovarian cystadenomas is made up of several cell types, either columnar or cuboidal, ciliated and microvillous cells of tubal, endometrial and endocervical type and of undifferentiated smaller basal cells (Roberts *et al.*, 1970; Gondos, 1971; Fox and Langley, 1976; Blaustein, 1976; Klemi and Nevalainen, 1978; Stenbäck, 1981). The cell types seen by SEM in the serous tumors resemble cells of the fallopian tube (Fredricsson and Björkman, 1962), epithelia of the endocervical canal and ovarian cystadenofibromas (Laguens *et al.*, 1967; Czernobilsky *et al.*, 1974; Papadaki and Beilby, 1975), as well as endometrial cells

(Ferenczy and Richart, 1974). The epithelia of the endocervical canal originate from the Müllerian duct which develops early in life by invagination of the celomic epithelium. This celomic epithelium also covers the ovarian cortex and can give rise to the serous cystadenomas directly or via the formation of the inclusion cysts (von Numers, 1965; Roberts *et al.*, 1970; Radisavljevic, 1977). An origin from epithelial inclusion cysts by a metaplastic process was proposed by Fenoglio *et al.* (1977) in their study on the ultrastructure of ovarian cystadenomas.
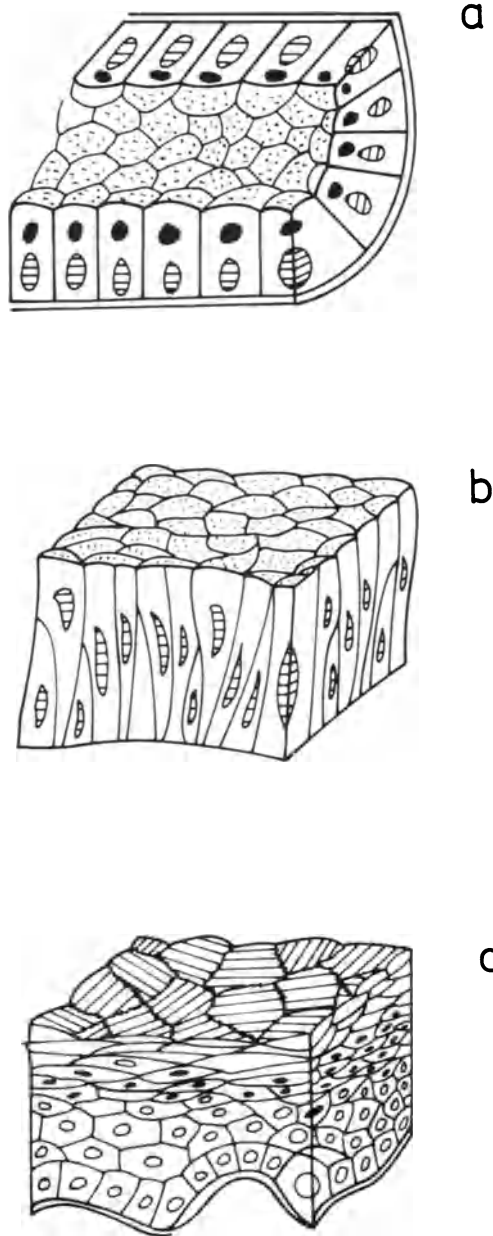
Figure 3 Surface epithelium of ovarian tumors
a: Mucinous cystadenoma
b: Serous cystadenoma
c: Teratoma

Surface analysis of benign cystadenomas shows elongated or cuboidal cells (Figure 3b), which occasionally appeared columnar resembling those lining the fallopian tube. In the surface epithelium, four types of cells were recognized: microvillous, ciliated and secretory in addition to someunclassifiable cells (Table 2). Some cells had a mixture of branched microvillous projections and cilia (Figure 16) similar to those of endometrium, others evidenced numerous cytoplasmic projections arranged in a wavelike pattern extending into the lumen.

The surface structures were not as well developed in borderline cystadenomas as in benign tumors. Most of the epithelial cells were non-ciliated low columnar or cuboidal cells, with an irregular surface. The surface

Table 2 Some histological and SEM characteristics of surface of ovarian tumors

	Mucin and glycogen	Goblet cells	Columnar or cuboidal cells	Hobnail cells	Argyrophil and argentaffin cells	Well-preserved microvilli	Well-preserved cilia	Secretory granules
Serous cystadenoma								
benign	1	1	4	1	0	4	4	1
borderline	1	1	4	0	0	3	3	1
malignant	1	1	3	0	0	2	2	1
Mucinous cystadenoma								
benign	4	4	4	0	3	4	3	4
borderline	3	3	4	0	3	3	2	3
malignant	2	3	3	0	3	2	1	2
Endometrioid lesions								
benign	3	4	4	0	2	4	3	4
borderline	3	3	4	0	2	3	2	3
malignant	2	3	3	0	1	2	1	2
Mesonephrioid cystadenoma								
malignant	4	1	3	4	0	3	3	3
Brenner								
benign	2	1	3	0	3	2	3	3
malignant	2	1	3	0	3	2	2	3
Teratoma								
cystic	0–3	0	3	0	3	2	2	2

0 = not noted
1 = extremely rare
2 = rare
3 = common
4 = very common

cells slightly irregular in size and shape were covered by microvilli. The ciliated cells were not as numerous as in the benign cystadenomas. Frequently focal denuded areas with histological atypias occurred.

Ultrastructural studies of malignant serous cystadenomas showed the main cell type to be the non-ciliated cell, covered by microvilli, few in number and small in size, arranged in irregular heaps and piles (Figure 7). The intercellular space was widened with grooves and indentations. The tumor cells varied in size

Figure 4 (opposite) Cortical inclusion cysts in human ovarian tumors
a: Low magnification of SEM. The arrow indicates cortical inclusion cysts of a cross-sectioned ovary (×25)
b: Low magnification of SEM. The arrow indicates cortical inclusion cysts of a cross-sectional ovary (×300)
c: Higher magnification of 4b (×500)
d: Higher magnification of 4c. Note the ciliated and non-ciliated cells. The luminal microvilli are well developed, occasionally accompanied by solitary cilia (arrows) (×2000)
e,f: Higher magnification of 4d. Note the fused stubby cilia and secretory protrusions (arrows). e (×2500); f (×5000)
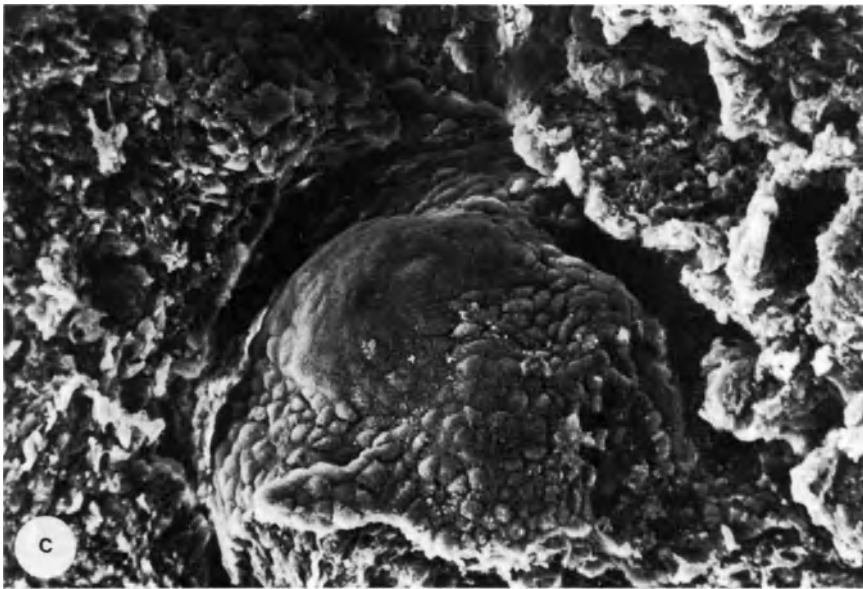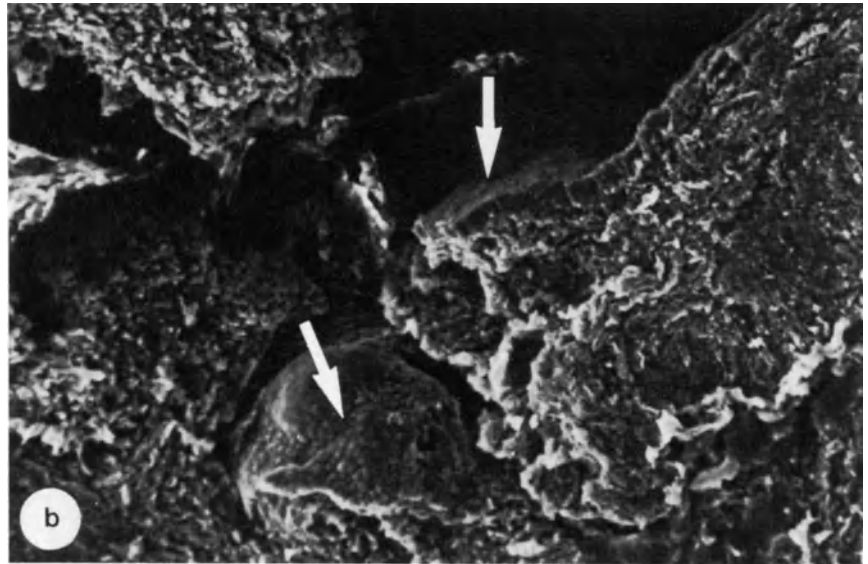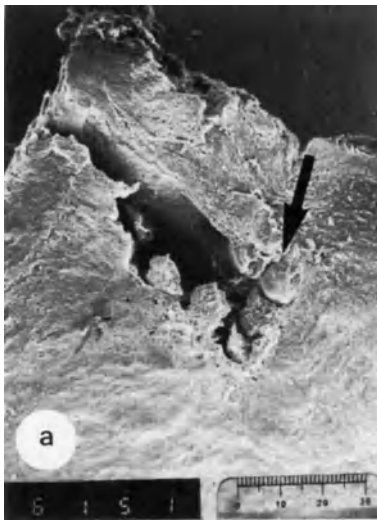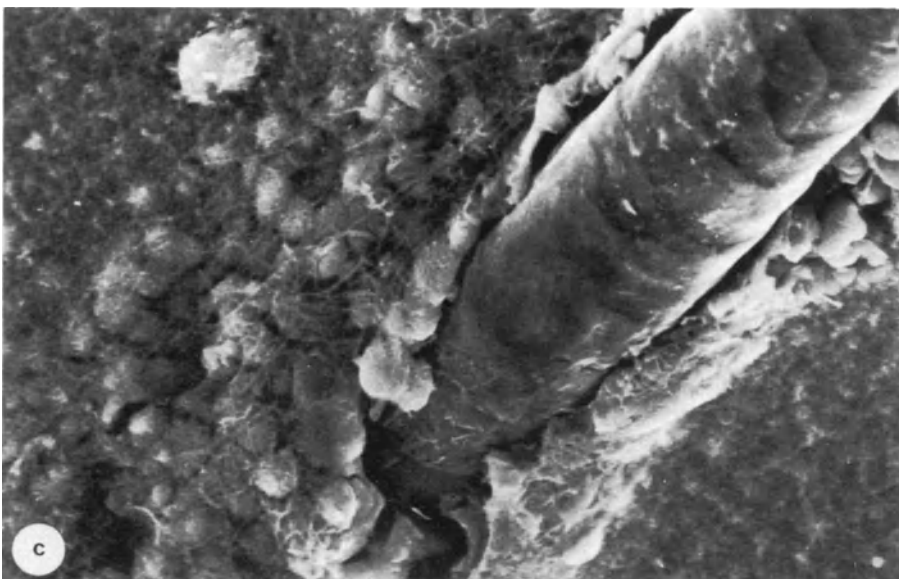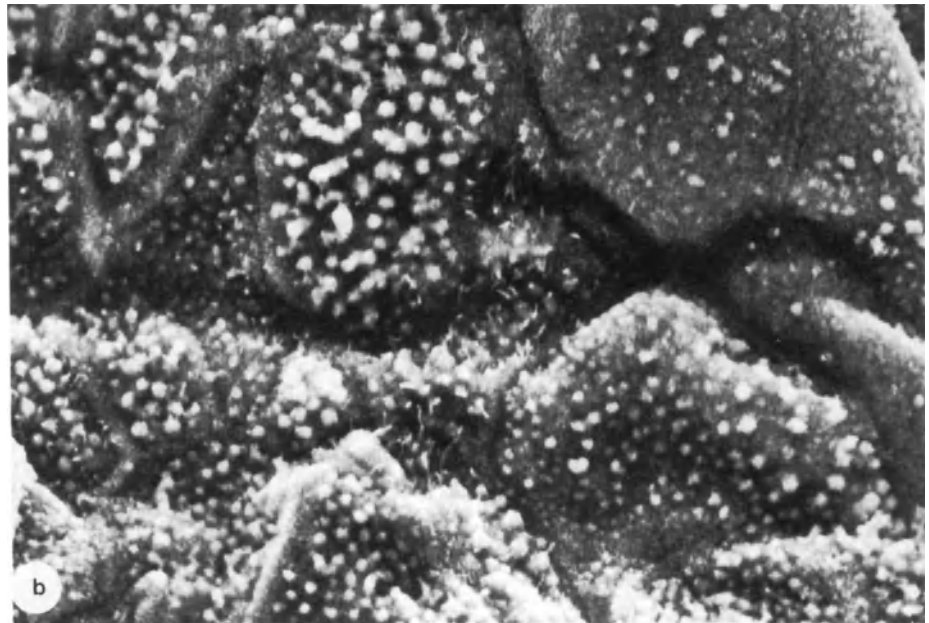
Figure 4
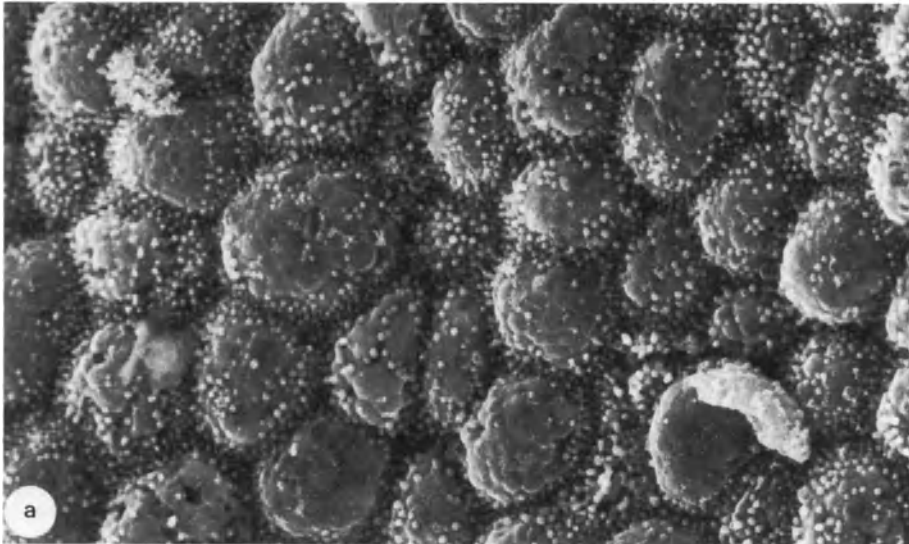
Figure 5
a: Mucinous cystadenoma show-
ing regular arranged cells in a
pavement-like fashion and partly
denuded areas (×1275)
b: Cystic teratoma showing cells
having a partly squamous con-
figuration but also small
microvilli (×1275)
c: Ovarian teratoma with
squamoid cells and abortive hair
(×731)

Figure 6

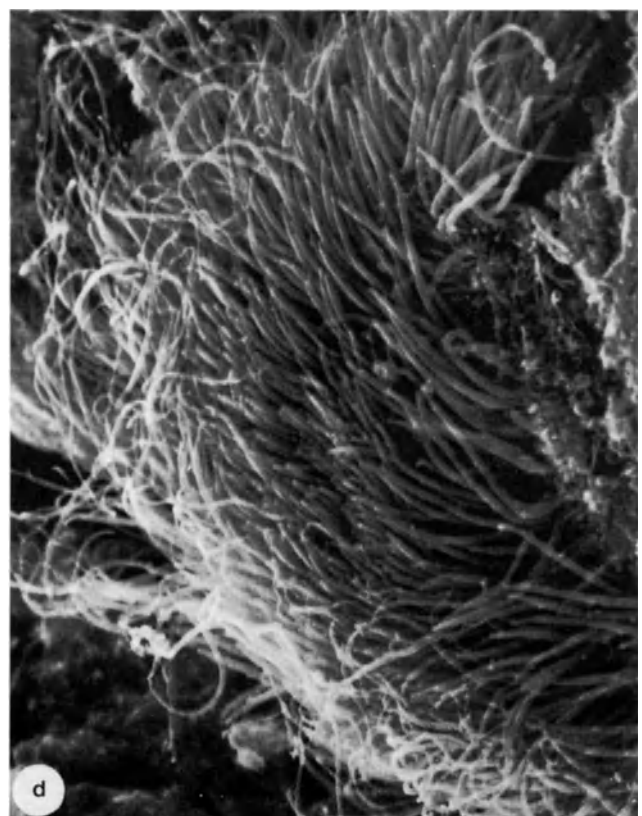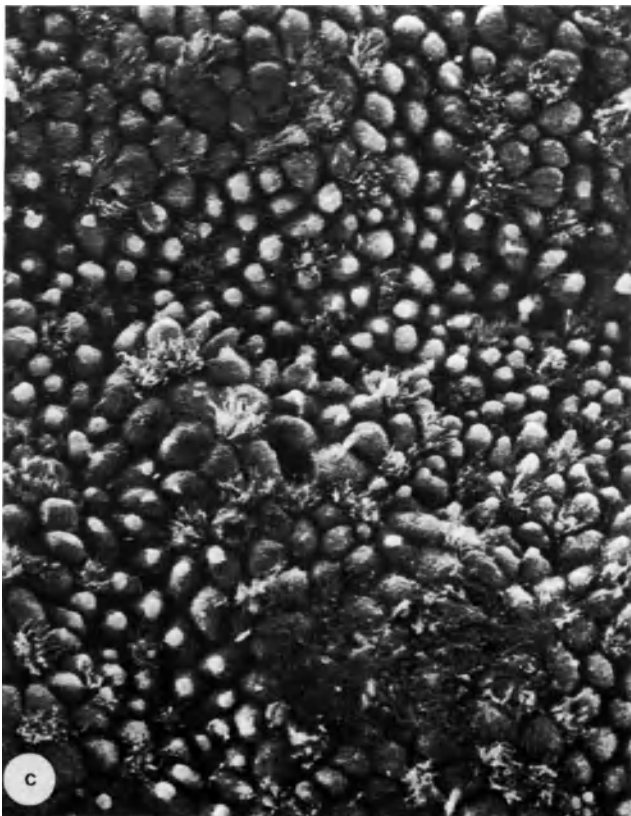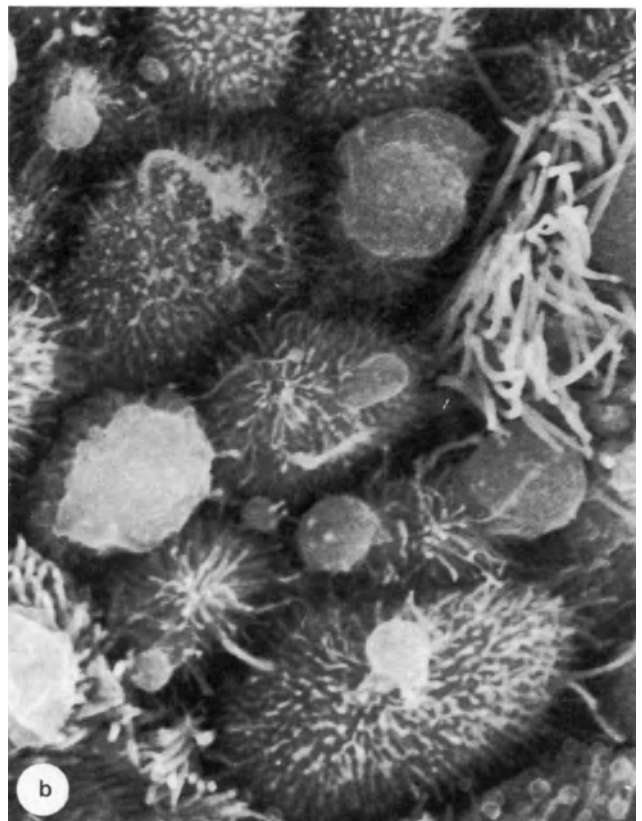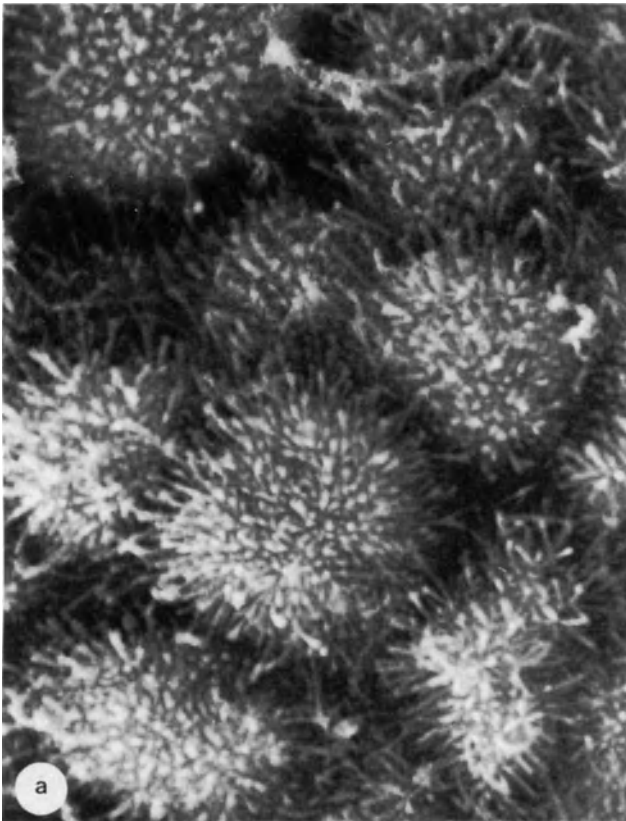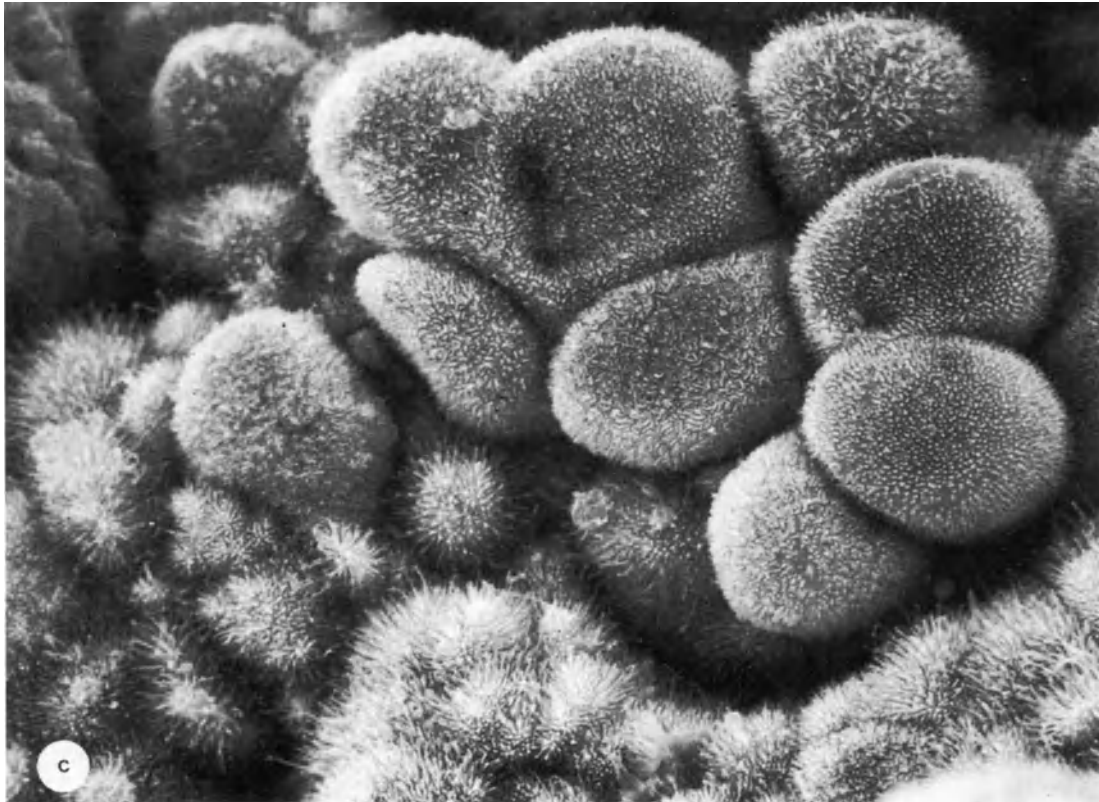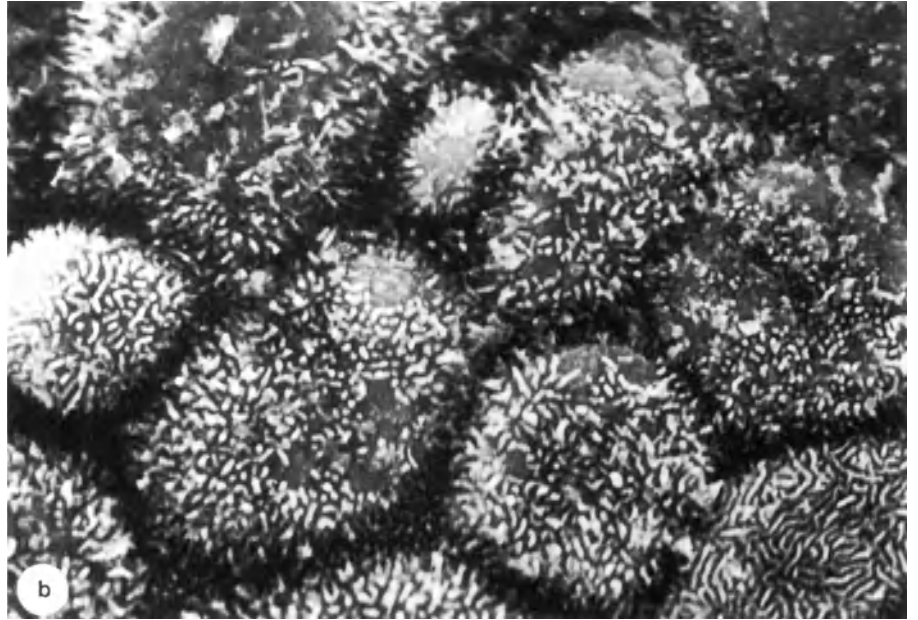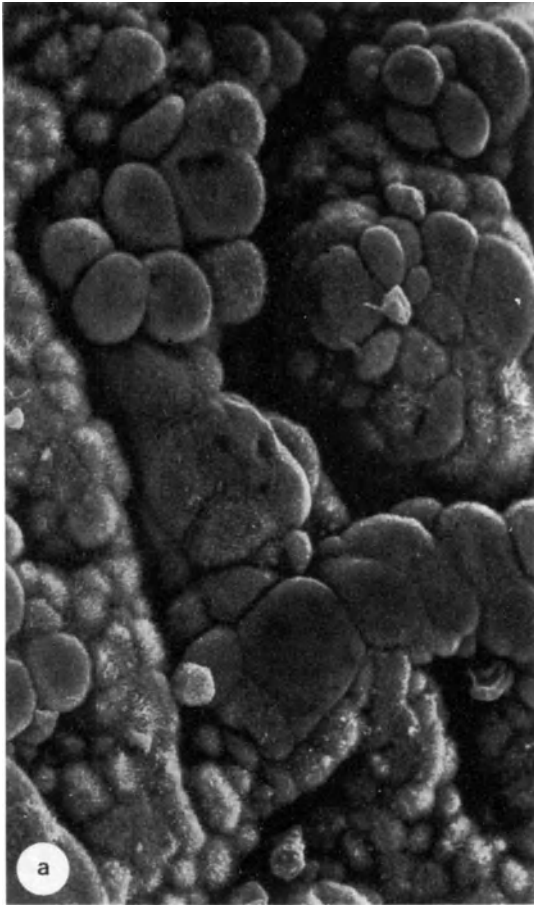a: Serous cystadenoma of the ovary with ciliated cells, well preserved surface structures (×2550)

b: Serous cystadenoma with regular ciliated and microvillous cells (×2550)

c: Serous cystadenoma showing numerous microvillous and few ciliated cells (×2550)

d: Well developed tall cilia on surface of ovarian cystadenoma (×2550)

Figure 7

a: Ovarian serous cystadenocarcinoma showing papillary arrangements of irregular cells, varying in size and shape (×1500)

b: Ovarian cystadenocarcinoma showing small undeveloped microvilli and partly denuded cell surfaces (×3000)

c: Ovarian cystadenocarcinoma with irregular surface and varying number of microvilli (×3000)
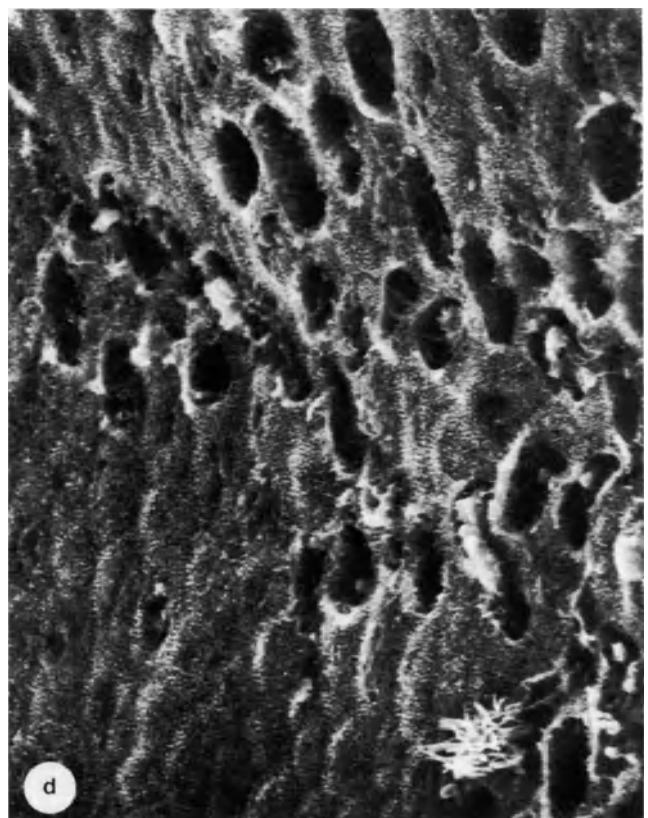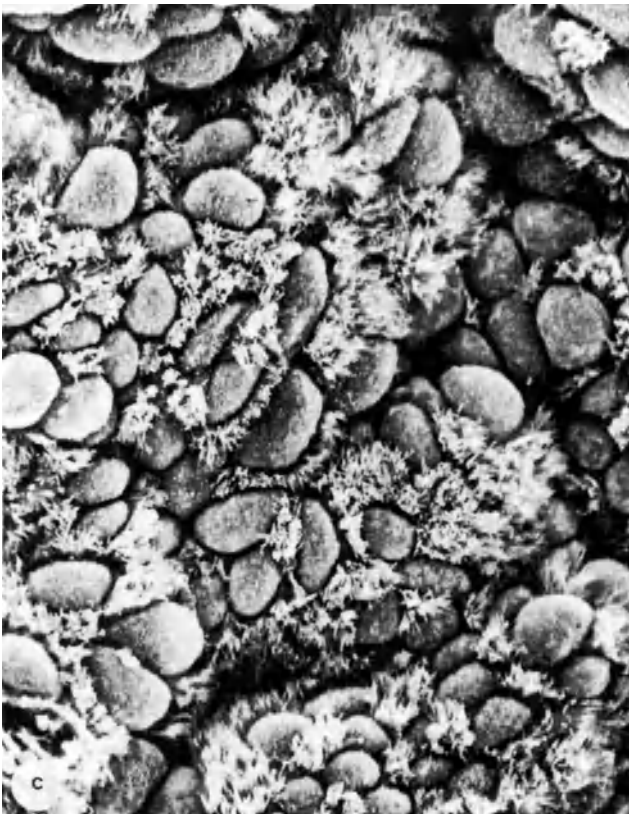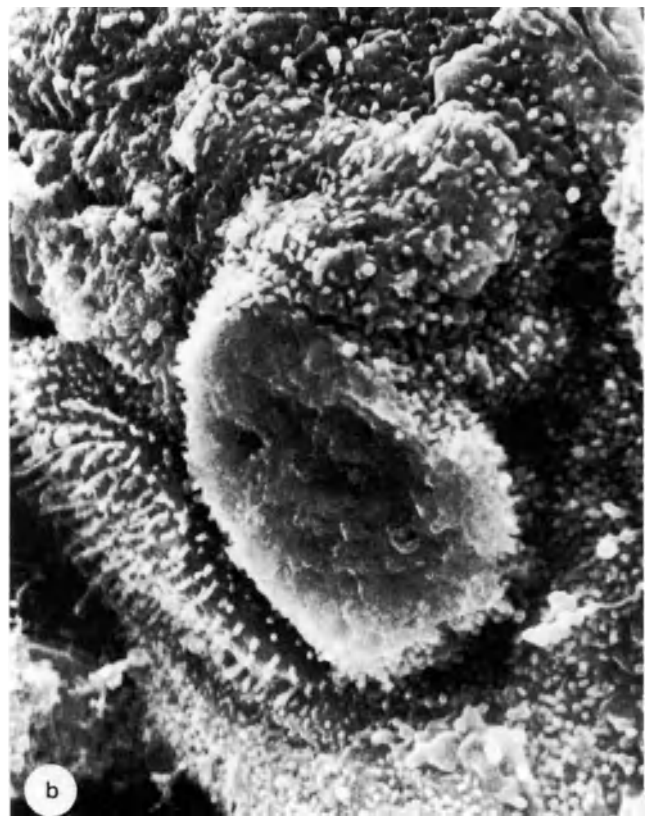
Figure 8
a: Undulating surface of endometrioid ovarian adeno-carcinoma ($\times 120$)
b: Endometrioid ovarian adenocarcinoma with irregular cells and partly developed surface structures ($\times 1700$)
c: Mucinous cystadenoma of the ovary with cells having centralled located microvilli and peripheral well-developed cilia ($\times 1200$)
d: Mucino cystadenoma showing holes capable of secretion of the surface ($\times 800$)
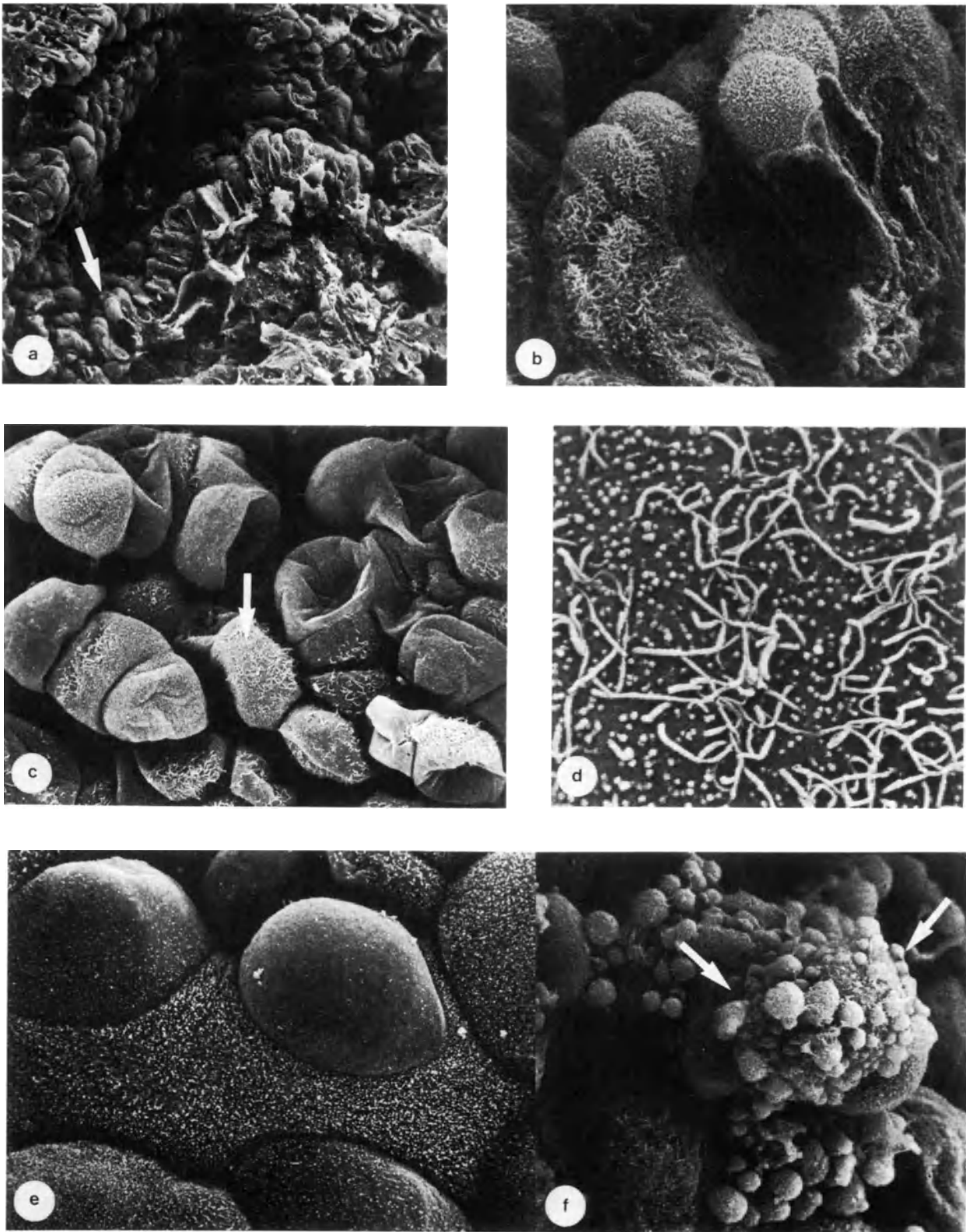
Figure 9 Clear cell adenocarcinoma in human ovarian tumors
a: Scanning electron micrograph of the sectional surface of clear cell adenocarcinoma. Clear cells are indicated by arrow. Note the clear cell forming glandular structures ($\times 255$)
b: Higher magnification of the arrow area of Figure 9a. Note the luminal microvilli ($\times 1700$)

c: Similar feature of Figure 9b. Also note the prominent microvilli ($\times 850$)
d: Higher magnification of Figure 9c. Note the slender microvilli and short microvilli ($\times 8500$)
e: Emerging clear cells have barely noticeable short microvilli ($\times 1700$)
f: In other areas, predominant aggregations of various-sized secretions are noted (arrow) ($\times 1700$)
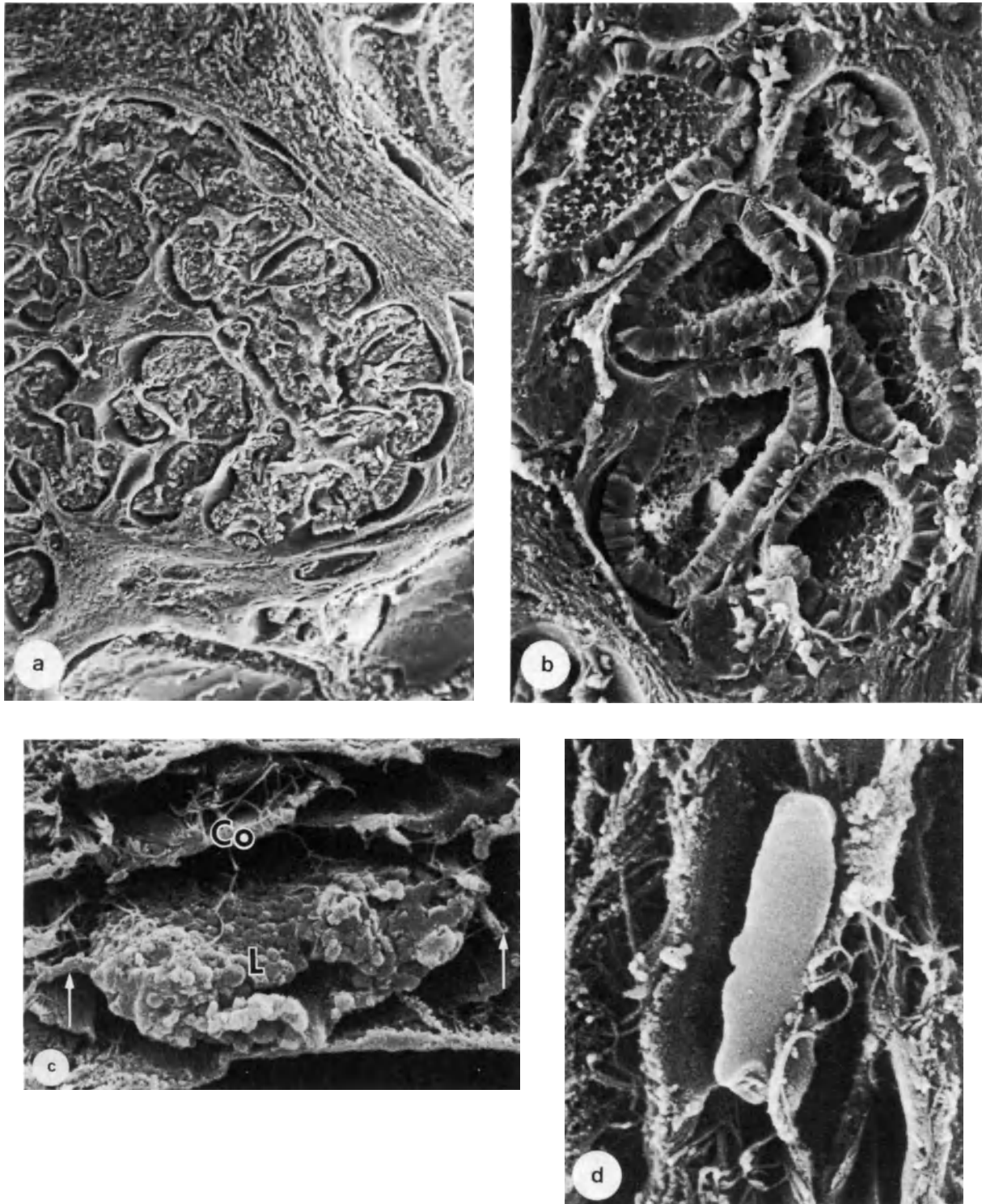
Figure 10   Sertoli–Leydig cell tumors (human ovaries)
a: Typical Sertoli–Leydig cell tumor (×80)
b: The tumor is well differentiated. The tubules lined with cuboidal to columnar Sertoli cells are arranged in lobules (×250)

c: Leydig cell (L) in intertubular stroma. Cytoplasmic processes (arrow) extend to collagenous stroma (Co) (×3750)
d: A crystal of Reinke in cytoplasm (×4000)

and shape, some being elongated or angular, others kidney-shaped or rounded. The remaining preserved surface structures were also altered with branched angular or S-shaped formations (Figure 12).

Evaluation of the degree of malignancy based upon surface structure can be done on the ultrastructural level. Papillary structures are common in malignant tumors (Julian and Woodruff, 1972). Many of the tumor cells display cilia and some assume a rounded shape with abundant cytoplasm referred to as 'mesothelial' cells. Ciliated cells are common in benign serous cystadenomas, less frequent in borderline tumors and rare in the malignant epithelium except in well-differentiated areas. The absence of ciliated cells in a serous cystadenoma may indicate malignancy of the tumor, but the presence of ciliated cells is not diagnostic for benign tumors (Roberts et al., 1970; Blaustein, 1976). Transitions from one type of epithelium, benign, borderline and malignant, to another is observed, indicating that all ovarian cystadenomas have the same origin, and that they develop into more malignant ones by malignant transformation from their benign counterparts.

ENDOMETRIOID TUMORS

A large proportion of ovarian tumors have been known for years as simple or unclassified adenocarcinoma of the ovary (Table 1). The term endometrioid adeno-carcinoma indicates some morphological similarity between this type of primary ovarian carcinoma and carcinoma of the endometrium (Thompson, 1957; Long and Taylor, 1964; Cummins et al., 1974). The relation to other surface tumors, mucinous, serous, clear cell and Brenner tumors, is also unclear, as serous and mucinous elements occur in endometrioid tumors as well as argentaffin cells (Anderson, 1972; Serov et al., 1973). The definite development of endometrial adenocarcinomas is also unsettled, being either development from pre-existing endometriosis, implants from the endometrium or as primary malignant tumors (Scott, 1953; Scully et al., 1966; Gricouroff, 1968; Stenbäck et al., 1980; Stenbäck and Kauppila, 1981b).

Ultrastructural analysis of the surface of endometrioid ovarian tumors shows glandular arrangements of columnar cells occasionally with club-like, rod-shaped structures on the surface. Frequently apical borders of the surface of these tumors are covered with short and irregular microvilli similar to that of proliferative endometrium. Some cells show grooves and ridges on a fairly smooth surface (Figures 8a, 8b).

TERATOMAS

The second most common group of ovarian tumors after surface epithelial lesions are tumors of germ cell origin. They develop from the totipotential germ cells of the definitive gonad. These are formed when the primitive germ cells in the embryo migrate from the yolk sac to the urogenital ridge and there ultimately develop. Neoplastic transformation and proliferation of germ cells with differentiation principally along embryonic, rather than extraembryonic, lines are

considered teratomas (Fox and Langley, 1976). The teratomata have commonly been divided into benign cystic teratomas, benign cystic teratomas with malignant change, solid teratomas and monophyletic teratomas (Fox and Langley, 1976). Another type of classification is the use of simple and complex types (Caruso et al., 1971). Both types usually contain mature, well-differentiated adult tissue though sometimes in bizarre and chaotic arrangements. The simple variety, the epidermoid cyst, is devoid of adnexal structures. The dermoid cyst consists of skin with hair follicles and sebaceous glands with few or no other combinations of heterotopic tissue, representing derivatives of different germ layers in various proportions.

Examinations of the surface ultrastructure of cystic ovarian teratomas shows extensive squamous epithelium with abnormal maturation and keratinization of surface cells causing keratinous flakes occasionally in polypoid configurations. The respiratory epithelium shows an abundance of microvillous and ciliated cells, areas with disorganized surface structures. Piling up of squamous cells in heaps, piles, cauliflower or onion-like arrangements is also found (Figures 5c, 5d).

OTHER TUMORS

As shown in Table 1 a number of other tumors are found in the ovary (Pedowitz and Pomeranze, 1962; Novak et al., 1975; Melis and Carpino, 1980), SEM information is, however, scanty. Clear cell adenocarcinoma types are shown in Figure 9. These tumors are surface epithelial lesions characterized by abundant glycogen in the cytoplasm (Fox and Langley, 1976). Sertoli–Leydig cell tumors are derived from the specialized ovarian stroma. Their morphology (Figure 10) and histogenesis is disputed (Jensen and Fechner, 1969; Kalderon and Tucci, 1973; Roth et al., 1974; Ramzy and Bos, 1976).

References

Anderson, M. C. (1972). Endometrioid tumor of the ovary with mucinous and serous components. Am. J. Obstet. Gynecol., 113, 686

Blaustein, A. (1976). Papillary serous tumours of the ovary: an electron microscopic study. Gynec. Oncol., 4, 314

Caruso, P. A., Marsh, M. R., Minkowitz, S. and Karten, G. (1971). An intense clinicopathologic study of 305 teratomas of the ovary. Cancer, Philad., 27, 343

Cummins, P. A., Fox, H. and Langley, F. A. (1974). An electron microscopic study of the endometrioid adeno-carcinoma of the ovary and a comparison of its fine structure with that of normal endometrium and of adenocarcinoma of the endometrium. J. Pathol., 113, 165

Czernobilsky, B., Borenstein, R. and Lancet, M. (1974). Cystadenofibroma of the ovary. Cancer, Philad., 34, 1971

Fenoglio, C. M., Castadot, M. J., Ferenczy, A., Cottral, G. A. and Richart, R. M. (1977). Serous tumors of the ovary. Gynecol. Oncol., 5, 203

Fenoglio, C. M., Ferenczy, A. and Richart, R. M. (1976). Mucinous tumors of the ovary II. Ultrastructural features of mucinous cystadenocarcinomas. Am. J. Obstet. Gynecol., 125, 990

Ferenczy, A. and Richart, R. M. (1974). *Female Reproductive System: Dynamics of Scan and Transmission Electron Microscopy*, pp. 286–94. (New York: Wiley)

Fox, H., Kazzas, B. and Langley, F. A. (1964). Argyrophil and argentaffin cells in the female genital tract and in ovarian mucinous cysts. *J. Pathol. Bacteriol.*, **88**, 479

Fox, H. and Langley, F. A. (1976). *Tumors of the Ovary*, (London: Heinemann Medical Books)

Fredricsson, B. and Björkman, N. (1962). Studies on the ultrastructure of the human oviduct epithelium in different functional states. *Z. Zellforsch.*, **58**, 387

Freeman, J. A. (1966). Goblet cell fine structure. *Anat. Rec.*, **154**, 121

Gondos, B. (1971). Electron microscopic study of papillary serous tumours of the ovary. *Cancer, Philad.*, **27**, 1455

Gondos, B. (1975). Surface epithelium of the developing ovary *Am. J. Pathol.*, **81**, 303

Gricouroff, G. (1968). Endometrioid Tumors of the Ovary. *Ovarian Cancer*, pp. 23–39. UICC monograph series, Vol. 11 (ed. by Gentil, F. and Junqueira, A. C.) (New York: Springer-Verlag)

Janovski, N. A. and Paramanandhan, T. L. (1973). *Major Problems in Obstetrics/Gynecology*. Vol. 4: *Ovarian Tumors*. (Philadelphia: W. B. Saunders)

Jensen, A. B. and Fechner, R. E. (1969). Ultrastructure of an intermediate Sertoli–Leydig cell tumor: a histogenetic misnomer. *Lab. Invest.*, **21**, 527

Julian, C. G. and Woodruff, J. D. (1972). The biologic behavior of low-grade papillary serous carcinoma of the ovary. *Obstet. Gynecol.*, **40**, 860

Kalderon, A. E. and Tucci, J. R. (1973). Ultrastructure of a human chorionic gonadotropin and adenocorticotropin responsive functioning Sertoli-Leydig cell tumor (type I). *Lab. Invest.*, **29**, 81

Katzenstein, A.-L. A., Mazur, M. T., Morgan, T. E. and Kao, M. (1978). Proliferative serous tumors of the ovary. Histologic features and prognosis. *Am. J. Surg. Pathol.*, **2**, 339

Kaye, G. I., Fenoglio, C. M., Pascal, R. R. and Lane, N. (1973). Comparative electron microscopic features of normal, hyperplastic, and adenomatous human colonic epithelium. *Gastroenterology*, **64**, 926

Klemi, P. J. and Nevalainen, T. J. (1978). Pathology of mucinous ovarian cystadenomas. 2. Ultrastructural findings. *Acta Pathol. Microbiol. Scand.*, Sect. A, **86**, 471

Laguens, R. P., Lagrutta, J., Koch, O. R. and Quijano, F. (1967). Fine structure of human endocervical epithelium. *Am. J. Obstet. Gynecol.*, **98**, 773

Langley, F. A., Cummins, P. A. and Fox, H. (1972). An ultrastructural study of mucin secreting epithelia in ovarian neoplasms. *Acta Pathol. Microbiol. Scand.*, A., Suppl. **233**, 76

Long, M. E. and Taylor, H. C. (1964). Endometrioid carcinoma of the ovary. *Am. J. Obstet. Gynecol.*, **90**, 936

Melis, M. and Carpino, F. (1980). In Motta, P. and Hafez, E. S. E. (eds). *Ovarian Tumors in Biology of the Ovary*. (The Hague: Martinus Nijhoff)

Nevalainen, T. J. and Järvi, O. H. (1977). Ultrastructure of intestinal and diffuse type gastric carcinoma. *J. Pathol.*, **122**, 129

Novak, E. R., Jones, S. G. and Jones, H., Jr. (1975). *Textbook of Gynecology*. (Baltimore: Williams & Wilkins)

Numers, V. von (1965). Observations on metaplastic changes in the germinal epithelium of the ovary and on the etiology of ovarian endometriosis. *Acta Obstet. Gynecol. Scand.*, **44**, 107

Papadaki, L. and Beilby, J. O. W. (1975). Ovarian cystadenofibroma: A consideration of the role of estrogen in its pathogenesis. *Am. J. Obstet. Gynecol.*, **121**, 501

Pedowitz, P. and Pomerance, W. (1962). Adrenal-like tumors of the ovary; review of literature and report of 2 new cases. *Obstet. Gynecol.*, **19**, 183

Radisavljevic, S. V. (1977). The pathogenesis of ovarian inclusion cysts and cystomas. *Obstet. Gynecol.*, **49**, 424

Ramzy, I. and Bos, C. (1976). Sertoli cell tumors of the ovary: light microscopic and ultrastructural study with histogenetic considerations. *Cancer Philad.*, **38**, 2447

Roberts, D. K., Marshall, R. B. and Wharton, J. T. (1970). Ultrastructure of ovarian tumors. *Cancer. Philad.*, **25**, 947

Roth, L. M., Cleary, R. E. and Rosenfield, R. L. (1974). Sertoli–Leydig cell tumor of the ovary with an associated mucinous cystadenoma: an ultrastructural and endocrine study. *Lab. Invest.*, **31**, 648

Scott, R. B. (1953). Malignant changes in endometriosis. *Obstet. Gynecol.*, **2**, 283

Scully, R. E. (1970a). Germ cell tumors of the ovary. In Sturgis, S. H. and Taylor, M. L. (eds) *Progress in Gynecology*, vol. 5. (New York: Grune & Stratton)

Scully, R. E. (1970b). Gonadoblastoma. *Cancer Philad.*, **25**, 1340

Scully, R. E. (1953). Gonadoblastoma: a gonadal tumor related to the dysgerminoma (seminoma) and capable of sex-hormone production. *Cancer*, **6**, 455

Scully, R. E., Richardson, G. S. and Barlow, J. F. (1966). The development of malignancy in endometriosis. *Clin. Obstet. Gynecol.*, **9**, 384

Serov, S. F., Scully, R. E. and Sobin, L. H. (1973). *Histological Typing of Ovarian Tumours*, pp. 37–42. (Geneva: WHO)

Stenbäck, F. (1980). Morphology of mucinous cystadenoma of the ovary: surface ultrastructure, development and biological behavior. *Int. J. Gynaecol. Obstet.*, **18**, 157

Stenbäck, F. (1981). Benign, borderline and malignant serous cystadenomas of the ovary. A transmission and scanning microscopical study. *Pathol. Res. Pract.*, **172**, 58

Stenbäck, F. and Kauppila, A. (1981a). Development and classification of parovarian cysts. An ultrastructural study. *Gynecol. Obstet. Invest.*, **12**, 1

Stenbäck, F. and Kauppila, A. (1981b). Endometrioid ovarian tumors: Morphology and relation to other endometrial conditions. *Gynecol. Obstet. Invest.*, **12**, 57

Taylor, C. R., Klirman, R. J. and Warner, N. E. (1978). The potential value of immunohistologic techniques in the classification of ovarian and testicular tumors. *Hum. Pathol.*, **9**, 417

Teilum, G. (1977). *Special Tumors of Ovary and Testis and Related Extragonadal Lesions*, 2nd edn (J. B. Lippincott, Philadelphia)

Thompson, J. D. (1957). Primary ovarian adenoacanthoma: its relationship to endometriosis. *Obstet. Gynecol.*, **9**, 403

Wilson, J. R.., Beecham, T. C. and Carrington, E. R. (1975). *Obstetrics and Gynecology*. St Louis: Mosby)

Zuckerman, L. and Weir, B. J. (eds) (1977). *The Ovary*, 2nd edn. (New York: Academic Press)

17

The mammary gland

E. SPRING-MILLS*†, M. O. BROPHY* and P. J. NUMANN‡

* Department of Anatomy* and Urology†, and Surgery‡, State University of New York, Syracuse, New York

THE NORMAL BREASTS

The breasts are specialized skin glands which undergo maturational changes at puberty but only achieve full structural and functional development during lactation. The structural and physiological status of these glands usually is in excellent agreement with the age, reproductive stage and hormonal balance of the individual. In mature, non-pregnant women each breast contains 15–20 lobes radiating from the nipple or mammary papilla. Each lobe is an independent gland containing an arborizing duct system. The ducts converge to form a single lactiferous duct that dilates to form a lactiferous sinus and then narrows as it opens onto the nipple. Dense irregular connective tissue occurs between lobes. Loose, moderately cellular connective tissue subdivides the lobes into lobules, the basic structural units. Ducts (i.e., primary/lactiferous, secondary/interlobular and tertiary/intralobular) are the chief epithelial components. Most ducts contain bi-layered, stratified cuboidal or columnar epithelium. There are two cell types, glandular and myoepithelial. True alveoli with simple, cuboidal epithelium and an incomplete layer of basal myoepithelial cells are rare in the breasts of nulliparous young women. However, a moderate number of alveoli are present in breasts of nulliparous older women and in breasts from non-pregnant multiparous women who are premenopausal. In postmenopausal women the glands involute and little epithelium remains except beneath the areola and in the upper, outer quadrants.

SURFACE CHARACTERISTICS OF NORMAL AND ABNORMAL BREAST CELLS

Scanning electron microscopy of the breast is technically difficult because: the epithelium is very sparse in relationship to the amount of connective and adipose tissue; ducts often cannot be located with certainty in an unfixed specimen even with a dissecting microscope; and the proteinaceous fluid secreted by the epithelium adheres strongly to the apical surfaces and microvilli. In addition, variation in breast architecture produced by regional differences among the independent glands and gland fields, as well as the changes associated with the menstrual cycle and hormonal milieu, complicate interpretation and recognition of the range of normal structural variation. Usually, however, the apical surfaces of normal breast epithelial cells are covered by numerous microvilli (Spring-Mills and Elias, 1975, 1976, 1978). The microvilli on the glandular cells are longer, more regular and closer together than the microvilli on the myoepithelial cells.

In 1975, Spring-Mills and Elias observed more variation in the size, shape, distribution and number of microvilli on duct cells from cancerous breasts than on duct cells from tumor-free breasts. Subsequent observations of breast tissues from women undergoing reduction mammoplasty, biopsy or mastectomy indicate that infiltrating duct carcinoma cells can be identified in the breast stroma with the SEM on the basis of shape and surface characteristics, and that dramatic changes in cell surfaces also occur in non-proliferative and benign proliferative breast diseases (Spring-Mills and Elias, 1976, 1978). While normal mammary epithelial cells usually are similar in size and shape and contain regular, moderately long microvilli, abnormal mammary epithelial cells can assume a variety of shapes, sizes and surface characteristics. Although no single cellular alteration has been found in only one disease, some changes are more commonly associated with certain breast diseases than with others. Depending upon the disease process, the surface alterations may be focal or disseminated.

DYSPLASIA (fibrocystic disease, chronic cystic mastitis, Schimmelbusch's disease, mazoplasia, etc.)

Mammary dysplasia usually is found in women during the decade prior to the onset of menopause (McDivitt *et al.*, 1968; Haagensen, 1971). The breast becomes lumpy because of an increase in the interlobular connective tissue and/or disturbances in the ductal

Table 1 Common surface features of abnormal human breast cells

Condition	Cell shape	Cell size	Shape of apical surface	Microvilli Number	Length	Distribution	Pleomorphism
Benign mammary dysplasia	usually cuboidal to columnar; squamous in some cysts	usually slight to moderate variation; often pronounced in hyperplastic areas	slightly domed; flat in areas of squamous changes	2–3	2–3	usually uniform	0–1
Fibroadenoma	usually cuboidal	slight to moderate variation	usually flatter than normal	2	2–3	uniform or marginated	0–1
Plasma cell mastitis	cuboidal to squamous	slight variation	flat, spindle shape	2	1	uniform	0–1
Carcinoma (infiltrating duct) ducts	cuboidal to columnar	moderate to highly variable	usually domed	1–2	1	variable	2–3
carcinoma cells	spherical or pear shape	slight variation	flatter than duct cells	0–1	1	variable	1

Key: 0 = none; 1 = some, little or short; 2 = moderate; 3 = extensive or long

epithelium such as hyperplasia, dilatation and cyst formation with or without proliferation of the intralobular stroma (Haagensen, 1971; Minkowitz et al., 1973). Most often the condition is bilateral and a deficiency of progesterone with a real or relative excess of estrogens may promote or exacerbate it. Women with dysplasia, especially those with gross fibrocystic disease, have an increased risk of developing breast carcinoma, but it is uncertain whether the two disease processes are obligatorily or coincidentally related (Davis et al., 1964; McDivitt et al., 1968; Haagensen 1971).

At the light microscopic level (Figures 1a,b) mammary dysplasia is characterized by varying combinations of epithelial proliferation, fibrosis, cystic dilatation of ducts and lymphocytic infiltration. The disturbance may be limited and focal, or patches of dysplastic tissue may be found throughout the breast. The duct cells often are not uniform in size or shape (Figure 1c,d). Although some cells may contain more microvilli than other cells (Figure 1d), the microvilli are fairly evenly distributed in all but the most severe cases. In contrast to extralobular ducts, intralobular duct cells and alveolar cells may contain secretory blebs on their apical surfaces (Figure 1e). Blue dome cysts, gross cysts, microcysts and apocrine cysts often are encountered and have been described previously (Spring-Mills and Elias, 1975, 1976, 1978). Columnar cyst cells almost always have numerous regular or irregular microvilli. As the apical surfaces flatten and the cyst cells become cuboidal or squamous, most of the microvilli become reduced in height; however, the marginal microvilli that encircle the region above the junctional complex remain elongated and are very conspicuous (Spring-Mills and Elias, 1976). In hyperplastic regions the cells are crowded. Within the ducts they often form roughly circular plaques and ridges covered by cells exhibiting variations in size, shape and microvilli (Figure 2a).

FIBROADENOMA (intracanalicular or pericanalicular fibroadenoma, fibroma, adenofibroma)

Fibroadenomas are very common benign breast tumors. Most occur in nulliparous women before the age of 35. Tumor growth is slow except during pregnancy and lactation. Usually only one breast is involved; however, we have several patients with bilateral breast tumors and two with accessory fibroadenomas which arise along the trunk in what presumably are vestiges of the embryonic milk ridge. The ultrastructural observations of Murad et al. (1967) indicate that epithelial cell proliferation is secondary to stromal cell expansion.

Fibroadenomas are lobulated tumors composed of epithelial and stromal tissue (Figure 2b). Usually the epithelium is bilayered and inactive in appearance, but papillary proliferation and adenosis-like areas may be found as well. In some specimens the epithelial cells

Figure 1

a: Light micrograph showing dilated primary duct with some eosinophilic secretion and portions of lobules. Benign mammary dysplasia (×50)

b: Light micrograph showing portion of lobule with many microcysts. The cysts are formed from dilated ducts. As secretion continues the cysts become progressively more distended. Large cysts may lose their lining epithelium. Benign mammary dysplasia (×75)

c: In this low-power scanning electron micrograph, the slight to moderate variation in epithelial cell shape that usually is associated with this condition can be seen. Benign mammary dysplasia

d: Microvilli exhibit some variation in length, number and distribution on glandular cells from dysplastic ducts

e: Secretory blebs form on the surfaces of some duct cells. Material contained within the blebs contributes to the amorphous eosinophilic material within the lumen
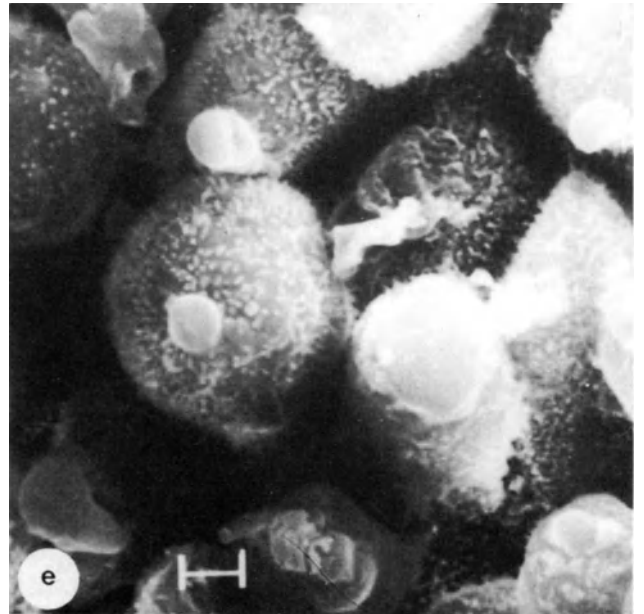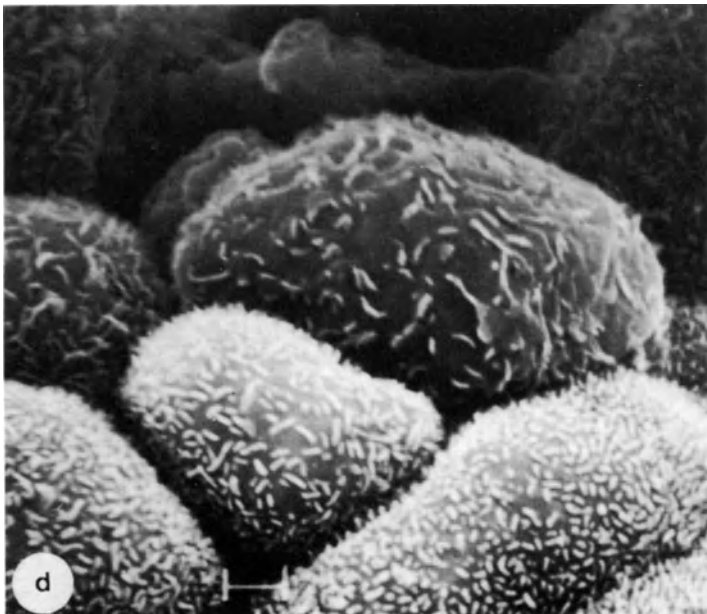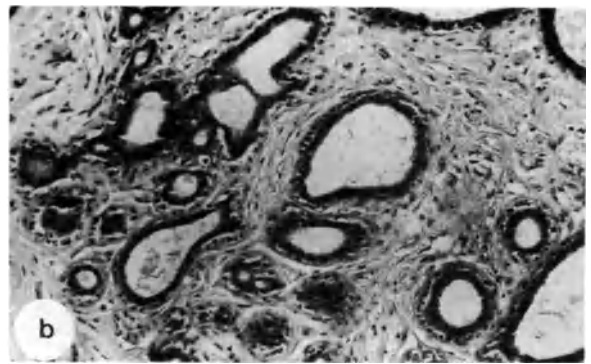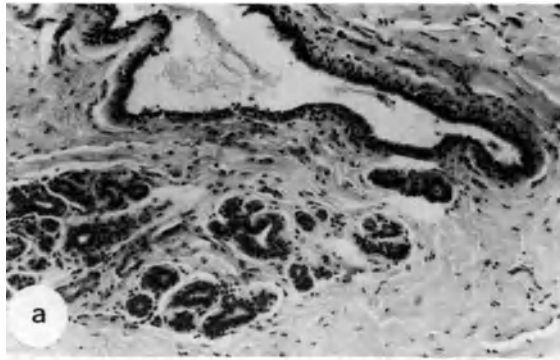
Figure 1

lining the wide ducts or clefts within the tumor are covered with a rather sparse coat of long microvilli. Sometimes the epithelial cells may have a flattened apical surface, short microvilli and exhibit moderate variations in size and shape (Figure 2c). In a few patients secretory blebs have been found on some of the epithelial cells lining the clefts (Figure 2d). Outside the tumor, duct cells usually are normal or minimally altered in appearance.

PLASMA CELL MASTITIS (mammary duct ectasia, comedomastitis, periductal mastitis)

Clinically evident plasma cell mastitis is uncommon. Usually it is detected as a lump beneath the areola in multiparous older or postmenopausal women. Little is known of its etiology; however, it is of widespread interest because the production of a palpable tumor, reactive fibrosis and retraction of skin below the areola stimulate mammary carcinoma.

Plasma cell mastitis presumably is an end-stage of mammary duct ectasia (dilation). It usually begins in the primary ducts beneath the nipple and areola. The ducts become filled with a complex mixture of cellular and fatty debris that may be discharged from the nipple. As the disease progresses it is presumed that some of the debris seeps into the periductal tissue. The walls of the dilated ducts eventually thicken because of reactive fibrosis and the infiltration of lymphocytes, plasma cells, foam cells (lipid-laden macrophages), eosinophils and neutrophils. At the light microscopic level, the epithelium usually appears squamous and atrophic (Figure 2e). The epithelial cells lining the ectatic ducts appear as flattened, elliptical plates covered by numerous short, regular microvilli. Usually there is little variation in cell size, shape or surface characteristics within the affected ducts, a finding consistent with the atrophic nature of the disease process (Figure 2f).

CARCINOMA

Carcinoma of the breast exhibits a bimodal age distribution. Over half of the cases are detected in women prior to the age of 49. The left breast is more prone to the disease than the right breast, and one-third or more of all carcinomas arise in the upper, outer quadrant (Haagensen, 1971). In the United States, approximately one out of every 15 women eventually develops breast cancer. Most carcinomas appear to arise from duct epithelium, and 40–50% of the cases have axillary metastases at the time of surgery. Since little can be done to cure these patients, much attention has been devoted to the recognition and detection of so-called 'early' lesions – cancer confined to the breast's ducts and lobules. The SEM is being used to define the surface features of these lesions.

Infiltrating duct carcinoma is the most common type of mammary carcinoma (McDivitt et al., 1968; Haagensen, 1971; Fisher et al., 1975). The cells are often closely packed in clusters or in single file. The cells may be fairly uniform in size, shape and staining characteristics. However, giant cells and highly pleomorphic, hyperchromatic cells are not uncommon. The tumor cells tend to infiltrate the stroma along ducts

and fascial strands. Reactive fibrosis is common, so that most carcinoma cells usually lie between strands of collagen and elastic fibers. Infiltrating duct carcinoma cells usually are oval to pear shape. They contain very few microvilli (Figure 3d,e). Within the stroma the tumor cells actively climb over each other and the connective tissue cells.

The apical surfaces of duct cells from breasts containing carcinoma are almost always atypical. Although no single surface feature is unique to this condition, duct cells from carcinoma patients usually contain fewer and shorter microvilli than duct cells from normal or dysplastic breasts. In addition, the microvilli are more pleomorphic (Figure 3c). When present, these changes are best seen in so-called non-involved areas close to the tumor; however, in more than half of the specimens studied the profound surface alterations were present in ducts at considerable distance from the tumor. As infiltrating duct carcinoma cells break through the basal lamina, there is a further reduction in microvilli and a profound change in cell shape. Whether the surface changes are directly or indirectly related to neoplasia and/or metastasis has not been determined.

Acknowledgements

References

Davis, H. H., Simons, M. and Davis, J. B. (1964). Cystic disease of the breast and relationship to carcinoma. *Cancer*, 17, 957

Fisher, E. R., Gregorio, R. M. and Fisher, B. (1975). The pathology of invasive breast cancer. *Cancer*, 36, 1

Haagensen, C. D. (1971). *Diseases of the Breast.* (Philadelphia: W. B. Saunders)

Figure 2 (opposite)

a: Intraductal ridges are formed by glandular cell proliferation in some hyperplastic ducts and cysts. In hyperplastic foci there may be considerable variation in cell size, shape and surface characteristics. Benign mammary dysplasia.

b: Light micrograph showing a fibroadenoma. These benign tumors may exhibit various growth patterns; however, malignant epithelial cell changes are rarely seen in fibroadenomas (×125)

c: The surfaces of the glandular epithelial cells often are slightly flattened and there is some variation in cell size and shape in fibroadenomas

d: Occasionally secretory blebs form on the epithelial cells within a fibroadenoma but most specimens contain cells that appear less active

e: An ectatic duct is shown in this light micrograph. Note its thick wall and the flattened cells surrounding the lumen. Plasma cell mastitis (×100)

f: The epithelial cells lining ectatic ducts are flatter than normal gland cells and contain short, regular microvilli. Plasma cell mastitis
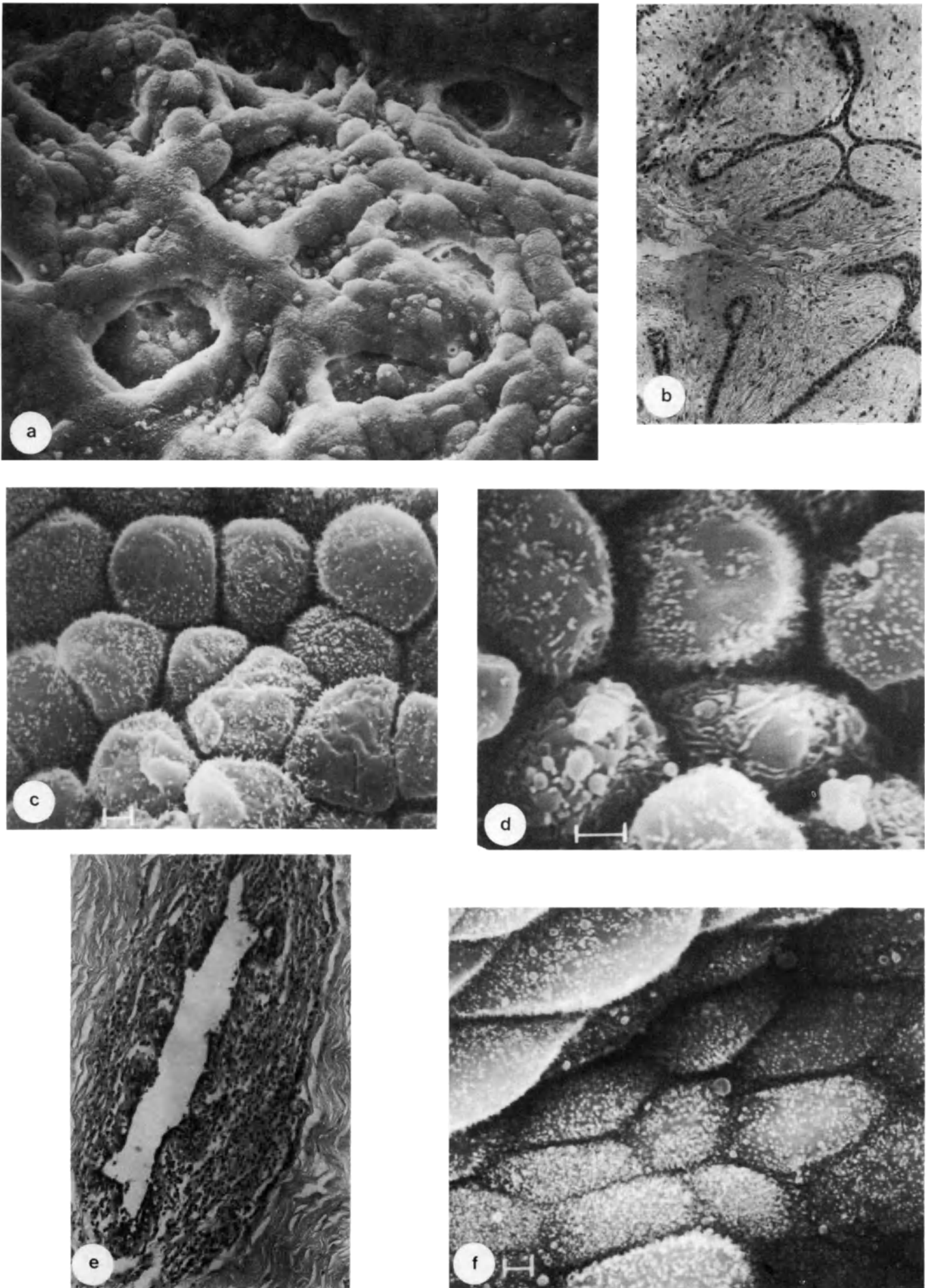
Figure 2

McDivitt, R. W., Stewart, F. W. and Berg, J. W. (1968). *Tumors of the Breast*, 2nd series, Fascicle 2, Atlas of tumor pathology. (Washington DC: Armed Forces Institute of Pathology)

Minkowitz, S., Hedayati, H., Hiller, S. and Gardner, B. (1973). Fibrous mastopathy. *Cancer*, 32, 913

Murad, T. M., Greider, M. H. and Scarpelli, D. G. (1967). The ultrastructure of human mammary fibroadenoma. *Am. J. Pathol.* 51, 663

Murad, T. M. and von Ham, E. (1968). The ultrastructure of fibrocystic disease of the breast. *Cancer*, 22, 587

Spring-Mills, E. and Elias, J. (1975). Cell surface differences in ducts from cancerous and noncancerous human breasts.

Science, 188, 947

Spring-Mills, E. and Elias, J. E. (1976). Cell surface changes associated wth human breast cancer. *SEM/1976 II*, pp. 1–10

Spring-Mills, E. and Elias, J. (1978). The mammary glands. In Hafez, E. S. E. (ed) *Scanning Electron Microscopy of Human Reproduction*, chapter 13, pp. 193–202. (Ann Arbor: Ann Arbor Science)

Spring-Mills, E., Berg, N. B. and Hafez, E. S. E. (1980). Lactation and fertility regulation. In Hafez, E. S. E. (ed.) *Human Reproduction*, chapter 14, pp. 355–70. (Hagerstown: Harper & Row)

Figure 3 (opposite)

a: Light micrograph showing histologic appearance of colloid carcinoma. The tumor cells secrete a mucinous material which accumulates in the stroma. Areas of mucin accumulation appear as spaces in fixed and sectioned specimens. Patients with colloid carcinomas have a better survival rate than patients with infiltrating duct carcinoma (×200)

b: The ducts from a patient with colloid carcinoma contain cells with many different sizes and surface characteristics (×8100)

c: Duct cells from patient with infiltrating duct carcinoma showing pronounced variation in cell size, shape and microvilli

d: Infiltrating duct carcinoma cells are shown in this light micrograph (×150)

e: Infiltrating duct carcinoma cells can be seen crawling over each other in this scanning electron micrograph
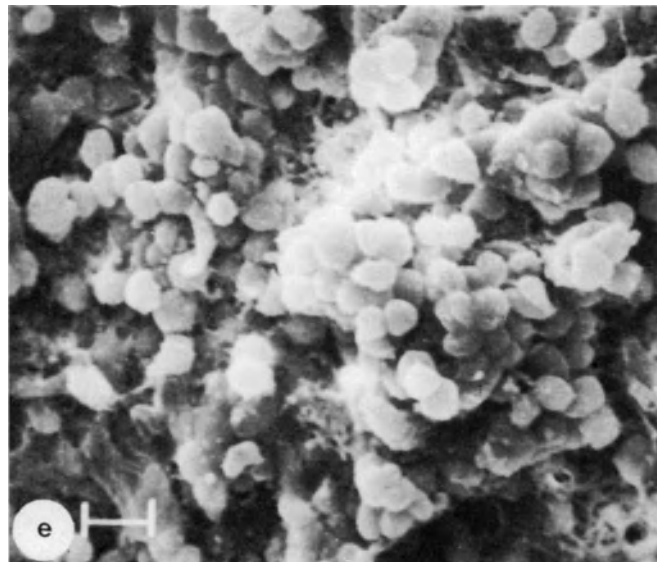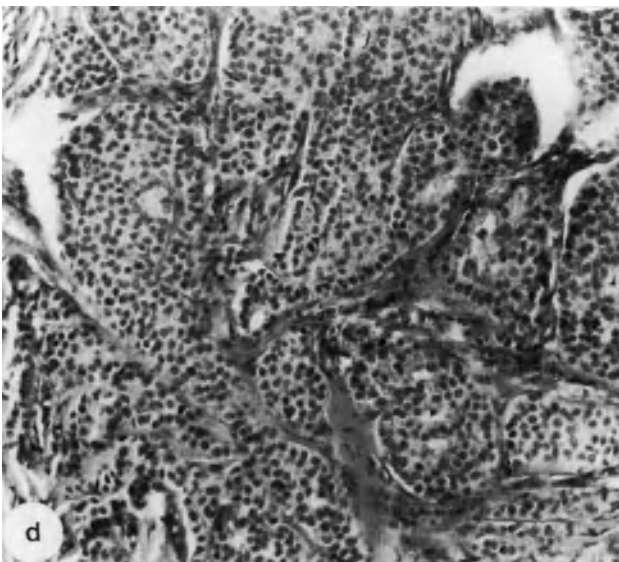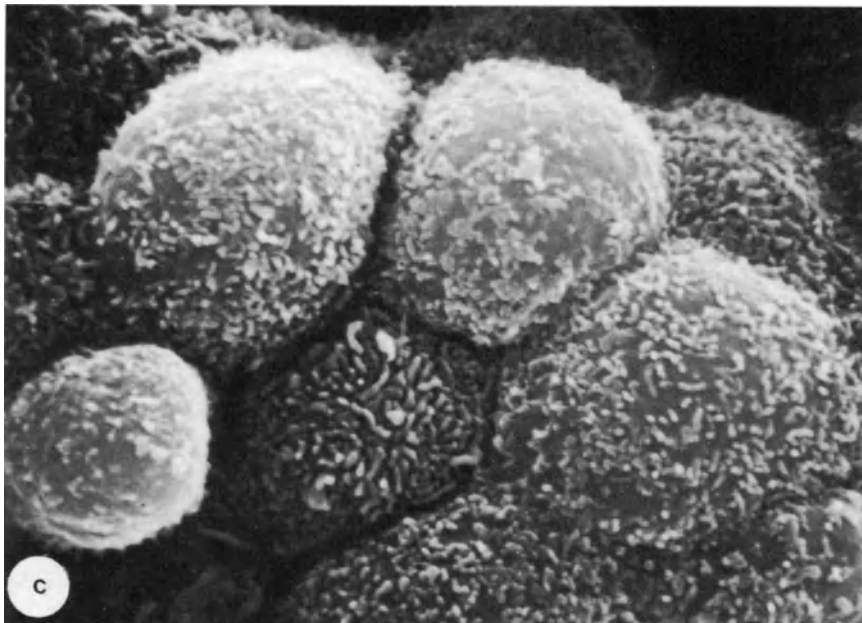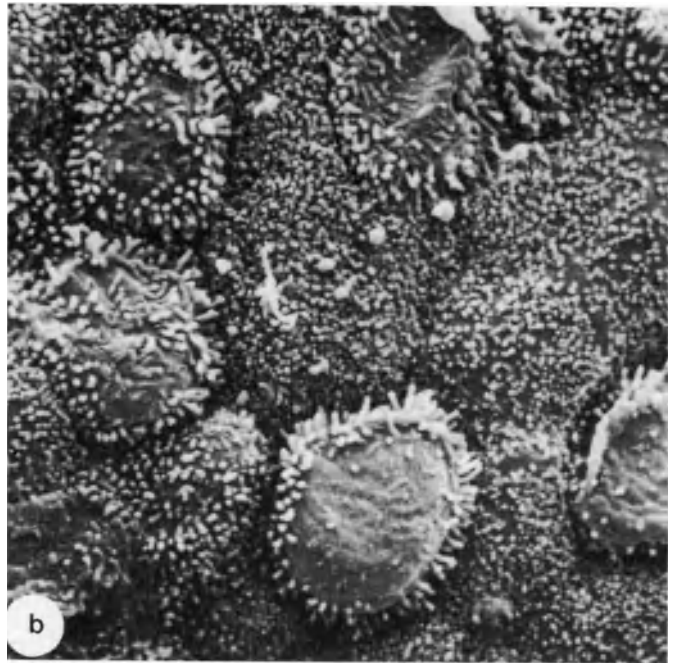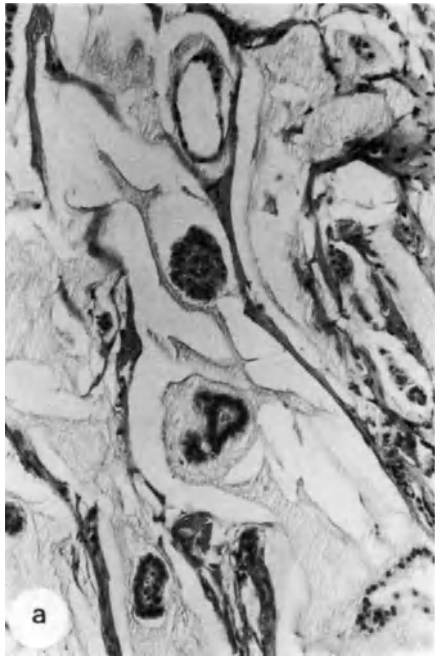
Figure 3

II ANDROLOGY

18

The seminal vesicle

E. SPRING-MILLS*†, and M. BUSH*

* Departments of Anatomy* and Urology†, State University of New York, Syracuse, New York

The seminal vesicles are elongated (~ 1–2 × 6 cm), paired male accessory sex glands which lie, one on each side of the midline, posterior to the urinary bladder, superior to the prostate and lateral to the vas deferens. There is moderate variation among individuals in how and precisely where the seminal vesicles join the vas deferens to form the ejaculatory ducts as well as the extent to which each gland coils upon itself. When the connective tissue binding the coils is cut, the glands usually unravel to form tubular structures (~ 15 cm long) composed of a mucosa, muscularis and adventitia.

Most normal specimens have a moderately well defined central lumen. A variable number of side branches and saccular recesses extend from the central lumen. The complexity and the variety of sizes and shapes of the projections along the mucosal surface is best appreciated when routine histologic sections are compared to scanning electron micrographs of these glands (Figure 1a,b). Both circular and longitudinal ridges are present along the central lumen and many of the branches and cavities. Some ridges are solid, while others with lumens allow communication and passage of secretion between segments. The thickness of the ridges varies considerably. It is not unusual to find projections which are thinner at the base than at the apex. The cavities also vary in size and the amount of contained secretion.

MUCOSA

The mucosa contains principal and basal cells. Most principal cells are columnar in shape and play a prominent role in the secretory process. Their nuclei are oval and situated in the lower half of the cytoplasm. After the age of 30, the nuclei become irregular in shape, size and staining affinity (Droese and Voeth, 1976; Koivuniemi and Tyrkkö, 1976). Hyperchromatic, polyploid nuclei with marginated heterochromatin and inclusions are often present in principal cells from old men (Meisels and Ayotte, 1976).

Rough endoplasmic reticulum and free ribosomes are abundant, especially in the basal cytoplasm of principal cells. The Golgi usually occupies a large crescent-shaped band of cytoplasm immediately above the nucleus. The granules are eosinophilic and osmiophilic. They occupy only a fraction of the membrane-limited vacuoles, the remainder being composed of a structureless matrix or empty space. The secretory granules are released at the apex of the cell via exocytosis. Apical junctional complexes and marginal flaps or folds are present between adjacent principal cells. The infranuclear cytoplasm contains much rough endoplasmic reticulum and a few medium mitochondria. The basal plasmalemma is regular and contains many hemidesmosomes. Membrane-bound lipopigment granules are common. In histologic sections they are yellowish-brown. At the ultrastructural level, however, their contents vary greatly in appearance and increase in number with increasing age (Koivuniemi and Tyrkkö, 1976; Aumüller, 1977). Nevertheless, seminal vesicle cells that are loaded with these pigments are not inactive. Instead, certain types of complex lipid metabolism and lipopigment formation may be coupled to secretory or absorptive activity (Aumüller, 1977).

The basal cells form an incomplete layer and lie immediately adjacent to the basal lamina. Their apical surfaces do not reach the lumen. The nuclei have no prominent nucleoli. The paucity of mitochondria, Golgi components and elements of the rough endoplasmic reticulum suggests that these cells probably are not actively synthesizing secretory products or export proteins.

Although two types of epithelial cells can be identified in histologic sections, usually only the surfaces of the glandular or principal cells can be seen in scanning electron micrographs unless the ridges are cut prior to observation (Figures a–d). The three-dimensional organization of the mucosa and the arrangement of the epithelial cells vary from one area of the gland to another in specimens obtained from accident victims and men who died from non-malignant diseases of the cardiovascular and gastrointestinal systems. In some regions the epithelium is simple columnar, in other regions it is pseudostratified. The
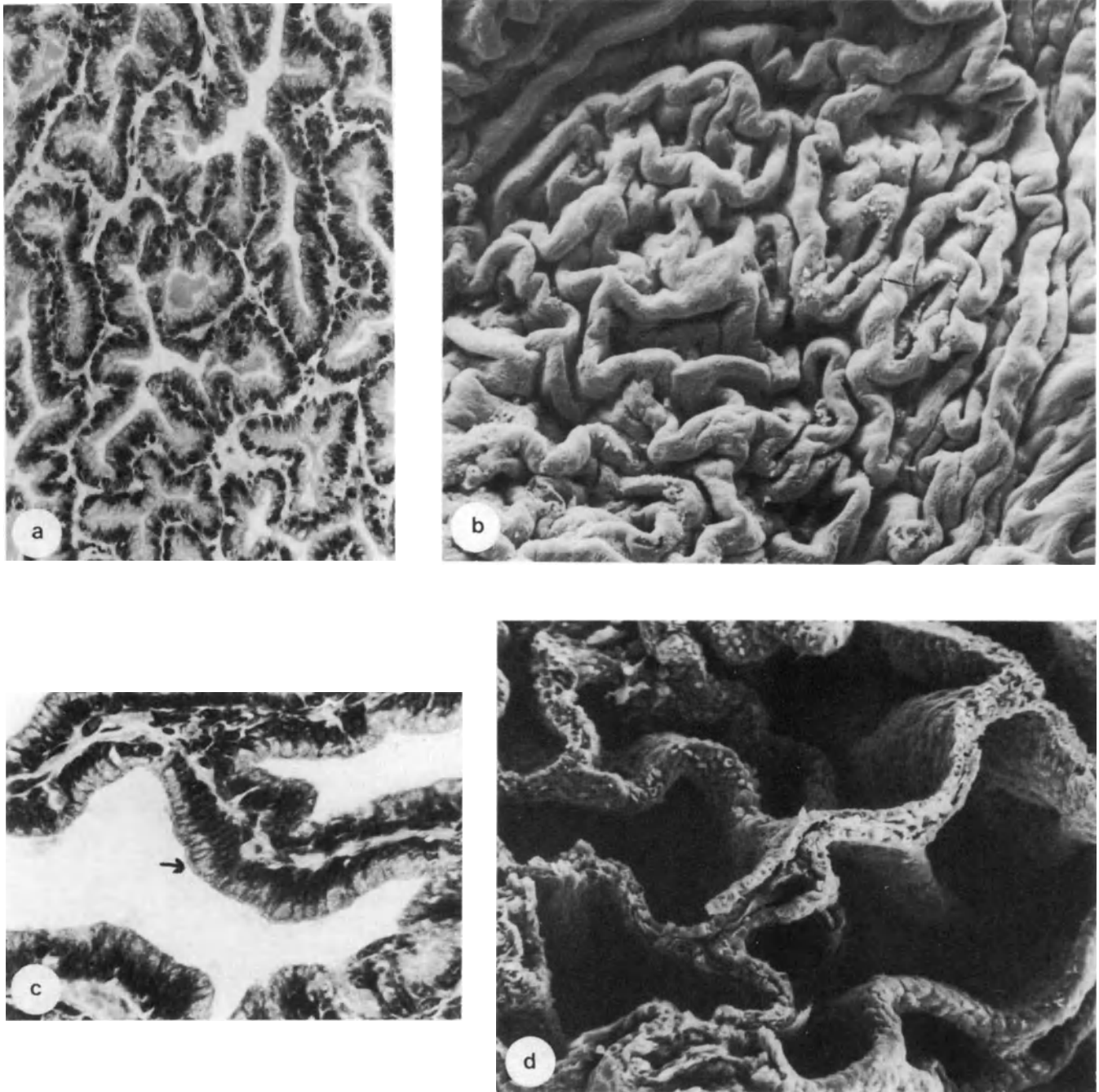
Figure 1

a: This light micrograph shows a section of the seminal vesicle. Many mucosal folds project into the central lumen (H and E, ×125)

b: Low-power scanning electron micrograph showing surfaces of mucosal ridges and folds which project into the central lumen. This region is comparable to that shown in Figure 1a, and is taken from the same individual (×150)

c: Light micrograph showing portion of a mucosal ridge at higher magnification. The columnar principal cells contain

elongated oval nuclei. In the supranuclear cytoplasm the Golgi apparatus appears as a negative image. A striated border of microvilli is obvious on some cells (arrow). A thin layer of highly vascular, loose connective tissue forms the core of the ridge (H and E, ×200)

d: The three-dimensional arrangement of the mucosal ridges is shown in this scanning electron micrograph. In several areas the ridges have been cut and the epithelium and connective tissue cores are shown (×150)

---

epithelial cells are supported by highly vascularized cores of lamina propria (Figures 1a, 1c, 1d, 2a). The apical surfaces of the principal cells either contain many or very few microvilli (Figure 2b). A solitary filopodium, which may be a cilium, often projects from the center of the apical membrane. In normal specimens, principal cells with few microvilli usually have many apical bulges. The bulges on such cells contain secretory granules. Nevertheless, it should be pointed out that it has not been determined whether microvilli disappear from the plasmalemma as the secretory granules move towards the cell surface or whether secretory granules are made only by cells with few microvilli.
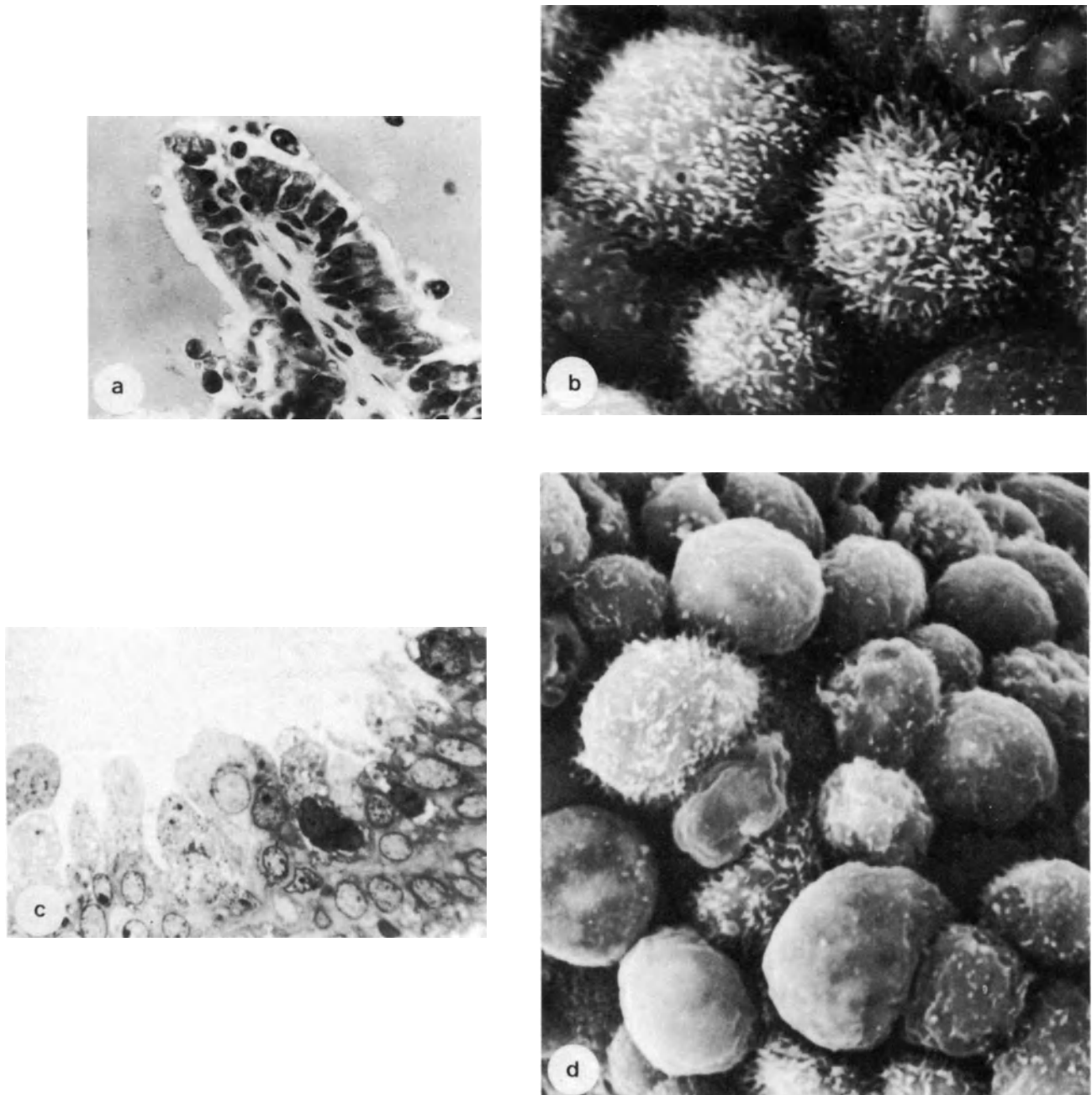
Figure 2

a: Light micrograph showing the tip of a mucosal ridge and surrounding secretion. Sloughed mucosal cells round up and lose their columnar shape. Most of the secretion is eosinophilic and uniform in texture. Sloughed seminal vesicle cells, migrating leukocytes and macrophages are suspended in the secretion (H and E, ×250)

b: The apical surfaces of principal cells can be seen in this scanning electron micrograph. Most cells have many moderately long microvilli. Cells similar to the one in the upper right corner with many secretory bulges usually have few microvilli (×3500)

c: Light micrograph showing thick plastic section of mucosa of seminal vesicle from a patient with prostatic carcinoma. The cells are crowded. In many areas the epithelium has become stratified. The cells show considerable variation in size, shape, cytoplasmic organization and nuclear morphology (×700)

d: Scanning electron micrograph showing surfaces of seminal vesicle cells from patient with prostatic carcinoma. Same patient as Figure 2c. The variation in cell size, shape and surface morphology are obvious (×3000)

Data gathered from light, transmission and scanning electron micrographs indicate that the secretion of these glands is a mixture of materials. Some is obviously exocytosed but other portions are derived from sloughed epithelial cells and intraepithelial migratory cells such as lymphocytes, neutrophils, eosinophils and macrophages. in rats, the number of migratory cells increases with age; however, a similar phenomenon has not been demonstrated in humans (Allison and Cearley, 1972).

Following castration, the principal cells atrophy and secretion diminishes or stops. The organelles associated with active secretion such as the rough endoplasmic reticulum and Golgi decrease in size and may become

disrupted. Lysosomes, however, tend to increase in size and activity. Appropriate androgen replacement therapy usually causes a prompt reversal of the effects of castration.

STROMA

A delicate lamina propria supports the mucosal folds. Fibroblasts, collagen and reticular fibers as well as numerous capillaries and venules are present in this loosely organized layer.

The muscularis forms robust layers. Usually the inner layers of smooth muscle cells are circularly arranged and the outer layers are longitudinal in orientation; however, it is not uncommon to find a large number of interlacing oblique fibers throughout the muscularis.

The adventitia is thin. It contains many blood vessels, collagen and elastic fibers.

ALTERATIONS IN PATIENTS WITH PROSTATIC CARCINOMA

Since needle biopsies are difficult to perform and the clinical signs of seminal vesicle disease are not clear-cut, little is known about the histopathology of these glands. Primary tumors seem to be rare (Boreau, 1977). A few papillary carcinomas and sarcomas have been reported (Mostofi and Price, 1973). Most of what we know about the morphology of these glands in humans has come from examination of the seminal vesicles removed from patients undergoing prostatectomy for prostatic carcinoma. The principal cells often undergo marked changes in these patients, especially if the prostatic tumor has entered the gland via direct extension. The principal cells may increase in height up to 150 or 200 μm and their shape also may become distorted. The nucleus may move from the central or basal regions to the apical cytoplasm and protrude into the lumen. Hyperplasia and crowding of cells within the mucosa is not uncommon. The number of pleomorphic microvilli usually increases and there often is a reduction in the number of microvilli or the principal cells (Figures 2c,d).

SURFACE CHANGES DURING POSTNATAL DEVELOPMENT AND AFTER CASTRATION IN RODENTS

In the guinea pig, the seminal vesicle epithelium undergoes striking changes during normal postnatal growth and development (Barham et al., 1979). As the animal matures, microvilli become more numerous on the cell surfaces. Maximum microvillus density occurs at puberty; however, the microvilli continue to increase in length during early adulthood. Secretory blebs are minimal or absent until shortly before puberty and then increase in number.

Castration of mature guinea pigs or rats (Barham et al., 1979; Thompson et al., 1979) produces changes in surface architecture prior to the onset of significant intracellular alterations. Apical cell surfaces usually flatten. Microvilli are reduced in number and shorter than in intact control animals. The secondary and tertiary mucosal folds become less deep. In long-term (90-day) castrated guinea pigs, the surface alterations are very pronounced but do not resemble those observed in the prepubertal animal (Barham et al., 1979). Hence, it has been concluded that the metabolic status of the long-term castrated animal probably is quite different from that of the intact immature animal. Whether these two groups also will show different surface responses to identical hormonal treatments is under investigation, and should provide important information regarding real or potential differences between the epithelium of prepubertal and long-term castrates.

References

Allison, V. F. and Cearley, G. W. (1972). Electron microscopic study of cells within the epithelium of the seminal vesicle of aging rats. Anat. Rec., 172, 262

Aumüller, G. (1977). Lipopigment fine structure in human seminal vesicle and prostate gland epithelia. Virchows. Arch. Cell Pathol., 24, 79

Barham, S. S., Lieber, M. M. and Veneziale, C. M. (1979). Ultrastructural surface alterations of guinea pig seminal vesicle epithelium during postnatal development and after castration. Invest. Urol., 17, 248

Boreau, J. (1977). Diagnosis and treatment of primary malignant tumors of the seminal vesicles. In Grundmann, E. and Vahlensiech, W. (eds), Tumors of Male Genital System (New York: Springer Verlag)

Droese, M. and Voeth, C. (1976). Cytologic features of seminal vesicle epithelium in aspiration biopsy smears of the prostate. Acta Cytol., 20, 120

Koivuniemi, A. and Tyrkkö, J. (1976). Seminal vesicle epithelium in fine-needle aspiration biopsies of the prostate as a pitfall in the cytologic diagnosis of carcinoma. Acta Cytol., 20, 116

Meisels, A. and Ayotte, D. (1976). Cells from the seminal vesicles: contaminants of the V-C-E smear. Acta Cytol., 20, 211

Mostofi, G. P. and Price, E. B. Jr. (1973). Atlas of Tumor Pathology. Tumors of the Male Genital System, (Washington, DC: Armed Forces Institute of Pathology)

Spring-Mills, E. (1980). The seminal vesicles. In Spring-Mills, E. and Hafez, E. S. E. (eds), Male Accessory Sex Glands, chap. 4. (Amsterdam: Elsevier/North Holland)

Spring-Mills, E. and Hafez, E. S. E. (1980). Male accessory sexual organs. In Hafez, E. S. E. (ed.) Human Reproduction, chap. 3. (Hagerstown: Harper & Row)

Thompson, S. A., Rowley, D. R. and Heidger, P. M. Jr. (1979). Fine structural studies of rat seminal vesicle in castrated and intact animals following estrogen treatment. Am. J. Anat., 154, 525

19

The vas deferens and seminal coagulum

L. J. D. ZANEFELD*, P. F. TAUBER† and E. E. BRUESCHKE‡

* Departments of Physiology and Biophysics, and Obstetrics and Gynecology, College of Medicine, University of
  Illinois at the Medical Center, Chicago, Illinois, USA
† Department of Obstetrics and Gynecology, University of Essen, Essen, West Germany
‡ Department of Family Practice, Rush Medical School, Chicago, Illinois, USA

THE VAS DEFERENS

Introduction

With a large proportion of biomedical experimentation and research, it is impossible to use the subject for which the research is intended, i.e., man himself. One of the most important considerations is selecting a suitable animal model is the similarity of structure of the organ to be studied. For micromorphological examination and comparison of the vas deferens of different species, three-dimensional study (with the scanning electron microscope, SEM) has certain advantages over studies which base their interpretations on evaluations by light or transmission electron microscopy. This investigation was performed as part of a study to develop a reversible vas deferens occlusive device. The first goal of the study was the characterization of the normal vasal micromorphologies of the mature man and dog in order to determine whether their vasa deferentia were of similar size, topography, musculature and structure of epithelial lining. Subsequently, the changes in morphology after implantation of the device were assessed.

Methodology

Sections of the vas deferens were fixed in a solution of 2.5% glutaraldehyde in Millonig's phosphate buffer (pH 7.4) containing 0.1% dipotassium ethylenediaminetra-acetate. K_2EDTA appeared to act as a mucus solvent which was useful because the luminal surface of the vas is often covered by a layer of mucus. For retention of the normal mucosal lining with free-standing microvilli, a section of the vas was immersed in the fixative. After a fixation period of 4–5 days the vas was sliced open with a scalpel either longitudinally or transversely to expose the luminal surface. Fixation was continued for one more day. When the vas was sectioned prior to fixation and/or

syringe-flushed with a stream of 0.1% glutaraldehyde in Millonig's buffer, the columnar cells were usually removed completely or in patches, allowing study of the basal (cuboidal) cells. Longitudinal sectioning of the vas, and pinning the specimen flat prior to fixation, usually resulted in the removal of both the columnar and basal cells and all or part of the basement membrane, permitting observation of the underlying connective tissue.

All sections were thoroughly rinsed for three 20-min periods in distilled water. Slight agitation accompanied the rinsing of all specimens. Vigorous agitation tended to remove luminal contents (generally spermatozoa) and epithelial cells. Specimen dehydration was accomplished with 20-min changes of 20, 40, 60, 80, 90, 95 and 100% (twice) ethyl alcohol in distilled H_2O, followed by 20-min substitutions of 25, 50, 75 and 100% (twice) amyl acetate in ethanol. Critical-point drying with bone-dry grade liquid CO_2 produced minimal specimen shrinkage. This varied between 8 and 15% as compared to 20% with freeze-drying from Camphene or 35% with air-drying from ethanol. The sections were cemented to stubs with Duco cement, coated with carbon/gold and observed under a JEOL electron microscope.

Observations

Very few differences are present between the human and dog vas deferens. In both species, musculature of the vas deferens consists of three concentric rings of smooth muscle. A circular layer is surrounded by two longitudinal layers. Connective tissue composed of a dense network of collagen fibers surrounds the muscle layer immediately beneath a basement membrane. This membrane limits the luminal epithelium which consists of cuboidal and ciliated columnar cell types. Possibly due to the contractile stage of the vas at the time of fixation, the luminal surfaces of the dog or man can appear slightly rippled or highly convoluted.
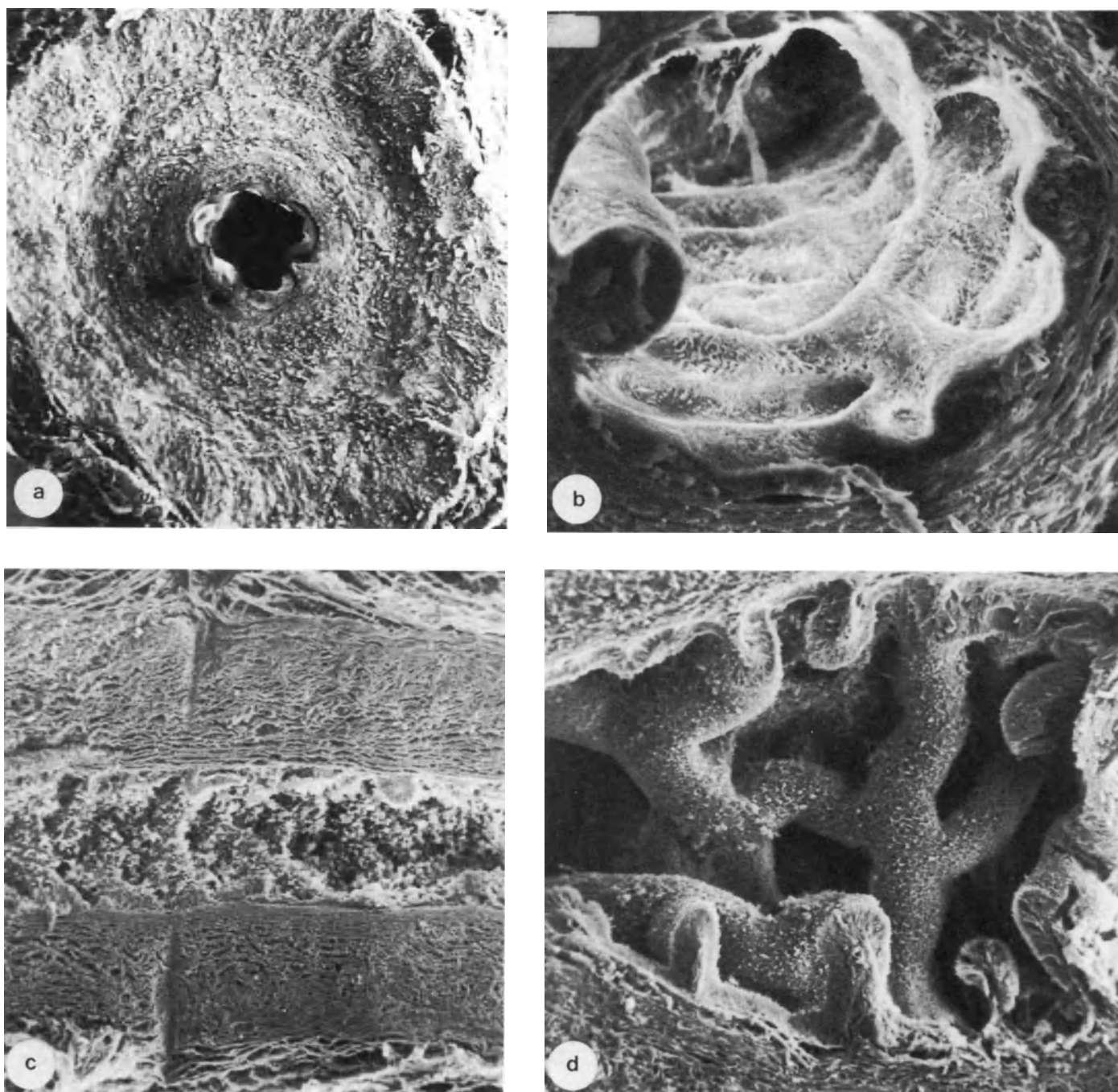
173

Figure 1   Human (a and b) and dog (c and d) vas deferens.
Figures a and b are cross-sections, c and d are longitudinal
sections. Note extreme convolutions of the luminal surface in
d (a ×40; b ×200; c ×60; d ×125)

The size of the vas lumen (taken from transverse sections) varies from 0.25 to 0.55 mm, averaging 0.4 mm, and is similar in man and dog. This is somewhat smaller than that found during surgery *in situ* using probes (human vas: 0.85–1.06 mm; dog vas: 0.77–0.98 mm). The external diameter of the human vas *in situ* ranges from 2.0 to 4.0 mm, averaging 2.85 mm.

Two types of cells make up the vas deferens epithelium: columnar cells and basal cells. It is difficult to obtain preparations with the columnar cells still intact, since they are easily removed from the underlying basement membrane. Columnar cells are situated above basal cells and adhere to the basement membrane via a single point of attachment. If dislodged, the columnar cells are usually removed as a layer although intact areas are occasionally left behind.

Two different types of columnar cells are present, one a 'rectangular' cell being long, narrow and straight (approximately 20 μm long and 5 μm in diameter), and the other a 'stalked' cell possessing a narrow base of varying length (5–10 μm) but rather constant width (2 μm) and a rounded upper portion (10–15 μm long and
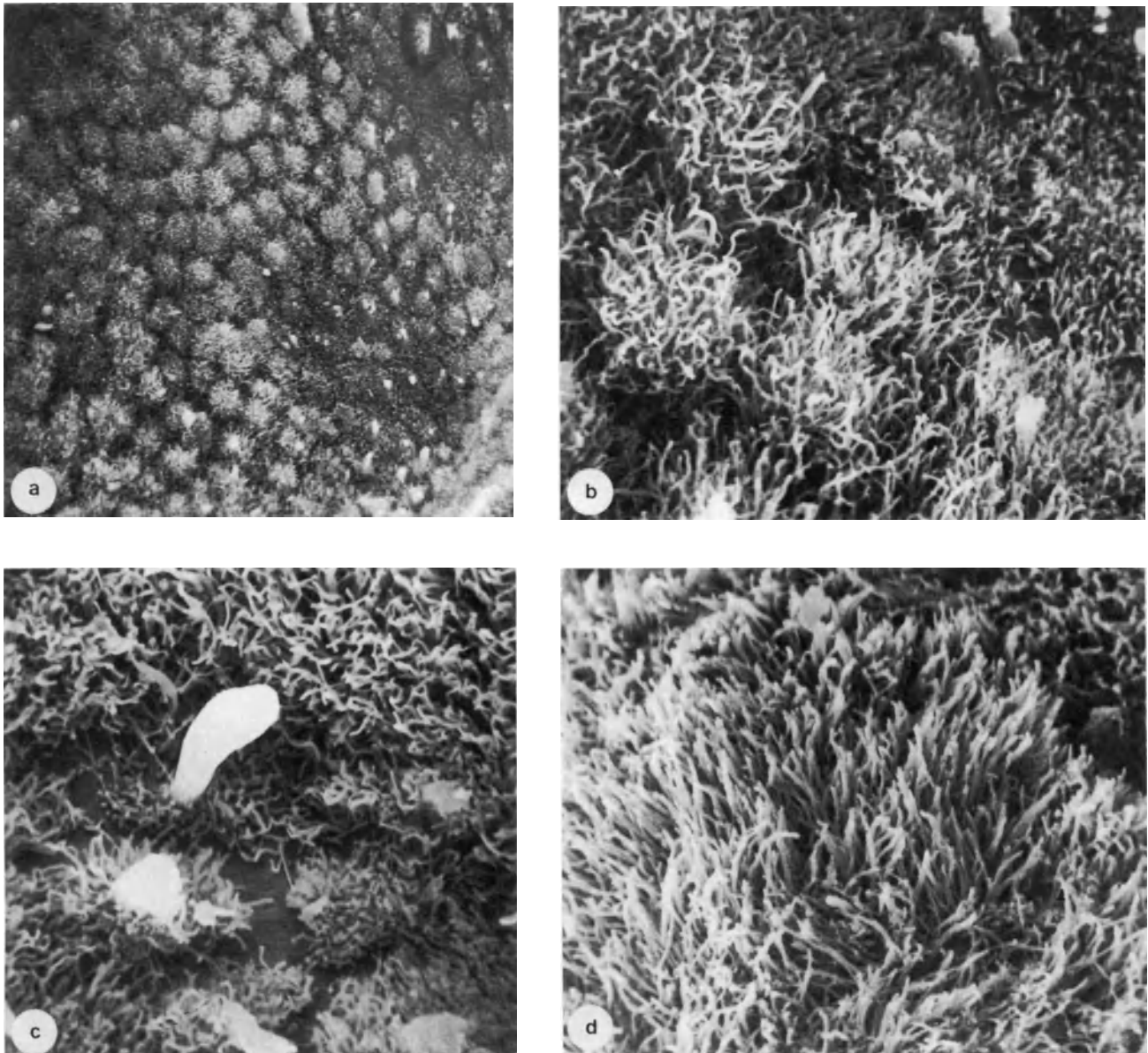
Figure 2 Luminal surface of the human (a,b and c) and dog
(d) vas deferens showing the microvilli (stereocilia) (a ×850;
b ×4250; c ×5100; d ×4250)

5 μm in diameter). The rectangular and stalked columnar cells closely adhere to each other by connective material. Both types of columnar cells appear simply to rest on the basement membrane, between the basal cells, explaining the ease with which they are removed.

Microvilli (stereocilia) cover the interior surface of the vas and originate from the luminal surfaces of the columnar cells. The microvilli of the human are usually spread patch-like over the vas surface, each patch representing an individual columnar cell. By contrast, the microvilli are evenly spread over the luminal surface of the dog vas deferens. The microvilli of both species are approximately 2–3 μm long and 0.15–0.2 μm wide.

Large numbers of basal (cuboidal) cells are spaced evenly over the surface of the basement membrane. The basal cells are usually rounded and about 15–20% of

the height of the columnar cells. Although their shape may vary, they are approximately 5 μm wide and 10 μm long. Tentacles extend between the lower portions of the basal cells, connecting one cell to the other, and also to the basement membrane. These tentacles appear to be anchoring structures. Situated under the basal cells, surrounding the vasal epithelium, is the smooth basement membrane. Outward of the membrane are the collagen fibers of the connective tissue which is surrounded by the muscle layers described previously.

From these observations one can conclude that the vasa deferentia of the human and dog have highly similar micromorphologies, and agree very closely in size, topography, musculature and structure. Where vas deferens morphology is concerned, the dog appears to be a good animal model for human experimentation. It was therefore used to evaluate the effects of long-term implantation of a vas deferens device that
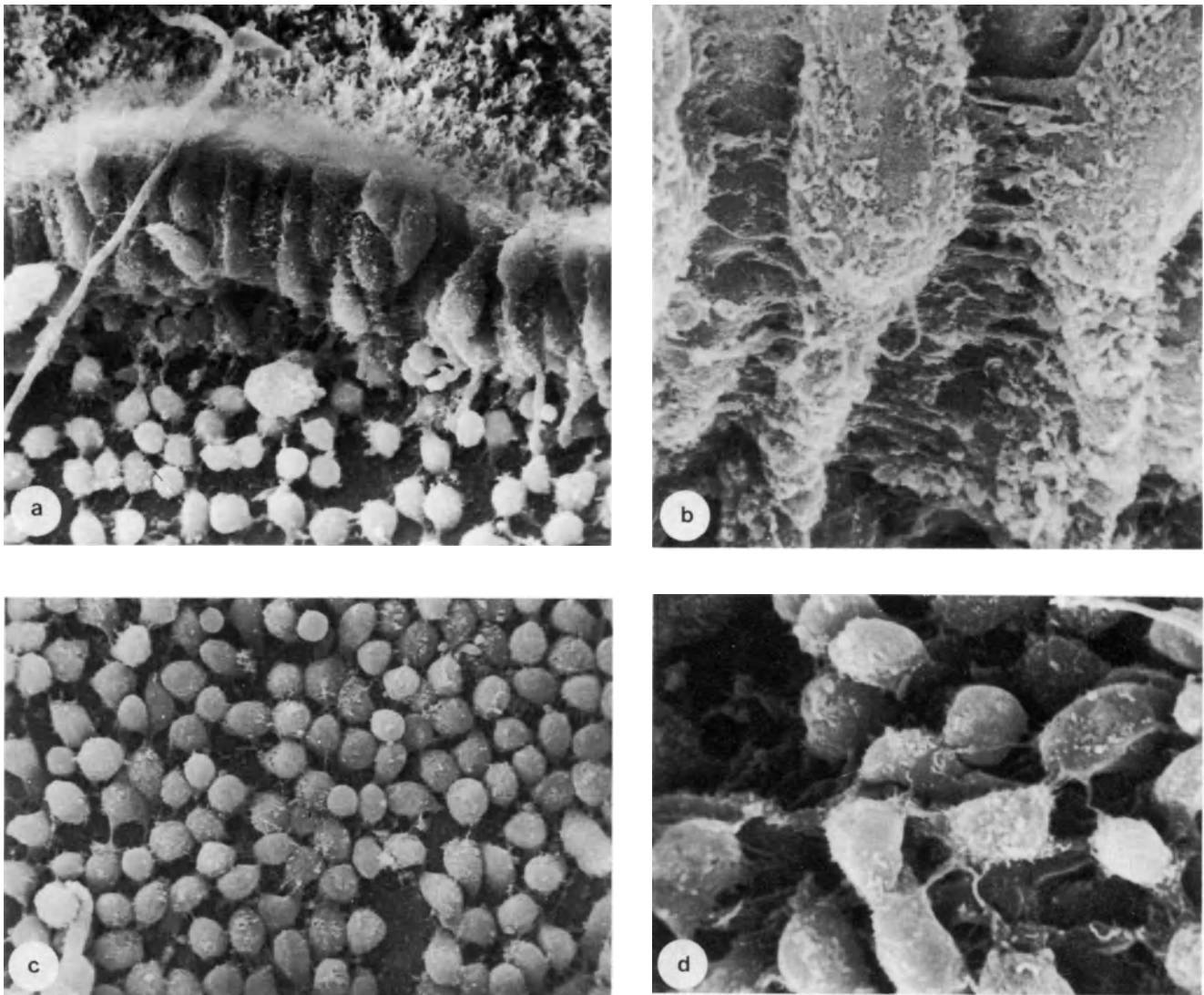
Figure 3   Columnar and basal cells of the luminal epithelium
of the human (a, b and c) and dog (d) vas deferens. Note the
connective strands between the columnar cells (b) and the
tentacles of basal cells (d) (a ×1000; b ×5000; c ×1200;
d ×3000)

reversibly blocks sperm transport. This device consists
of a body in which a valving mechanism is located, a
conducting tube that runs through the body, and pilot
tubes that extend from each side of the device body.
The luminal diameter of the tubes is 0.3 mm and the
external diameter of the pilot tube is 0.6 mm, which
allows ready implantation into the human and dog vas
deferens while forming a fairly snug fit. Except for the
valving mechanisms, the device is made entirely of
silicone rubber. The device possesses a Dacron velour
suture ring that surrounds the pilot tube at its junction
with the body. This suture ring is bonded to the silicone
rubber with Dow Corning type A medical-grade
adhesive. The velour allows tissue ingrowth and forms
an effective seal with the cut edges of the vas deferens.

The devices were implanted in dogs in one of the
following fashions:

(1) the open mode and left this way for 27–44 months;

(2) the closed mode and kept this way for 11–12
     months before the valves were reopened;
(3) either the closed or open mode and cycled to the
     opposite mode every 3 months (four or five cycles);
     or
(4) either the closed or open mode and cycled to the
     opposite mode every 6 months (two or three
     cycles).

Semen analyses were regularly performed on all of the
dogs and a number of the animals were bred during the
experiments. The results showed that:

(1) the devices can be opened and closed successfully
     over long periods, respectively allowing and
     preventing sperm transport;
(2) the breeding ability of the animals is not impaired
     while the devices are in the open mode; and
(3) the devices do not result in an enhanced incidence
     of congenital abnormalities in the offspring.
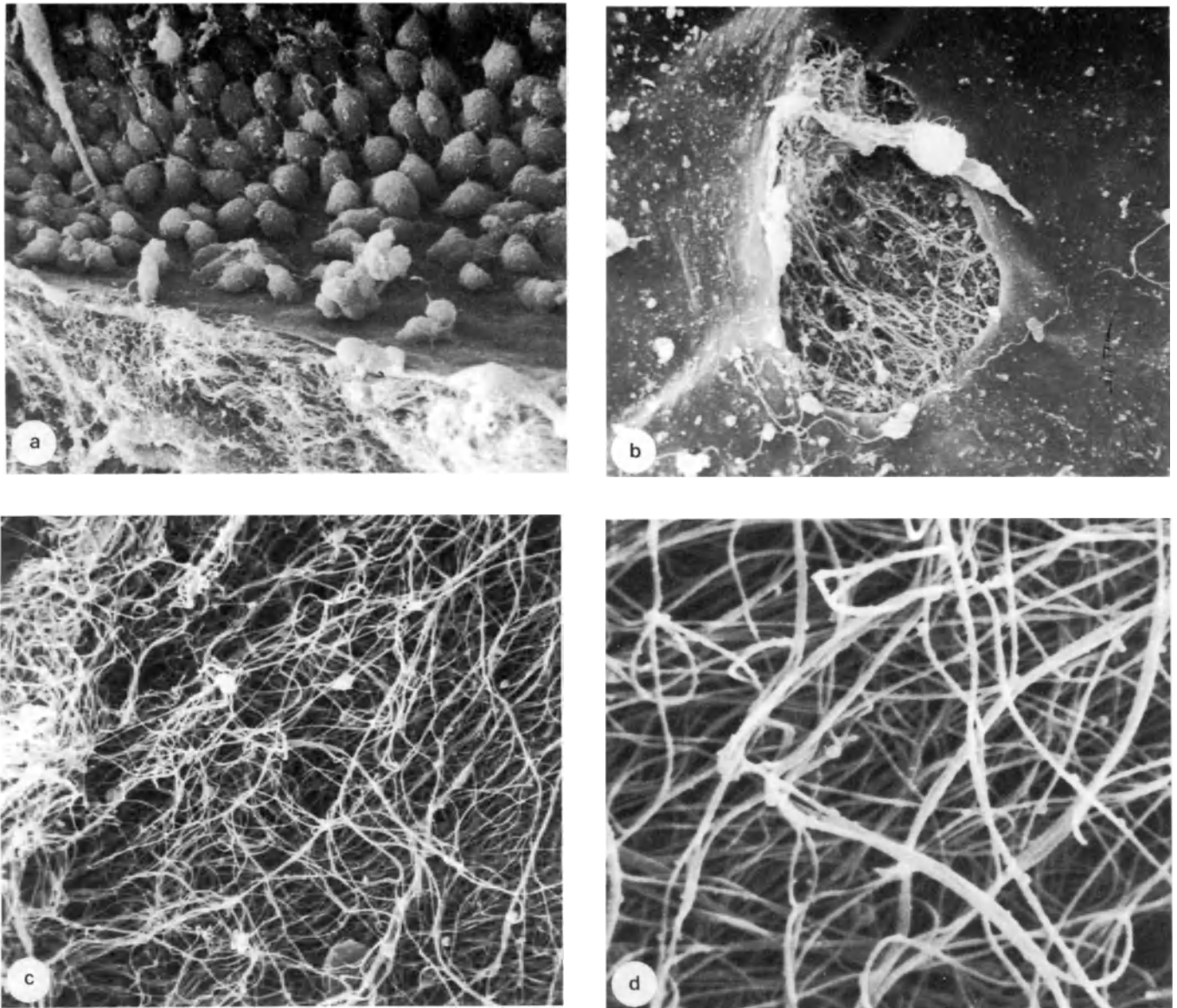
Figure 4 The basement membrane and connective tissue colagen fibers of the human (a and b) and dog (c and d) vas deferens (a ×850; b ×1700; c ×2550; d ×5950)

Scanning electron microscopic and histologic observations of the vasa deferentia showed that no morphological alterations occur in the vas distal to the device, i.e., towards the prostate. However, the portion of the vas deferens between the device and the epididymis possessed an enlarged lumen (approximately twice its normal size) and showed some disappearance of stereocilia and a thinning of the muscle wall. The overall (outer) diameter of the vas increased by an average of 24% over normal. These changes are no worse than those observed after a vasectomy, indicating that they do not represent permanent damage to the vas and that they do not impair the functional activity of the organ.

Scanning electron microscope studies of the devices showed:

(1) excellent tissue ingrowth into the Dacron velour material of the implanted device;

(2) the build-up of material, consisting in part of spermatozoa, in the device lumen and on the valve stem; and

(3) the absence of surface degradation of either the Silastic material or the valve stem of the device.

Although the build-up of material constitutes some potential danger in that it may obstruct the lumen of the device, all other observations are very encouraging and justify continued work with the device to make it a clinical reality.

THE SEMINAL COAGULUM

Introduction

Distinct differences exist in the coagulation and liquefaction properties of the ejaculates among
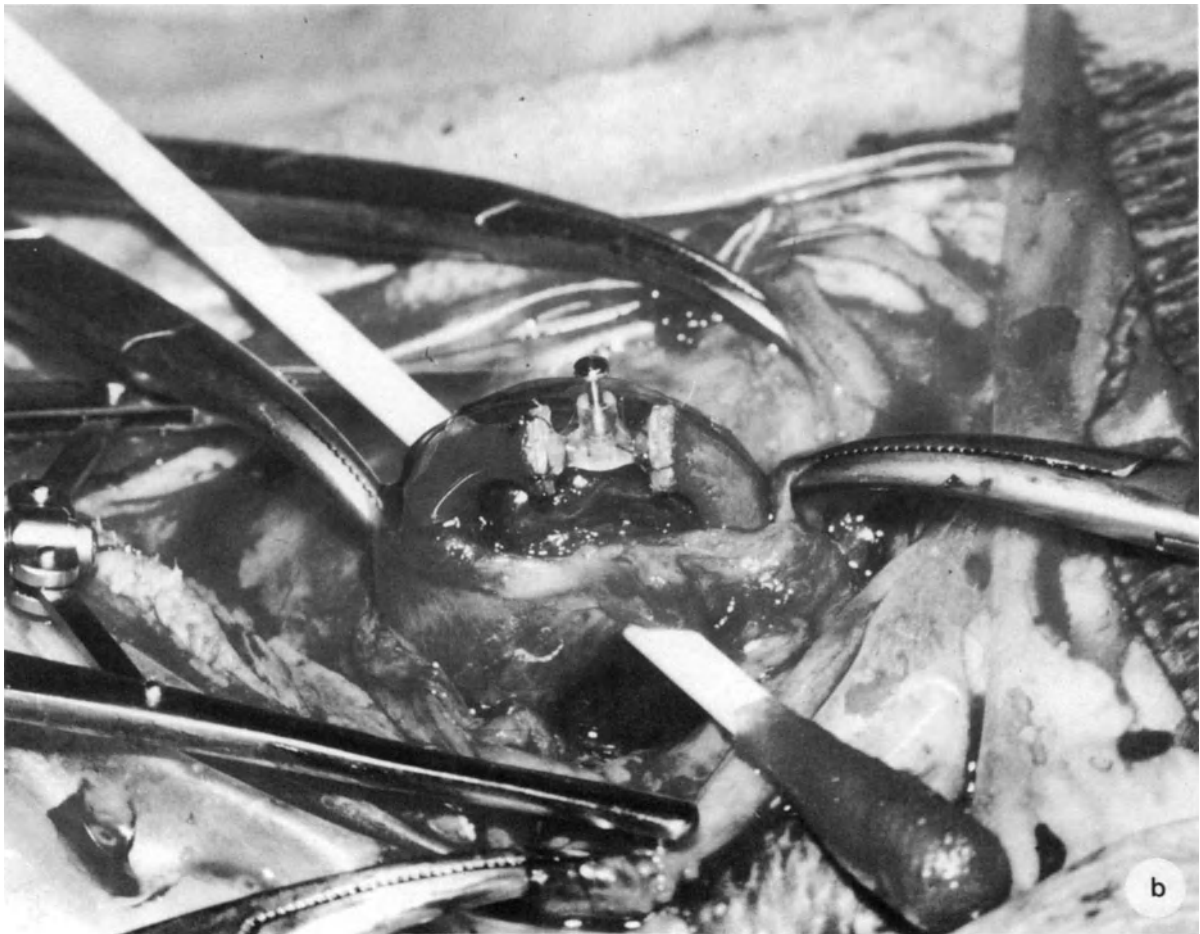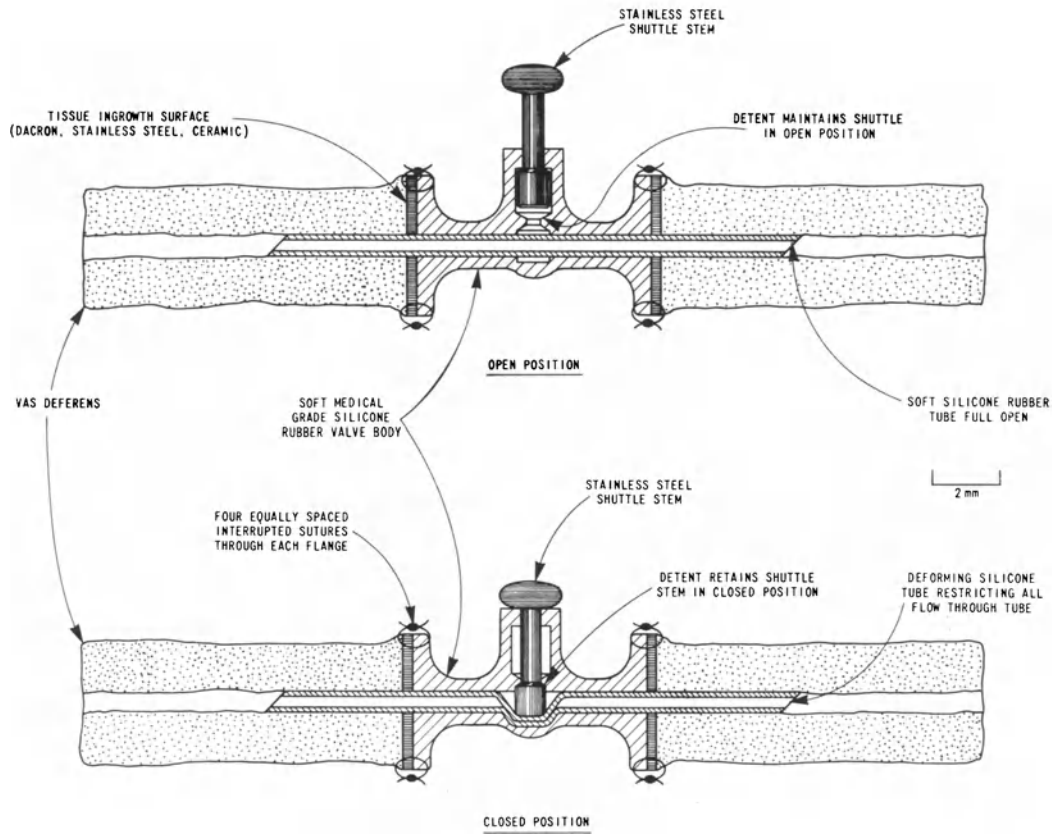
Figure 5 Reversible vas deferens occlusive device; schematic
representation (a) and implanted in the dog vas deferens (b)
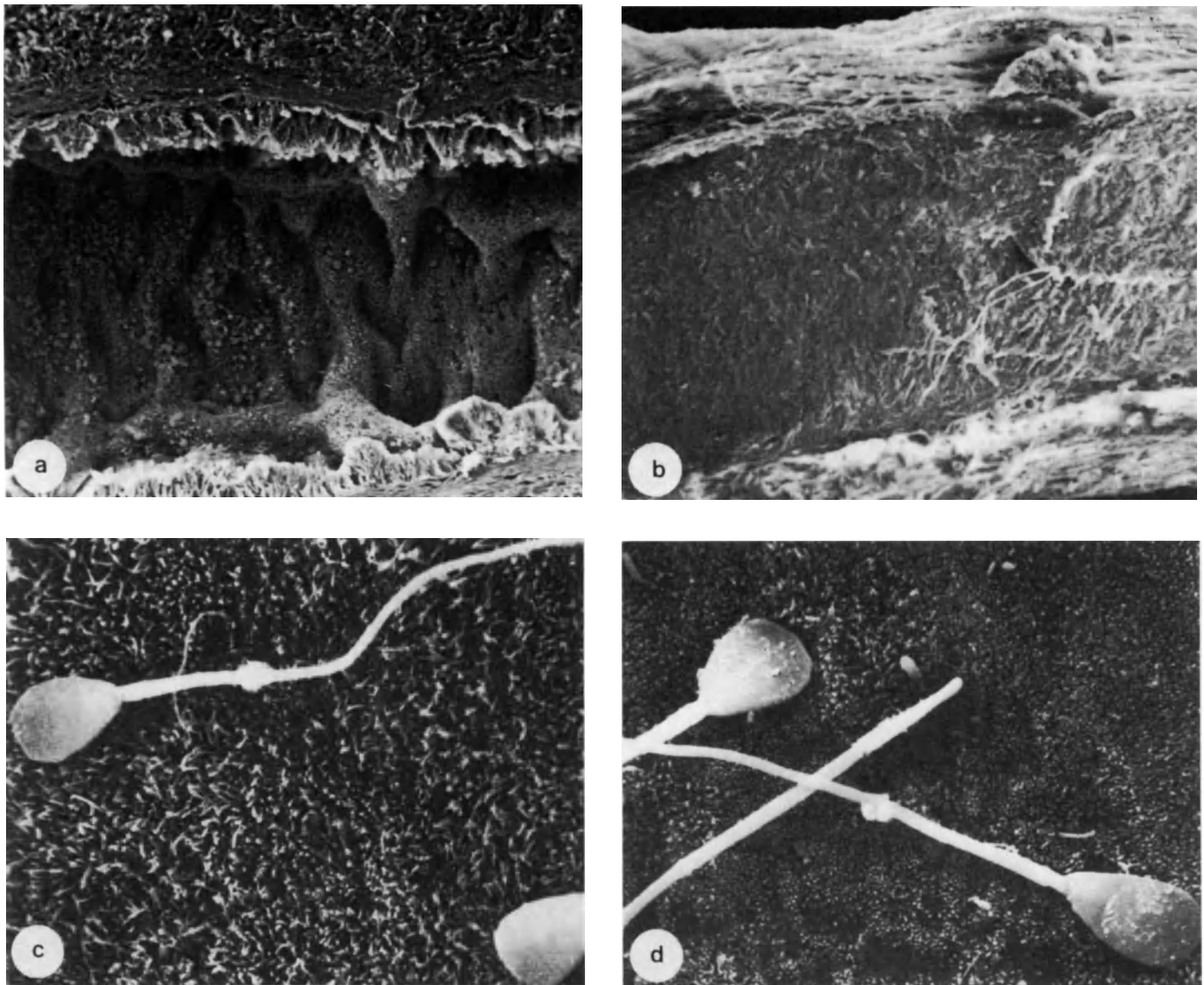
Figure 6 Dog vas deferens after device implantation
a: Unimplanted vas deferens (×150)
b: Vas deferens testicular to the implanted device. Note the rather smooth luminal surface and the thinning of the muscle wall (×125)

c: Spermatozoa on the luminal surface of the vas, prostatic to the device (×5000)
d: Spermatozoa on the luminal surface, testicular to the device; note the decrease in number and height of the microvilli (×5000)

different species of animals. The human ejaculate coagulates immediately after ejaculation and normally liquefies again within 15–20 min. Abnormally liquefying coagula of men may require more than 1 h to liquefy or may not liquefy at all. Such slowly liquefying ejaculates may be infertile. The ejaculates of the bull and dog do not coagulate at all, whereas the rodent ejaculates a fluid portion first followed by a firm coagulum ('plug') that does not liquefy. The primate ejaculate is more similar to that of man since it forms a solid coagulum that partially liquefies. It is of interest to compare the different species in regard to the morphological aspects of the coagulum. Since the coagulum is 'gel-like', this is difficult to do histologically or by the transmission electron microscopy; and the scanning electron microscope is the instrument of choice.

Methodology

At certain periods of time after ejaculation, samples of human semen were pipetted into a 2.5% glutaraldehyde in 0.05 mol/l phosphate buffer, pH 7.0. This stops the liquefaction process immediately. The final fraction of a split, slowly liquefying ejaculate from a donor, as well as coagula collected from the vagina, were treated in a similar fashion. Rhesus monkey coagula, obtained by electroejaculation, and a urethral (seminal) plug from a guinea pig were washed three times in physiological saline to remove the supernatant sperm and were also submerged in fixative. After 5–10 days, at least one change of fixative, the samples were washed, dehydrated, sectioned, critical-point dried, coated with carbon and two layers of gold, and observed with a Mark II Cambridge stereoscan electron microscope.
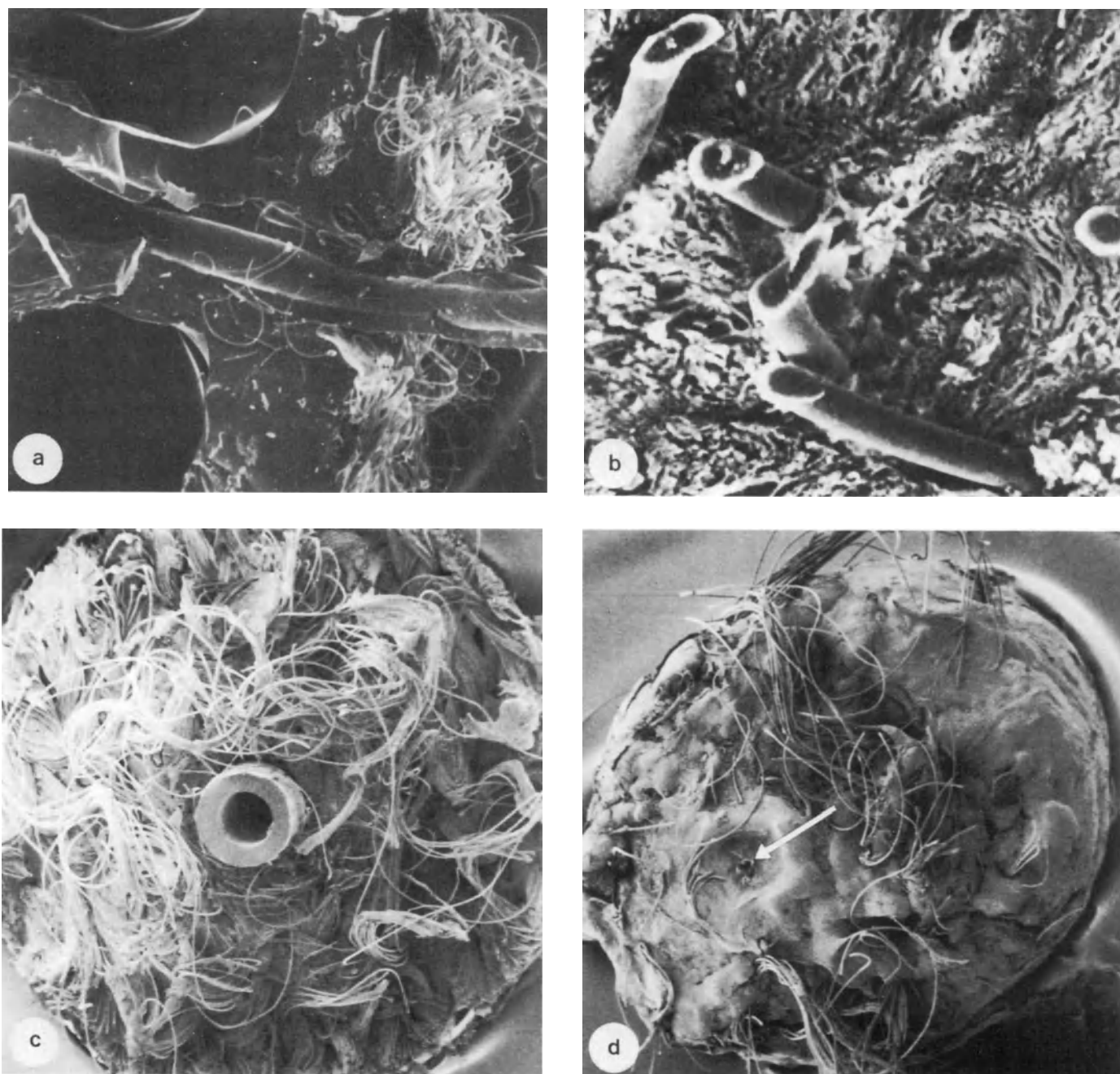
Figure 7   Dacron velour portion of the reversible occlusive device before (a and c) and after (b and d) implantation in the dog vas deferens. Note the tissue ingrowth in b and d. a: longitudinal section of the device showing conduction tube and pilot tube (×25); (b ×600; c ×35; d ×25)

Observations

The human coagulum consists of a dense, organized network of long, narrow fibers approximately 0.15 μm thick. The spaces between the fibers are so small that movement of the spermatozoa that are trapped in large numbers throughout this network is not possible. During liquefaction, the spaces between the fibers increase. After about 6–10 min, small spherical globules appear at the surface of the fibers, approximately 0.15–3.0 μm in diameter. Subsequently, the coagulum loses its structure as the fibers disappear and the globules take over. After 10–20 min, only globules can be found, forming smaller or larger clumps from which the spermatozoa can escape.

A slowly liquefying human seminal coagulum possesses some very large fibers that measure 0.8–1.8 μm in width, and are interconnected by a meshwork of smaller fibers of approximately the same size as those of the normally liquefying coagulum. If it liquefies at all, the slowly liquefying coagulum shows the same changes in morphology as the normal ejaculates, although the alterations occur much more slowly. The rate of liquefaction, even that of slowly liquefying semen samples, appears to be increased when the semen
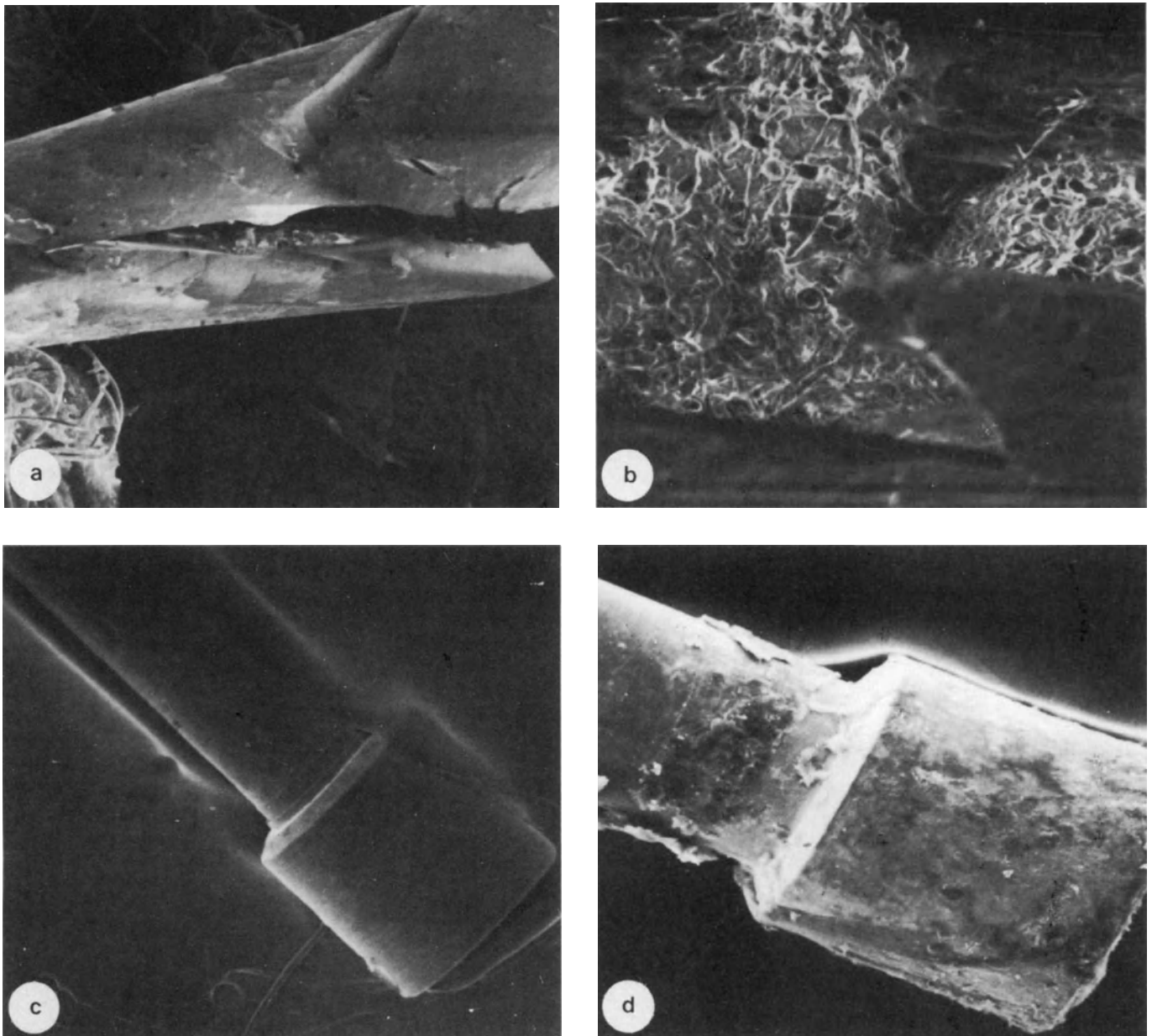
Figure 8 Material build-up in the device after implantation in the dog vas deferens
a: Sliced pilot tube with material inside the lumen ($\times 200$)
b: Material within the lumen of the pilot tube ($\times 1000$)

c,d: Stainless steel valve stem before (c) and after (d) implantation of the device. Note build-up of material on the stem (d); (c $\times 40$; d $\times 50$)

is ejaculated vaginally. Otherwise, the morphological appearance of the coagulum before and during liquefaction in the vagina, is identical to semen ejaculated *in vitro*. It is not known how the vaginal milieu enhances the liquefaction rate of the human coagulum.

The guinea pig and monkey coagula appear to be much more solid than the human coagulum. The guinea pig plug is a rigid, tubular structure with a sponge-like appearance. Short flattened fibers (0.6 μm thick) form a dense narrow-spaced network. By contrast, the monkey coagulum possesses a disorganized array of fibers of different thicknesses, varying from 0.2 to 0.7 μm. The spaces in the monkey and guinea pig coagula are much larger than those of man. Occasionally, a few

spermatozoa are present within the monkey coagulum although most of them are located on its surface. Some adhesive properties may exist between the monkey coagulum and its spermatozoa because the coagulum had been washed quite extensively before fixation. No spermatozoa are located inside or on the surface of the guinea pig coagulum.

Acknowledgements and References

Figure 9 The human seminal coagulum, 3 min after ejaculation (a ×30; b ×100; c ×600; d ×600; e ×3000)
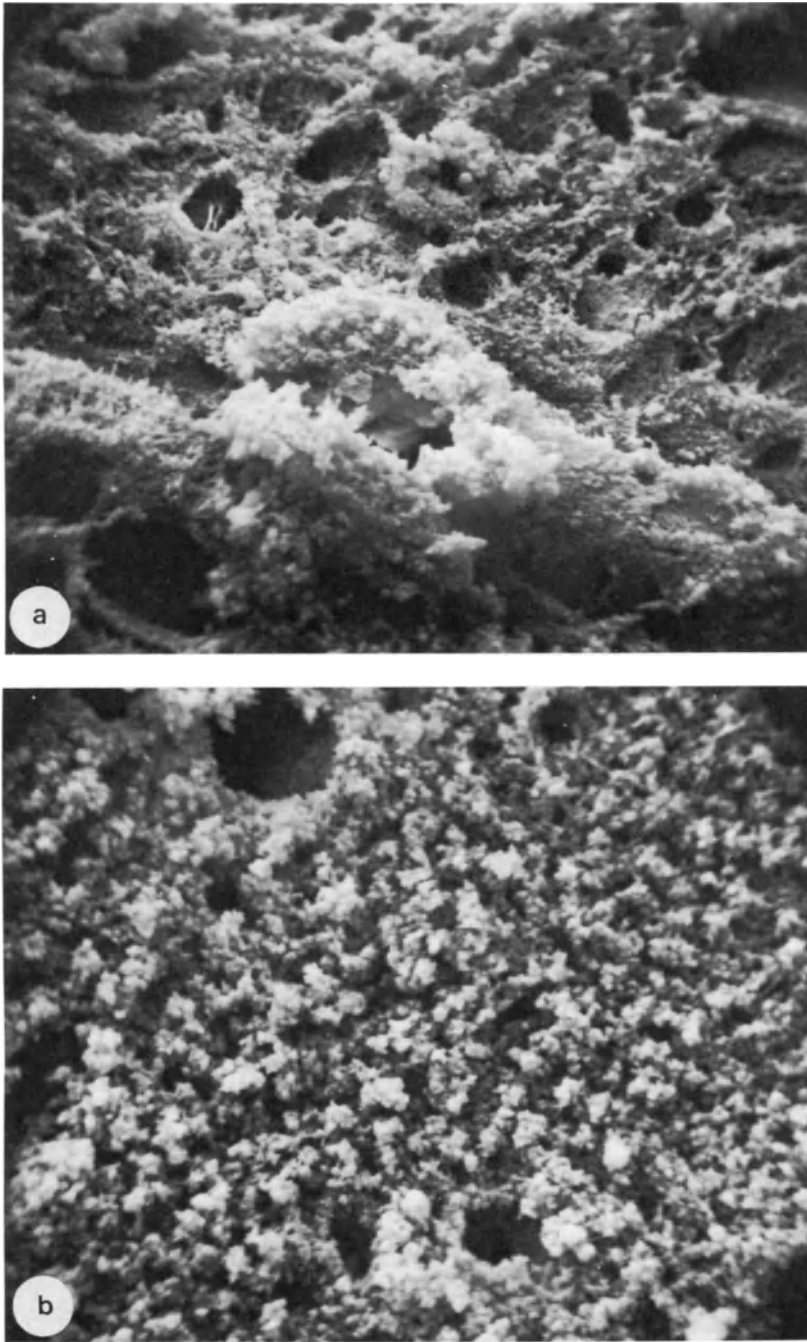
Figure 10 Liquefying human seminal coagulum, 6 min after ejaculation (a ×1200; b ×3100)

of a reversible vas deferens occlusive device: III. Morphology of the human and dog vas deferens: a study with the scanning electron microscope. *Fertil. Steril.*, 25, 687. Figure 5 is from Brueschke, E. E., Zaneveld, L. J. D., Rodzen, R., Mayerhofer, K., Burns, M., Maness, J. H. and Wingfield, J. R. (1975). Development of a reversible vas deferens occlusive device: V. Flexible prosthetic devices. *Fertil. Steril.*, 26, 40. Figures 6b, c and d; 7a and b; and 8 were first published in Brueschke, E. E., Kaleckas, R. A.,

Wingfield, J. R., Welch, T. J. and Zaneveld, L. J. D. (1980). Development of a reversible vas deferens occlusive device: VII. Physical and microscopic observations after long term implantation of flexible prosthetic devices. *Fertil. Steril.*, 33, 167. Figures 9a, d and e; 10; 11a and c; 12 and 13, are from Zaneveld, L. J. D., Tauber, P. F., Port, C., Propping, D. and Schumacher, G. F. B. (1974). Scanning electron microscopy of the human, guinea pig and rhesus monkey seminal coagulum. *J. Reprod. Fertil.*, 40, 223.
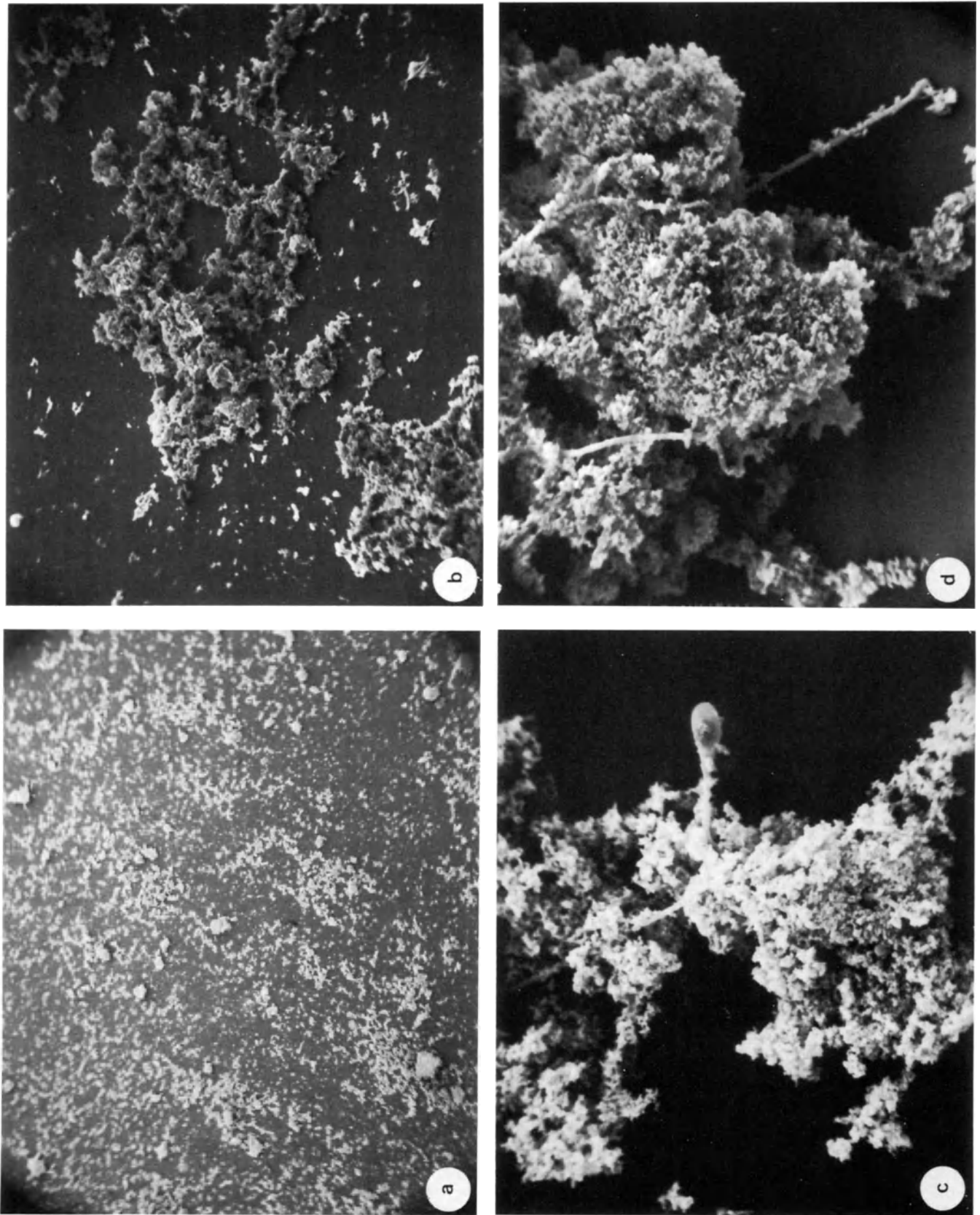
Figure 11   Liquefied human seminal coagulum, 15 min after ejaculation (a ×30; b ×100; c×1200; d ×1200)
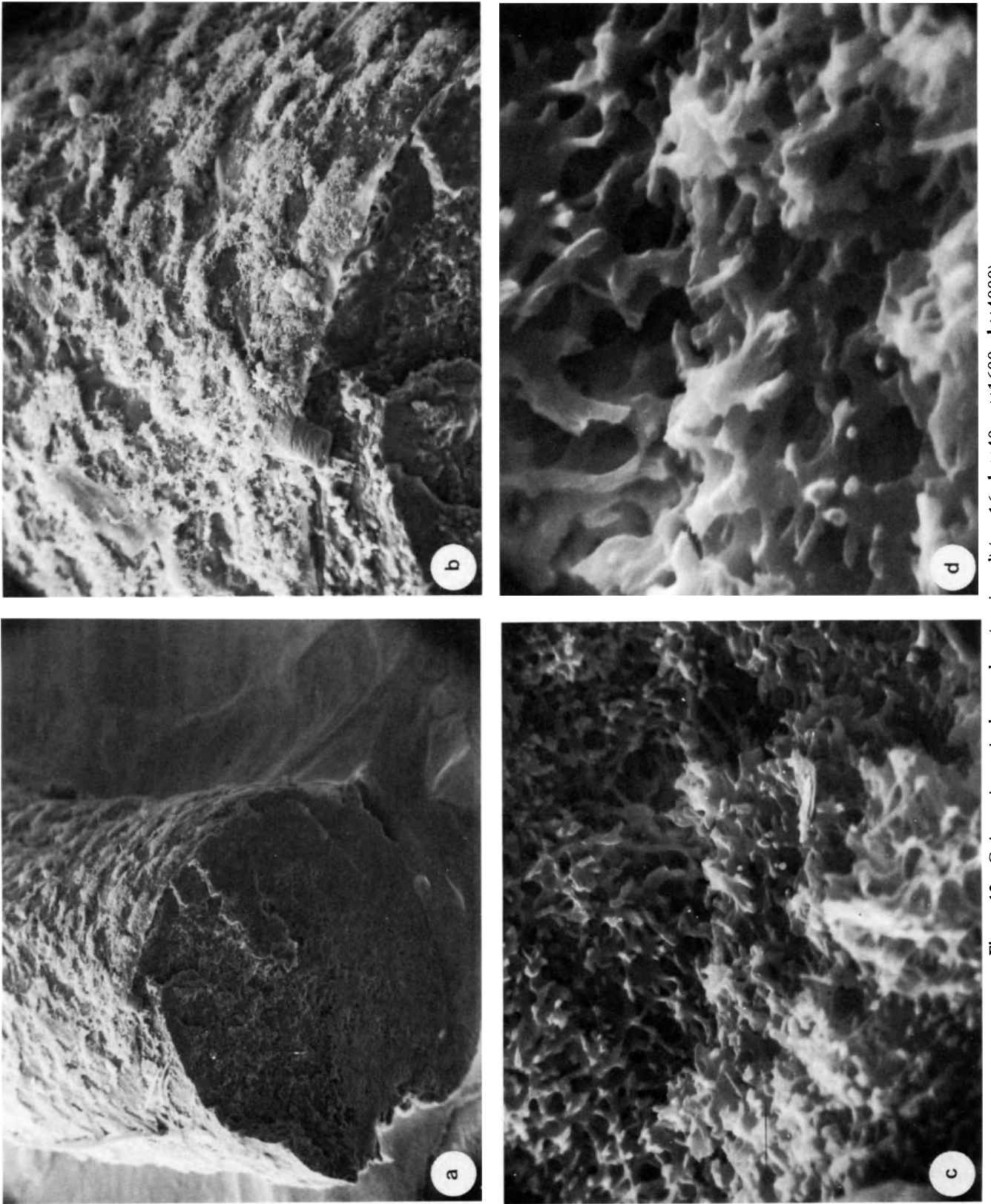
Figure 12 Guinea pig seminal coagulum (sectioned) (a ×16; b ×40; c ×1600; d ×4000)
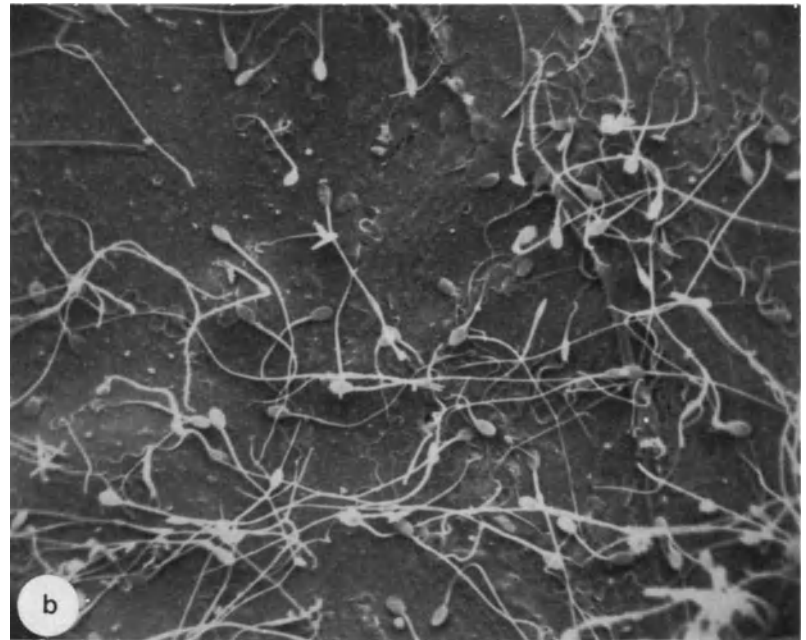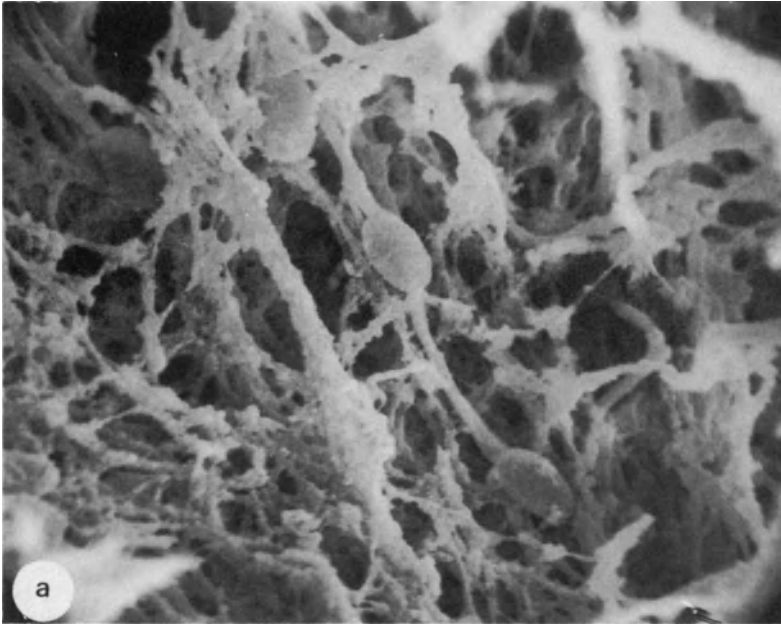
Figure 13 Spermatozoa within (a) or on the surface (b and c) of the primate seminal coagulum (a ×1300; b ×310; c ×660)

20

The vas deferens in man and monkey: spermiophagy in its ampulla

M. MURAKAMI, A. SUGITA and M. HAMASAKI

Department of Anatomy, Kurume University School of Medicine, Kurume, Japan

Extensive research concerning function and structure of the vas deferens has been accumulated in various mammalian species, including man, by using light and transmission electron microscopy. In recent years the vas has attracted the considerable attention of morphologists regarding the problems of fertility or sterility. More recently, surface topography of the vas deferens of rats, dogs and humans viewed by SEM has indicated that there exist not only species differences in luminal configuration, but regional variations along the longitudinal axis of the vas deferens (Nowell and Faulkin, 1974; Zaneveld and Brueschke, 1975; Hamilton and Cooper, 1978; Kennedy and Heidger, 1979).

In the present study the luminal surfaces of the vas deferens of humans and monkeys were observed by SEM and compared with each other with special attention to that surface in the ampullary region.

The human vas deferens was obtained from four adult men, who were subjected to total vasectomy for early cancer of the prostate or urinary bladder. All the segments of the vas deferens examined were free from tumor and remained intact. Immediately after surgical removal the vas was immersed en masse in buffered paraformaldehyde–glutaraldehyde mixture (pH 7.2).

The vas deferens of the monkey was taken from two healthy adult Japanese monkeys, which were housed in an individual cage. The animals were, under nembutal anesthesia, perfused through the ascending aorta with paraformaldehyde–glutaraldehyde mixture and were immersed in the same fixative.

The specimens of both species thus pre-fixed were then processed routinely for SEM.

The vas deferens is a thick-walled duct which conveys spermatozoa from the epididymis to the urethra, and it originates at the cauda epididymis in the scrotum (scrotal region), ascends up to the inguinal canal, traverses the canal (inguinal region) and runs into the pelvic cavity (pelvic region). At the terminal portion the vas deferens of human and monkey becomes gradually dilated and tortuous to form the ampulla distal from which the vas is joined with the excretory duct of the seminal vesicle. Thereafter, the vas penetrates the prostate where it is termed the ejaculatory duct, and finally enters the urethra.

The wall of the vas deferens is made up of mucosa, three dense concentric layers of smooth muscle and adventitia, as a common structure in mammals. With regard to configuration of the mucosa, individual differences can be seen but even in the same individual side differences is recognized. No basic difference in vas morphology exists between the species. The following description applies commonly to both human and monkey.

In the monkey there are occasionally foldings of the lining mucosa together with underlying lamina propria in the section from the scrotal region to the pelvic region. These foldings in the scrotal region are circular, becoming smooth, and unfold gradually in the inguinal region. They are longitudinal in the pelvic region. The lumen of the vas becomes more folded as it approaches the ampullary region. The luminal surface of the human vas is essentially similar in the pattern of fold formation, but appears a little more rippled or convoluted as compared with the monkey (Figure 1a,b). The mucosal lining is composed of pseudostratified, tall columnar epithelial cells with stereocilia and occasional basal cell of stellate shape as generally known in human and other mammals. When viewed with SEM, the apical surface of the individual columnar cell is more or less protruded into the lumen and densely covered by the tuft-like microvilli termed stereocilia in both species (Figures 1c; 2a,b). A few spermatozoa are located on or among the microvilli of the epithelial cells through the entire length of the vas deferens, but are never found to be in a process of penetration into the epithelial cells. In the human vas deferens there are two types of the columnar cells; i.e., mitochondria-rich cell and narrow pencil cell, as shown by TEM (Popvic et al., 1973; Hoffer, 1976) in addition to the principal columnar cell. The lumen of

the vas deferens of the human and the monkey is uniformly covered by principal columnar cells with stereocilia, and two types of the cells described above are not identified by the surface SEM view.

In the ampullary region of the vas deferens its mucosal lining is functionally specific, though the transition from pelvic region to ampullary region is not abrupt but gradual. The mucosa in the ampullary region is folded in a complex manner to divide the lumen into a labyrinth of space. As compared with the monkey vas, the lumen of the human vas is slightly wider and its mucosa is much more folded (Figure 2c). The epithelium lining the lumen is a simple or two-cell-thick pseudostratified columnar epithelium. Most of the epithelial cells contain abundant spherical uniform granules, probably secretory in nature, and a few residual bodies of varying sizes and shapes which increase in number with age (Figures 3a,b). Similar findings of the secretory epithelial cells of the human ampullary vas were otherwise demonstrated by using TEM (Aumüller and Brühl, 1977). The epithelium of the ampullary vas resembles that of the human or monkey seminal vesicle. The apical surface of individual epithelial cells protrudes slightly into the lumen. These cells are almost devoid of stereocilia, but instead provide short, stubby microvilli which vary in distribution from cell to cell (Figures 3c,d; 4a,b). In the human vas the ciliated cells are interspersed among non-ciliated cells while the monkey ampullary region entirely lacks the ciliated cells (Figure 4c). The functional significance of the ciliated cells in the human ampullary vas remains to be solved. Spermatozoa are also located singly or in clusters on the apical surface of each epithelial cell in the ampullary region, as in the other regions of the vas deferens.

In the ampullary region of both human and monkey, various modes and stages of spermiophagy by the epithelial cell are visible in SEM photographs. Spermatozoa encountered are in the process of incorporation into the epithelial cells. They are ingested, in many cases, along their long axis, and sometimes trapped by a cuff-like ridge projecting from the epithelial cells. Most of spermatozoa are ingested

vertically from their head (Figures 4d,e; 5a,b), but others are taken up from the tail (Figures 5c,d). Intraepithelial digestion of spermatozoa incorporated is also apparent (Figure 5e). Thus, epithelial cells of the ampullary vas deferens of both species are capable of phagocytosis of spermatozoa; however, the spermiophagy is encountered less in rate in the human than in the monkey. Cooper and Hamilton (1977) first reported spermiophagy by the epithelial cells lining the lumen of the terminal vas deferens of the rat by means of light microscopy and TEM, and stated that it might involve the removal of surplus spermatozoa. As in the rat, the terminal region of the vas deferens of such primates as human and Japanese monkey may play the role in removing spermatozoa in addition to storing them, although it is not yet known whether the epithelial cells ingest selectively damaged or dead spermatozoa only, or possibly also living ones.

References

Aumüller, G. and Brühl, B. (1977). Uber die Bau der Ampulla ductus deferentis des Menschen. *Verh. Anat. Ges.*, 71, 561

Cooper, T. G. and Hamilton, D. W. (1977). Phagocytosis of spermatozoa in the terminal region and gland of the vas deferens of the rat. *Am. J. Anat.*, 150, 247

Hamilton, D. W. and Cooper, T. C. (1978). Gross and histological variations along the length of the rat vas deferens. *Anat. Rec.*, 190, 795

Hoffer, A. P. (1976). The ultrastructure of the ductus deferens in man. *Biol. Reprod.*, 14, 425

Kennedy, S. W. and Heidger, P. M. (1979). Fine structural studies of the rat vas deferens. *Anat. Rec.*, 194, 159

Nowell, J. A. and Faulkin, L. J. (1974). Internal topography of the male reproductive system. In *Scanning Electron Microscopy*, Part III, pp. 639–646. (Chicago IL 60616, IIT Research Institute)

Popovic, N. A., McLeod, D. G. and Borski, A. A. (1973). Ultrastructure of the human vas deferens. *Invest. Urol.*, 10, 266

Zaneveld, L. J. D. and Brueschke, E. E. (1975). The vas deferens. In Hafez, E. S. E. (ed). *Scanning Microscopic Atlas of Mammalian Reproduction*, pp. 99–105. (Stuttgart: Thieme)

Figure 1 (opposite)

a: Section of the inguinal vas deferens of the monkey. The luminal surface is relatively smooth (×200)

b: Section of the inguinal vas deferens of the human. The luminal surface appears a little more rippled when compared to the monkey (×160)

c: Higher magnification view of stereocilia in the human inguinal vas deferens. A cord-like structure lying among microvilli is a portion of one spermatozoon (×19 500)
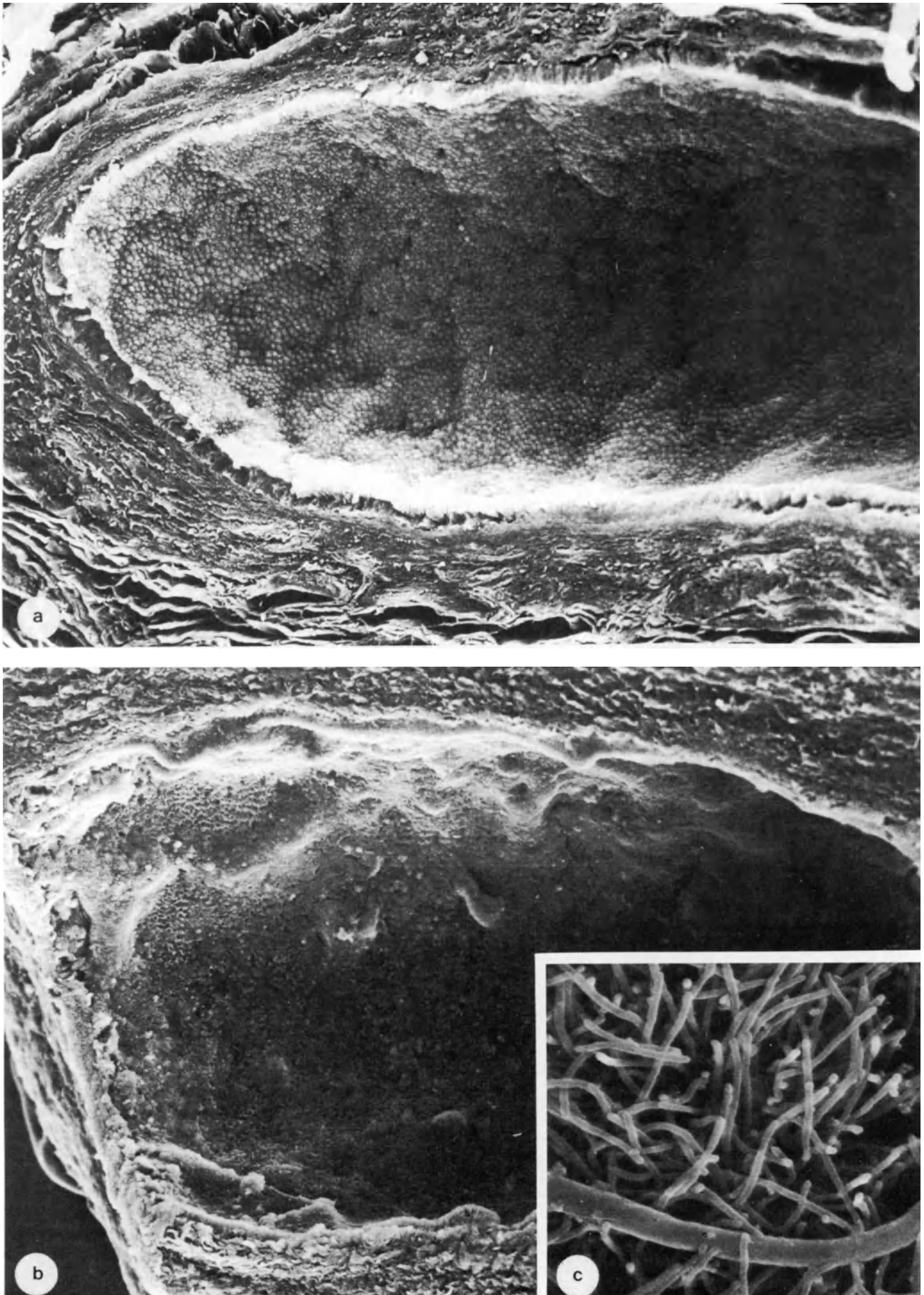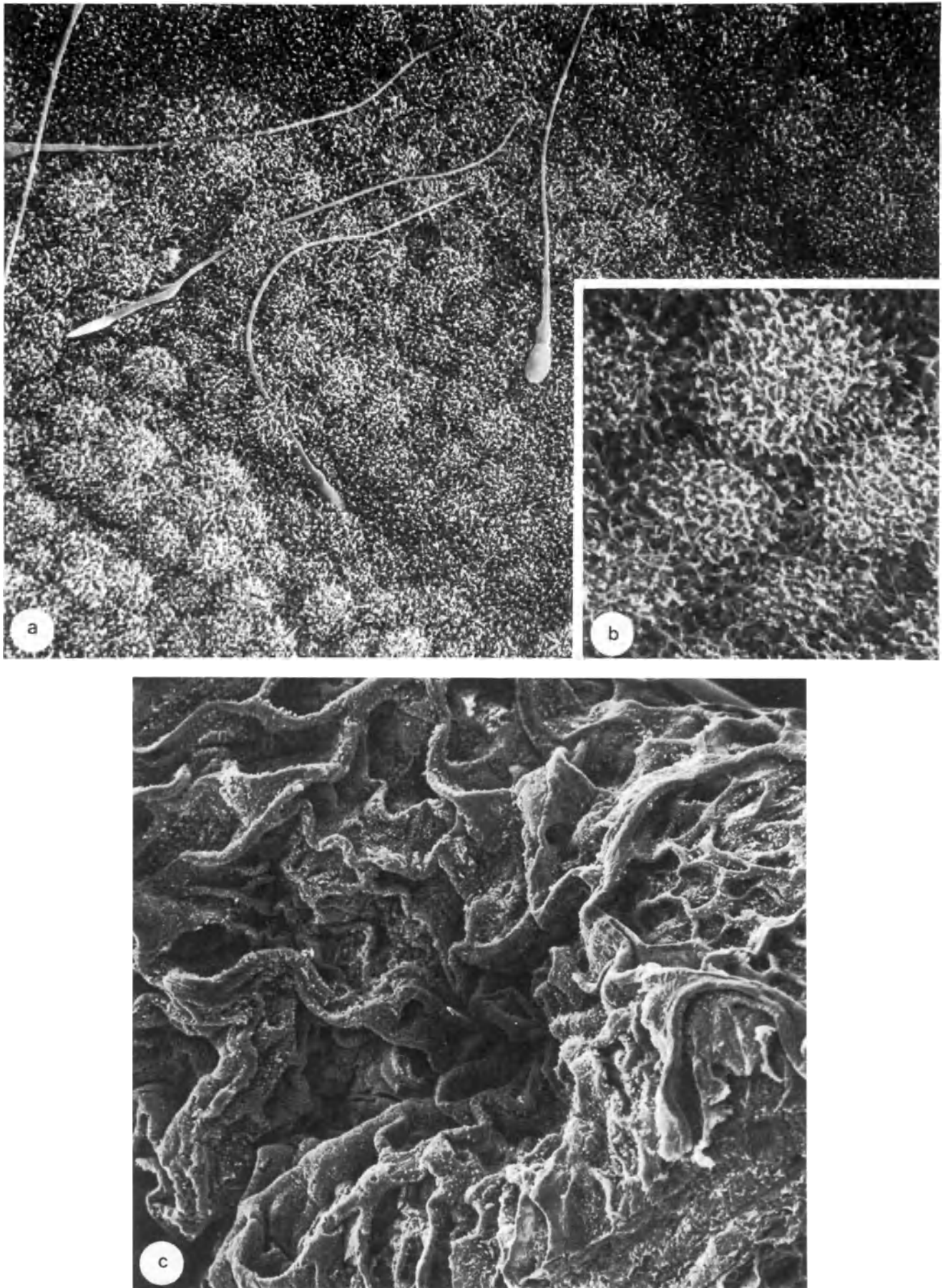
Figure 1

Figure 2

a: Luminal surface of the inguina vas deferens of the monkey. Individual epithelial cel s are covered densely with stereocilia. A few spermatozoa are located on or among the microvilli of the epithelial cells (×1600)

b: Higher magnification view of stereocilia (×5600)

c: Low magnification view of the human ampullary vas deferens. The luminal surface is thrown into extensive foldings of the mucosa. The lumen of the ampullary vas of the monkey is narrower than that of the human (×70)
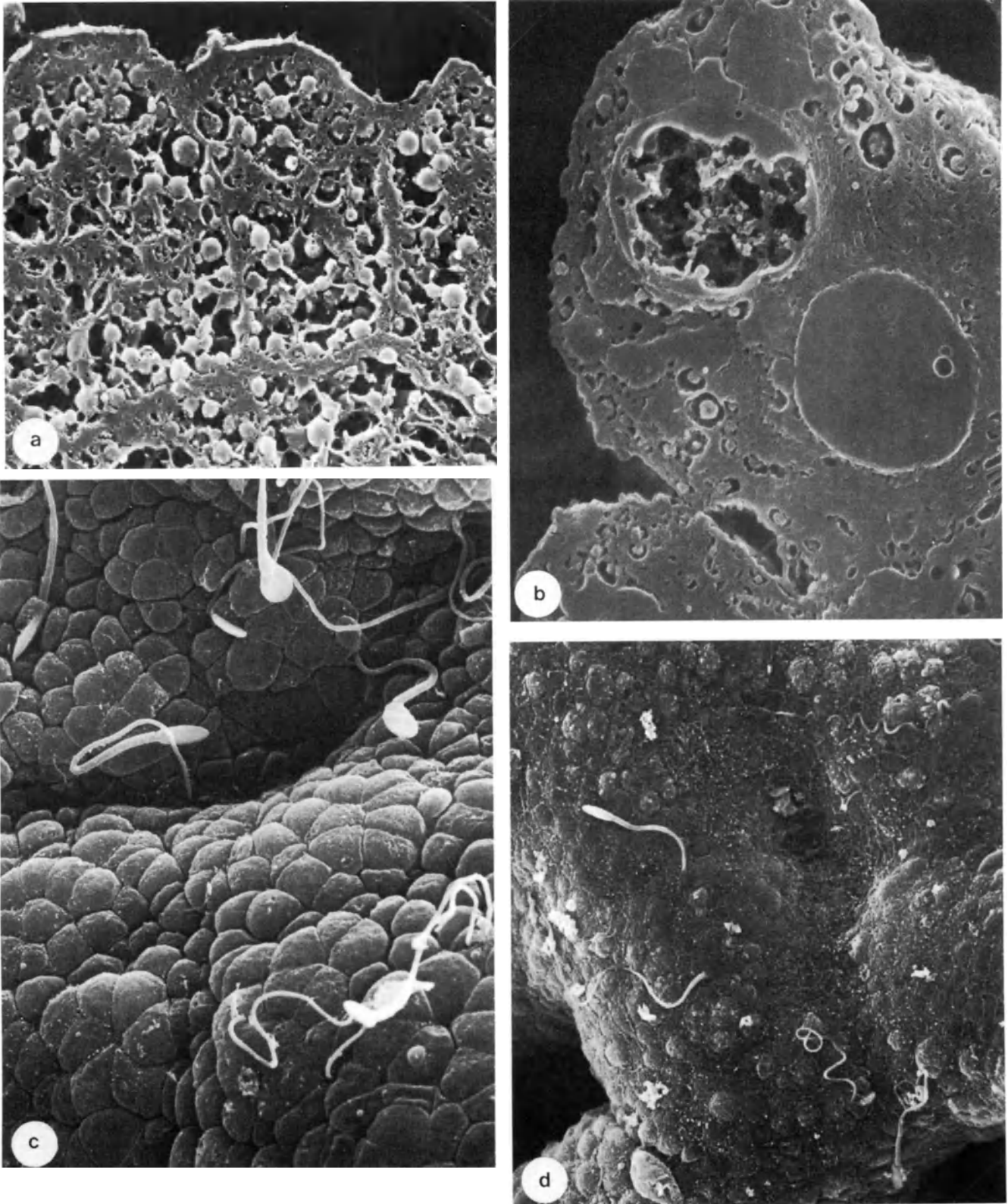
Figure 3

a,b: Fractured surface of the epithelial cells in the monkey (a) and the human (b) ampullary vas deferens, showing abundant secretory granules. In the human the cytoplasm of the epithelial cells contains many residual bodies of varying sizes and contents in addition to the secretory granules (a ×11 200; b ×12 000)

c,d: Survey micrograph of the luminal surface of the ampullary vas deferens in the monkey (c) and the human (d). The epithelial cells are slightly protruded into the lumen and arranged in a fashion of cobblestone pavement. A few spermatozoa are visible attached to the epithelial free surface in each species. (c ×1800; d × 1050)

Figure 4 (opposite)

a–c: Mid-range magnification view of the apical surface of the epithelium in the monkey (a) and the human (b) ampullary vas deferens. Surface configuration of epithelium of the ampullary vas deferens is essentially identical in two species. The epithelial cells are devoid of stereocilia, but covered with short stubby microvilli. In the case of the human, occasional ciliated cells are scattered among non-ciliated cells as shown in c. (a ×3200; b ×3100; c ×7600)

d: SEM view of spermiophagy by the epithelial cells of the monkey ampullary vas deferens. Spermatozoa are ingesting vertically from their heads into the epithelial cells (×17 800)

e: Higher magnification view of spermiophagic process by an epithelial cell (×20 000)
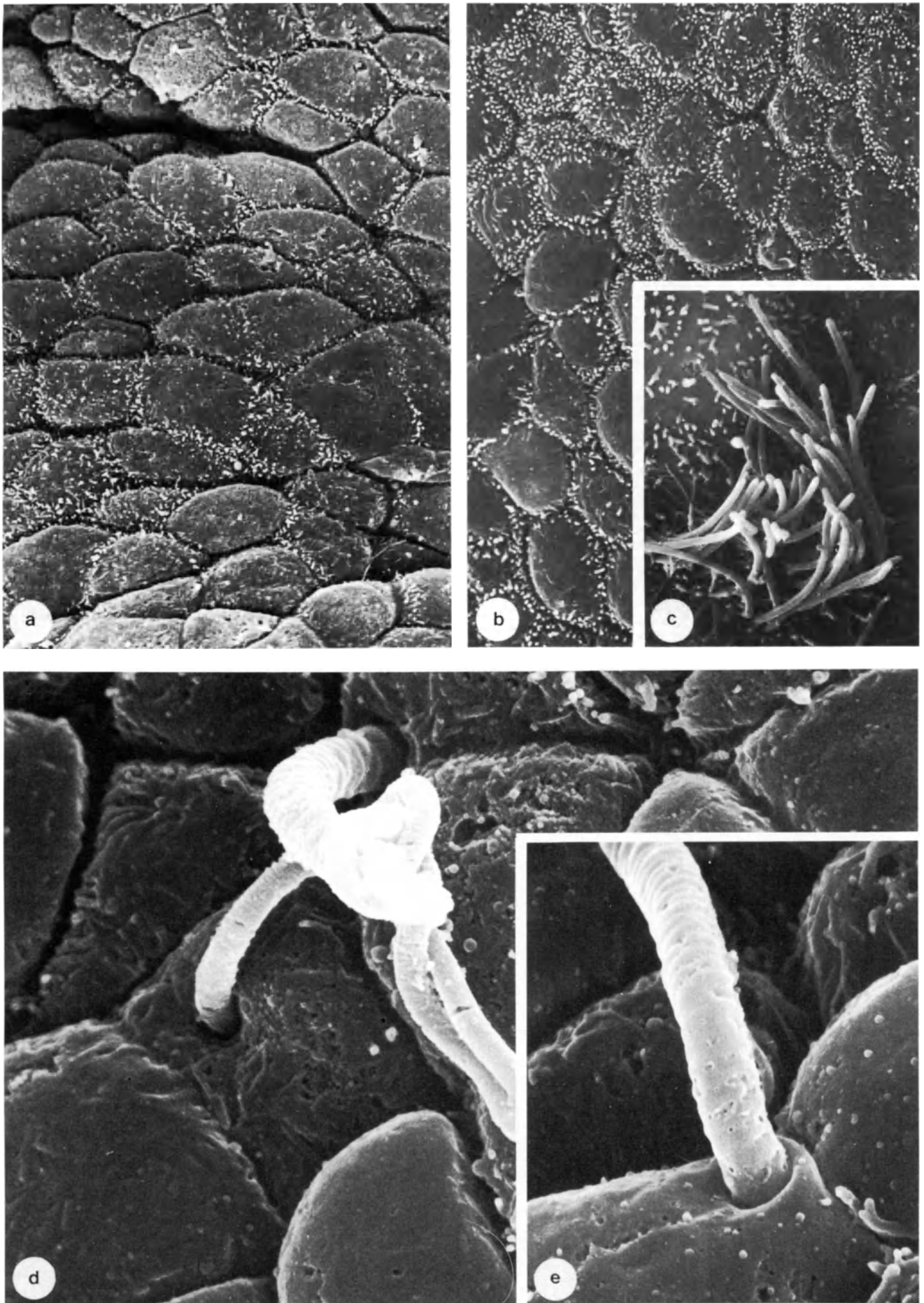
Figure 4

Figure 5 (opposite)

a: SEM view of human ampullary vas deferens showing
      spermiophagy by the epithelial cells (×4000)
b: Higher magnification view of spermiophagic process by
      an epithelial cell in a (×18 500)
c,d: SEM view of spermiophagy by the epithelial cells of the
      monkey (c) and the human (d) ampullary vas deferens.
      Spermiophagy by this epithelial cell proceeds in a
      direction reverse to the previous four figures (c ×8000;
      d ×4500)
e: Fractured surface of an epithelial cell of the monkey
      ampullary vas deferens. Profile of ingested spermatozoa
      can be seen within the cytoplasm of the epithelial cell
      (×9000)
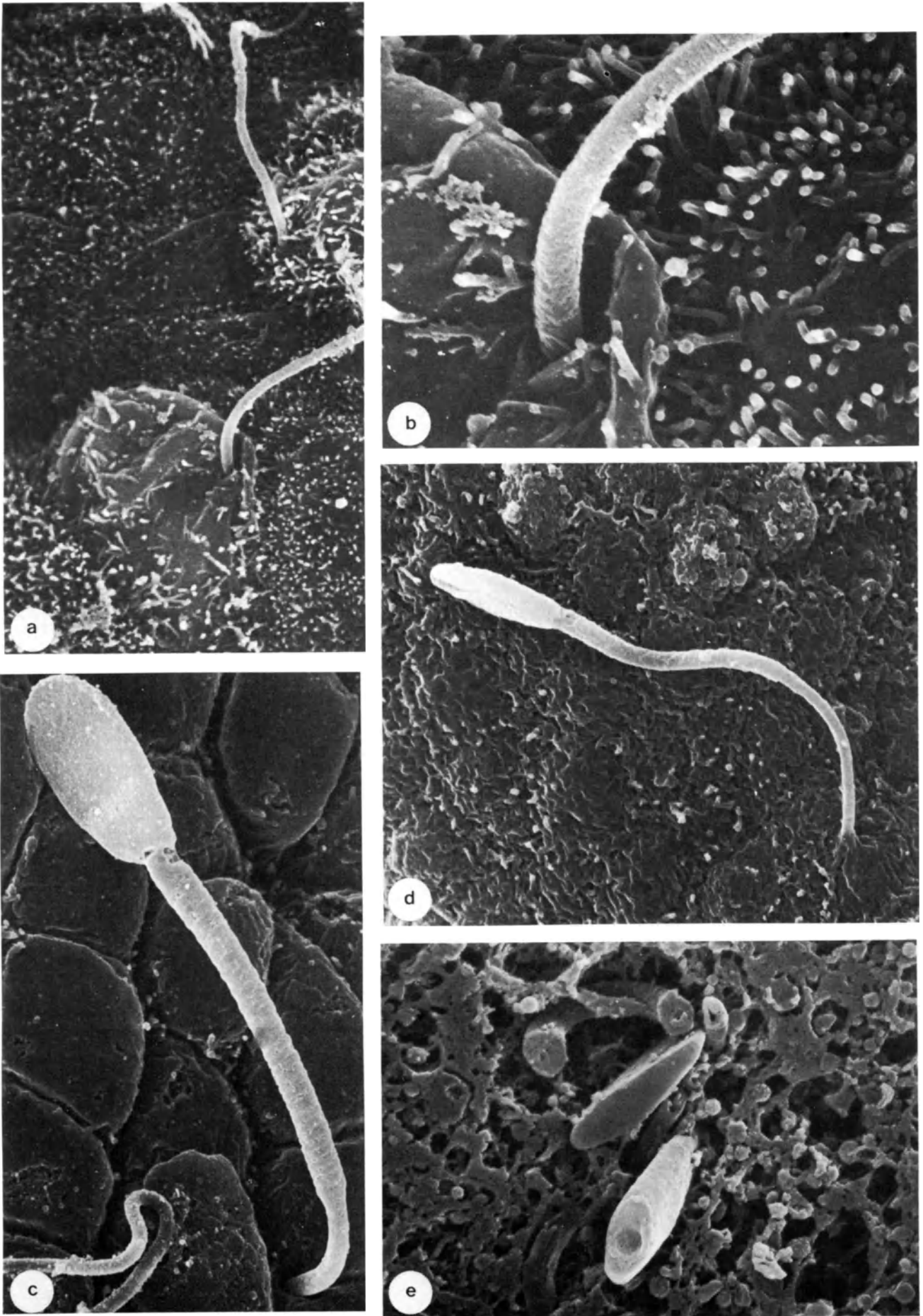
Figure 5

21

Spermatozoa

B. BACCETTI*, E. S. E. HAFEZ† and K. G. GOULD‡

* Universita di Siena, Istituto de Zoologia, Siena, Italy
† Department of Gynecology/Obstetrics, School of Medicine, Wayne State University, Detroit, Michigan, USA
‡ Division of Reproductive Biology, Emory University, Atlanta, Georgia, USA

The ejaculate contains millions of spermatozoa, but there are remarkable individual variations in semen characteristics; e.g. sperm count (concentration, total number of spermatozoa, motility and viability). The human semen is unique when compared with other mammalian semen. For example, there is a high percentage of morphological abnormal spermatozoa in highly fertile men.

NORMAL SPERMATOZOA

The average dimensions of human spermatozoa are as follows:

sperm head: 4.5 μm long and 3 μm wide; it is relatively
    thick in its posterior part
sperm tail
    middle piece: 5–7 μm long and 1 μm in diameter
        wrapped in 10–15 mitochrondrial gyres;
    principal piece: 45 μm long with decreasing
        diameter;
    end piece: 5 μm long, and thinner in diameter than
        the principal piece.

Normal human spermatozoa are characterized by flattened and ovoid heads covered anteriorly by a rough rigid surface and posteriorly by a smooth surface with few granules (Figure 1). There is a marked depression in the head's anterior portion. The acrosome contains proteolytic enzymes which probably facilitate sperm penetration in cervical mucus and in luminal fluids in the uterus and zona pellucida. Remnants of either the plasmalemma or a disrupted cytoplasmic droplet are present immediately posterior to the head, obscuring the junction piece. There are considerable variations in the morphology and thickness of the neck of spermatozoa. In some spermatozoa the neck appears as a thickening or as a slight constriction connecting the head midpiece with the tail. The neck region contains the proximal centriole and the remnant of the distal centriole, surrounded by nine striated columns. The axoneme shows the classical structure '9 + 2': nine double tubules surrounding two central single tubules. The doublet bears two arms of the dynein protein ATPase, responsible for the sliding of each doublet to the other during movement. Radial spokes, peripheral links and other structures also provide a system of cross-links controlling the flagellar movement. The axoneme is surrounded by nine, coarse accessory fibers made up of a specific protein (Baccetti et al., 1976). This arrangement is surrounded by 12 gyres of a mitochondrial helix in the midpiece and by a spiral fibrous sheath in the principal piece (Figures 2–4). In order to obtain this peculiar arrangement (André, 1962; Favard and André, 1970), the mitochondria of the male germinal epithelium undergo extensive rearrangement during spermiogenesis. Actin filaments are found around the mitochondria as shown by immunofluorescence, immunoelectron microscopy and by heavy meromyosin labeling (Baccetti et al, 1980a).

PATHOLOGY OF HUMAN SPERMATOZOA

Abnormal spermatozoa are normally found in the ejaculate of all fertile and infertile men (Tables 1 and 2). Amorphous spermatozoa have structural defects in the shape or size of the head. Anomalies in the shape of sperm head include conical, spherical or more irregular shapes (Figures 5 and 6). Agenesis and hypogenesis of the acrosome and postnuclear cap are also noted (Figures 7–11).

The distorted or bent neck, or a bent head resembling a golf club, are common in the spermatozoa of certain infertile patients. In this type of anomaly, a cytoplasmic droplet is often present. Undersized and rudimentary or a large and monstrous head, as well as stumpy tail, are most frequently seen (Fujita et al., 1971; Hafez and Kanagawa, 1973). Oval, large, small, immature, tapering or bicephalic (two) heads, and malformation of sperm nucleus, are also observed.
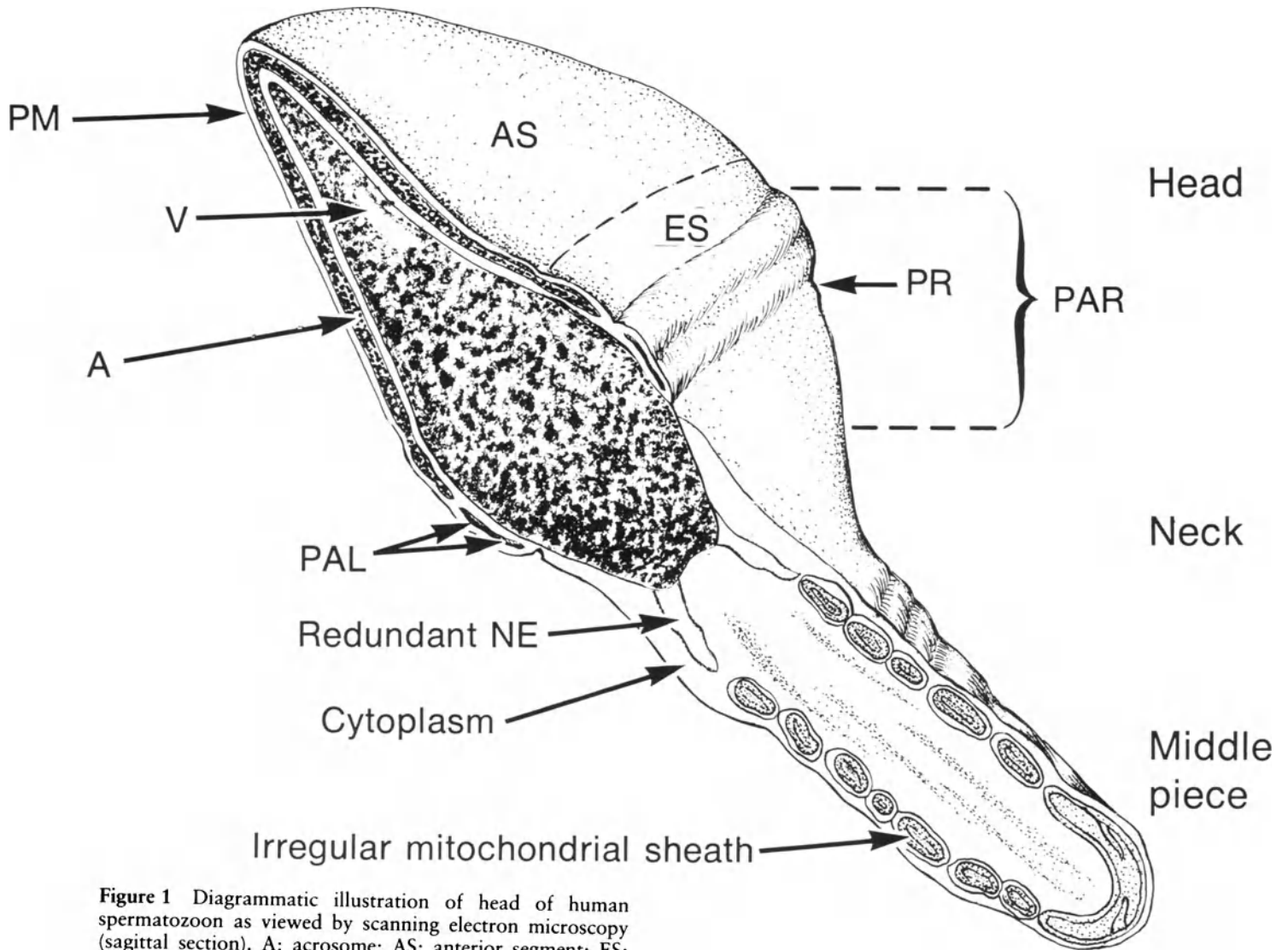
Figure 1 Diagrammatic illustration of head of human spermatozoon as viewed by scanning electron microscopy (sagittal section). A: acrosome; AS: anterior segment; ES: equatorial segment; NE: nuclear envelope; PAL: postacrosomal lamina; PAR: postacrosomal region; PM: plasma membrane; PR: posterior ring; V: nuclear vacuole (Flechon and Hafez, 1976)

Table 1 Some surface and ultrastructural anomalies in human spermatozoa from fertile and infertile men

Anatomical regions	Surface and ultrastructural anomalies
Head	
plasmalemma	discontinuous, vesicular, granular, wavy, swollen
postacrosomal cap	absent, abnormal, discontinuous or detached
Middle piece	
cytoplasmic excess	absent, large, small or granular
mitochondria	dispersed, high or low number, discontinuous external membrane, indistinct architecture, cristae peripherally placed, dilated, narrowed or of variable thickness
Principal piece	
plasmalemma	irregular, swollen, granular or discontinuous
coarse fibers	absent, indistinct contour, abnormal disposition, fibers separated from tubules
fibrous sheath	indistinct contour, discontinuous, circumferential strands massed or dissociated, increased, reduced or variable thickness

Abnormalities of the midpiece include parts of thin and constricted midpieces, enlargement, breakage and duplication. The morphological anomalies may be a result of trauma, illness, or the use of antispermatogenic compounds.

A common defect is the cytoplasmic droplet, accumulation of cytoplasm at the neck and midpiece. Variable contents of the droplet have been observed by TEM (Fujita et al., 1971; Zambone et al., 1971). The droplet is usually represented by an oval thickening in the middle of the midpiece, thickening in the neck of the spermatozoa, or by various deviations in shape, surface structure and position of the droplet. A thickened midpiece may be due to an accumulation of cytoplasmic substance or to superficial mitochondria.

Complete or incomplete absence of mitochondria in the midpiece is a common anomaly in infertile sperm. Mitochondrial hypogenesis is represented in different degrees: slight defect, slight thickenings reminiscent of mitochondrial windings, or complete exposure of the axis of the midpiece as a result of mitochondrial
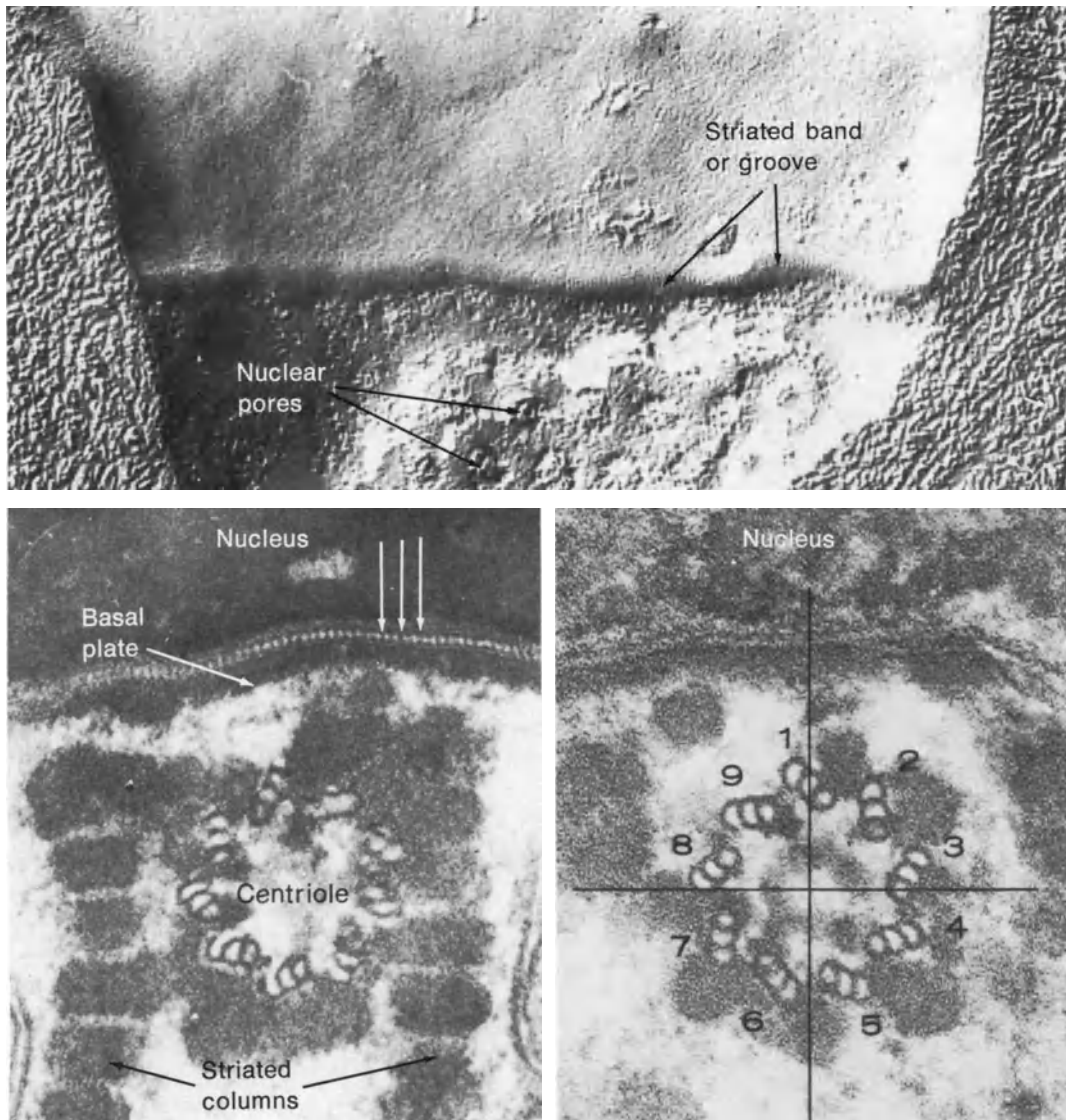
Figure 2

Top: Freeze cleaving preparation of postacrosomal and neck regions of human spermatozoon. Striated band, or groove, also referred to as posterior ring, encircles head. Fine striation is discernible in depths of groove. Along this band, cell membrane appears to be fused to membranes of underlying nuclear envelope. Caudal to this line of fusion, redundant fold of nuclear envelope extends back into neck. Where fracture plane has broken through cell membrane, several pores in close hexagonal array can be seen in nuclear envelope (from Pedersen, 1972b)

Bottom left: Electron micrograph of longitudinal section through base of nucleus and proximal portion of connecting piece. Note centriole in interior of connecting piece and periodic densities (arrows) transversing narrow cleft between outer and inner membranes of nuclear envelope where it lines implantation fossa (from Pedersen, 1972a)

Bottom right: Micrograph of neck region. Juxtanuclear centriole has constant orientation. Line drawn through triplet nearest basal plate and between two opposite triplets coincides with long axis of tail. Conventional system of numbering triplets is suggested (from Pedersen, 1972a)
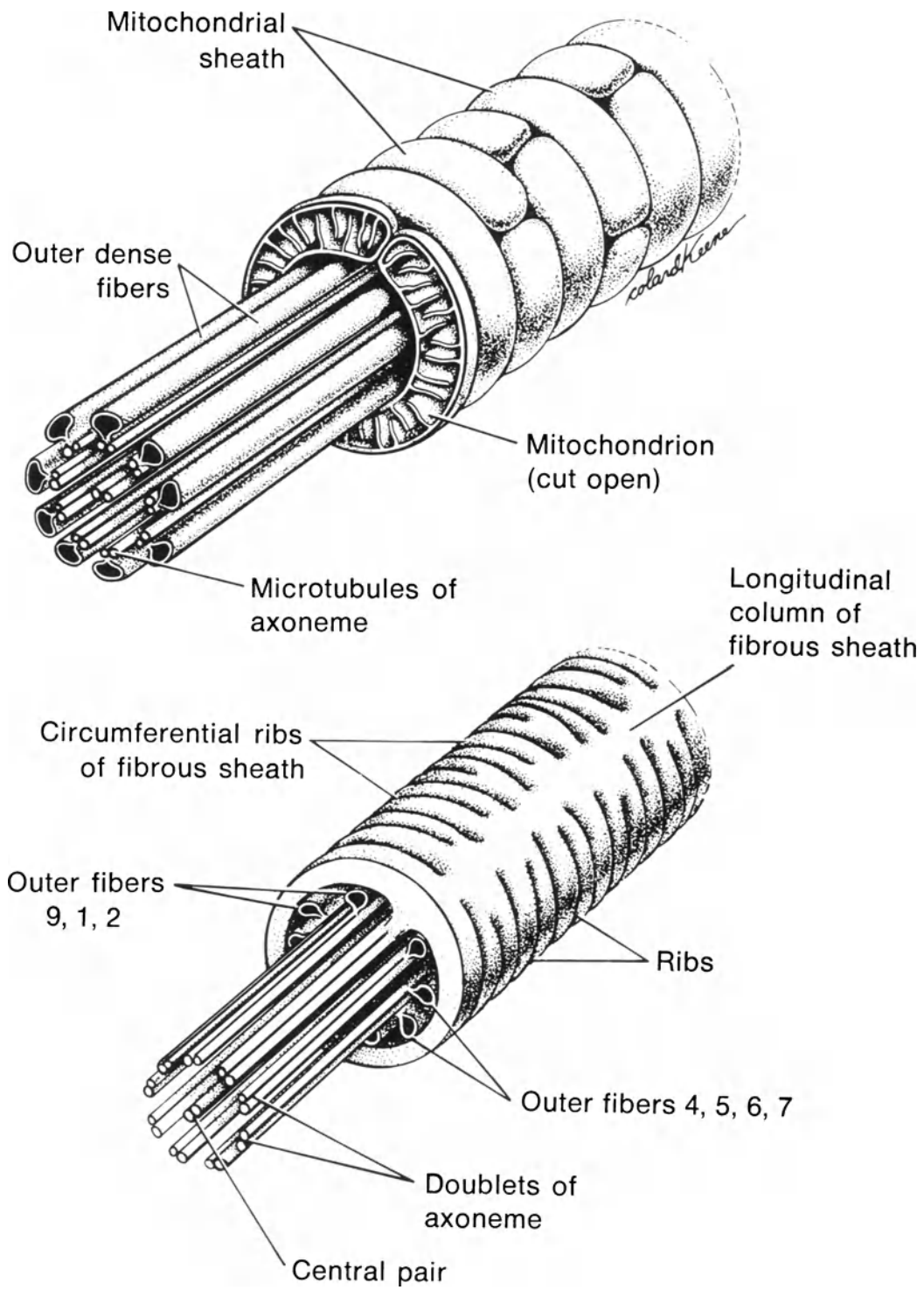
Figure 3 Organization of middle piece (above) and principal piece (below) of human sperm tail (from Pedersen and Fawcett, 1976)
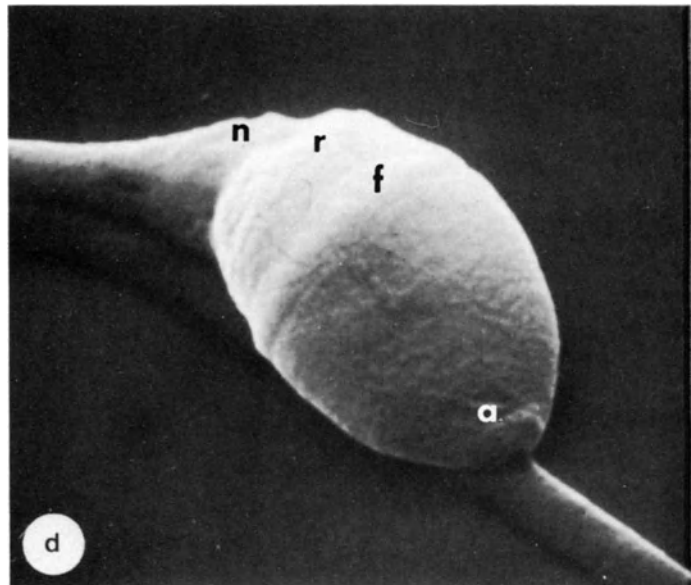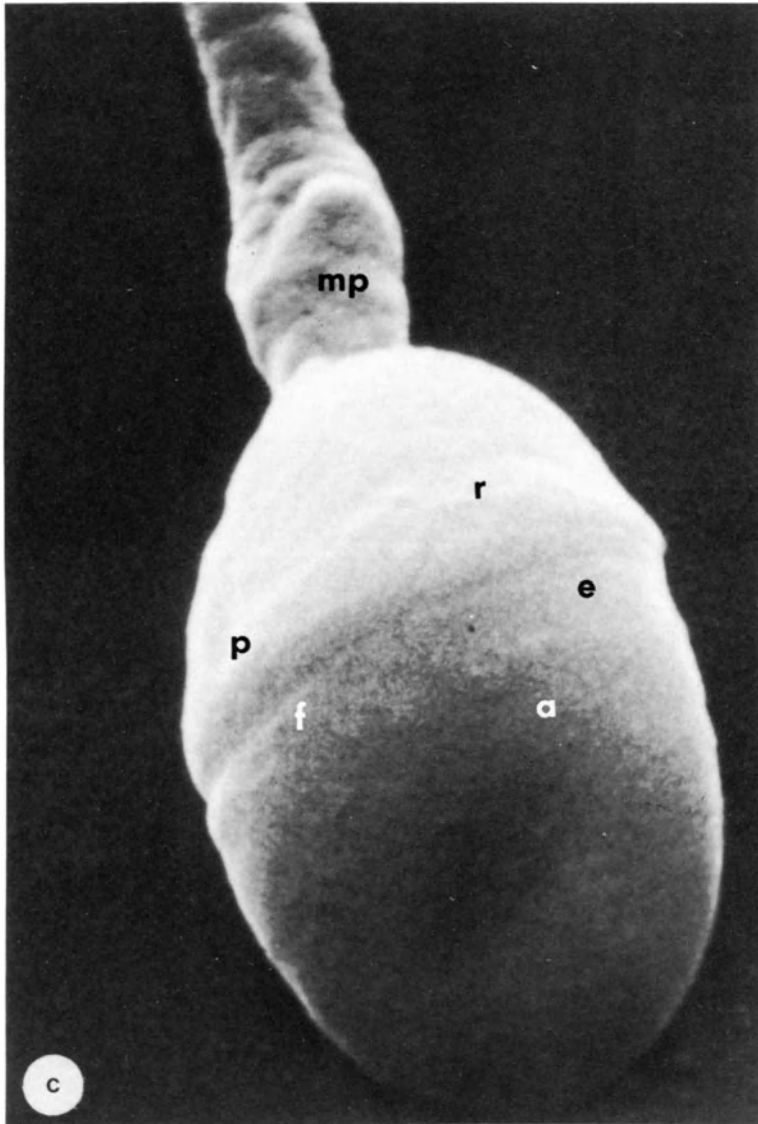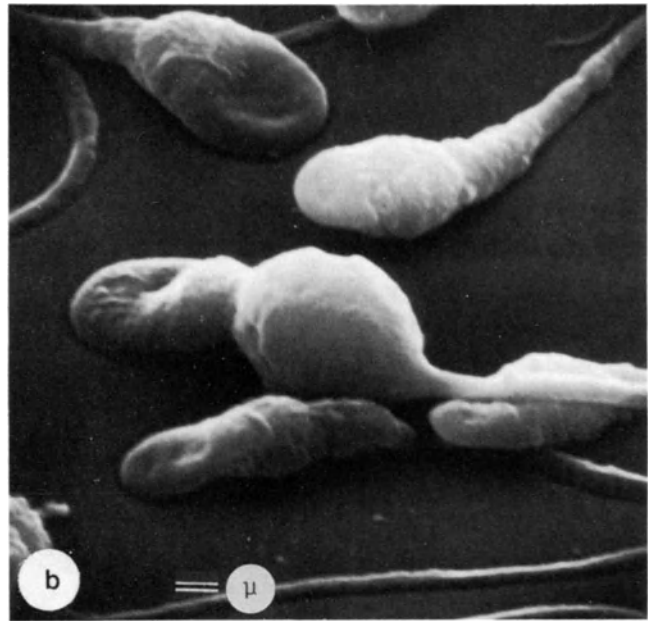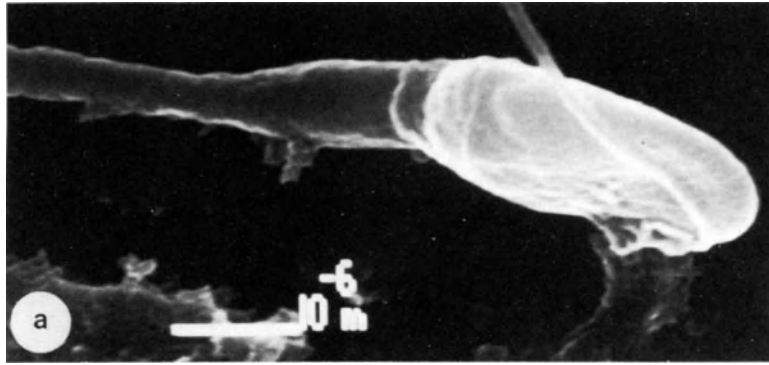
Figure 4   SEM of normal spermatozoa from fertile men

a: The relatively flat structure of the head and the smooth acrosome membrane is evident, as is the smooth membrane over the mitrochondria of the midpiece. The underlying mitochondria are more evident in SEM if the specimens are air-dried and the membrane contracts down onto the underlying structure.

b: Of the five spermatozoa only two (upper) are normal. The sperm in the center is immature as judged by the presence of cytoplasmic droplet around the midpiece. The other two sperm have excessively small heads

c: Anterolateral view of head with typical 'oval' shape, Acrosomal surface is finely granular and somewhat depressed. A fine line may separate anterior (a) and equatorial (e) segments of acrosome. Profound furrow (f) is visible in front of thicker postacrosomal region (p), which is divided in two parts by posterior ring (r). Note irregularity of mitochondrial sheath of middle piece (mp) ($\times 16\,500$)

d: Anterolateral aspect of ovoid sperm head. Acrosome (a) surface is rough. Note furrow (f) and postacrosomal region, including posterior ring (r). Two distinct bands appear in postacrosomal region between furrow and posterior ring. Neck (n) is bent and thickened by cytoplasmic remnants. ($\times 8800$) (a and b from Gould *et al.*, 1971; c and d from Flechon and Hafez, 1976)
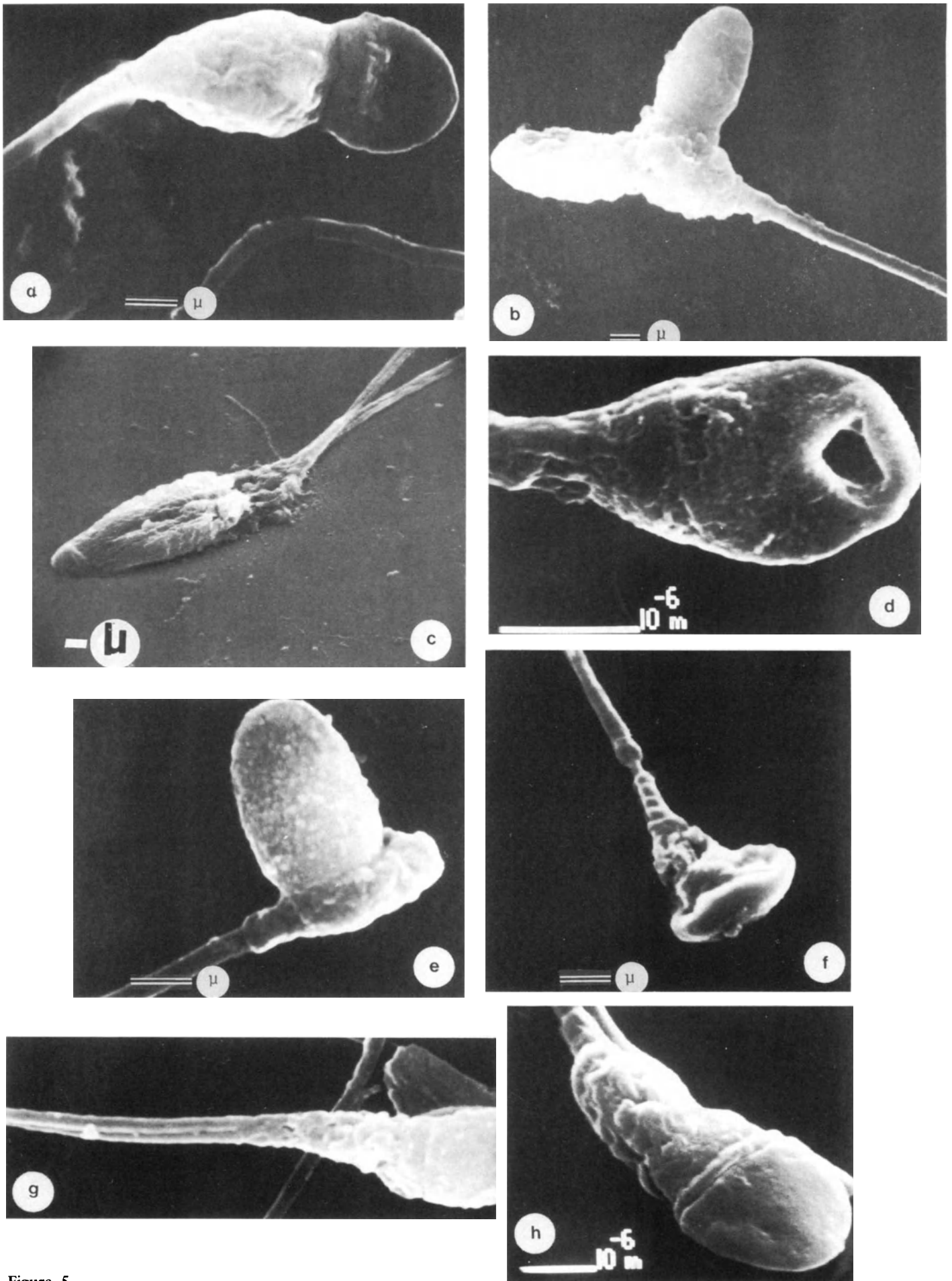
Figure 5
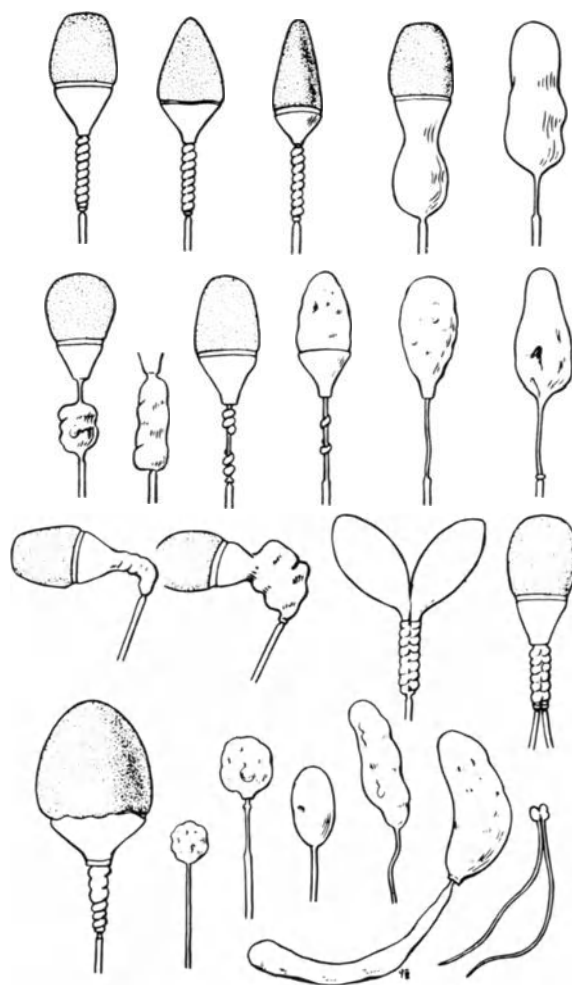
Figure 6 Diagrammatic depictions of abnormal human spermatozoon as observed by scanning electron microscopy (from Fujita, 1975)

Figure 5 (opposite) SEM of abnormal human spermatozoa from fertile and infertile men

a: Immature human sperm. The head is round and paddle-shaped, and there is an excess of cytoplasmic material obscuring the midpiece. Such sperm are frequently motile, but probably infertile. They are usually present in low numbers (≤1%) in a normal ejaculate

b: Two-headed sperm. The nuclei appear relatively normal, but there is clearly disorganization in the midpiece and a single tail. Such sperm are infertile

c: Abnormal sperm with a double tail and excessively large head. The normal morphology of midpiece is lost

d: Sperm head showing severe cavitation. It is not unusual for TEM of human sperm to demonstrate defects in the nucleus. Such defects occasionally communicate with the exterior.

e: Certain ejaculates demonstrate a uniform malformation of the midpiece. Note sequential double fold in the midpiece which results in the appearance of the head being mounted midway along the midpiece

f: Abnormal sperm with loss of normal head structure and bizarre neck structure. Mitochondria of the midpiece appear to be present

g: Sperm with double tail. Note the disorganization of the midpiece

h: This sperm shows a frequently observed form of the head in which the posterior acrosome margin is extremely obvious and, frequently, a second annular structure is present posterior to the acrosome margin. This sperm was in an ejaculate from a fertile man (photos by K. Gould)

Table 2 Some structural and ultrastructural anomalies of human spermatozoa which may be associated with male infertility or related syndromes

Structural and ultrastructural anomalies	Authors
(1) 'Round-headed spermatozoa': a specific defect affecting the whole sperm population: absence of acrosome and postacrosomal sheath; round head; infertility. An occurrence of round-headed spermatozoa in two brothers suggests that the defect may have a genetic origin Abortive development of acrosome, whose primordium failed to attach to nucleus and expand, and instead regressed. Nucleus failed in shaping and retarded in maturing, a disturbance apparently associated with the aplasia or hypoplasia of sperm manchette; possible role of zinc in nuclear differentiation and the shape of head in the movement pattern	Holstein et al. (1973) Pedersen and Rebbe (1974) Kullander and Rausing (1975)
(2) Paddle-shaped head, normal head, posterior thickening of nucleus; the acrosome covers the anterior half to two-thirds of head In other types, the midpiece is completely flexed back upon itself and appears to occupy the position of the sperm head which is central in the micrograph; severe distortion of midpiece can be associated with infertility	Gould et al., (1971) Fujita (1975) Fujita et al. (1970, 1971)
(3) Excessive large sperm head. In form it is basically pyriform, but SEM does not permit identification of nuclear size. The acrosomal membrane is smooth but appears to cover approximately two-thirds of the head. Such sperm heads are frequently associated with diploid chromosome content	Hafez (1975)
(4) Bizarre and degenerate form, sperm may be actively motile, uncertain fertilizing capacity, the head is basically paddle-shaped, but there is evidence of anterior swelling of acrosome. Sperm neck is distorted with excess membrane present, midpiece is short, and mitochrondria are clearly visible	Hafez and Kanagawa (1973)
(5) 'Kartagener's syndrome': immotility of all spermatozoa of an individual (epithelial cilia are also immotile) Apparently normal-shaped spermatozoa; absence of doublet arms (and consequently of most of the ATPase dynein)	Afzelius et al. (1975) Pedersen and Rebbe (1975) Baccetti et al. (1981)
(6) Absence of central tubules and projections forming the central sheath; electrophoretic analysis of the high molecular weight polypeptide chains attributed to dyneins shows constant absence of one chair, possible location of a dynein chain in central structures usually belonging to the '9 + 2' model	Baccetti et al. (1979a)
(7) 'Empty tails': infertile patients with all immotile spermatozoa, flat and unusually curved sperm tails, length and proportions of the cell are normal. This defect consists in an axonemal alteration able to modify the cell outline. The '9 + 0' basic structure of the axoneme is completely missing and only the set of nine accessory fibers is present. Absence of '9 + 2' axoneme is accompanied by absence of dynein proteins and motility	Baccetti et al. (1980b)
(8) 'Short tails': sperm tail is constantly extremely short, with two imperfect brief axonemes arising from both centrioles, accessory fibers are present, the tubules rarely arranged in doublets and without arms, tubulin and the protein of accessory fibers are present, dynein absent (anomaly found in two unrelated patients)	Baccetti et al. (1975)

Structural and ultrastructure anomalies	Authors
(9) Abnormal sperm tails: e.g. with deficient accessory fibers; or disordered or half axonemes	Ross et al. (1971, 1973) Renieri (1974)
(10) 'Double spermatozoa': sperm anomaly associated with 'hyperprolactinemy' due to pituitary adenoma Almost all spermatozoa are double, with a common bilocular acrosome, two paired nuclei and two tails which run free from the level of the midpiece or from the principal piece; sperm are motile, but they can progress only if the two flagella beat synchronously, a few sperm are triple or quadruple Abnormal prolactin levels seem to inhibit cell division during the late spermatogenetic stages after treatment with 2-brom-a-ergocryptine the prolactin level is corrected only normal, single spermatozoa are produced	Baccetti et al. (1978, 1979c)
(11) Persistence in mature sperm of some characteristics normally found only in spermatids	Fujita et al. (1970) Lacy et al. (1974) Renieri (1974)
(12) 'Aged spermatozoa' from donors older than 65 years with low sperm count (10 and 20 million per ml) and a poor level of motility (less than 10%). The structure of the ejaculated cells is peculiar, immature stages are absent, spermatozoa are all devoid of cytoplasmic droplets, meager and sometimes straight, and unusually thin	Gould et al. (1971) Hafez (1975)

agenesis. Mitochondrial defects in the midpiece may occur in combination with the absence of acrosome.

Certain anomalies of the axoneme may be of genetic origin. One common defect is the complete absence of tubulin and dynein from the tail, which is made up only by accessory fibers. Another defect is the absence of central tubules (and the axoneme assumes the arrangment '9+ 0') or of dynein arms from the doublets. This last defect is named Kartagener's syndrome. Patients with this syndrome are infertile due to immotility of spermatozoa. Such patients apparently have situs inversus of the heart and chronic pulmonary symptoms that are characteristic of Kartagener's syndrome (Table 2). It was then demonstrated that the basic mechanism in this syndrome might be a lack of dynein arms, both in the sperm flagella and in the cilia of their respiratory tract and of the embryo (Afzelius et al., 1975; Pedersen and Rebbe, 1975).

ABNORMAL SPERM AND MALE INFERTILITY

Classification of abnormal spermatozoa has been attempted using light microscopy (Freund, 1966; MacLeod, 1970). SEM has been used in conjunction with TEM to examine the relationship of morphological abnormality and infertility in man (Fujita et al., 1970). Some of the atypical spermatozoan types are found in fertile semen, whereas other forms are encountered only in sterile patients. For example, certain abnormal forms may be characteristic of post-traumatic or postinfectious infertility, whereas others characterize infertility due to endocrine balance. A few forms are associated with congenital sterility,

particularly the round shape of the head: associated with the absence of the acrosome and all the defects of the tail, occurring in the whole sperm population of some individuals, are constantly responsible for an irreversible sterility. A defect in a certain subcellular portion of the spermatozoa may possibly be associated with that of another type. For example, deformation of the acrosome of the head may be associated with abnormalities of the mitochondrial sheath of the midpiece (Fujita, 1975). The mechanisms involved in the formation of sperm anomalies and the association of such anomalies should be analyzed on the basis of morphological observations of spermatogenesis in sterile patients. The origin of binucleate spermatozoa in the human testis has been studied using TEM.

SPERM–EGG INTERACTIONS AND DYNAMICS OF FERTILIZATION

The surface ultrastructure of unfertilized and fertilized eggs of women, rabbits and rats was studied using SEM and TEM. The zona pellucida had an outer surface with fibrous meshwork containing numerous pores or channels, and an inner surface with relatively smooth pores corresponding to the microvilli of the vitellus of the ovum. The zona pellucida acts as a barrier to sperm penetration and prevents polyspermy in some species (Dudkiewicz and Williams, 1977). Unfertilized ova are uniformly covered with microvilli except for a small polar region overlying the second metaphase spindle. The membrane covering the first polar body, which is extruded before ovulation, is smooth and non-villous and is near a non-microvillous area of the egg surface
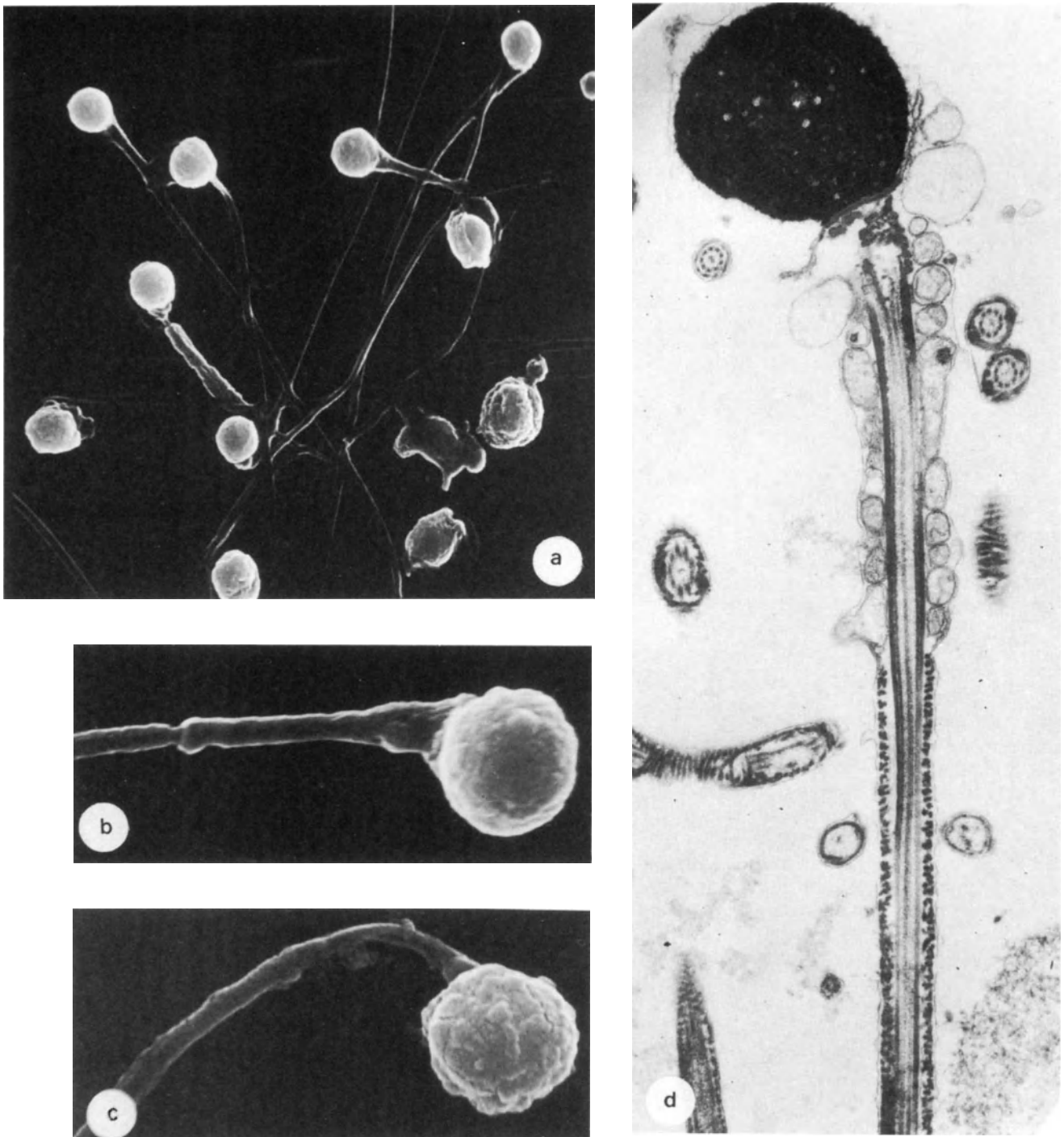
Figure 7 SEM and TEM of 'round-headed' human spermatozoa
a: ×3000
b,c: ×10 000

d: TEM of longitudinal section: Ax, axoneme; M. mitochondrial; N. nucleus (×19 000) (Baccetti *et al.*, 1977)
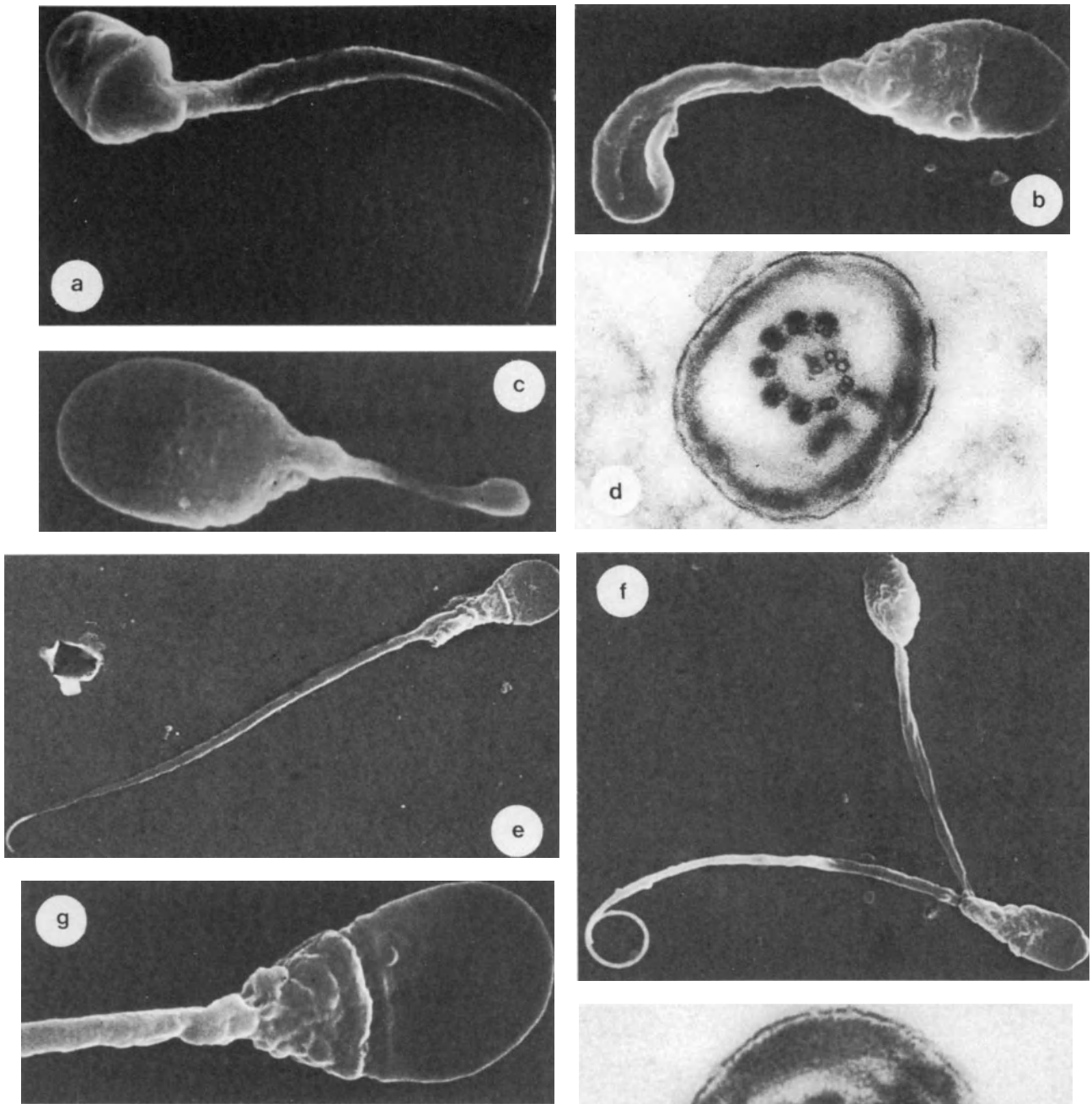
Figure 8 SEM and TEM of 'short-tailed' and '9 + 0' human spermatozoa

a,b: 'Short-tailed' spermatozoa. The tail is quite short, immotile and lacking dynein arms (×6000)

c: Higher magnification of the same (×10 000)

d: 'Short-tailed' spermatozoon. Cross-section of the tail. Axonemal elements are disordered and dynein arms lacking (×80 000)

e–g: '9 + 0' spermatozoa. The tail region appears straight, the head is normal (f). (e × 2400; f ×3000; g ×10 000)

h: Cross-section of the tail is '9 + 0' spermatozoon (Baccetti et al., 1975, 1979a)
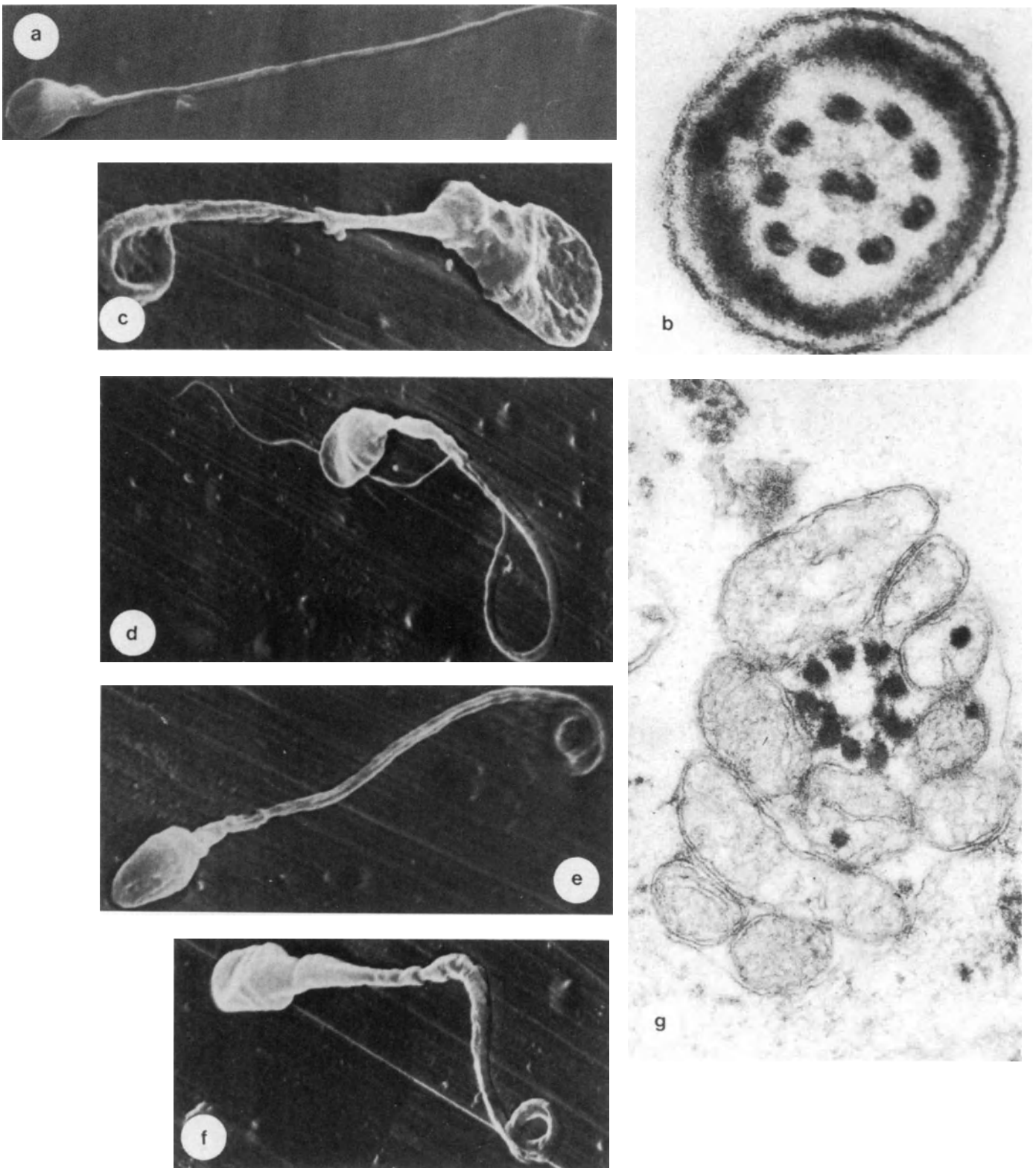
Figure 9 SEM and TEM of 'arm-less' and 'empty-tailed' human spermatozoa

a: 'Arm-less' sperm. The tail is straight (×3000)

b: Cross-section of the tail region in an arm-less spermatozoon. The dynein arms of the doublet tubules are absent (×170 000)

c–f: 'Empty-tailed' spermatozoa. Tails appear empty and flattened. (c ×7000; d–f ×5000)

g: 'Empty-tailed' spermatozoon. Cross-section of the middle piece. The '9 + 2' axoneme is absent. Only the accessory fibers are present (×62 500)

(a–g from Baccetti et al., 1980b, 1981)
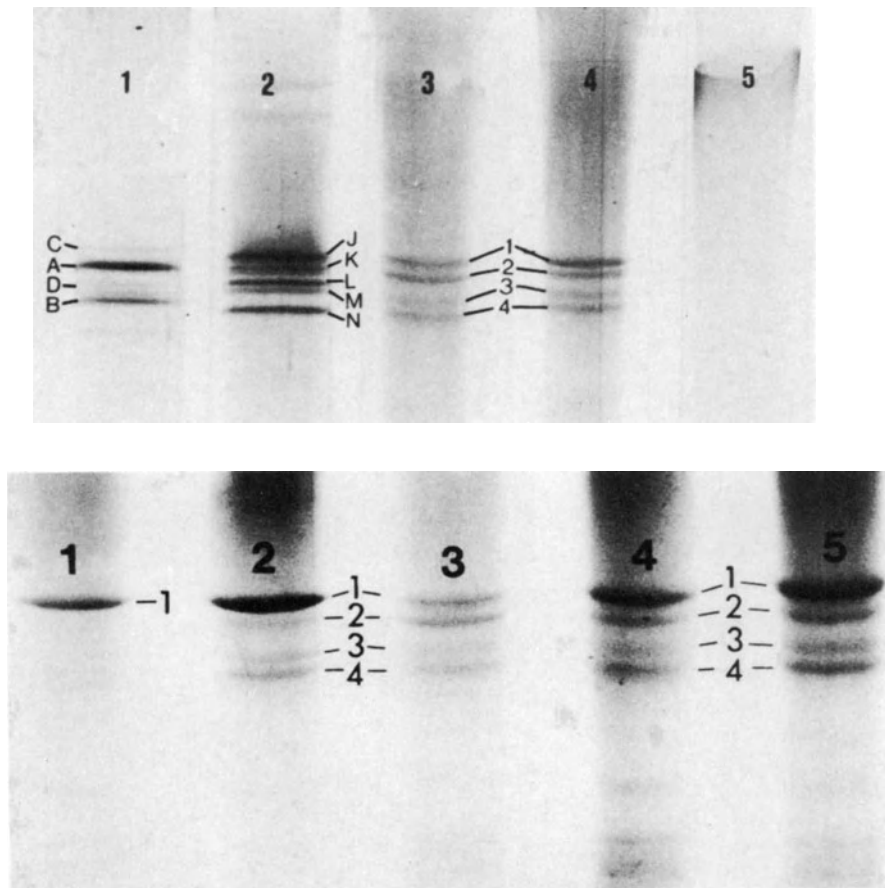
Figure 10 SDS gel electrophoresis on high molecular weight polypeptide chains of spermatozoa

Top: High molecular weight polypeptides of sea urchin, bull and human spermatozoa

Gel 1: sea urchin sperm flagella, 30 μg of total protein

Gel 2: SDS extract from ~4 mg of ejaculated, motile bull spermatozoa

Gel 3: SDS extract from 4 mg of normal human spermatozoa

Gel 4: SDS extract from 4 mg of acrosome-less, motile human spermatozoa

Gel 5: SDS extract from 4 mg of axoneme-less immotile human spermatozoa

Bands in the dynein region are labeled from A to D according to Pallini and Gibbons in bull and from 1 to 4 in human spermatozoa

Bottom: SDS gel electrophoresis on high molecular weight polypeptide chains of human spermatozoa bearing different axoneme defects

Gel 1: arm-less axoneme

Gel 2: '9 + 0' axoneme

Gel 3: normal axoneme

Gel 4: coelectrophoresis of normal and arm-less sperm

Gel 5: coelectrophoresis of '9 + 0' and normal human spermatozoa

The dynein bands are labeled from 1 to 4. SDS extracts from ~4 mg of cells for each cell type were used in the electrophoretic runs. (Baccetti et al., 1981)

which is an area of low sperm attachment and contains no cortical granules (Calarco and Epstein, 1973). At the outer surface of the zona pellucida, spermatozoa undergo the acrosome reaction and the outer acromosomal membrane and plasmalemma separate from the head of the spermatozoon. Several acrosomal caps are noted at the surface of the zona. The outer acrosome and plasmalemma undergo extensive vesiculation. The spermatozoa penetrate the zona pellucida through a furrow. The first interaction of the fertilizing spermatozoon with the oocyte surface involves the microvilli, with an initial contact in the region posterior to the.portion of the head previously covered by the acrosome. This is followed by fusion between the membranes of the gametes with the head

and portions of the tail being incorporated within the vitellus. The entire tail becomes covered with surface microvilli and is eventually incorporated into the oocyte (Sugawara et al., 1975). Fertilization is associated with numerous cytological changes; e.g. lack of cortical granules, presence of acrosomal membranes and rough endoplasmic reticulum in cumulus cells (Gwatkin et al., 1976; Lin et al., 1975).

References

Afzelius, B. A. R., Eliasson, O., Johnsen and Lindholmer, C. (1975). Lack of dynein arms in immotile human spermatozoa. *J. Cell Biol.*, 66, 225

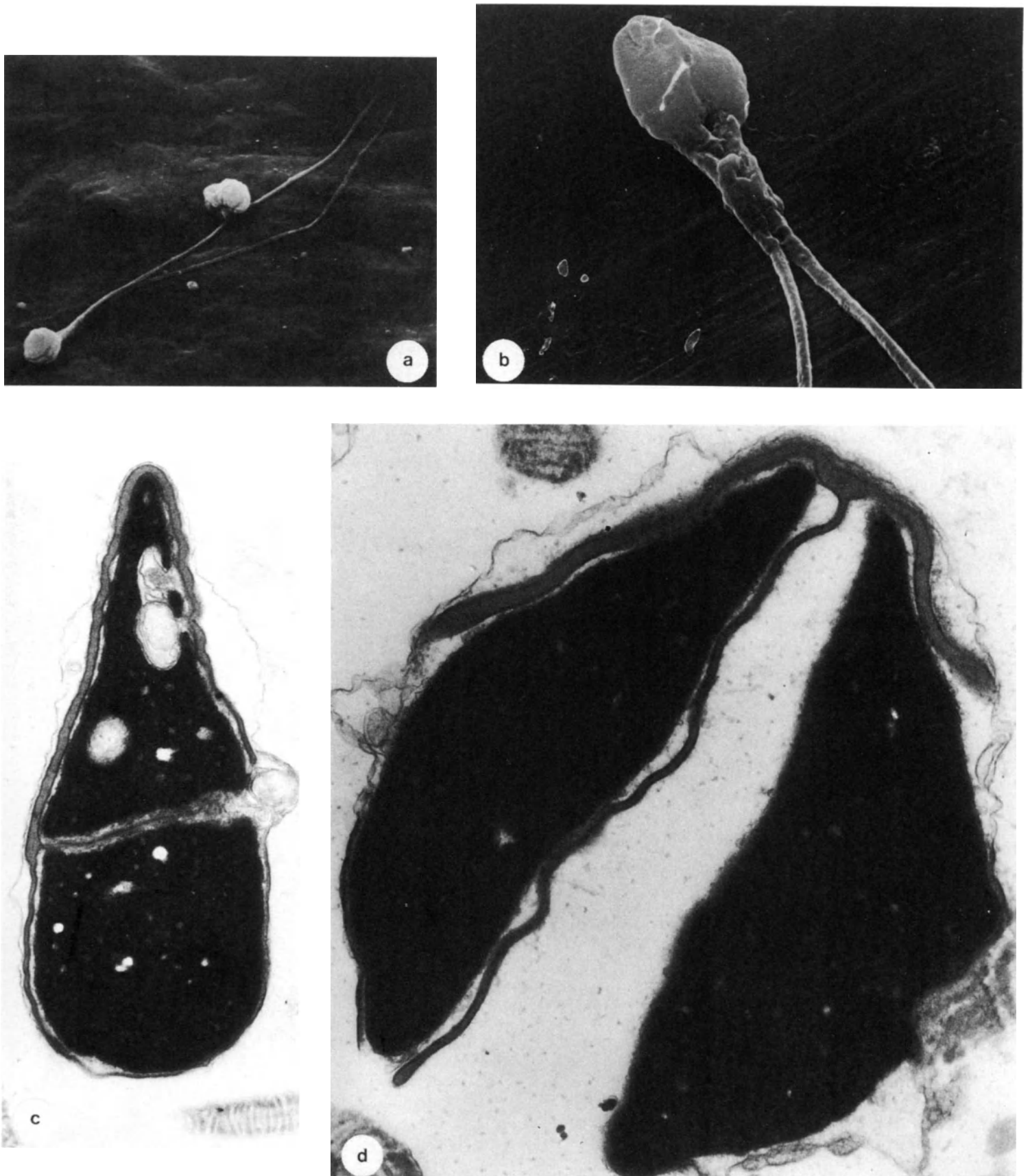**Figure 11** SEM and TEM of 'double' spermatozoa from hyperprolatinaemic men
a: From an apparently single head, two tails arise (×2000)
b: Higher magnification of the anterior region in the spermatozoa of the same individual (×10 000)
c: Longitudinal section of the head in a double spermatozoon of a hyperprolactinemic man. An apparently unique acrosome surrounds a double nucleus (×30 000)
d: Longitudinal section of the head region in the spermatozoon of a hyperprolactinemic man. The acrosome is bipartite with two nuclei (×47 500) (Baccetti *et al.*, 1978)

André, J. (1962). Contribution a la connaissance du chondriome. Etude de ses modifications ultrastructurales pendant la spermayogenese. *J. Ultrastruct. Res.*, 3 (Suppl), 1

Baccetti, B. and Afzelius, B. A. (1976). *The Biology of the Sperm Cell*. (Basel: S. Karger)

Baccetto. B., Burini, A. G., Maver, A., Pallini, V. and Renieri, T. (1979a). '9 + 0' immotile spermatozoa in an infertile man. *Andrologia*, 11, 437

Baccetti, B., Bigliardi, E., Burrini, A. G. and Pallini, V. (1980a). Actin filaments and mitochondrial movement in vertebrate-spermiogenesis. *Gamete Res.*, 3, 203

Baccetti, B., Burrini, A. G. and Pallini, V. (1980b). Spermatozoa and cilia lacking axoneme in an infertile man. *Andrologia*, 12, 525

Baccetti, B., Burrini, A., Pallini, V., Renieri, T., Rosati, F. and Menchini Fabris, G. F. (1975). The short-tailed human spermatozoa. Ultrastructural alterations and dynein absence. *J. Submicr. Cytol.*, 7, 349

Baccetti, B. A. G., Burrini, R. and Pallini, V. (1979b). The dynein electrophoretic bands in axonemes naturally lacking the inner of the outer arm. *J. Cell Biol.*, 80, 334

Baccetti, B., Burrini, A. G., Pallini, V. and Renieri, T. (1981). Human dynein and sperm pathology, *J. Cell Biol.*, 88, 102

Baccetti, B., Fraioli, F., Paulucci, D., Selmi, G., Spera, G. and Renieri, T. (1978). Double spermatozoa in a hyperprolactinemic man. *J. Submicr. Cytol.*, 10, 240

Baccetti, B., Fraioli, F., Paolucci, D., Selmi, G., Spera, G. and Renieri, T. (1979c). High prolactin level and double spermatozoa. *Gamete Res.*, 2, 193

Baccetti, B., Pallini, V. and Burrini, A. G. (1976). The accessory fibers of the sperm tail. III. High-sulfur and low-sulfur components in mammals and cephalopods. *J. Ultrastruct. Res.*, 57, 289

Baccetti, B., Renieri, T., Rosati, F., Selmi, M. G. and Casanova, S. (1977). Further observation on the morphogenesis of the round-headed human spermatozoa. *Andrologia*, 9, 255

Calarco, P. G. and Epstein, C. J. (1973). Cell surface changes during preimplantation development in the mouse. *Devel. Biol.*, 32, 208

Dudkeiwicz, A. B. and Williams, W. L. (1977). Fine structural observations of the mammalian zona pellucida by scanning electron microscopy. *SEM/IITRI*, 10, 317

Favard, P. and André, J., (1970). The mitrochondria of spermatozoa. In Baccetti, B. (ed.) *Comparative Spermatology*, pp. 415–29. (New York: Academic Press)

Fawcett, D. W. and Phillips, D. M. (1969). The fine structure and development of the neck region of the mammalian spermatozoon. *Anat. Rec.*, 165, 153

Flechon, J. E. and Hafez, E. S. E. (1976). Scanning electron microscopy of human spermatozoa. In Hafez, E. S. E. (ed.) *Human Semen and Fertility Regulation in Men*, pp. 76–82. (St Louis: Mosby

Freund, M. (1966). Standards for the rating of human morphology. *Int. J. Fertil.*, 11, 97

Fujita, T. (1975). Abnormal spermatozoa and infertility (man). In Hafez, E. S. E. (ed.) *Scanning Electron Microscopical Atlas of Mammalian Reproduction*, pp. (New York: Springer Verlag)

Fujita, T., Miyoshi, M. and Tokunaga, J. (1970). Scanning and transmission electron microscopy of human ejaculate spermatozoa with special reference to their abnormal forms. *Z. Zellforsch.*, 105, 483

Fujita, T., Tokunaga, J. and Inove, H. (1971). *Atlas of Scanning Electron Microscopy in Medicine*, pp. 90–93. (Amsterdam: Elsevier)

Gould, K. S., Zaneveld, L. J. D. and Williams, W. L. (1971). Scanning electron Microscopy of Mammalian Gametes. *Arch. Gynakel.*,

Gwatkin, R. B. L., Carter, H. W. and Patterson, H. (1976). Association of mammalian sperm with the cumulus cells

and the zona pellucida studied by scanning electron microscopy. *SEM/IITRI*, 9, 379

Hafez, E. S. E. (ed.) (1975). *Scanning Electron Microscopical Atlas of Mamalian Reproduction*. (New York: Springer Verlag)

Hafez, E. S. E. and Kanagawa, H. (1973). Scanning electron microscopy of human monkey and rabbit spermatozoa. *Fertil. Steril.*, 23, 393

Holstein, A. F., Schirren, C. and Schirren Sen., C. G. (1973). Human spermatids and spermatozoa lacking acrosomes. *J. Reprod. Fertil.*, 35, 489

Kincaid, H. L., Gibbons, B. H. and Gibbons, I. R. (1973). The salt extractable fraction of dynein from sea urchin sp erm flagella: an alalysis by gel electrophoresis and by adenosine tripholphatase activity. *J. Supramol. Struct.*, 1, 461

Kullander, S. and Rausing, A. (1975). On round-headed human spermatozoa, *Int. J. Fertil.*, 20, 33

Lacy, D., Petitt, A. J., Pettitt, J. M. and Martin, B. S. (1974). Applications of scanning electron microscopy to semen analysis of the subfertile man utilising data obtained by transmission electron microscopy as an aid to interpretation. *Micron*, 5, 135

Lin, T. P., Glass, R. H., Bronson, R., Florence, J. and Maglio, M. (1975). Interspecies sperm–egg interaction. In Hafez, E. S. E. (ed.) *Scanning Electron Microscopic Atlas of Mammalian Reproduction*, pp. 300–5. (Tokyo: Igaku Shoin)

MacLeod, J. (1970). The significance of deviations in human sperm morphology. In Rosenberg, E. and Paulsen, C. A. (eds). *The Human Testis*, pp. 481–94. (New York: Plenum)

Pedersen, H. (1972a). Further observations on the fine structure of the human spermatozoon. *Z. Zellforsch, Mikrosk. Anat.*, 123, 305

Pedersen, H. (1972b). The postacrosomal region of the spermatozoa of man and *Macaca arctoides. J. Ultrastruct. Res.*, 40, 366

Pedersen, H. (1981). Ultrastructure of immobile human spermatozoa. Abstract #36: 'Human Reproduction in three Dimensions'. SEM Symposium, Nijmegen, The Netherlands

Pedersen, H. and Fawcett, D. W. (1976). Functional anatomy of human spermatozoon. In Hafez, E. S. E. (ed.) *Human Semen and Fertility Regulation in Men*, pp. 65–75. (St Louis: Mosby)

Pedersen, H. and Rebbe, H. (1974). Fine structure of round-headed human spermatozoa. *J. Reprod. Fertil.*, 37, 51

Pedersen, H. and Rebbe, H. (1975). Absence of arms in the axoneme of immotile human spermatozoa. *Biol. Reprod.*, 12, 541

Renieri, T. (1974). Submicroscopical observations on abnormal human spermatozoa. *J. Submicr. Cytol.*, 6, 42]

Ross, A., Christie, S. and Kerr, M. G. (1971). An electron microscope study of a tail abnormality in spermatozoa from a subfertile man. *J. Reprod. Fertil.*, 24, 99

Ross, A., Christie, S. and Edmond, P. (1973). Ultrastructural tail defects in thespermatozoa from two men attending a subfertility clinic. *J. Reprod. Fertil.*, 32, 243

Schirren, Sr. C. G., Holstein, A. F. and Schirren, C. (1979). Uber die Morphogenese rundkopfiger Spermatozoen des Menschen. *Andrologie*, 3, 117

Sugawara, S., Takeuchi, S. and Hafez, E. S. E. (1975). Sperm penetration. In Hafez, E. S. E. (ed.) *Scanning Electron Microscopic Atlas of Mammalian Reproduction*, pp. 280–7. (Tokyo: Egaku Shoin)

Vegni Talluri, M., Bigliardi, E. and Soldani, P. (1978). Unuaual incidence of binucleate spermatids in human crypotorchidism. *J. Submicrosc Cytol.*, 10, 357

Zamboni, L., Zemjanis, R. and Stefanini, M. (1971). The fine structure of monkey and human spermatozoa. *Anat. Rec.*, 169, 129

22

Spermophagy

J. K. KOEHLER, R. E. BERGER, D. SMITH and L. E. KARP

Departments of Biological Structure, Urology, and Obstetrics/Gynecology, University of Washington School of Medicine, Seattle, Washington, USA

PHAGOCYTOSIS IN THE FEMALE TRACT

The uptake of mammalian spermatozoa by phagocytes under a variety of *in vivo* and *in vitro* conditions has been recognized for many years. Infiltration of leukocytes into the uterine lumen and their activation to ingest sperm following mating appears to be a major mechanism for the removal of these cells from the female tract (Austin, 1957; Yanagimachi and Chang, 1963). Bedford (1965) has shown by electron microscopy that rabbit sperm were indeed taken into phagocytic vacuoles and digested by macrophages, and that the phagocytosed sperm need not have been initially damaged or necrotic. *In vitro* experiments were also carried out by Bedford (1965) suggesting that under these conditions leukocytes preferentially took up damaged sperm.

VASECTOMY

Extensive phagocytosis of spermatozoa was also seen in the epididymis and other excurrent ducts following vasectomy. In the monkey such spermophagy has been noted many years following vasectomy (Alexander, 1975). The phagocytosis is the result of white cell migration into the lumen of the ducts and not due to the activity of epithelial cells. Alexander (1975) has further shown that vasectomy is followed by a sharp increase in circulating antisperm antibodies in a number of experimental animals as well as man; an event which may be closely related to the increase in phagocytic activity of leukocytes.

MALE INFERTILITY

In the male tract, a high seminal white cell count has been associated with poor semen quality (Svendson, 1948; Ulstein *et al.*, 1976; Harrison and Johnson, 1979). Infections of accessory glands such as the prostate many contribute to such high bacterial and white cell counts and there is a considerable literature on the treatment of such cases with antibiotics and

resultant increases in sperm quality (see, for example, Berger *et al.*, 1979). There are, however, great variations in the quality and quantity of seminal bacterial flora of fertile and infertile individuals that make it very difficult to correlate any particular strains or levels of infection with infertility. As a case in point, *Ureaplasma urealyticum* has recently been implicated as an important cause of infertility and yet Bowie *et al.* (1977) had found that 69% of normal males are positive for this organism.

There are high white cell counts and extensive phagocytosis of sperm in the semen of a number of men with idiopathic infertility. These men do not have abnormal bacterial or mycoplasma levels and yet produce ejaculates showing massive infiltration by neutrophils and macrophages containing sperm in various stages of digestion (Figures 1a–3a). Very often several sperm seem to be associated with a single phagocyte (Figures 1b and 3a). Usually the sperm heads appear to be engulfed first, leaving the flagellum extending from the ruffled cytoplasm (Figures 2a,b). This may be due to specific interactions between antigenic components of the sperm head and the phagocytes, or simply a result of the mechanical difficulty of engulfing moving flagellae as compared to the more manageable sperm head. Thin sections illustrate that the internalized sperm are in various stages of digestion within phagocytic vacuoles (Figures 3a,b). The nucleochromatin due to its sheer mass seems to be less easily digested than membranous components and the dense fibers of the flagellum also appear to remain after many of the other cytoplasmic components have disappeared.

When sperm from normal, fertile donors are mixed with isolated white cells from the blood of the same individual, sperm can also be seen to be engulfed within several hours of incubation. Images of macrophages containing sperm prepared for electron microscopy of such samples are indistinguishable from those obtained from the abnormal ejaculates discussed above (Figure 3b).
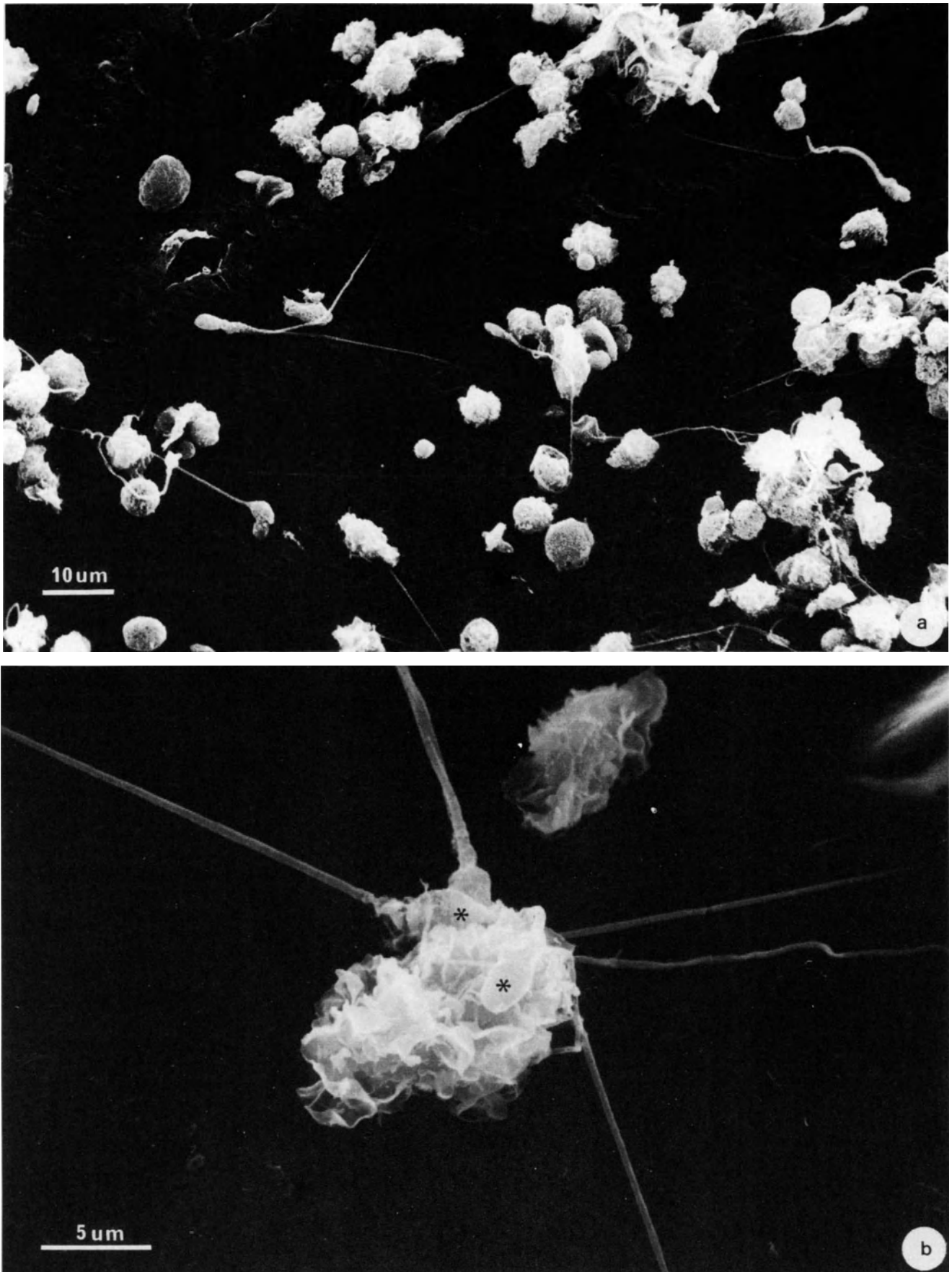
Figure 1

a: Survey scanning micrograph of an ejaculate from a patient with idiopathic infertility showing massive infiltration of leukocytes. Very few 'free' sperm are present, most being associated with the ruffled white cells. The smooth contoured, rounded cells may be immature forms of early spermatids (×13 000)

b: Several sperm are seen associated with a ruffled phagocytic cell. Sperm heads are seen adsorbed onto the cell surface (asterisks) and in this case, it is not clear if some of the sperm have actually been incorporated into the phagocyte (×4100)
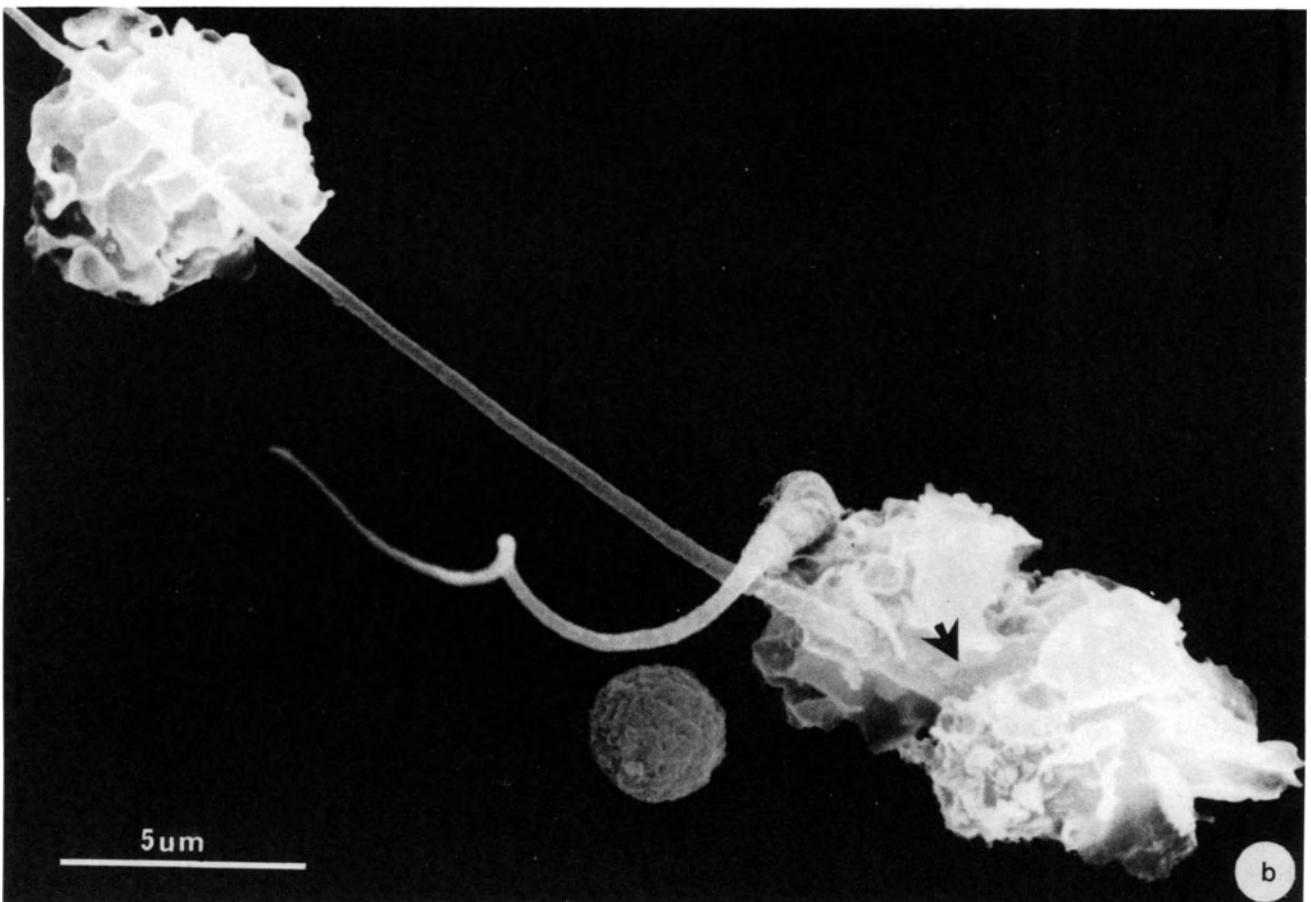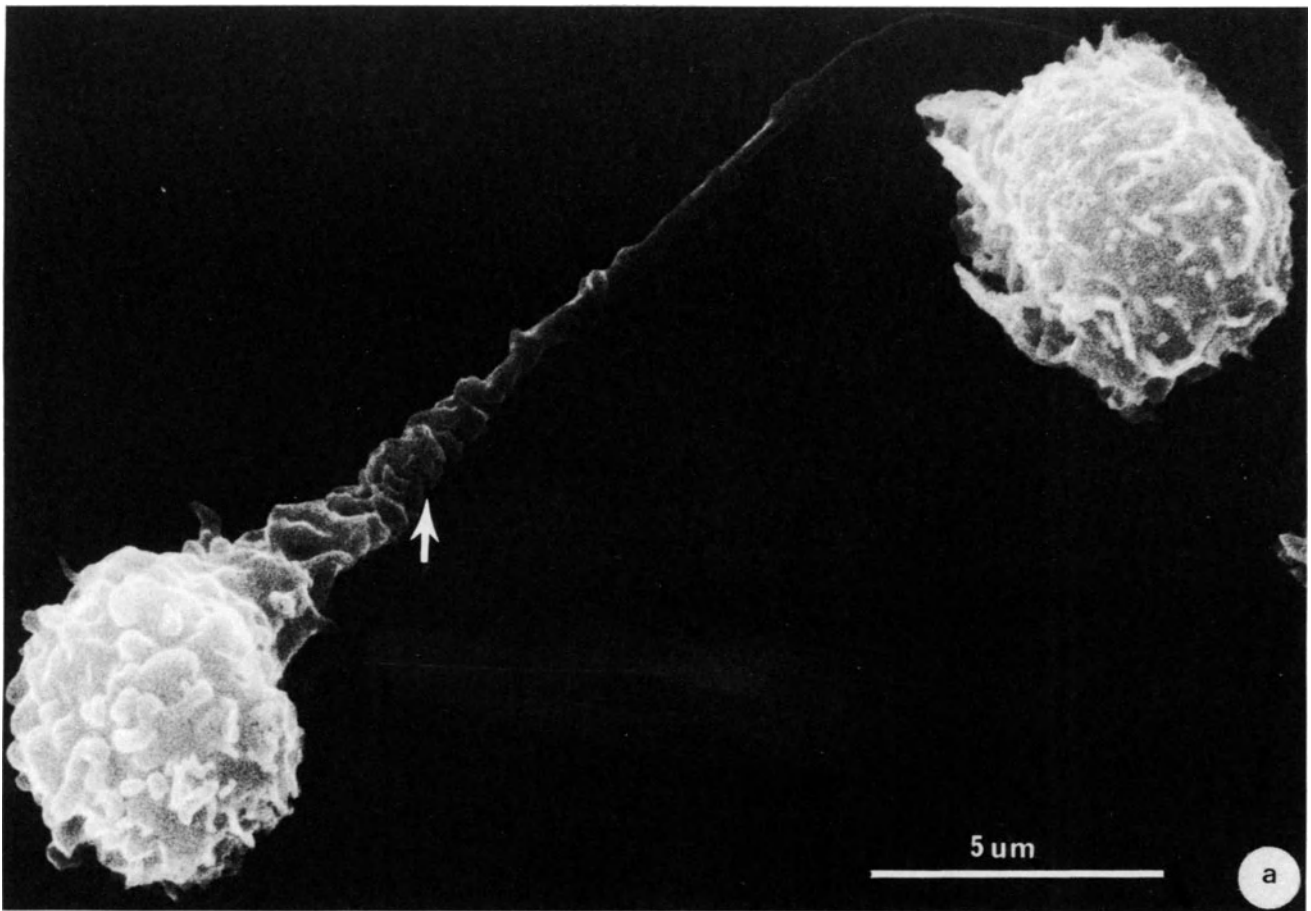
Figure 2

a: The rounded cell at bottom left has phagocytosed a human sperm head. The pseudopodial ruffles are working their way up the flagellum (arrow) (×7700)

b: Several phagocytes and sperm are seen. In one case the sperm head clearly is being incorporated into the cytoplasm (arrow) (×6300)
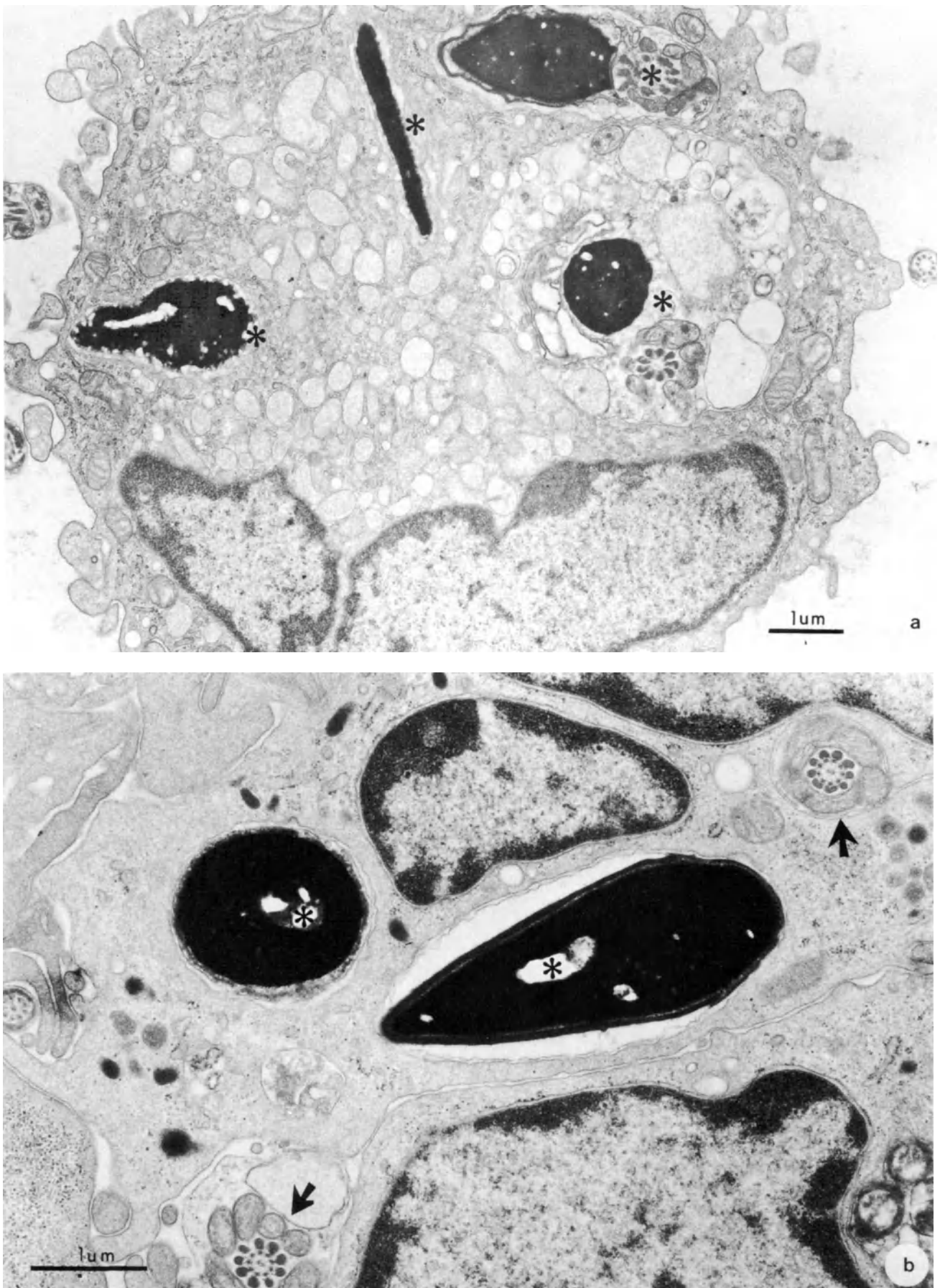
Figure 3

a: Thin section of macrophage from ejaculate displaying portions of four spermatozoa in various stages of digestion (asterisks). Note that the nucleochromatin is still relatively intact, although extensive membrane disruption has occurred (×14 000)

b: Just 2 hours after incubation of normal ejaculated sperm with a white blood cell fraction from the same fertile donor. Extensive phagocytosis has occurred. Portions of sperm heads (asterisks) and tails (arrows) can be seen in various stages of incorporation and digestion (×21 500)

Observations on the chemotaxis of neutrophils toward spermatozoa by Maroni *et al.* (1972) suggested that the complement system is necessary for the interaction of these cell types. Clark and Klebanoff (1976) have further shown by using a chemotaxis assay that the C5a cleavage fragment of complement is produced during these interactions and is the most likely active factor in stimulating chemotaxis of leukocytes toward sperm, culminating in their phagocytosis.

A great deal of further work is required in determining the relationships between male infertility and phagocytic activity, especially when infective agents do not seem to be playing a major role. The relative isolation of the male germ cells from the immune system by virtue of the blood–testis barrier makes autoimmune interactions a possible candidate for such non-pathogen mediated phagocytosis.

References

Alexander, N. J. (1975). Immunologic and morphologic effects of vasectomy in the rhesus monkey. *Fed. Proc.*, **34**, 1692

Austin, C. R. (1957). Fate of spermatozoa in the uterus of the mouse and rat. *J. Endocrinol.*, **14**, 335

Bedford, J. M. (1965). Effect of environment on phagocytosis of rabbit spermatozoa. *J. Reprod. Fertil.*, **9**, 249

Berger, R. D., Alexander, E. R., Harmisch, J. P., Paulsen, C. A., Monda, G. D., Ansell, J. and Holmes, K. K. (1979). Etiology, manifestations and therapy of acute epididymitis: prospective study of 50 cases. *J. Urol.*, **121**, 750

Bowie, W. R., Pollock, H. M., Forsyth, P. S., Floyd, J. F., Alexander, E. R., Wang, S. P. and Holmes, K. K. (1977). Bacteriology of the urethra in normal men and men with nongonococcal urethritis. *J. Clin. Microbiol.*, **6**, 482

Clark, R. A. and Klebanoff, S. J. (1976). Generation of a neutrophil chemotactic agent by spermatozoa: role of complement and regulation by seminal plasma factors. *J. Immunol.*, **117**, 1378

Harrison, K. L. and Johnson, D. K. (1979). Chronic asymptomatic genital tract infection and semen quality. *Pathology*, **11**, 289

Maroni, E. S., Symon, D. N. K. and Wilkinson, P. C. (1972). Chemotaxis of neutrophil leucocytes towards spermatozoa and seminal fluid. *J. Reprod. Fertil.*, **28**, 359

Svendson, M. (1948). Leukocytes and bacteria in human semen. *J. Pathol. Bacteriol.*, **60**, 131

Ulstein, M., Capall, P., Holmes, K. K. and Paulsen, C. A. (1976). Nonsymptomatic genital tract infection and male infertility. In Hafez, E. S. E. (ed.). *Human Semen and Fertility Regulation in Men*, pp. 355–62. (St. Louis: C. V. Mosby)

Yanagimachi, R. and Chang, M. C. (1963). Infiltration of leucocytes into the uterine lumen of the golden hamster during the oestrous cycle and following mating. *J. Reprod. Fertil.*, **5**, 389

23

Sperm cell–cervical mucus interaction

F. C. CHRÉTIEN

Travaux Pratiques de Biologie Animale du PCEM, Paris, France

PHYSICOCHEMICAL NATURE OF CERVICAL MUCUS

The receptivity or hostility of the cervix to spermatozoa is fully dependent upon the overall physical condition of the cervical mucus. In various stages of the reproductive life during which spermatozoa are not able to penetrate, the cervical mucus shows a similarity in macroscopic appearance, as well as in ultrastructure.

The cervical mucus is an extremely complex and heterogeneous secretion. As a whole, it consists of a hydrogel with a low-viscosity 'liquid' phase, and a high-viscosity 'solid' phase.

Its liquid phase usually contains about 92–94% of water, peaking up to 98% during ovulation – at which time the mucus is most abundant. The liquid phase contains many insoluble and soluble components which are subjected to fluctuations throughout the cycle. The solid phase of the mucus hydrogel contains a characteristic glycoprotein, the most plausible structure of which is a long polypeptide backbone with a large number of branched sugar chains attached via glycosidic linkages.

Changes in viscosity and 'Spinnbarkeit' occurring in the cervical mucus coincide with variations in its penetrability by sperm cells. The phenomenon could be based on a mechanism located in the solid phase at the macromolecular level. On the basis of a combined nuclear magnetic resonance and rheologic approach, a theoretical model was proposed by Odeblad (1968) for the ultrastructure of the solid phase of cervical mucus and is known as the 'tricot-like macromolecular gel arrangement'. According to this model, glycoprotein chains would form a dense, compact network in the luteal phase acting as a mechanical obstacle impervious to spermatozoa. During the time of ovulation, the micelles – in a parallel order with each other – form a significantly larger network. In addition, Odeblad substantiated the observation of Tampion and Gibbons (1962) which stated that sperm cell migration occurs within the aqueous channels dividing the micelles.

THE ULTRASTRUCTURE OF CERVICAL MUCUS

In 1973 scanning electron microscopy (SEM) provided the first three-deimensional pictures of the human mid-cycle mucus. From these micrographs the solid phase could be described as a net-like structure formed of anastomosed filaments of varying thickness (Chrétien et al., 1973). Two types of spatial arrangement can be observed in midcycle cervical mucus depending on whether or not they have been submitted to a stretching action prior to fixation. Cervical mucus molded mechanically to the shape of a thread shows a preferential alignment of most of the filaments in a direction parallel to that of elongation. It closely resembles the 'tricot-like' model proposed by Odeblad (Figure 1a). However, cervical mucus fixed without preliminary stretching does not appear aligned in a particular manner. Instead, it exhibits entangled filaments arranged at random, without any preferential orientation, and is similar in appearance to a skein of yarn (Figure 1b). During the time of ovulation the mesh dimension may exceed 10 μm. Several authors using SEM techniques corroborate these findings (Chrétien, 1977; Gould et al., 1976; Zaneveld et al., 1975), with the exception of Daunter et al. (1976).

Outside of the ovulatory period, during pregnancy and after menopause, the cervical mucus exhibits an important decrease of its 'Spinnbarkeit'. It is sticky and gelatinous and obstructs the cervical canal. At the end of menstruation the mucous infrastructure forms a very compact meshwork with extremely small meshes (0.5 μm). After that time, the solid woof slackens progressively until the day of ovulation, at which time the widening of the meshes reaches a maximum. During the second part of the cycle the dimension of the meshes decreases until the 28th day, but does not exceed 0.5 μm. The woof density becomes increasingly intense as the luteal phase continues (Figure 1c).

During pregnancy, and after menopause, a striking thickening of the cervical mucus ultrastructure occurs very rapidly, thus forming a much more compact meshwork. The mean mesh dimension is smaller than
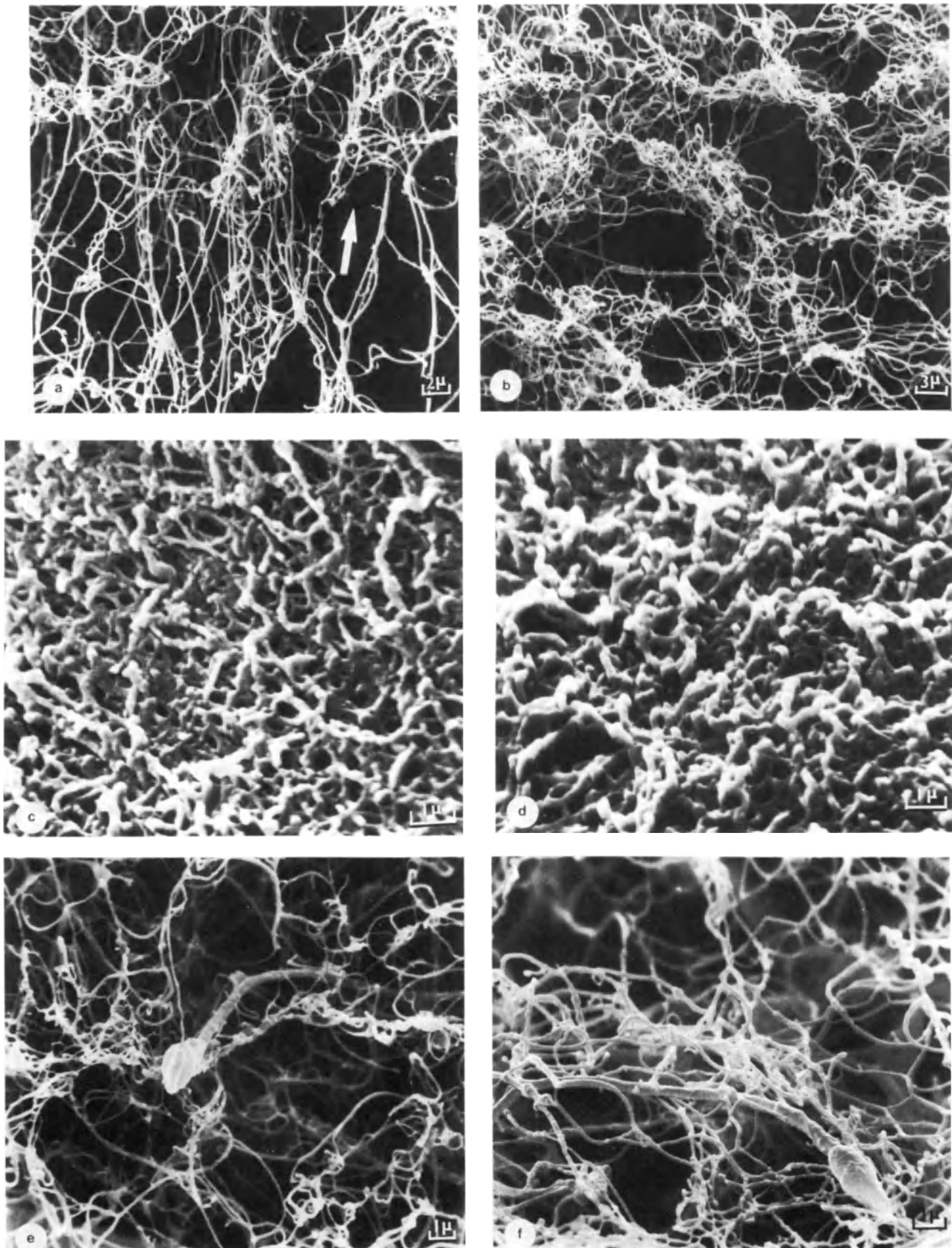
Figure 1 Ultrastructure of pervious and impervious cervical mucus as shown by SEM

a: Pervious cervical mucus during the time of ovulation (14th day), submitted to a slight stretching action prior to fixation. Note the preferential alignment of the filaments that run parallel to the lines of force (arrow) (×2380)

b: Relaxed pervious cervical mucus during the time of ovulation. Note the random arrangement of the mesh-work, without any preferential orientation (×1820)

c: Impervious mucus during the late luteal phase (28th day).

Note the distorted appearance of the filaments by median or lateral swellings (×8400)

d: Impervious mucus during the last week of pregnancy (×7210)

e: Pervious cervical mucus on 14th day of the cycle. Sperm cell is seen moving in the central part of loose relaxed mucus; incubation: 60 seconds (×4410)

f: The influence of micellular orientation on sperm migration (14th day). Sperm cell following the lines of strain in slightly stretched mucus; incubation: 60 seconds (×5390)
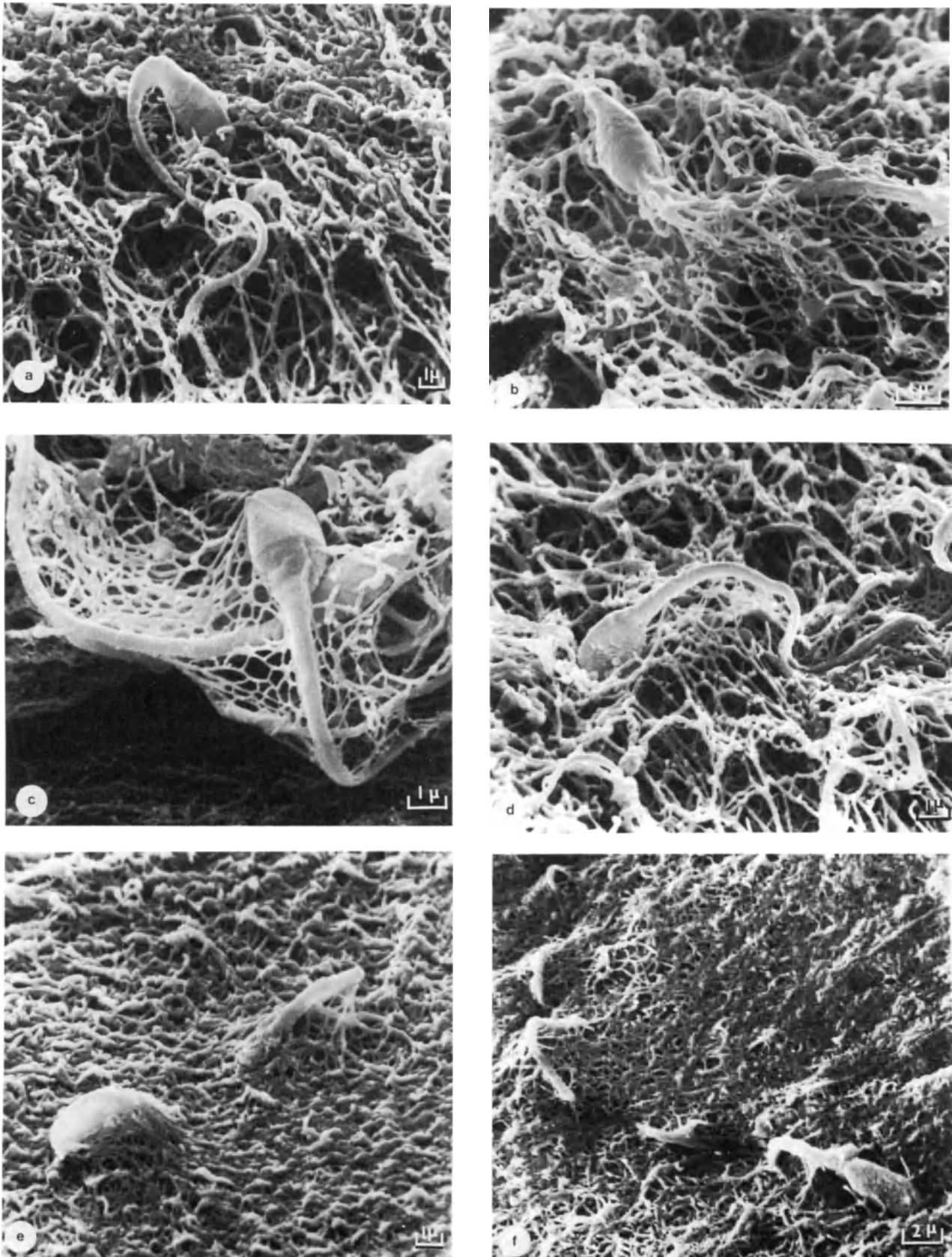
Figure 2 Sperm cells in impervious cervical mucus

a: Menstrual cycle (4th day). Despite its sudden leaps, this sperm cell will not succeed in wrenching itself free from the mucus meshwork; incubation: 3 minutes (×4410)

b: Menstrual cycle (10th day). Sperm cell enmeshed within the meshwork; incubation: 3 minutes (×7140)

c: Menstrual cycle (24th day). These sperm cells are similar in appearance to eels trying to escape from the net; incubation 1:30 minutes (×7000)

d: Menstrual cycle (28th day). Sperm cell is embedded superficially in the mucus framework; incubation: 3 minutes (×4340)

e: Last week of pregnancy. The sperm cell looks like a sea serpent. Incubation: 4:30 minutes (×4410)

f: Cervical mucus under the influence of low-dose pure progestogen (0.35 mg of norgestrienone); 13th day of the first cycle. By plunging and emerging several times from the mesh, this sperm cell takes on the appearance of some Loch Ness Monster (×3290)

0.5 μm at the end of pregnancy and during post-meno-pause (Chrétien, 1978).

SPERM–MUCUS INTERACTION

On the basis of SEM findings, variations in the pattern and mesh dimension of the framework are apparently responsible for the valve effect of cervical mucus towards sperm cells. The mucous viscosity and its ability to be penetrated by spermatozoa may be directly related to the degree of cross-linkage amongst the long-chain glycoprotein filaments. This hypothesis is confirmed by investigations which correlate SEM observations with spermatozoal penetration tests (Chrétien and David, 1978). Whether or not spermatozoa can enter this framework depends on the size ratio between the sperm head and glycoprotein meshes. The width must become large enough to enable the male gametes to pass through. The mesh diameter is at least equal to and, more often than not, notably larger than that of the sperm head during a period of 6–7 days around ovulation (Figures 1e,f).

In the various stages of the reproductive life, the cervical mucus acts as an effective barrier against spermatozoal invasion of the uterine cavity. The inadequate mesh dimension is notably smaller than that of the sperm head which opposes a succession of physical obstacles to these sperm cells, thus rendering sperm penetration practically impossible (Figures 2a–e).

SEM of cervical mucus under the influence of oral contraceptives shows reduced dimension of the meshed woof which must be held responsible for the obstructive effect. The more marked effect has also been observed with the recent use of low-dose pure progestogens (Figure 2f).

CONCLUDING REMARKS

SEM enables an appropriate estimation of the behavior of spermatozoa entering the mucus in either the vagina or the cervix. In agreements with previous results (Tampion and Gibbons, 1962), SEM obser-vations demonstrate that the preferential alignment of most glycoprotein filaments constitutes a real advantage for spermatozoa crossing the mucous framework. Indeed, SEM offers evidence which suggests that relaxed mucus hinders the penetration of spermatozoa by opposing an entangled skein of filaments. However, spermatozoa can enter stretched ovulatory mucus quite readily by migrating along the lines of strain in a direction parallel to that of elongation of the molecules.

During the time of ovulation the midcycle widening of the mucus meshwork enables the sperma-tozoa to enter. Outside this period the cervical mucus acts as an effective barrier against spermatozoal invasion of the uterine cavity by forming a framework of extremely small meshes. Since sperm cells would have had access to the upper female genital tracts outside of the ovulatory period *without* inducing serious physiological consequences, the question of what is the finality of such a precise and complex obstructive mechanism still remains.

References

Chrétien, F. C. (1977). Technical problems involved in SEM observation of cervical mucus framework. In Insler, V. and Bettendorf, G. (eds), *The Uterine Cervix in Repro-duction*, Workshop Conference Rottach-Egern, p. 44. (Stuttgart: Georg Thième)

Chrétien, F. C. (1978). Ultrastructure and variations of human cervical mucus during pregnancy and the menopause. *Acta Obstet. Gynecol. Scand.*, 57, 337

Chrétien, F. C. and David, G. (1978). Temporary obstructive effect of human cervical towards mucus spermatozoa throughout reproductive life: a SEM study. *Eur. J. Obstet. Gynecol. Reprod. Biol.*, 8, 307

Chrétien, F. C., Gernigon, C., David, G. and Psychoyos, A. (1973). The ultrastructure of human cervical mucus under scanning electron microscopy. *Fertil. Steril.*, 24, 746

Daunter, B., Chandler, E. N. and Elstein, M. (1976). The scanning electron microscopy of human cervical mucus in the non-pregnant and pregnant states. *Br. J. Obstet. Gynaecol.*, 83, 738

Gould, K. G., Martin, D. E. and Graham, C. E. (1976). Analysis of cervical mucus with SEM/EDX. *Proc. Workshop on SEM in Reproductaive Biology*, Part VI. (Chicago: ITT Research Institute)

Odeblad, E. (1968). The functional structure of human cervical mucus. *Acta Obstet. Gynecol. Scand.*, 47, suppl. 1, 59

Tampion, D. and Gibbons, R. A. (1962). Orientation of spermatozoa in mucus of the cervix uteri. *Nature (London)*, 194, 381

Zaneveld, L. J. D., Tauber, P. F., Port, C., Propping, D. and Schumacher, G. F. B. (1975). Structural aspects of human cervical mucus. *Am. J. Obstet. Gynecol.*, 122, 650
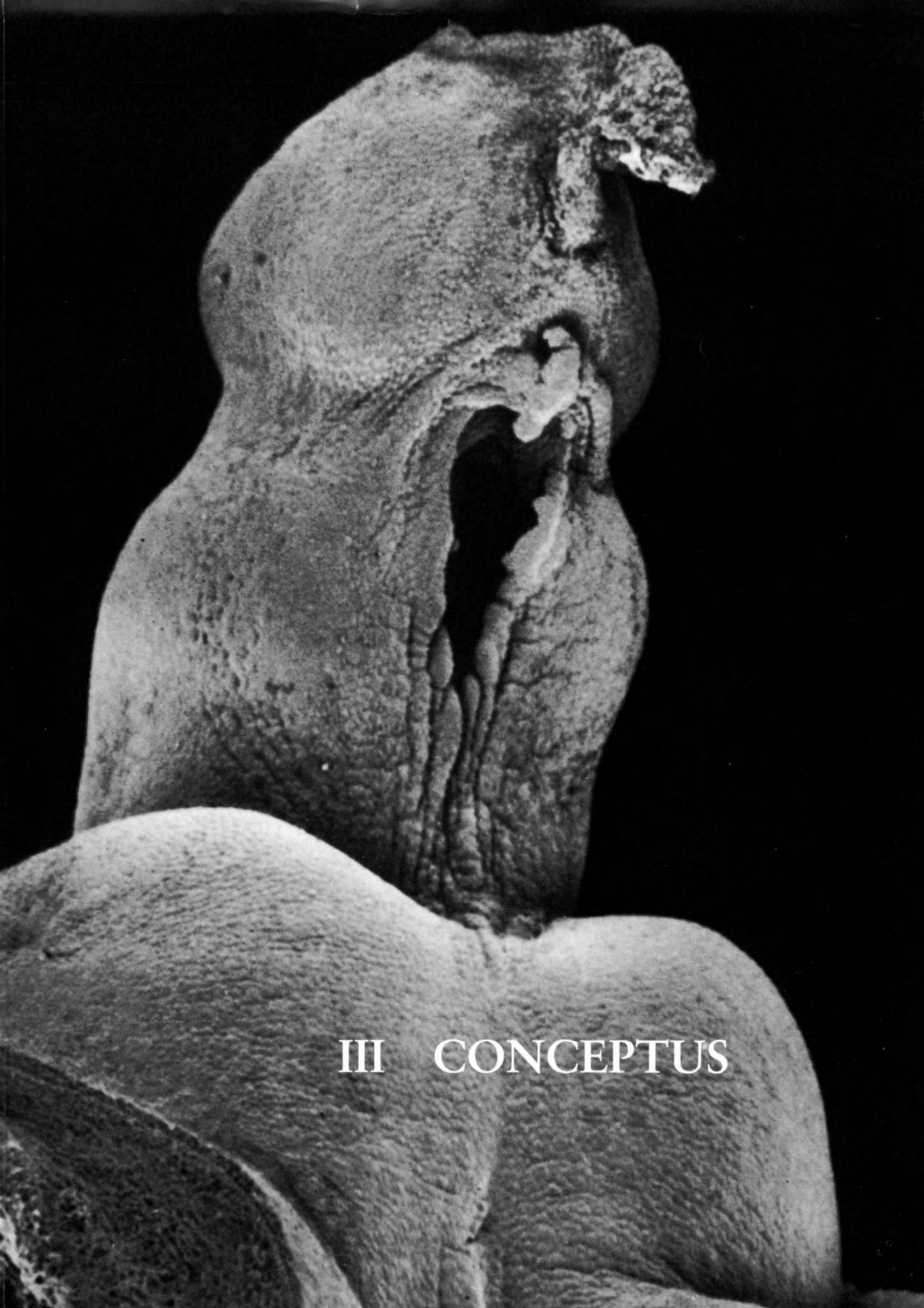
III CONCEPTUS

24

Interaction between spermatozoa and ovum *in vitro*

P. SUNDSTRÖM

Department of Obstetrics and Gynecology, Malmö Allmänna Sjukhus, S-214 01 Malmö, Sweden

The first to test the feasibility of *in vitro* fertilization of human oocytes were Rock and Menkin (1944). However, in 1969 Mastroianni and Noriega (Mastroianni and Noriega, 1970) concluded that *in vitro* fertilization had not yet been accomplished in the human if rigid criteria were applied; *viz.* the presence of two polar bodies in the perivitelline space, the presence of two pronuclei in the cytoplasm, and the presence of remnants of the fertilizing sperm flagellum within the ooplasm.

Successful fertilization requires mature oocytes – oocytes in which the first polar body has been extruded, and capacitated sperm – sperm capable of penetrating the zona pellucida. Capacitation includes a reaction leading to exposure of the inner acrosomal membrane which appears to be the site (Stambaugh and Buckley, 1969) of the acrosomal proteinase (Newsletter from the Editors, 1972). This is necessary for spermatozoa to pass through the zona pellucida. In 1969 Bavister *et al.* identified by light microscopy for the first time remnants of a spermatozoon in a fertilized ovum in the pronuclear stage. The ultrastructure of a pronuclear ovum obtained from the tuba had been described in an earlier article (Zamboni *et al.*, 1966), but provided no information on how the spermatozoon had penetrated the zona pellucida.

The ultrastructure of a human oocyte fertilized *in vitro* was described by Soupart and Strong (1974). The remnants of the fertilizing spermatozoon were found close to the pronuclear membrane. On the zona pellucida lay spermatozoa with the flat side of the head on the outer surface or touching it with the tip of the head. Penetrating spermatozoa had pursued a curved path starting almost tangentially to the outer surface of the zona.

Transmission electron microscopic (TEM) investigation of early interaction between oocytes and spermatozoa is, however, limited to the part of a spermatozoon and oocyte that happens to be in the field of a section. Scanning electron microscopy (SEM) should provide better possibilities for these studies because it allows a general view of many of the attached and penetrating spermatozoa. In only one study have micrographs of the interaction between human oocytes and spermatozoa by means of SEM hitherto been published (Nilsson, 1975). This chapter will describe in greater detail the morphology of human oocytes and their early interaction with spermatozoa *in vitro*. Further, since human semen normally contains many morphologically abnormal spermatozoa (Dadoune and Fain-Maurel, 1977; Flechou and Hafez, 1975; Fujita, 1975), it was studied whether abnormal spermatozoa adhere to the zona pellucida.

MATERIAL

Forty-five human oocytes in different stages of maturation were aspirated from follicles in women operated upon because of infertility (mainly due to tubal failure) or for voluntary sterilization. Oocytes were classified as preovulatory or non-ovulatory by their appearance in the light microscope. Preovulatory oocytes are surrounded by a large, sticky and loose cumulus mass (Edwards and Steptoe, 1974; Lopata *et al.*, 1978); non-ovulatory oocytes are surrounded by a small cumulus mass or by corona cells only. In this stage polar bodies are obscured by corona cells and can therefore not always be identified. About half of the oocytes studied were classified as preovulatory and half as non-ovulatory. Fresh sperm samples for *in vitro* fertilization were obtained from healthy fertile donors. The oocytes were incubated in sperm suspensions for 24 hours and then in culture medium for various periods (Sundström *et al.*, 1981). The oocytes were fixed in 2.5% glutaraldehyde in culture medium without serum, dehydrated in acetone, and prepared for SEM with critical-point drying and gold coating.
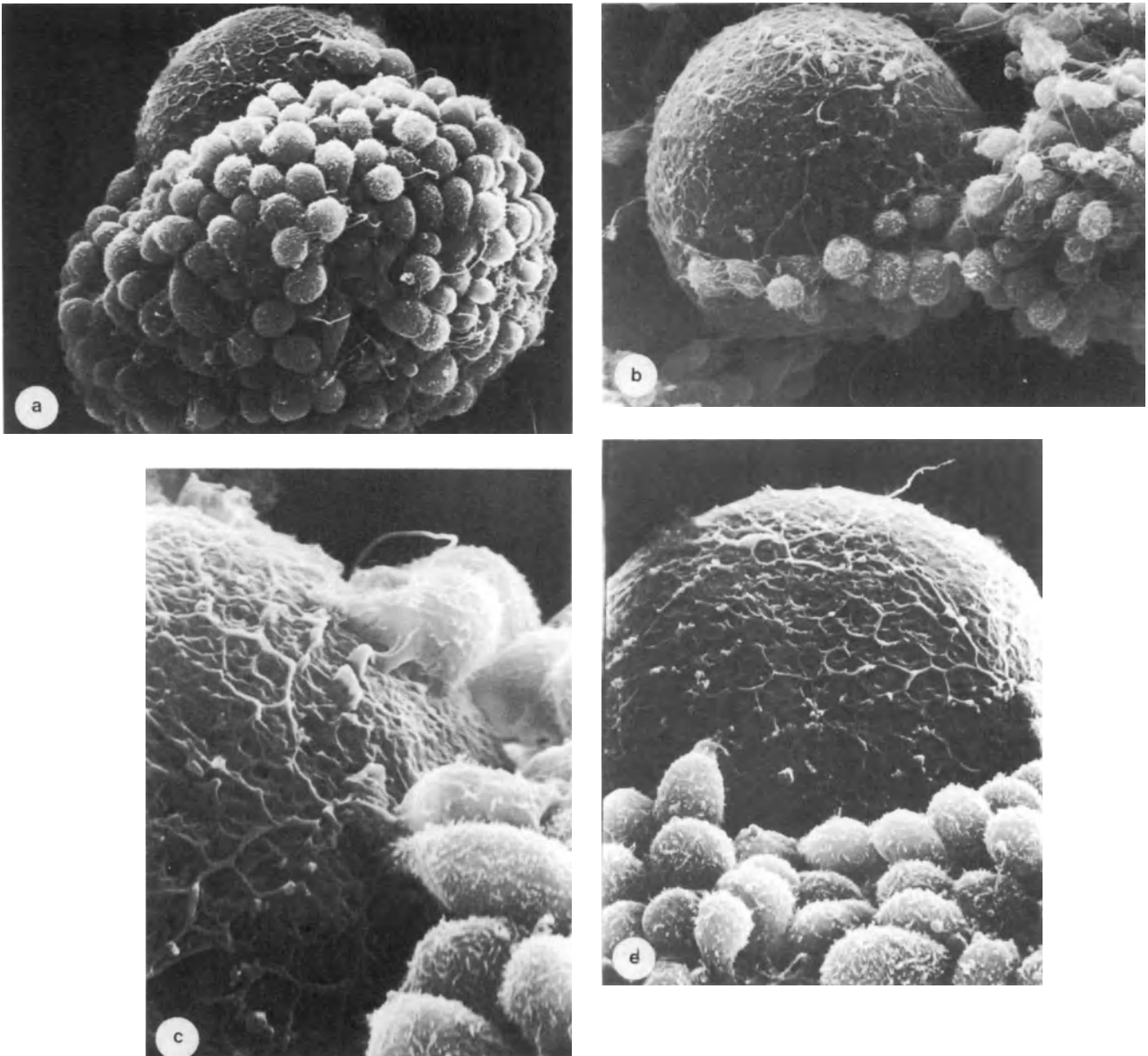
225

Figure 1 Scanning electron micrographs of human oocytes and spermatozoa

a: Human preovulatory oocyte partially surrounded by corona cells. Tails of spermatozoa can be seen in between the corona cells (×520)

b: Preovulatory oocyte surrounded by corona cells which are retracted from the zona and only attached to the oocyte by mucous threads (×640)

c: Same oocyte as in a. The surface of the oocyte – the zona pellucida – has a net-like structure. Cytoplasmic projections from the corona cells extend into the zona (×2000)

d: Same oocyte as in a. One spermatozoon has penetrated the corona cell layer and its tail can be seen projecting from the zona (×1000)
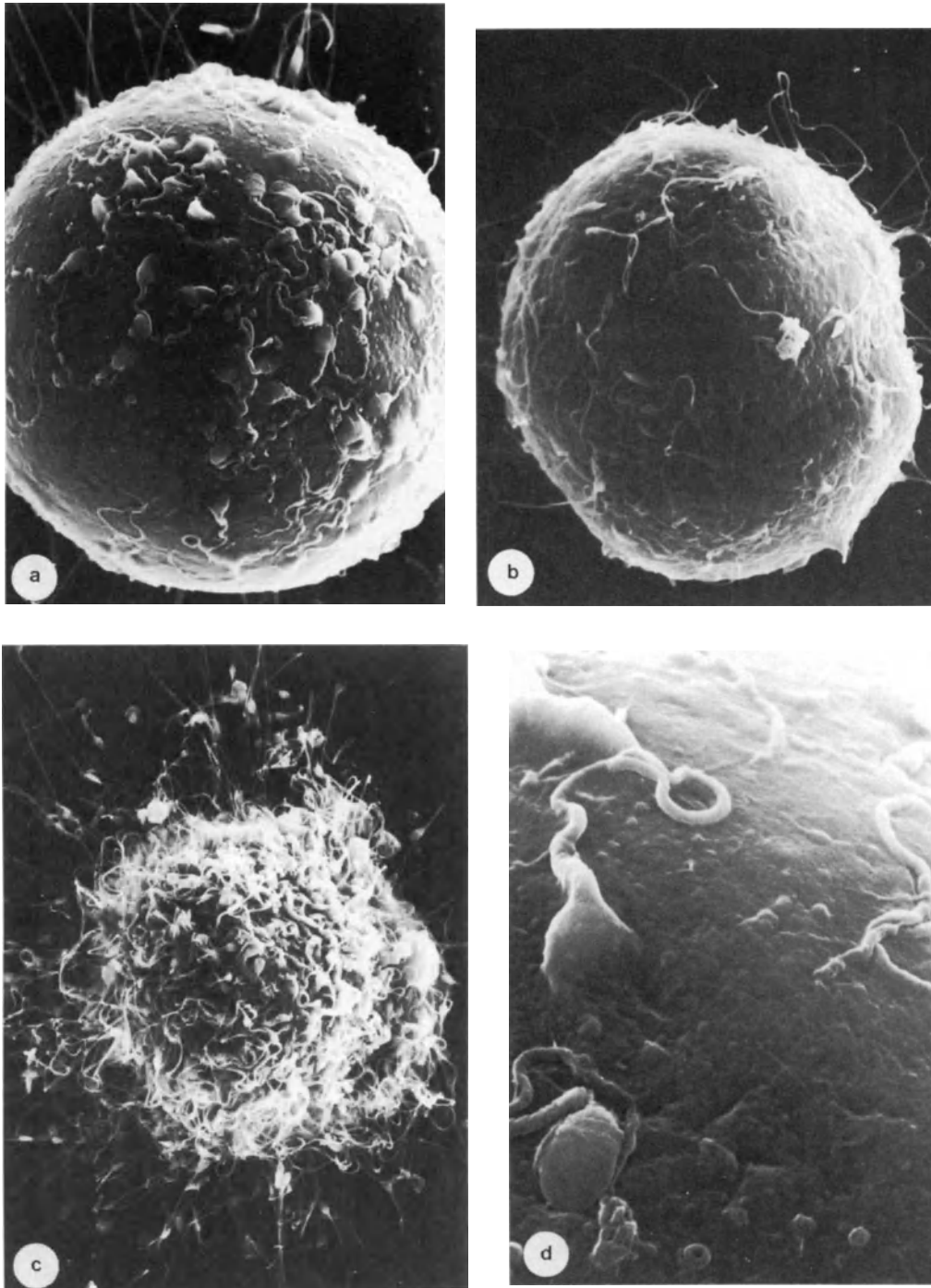
Figure 2

a-c: Scanning electron micrographs of human oocytes and spermatozoa

a: The surface of the zona pellucida was sometimes smooth, which made it easy to study the structure of attached and penetrating spermatozoa (×800)

b: The number of attached spermatozoa varied, usually 30–40 spermatozoa were found as on the illustrated embryo in an early stage of cleavage. Observe the slight depression of the zona between two of the blastomeres (to the right ×720)

c: Occasionally more than 100 spermatozoa were seen on non-ovulatory oocytes (×520)

d: Details of the interaction between human oocytes and spermatozoa. The spermatozoa are penetrating the zona almost tangentially and mostly with their flat side facing the surface. The head merges with the zona (×4000)
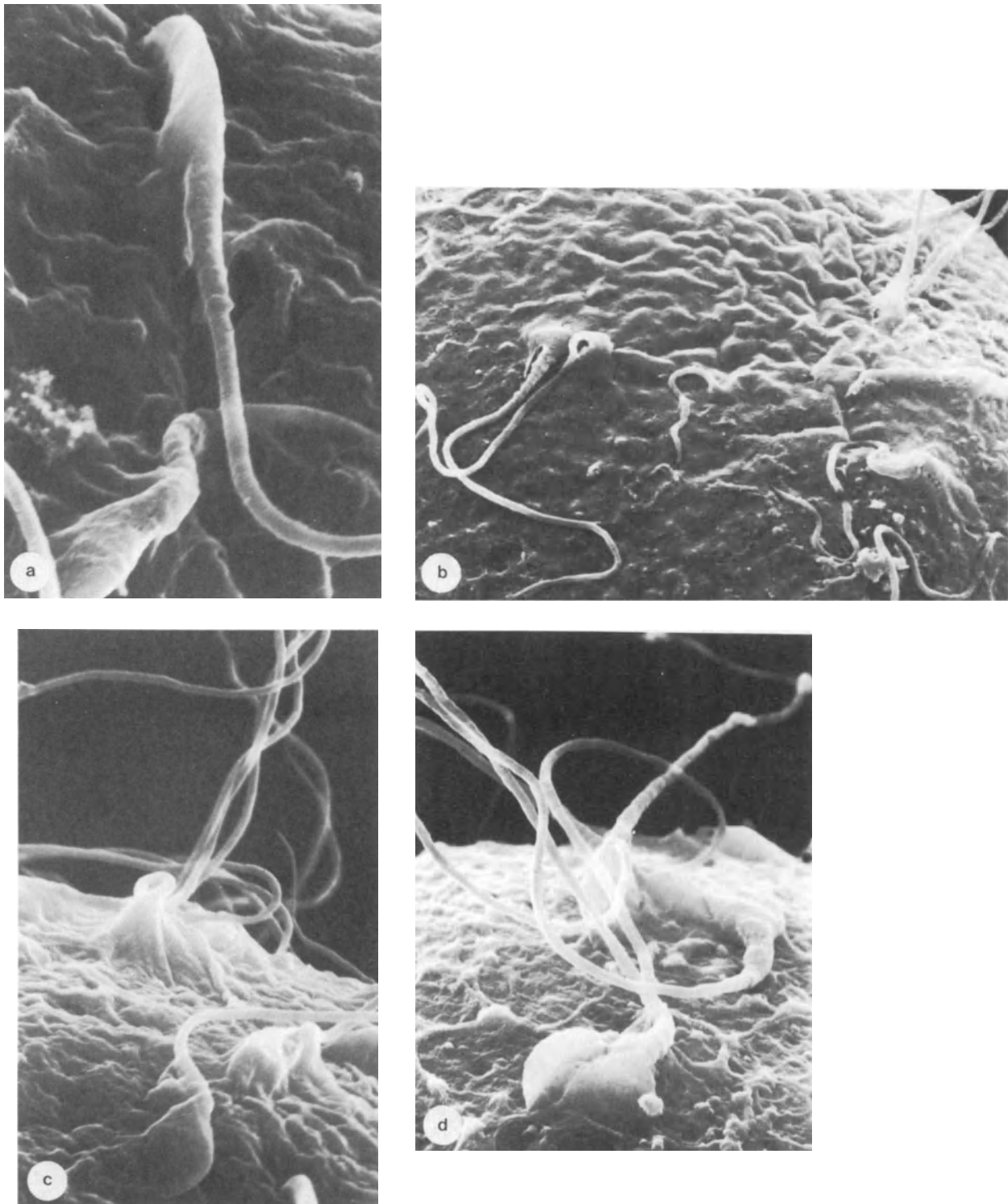
Figure 3 Details of the interaction between human oocytes and spermatozoa

a: Spermatozoa penetrating the zona with the side of the head are sometimes seen (×8000)

b: The tail is the last structure to enter the surface. Three spermatozoa in different stages of penetration are observed to the left (×2400)

c: Part of a fertilized and cleaved oocyte (same as in Figure 2b). The tails lie flat on the surface or project from it. One spermatozoon is penetrating and the diffuse contour of the head resembles a tent (×4000)

d: Shallow penetration of spermatozoa (×4000)
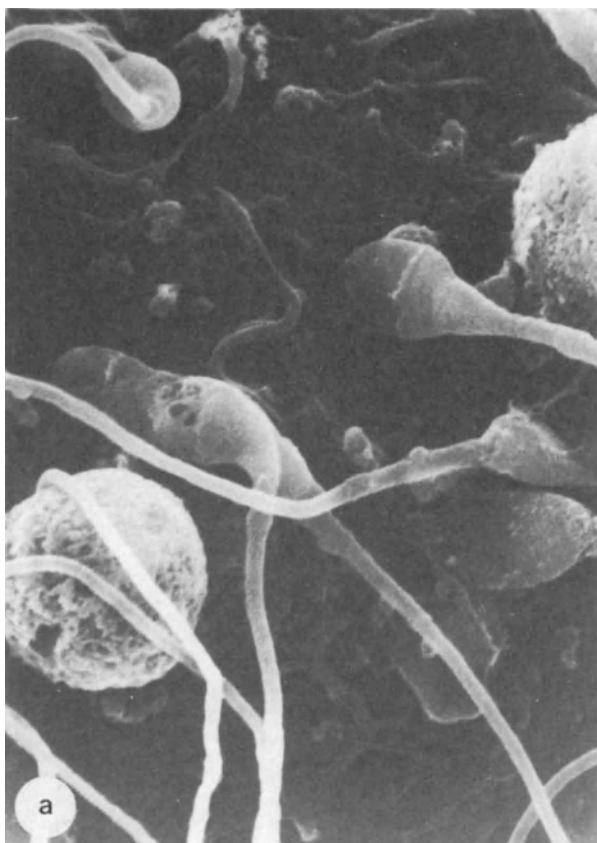
Figure 4 Details of the interaction between human oocytes and spermatozoa

a: Abnormal spermatozoa are rarely seen attached to the oocytes, but one abnormal spermatozoon can be seen in the center of the picture (×4500)
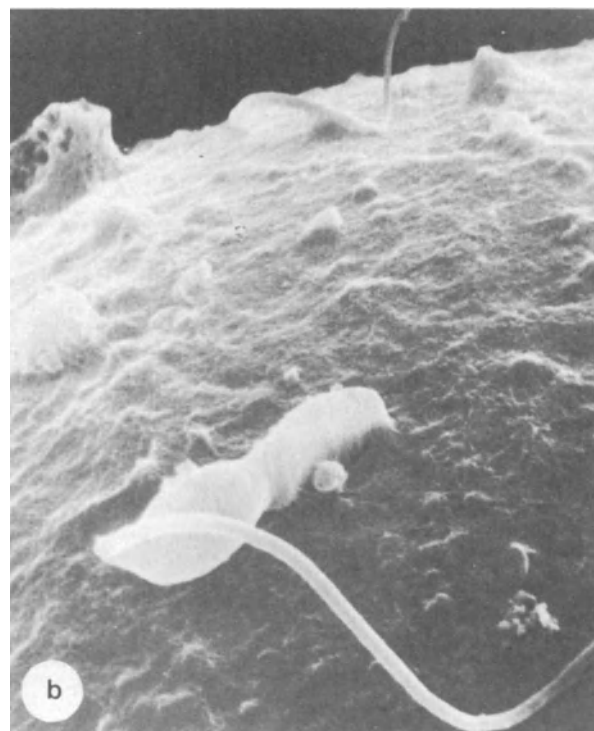
b: Abnormal shape of a shallowly penetrating spermatozoa (×5000)

OBSERVATIONS

The outer surface of the zona pellucida usually displays a porous net-like appearance, but oocytes with a smoother or completely smooth surface of the zona are also seen. A smooth surface seems to be more common among non-ovulatory oocytes, but no consistent differences in morphology due to the maturity of the oocytes can be found.

The corona cells still surrounding some oocytes after culture are round or elongated with short microvilli. In between the corona cells numerous spermatozoa are seen trapped or on their way to the oocyte. Cytoplasmic projections from the corona cells penetrate the underlying zona pellucida but most of the projections are retracted, leaving a naked zona.

The number of spermatozoa on the oocytes varies. Mostly, about 20 to 40 spermatozoa are seen on an oocyte. Occasionally, however, there were more than 100, but then only on non-ovulatory oocytes surrounded at most by a few layers of corona cells. This phenomenon might perhaps be explained by an easier access of the spermatozoa to the oocyte, the cumulus mass and corona cells probably making it difficult for an excessive number of spermatozoa to make their way to the oocyte normally. Another reason might be that a possible zonal barrier preventing attachment of too large a number of spermatozoa is lacking in some non-ovulatory oocytes.

Some oocytes – both preovulatory and non-ovulatory – show no spermatozoa at all. In one case, the spermatozoa from a donor with proven fertility failed to become attached to some oocytes on some occasions while on others they seemed to function normally and were seen penetrating the zona pellucida in the same way as spermatozoa from other donors. No explanation can be offered for this difference of the spermatozoa–oocyte interaction. The specimens were incubated in the same way as the others, and the number of spermatozoa/ml was about the same. The problem deserves further attention for such lack of attachment might be one of the causes of childlessness of some seemingly normal couples (Shivers and Dunbar, 1977; Trounson *et al.*, 1980).

Spermatozoa are seen attached or penetrating the oocytes. The anterior part of the sperm head penetrates the zona almost tangentially, mostly with its flat side facing the surface. The head then forms an indistinguishable structure with the zona. The tail – being the last structure to penetrate the zona – is either lying flat on the surface or projecting from the zona. Most of the penetrating spermatozoa are seen in an early stage of penetration, i.e. only a small portion of the head is embedded in the zona. Only occasionally was but part of the tail still demonstrable. It must be that the first penetrating spermatozoon causes some reaction of the zona pellucida – the zona reaction (Soupart and Strong, 1974) – making it more difficult

for other spermatozoa to penetrate deep into the zona.

The structure of those attached spermatozoa that are clearly visible is judged as abnormal in only a few cases. Penetrating spermatozoa can not be properly judged fully but the visible parts – i.e. part of the head and/or of the tail – invariably appear normal. It would appear that abnormal spermatozoa rarely adhere to the zona pellucida *in vitro*. This is interesting since about 40% of the germ cells in the semen droplets used were presumably morphologically abnormal. One of the functions of the cervical mucus *in vivo* is to filter off abnormal spermatozoa, allowing only mobile spermatozoa of normal shape into the upper genital tract (Elstein, 1978). Although this mechanism is lacking *in vitro*, only very few abnormal spermatozoa appear to find their way to the oocyte. They might perhaps be held back by some barrier in the surrounding corona cells and/or on the zona pellucida.

In conclusion, of about 250 000 spermatozoa in a fertilization droplet only about 30–40 adhere to the zona pellucida (of these very few are abnormal), suggesting a selective function of the zona. The zona may have spermatozoa-binding sites which are occupied already a couple of minutes after contact with the spermatozoa (Propping *et al.*, 1978). Only rarely no spermatozoa, or more than 100 spermatozoa, adhere to the zona – indicating an altered function of the surface of the zona pellucida of some oocytes.

References

Bavister, B. D., Edwards, R. G. and Steptoe, P. C. (1969). Identification of the mid-piece and tail of the spermatozoa during fertilization of human eggs in vitro. *J. Reprod. Fertil.*, **20**, 159

Dadoune, J.-P. and Fain-Maurel, M.-A. (1977). A routine technique for processing human ejaculate spermatozoa for scanning electron microscopy with special reference to their abnormal forms. *Biol. Cell.*, **29**, 215

Edwards, R. G. and Steptoe, P. C. (1974). Control of human ovulation, fertilization and implantation. *Proc. R. Soc. Med.*, **67**, 30

Elstein, M. (1978). Morphology of cervical mucus and its clinical assessment. In Ludwig, H. and Tauber, P. F. (eds),

Human Fertilization, pp. 68-79. (Stuttgart: Thième)

Flechou, J. E. and Hafez, E. S. E. (1975). Scanning electron microscopy of human spermatozoa. *Int. Conf. Androl.*, *Detroit, Mich., USA*

Fujita, T. (1975). Abnormal spermatozoa and infertility (man). In Hafez, E. S. E. (ed.), *Scanning Electron Microscopic Atlas of Mammalian Reproduction*, pp. 82-7. (Stuttgart: Thième)

Lopata, A., Brown, J. B., Leeton, J. F., McTalbot, J. and Wood, C. (1978). *In vitro* fertilization of preovulatory oocytes and embryo transfer in fertile patients treated with clomiphene and human chorionic gonadotropin. *Fertil. Steril.*, **30**, 27

Mastroianni, L. Jr. and Noriega, C. (1970). Observations on human ova and the fertilization process. *Am. J. Obstet. Gynecol.*, **107**, 682

Newsletter from the Editors (1972). Acrosomal enzyme. *Biol. Reprod.*, **6**, 176

Nilsson, L. (1975). A portrait of the sperm. In Afzelius, B. A. (ed.), *The Functional Anatomy of the Spermatozoon*, pp. 79-82. (Oxford: Pergamon Press)

Propping, D., Tauber, P. F. and Zaneveld, L. J. D. (1978). Fertilization and implantation. In Ludwig, H. and Tauber, P. F. (eds), *Human Fertilization*, pp. 152-64. (Stuttgart: Thième)

Rock, J. and Menkin, M. F. (1944). In vitro fertilization and cleavage of human ovarian eggs. *Science*, **100**, 105

Shivers, C. A. and Dunbar, B. S. (1977). Autoantibodies to zona pellucida: a possible cause for infertility in women. *Science*, **197**, 1082

Soupart, P. and Strong, P. A. (1974). Ultrastructural observations on human oocytes fertilized in vitro. *Fertil. Steril.*, **25**, 11

Stambaugh, R. and Buckley, J. (1969). Identification and subcellular localization of the enzymes effecting penetration of the zona pellucida by rabbit spermatozoa. *J. Reprod. Fertil.*, **19**, 423

Sundström, P., Nilsson, O. and Liedholm, P. (1981). Cleavage rate and morphology of early human embryos obtained after artificial fertilizaion and culture. *Acta Obstet. Gynecol. Scand.*, **60**, 109

Trounson, A. O., Shivers, C. A., McMaster, R. and Lopata, A. (1980). Inhibition of sperm binding and fertilization of human ova by antibody to porcine zona pellucida and by human sera. *Arch. Androl.*, **4**, 29

Zamboni, L., Mishell, D. R. Jr., Bell, J. H. and Baca, M. (1966). Fine structure of the human ovum in the pronuclear stage. *J. Cell Biol.*, **30**, 579

25

The normal placenta

H. P. VAN GEIJN*, M. CASTELLUCCI†, P. KAUFMANN‡ and P. KENEMANS§

* Department of Obstetrics and Gynecology, Academisch Ziekenhuis der Vrije Universiteit, Amsterdam, The Netherlands
† Department of Electronmicroscopy, Medizinische Hochschule, Hannover, West Germany
‡ Department of Anatomy, University of Hamburg, Hamburg, West Germany
§ Department of Obstetrics and Gynecology, University Hospital Sint Radboud, Nijmegen, The Netherlands

The human placenta acts as a barrier separating the blood circulations of the mother and the fetus throughout the entire pregnancy. Fetal blood circulates in vessels located within the chorionic villi while maternal blood circulates around the villi in the intervillous space. Chorionic villi are the functional and morphologic units of the placenta. They are composed of the trophoblast and its basement membrane, the connective tissue of the villous core and the fetal vessels (Fox, 1978; Sandstedt, 1979).

Attention is focused on the three-dimensional organization of the chorionic villous tree and the changes which occur at the outer and inner surfaces of the chorionic villi throughout gestation. The trophoblast and its microvilli, the connective tissue with the fixed stromal and Hofbauer cells, and the walls of the fetal vessels have been visualized.

OUTER SURFACE OF CHORIONIC VILLI

During early pregnancy (9–10 weeks), the chorionic villi are relatively large and plump or sausage-shaped. From the surfaces of the chorionic villi, villous sprouts emerge which vary greatly in size and shape. Most are elongated and have a small basis with a large expanded apex (Figures 1a–c). The distance between the chorionic villi is relatively large, leading to a rather wide intervillous space.

A continuous layer of microvilli covers the surfaces of the chorionic villi and of the villous sprouts (Figure 1d). Most of the microvilli have a leaf-like form. This layer of microvilli is observed throughout gestation. Cell boundaries cannot be seen at the outer surfaces of the chorionic villi.

During the second trimester of pregnancy the chorionic villi remain plump (Figure 2a). Trophoblastic protrusions are fewer in number and have a less variable form than those in the first trimester placenta. Most of

the protrusions have a bulbous appearance at this stage (Figure 2b), and occasionally appear as cord-like structures. The villous surface is still covered with a brush border of slender, interbranching microvilli.

During the third trimester considerable branching of the villous tree occurs. Stem, intermediate and terminal villi are present at this time (Kaufmann, 1981; Figures 2c,d and 3a). The generally short terminal villi are the final branches of the villous tree and originate primarily from the intermediate villi. The terminal villi are characterized by dome-shaped swellings (Figure 3b). These swellings correspond morphologically to the so-called epithelial plates, which are very probably areas involved in numerous metabolic and transport processes. They can easily be visualized through transmission electron microscopy (TEM) (Figure 3c).

The finger-like syncytial sprouts seen by scanning electron microscopy (SEM) in the first trimester are absent in the third trimester. Near term, the intervillous space has been altered from a wide space with large distances between the villi into an intricate labyrinth of closely opposed intermediate and terminal villi (Kenemans et al., 1975; Van Geijn et al., 1975).

INNER SURFACE OF CHORIONIC VILLI

At the onset of pregnancy, until the 7th–8th week, the connective tissue of the chorionic villi is mainly composed of a tight network of tiny bundles of collagen fibrils. These fibrils enmesh numerous fixed stromal cells, Hofbauer cells and fetal vessels (Figure 4). The fixed stromal cells have an elongated form while the Hofbauer cells appear roundish (Castellucci et al., 1980). While pregnancy progresses, from the 8th week onward, the fixed stromal cells form sail-like processes, lining a system of intercommunicating channels (immature intermediate villi) (Figure 5a). These usually run parallel to the major axis of the chorionic villus
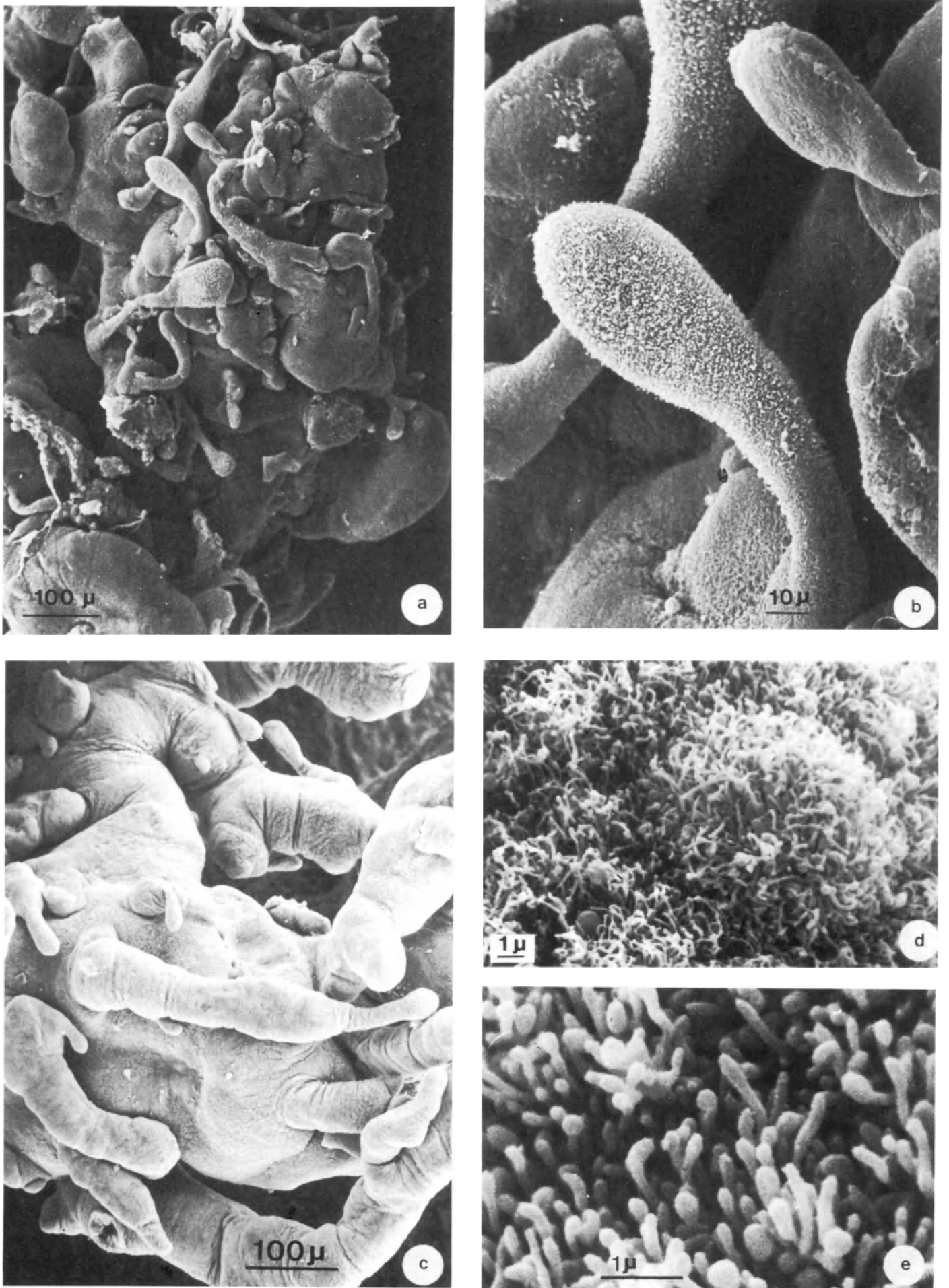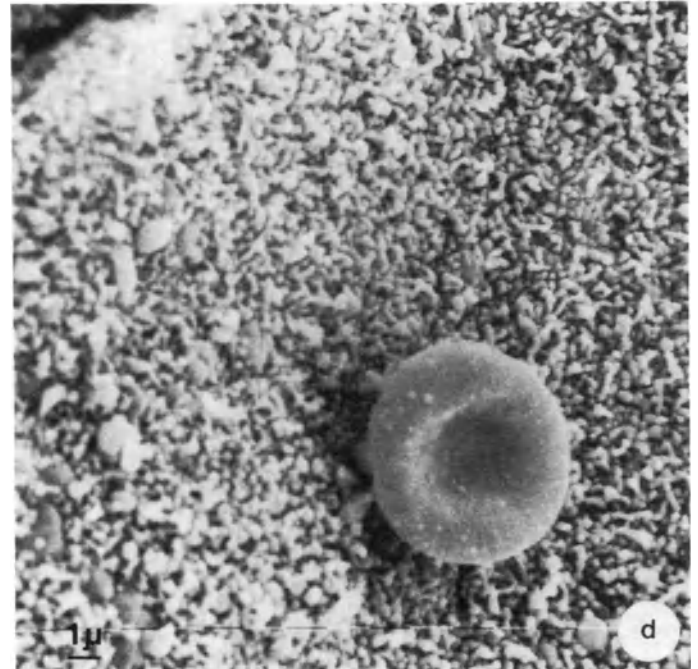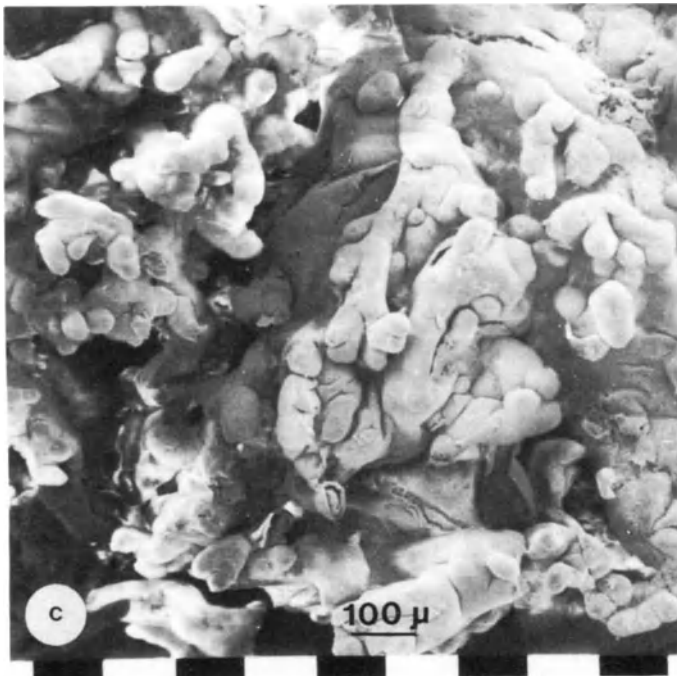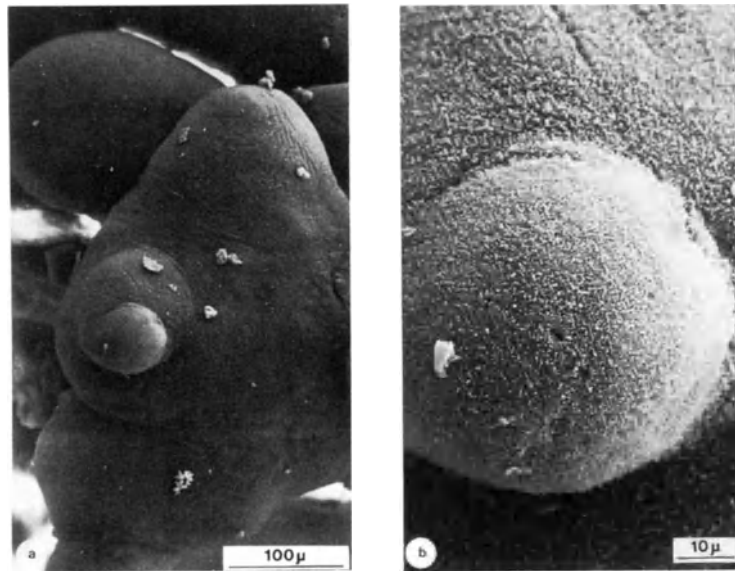
Figure 1

Figure 2
a: Second trimester placenta, 23 weeks of gestation, plump chorionic villi with few bulbous (and sometimes cord-like) protrusions are present
b: Same placenta at higher magnification showing brush-border of microvilli covering a bulbous swelling

c: General structure of the villous tree at 30 weeks of pregnancy. Stem, intermediate and terminal villi are present
d: Maternal erythrocyte situated on top of the microvilli covering the outer surfaces of a chorionic villus
(van Geijn and Kenemans, 1975)

Figure 1 (opposite)
a: First trimester placenta, 8th week of pregnancy, example of the villous tree. Note the presence of plump stem villi and elongated villous protrusions
b: Same placenta; two protrusions with a small basis and broad apex are shown at a higher magnification

c: First trimester placenta, showing the variety of villous protrusions originating from a stem villus
d: First trimester placenta, two examples of the brushborder of microvilli covering the surfaces of the villous tree during gestation
(van Geijn and Kenemans, 1975; Exalto, 1979; Castellucci and Kaufmann, 1981)
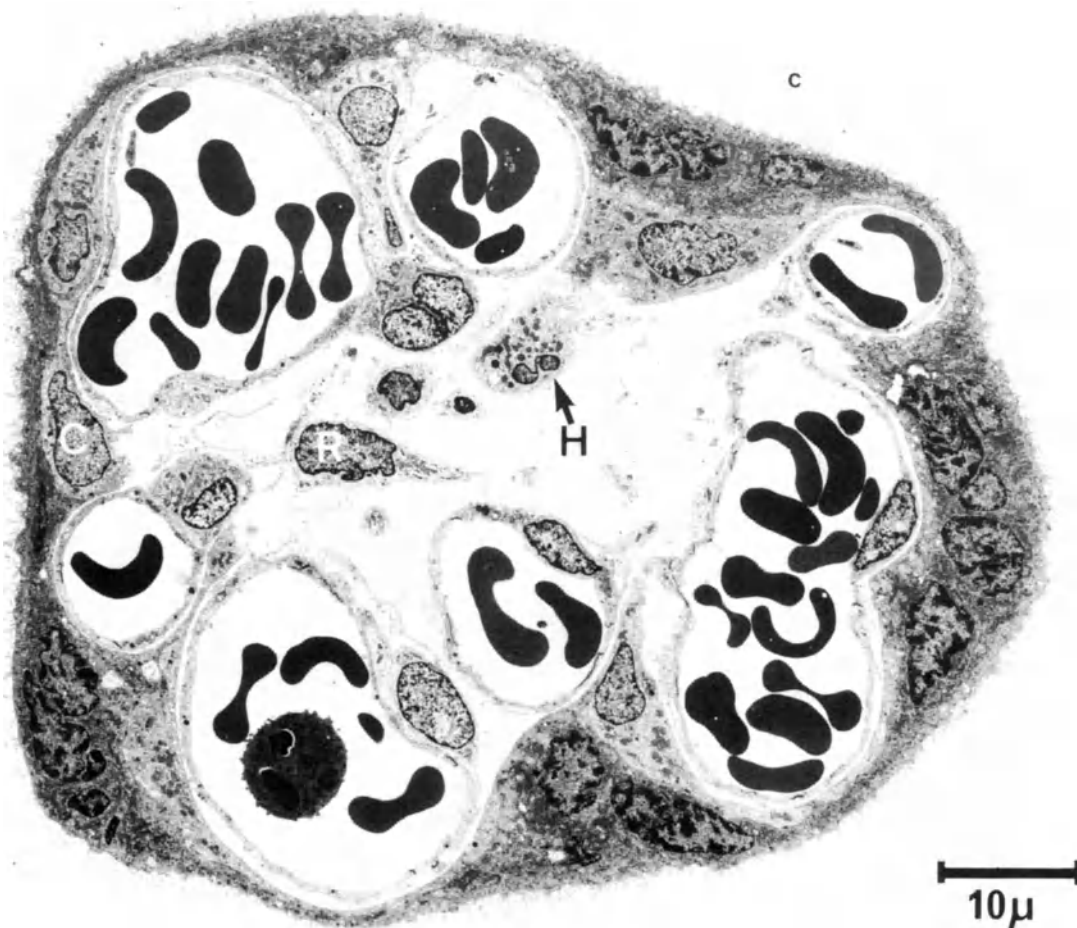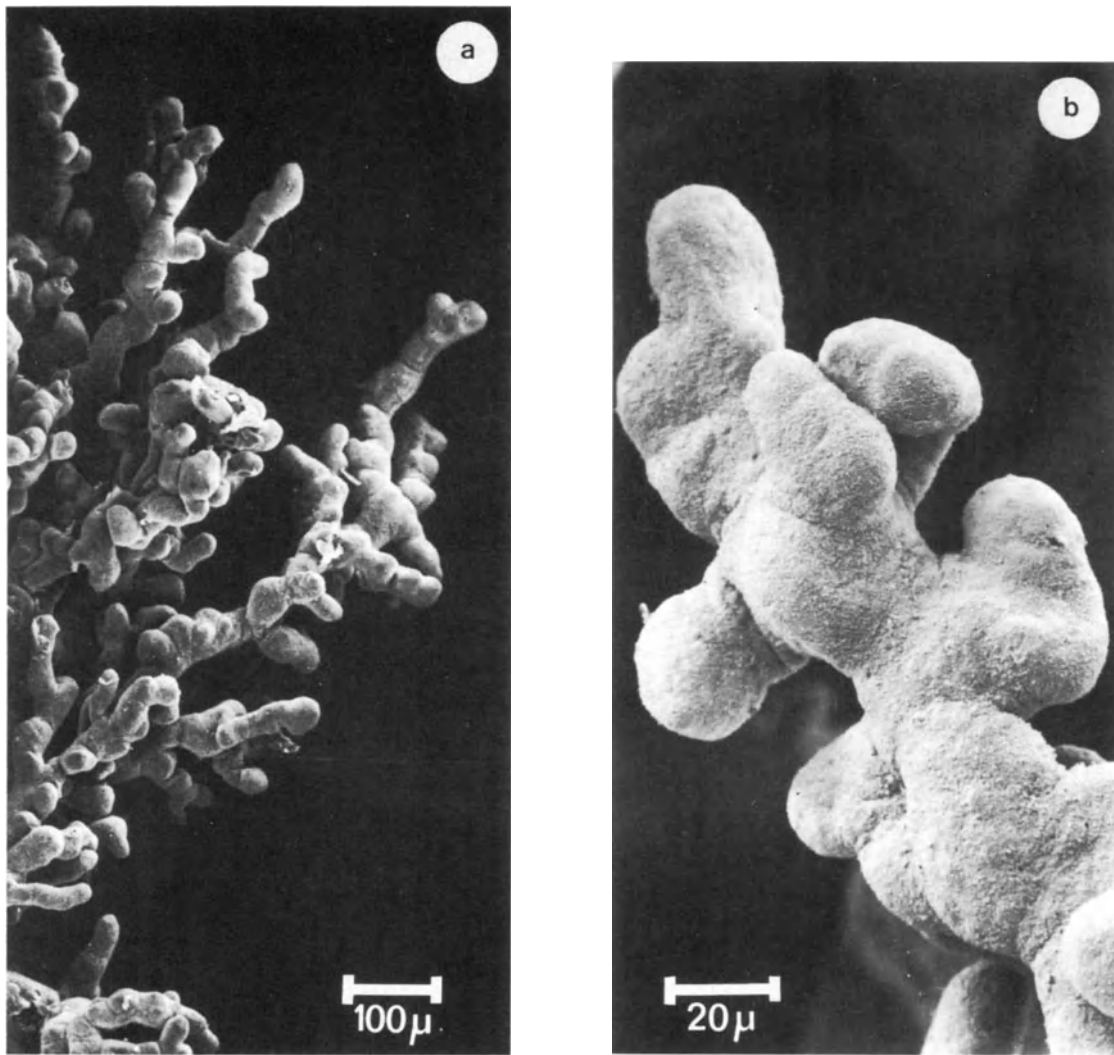
Figure 3
a: Spatial configuration of the villous tree in the near-term placenta. Stem, intermediate and terminal chorionic villi are present
b: Terminal villi that originate from an intermediate villus are visualized
c: TEM of a section through a terminal chorionic villus. Fetal capillaries are closely apposed to the trophoblastic surface. Cytotrophoblastic (C), Hofbauer (H) and reticulum (R) cells are present in the stromal tissue of the chorionic villus
(Kaufmann, 1981)
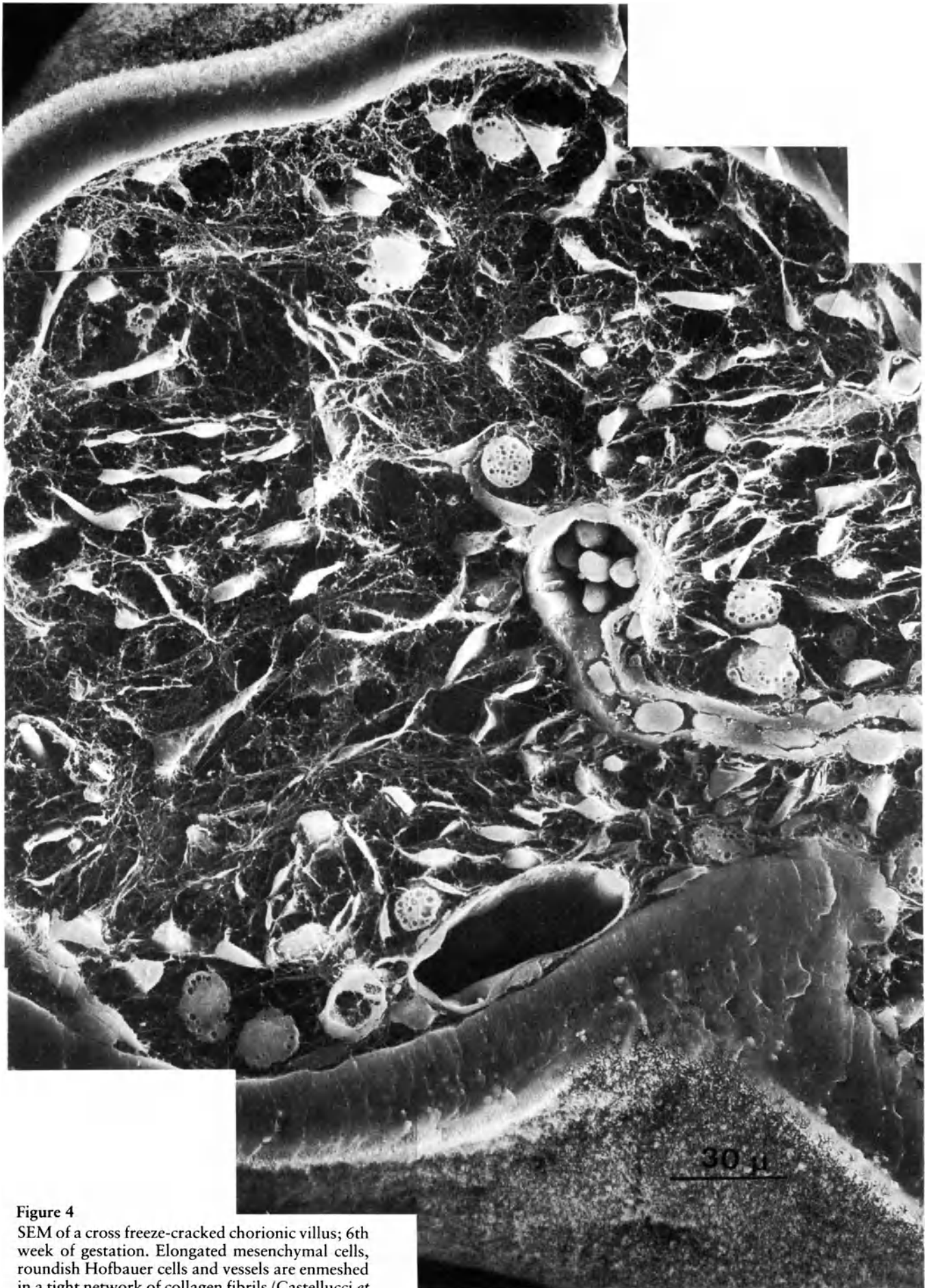
Figure 4
SEM of a cross freeze-cracked chorionic villus; 6th week of gestation. Elongated mesenchymal cells, roundish Hofbauer cells and vessels are enmeshed in a tight network of collagen fibrils (Castellucci *et al.*, 1980)
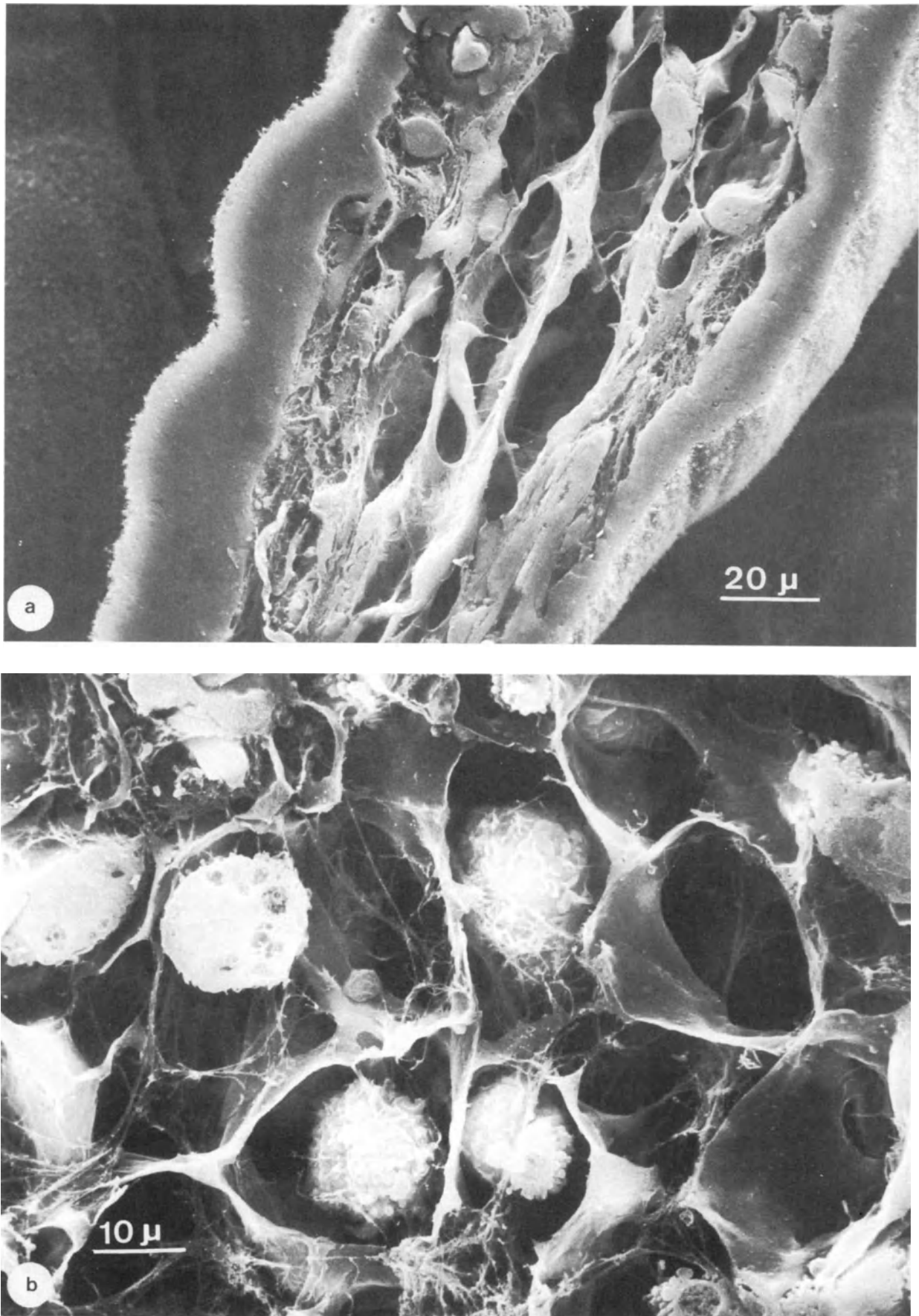
Figure 5

a: Longitudinal fractured immature intermediate villus. A system of differently sized intercommunicating channels is visible

b: SEM of a cross, freeze-cracked chorionic villus; 12th week of gestation. Cross fractured stromal channels appear as deep rooms or compartments which are delimited by the sail-like processes of the fixed stromal cells. Numerous compartments are occupied by Hofbauer cells which surfaces are characterized by microplicae and blebs

(Castellucci *et al.*, 1980)
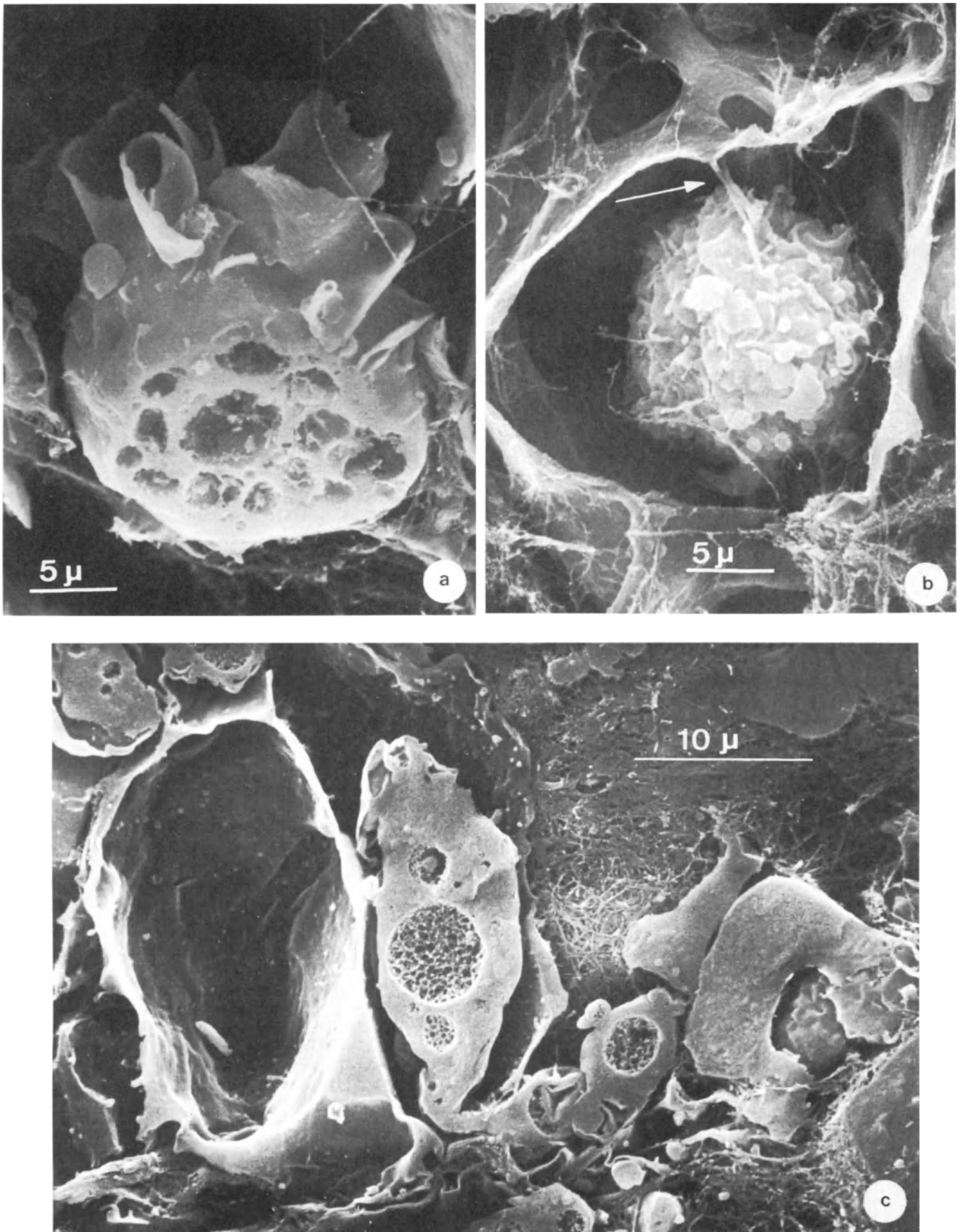
Figure 6

a: Large lamellipodia characterize a highly vacuolated Hofbauer cell; 9th week of gestation

b: Hofbauer cell lying in a stromal channel; 12th week of gestation. Note the thin cytoplasmic filaments (arrow) connecting a Hofbauer cell to a fixed stromal cell

c: Elongated Hofbauer cell situated within a stromal channel and extending partly into the intercellular substance

(Castellucci *et al.*, 1980)
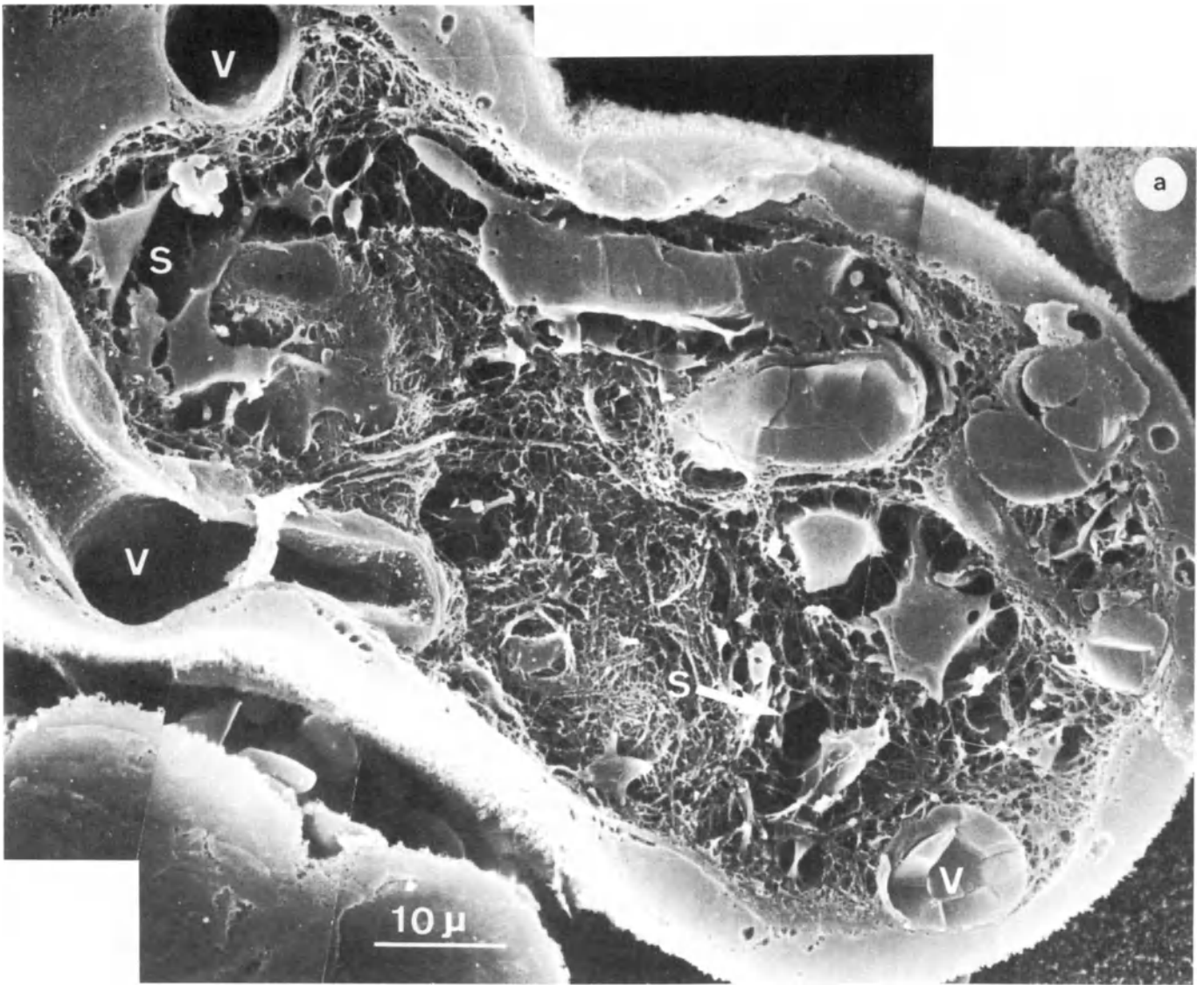
Figure 7
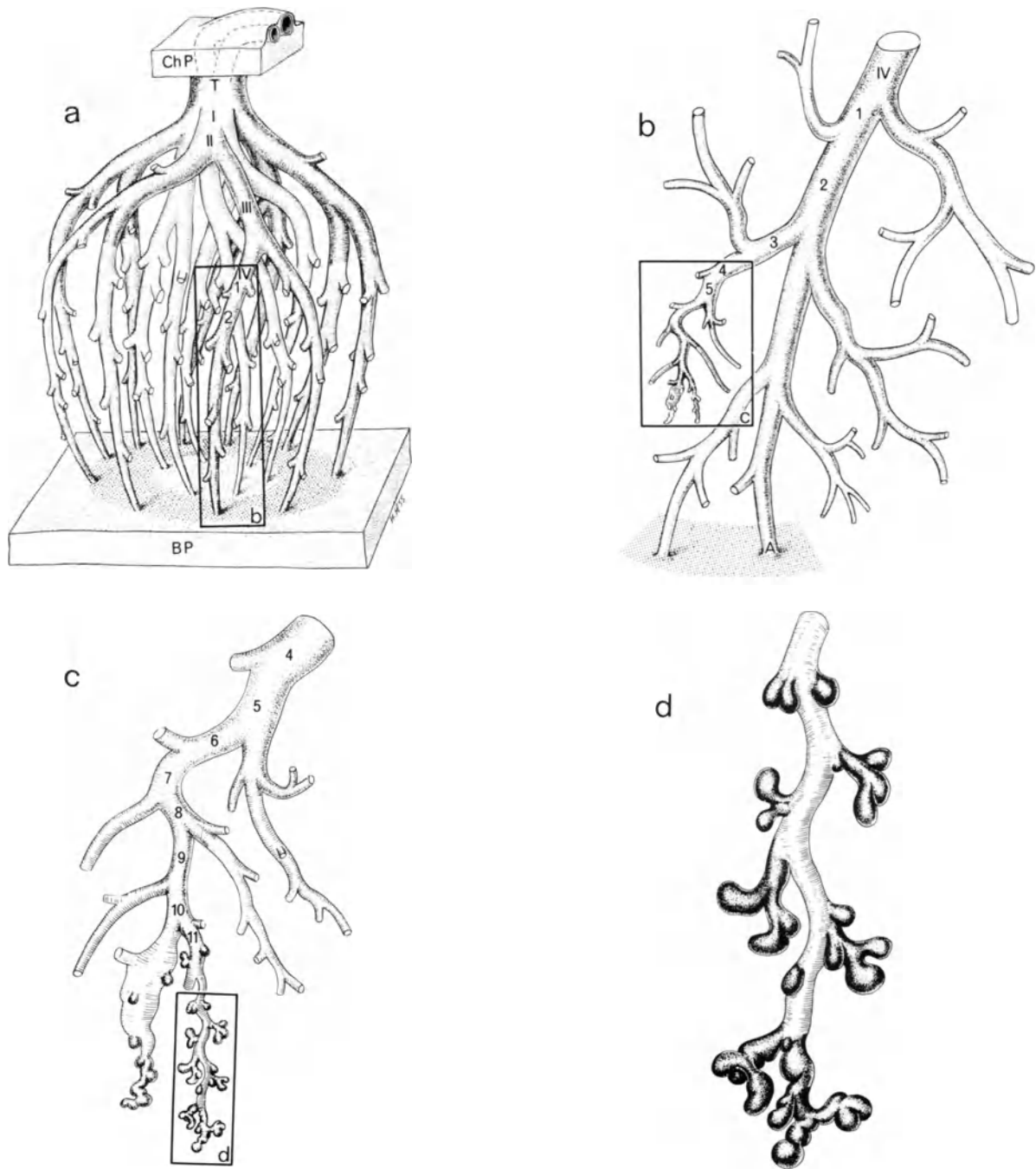
Figure 8 Schematic diagram of villous branching patterns

a: Fetal cotyledon showing truncus (T), ramus I to IV (dense shading) and the first generations of ramuli. The larger branches form an outer ring (shaded) and an inner core. The rami show equal dichotomous branching near the chorionic plate (ChP)

b: Ramus IV and following generations of ramuli (1-5). Some are attached to the basal plate (anchoring villi, A). Note the unequal dichotomous branching of the ramuli (see also Figure 8c)

c: Ramulus 4 and smaller ramuli terminating in an immature (left, lower) and mature (right) intermediate villus. Terminal villi (dense shading) are seen to arise from both types (see also Figure 8d)

d: Mature intermediate villus. Note the characteristic long, poorly branched appearance. Terminal villi (dense shading) arise either directly or with a neck region. They branch repeatedly, particularly at the end of the intermediate villus. (Reprinted, with permission, from Kaufmann, P., Sen, D. K. and Sweikhart, G. (1979). *Cell Tissue Res.*, **200**, 409)

Figure 7 (opposite)

a: Cross-fractured mature intermediate villus; 40th week of gestation. The villous core shows a compact fibrous network of vessels (V). Only few very narrow stromal channels (S) are present

b: Longitudinal-fractured terminal villus; 40th week of gestation. The major part of the villous core is occupied by sinusoidal vessels. Their luminal endothelial surface is characterized by numerous small blebs. The arrows point to two areas where the thickness of the placental barrier is extremely reduced (compare with Figure 3c) (Castellucci *et al.*, 1980)
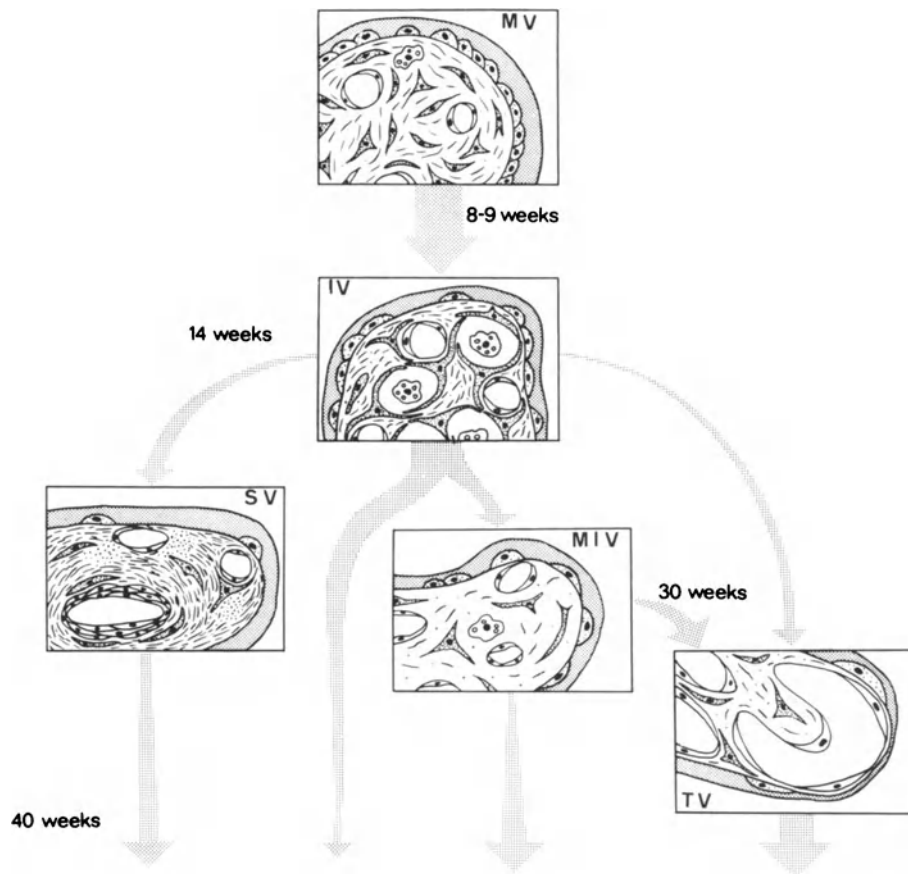
Figure 9 Schematic drawing summarizing the modifications occurring in the villous core of human placental villi throughout pregnancy. MV: mesenchymal villus; IV: immature intermediate villus; SV: stem villus; MIV: mature intermediate villus; TV: terminal villus (Castellucci and Kaufmann, 1981)

Table 1 Changes in appearance of the chorionic villi throughout pregnancy, as viewed by SEM

Trimester	Outer surface	Inner surface
1st	Large and plump/sausage-shaped chorionic villi	Connective tissue consists of collagen fibrils
	Large distance, wide space in between villi	Elongated fixed stromal cells
	Villous sprouts emerge	Roundish Hofbauer cells within stromal channels
	Continuous layer of microvilli	Stromal cells line the immature intermediate villi
2nd	Chorionic villi remain plump	New branches appear
	Fewer, bulbous-like trophoblastic protrusions	Compact network of connective tissue
	Microvilli increase in number, decrease in length and diameter	Stromal channels are few and narrow; Hofbauer cells are mainly absent
3rd	Villous tree branches greatly	Terminal villi develop, showing sinusoidal-dilated capillaries
	Stem, intermediate and terminal villi appear	
	Intervillous space changes into labyrinth	

(Castellucci and Kaufmann, 1981). Within these stromal channels the Hofbauer cells are present. Their cut surfaces (by freeze-cracking) exhibit numerous vacuoles in the cytoplasm (Figure 5b). At the external surface of the Hofbauer cells, blebs, microplicae and lamellipodia are visible (Figures 5b and 6a,b). Some of the Hofbauer cells extend one portion of their body within the stromal channel and range outside it with the other portion (Figure 6c). The presence of the lamellipodia, together with the elongated shape of some of the Hofbauer cells suggest motility of these cells.

From the 14th week onward, the described stromal channels become less apparent. Condensed meshworks of collagen fibers begin to appear in the villi proximal to the chorionic plate (stem villi) and proceed gradually toward the peripheral ramifications. In the second half of pregnancy the new branches of chorionic villi have a compact network of connective tissue fibers surrounding very few short and narrow stromal channels (mature intermediate villi). Hofbauer cells are seldom seen inside or outside these stromal channels. At around the 30th week of pregnancy small outgrowths (terminal villi), showing sinusoidal-dilated capillaries (Figures 7a,b), begin to develop particularly along the surface of the mature intermediate villi.

CONCLUDING REMARKS

The maturational changes occurring in the human placenta with the advance of gestation, as seen by SEM, are as follows (Figures 8 and 9): The chorionic villi increase in number and length, decrease in diameter and change toward a more uniform size; stem, intermediate and terminal chorionic villi develop. The villous protrusions decrease in number and length; they change from being elongated to dome-shaped. The microvilli increase in number, while their length and diameter decrease. The intervillous space progresses from widely organized, large distances into labyrinths. Intercommunicating channels develop in the villous core and characterize the immature intermediate villi. The channels could facilitate the macrophagic and immunologic task of the Hofbauer cells which are particularly numerous in this type of villi. The stem villi (SV) are characterized by a compact network of collagen fibers and large fetal vessels. The mature intermediate villi (MIV) show narrow and short stromal channels, surrounded by a rather tight network of collagen fibrils. The terminal villi (TV) contain sinusoidal-dilated capillaries and a small amount of connective tissue.

SEM is a simple technique, yet most appropriate for studying the outer and inner surfaces of placental chorionic villi in three dimensions. It allows the observer to combine a wide spatial view of the chorionic surface with detailed observations of the ultrastructure of stromal tissues. Stem, mature (and some immature) intermediate, and terminal villi can be seen in the full-term placenta. Stromal channels and their relationships with the other components of the villous core can be visualized, including collagen fibrils, fixed stromal cells, Hofbauer cells and fetal vessels.

References

Castellucci, M., Zaccheo, D. and Pescetto, G. (1980). A three-dimensional study of the normal human placental villous core. I. The Hofbauer cells. *Cell Tissue Res.*, **210**, 235

Castellucci, M. and Kaufmann, P. (1981). A three-dimensional study of the normal human placental villous core. II. Stromal architecture. *Placenta* (In press)

Exalto, N. (1979). De jonge zwangerschap. *Thesis*: Nijmegen, The Netherlands

Fox, H. (1978). *Pathology of the Placenta*. (London: W. B. Saunders)

Geijn, H. P. van, Kenemans, P., Hodde, K. C. and Eskes, T. K. A. B. (1975). The human placenta: surface of chorionic villi. *Proceedings of the X International Congress of Anatomists, Tokyo*, p. 416

Kaufmann, P. (1981). Entwickelung der Plazenta. In Becker, V., Schiebler, Th. H. and Kubli, F. (eds). *Die Plazenta des Menschen*. (Stuttgart: Thième)

Kenemans, P., Geijn, H. P. van, Hodde, K. C. and Eskes, T. K. A. B. (1975). The human placenta: surface structure of chorionic villi in different gestational stages. *J. Microsci. Biol. Cell.*, **24**, 186

Sandstedt, B. (1979). The placenta and low birth weight. In Grundmann, E. (ed). *Perinatal Pathology*. (Berlin: Springer Verlag)

26

The pathological placenta

P. KENEMANS*, H. P. VAN GEIJN†, K. C. HODDE‡ and E. S. E. HAFEZ§

* Department of Obstetrics/Gynecology, Catholic University, Nijmegen, The Netherlands
† Department of Obstetrics/Gynecology, Free University, Amsterdam, The Netherlands
‡ Laboratory for Surgical Research, Wilhelmina Gasthuis University of Amsterdam, Amsterdam, The Netherlands
§ Department of Gynecology/Obstetrics, Wayne State University School of Medicine, Detroit, Michigan 482012, USA

The placenta is the biggest fetal organ. It is the organ of contact between the fetal circulation and the maternal circulation.

Until the 38th week of gestation the normal placenta, and all its components, grow in a definite pattern during the course of gestation, but not all show a similar growth rate. Using light microscopy (LM) and stereological methods Bouw (1975) found the following: 'The growth rate of the intervillous space, the volume of the villi as a whole and the villous stroma alone do not differ from the growth rate of the placenta as a whole. The growth rate of the villous vessels (volume, surface and length) exceeds the growth rate of the placenta. The same is valid for the surface of the trophoblast. The trophoblast does not grow as fast as the placenta but becomes thinner because of the branching of the villi and gets a larger exchanging surface with the intervillous space. The placenta does not grow as fast as the child.'

Scanning electron microscopy (SEM) also shows a gradual alteration in shape as well as in surface ultrastructure of the terminal chorionic villi in relation to gestational age (Herbst et al., 1968; Multier et al., 1969; Herbst and Multier, 1970; Kaufmann, 1971; Ludwig, 1971, 1974; Lerat et al., 1973; Sheppard and Bonnar, 1974; Fox and Agrafojo-Blanco, 1974; Kenemans et al., 1975; Kuppe, et al., 1975; Ludwig et al., 1975; King and Menton, 1975). During maturation the terminal villi show an increase in number combined with a diminution of diameter resulting in enlargement of the total trophoblastic surface. As they become interlaced, the intervillous space is transformed into an intricate labyrinth. Trophoblastic protrusions of different shape (sprouts, ridges), numerous in early stages (Bergstrom, 1971), are sparse at term.

The syncytiotrophoblastic surface shows a brush border of microvilli. With advance of gestation there is a decrease in length, diameter and shape variation in these microvilli, with a tendency to greater density. The microvilli increase the plain syncytial surface twenty-fold, thus giving a total of approximately 200 m² actual surface (Sandstedt, 1979). This surface area cannot be studied by light microscopy. However, it is most important, because it is an area of high metabolic activity, and of maternal–fetal exchange of oxygen and nutrients, and highly essential, therefore, for embryonic differentiation and fetal growth.

For the study of the surface of the chorionic villi scanning electron microscopy is a particularly appropriate method, as it permits the examination of relatively large areas of tissue, with correlation of local changes in the surface ultrastructure to changes in the overall spatial organization. However, reports on SEM studies of abnormal trophoblast are almost completely lacking.

INTRAUTERINE FETAL DEATH

Gross lesions of the placenta, such as retroplacental haematoma or massive infarction, can sometimes be found as a cause of intrauterine fetal death. Such conditions lead to impaired functioning of the placenta, with ultrastructural pathology of the adjacent chorionic villi (Figure 1).

In other instances one can only hope to find a histological sign as to the causal factor for fetal demise. However, after fetal death the trophoblast, although remaining fully viable, will undergo a sequence of morphological changes (Figure 2) obscuring the original characteristics as a result of cessation of fetal circulation within the villi. SEM observations on fetal post-mortem placental changes have not been reported so far.

LOW BIRTHWEIGHT

The syndrome of low birthweight for gestational age is not a homogeneous entity, neither as to etiological

factors, nor with regard to placental morphology. When leaving aside low birthweight on the basis of fetal congenital malformation, the most important group is that of so-called placental insufficiency. Poor intrauterine fetal growth in normotensive (uncomplicated) pregnancies may differ from that in hypertensive (pre-eclamptic) pregnancies, and so may the placental morphology. In the former the placenta may be small because the fetus is small, and in the latter the fetus may be small because the placenta is small (Fox, 1978). However, Sheppard and Bonnare (1976) have claimed to see (with SEM and TEM) identical pathology of the uteroplacental vessels in both groups.

Preliminary SEM studies (Van Geijn et al., 1975; Sandstedt, 1979) suggest differences in morphology of the chorionic villi between both groups, describing the normotensive low birthweight placenta as the 'retardation type', showing maturation arrest of the chorionic villi, and the hypertensive type as the 'compensation type', in which degenerative features are found next to compensation phenomena (Table 1; Figure 3).

MATERNOFETAL RHESUS INCOMPATIBILITY

Only a small proportion of the placenta from cases of hemolytic disease of the neonate on basis of maternofetal rhesus incompatibility show an abnormal morphology. These 'hydropic' placentae are heavy, bulky and edematous, with areas of marked pallor. Intervillous thrombosis is common. The maturation of the chorionic villi seems overall delayed, with some very young villi present. There is a large regional variability within one placenta. Small foci of syncytial necrosis within large areas of normal villous syncytiotrophoblast, with local loss or distortion of microvilli, were observed using SEM (see Fox, 1979). SEM pictures of hydropic placentae (Figure 4) have not been published, as far as we know.

DIABETES MELLITUS

The description of the placental morphology in diabetes mellitus varies considerably with the author, and with the degree of severity of the maternal disease.

Our limited SEM observations reveal in near-term placental tissue of insulin-treated patients plump chorionic villi, numerous bulbous protrusions and a widely organized intervillous space, all consistent with decelerated maturation. Microvilli were in some instances unusually sparse (Figures 4c-f).

HYDATIDIFORM MOLE

Trophoblastic proliferation, hydropic swelling of the villi, and absence of blood vessels are the characteristic morphological changes in hydatidiform mole. There is a close surface similarity between the molar and the immature trophoblast, as revealed with SEM (Ferenczy and Richart, 1972). The vesicular surface is slightly undulant and contains several varying-sized, polymorph, mostly cylindrical, syncytial protrusions (Figure 5). After fracturing of the vesicle the inner surface shows connective tissue fibers, primitive mesenchymal cells, and lack of vessels (Figure 6).

CONCLUDING REMARKS

SEM is a simple and appropriate method for the study of the placental chorionic villi, notably because it gives a wide, spatial view of the chorionic surface, which is the most important site of fetal maternal exchange.

Maturation in the normal, and retardation, degeneration and compensation phenomena in the pathological material can be seen with low and high magnification, thus allowing local changes to be related to overall spatial alterations.

In severe pre-eclampsia the villous surface shows, besides compensation characteristics such as enlargement of trophoblastic surface by a multitude of small slender terminal villi, also degenerative features, such as fibrin deposition, extensive areas of damage and a corrugated surface. Similar degenerative changes are seen in some placentae of pregnancies complicated by severe rhesus incompatibility. The villous organization in diabetic pregnancy shows signs of a decelerated maturation.

In the low birthweight group two types of placental outgrowth are distinguishable. In type I – the retardation type – sparse short villi with only few protrusions sprout from plump main villi. The microvilli are tall and slender. A second type – the compensation type – shows abundant, slender, multiple branching terminal villi sprouting from small main villi.

Table 1 Low birthweight

Type	I. Compensation type	II. Retardation type
Main villi	small	plump
Terminal villi	slender, abundant, multiple branching	short, sparse, occasional branching
Protrusions	numerous	sparse
Intervillous space	labyrinthine	wide
Microvilli	slender, irregular, many apical promontories	tall, slender, apical promontories

Figure 1 (opposite) Placental infarction: area of placental infarction and adjacent chorionic villi.
a: Low magnification view of damaged area (×50)
b: Cut surface through infarct (×500)
c: Altered chorionic villi at the border of the placental infarction (×100)
d: Higher magnification of c, showing altered shape of the terminal villi (×500)
e: Higher magnification of d, showing abnormal microvillous patterns (×2000)
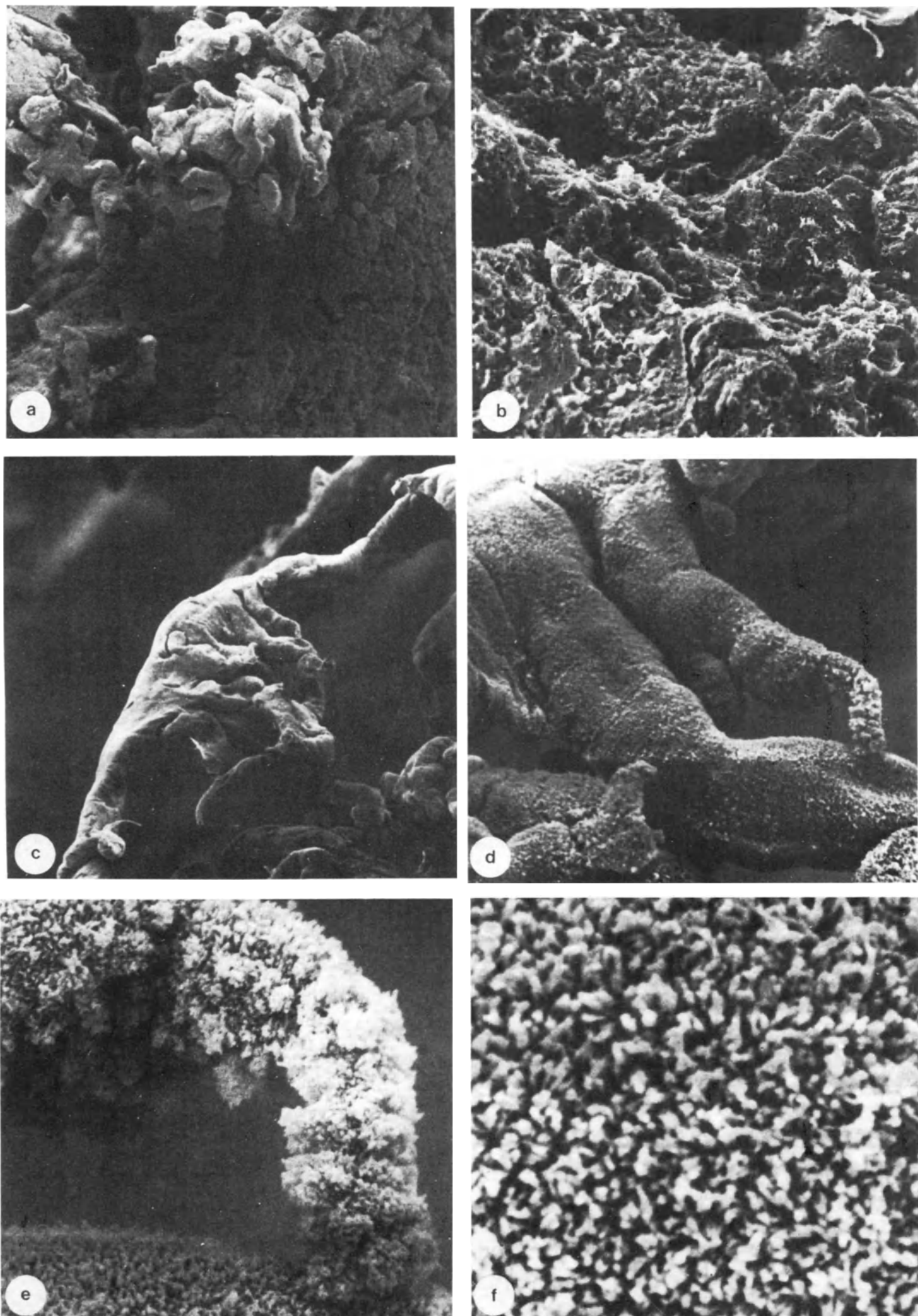f: Microvilli, with rather normal appearance on neighbouring villus (×5000)

Figure 1

The intervillous space is transformed into an intricate labyrinth. The irregular microvilli have many apical promontories.

These preliminary results need further confirmation. Placentae from small for gestational age infants obviously form a heterogeneous group. Ultrastructural studies have not proved to be very rewarding (Fox, 1978). Moreoever, there is a necessity to standardize the acquisition and the processing of the placenta (e.g. time of cord clamping, topographical sampling errors, fixation shrinkage). SEM of microcorrosion casts of the fetal vascular systems, which could give new insights in angioarchitectural questions, have not been reported thus far.

References

Bergstrom, S. (1971). Surface ultrastructure of human amnion and chorion in early pregnancy. *Obstet. Gynecol.*, 38, 513

Bouw, G. M. (1975). Growth and growth retardation of the human placenta. *Thesis*, Free University, Amsterdam

Ferenczy, A. and Richart, R. M. (1972). Scanning electron microscopic study of normal and molar trophoblast. *Gynecol. Oncol.*, 1, 95

Fox, H. (1978). *Pathology of the Placenta*. (London: Saunders)

Fox, H. and Agrafojo-Blanco, A. (1974). Scanning electron microscopy of the human placenta in normal and abnormal pregnancies. *Eur. J. Obstet. Gynecol. Reprod. Biol.*, 4, 45

Herbst, R., Multier, A.-M. and Inatsugi, Y. (1968). Die räumliche Darstellung der menschlichen Chorionzotten mit dem JEOL-Raster-Elektronenmikroskop. *Beitr. z. Elektronenmikroskopischen Direktabbildung von Oberflächen*, 1, 297

Herbst, R. and Multier, A. M. (1970). Les microvillosites à la surface des chorioniques du placenta human. *Gynécol. Obstét.*, 69, 609

Kaufmann, P. (1971). The demonstration of cytoplasmic polyps from the human trophoblast by scanning electron microscopy. *Arch. Gynekol.*, 211, 523

Kenemans, P., van Geijn, H. P., Hodde, K. C. and Eskes, T. K. A. B. (1975). The human placenta: Surface structure of chorionic villi in different gestational stages. *J. Microsc. Biol. Cell.*, 24, 186

King, B. F. and Menton, D. N. (1975). Scanning electron microscopy of human placental villi from early and late in gestation. *Am. J. Obstet. Gynecol.*, 122, 824

Kuppe, G., Metzger, H. and Ludwig, H. (1975). Ultrastructural changes of the human placenta as seen by scanning electron microscopy. In Hafez, E. S. E. (ed). *The Mammalian Fetus*, pp. 49–67. (Springfield, Ill.: Charles C. Thomas)

Lerat, M. F., Connehaye, P., Richomme, J., Magre, J. and Bonnaille, J. (1973). Etude du placenta humain au microscope électronique à balayage *J. Gynecol. Obstet. Biol. Reprod.*, 2, 233

Ludwig, H. (1971). Surface structure of the human term placenta and of the uterine wall postpartum in the screen scan electron microscope. *Am. J. Obstet. Gynecol.*, 111, 328

Ludwig, H. (1974). Surface structure of the human placenta. In Moghissi, K. S. and Hafez, E. S. E. (eds), *The Placenta. Biological and Clinical Aspects*, pp. 40–64. (Springfield, Ill.: Charles C. Thomas)

Ludwig, H., Metzger, H. and Wolf, H. (1975). The placenta (man). In Hafez, E. S. E. (ed.), *SEM Atlas of Mammalian Reproduction*, pp. 346–57. (Tokyo: Igaku Shoin)

Multier, A.-M., Herbst, R. and Blaschke, R. (1969). Face maternelle due placenta et villosités choriales observées au Scanning Microscope. *Féd. Soc. Gynécol. Obstétr. Langue Franq.*, 22, 411

Sandstedt, B. (1979). The placenta and low birth weight. In Grundmann, E. (ed.), *Perinatal Pathology*, pp. 2–55. (Berlin: Springer-Verlag)

Sheppard, B. L. and Bonnar, J. (1974). Scanning electron microscopy of the human placenta and decidual spiral arteries in normal pregnancy. *J. Obstet. Gynaecol. Br. Commonw.*, 81, 20

Sheppard, B. L. and Bonnar, J. (1976). The ultrastructure of the arterial supply of the human placenta in pregnancy complacated by fetal growth retardation., *Br. J. Obstet. Gynaecol.*, 83, 948

Van Geijn, H. P., Kenemans, P., Hodde, K. C. and Eskes, T. K. A. B. (1975). The human placenta: surface structure of chorionic villi in pathological conditions. *J. Microscopie Biol. Cell.*, 24, 183

Figure 2 (opposite) Intrauterine fetal death with post-mortem placental changes. Extensive areas of damage and corrugated surface structures are present in this material of a patient with severe pre-eclampsia and fetal death (a, ×200; c, ×100; e, ×1000). The microvilli show high variability in shape, both within and between various regions. Next to areas with impaired microvillous function (b), other terminal chorionic villi (d,f) show abundantly present, tightly packed, and highly pleomorphic microvilli with many apical promontories (b, ×5000; d, ×10 000; f, ×5000)
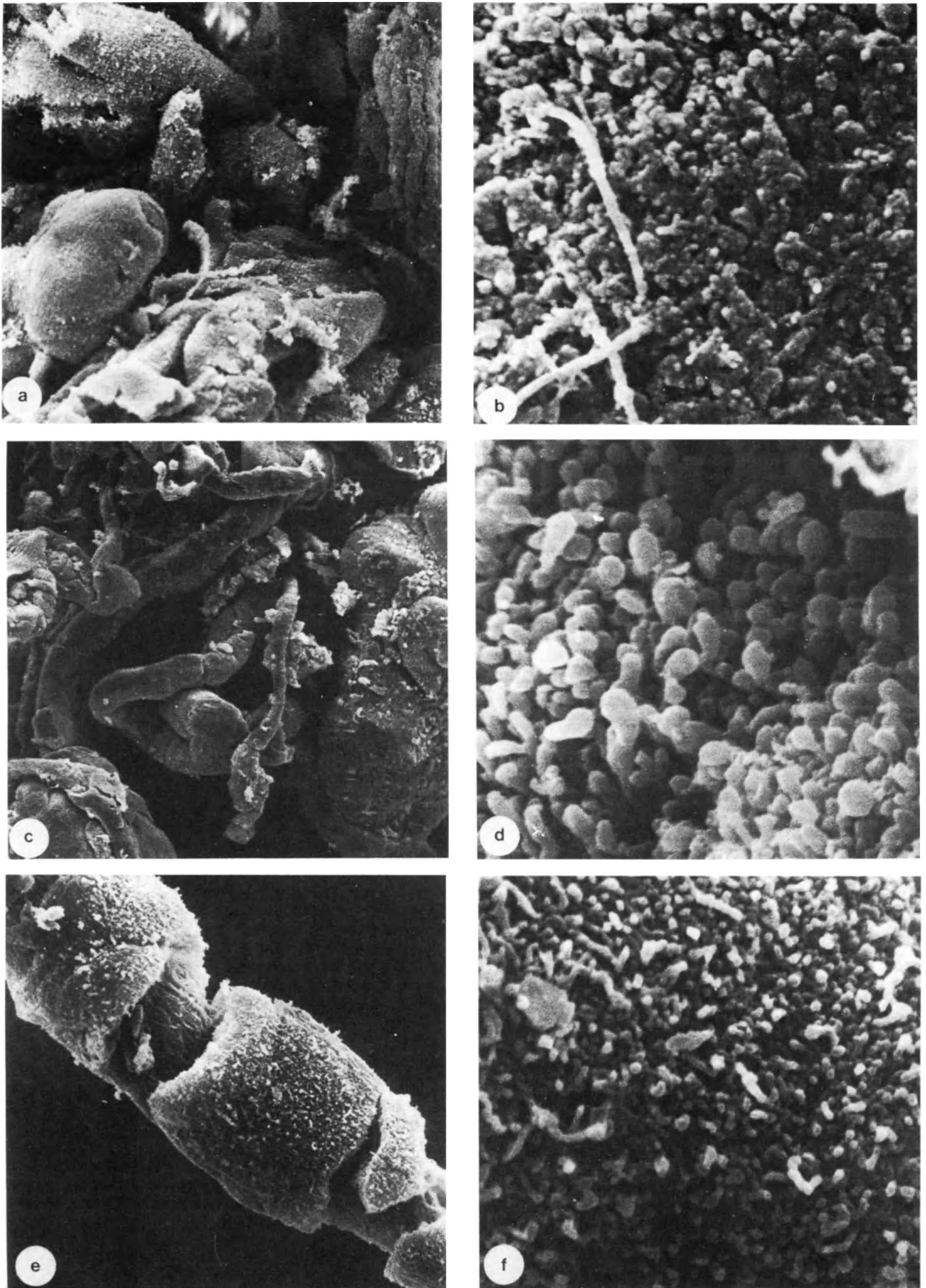
Figure 2

Figure 3 (opposite) Low birthweight. Preliminary SEM studies suggest difference in morphology of the chorionic villi between the two major groups of low birthweight placentae. In type I – the compensation type, associated with maternal vascular disturbances – abundant, slender, multiple branching terminal villi sprout from small main villi. Protrusions are numerous. By interlacing of terminal villi the intervillous space is transformed into an intricate labyrinth (a). The slender microvilli have an irregular shape and show many apical promontories. Fibrinoid depositions are common (c). In type II – the retardation type, associated with unexplained low birthweight – sparse short occasional branching villi sprout from plump main villi. Trophoblastic protrusions are few in number. The intervillous space is wide (b). The microvilli are tall and slender and have relatively many apical promontories (d). (c, ×18 000; d, ×4500)

50 μ   a

50 μ   b

c

d
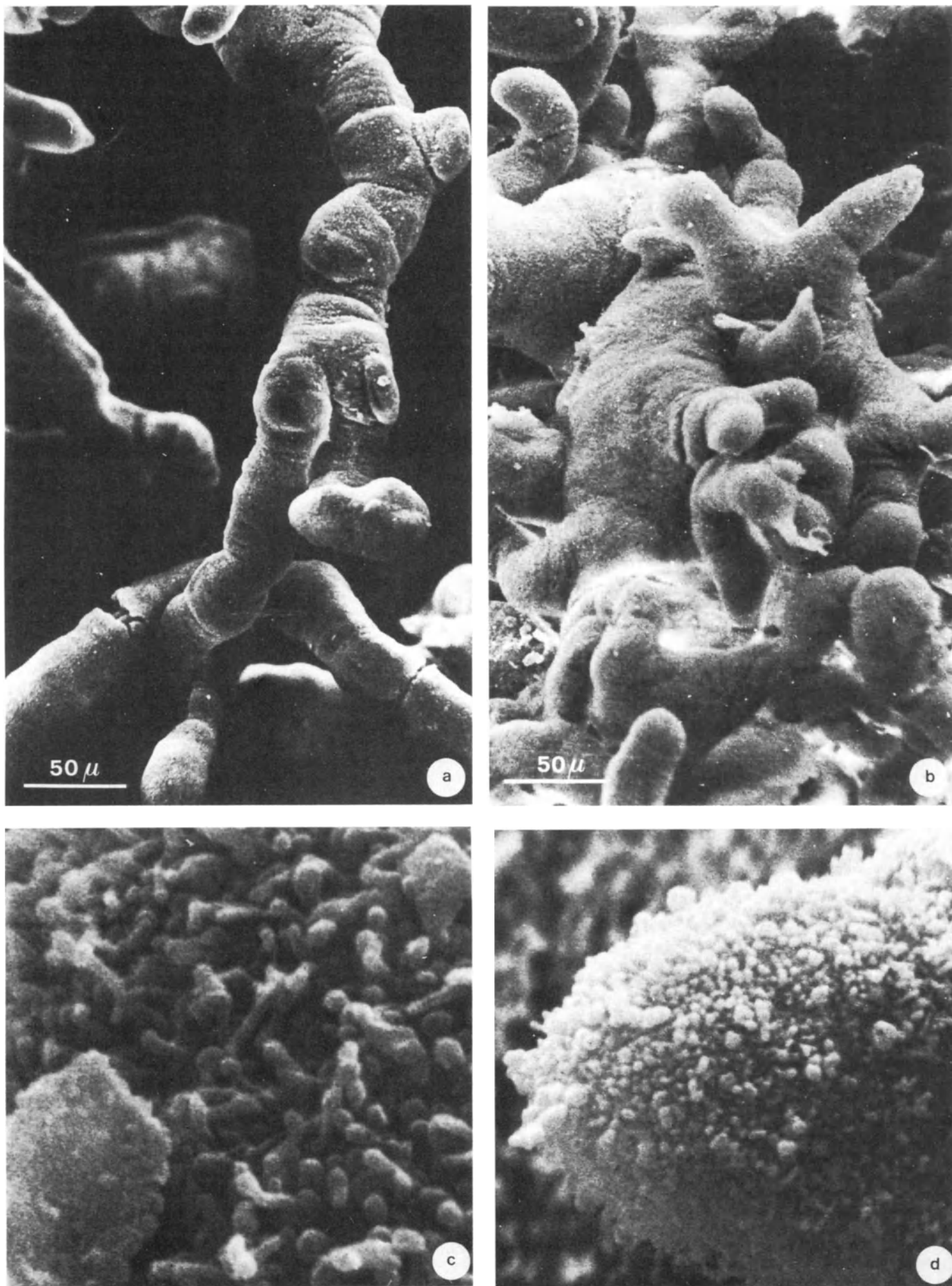
Figure 3

Figure 4 (opposite) Maternofetal rhesus incompatibility and diabetes mellitus

a,b: Rhesus incompatibility. A placenta from a case of hemolytic disease of the neonate on the basis of maternofetal rhesus incompatibility shows a rather normal morphology (a), although macroscopically this was a heavy, edematous and pale placenta. There are many areas with pleomorphic microvilli, with some large, solitary processes (b) (a, ×500; b, ×10 000)

c–f: Diabetes mellitus. The placental morphology in diabetes mellitus varies considerably. However, in a considerable percentage SEM observations reveal in near-term placentae of (treated) patients plump chorionic villi, numerous bulbous protrusions and a widely organized intervillous space, all consistent with arrest of maturation (c–e). Microvilli were in some instances unusually sparse (f). (c, ×500; d, ×1000; e, ×160; f, ×5000)
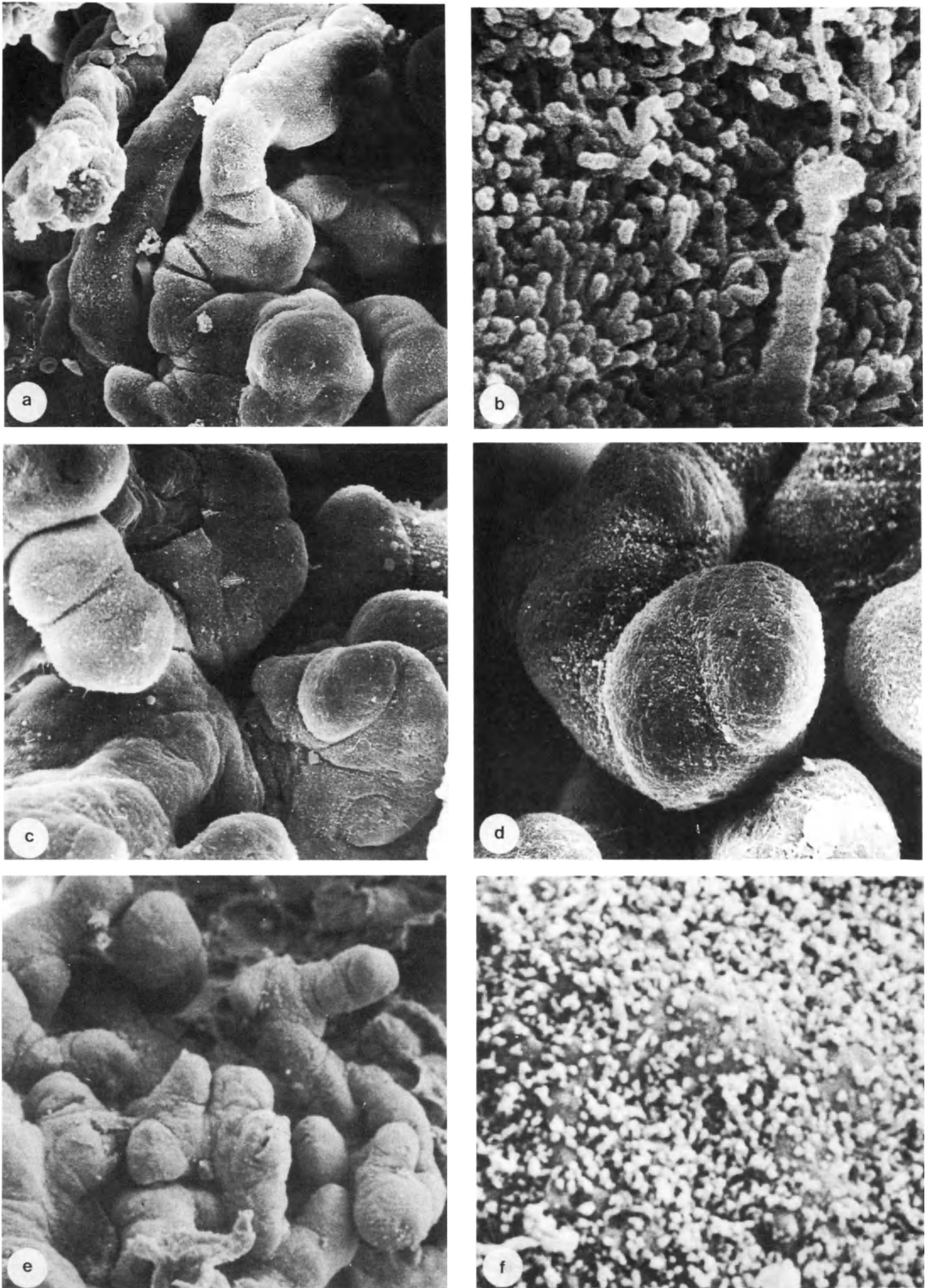
Figure 4

Figure 5 (opposite) Hydatidiform mole

a–c: Outer surface of molar vesicle. Besides many polymorph, mostly cylindrical protrusions, flat overgrowths are visible. Both structures are composed of cyto- and syncytiotrophoblast, and their presence probably indicates high activity of trophoblastic growth (a, ×80; b, ×80; c, ×160)

d,e: Inner aspect of a molar vesicle. In order to study the inner surface the vesicle was artificially ruptured. The structures on the bottom are almost certainly stromal elements (d), which are compressed into a thin network of connective tissue fibrils (e) flattened out against the vesicle wall. There are no vascular structures (d, ×320; e, ×500)

Figure 5

27
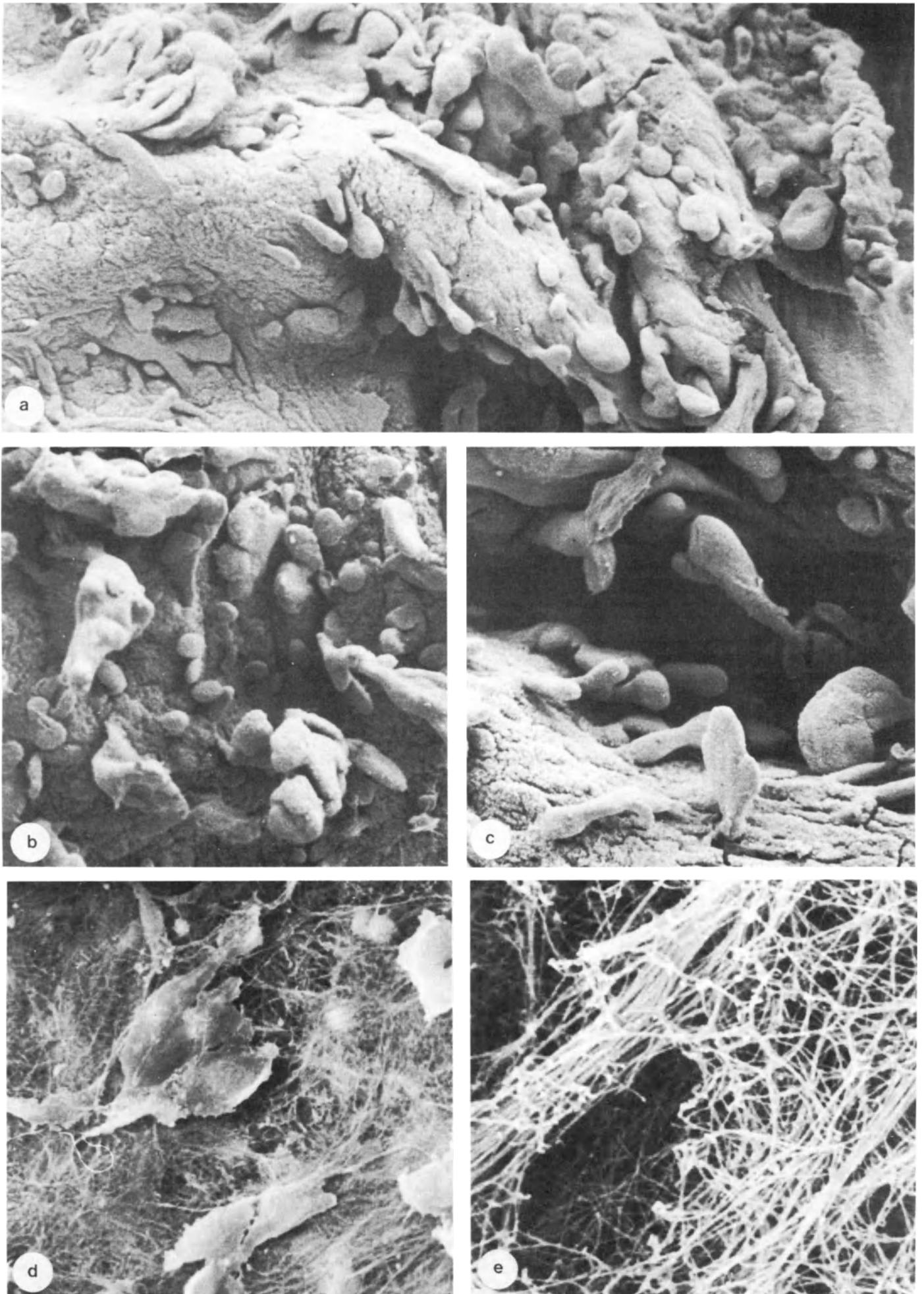
Amniotic fluid cells and placental membranes

O. TYDÉN

* Department of Obstetrics and Gynecology and Department of Anatomy, University of Uppsala, Uppsala, Sweden

The amniotic fluid lies in a cavity lined by the amniotic epithelium and reflects fetal metabolism and maturation.

AMNIOTIC FLUID CELLS

These cells are important fetal messengers throughout pregnancy. In early pregnancy they have become a tool in the detection of genetic and biochemical disorders of the fetus. Gradually the total number of cells increases during pregnancy. A lipid dye (Nile blue) stains neutral lipids orange and discriminates two distinct subpopulations of exfoliated cells, namely *lipid-carrying* and *lipid-free*. Shortly before term there is a steep increase in the lipid-carrying cells in the amniotic fluid, indicating fetal maturity (Brosens and Gordon, 1966).

Classification

Differences in the surface ultrastructure allow distinction between four groups of amniotic fluid cells at mid-gestation: spherical cells, bladder cells, microridge cells and amorphous cells (Tydén *et al.*, 1981). At term only the latter two types are encountered. In a combined study of fixed and Nile blue stained cell suspensions processed through freeze-drying, correlative observations were made to establish the appearance at LM and SEM of one and the same cell in a series of cells. A direct clue to ultrastructural distinctions between cell populations differing at LM could thereby be obtained. Amorphous cells proved to be the ultrastructural counterpart to lipid-carrying cells, while microridge cells corresponded to the lipid-free type (Figure 1) (Bergström *et al.*, 1982).

Tissue contribution to cells

A study of the origin of the cell subpopulations requires parallel electron microscopy of amniotic fluid cells and fetal tissue specimens. Extensive tissue sampling cannot be carried out in human liveborn infants. We have therefore used two fetal Rhesus monkeys, which display a fetal development parallel to that in humans. To extend this study, six human fetuses from legal mid-trimester abortions were investigated. Tissue samples were taken from areas facing or communicating with the amniotic cavity. The tissue contribution to cellular populations in the amniotic fluid was found to be dependent upon cell shedding events on several fetal organ surfaces. It became obvious that some organ surfaces did not contribute at all, whereas others contributed extensively (Tydén *et al.*, 1981).

Non-shedding epithelia were observed in the respiratory tract, the urinary bladder and the amniotic membranes. Two principal shedding mechanisms of *shedding epithelia* seemed to be operative in mid-gestation, namely detachment and exfoliation. *Detachment* occurs in the periderm and in the cords (see below) and implies a mechanism of shedding cell fragments. *Exfoliation* reflects cell turnover with shedding of whole cells and takes place in various squamous epithelia and from fetal skin (Figures 2a,b). Bladder cells are shed during the final stage of periderm regression, while microridge cells are derived from various squamous epithelia, for example in the vagina and oral cavity and in the cord at term. The amorphous cells exfoliate from the nasal mucosa, but the main source seems to be the cornified epidermis (Tydén *et al.*, 1981; Bergström *et al.*, 1982).

Maturity testing by cytological examination of amniotic fluid cells thus reflects maturational events in fetal skin.

AMNIOTIC EPITHELIUM

Amniotic epithelium has a homogeneous appearance with cells covered by microvilli. Intercellular openings in three cell junctions are a marked feature of this tissue (Figures 3a,b). TEM studies have revealed a complicated ultrastructure (see van Herendael *et al.*, 1978, for review), which suggests that the amnion has multiple specialized functions to perform, such as active epithelial secretion and intensive intercellular and transcellular transport.
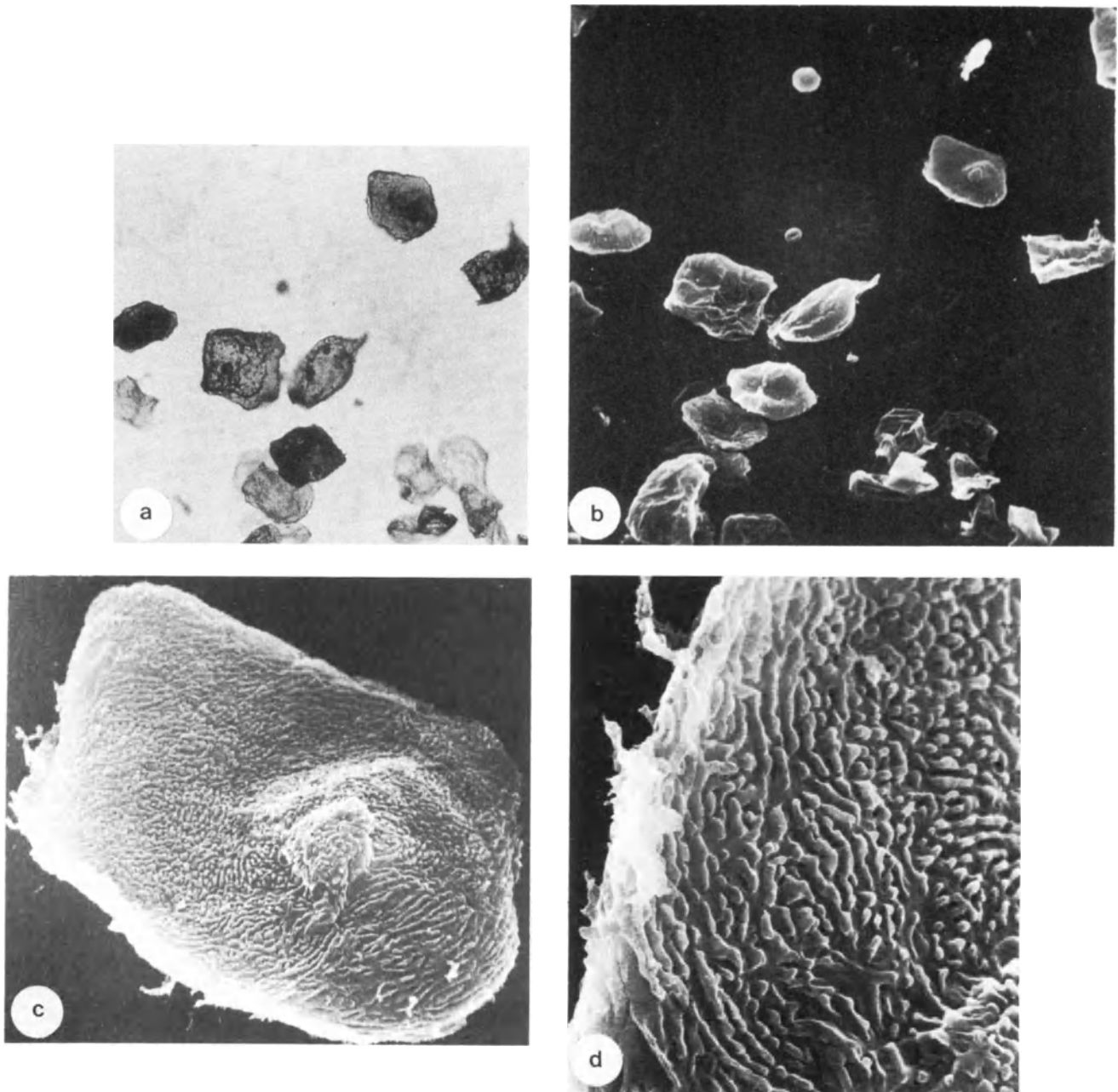
Figure 1

a. Nile blue stained human amniotic fluid cells at term. Prior to staining, glutaraldehyde fixation was performed. Note the correlative mapping in Figures 1a and 1b. The appearance of one microridge cell at light microscopy is shown; its surface ultrastructure is seen in Figures 1a–c. Also visible are amorphous cells and a red blood cell (×1300)

b: Corresponding SEM field of the wet smear in Figure 1c (×1300)

c: Microridge cell (SEM), detail of Figure 1b. The polygonal shape and protruding center are characteristic features of this cell type. The microridge pattern is discernible all over the cell surface (×7700)

d: Detail of Figure 1c. Note the microridges and their random organization. Intermingled with these ridges are areas with microvilli (×13 200)
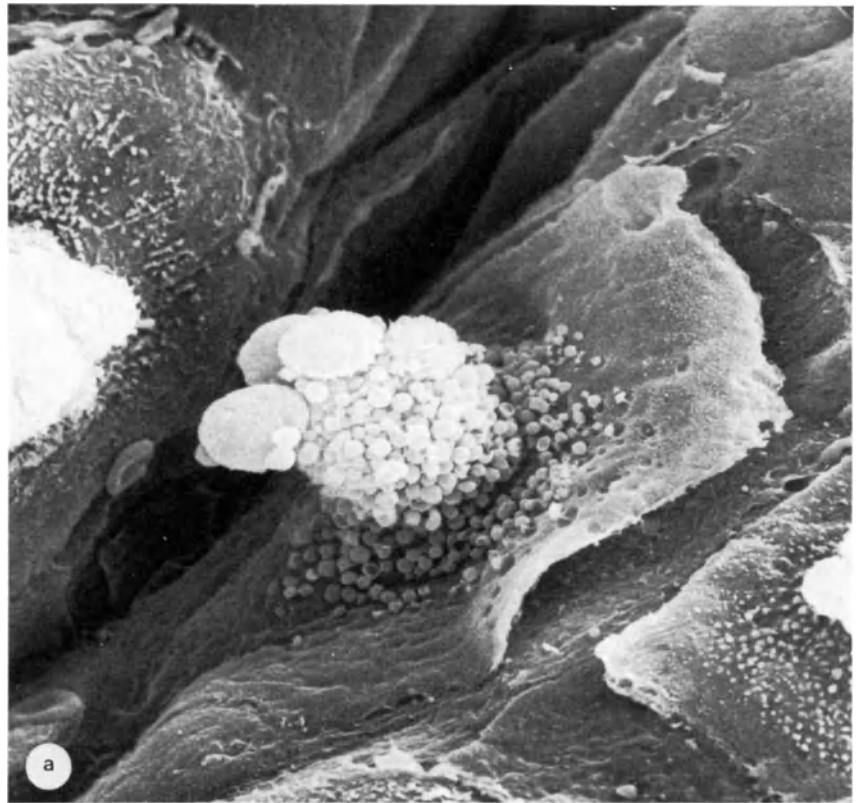
Figure 2
a: Sole of the foot from the mid-gestational monkey fetus, showing an exfoliating bladder cell with numerous buddings and a protruding center. Note the amorphous area below the exfoliated part of the bladder cell. This amorphous area probably represents the keratinized stratum corneum ($\times 1050$)
b: Exfoliating amorphous cell clusters from the sole of a human fetal foot in the 24th week of gestation ($\times 5400$)
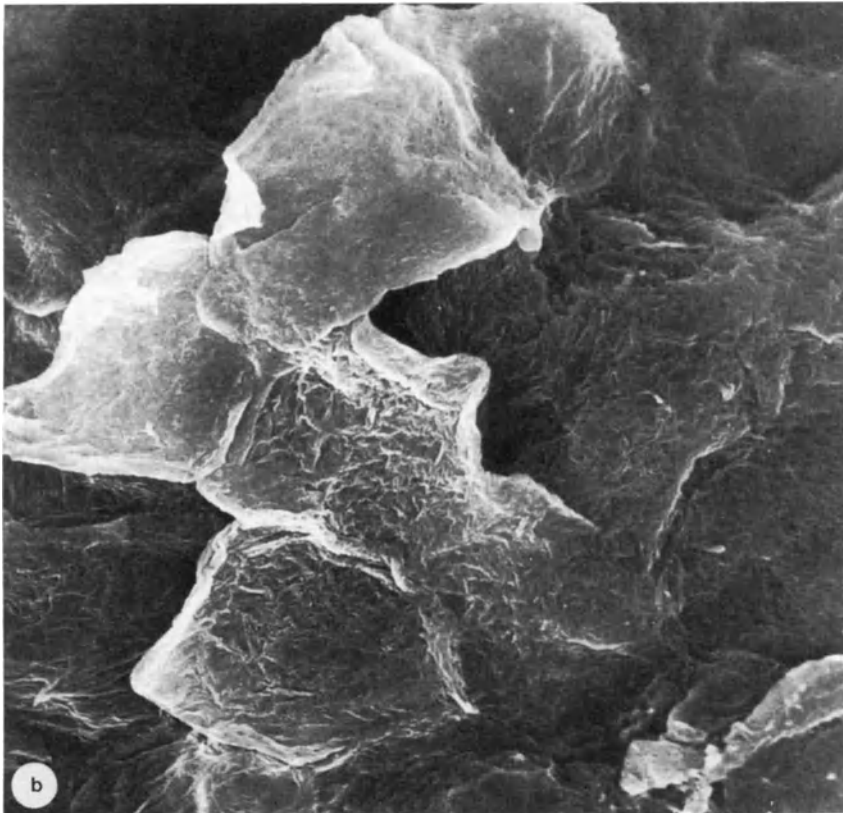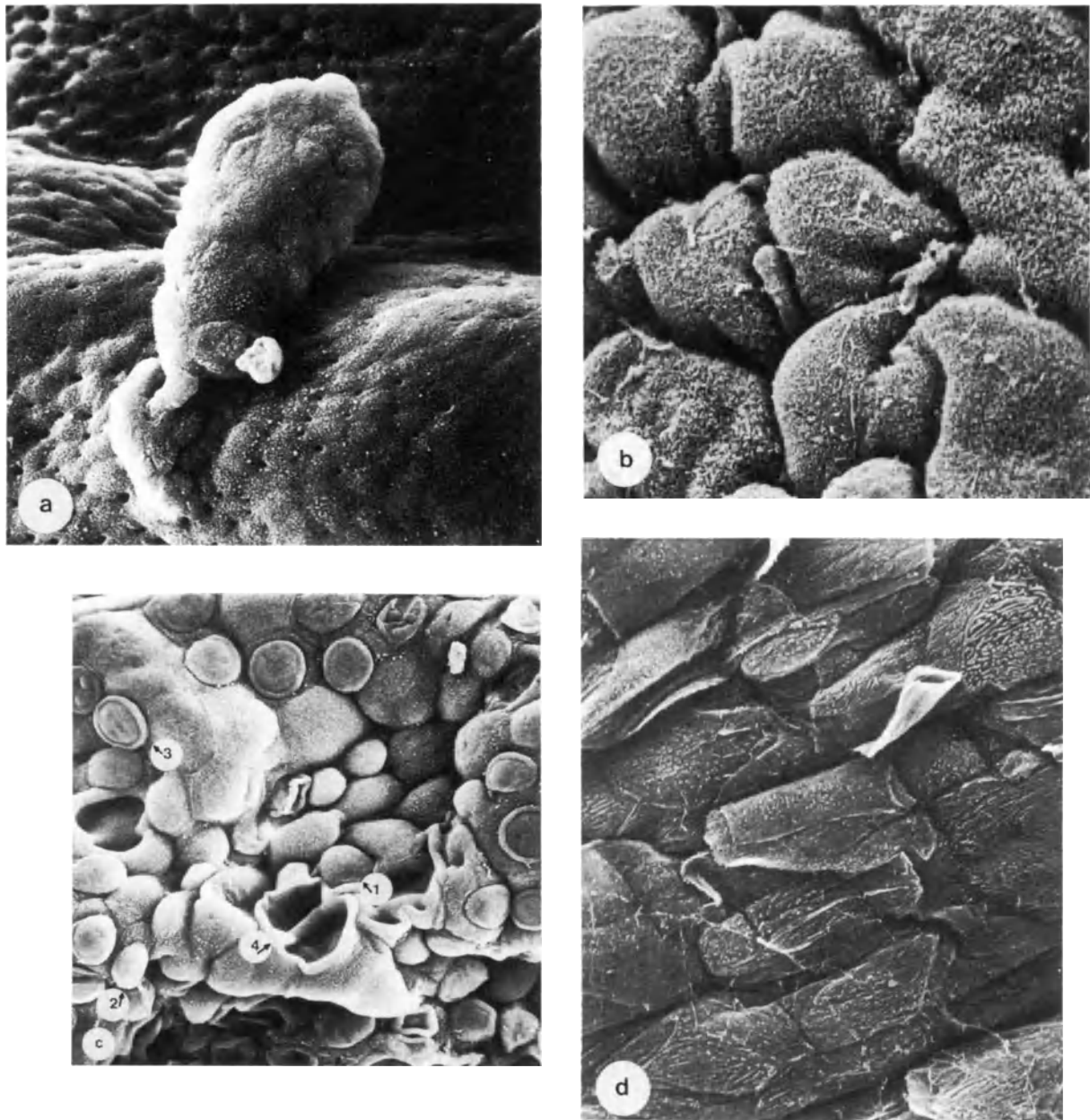
Figure 3

a: The reflected amniotic membrane, showing the shedding of 25–50 cells. This event was only observed once. Note also the absence of exfoliation of single cells. Between the cells intercellular channels are seen (arrows) (×450)

b: Placental amnion. Individual cells are protruding and show deep intercellular ditches. The apical cell areas are densely microvillous (×1500)

c: Umbilical cord from an 18-week fetus, showing the development leading to detachment of spherical cells. The

consecutive stages of detachment are indicated by numbers. Apical cell protrusions (1) are gradually being undermined by indentation of the surface membrane (2, 3). Occasional craters are observed, presumably representing apical sites where detachment has occurred (4) (×650)

d: Middle portion of umbilical cord from a fetus at term. Mainly microridge-bearing surfaces are seen on the cells (×550)

THE UMBILICAL CORD

The umbilical cord displays ridges and furrows at low magnification. The regional surface variation may be described in three parts. At the placental insertion (1) the cell surface pattern is similar to that of the amniotic epithelium. In the mid-portion (2) the surface ultrastructure differs during gestation. In early mid-pregnancy the cell pattern is reminiscent of that of the amniotic epithelium. During a limited period of time, at about 18–23 weeks of gestation, indentations in the surface membranes result in the formation of spherical cell fragments and deep pits remain in the cell surface after detachment (Figure 3c). This process probably reflects a functional activity, possibly with controlling influence over the amniotic fluid (Tydén et al., 1981). At term the surface cells are uniform and display a pattern of microridges (Figure 3d) (Tydén et al., 1981; van Herendael et al., 1978). Close to the fetus a transitional zone (3) is apparent.

SEM has proved to be a convenient tool in studying tissue surfaces; the ultrastructure of intact surfaces can be observed, large tissue areas can rapidly be screened and a resolution down to 15 nm or even lower can be achieved. Detailed ultrastructural features of cell shedding can therefore be revealed (Tydén, 1980).

References

Brosens, I. A. and Gordon, H. (1966). The estimation of maturity by cytological examination of the liquor amnii. *J. Obstet. Gynaecol. Br. Commonw.*, **73**, 88

Tydén, O., Bergström, S. and Nilsson, B. A. (1981). Origin of amniotic fluid cells in mid-trimester pregnancy. *Br. J. Obstet. Gynaecol.*, **88**, 278

Bergström, S., Tydén, O. and Nilsson, B. A. (1982). Light and electron microscopic correlation of human amniotic fluid cells in late pregnancy. *Obstet. Gynecol.* **59**, 172

Tydén, O., Bergström, S. and Nilsson, B. A. (1981). Surface ultrastructure of amniotic fluid cells and various fetal tissues of the Rhesus monkey. *Acta Obstet. Gynecol. Scand.*, **60**, 277

Tydén, O. (1980). Amniotic fluid cells. A morphological and clinical study. *Doctoral thesis, Acta Universitatis Upsaliensis*, 354

Van Herendael, B. J., Oberti, C. and Brosens, I. (1978). Microanatomy of the human amniotic membranes. *Am. J. Obstet. Gynecol.*, **131**, 872

28

Human embryo and fetus

R. E. WATERMAN

Department of Anatomy, School of Medicine, University of New Mexico, Albuquerque, New Mexico 87131, USA

The few existing SEM studies of developing human tissues deal mainly with older fetal stages (Gondos *et al.*, 1978; Waterman, 1979; Blick, 1979). Examination of early embryonic stages is restricted in part by their limited availability, and by the desire to maximize recovery of information by embedding and serial sectioning. The circumstances resulting in spontaneous abortion and the methods used for surgical interruption of pregnancy (for example: suction curettage, saline injection, prostaglandin infusion) may also introduce pre-fixation artifact and often preclude recovery of intact specimens making accurate staging (O'Rahilly, 1973; Shepard, 1975; Gasser, 1975; Corliss, 1976; Moore, 1977), and assessment of normality, difficult. In addition, the fixative used initially in the clinical setting may not be the most appropriate for ultrastructural preservation, and although smaller stages or fragments may be adequately preserved by immersion in a fixative solution, organs of larger embryos and fetal stages may suffer from lack of perfusion of fixative through the vascular system (Waterman, 1980). In spite of these difficulties, SEM observations are of proven value in visualizing the three-dimensional architecture of organs and tissues in developing organisms.

The purpose of this chapter is to illustrate the usefulness of the SEM for examining developing human tissues obtained and preserved by routine methods during the interval encompassing the end of the embryonic and beginning of the fetal periods (6–12 weeks post-fertilization). The reproductive system is emphasized. The cardiovascular, respiratory, muscular, and skeletal systems are not included due to limitations of space. References to SEM studies of these systems may be found in Waterman (1979) and Pexieder (1981).

REPRODUCTIVE SYSTEM

Developments of the reproductive and urinary systems are closely interrelated. The gonads, reproductive ducts (mesonephric or Wolffian; paramesonephric or Müllarian), and external genitalia pass through an 'indifferent' or bisexual period before sexual differences become morphologically identifiable near the end of the 2nd month of development. No sexual differences can be discerned in the urogenital duct system until the late 8th or early 9th week, and in the external genitalia until about 1 week later, (O'Rahilly and Muecke, 1972; Glenister, 1954).

External genitalia

During the indifferent stage, the external genitalia consist of: (1) a genital tubercle; (2) a urogenital groove flanked laterally by the urogenital folds; and (3) genital (scrotolabial) swellings on either side of the genital tubercle (Figure 1) (Spaulding, 1921; Glenister, 1954). The urogenital sinus opens into the urethral groove following breakdown of the urogenital membrane near the end of the 6th week. A group of epithelial cells extends for a time from the tip of the genital tubercle in both sexes. This 'epithelial tag' is eventually lost.

In the female, the urethral folds remain unfused as the labia minora. The urethral groove thus remains open as the vestibule. The genital tubercle becomes the glans clitoris and the genital swellings elongate around the base of the clitoris as the labia majora which fuse caudal to the vestibule to form the posterior commissure. These structures are present by 3 months.

In the male, the genital tubercle enlarges to form the penis, and the urethral folds progressively fuse along the ventral aspect of the developing phallus converting the urogenital groove into the penile portion of the urethra (Figure 2). The male urethra is completed during the 4th month by canalization of a plate of cells (urethral plate) within the glans. The genital swellings enlarge and grow towards each other in the ventral midline; overgrowing the proximal portion of the fused urogenital folds.

Genital tract

During the indifferent period, the primordia of two

sets of reproductive ducts are present. These develop into different structures in males and females. The primordia of the genital ducts are already recognizable when differentiation of the gonad begins. The mesonephric (Wolffian) ducts which originate as a component of the urinary system during the 4th week drain the tubules of the mesonephric kidneys into urogenital sinus. The paramesonephric (Müllarian) ducts develop lateral to the mesonephric ducts. The cranial end of each paramesonephric duct appears initially as a funnel-shaped depression in the celomic epithelium. The caudal ends of the paramesonephric ducts grow caudally as cellular cords which reach the urogenital sinus at about 10 weeks. The mesonephric and paramesonephric ducts on each side form the two urogenital ridges which approach each other caudally and unite in the midline posterior to the cloaca (Figures 3a,b,d,e). The paramesonephric ducts which lie lateral to the mesonephric ducts cranially, move medially as they approach the cloaca and fuse in the midline to form the blind Müllarian tubercle, which protrudes, but does not open, into the posterior wall of the urogenital sinus (Figures 3d,e,g) (Jones, 1968b).

In the male, the mesonephric duct persists as the outflow tract of the testis. The cranial end becomes highly coiled, forming the bulk of the epididymidis. The continuation of the duct becomes the ductus deferens which opens into the posterior wall of the developing urethra. The cranial 10–15 mesonephric tubules of each mesonephros persist as the ductuli efferentes which anastomose with tubules of the rete testis. Development of the caudal end of the mesonephric duct is closely related to that of the primordia of the ureters of the metanephros and of the seminal vesicles, which evaginate from the wall of the dilated portion of the mesonephric ducts during the 3rd month. Except for a few minor remnants, the paramesonephric ducts largely degenerate on the male.

In the female the paramesonephric ducts develop into the oviducts and uterus, and the mesonephric ducts begin to degenerate around the 10th week. The fused caudal ends of the paramesonephric grow caudally as a cellular cord, the vaginal plate, which eventually develops a continuous lumen at about 6 months. The unfused cranial portions of the paramesonephric ducts become the uterine tubes, the epithelium of which becomes ciliated during fetal life (Ludwig and Metzger, 1977).

In both sexes a strand of connective tissue extends from the urogenital fold into the connective tissue of the genital swellings (Figures 3a,d,e). In the male this structure (gubernaculum) becomes ultimately located at the inferior pole of the testis within the scrotum. In the female it persists as the ovarian ligament between the ovary and uterine wall and continues into the connective tissue of the labia majora as the ligmentum teres of the uterus.

Gonads

The indifferent period of gonadal development persists from about the beginning of the 5th week when the gonadal ridges form at the medial side of the mesonephric kidneys, through the recognition of

testicular development between 6 and 7 weeks. By the 6th week the gonad consists of a cortex containing germ cells and a medulla containing sex cords which also include germ cells (Vossmeyer, 1971).

The testis becomes identifiable histologically in embryos during the 6th week as the germ cells disappear from the cortex and a tunica albuginea forms (Vossmeyer, 1971; O'Rahilly and Muecke, 1972). Interstitial cells become recognizable about 10 weeks and increase until 5–6 months when they suddenly 'shrink and degenerate'. The rete testis develops in the mesentery between gonad and mesonephros as the testis enlarges and the mesonephros decreases in size (Figures 3c,f).

The ovary can be recognized during the 6th week by its failure to exhibit the characteristics of a testis, but the ovary does not become well differentiated morphologically until later in fetal life. Ovarian development is characterized by an increase in the size of the cortex at the expense of the medulla. Follicles consisting of oocytes surrounded by granulocytes are present in the center of the ovary in embryos near the middle of the 6th month (Jones, 1968b).

The gonads change position within the body during development, coming to lie within the pelvis at the end of the embryonic period. The testes further descend into the scrotum by term.

KIDNEY

The tubules and duct systems of the kidneys develop within the mesoderm of the bilateral nephrogenic ridges

---

Figure 1 (opposite)   Stages of external genitalia development

a: Ventral surface of a genital tubercle near the beginning of the 8th week. The urogenital groove between the urogenital folds is separated from the sinus within the tubercle at this stage by the urogenital membrane. Small genital (labioscrotal) swellings are present at the lateral aspects of the genital tubercle. An epithelial tag is present at the tip of the tubercle (*). Sexual differences in external genitalia are not yet apparent (bar=100 μm)

b: Genital tubercle during the 8th week. The urogenital groove is deeper and the genital swellings are larger. The urogenital membrane has ruptured. This is still the 'indifferent' stage (bar=100 μm)

c: Genital tubercle late in the 8th week. The urogenital groove is separated from the proctodeal depression by the perineal body (arrow) (bar=100 μm)

d: Higher magnification of opposed margins of the urogenital groove of a genital tubercle from an embryo similar to that in Figure 1c. The apical surfaces of the periderm cells are rounded and covered with short microvilli. Small groups of epithelial cells frequently project from the surface near the margin of the urogenital fold (bar=5 μm)

e: The remnant of the tail (arrow) is seen caudal to the genital tubercle (at left) of an embryo early in the 8th week (see Figure 1f) (bar=50 μm)

f: Tail remnant of the embryo in Figure 1e shown at higher magnification. The human tail reaches its maximum length of about 1 mm near the beginning of the 7th week. It then diminishes in size due to cell death of the subepithelial components and relative overgrowth of the trunk, and is no longer present by the middle of the 8th week. (Fallon and Simandl, 1978) (bar=10 μm)
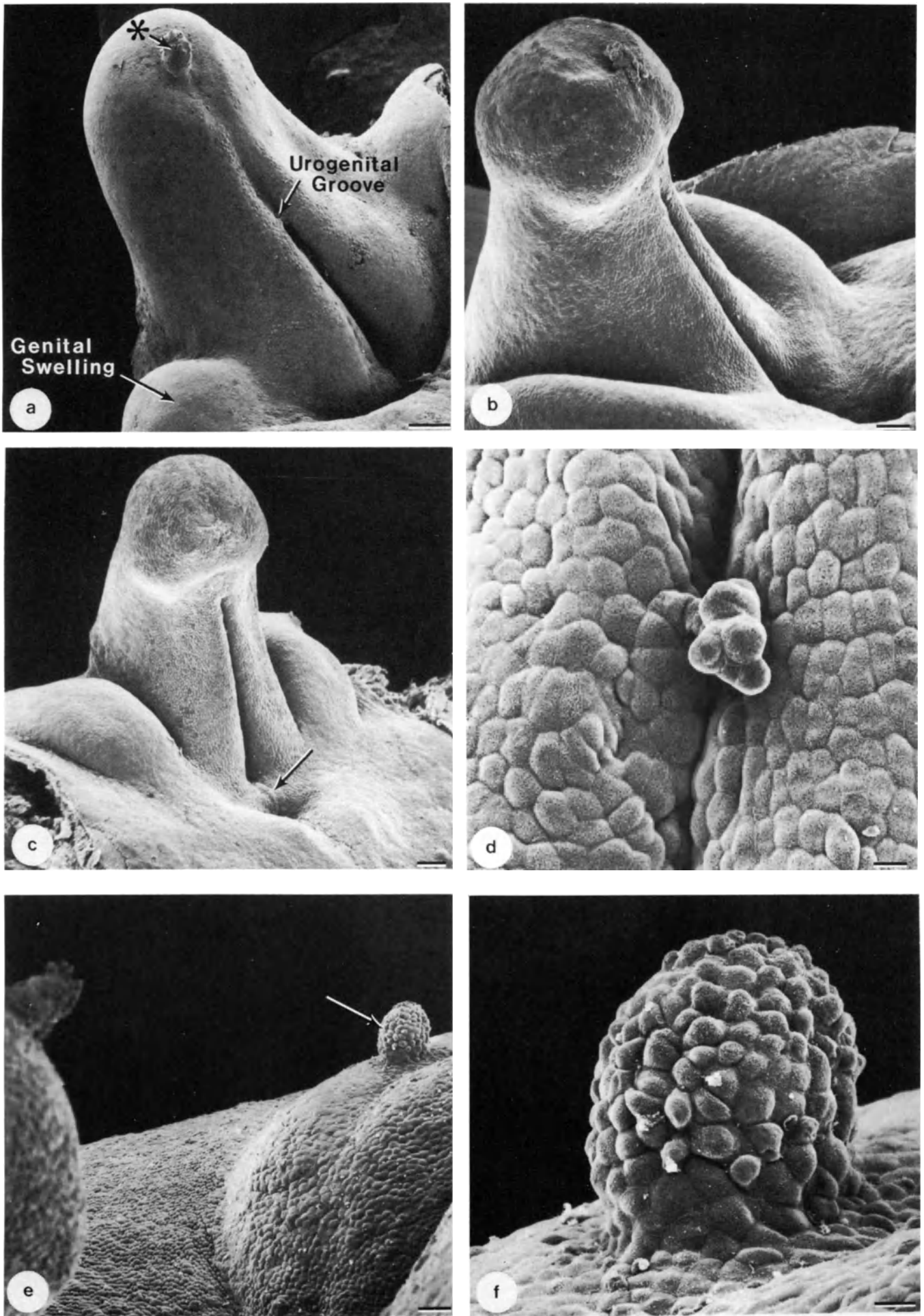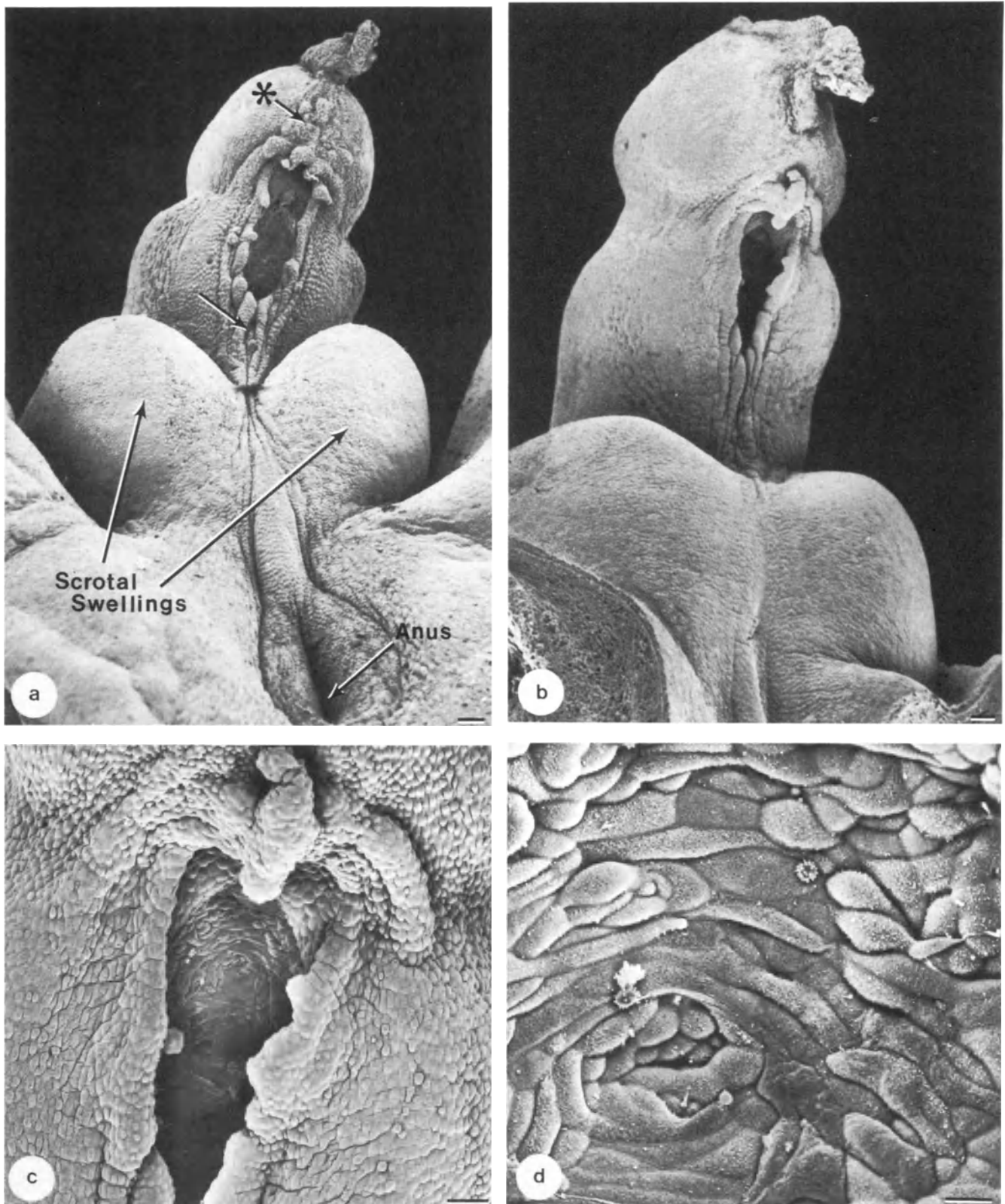
Figure 1

Figure 2 Stages of external genitalia development

a: Ventral view of the phallus of a male fetus at the end of the 9th or early 10th week. The proximal ends of the irregular margins of the urogenital folds (arrow) are in the process of fusing to elongate the penile urethra. The relatively large scrotal swellings are approaching one another in the midline. The location of the urethral plate within the developing glans penis is indicated by surface irregularities (*) in the midline between the urogenital groove and epithelial tag. The male urethra is completed during the 4th month by canalization of this epithelial plate (bar=100 μm)

b: Developing penis from an embryo slightly older than that in Figure 2a. Fusion between the urogenital folds to form the penile urethra has increased. The line of fusion will be marked by the midline penile raphé which is continuous with the raphé between the joined scrotal swellings. Fusion of the urogenital folds is complete by the end of week 12 (bar=100 μm)

c: Higher magnification of the unfused urogenital folds from the penis shown in Figure 2b. Cells of the urethral plate which line the developing urethra may be seen through this opening and are shown at higher magnification in Figure 2d (bar=50 μm)

d: Many cells of the urethral plate indicated in Figure 2c are elongated, and the surface is quite irregular (bar=10 μm)

along the dorsal body wall. The first few sets of tubules form early in the 4th week and have been referred to as the pronephros, although this may not be appropriate (O'Rahilly and Muecke, 1972). Subsequent generations of tubules which develop sequentially in a cranio-caudal manner constitute the mesonephros. These mesonephric tubules fuse with the mesonephric duct which grows toward, and eventually opens into, the developing urinary bladder.

The adult kidney, or metanephros, begins to develop late in the 4th week from two primordia:

(1) the future ureters and collecting ducts develop from ureteric buds which appear as diverticula from each mesonephric duct near the wall of the bladder; and

(2) nephrogenic tubules which form from mesodermal cells of the nephrogenic ridges into which the ureteric buds grow.

The mesonephros largely degenerates as the metanephros enlarges, except for those portions which remain associated with the reproductive organs – particularly in the male. The metanephros appears to grow cranially into the abdominal cavity, which it reaches during the 8th week. Formation of glomeruli begins during the 8th week and continues during the fetal period (Figures 4a,c,e,g). While SEM studies of the complex cellular morphology of the kidney tubules and collecting ducts have been done in other species, similar information is lacking for the human.

ADRENAL GLAND

The adrenal glands in man form from two separate primordia; the medulla containing chromaffin cells of neural crest origin, and the cortex derived from mesoderm. The adrenal glands of the late embryonic and fetal periods are large organs relative to the metanephric kidneys (Figures 3a and 4a). Their size is due in large part to a collection of cells termed the 'fetal cortex' lying between the regions which will become the cortex and medulla of the adult gland (Figures 4b,e). The maximal size of the adrenal glands relative to the metanephric kidneys is reached at about 4 months. They are about one-third the size of the kidney at birth, and the fetal cortex rapidly involutes after birth (Jones, 1968a).

EPIDERMIS

The epidermis is generally two cells thick by the end of the 8th week. The outer cellular layer, or periderm, exhibits a series of morphological changes and is lost when epidermal karatinization is complete (Holbrook and Odland, 1975). Although significant variations exist over the body surface (Figure 5), several stages of periderm morphology can be discerned. Prior to 36 days, the epidermis is one cell thick. A layer of the squamous periderm cells then appears. By 11–12 weeks many periderm cells begin to develop a central bleb of various morphology, and these are characteristic of all periderm cells from 85 to 110 days. They contain glycogen and become increasingly more complex in

shape as the periderm cells enlarge. The blebs then regress, and are nearly absent by about 160 days.

Complex blebs may detach and be recovered from the amniotic fluid. Complete periderm cells, however, are usually recovered only during regression of the periderm following keratinization of underlying epidermal cells.

ORAL CAVITY

Epithelial surfaces of the oral cavity have been examined by SEM in the human and compared to epithelial differentiation of the periderm of the epidermis (Adams, 1974). The tongue begins to develop near the end of the 4th week and by the 6th week consists of a set of elevations at the floor of the oral cavity (Figure 6a). These merge to form the characteristic shape of the tongue and papillae develop on its surface (Figures 6b–d). The palatal shelves (Figures 6e–g) have also been examined in some detail because of their importance to formation of the secondary palate in the interval from 7 to 12 weeks. A pattern of alterations in surface morphology which proceeds and mimics the pattern of contact and fusion between the medial edges of the bilateral shelves has been observed by SEM and correlated with histological and ultrastructural changes in the underlying region of presumptive fusion (Waterman and Meller, 1974; Meller and Barton, 1978). Some of these observations are summarized in Table 1.

CENTRAL NERVOUS SYSTEM (CNS) AND ORGANS OF SPECIAL SENSE

The CNS and associated organs of special sense present opportunities for examining the establishment of complex cellular organization which have not yet been adequately explored by SEM techniques in the human (Hattori and Fujita, 1974) (Figure 7). The neural folds begin to fuse early in the 4th week, and formation of the neural tube is completed with closure of the caudal neuropore a few days later (O'Rahilly and Gardner, 1971). Cells forming the wall of the neural tube then undergo a sequence of organized cell divisions and reorganizations to form the increasingly complex layers, nuclei and tracts which characterize the CNS (Figure 7d).

The cells forming the walls of the optic cups, which form as outgrowths of the diencephalic region of the neural tube, undergo a similar sequence of organized morphogenetic events leading to the establishment of the pigmented and neural components of the retina (Figures 7a–c).

The complex, changing patterns of blood vessels within embryonic and fetal organs, exemplified by the tunica vasculosa lentis which surrounds the lens (Figure 7e), may also be studied with the SEM. Such vascular beds are also potentially accessible to a variety of vascular casting and corrosion techniques similar to those successfully applied to non-human species.

CONCLUDING COMMENTS

Specimens for this study were obtained by suction

Table 1 Ultrastructural changes in medial edge epithelium of palatal shelves prior to and during formation of the secondary palate

Stage of palate development	Estimated age P.O.*	Anterior third	Middle third	Posterior third
I (Shelves vertical)	44–54 days	epithelium along entire medial edge two cells thick; surface cells polygonal, glycogen-filled, with numerous microvilli ('cobblestone' appearance); basal lamina intact		
II (Anterior ends horizontal and bulging)	54 days	surface cells flattened and elongated in small region overlying bulge; basal cells cuboidal	(as above)	(as above)
III (Shelves horizontal but not in contact)	54–57 days	surface alterations more prominent and spread to middle third; many cells flattened, intercellular gaps; thickness of medial edge epithelium variable; basal cells protrude into subjacent mesenchyme; sharp boundary between flattened medial epithelium and 'cobblestone' appearance of oral and nasal surface	(as above)	
IV (Shelves partially fused)	57 days	fused except for gap between shelves and primary palate	fusing	unfused; narrow band of surface alteration extends to posterior tip; surface cells flat; Ruthenium-red (R-R) binding to intercellular material within superficial layers of epithelium
V (Fused shelves united with primary palate-post ends unfused)	9 weeks	fused	fused	band of surface alterations is wider and more distinct; epithelial projections into mesenchyme; R-R binding by intercellular material
VI (Completion of soft palate and uvula)	10–12 weeks	(fused) midline ridge of elongated cells on oral and nasal surface marks site of fusion	(fused)	(fused) small midline cleft at tip of uvula as it forms and is rounded out

* Gestational ages based on information kindly supplied by Dr. R. O'Rahilly. These corrected estimates differ slightly from those in the original publications

Figure 3 (opposite)
a–g illustrate various features of the developing gonad and associated structures.

a: The anterior body wall and intestine have been removed from an embryo late in the eighth week to visualize the gonads, urogenital ridges which contain the paramesonephric and mesonephric ducts, metanephric kidneys, and adrenal glands. The gonads overlie the mesonephros. The caudal ends of the urogenital ridges join between the colon (posteriorly) and developing bladder (anteriorly) (see Figure 3d). Gubernacular folds extend laterally from the urogenital ridges and eventually merge with the connective tissue of the genital swellings. The cranial end of the left gonad is bent slightly toward the midline to allow visualization of the small fimbria (*) at the end of the paramesonephric duct. (Bar=100 μm).

b: The cranial ends of the gonad and fimbria (*) of the paramesonephric duct of an embryo in the eighth week. Bulge at lower right contains the mesonephros and mesonephric duct. (Bar=50 μm)

c: The relationship of the gonad, mesonephros, and urogenital ridge containing the mesonephric and paramesonephric ducts during the eighth week are seen in this cryofractured specimen. The pattern of sex (semi-niferous) cords within the gonad and the presence of a

developing tunica albuginea indicate this is a testis (Vossmeyer, 1971). The gonad is suspended by a mesorchium from the anterior aspect of the mesonephros. The smaller cellular cords within the gonad near the mesorchium represent the developing rete testis. (Bar=50 μm)

d: An embryo similar to that shown in Figure 3a dissected to illustrate the relationships of the gonad, fused urogenital folds (arrow), colon, gubernacular folds, and bladder. The umbilical arteries are seen on either side of the bladder (bar=100 μm)

e: An embryo similar to that in Figure 3d. The bladder has been dissected away except for a small projection, the Müllarian tubercle (arrow) on its posterior wall. This marks the caudal ends of the fused paramesonephric ducts and is shown at higher magnification in Figure 3g (bar=100 μm)

f: A portion of the gonad in Figure 3c is seen at higher magnification. The anastomosing sex cords containing both germ cells and supporting (Sertoli) cells are separated by cells of the interstitial mesenchyme (bar=10 μm)

g: The epithelium covering the Müllarian tubercle is seen in the midline of the posterior wall of the bladder between the openings of the mesonephric ducts. Compare relationships in Figures 3a, d and e (bar=10 μm)
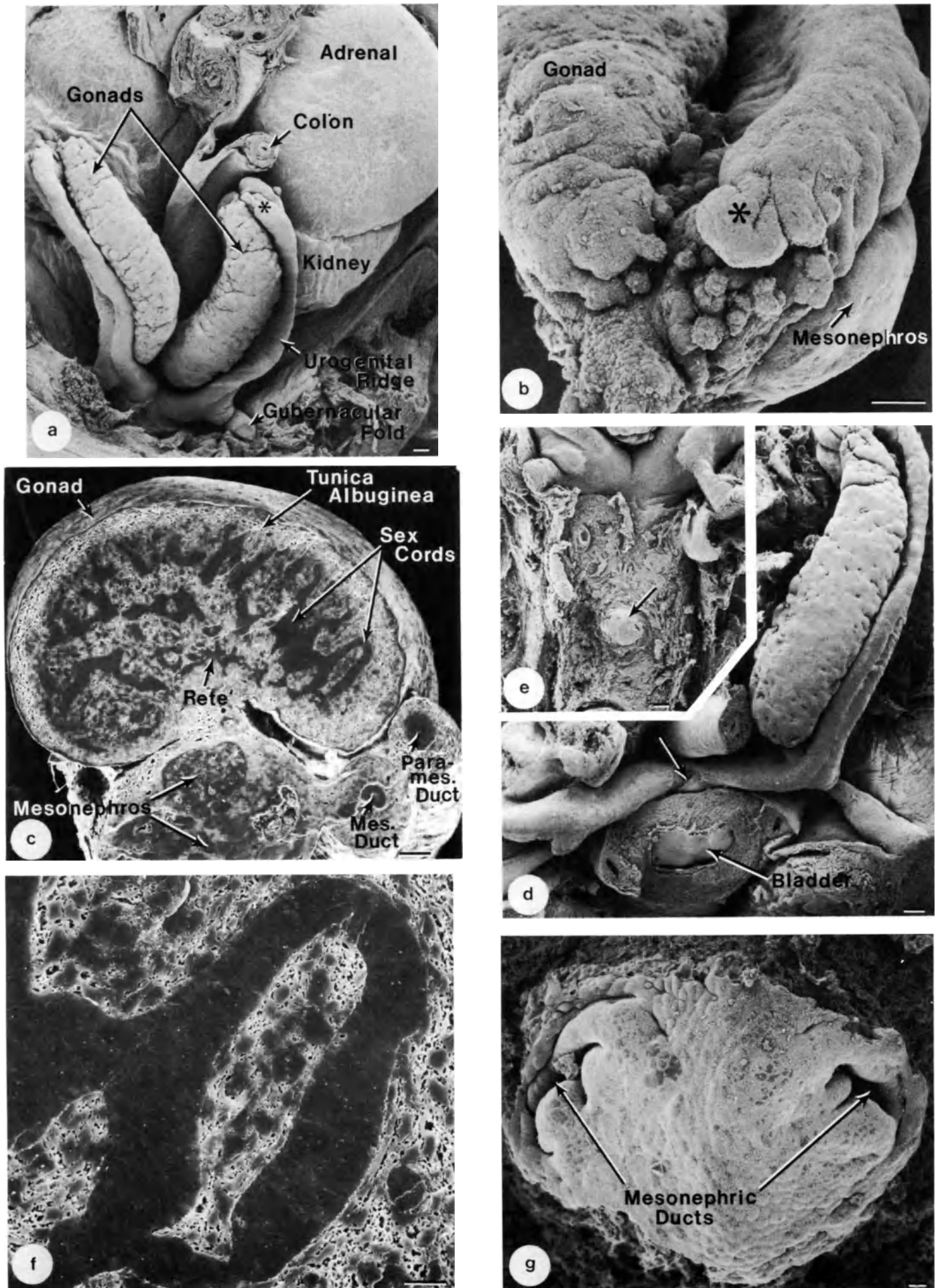
Figure 3

curettage and rapidly fixed by immersion in PAFG (Ito and Karnovsky, 1968) in which they remained for 7–8 years prior to dissection and examination. The quality of the images provided in this chapter suggest that many currently available embryonic specimens which have been stored in fixative for extended periods may be profitably examined by SEM. In addition, obtaining specimens specifically for SEM examination would allow rapid fixation and dissection to expose surfaces of interest, plus the use of procedures to minimize specimen shrinkage and other sources of artifact peculiar to SEM techniques. This should improve our understanding of the rapidly changing surface topography of developing organ systems in man. It is further hoped that examination of surface details by detection of secondary electrons will be combined in future investigations with the ability to embed and section scanned specimens, plus other currently available techniques of SEM methodology, to maximize the amount of information gathered from single specimens of known developmental age.

References

Adams, D. (1974). Surface coatings of cells in the oral epithelium of the human fetus. *J. Anat.*, 118, 61

Blick, U. (1979). Zur Entwicklung der Haut der Fingerbeere in der frühen Fetalperiode. *Virchows Arch. A. Pathol. Anat. Histol.*, 384, 213

Corliss, C. E. (1976). *Paten's Human Embryology*, pp. 1-470. (New York: McGraw-Hill)

Fallon, J. F. and Simandl, B. K. (1978). Evidence of a role for cell death in the disappearance of the embryonic human tail. *Am. J. Anat.*, 152, 111

Gasser, R. F. (1975). *Atlas of Human Embryos*. (Hagerstown, Md.: Harper & Row)

Glenister, T. W. (1954). The origin and fate of the urethral plate in man. *J. Anat.*, 88, 413

Gondos, B., Connell, C. J. and Lai, C. E. (1978). Scanning electron microscopy study of the human fetal testis. *SEM Symposium/1978*, pp. 1099–1104

Hattori, T. and Fujita, S. (1974). Scanning electron microscopic studies of matrix cells, and on development of neuroblasts in human and chick embryos. *J. Electron Microsc.*, 23, 269

Holbrook, K. A. and Odland, G. F. (1975). The fine structure of developing human epidermis: light, scanning, and transmission electron microscopy of the periderm. *J. Invest. Dermatol.*, 65, 16

Ito, S. and Karnovsky, M. J. (1968). Formaldehyde-glutaraldehyde fixatives containing trinitro compounds. *J. Cell Biol.*, 39, 168a

Jones, G. S. (1968a). Development of the adrenal. In Barnes, A. C. (ed.), *Intra-Uterine Development*, pp. 273–80. (Philadelphia: Lea & Febiger)

Jones, H. W. (Jr.) (1968b). Development of the genitalia. In Barnes A. C. (ed.), *Intra-Uterine Development*, pp. 253–72. (Philadelphia: Lea & Febiger)

Ludwig, H. and Metzger, H. (1977). Ciliogenesis in the human fetal oviduct. *SEM/IITRI*, 10, 361

Meller, S. M. and Barton, L. H. (1978). Extracellular coat in developing human palatal processes: electron microscopy and ruthenium red binding. *Anat. Rec.*, 190, 223

Moore, K. L. (1977). *The Developing Human*, 2nd edn, pp. 1–411. (Philadelphia: W. B. Saunders)

O'Rahilly, R. and Gardner, E. (1971). The timing and sequence of events in the development of the human nervous system during the embryonic period proper. *F. Anat. Entwickl.-Gesch.*, 134, 1

O'Rahilly, R. (1973). Developmental stages in human embryos. Part A: Embryos of the first three weeks (stages 1-9). Carnegie Institute Publication No. 631, pp. 1–167

O'Rahilly, R. and Muecke, E. C. (1972). The timing and sequence of events in the development of the human urinary system during the embryonic period proper. *Z. Anat. Entwickl.-Gesch.*, 138, 99

Pexieder, T. (1981). Prenatal development of the endocardium: a review. *SEM Symposium*, 2, 223

Shepard, T. (1975). Normal and abnormal growth patterns. In Gardner, L. I. (ed.), *Endocrine and Genetic Diseases of Childhood*, pp. 1–6. (Philadelphia: W. B. Saunders)

Spaulding, M. H. (1921). The development of the external genitalia in the human embryo. *Contr. Embryol. Carneg. Inst.*, 13, 67

Vossmeyer, J. (1971). Zur Cytologie der pränatalen Gonaden-Entwicklung beim menschen. I. Die Histogenese des Hodens, an Eponschnitten untersucht. *Z. Anat. Entwickl.-Gesch.*, 134, 146

Waterman, R. E. (1979). Embryonic and foetal tissues of vertebrates. In *Biomedical Research Applications of Scanning Electron Microscopy*. Vol. 1, chap. 1, pp. 1–125

Waterman, R. E. (1980). Preparation of embryonic tissues for SEM. *SEM Symposium*, pp. 20–44

Waterman, R. E. and Meller, S. M. (1974). Alterations in the epithelial surface of human palatal shelves prior to and during fusion: a scanning electron microscope study. *Anat. Rec.*, 180, 111

Figure 4 (opposite) Aspects of the developing metanephric kidney and adrenal gland

a: Sectioned specimen showing the relationship and relative sizes of the metanephros and adrenal gland during the 11th week (bar=500 μm)

b: Portion of the adrenal gland in a late 10, or early 11-week-old fetus. Cords of cells separated by vascular sinusoids form the bulk of the fetal cortex. The more compact cellular region beneath the capsule represents the future adult cortex. A portion of the fetal cortex is shown at higher magnification in Figure 4d (bar=50 μm)

c: Fractured surface of the metanephros in an 11-week embryo. Profiles of collecting ducts and associated nephrogenic (renal) vesicles are prevalent in the developing cortex (bar=50 μm)

d: Higher magnification from Figure 4b. Fractured cords of epithelial cells and associated sinusoids from the 'fetal' cortex of the adrenal gland (bar=10 μm)

e: Surface of a cryofractured kidney early in the 9th week. The fracture plane passes through the developing glomerular region of two nephrogenic vesicles (*) (bar=10 μm)

f: Fractured kidney in the 8th week. Bowman's capsule (visceral layer, VL; parietal layer, PL) and glomerulus are seen in a developing nephron of the inner cortex (bar=10 μm)

g: Cells of the visceral epithelium of Bowman's capsule from the kidney shown in Figure 4f. These future podocytes do not yet exhibit the extensively branching foot processes characteristic of the adult (bar=5 μm)
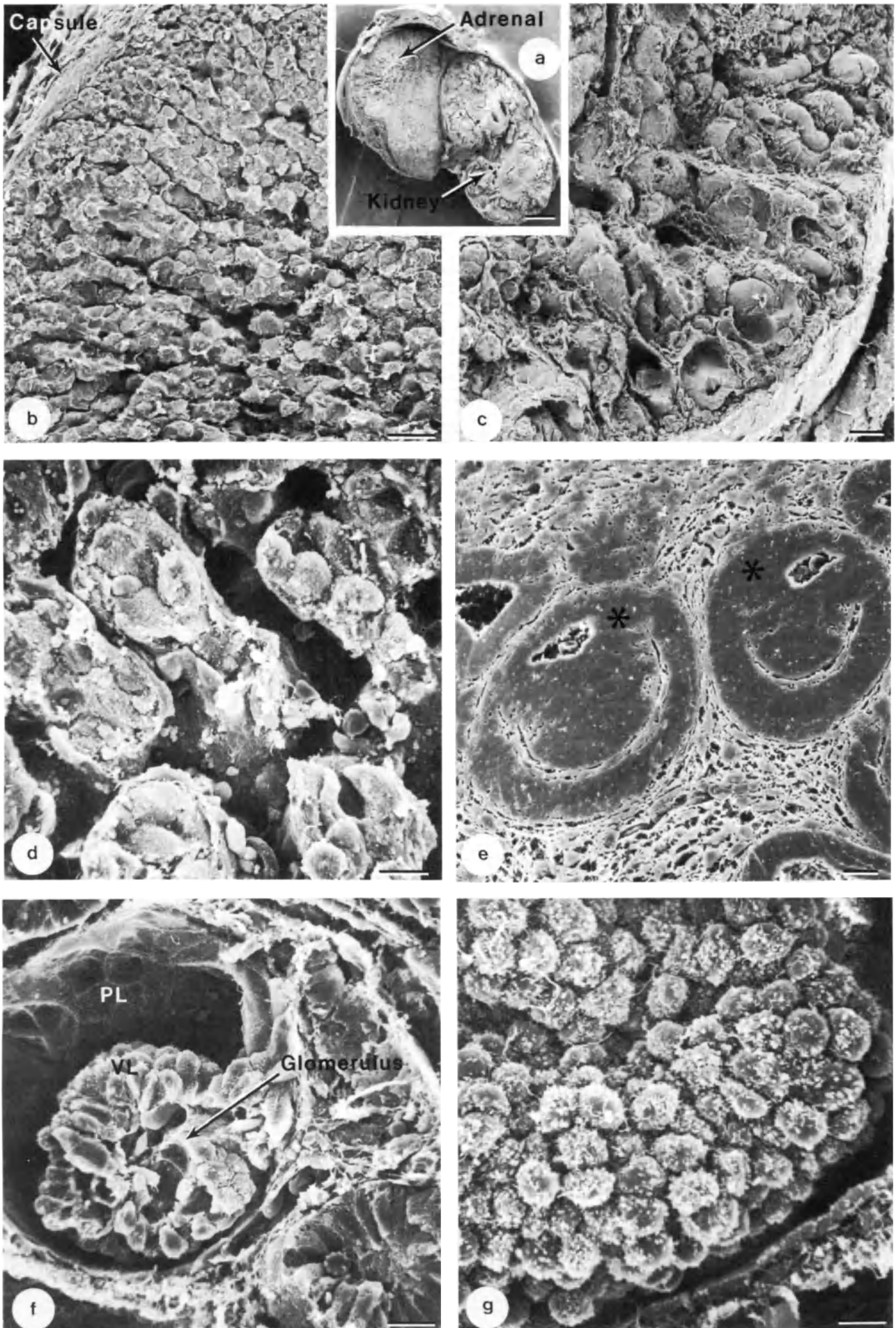
Figure 4

Figure 5 (opposite) Surface features of the developing integument

a: Plantar surfaces of the toes at the beginning of the 8th week. The enlargements on the dorsal surface at the tip of the digits are the nail fields (*) (bar=100 μm)

b: Periderm cells at the surface of the toes illustrated in Figure 5a are rounded and covered with short microvilli (bar=10 μm)

c: The surface of the nose during the 11th week. Each periderm cell has a central enlargement (bleb) projecting from the surface. These contain glycogen and represent a transient stage in the cycle of periderm differentiation (Holbrook and Odland, 1975) (bar=10 μm)

d: Transitional zone between the characteristic rounded periderm cells of the face and the squamous cells of the upper lip of an embryo in the 11th week (bar=10 μm)

e: Corneal surface and eyelids during the 8th week. The eyelids grow together and fuse completely during the 9th week (bar=100 μm)

f: External surface of the fused eyelids in a 10-week fetus. A ridge of epithelial cells marks the line of union between the upper and lower lids. The lids normally reopen during the 7th month (bar=10 μm)
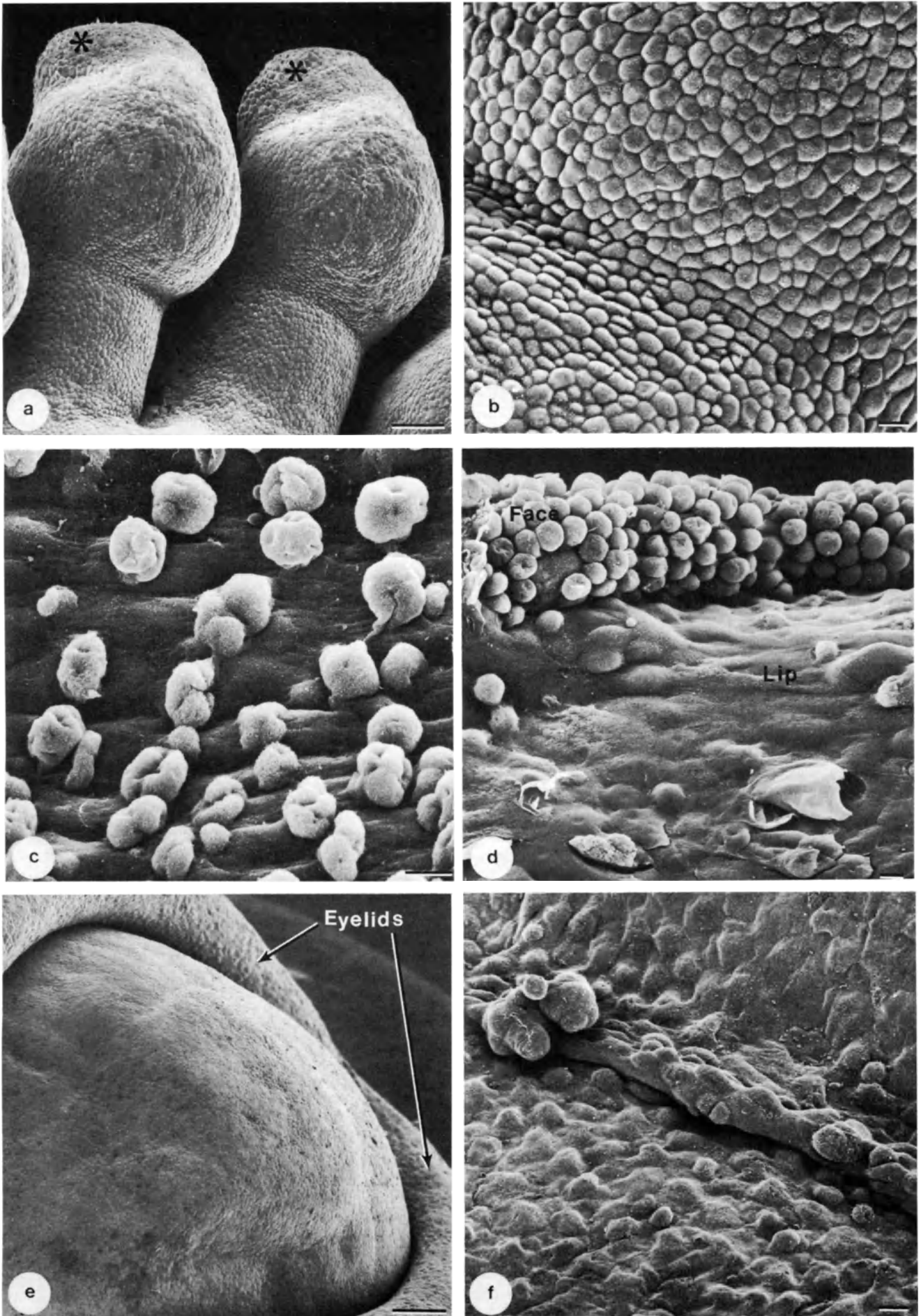
Figure 5

Figure 6 (opposite)

a–d illustrate the surface of the developing tongue

a: The floor of the oral cavity of an embryo in the 6th week has been exposed by cutting the pharyngeal arches and removing the roof of the oral cavity. The primordia of the developing tongue include the lingual swellings (LS) of the mandibular arch, the midline tuberculum impar (TI) and hypobranchial eminence (H), and contributions of the second and third arches (bar=100 μm)

b: Tongue from an embryo during the 8th week. The sulcus terminalis marks the approximate boundary between the anterior two-thirds and posterior third of the tongue. A midline depression, the foramen caecum (FC), marks the origin of the thyroid gland. The developing epiglottis (EP) is seen posterior to the base of the tongue (bar=100 μm)

c: The surface of the tongue during the 9th week is highly irregular due to the forming papillae (bar=100 μm)

d: Papillae at the lateral aspect of the tongue during the 11th week (bar=10 μm)

e–g represent three stages in formation of the secondary palate. The mandible and tongue have been removed to allow visualization of the oral surface of the palatal shelves. The upper lip and primary palate, formed during the 7th week, are toward the top

e: The shelves are vertically oriented at 54 days (stage 22; 8th week) (bar=500 μm)

f: The shelves have transposed to a horizontal position but have not begun to fuse in this 57-day embro (stage 23; early 9th week) (bar=500 μm)

g: Fusion between the medial margins of the palatal shelves and with the inferior surface of the nasal septum is nearly complete during the 9th week. Only a slight cleft is present at the posterior ends of the shelves in the region of the soft palate. Formation of the palate including the uvula is essentially complete by the 12th week (bar=500 μm)
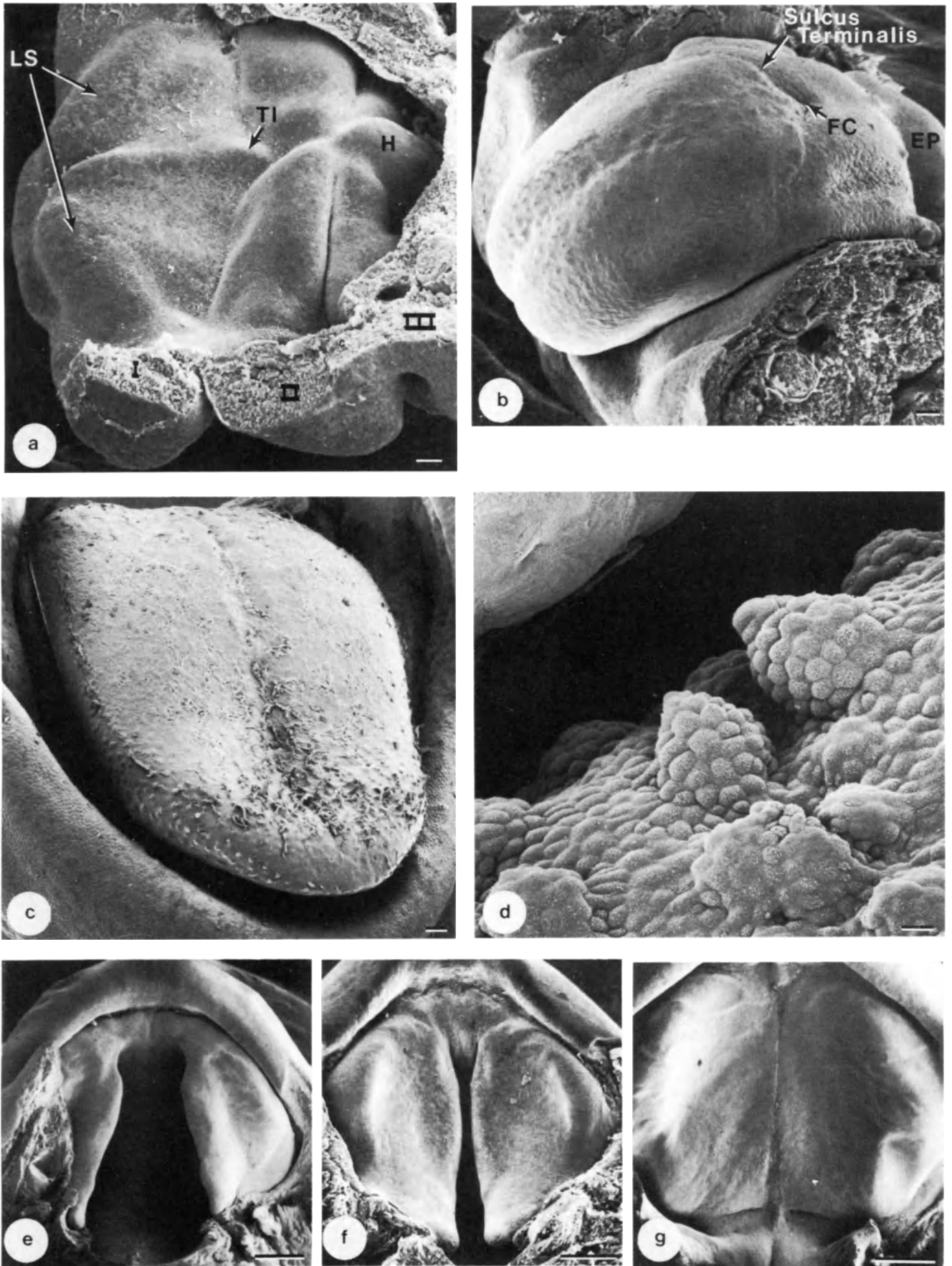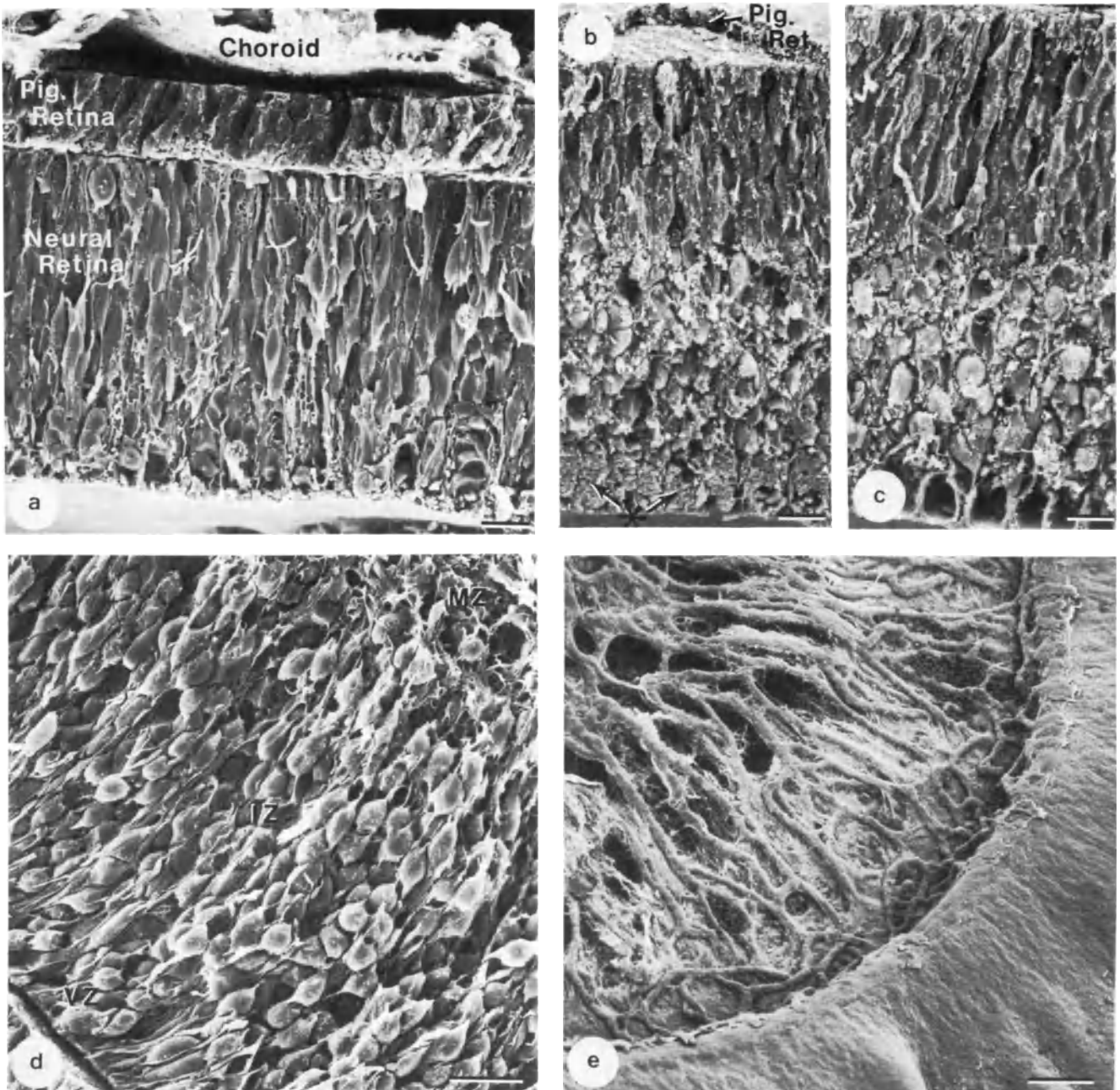
Figure 6

Figure 7

a: The pigmented and neural portions of the retina are demonstrated in this fracture through the equator of the eye near the beginning of the 8th week (bar=10 μm)

b,c: Nearly adjacent regions of the retina early in the 12th week illustrating the increased formation of cellular layers within the neural retina: (b) parallel bundles of axons coursing toward the optic nerve are present near the vitreal surface of the retina (*). These have been pulled away in (c) to show the processes of the Müller's cells which form compartments for, and align, the axons (bar b and c = 10 μm)

d: Fractured cross-section through the spinal cord during the 6th week. A ventricular zone (VZ) near the narrow lumen, intermediate zone (IZ) and narrow marginal zone (MZ) are present (bar=10 μm)

e: The lens has been removed from this eye of a 12-week-old fetus to allow visualization of the posterior aspect of the capillary network of the pupillary membrane which covers the anterior surface of the lens until the last month of fetal life when it is resorbed (bar=100 μm)

29

Hydatidiform mole

U. M. SPORNITZ* and E. S. E. HAFEZ†

* Anatomisches Institut der Universität Pestalozzistrasse 20, CH-4056 Basel, Switzerland
† Department of Gynecology and Obstetrics, Wayne State University, School of Medicine, Detroit, Michigan 48201, USA

A typical hydatidiform mole consists of grape-like clusters of vesicles of different sizes which contain an avascular edematous mesenchyme. The fluid-filled molar vesicles develop from chorionic villi. This trophoblastic lesion is believed either to originate from a so-called missed abortion of a blighted ovum, secondary to which the villous circulation has ceased (Hertig, 1968), or it is believed to be caused through a primary trophoblastic abnormality followed by a blighting of the embryo (Benirschke and Discroll, 1967). Much more controversial than the possible origin of hydatidiform moles, however, is their classification with respect to the origin of the lesion (cf. Scott, 1969). Hydatidiform moles represent only a part in the continuum of trophoblastic neoplasms ranging from hydatidiform degeneration to choriocarcinoma.

OUTER MOLAR SURFACE

There is a wide spectrum of trophoblastic growth and differentiation not only between different molar vesicles but also in different areas of the same vesicle. Four different surface modifications can be encountered (Figure 1):

(a) flat or smooth areas, which are sometimes slightly bulged, due to the underlying nuclei of the syncytiotrophoblast;
(b) areas with microridges, which often show a rhythmic pattern;
(c) areas with bulging folds, from which:
(d) hydropic villi often originate.

The varying amount of each of these modifications and their pattern of distribution on the molar surface are responsible for the great morphological variability observed in different hydatidiform moles.

Flat areas and microvilli

Molar vesicles originate from chorionic villi which have lost their fetal circulation and subsequently have accumulated large amounts of fluid. Concomitantly occurring with this accumulation of fluid there is a drastic alteration in the surface morphology which is caused through hyperplastic and anaplastic growth of the trophoblast.

In areas of the molar vesicles where this growth has not taken place, the surface closely resembles that of normal trophoblast of similar gestational age (Ferenczy and Richart, 1972). The syncytiotrophoblast is relatively flat and smooth and does not possess major undulations or projections in these areas. In contrast to normal trophoblast of the same gestational age, however, trophoblastic sprouts are relatively rare.

The free surface of the syncytium is covered by a profusion of two different types of microvilli. The most frequently occurring microvilli are of the ordinary straight type, which is similar to the normal microvilli of other tissues. The second type of microvilli are complexly branched (Figure 2). As many as 20–25 microvillous projections originate from a common stem. These branched microvilli can be found all over the surface of the molar vesicles. This branched type of microvillus is the most frequent one. The microvilli of both types (straight and branched) do not have a uniform thickness but very often have bulbous swellings at the ends. Nude areas are extremely rare (Figure 2).

Areas with microridges

One-third to one-half of the molar surface is covered with microridges, which do not resemble microridges described in other parts of the female genital tract (Sherman, 1977). They are formed by undulations in the apical plasmamembrane of the syncytium measuring 1–2 μm in width. The invaginations between the individual microridges are up to 6 μm deep (Figure 2b). These microridges occur in stacks of up to 100 or more arranged in parallel arrays (Figure 3). They interconnect between strands of flat areas
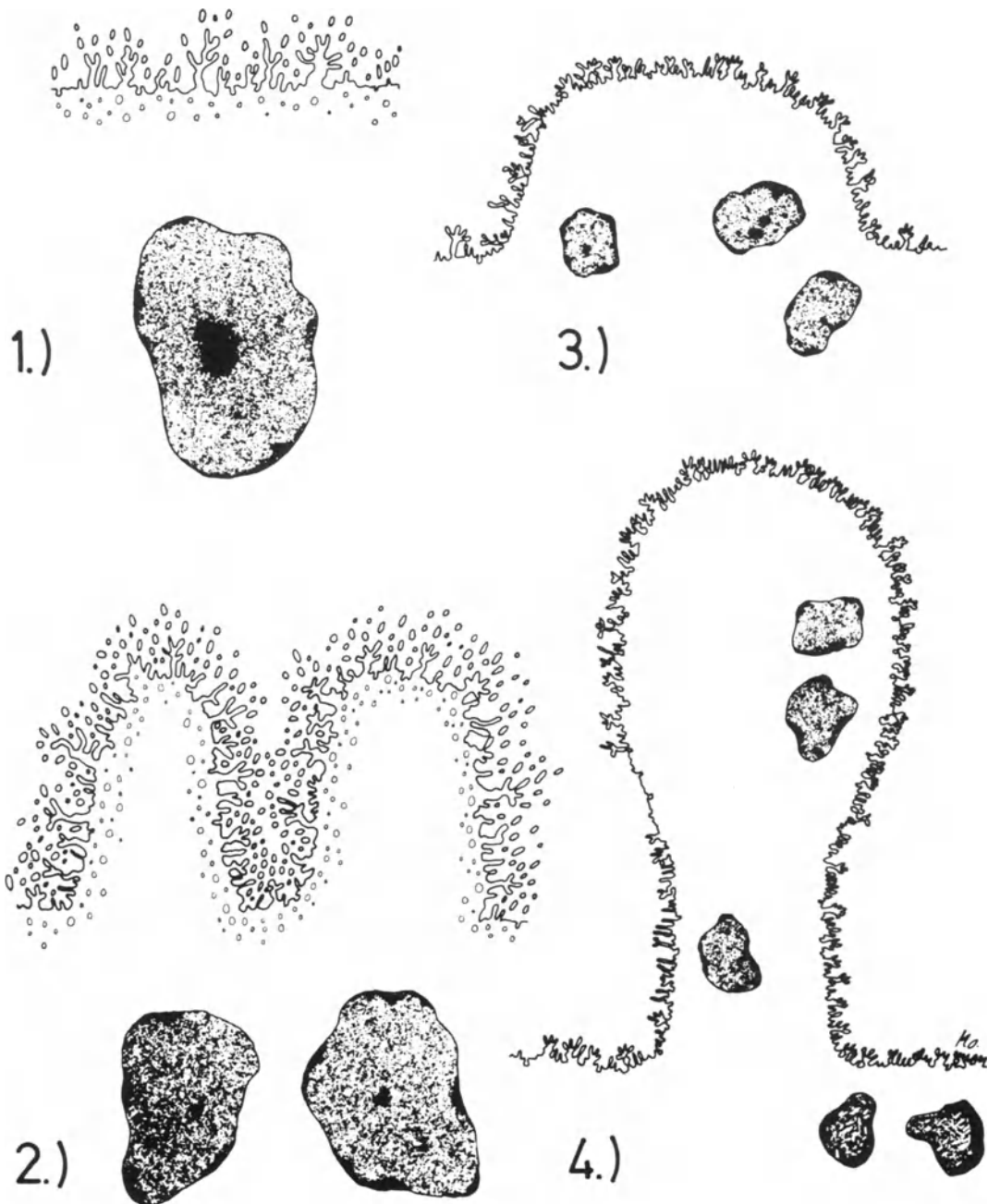
Figure 1 Schematic representation of four different surface specializations in hydatidiform moles:

a: flat area of syncytiotrophoblast with a mixture of normal and branched microvilli; note the pinocytotic vesicles

b: area with microridges also covered with branched microvilli

c: bulging folds which are formed by strands of flat overgrowth; these folds are closely related to the normal chorionic villi

d: hydropic villus which originates from trophoblastic sprouts; in many cases these hydropic villi have an edematous core

Figure 2 (opposite)

a: SEM of hydatidiform mole, showing two hydropic villi which are covered almost entirely by complexly branched microvilli. Up to 25 microvillous projections originate from a common stem. There are small nude areas on both hydropic villi (×1500)

b: TEM showing the apical region of the syncytiotrophoblast. The microridges formed in this

region are all covered with complexly branched microvilli, a fact which is hard to detect on TEM sections because of the unfavorable size of microvilli to thickness of section relationship. The apical cytoplasm is filled with lipid droplets and pinocytotic vesicles, the latter are particularly numerous in the microridges themselves (×8000)
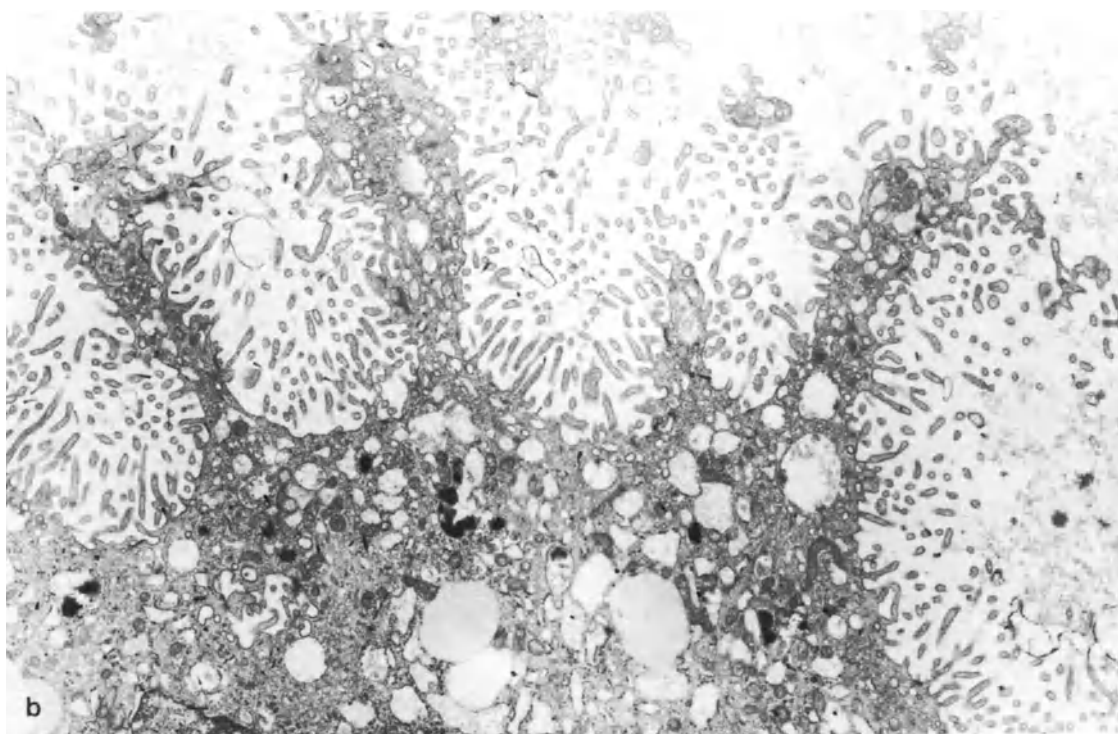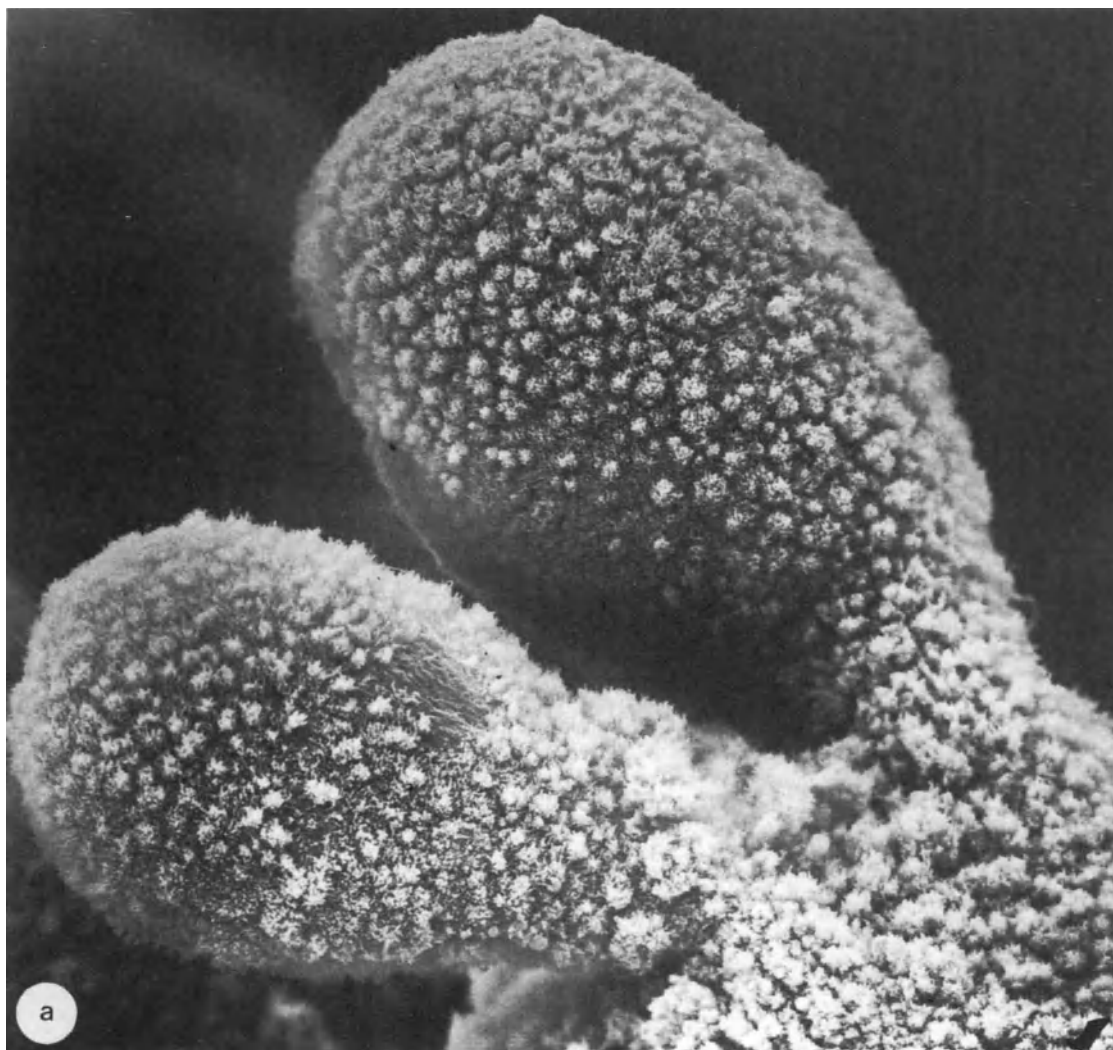
Figure 2

and/or bulging folds. The uppermost parts of these microridges are completely covered with complexly branched microvilli in contrast to the flat areas, or the areas of the bulging folds which are covered predominantly by the ordinary straight type of microvilli.

Areas with bulging folds

About one-third of the molar surface is covered with folds, which are either flat or bulging into the inter-villous space. These folds are up to 50 μm thick and 5–20 μm high. The largest parts of these folds are covered by the straight type of microvilli. In some areas, however, these folds are also covered with complexly branched microvilli (Figure 3).

The appearance of the folds ranges from bulging to flat overgrowths, where only the edges bordering the areas of the microridges are slightly rounded (Figure 3b). The folds are comparable to the cylindrical chorionic villi of the immature placenta. From the areas of the bulging folds very often the fourth surface modification of the molar vesicles originates, namely hydropic villi (Figure 4a).

Hydropic villi

Hydropic villi most frequently arise from the areas of the bulging folds. Contrary to the bulging folds themselves which are covered by the straight type of microvilli, the hydropic villi are covered by the complexly branched microvilli. The hydropic villi are very heterogeneous in appearance (Figures 4a,b). They range from very small sprouts comparable to the trophoblastic sprouts in immature placenta (Ferenczy and Richart, 1974), to very large hydropic villi, measuring up to 300 μm. Most of the hydropic villi have a drop-like shape and are connected to the underlying folds or microridges by means of a thin stem of trophoblast material. Because of the heterogeneity (compare e.g. Figures 4a,b) in size as well as in shape, these hydropic villi account for most of the variability in the morphology of the molar vesicles. Both the areas of the bulging folds and the hydropic villi appear to be actively growing, the growth, however, being rather uncontrolled. The smaller hydropic villi consist mainly of solid tissue, while the larger have an edematous core of mesenchyme-like connective tissue.

BASEMENT MEMBRANE

Through gaps in the underlying mesenchyme and the connective tissue elements, the basement membrane can be viewed from the luminal side. It has a very rough appearance which is caused through ruffles and ridges of very minute dimensions. Reticular or collagenous fibers inserting in the lamina densa of the basement membrane seem to be penetrating through the basement membrane. Some of them are apparently comparable to anchoring fibrils of other tissues (e.g. the cervix, Spornitz and Hafez, 1982). Globular structures ranging between 500 and 1500 Ångström in size also add considerably to the rough appearance of

the luminal face of the lamina densa. These particles seem to be permeating through the basement membrane.

After removal of the trophoblast, i.e. the syncytio- as well as the cytotrophoblast, relatively large areas of the basement membrane become exposed from the epithelial side. The appearance of the epithelial side of the basement membrane is much smoother than that of the luminal side. The large undulations which are present replicate exactly the undulations of the basis of the cytotrophoblast. At higher magnification, numerous fibers become clearly visible. These fibers are continuous with fibers from the other side. No discontinuities can be detected in the basement membrane, although an exchange of material through the basement membrane certainly must occur. The very few holes found in the basement membranes are due to mechanical injury during preparation.

FRACTURE FACES

Through intentonal fracturing, the molar vesicles expose a fracture face which corresponds to TEM sections. Despite the similarity shown by both methods, SEM fracture faces differ in certain aspects from TEM sections (Table 1). The trophoblast exposed by fracturing differs in thickness not only from one molar vesicle to another but also within the same molar vesicle. Much more differs, however, such as the amount of connective tissue under-lying the trophoblast. In smaller vesicles, the connective tissue elements fill out the vesicles completely, i.e. the smaller vesicles do not have a real lumen. In the smaller as well as in the larger vesicles most of the connective tissue consists of collagen, which forms a network in which on the one hand mesenchyme-like connective tissue cells are located and on the other hand the molar fluid has accumulated. The fracture faces also very clearly prove what has been known from TEM sections (Wynn and Davies, 1964), namely, that the connective tissue of molar vesicles is completely avascular (Figure 4c). In the larger molar vesicles, the connective tissue layer does not fill out the vesicles completely but forms a rim of connective tissue, which is between two and five times thicker than the layer of the trophoblast.

Figure 3 (opposite)
a: Area with microridges and folds. The microridges interconnect between the two major folds on this micrograph. Sometimes stacks of up to 100 individual microridges can be found. In contrast to the folds, the microridges are always covered with complexly branched microvilli (×1000)
b: The irregular and uncontrolled growth which occurs in some areas of the molar vesicles is best documented with these overgrowing folds. The folds are closely related to normal chorionic villi. Note the trophoblastic sprout in the lower right corner of the micrograph. There are several microridges interconnecting between folds on the right-hand side. The folds are covered with normal microvilli (×850)
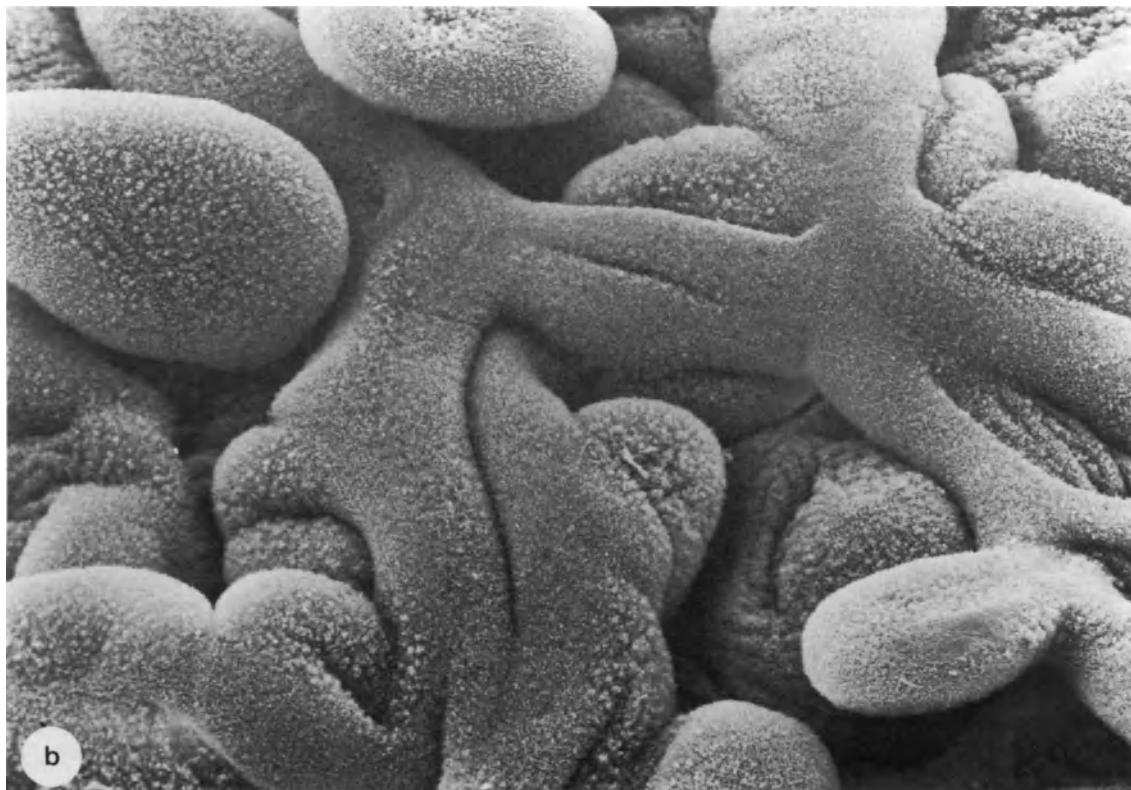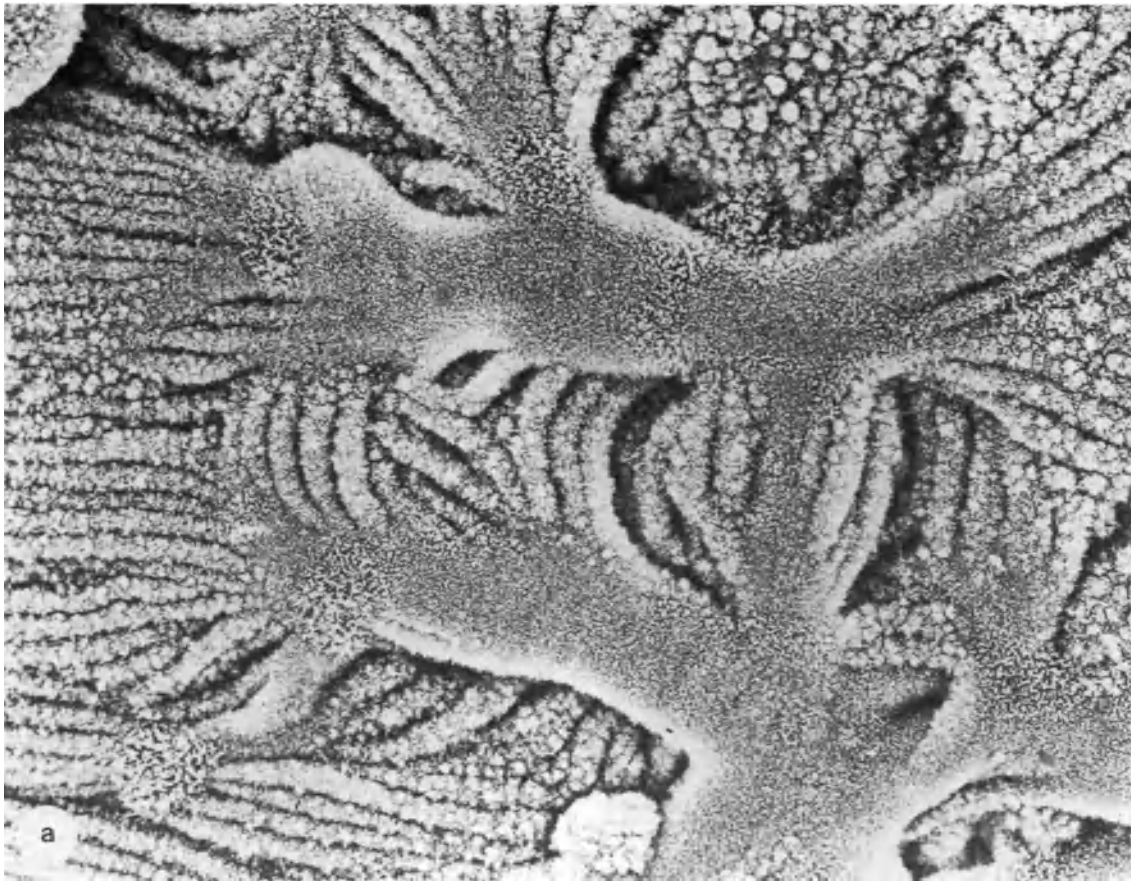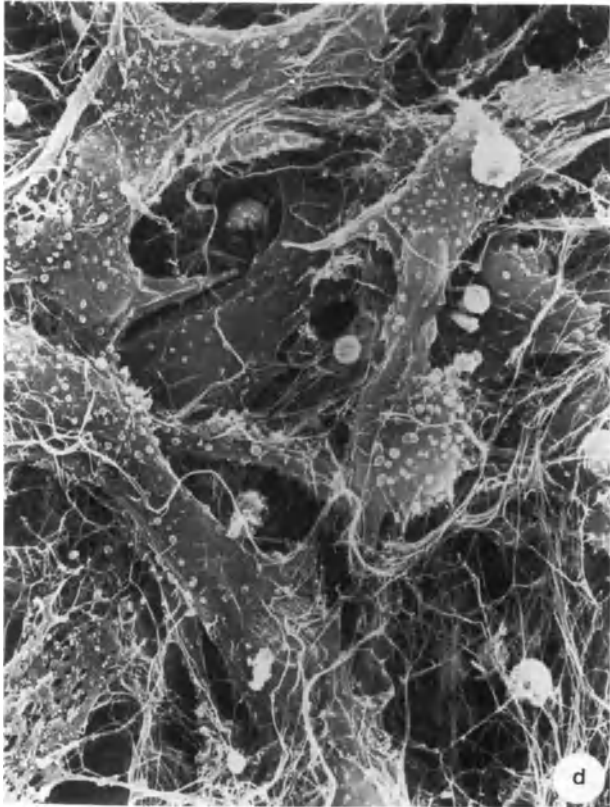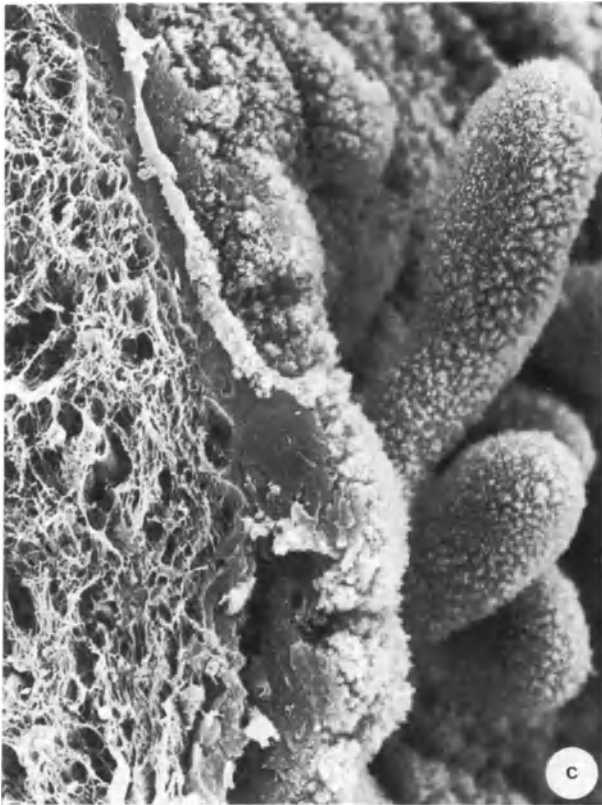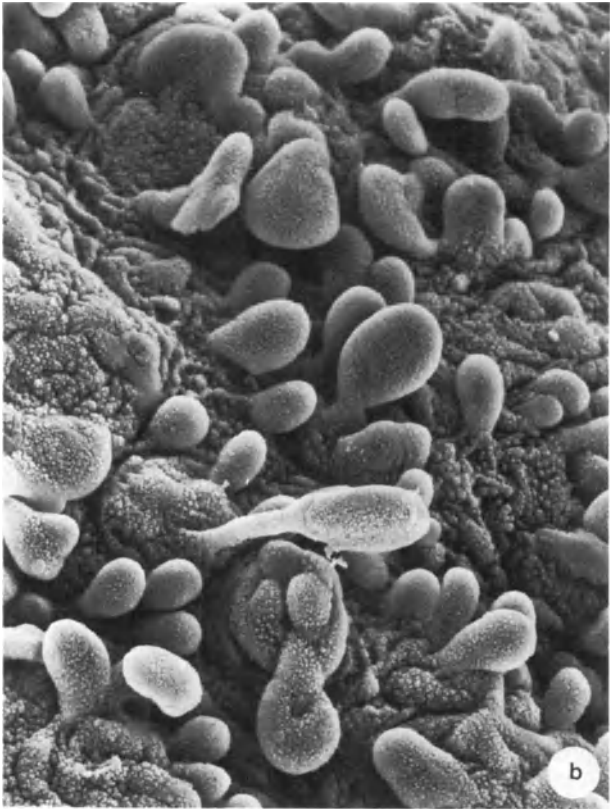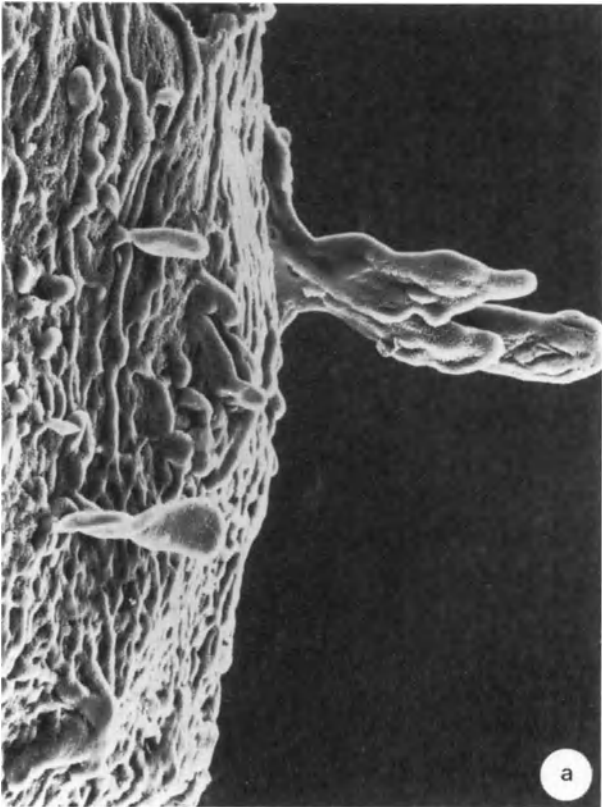
Figure 3

Figure 4

Table 1   Histological and ultrastructural characteristics of molar vesicles

Vesicles	Histological and ultrastructural characteristics
Syncytiotrophoblast	always present, syncytium in smaller molar vesicles interrupted by individual cells
pinocytosis	very pronounced, more than normal in syncytiotrophoblast (Ashley, 1965; Terzakis, 1963)
mitochondria	moderate number of small mitochondria
lipid droplets	high number ranging between 0.5 and 1 μm in diameter, always located in the apical region of the syncytium; related to steroid synthesis? (Gonzalez-Angulo, 1966)
RER	quite prominent, all over the syncytium, dilated; probably due to fixation (Schweikhart and Kaufmann, 1977)
SER	small areas scattered all over the syncytium, always associated with glycogen
Golgi apparatus	inconspicuous, mostly vesiculated
crystalline inclusion bodies	present in high numbers all over the syncytium (Figure 5b), related to HCG? (Midgley and Pierce, 1962)
nuclei	always in groups of three or four, some with irregular profiles as they frequently occur in immature placenta (Martin and Spicer, 1973)
Transitional cells (Intermediate cells)	absent in most cases, morphology intermediate between syncytio- and cytotrophoblast
Cytotrophoblast cells	occasionally absent, in which case the syncytiotrophoblast rests directly on the basement membrane
pinocytosis	not detectable
mitochondria	few but large, with well-developed cristae
lipid droplets	practically none
RER	not very pronounced
SER	not very pronounced
Golgi apparatus	4–5 dictyosomes present on the average section, appears to be active
glycogen	not detectable
nuclei	normal appearance, mitotic figures occasionally present
Basement membrane	always present, always continuous

Figure 4 (opposite)

a: Large areas of the molar vesicles are covered with trophoblastic sprouts and hydropic villi. The hydropic villi are connected to the underlying syncytiotrophoblast by means of a relatively thin stem (×212)

b: Some of the hydropic villi are extremely long. The group in the center of this micrograph measures about 350 μm. The heterogeneity of different molar vesicles is due to the varying percentage of the four molar surface specializations and their pattern of distribution (×127)

c: Intentionally fractured molar vesicle. This micrograph shows a relatively thin layer of trophoblast from which hydropic villi originate (upper part of the micrograph). The lower half of the micrograph shows the avascular connective tissue core of the molar vesicle. The fibers are mainly collagen fibers. Cellular elements are very sparse (×595)

d: Luminal surface of a smaller molar vesicle showing an area where mesenchymal cells form a typical network. The surface of the cells is studded with secretory droplets. The larger spherical structures like the one in the center of the micrograph are 'molar inclusion bodies' (×340)
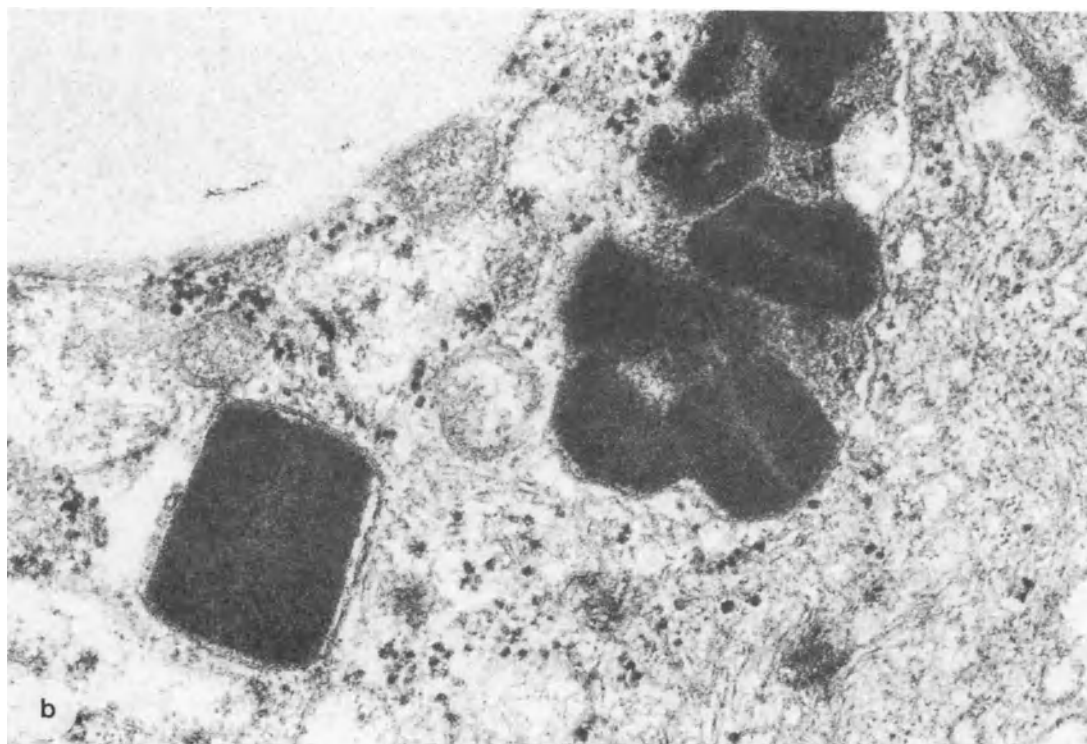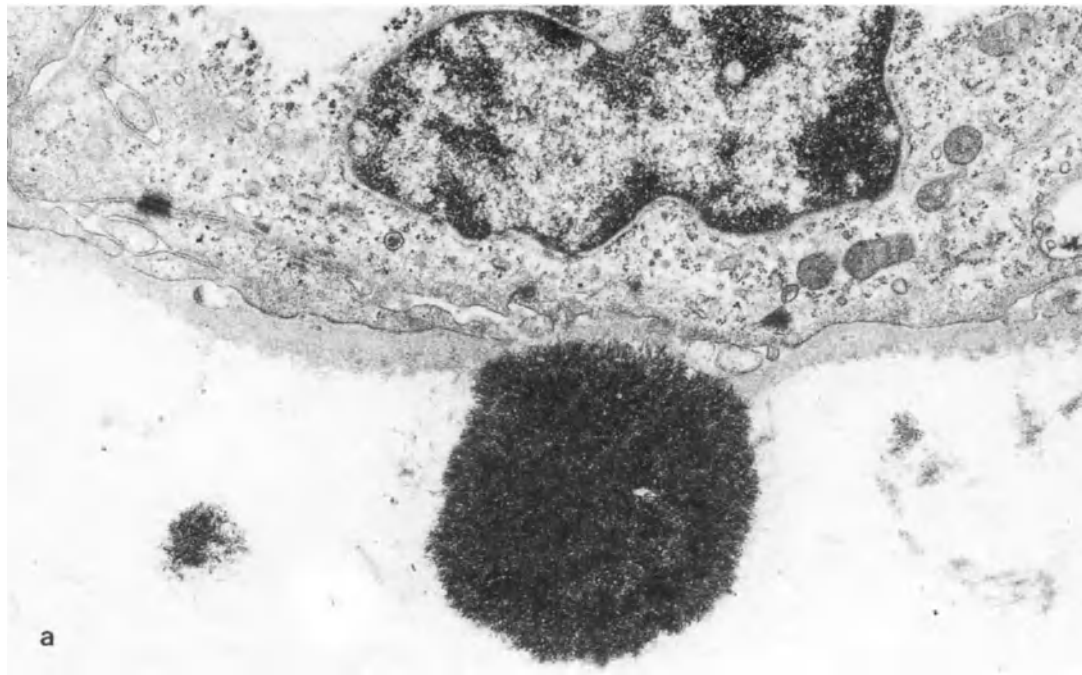
Figure 5

a: Typical molar inclusion body in direct contact with the basement membrane of a cytotrophoblast cell. Stained with uranyl acetate and lead citrate. The electron-dense substructure is, however, also present on unstained sections (×15 000)

b: The syncytiotrophoblast contains numerous para-crystalline inclusions which are bounded by a single membrane. These inclusions are present neither in cytotrophoblast cells nor in the transitional cells. They are probably related to HCG production which is elevated in patients with molar trophoblast (×60 000)

THE LUMINAL SURFACE

During the process of fixation, and particularly during dehydration, the elements of the spongy mesenchyme-like connective tissue do not remain suspended in the molar fluid and therefore collapse to become affixed to the vesicular wall, i.e. the trophoblast. For this reason the connective tissue as viewed from the luminal side appears to be much more compact than could be expected from both transmission and light micrographs. In most areas the luminal surface of the molar vesicles consists predominantly of collagen, which frequently is arranged in coarse bundles. The morphology and orientation of mesenchymal connective tissue cells is intermediate between mesenchymal cells and fibroblasts. The surface of most of these connective tissue cells is studded with bead-like particles ranging between 1 and 2 μm in size (Figure 4d). At higher magnification, some of these beads appear to be blebbing from the plasma membrane of the cells.

Despite the fact that vessels in the molar vesicles cannot be detected, red blood cells are present quite frequently in the network of the collagen fibers of the connective tissue. This is more often the case in the very large than in the smaller or medium-sized vesicles, and is perhaps due to a rupture of the molar vesicle as it occurs during suction evacuation of the molar tissue or as a result of a perforation of the vesicles due to an extreme accumulation of molar fluid.

CONTENTS OF MOLAR VESICLES
(EDX of molar inclusion bodies)

The fluid of the molar vesicles differs considerably in composition from the maternal serum. It contains less protein and more amino acids. It retains water on the fetal side of the early trophoblast against the force of higher osmotic pressure in the surrounding maternal serum. And finally, among many other differences, the iron and calcium contents of the vesicular fluid are much lower than in the maternal blood serum (McKay et al., 1955, 1958). TEM and semi-thin section prepared for light microscopic investigation reveal in molar vesicles a structural component suspended in the molar fluid. TEM pictures show these inclusion bodies to range between 2 and 5 μm in diameter (Figure 5a). They appear predominantly in the larger molar vesicles and are located in the vicinity of the basement membrane where they sometimes even seem to be incorporated into the basement membrane. They are also located in the layer of connective tissue where they are usually connected to collagen fibers. X-ray microanalysis shows that they contain among other less important elements calcium and iron (Figure 6). These molar inclusion bodies resemble bodies found in human placental villi during late pregnancy (Salazar and Gonzales-Angulo, 1967) and they also resemble bodies found in the chincilla placenta (King and Tibbitts, 1976). Salazar and Gonzalez-Angulo believed them to be the sites of blockage of iron transport. With the missing fetal circulation a need for further transport of calcium and iron is no longer given, thus it would only be logical that, if the trophoblast continues to transport iron and calcium from the maternal blood into the molar lumen, these two substances precipitate in the form of molar inclusion bodies. This might even be an explanation for the fact that eventually the iron and calcium content of the vesicular fluid is lower than that of the maternal serum (McKay et al., 1958).

CONCLUDING REMARKS

It is very difficult to interpret the surface morphology in three dimensions from TEM pictures. Therefore it has so far escaped the attention of most investigators that the surface of the molar trophoblast is not only bordered by straight microvilli but also complexly branched microvilli (e.g. Cesarini et al., 1967; Gonzalez-Angulo et al., 1966; Okudaira and Strauss, 1967; Wynn and Davies, 1964). Furthermore, the presence of bulging folds and particularly of microridges could not possibly have been reconstructed from transmission electron micrographs. However, with the information obtained from scanning electron micrographs it becomes very easy to detect not only the hydropic villi on TEM sections but also the bulging folds, microridges and complexly branched microvilli. It is important to realize that neither the absence nor presence of either the transitional cells or the cytotrophoblast cells influences the surface morphology of the syncytiotrophoblast.

The complexly branched microvilli and the microridges and folds may all be regarded as an increase in surface area, which is of particular importance since the maternal circulation is the only source of nutrition for the trophoblast. However, the microridges are unique structures which might well play a role other than just increasing the cell surface area, e.g. in the pathogenetic events leading to malignancy.

References

Ashley, C. A. (1965). Study of the human placenta with the electron microscope. Arch. Pathol., 80, 377

Benirschke, K. and Discroll, S. E. (1967). The Pathology of the Placenta. (New York: Springer Verlag)

Cesarini, J. P., Berebbi, M., Aymé, Y., Ruf, H. and Bonneau, H. (1967). Quelques aspects de l'ultrastructure d'un cas de môle hydatidiforme et d'un cas de chorio-epithéliome. Gyn. Obstet. (Paris), 66, 303

Ferenczy, A. and Richart, R. M. (1972). Scanning electron microscopic study of normal and molar trophoblast. Gynecol. Oncol., 1, 95

Ferenczy, A. and Richart, R. M. (1974). Female Reproductive System: dynamics of scan and transmission electron microscopy. (New York: John Wiley)
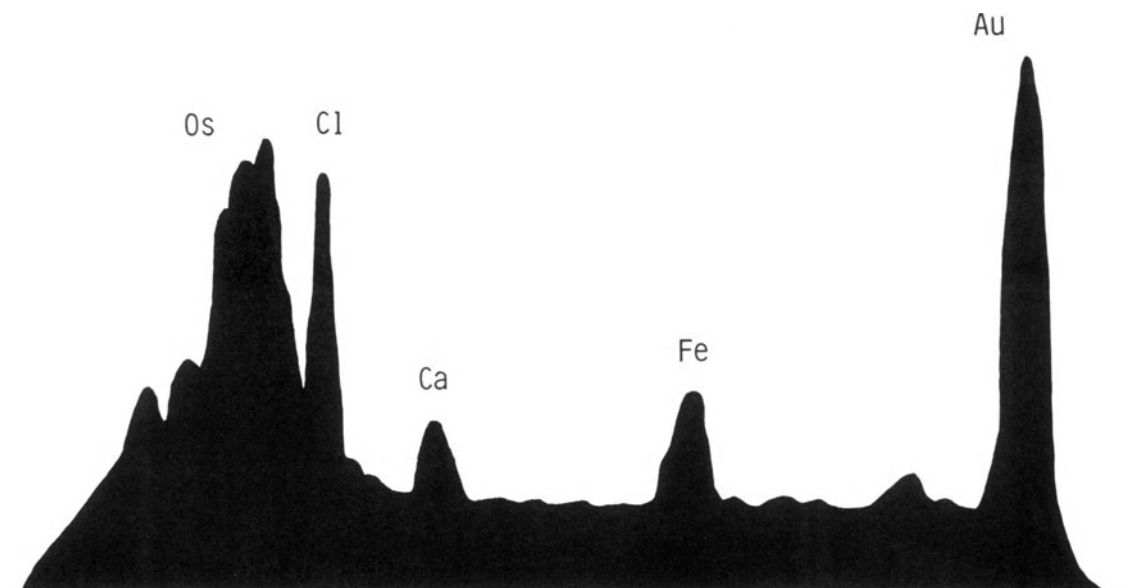
Figure 6 Energy-dispersive X-ray spectrogram (EDX). The Os, Cl and Au peaks are due to osmium fixation, epoxy-embedding and the gold grid used for X-ray analysis. The calcium and iron peaks are typical for molar inclusion bodies. In the absence of a fetal circulation the molar inclusion bodies can be regarded as precipitates caused through the continuing transport function of the trophoblast

Gonzalez-Angulo, A., Marquez-Monter, H., Zavala, B. J., Yabur, E. and Salazar, H. (1966). Electron microscopic observations in hydatidiform mole. *Obstet. Gynecol.*, **27**, 455

Hertig, A. T. (1968). *Human Trophoblast*. (Springfield: C. C. Thomas)

King, B. F. and Tibbitts, F. D. (1976). The fine structure of the Chinchilla placenta. *Am. J. Anat.*, **145**, 33

Martin, B. J. and Spicer, S. S. (1973) Ultrastructural features of cellular maturation and aging in human trophoblast. *J. Ultrastruct. Res.*, **43**, 133

Midgley, A. R. and Pierce, G. B. (1962). Immunohistochemical localization of human chorionic gonadotropin. *J. Exp. Med.*, **115**. 289

McKay, D. G., Roby, C. C., Hertig, A. T. and Richardson, M. V. (1955). Studies of the function of early human trophoblast. I. Observations on the chemical composition of the fluid of hydatidiform moles. *Am. J. Obstet. Gynecol.*, **69**, 722

McKay, D. G., Richardson, M,. V. and Hertig, A. T. (1958). Studies of the function of early human trophoblast. III. A study of the protein structure of mole fluid, chorionic and amniotic fluids by paper electrophoresis. *Am. J. Obstet. Gynecol.*, **75**, 699

Okudaira, Y. and Strauss, L. (1967) Ultrastructure of molar trophoblast. Observations on hydatidiform mole and chorioadenoma destruens. *Obstet. Gynecol.*, **30**, 172

Salazar, H. and Gonzalez-Angulo, A. (1967). The fine structure of human chorionic villi and placental transfer of iron in late pregnancy. *Am. J. Obstet. Gynecol.*, **97**, 851

Schweikhart, G. and Kaufmann, P. (1977). Problems of distinction of normal, arteficial and pathological structures of mature human placental villi. I. Ultrastructure of the syncytiotrophoblast. *Arch. Gynäkol.*, **222**, 213

Scott, J. S. 1969). Blasenmole und Chorionepitheliom. In Käser, O. (ed). *Gynakologie und Geburtshilfe. Vol. I. Die geschlechtsspezifischen Funktionen der Frau und ihre Störungen*. (Stuttgart: G.Thième)

Sherman, A. I. (1977). Comparison of cancer cell surfaces of the lower reproductive tract by scanning electron microscopy. *Am. J. Obstet. Gynecol.*, **129**, 893

Spornitz, U. M. and Hafez, E. S. E. (1982). The morphology of the basement membrane in carcinoma of the cervix.To appear in Hafez, E. S. E. and Smith, J. (eds). *Carcinoma of the Cervix*. (The Hague: Martinus Nijhof)

Terzakis, J. A. (1963). The ultrastructure of normal human first trimester placenta. *J. Ultrastruct.*, **9**, 268

Wynn, R. M. and Davies, J. (1964). Ultrastructure of hydatidiform mole: correlative electron microscopic and functional aspects. *Am. J. Obstet. Gynecol.*, **90**, 293

IV   SPECIAL TECHNIQUES
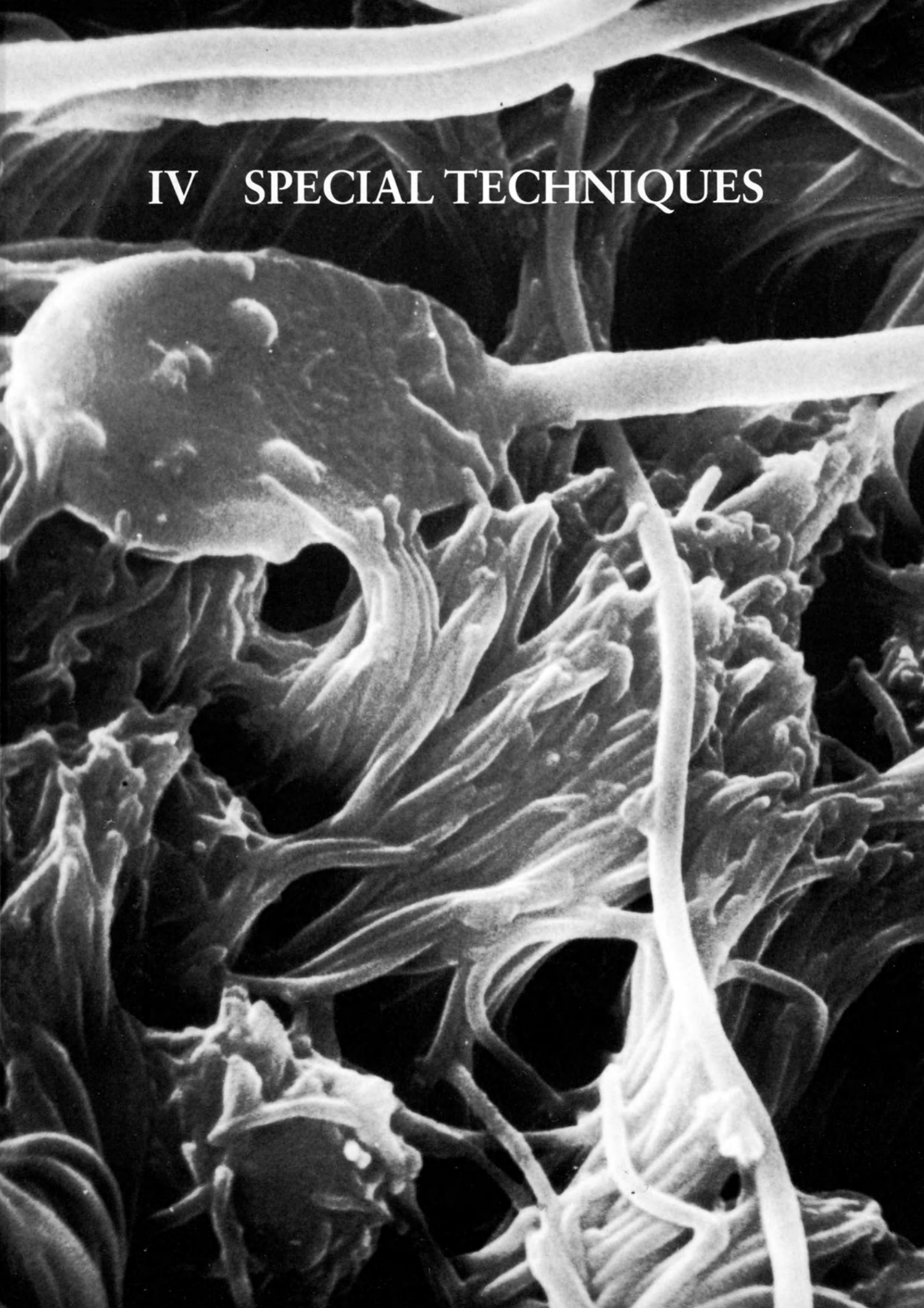
30

X-Ray microanalysis

G. M. ROOMANS

Wenner-Gren Institute, University of Stockholm, Norrtullsgatan 16, S–11345 Stockholm, Sweden

INTRODUCTION

X-ray microanalysis has greatly widened the scope of electron microscopy, by allowing elemental analysis of cellular structures in the electron microscope. Morphological information is complemented by chemical (elemental) information, and the link between cell structure and cell function strengthened: an extra dimension is added to electron microscopy. Energy dispersive X-ray microanalysis can simultaneously detect all elements from Na and heavier. The lowest concentration detectable is in the order of magnitude of 200–500 ppm, depending on the element of interest and the type of specimen. The lowest detectable amount of an element is about 10^{-18} g. In thin sections the resolution can be as good as 50 nm.

PRINCIPLES

Under the impact of the high-energy electrons from the electron beam, electrons from the inner shells of atoms in the specimen may be removed from their orbits. An electron from an outer orbit (with a higher energy level) will immediately fill this gap. The energy liberated in this process is emitted in the form of an X-ray photon with an energy equal to the energy difference between the two shells. Since this energy is characteristic for the element from which it originates and for the shells between which the electron transition occurs, these photons are called *characteristic X-rays* (Figure 1). Since, especially in heavy atoms, many electron transitions take place, many spectral emissions can occur. Not all transitions take place with the same frequency and hence the emissions vary in intensity; the most intense and hence most important X-ray emissions are listed in Table 1. The energy of the X-rays produced increases with increasing atomic number. However, since the energy difference between M and L shell is smaller than between L and K shell, the energy of L radiation is less than that of K radiation of the same element (Figure 2).

When incident electrons are inelastically scattered by the nucleus of atoms in the specimen, X-rays are produced that are not characteristic of the element, but which can have all energies from zero up to the energy of the incident electron. This X-ray radiation is called *continuum* or *white* or *background* radiation (Figure 1). The continuum radiation thus gives no information on the elemental composition of the specimen; however, its intensity is related to the total mass of the analyzed volume and determination of continuum intensity is therefore useful in quantitative analysis.

Not all X-rays produced in the specimen can emerge from the surface and be counted by the detector: some X-rays will be absorbed within the specimen. *X-ray absorption* depends on the energy of the X-rays, the wavelength of the X-rays in the specimen and the composition of the specimen. Low-energy X-rays, i.e. X-rays from light elements, are absorbed most (Figure 3). X-rays that are absorbed within the specimen can

Table 1 The most intense lines in the X-ray spectrum

Line	Electron transition			Relative intensity
$K_{\alpha,1}$	L_{III}	$\rightarrow$	K	100
$K_{\alpha,2}$	L_{II}	$\rightarrow$	K	50
$K_{\beta,1}$	M_{III}	$\rightarrow$	K	15–30
$K_{\beta,2}$	N_{III}	$\rightarrow$	K	1–10
$K_{\beta,3}$	M_{II}	$\rightarrow$	K	6–15
$L_{\alpha,1}$	M_V	$\rightarrow$	L_{III}	100
$L_{\alpha,2}$	M_{IV}	$\rightarrow$	L_{III}	10
$L_{\beta,1}$	M_{IV}	$\rightarrow$	L_{II}	50
$L_{\beta,2}$	N_V	$\rightarrow$	L_{III}	20
$L_{\gamma,1}$	N_{IV}	$\rightarrow$	L_{II}	1–10
M_α	N_{VII}	$\rightarrow$	M_V	100
M_β	N_{VI}	$\rightarrow$	M_{IV}	60

In the Bohr model of the atom the L shell consists of three subshells (L_I–L_{III}), the M shell of five (M_I–M_V) and the N shell of seven subshells (N_I–N_{VII}). The relative intensity is given in relation to the (α,1) line of each family of lines. Sometimes spectral lines, e.g. (α,1) and (α,2) are so close together that they cannot be resolved by the detector, and the line is simply denoted (α)
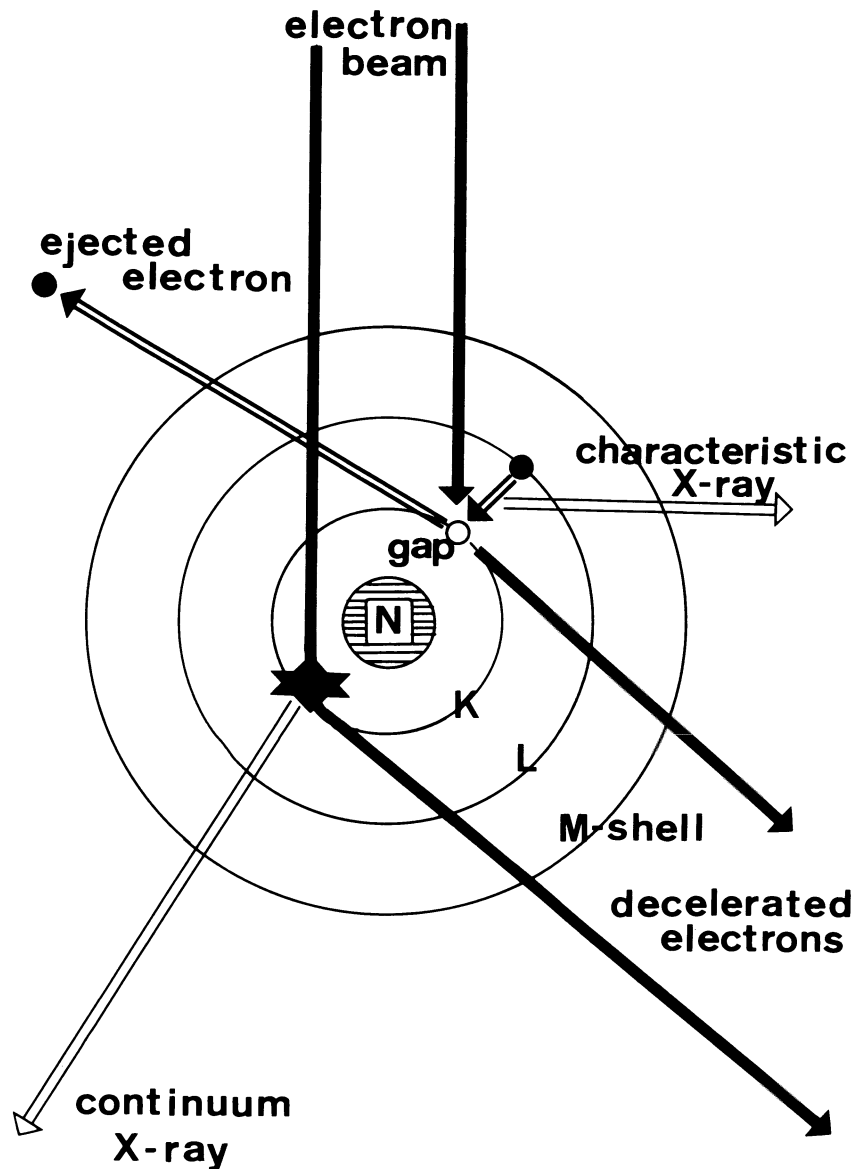
Figure 1 Generation of characteristic X-rays (involving an electron transition, here from L to K shell) and of continuum X-rays, involving interaction of a high-energy electron with the nucleus of an atom in the specimen

generate X-rays in the same way as electrons do, by creating a vacancy in an inner shell. Generation of X-rays by other X-rays is called *secondary fluorescence*. Both characteristic and continuum X-rays can be absorbed and can give rise to secondary fluorescence. X-ray absorption and secondary fluorescence are negligible in thin sections (for soft biological tissue up to 1-2 μm), but have to be taken into account in analysis of thicker specimens.

The incident electrons will penetrate several μm into the specimen before all their energy is lost. In addition, due to elastic scattering, electrons will diffuse laterally in the specimen. Most of the X-rays are not generated at the surface, but deeper in the specimen, in a volume much larger than the diameter of the electron beam would suggest. The *spatial resolution of analysis* is

usually defined as the volume from which 90% of the X-rays are generated (Figure 4), and can be distinguished into a *lateral resolution* and a *depth resolution*. In thin specimens, lateral diffusion occurs of course to a much smaller extent, and spatial resolution is much better. In thick specimens, spatial resolution depends on the accelerating voltage and on the density of the specimen (Figure 5).

INSTRUMENTATION

The instrumentation for energy-dispersive X-ray microanalysis consists of two main parts: *the electron optical system* (the electron microscope) and *the detection system* (Figure 6).

The two functions of the electron optical system are
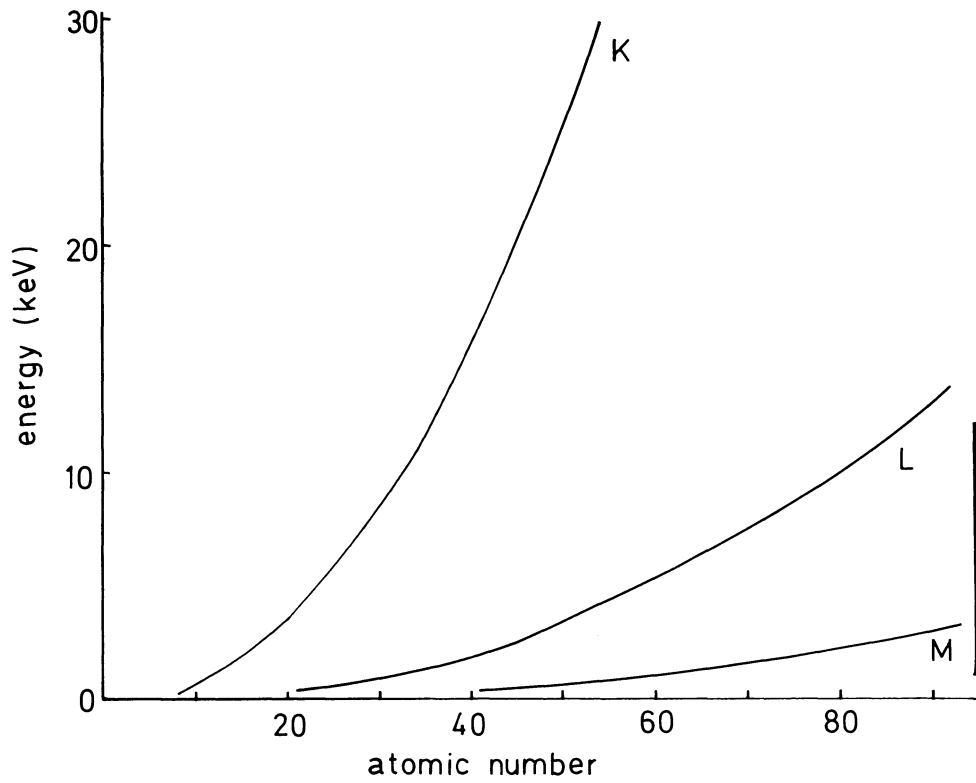
Figure 2 Energy of the principal K, L and M lines as a function of the atomic number of the atom. For analysis, usually lines in the energy range of about 1–12 keV are used
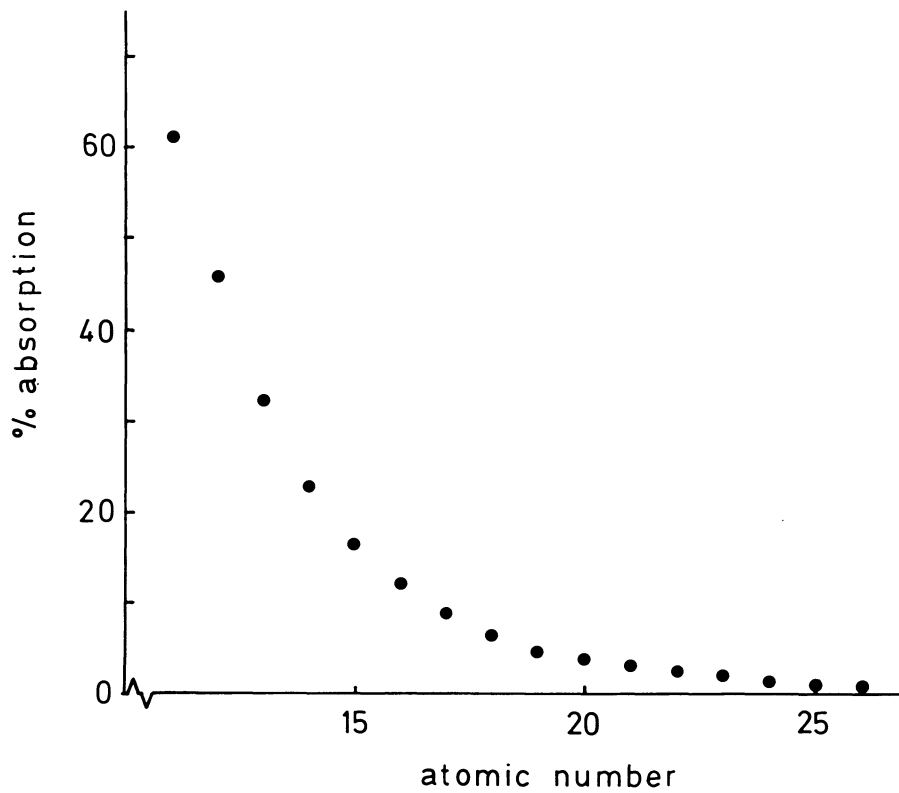
Figure 3 Absorption (in percentage) of K_α X-rays in a biological bulk specimen, as a function of the atomic number of the element emitting the X-rays. Calculated for an accelerating voltage of 20 kV
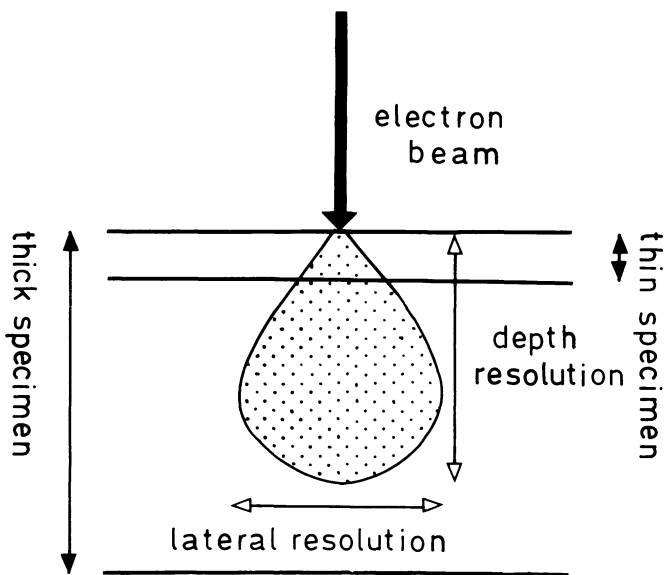
Figure 4 The pear-shaped volume in which (90% of) the X-rays are generated in a thick specimen. In a thin specimen the electron beam spreads less and the spatial resolution of analysis is much better
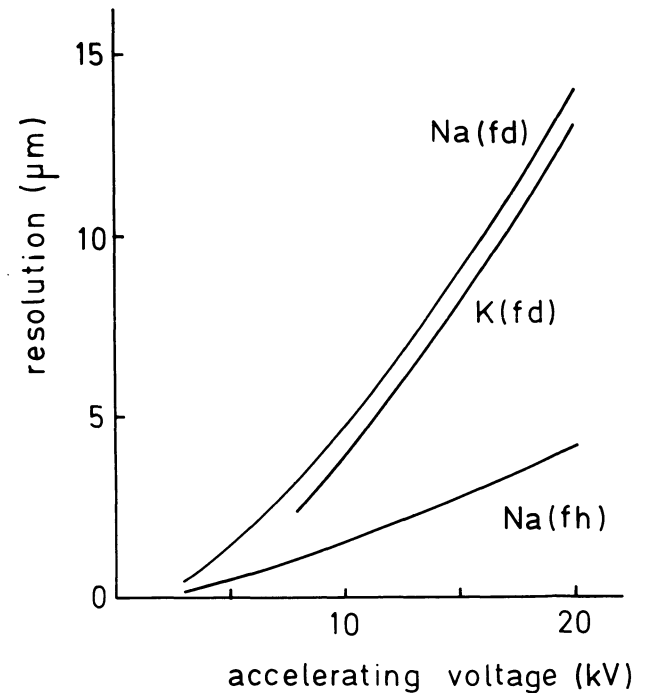
Figure 5 Spatial resolution of analysis as a function of the accelerating voltage in frozen-dried (fd: specific density 0.3 g cm^{-3}) and frozen–hydrated (fh: specific density 1.0 g cm^{-3}) biological thick specimens. The spatial resolution is also marginally dependent on the element emitting X-rays; this is shown for Na and K

to produce an electron beam that can be focused into a small probe, and to provide an image of the specimen. Because of the requirement to have as narrow a beam as possible, the scanning electron microscope has been the instrument of choice for X-ray microanalysis: SEM for thick specimens and STEM for sections. However, in some transmission microscopes the electron optics have been modified to allow the formation of a sufficiently narrow beam for analysis.

The detection system consists of the *X-ray detector*, the *multichannel analyzer*, and a computer and display system. The most commonly used type of detector in energy-dispersive X-ray microanalysis is the lithium-drifted silicon solid state semiconductor detector, in short Si (Li)-detector. Absorption of X-rays in the detector makes the semiconductor momentarily conducting. Electrons from the valence band are raised to the conduction band and the 'hole' left in the valence band behaves like a free positive charge. The amount of free charge created is, ideally, proportional to the energy of the X-ray. The charge is swept out of the semiconductor by an applied bias and collected as a charge pulse. To prevent the highly mobile lithium ions diffusing away, the detector is kept at liquid nitrogen temperature. In order to maintain the necessary purity of the detector material the detector is normally mounted in an evacuated encapsulation and separated from the microscope column by a thin (7–8 μm) beryllium window. This window absorbs low-energy X-rays and is an important factor responsible for the poor sensitivity of X-ray microanalysis to light elements (Figure 7).

Due to the statistical nature of the processes taking place in the detector, the characteristic X-ray signal, originally comprising a narrow energy band, is broadened. This may make it difficult to distinguish two elemental peaks with a small energy difference. The *energy resolution* depends on the quality of the detector; good detectors have a resolution of better than 150 eV. The charge pulse collected by the bias on the detector is converted to a voltage pulse in a field effect transistor (FET) in a preamplifier, and subsequently the signal is amplified. In the multi-channel analyzer (MCA) the pulses are sorted by voltage and stored in a memory, similar to that of a computer. The MCA breaks the signal from the amplifier, which is a continuum, into discrete channels of typically 10 or 20 eV wide. The MCA is connected to a (mini-) computer, that allows the spectra to be stored. Calculations on the spectra can be carried out on-line. The spectra can be displayed on a video screen or recorded on a chart recorder.

SPECIMEN PREPARATION

Specimen preparation for X-ray microanalysis should ideally preserve the localization of all elements of interest at the level of analytical resolution sought, and allow unequivocal identification of structures analyzed. These two requirements are often difficult to reconcile. Preparative methods for X-ray microanalysis of sections of biological material are shown in Table 2. Conventional specimen preparation for (S)TEM including fixation in buffered glutaraldehyde, post-
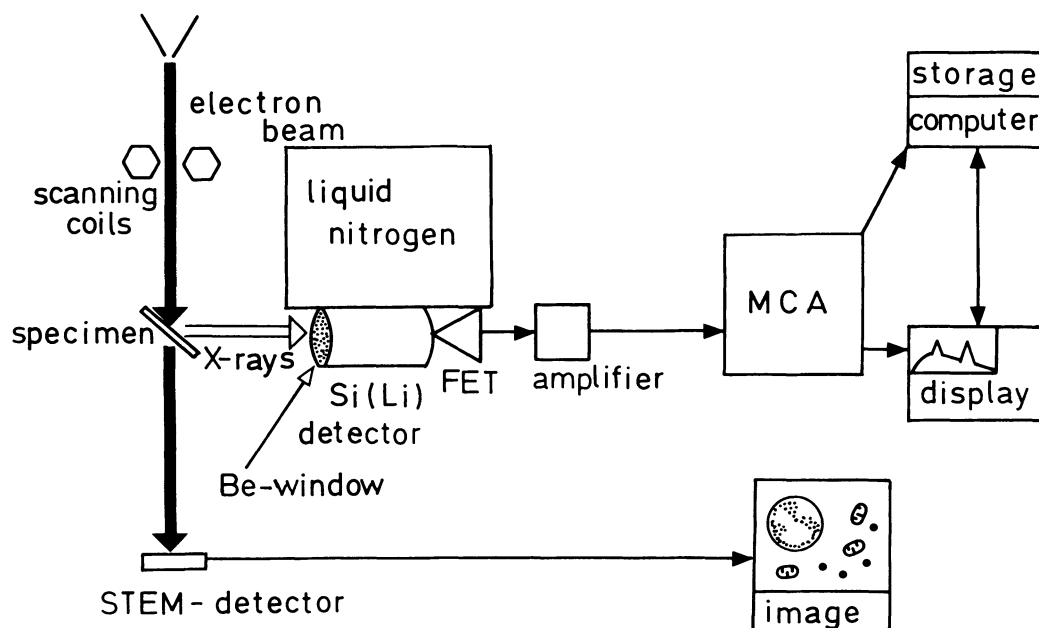
Figure 6 Schematic drawing of the instrumentation involved in X-ray microanalysis of a thin section. The detector and the FET are cooled with a cold finger kept at liquid nitrogen temperature
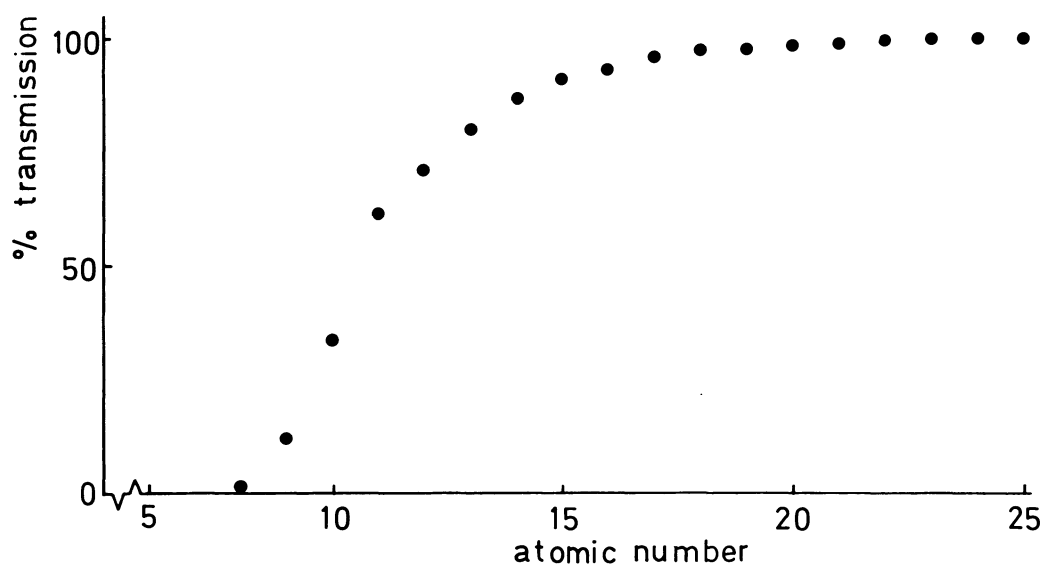
Figure 7 Fraction of the K_α X-rays transmitted by a beryllium window of 8 μm thickness, as a function of the atomic number of the element emitting the X-rays

fixation in osmium tetroxide, dehydration in an organic solvent, embedding in epoxy resin and staining of the sections with heavy metal salts gives the best morphological results, but important chemical changes occur (Table 3) and from the point of view of X-ray microanalysis the specimen can hardly be considered representative of the situation in vivo (Figure 8). Some of the drawbacks of the conventional preparation scheme can be avoided by omitting section staining and/ or osmium post-fixation, or by attempting to precipitate ions of interest during fixation. Precipitation

methods used for X-ray microanalysis are listed in Table 4. In general, none of these methods is completely effective (in some cases losses have even been reported to be larger in the presence of the precipitative agent) and there is doubt about the faithful localizaton of the ions precipitated.

For X-ray microanalysis, cryomethods are a much better alternative. The tissue is quickly frozen in subcooled freon or propane, or in nitrogen slush. Sectioning of the frozen tissue at very low temperature (typically about −100 °C and lower) is carried out on a

Table 2   Preparation of thin sections for X-ray microanalysis

Fixation	Dehydration	Embedding	Sectioning	Analysis
Conventional fixation				
Aldehyde and osmium	ethanol or acetone	epoxy resin	room temperature trough liquid: water	staining with uranyl and lead salts
Precipitation methods				
Aldehyde and/or osmium with precipitant	ethanol or acetone	epoxy resin	room temperature trough liquid: water or glycerol	
Cryomethods				
Rapid freezing	freeze-drying (osmium vapour staining	epoxy resin (under vacuum)	room temperature dry knife	
Rapid freezing	freeze-substitution e.g. ether/acetone at low temperature	epoxy resin	room temperature dry knife	
Rapid freezing			cryoultramicrotomy at low temperature	freeze-drying of sections
Rapid freezing			cryoultramicrotomy at low temperature	cryostransfer-frozen–hydrated (low temperature)

dry knife, i.e. without the use of a trough liquid. After sectioning, sections can be freeze-dried, or transferred to the microscope directly and examined at low temperature in the frozen–hydrated state. An alternative is to freeze-dry the frozen blocks of tissue, and to embed it under vacuum in resin. Sections can then be cut at room temperature with a dry knife. Also freeze-substitution, where the ice is (at low temperatures) exchanged for an organic solvent, and under gradual warming, the solvent is exchanged for resin, has been considered a useful method.

Since the cryotechniques do not involve treatment of the tissue with an aqueous solution, diffusible elements can be retained completely. The techniques are not problem-free, however: during freezing, ice crystals are formed that may cause elemental redistribution and distortion of the ultrastructure. Attempts are being made to reduce this problem by the use of sophisticated freezing techniques and high-molecular-weight cryoprotectants. As also can be seen from Figure 9, it is difficult to obtain a good image from an uncontrasted dry cryosection (and this is even more difficult with hydrated specimens).

For bulk specimens, rapid freezing followed by freeze-drying, or examination of the frozen–hydrated specimen in the scanning electron microscope, is the method of choice. Critical-point drying is not generally used in X-ray microanalysis. Occasionally a simple method such as air-drying can be used. This applies also to single cells from a cell suspension: freeze-drying is probably best but air-drying may be permissible (Figure 10). The specimen should not be coated with a heavy metal: carbon coating does not disturb the analysis and is therefore recommended.

In general, a consequence of the demands that X-ray microanalysis puts on specimen preparation is that the specimen is uncontrasted, which may lead to difficulties in obtaining a sufficiently detailed image. Omitting the fixation also leads to inferior image quality.

X-ray microanalysis offers a unique tool for the determination of the elemental composition of extremely small volumes of fluid. The liquid samples, with a size as small as 15 pl, are delivered from a specially constructed pipette onto a support, e.g. beryllium, carbon or a plastic-film covered grid. Freeze-drying generally gives the best results. Care should be taken to obtain only very small crystals, since in larger crystals X-ray absorption will occur.

Table 3   Elemental changes during conventional preparation for electron microscopy

Preparative step	Elements lost	Elements added
Glutaraldehyde fixation	Na, K, Mg, Cl, P (phosphate ions), Ca, Zn, other metals	As (cacodylate buffer), P (phosphate buffer)
Osmium fixation	Na, K, Mg, Cl, P, Ca, Zn, other metals	Os
Dehydration	P (phospholipids)	
Embedding		Cl (resin contaminant)
Sectioning	Na, K, Mg, Cl, Ca, Zn, other metals (to the water in the trough)	
Section staining	Ca	Pb, U
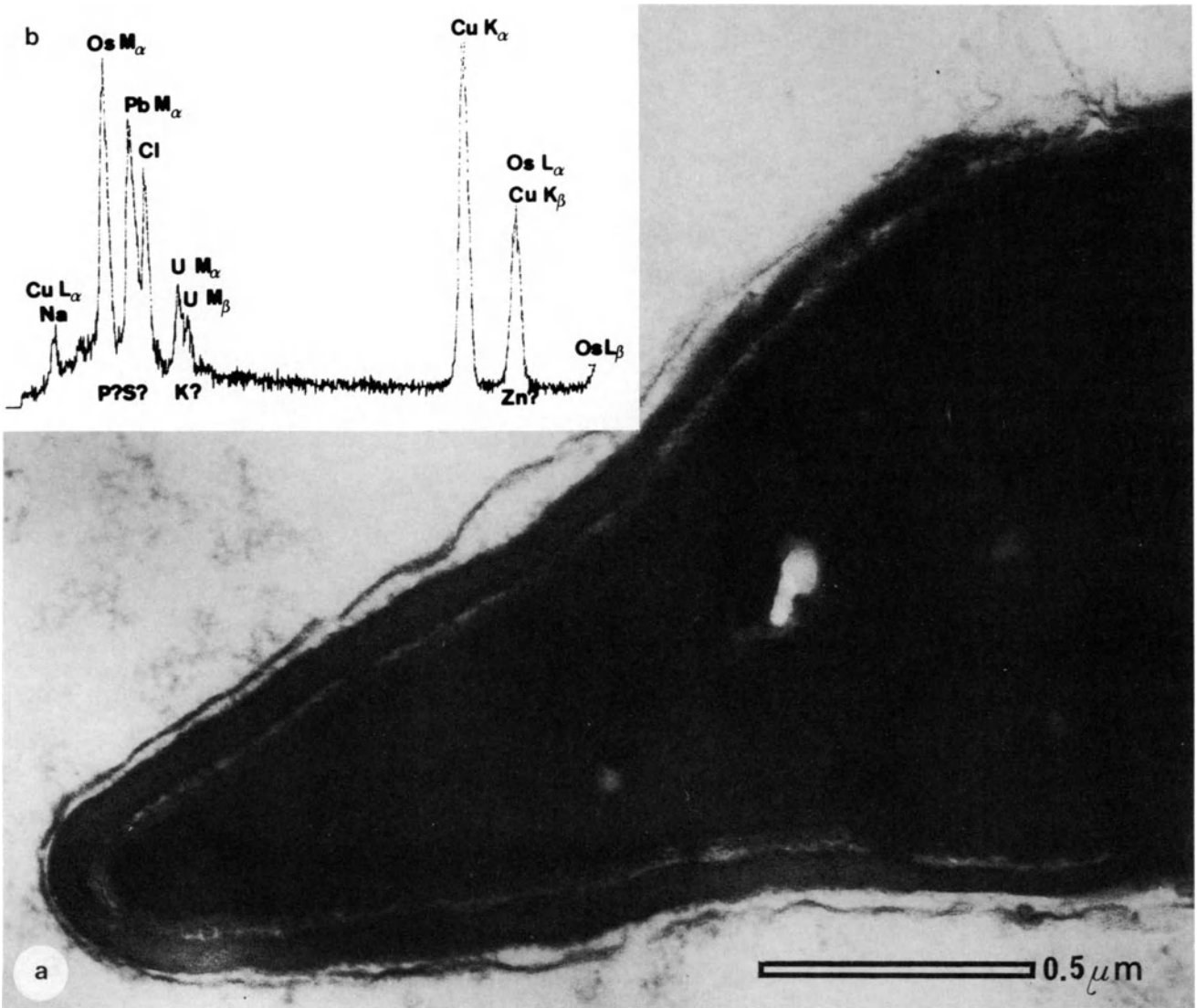
Figure 8 Section of a conventionally prepared human spermatozoon: (a) ultrastructure, (b) spectrum of X-ray microanalysis carried out in the nucleus. Os from osmium postfixation, Pb from lead citrate staining, Cl from the epoxy resin, U from uranyl acetate staining. The Cu signal is from the copper grid. This preparation method gives much ultra-structural information but virtually no chemical information about the specimen
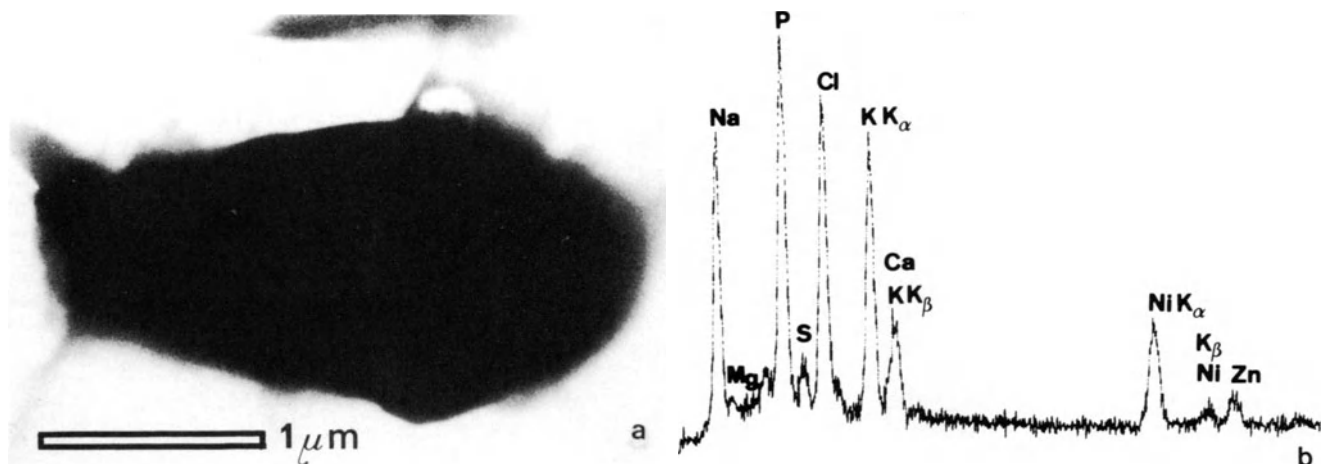
Figure 9 Uncontrasted dry-cut (at −100 °C) cryosection of a human spermatozoon showing a cross-section through the head (a) and a spectrum from the nucleus (b). The only extraneous signal detectable is a small Ni peak from the one-hole Ni grid used. Analytical information is very well retained (note the presence of Zn), but ultrastructural information is poor
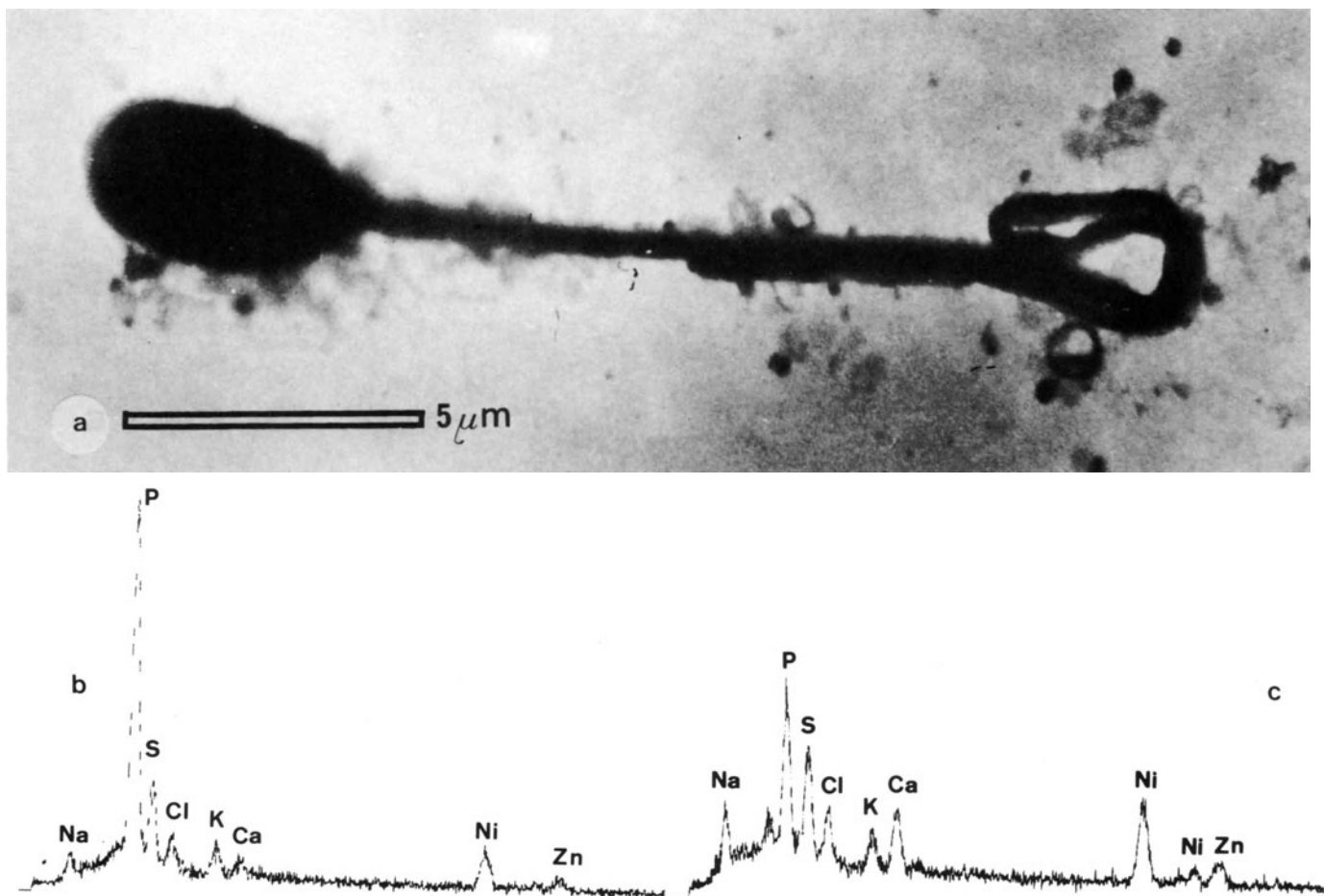
Figure 10   Air-dried human spermatozoon (a) with spectra from the head (b) and the midpiece (c); note the difference in phosphorus. The spermatozoa were centrifuged, the seminal fluid removed, and the cells resuspended in distilled water and immediately brought onto a Formvar film-covered nickel grid. If the spermatozoa are not rinsed, the analysis of the air-dried cells is complicated by the presence of the seminal fluid. The washing procedure seems to reduce the concentrations of Na, K and Cl (compare Figure 9), but Zn appears to be fairly well retained

SPECIMEN ANALYSIS

The goal of qualitative analysis is the demonstration of the presence (or absence) of the element of interest in a certain structure. A problem may be to distinguish a small characteristic peak from the background, especially because, due to the statistical nature of the process of X-ray generation, the background is not smooth, and the peak not a true Gaussian at the count rates common for biological specimens. To demonstrate a peak at 95% confidence level requires that the number of characteristic counts should be larger than twice the square root of the background intensity under the peak.

For qualitative analysis (and even more for quantitative analysis) it is important to choose optimal experimental conditions. For analysis of sections in STEM, the accelerating voltage should be high; 80–100 kV is generally used. Since the peak-to-background ratio increases with accelerating voltage, high voltage improves the sensitivity of the analysis. For analysis of thin specimens in SEM, one generally chooses the accelerating voltage as low as possible, but not lower than about 2.5 times the energy of the lines to

be detected. By taking a low accelerating voltage, spatial resolution is improved, and since the X-rays are generated at relataively low depth in the sample, X-ray absorption is minimized.

The spectrum obtained is not exclusively due to the part of the spectrum on which the beam is focused. Extraneous sources (e.g. grid bars or specimen holders) may contribute considerably to the spectrum. This may lead to an increase in the background (decreasing sensitivity) and give characteristic peaks that may interfere with signals from the specimen itself. Staining or coating of the specimen with heavy metals has, of

Table 4   Precipitation methods used in X-ray microanalysis

Precipitative agent	Precipitated ions
Potassium pyroantimonate	Na, Mg, Ca, K, Zn
Oxalate	Ca
Cobalt nitrite	K
Silver (Ag^+)	Cl
Sulfide	Hg and other heavy metals

Table 5 Common extraneous peaks and overlaps caused by these peaks

Extraneous peak	Possible source	Interferes with
Al (K_α)	specimen holder	Br (L_α)
Cu (K_β)	grid, specimen holder	Zn (K_α), Os (L_α)
Pd (L_α) ($L_{\beta,1}$)	coating	Cl (K_α) K (K_α)
Os (M_α) (L_α)	osmium post-fixation	Si (K_α), P (K_α) Zn (K_α)
Au (M_α)	coating	P (K_α), S (K_α)
Pb (M_α)	section staining	S (K_α), Cl (K_α)
U (M_α)	section staining	K (K_α)

course, a similar negative effect on the analysis. Although progress has been made in the development of computer programs to resolve peak overlaps, it is always better to avoid such overlaps. Common extraneous peaks and their effects are listed in Table 5.

During analysis, mass loss from the specimen may occur: especially light elements (C, H, N and O) are lost, but also some heavier elements (e.g. halogens) are notoriously unstable. On the other hand the specimen may be contaminated by hydrocarbons, chlorinated hydrocarbons (giving rise to an extraneous Cl signal) and silicon (from vacuum grease).

Identification of peaks is usually fairly straightforward. Complications may arise in the low-energy part of the spectrum where a peak could be a K, L or M line of three different elements. Generally, checking for other spectral lines of the element(s) in question will lead to unequivocal identification.

The first step in quantitative analysis is the separation of characteristic peaks from the background. The background has to be separated in a background due to the specimen itself and background from extraneous sources; only the background from the specimen is to be taken into account. The peak-to-background (P/B) ratio thus obtained is used in the rest of the quantitative procedure. The P/B ratio from the (unknown) specimen is compared with the P/B ratio from a standard with known composition. Standards are usually made up in such a way that they resemble the specimen in its physical and chemical properties. This reduces the importance of correction factors needed to correct for differences between specimen and standard, and provides some internal correction for mass loss. Low temperatures reduce mass loss and, ideally, quantitative analysis should be carried out in a cold stage. The type of standard to be used depends on the type of specimen; methods to make different types of standards are available (Roomans, 1979).

The theory of quantitation applied to biological thin sections has been developed by Hall (1971). With thick specimens, X-ray absorption and secondary

fluorescence may have to be taken into account, and quantitation may be somewhat more complicated (Roomans, 1981).

APPLICATIONS OF X-RAY MICROANALYSIS IN REPRODUCTIVE PHYSIOLOGY

Several aspects of reproductive physiology have been investigated by X-ray microanalysis. The most extensive studies on the male reproductive system have been carried out by Chandler (1980). These studies include an investigation of the localization of zinc in the prostate in an attempt to clarify the role of zinc in the secretion processes in the prostate. Also zinc–cadmium interactions were investigated. Attempts were made at localization of several elements in spermatozoa, but due to uncertainties inherent in the preparative methods used, and to possible contamination of the spermatozoa with seminal fluid, no firm conclusions have yet been drawn.

With regard to the female reproductive tract, studies have been made of the elemental composition of small volumes of fluids, e.g. in blastocysts, with the use of the microdroplet technique (Borland et al., 1977). Cameron and co-workers carried out studies of the basal layer of the vaginal epithelium in different stages of the cell cycle after estrogen stimulation (Cameron and Smith, 1980).

References

Borland, R. M., Biggers, J. D. and Lechene, C. P. (1977). Studies on the composition and formation of mouse blastocoele fluid using electron probe microanalysis. Dev. Biol., 55, 1

Cameron, I. L. and Smith, N. K. R. (1980). Energy-dispersive X-ray microanalysis of the concentration of elements in relation to cell reproduction in normal and in cancer cells. SEM/1980/II, 463

Chandler, J. A. (1980). Application of X-ray microanalysis in reproductive physiology. SEM/1980/II, 475

Hall, T. A. (1971). The microprobe assay of chemical elements. In Oster, G. (ed.), Physical Techniques in Biochemical Research, Vol. 1A, pp. 157-276. (New York: Academic Press)

Roomans, G. M. (1979). Standards for X-ray microanalysis of biological specimens. SEM/1979/II, 649

Roomans, G. M. (1981). Quantitative electron probe X-ray microanalysis of biological bulk specimens. SEM/1981/IV (In press)

Recommended Reviews

Chandler, J. A. (1977). X-ray microanalysis in the electron microscope. In Glauert, A. M. (ed.), Practical Methods in Electron Microscopy. Vol. 5, pp. 317-547. (Amsterdam: North Holland)

Hayat, M. A. (ed.) (1980). X-ray Microanalysis in Biology. (Baltimore: University Park Press)

31

Cell surface markers and labeling techniques

R. S. MOLDAY

Department of Biochemistry, Faculty of Medicine, University of British Columbia, Vancouver, BC, Canada

The detection and localization of specific molecules on cell surfaces has been achieved through the use of cell surface labeling techniques for microscopic analysis. These techniques generally involve labeling antigens or receptors on cell surfaces with high affinity, specific ligands, such as antibodies, lectins, toxins, hormones or drugs, which are directly or indirectly attached to markers visible under the light or electron microscope. Fluorescent dyes such as fluorescein and rhodamine have been widely used as visual markers for fluorescent light microscopy. Electron-dense markers such as ferritin, and enzymes such as horseradish peroxidase, have been extensively employed as transmission electron microscope (TEM) markers with thin sectioning. Macromolecular markers such as hemocyanin and viruses have also served as TEM markers for replica methods.

Visual markers which can be recognized on cell surfaces by their morphological features have been developed for scanning electron microscopy (SEM). These markers and labeling techniques have proven to be a valuable means of identifying and studying the three-dimensional morphological features of specific cells in complex, multi-cellular systems, and to analyze the topographical distribution and molecular properties of specific receptors and antigens on cell surfaces. In this chapter, SEM markers and labeling techniques are described and some examples of their application in identifying specific cells and in studying the organization of surface antigens and receptors are given.

CELL SURFACE MARKERS

Several biological macromolecular complexes and synthetic polymeric microspheres have been developed for visualization of cell labeling by SEM with the secondary electron mode of imaging (Table 1). These markers have distinctive sizes and shapes which permit them to be recognized on most cell surfaces on the basis of their morphological characteristics. The smallest SEM markers such as ferritin (Tokunaga et al., 1976), gold particles (Horisberger and Rosset, 1977) and silica spheres (Peters et al., 1976) are between 10 and 20 nm in diameter. These markers are most useful in high-resolution mapping of cell surface antigens and receptors. Small markers are also required when the antigens or receptors are sterically inaccessible to large

Table 1 Common SEM cell surface markers

Marker	Size (nm)	Shape	Primary interaction with ligands	Selected references
Ferritin	15	spherical	covalent bonding	Tokunaga et al. (1976)
Gold particles	16–150	spherical/ellipsoid	electrostatic adsorption	Horisberger and Rosset (1977)
Silica spheres	13–20	spherical	covalent bonding	Peters et al. (1976)
Hemocyanin	35 × 50	cylindrical	covalent bonding, specific binding to concanavalin-A	Brown and Revel (1976)
Copolymer microspheres	30–340	spherical	covalent bonding	Molday et al. (1975)
Tobacco mosaic virus	15 × 300	rod	covalent bonding, specific antigen–antibody binding	Hämerling et al. (1975); Nemanic et al. (1975); Kumon (1976)
Bacteriophage T-4	100 head 220 head–tail	hexagonal head and tail assembly	covalent bonding	Kumon (1976)
Polystyrene latex	230	spherical	hydrophobic adsorption	Linthicum and Sell (1975)

Figure 1

a

Ligand - Marker Conjugate   Antigen or Receptor   Labeled Cell

b

I^st Step

Specific Antibody   Surface Antigen   Antibody - Labeled Cell

2nd Step

Conjugate   Antibody - Labeled Cell   Conjugate - Labeled Cell
anti - Ig - marker
protein A - marker
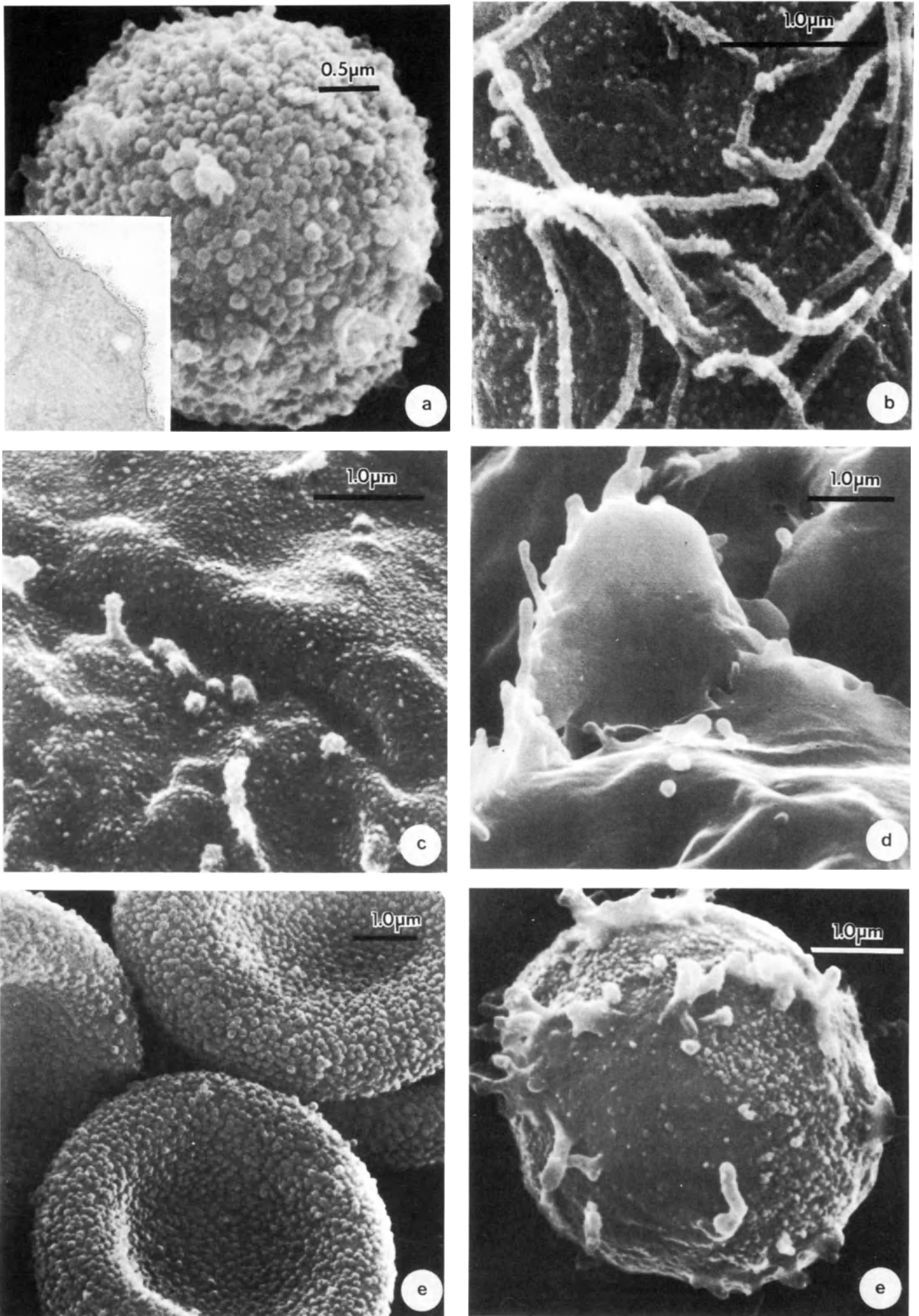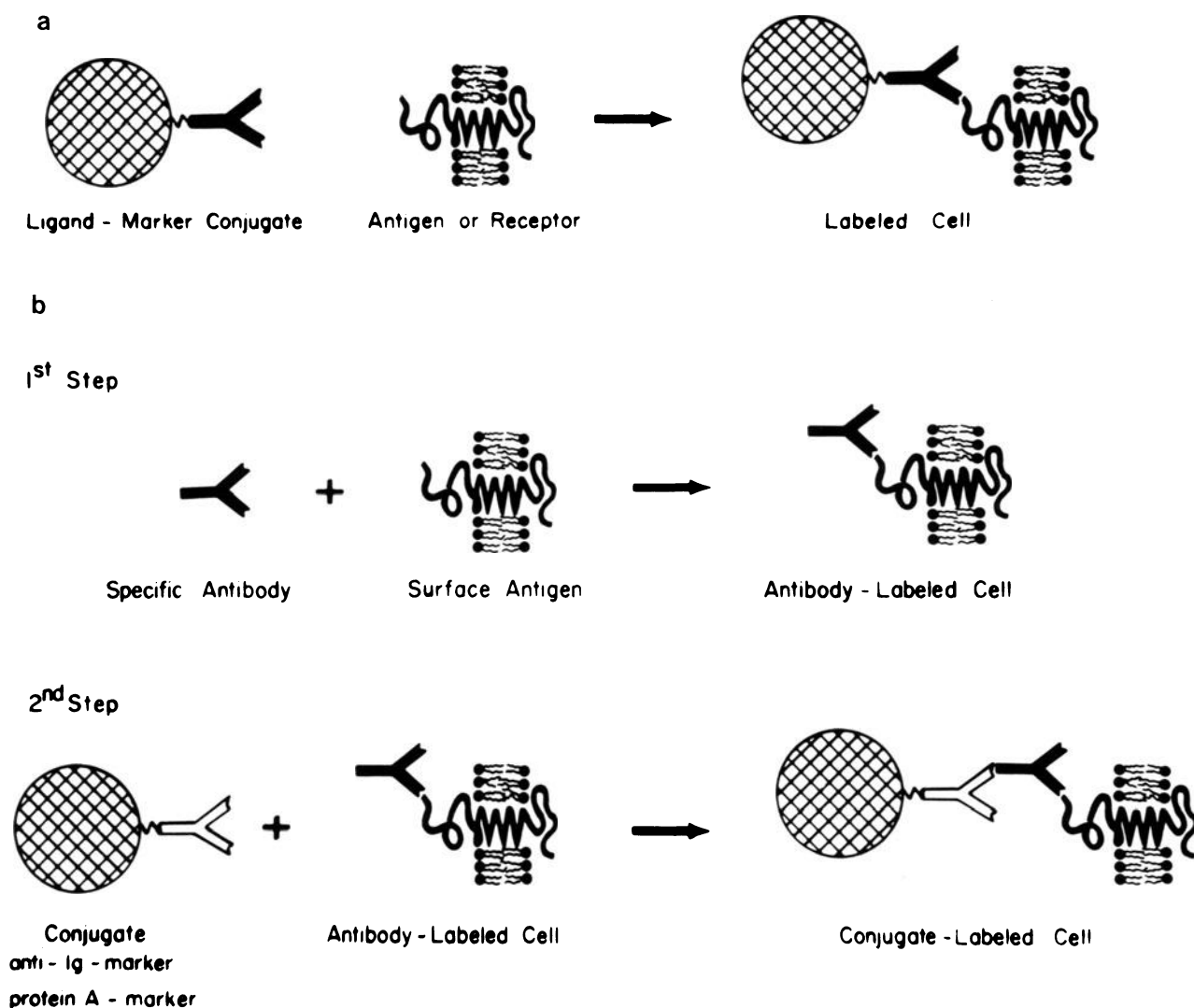
Figure 2

a: Scheme depicting the direct labeling methods in which cells are treated with previously prepared ligand–marker conjugates in a single step

b: Scheme depicting the standard indirect immunochemical

technique in which cells are first treated with the cell specific antibody (Ig) in the first step and subsequently labeled with anti-Ig antibody–marker or protein A–marker conjugates in the second step

---

Figure 1 (opposite) Electron micrographs of labeled cells.

a: SEM of a thymocyte indirectly labeled with monoclonal mouse anti-Thy 1 antibody followed by goat anti-mouse Ig–microsphere conjugate. The markers (90 nm in diameter) are densely and uniformly distributed over the cell surface. Inset: TEM of a thymocyte directly labeled with immunoferritin conjugates

b: Mouse 3T3 fibroblast labeled with wheat germ agglutinin–microspheres. Microsphere markers are randomly dispersed over the cell surface

c: *Dictyostelium discoideum* cells directly labeled with concanavalin-A microsphere conjugates. Microsphere markers (average diameter 35 nm) are densely distributed over the cell surface

d: *Dictyostelium discoideum* cells treated with concanavalin-A–microsphere conjugates in the presence of the inhibitor, α-methyl mannoside. The cell surface is essentially devoid of microspheres in this control experiment

e: SEM of human red blood cells (RBC) labeled for surface antigens with immunomicrospheres by the indirect 'sandwich' immunochemical method

f: SEM of immunoglobulin receptors localized in large patches on a mouse lymphocyte. Unfixed cells were first treated with rabbit anti-mouse Ig antiserum and then with goat anti-rabbit Ig–microspheres. Microsphere markers (average diameter 35 nm) are distributed in large patches over the cell surface.

markers. Markers of this size, however, are often difficult to recognize on irregular cell surfaces or on samples which have a thick metal coating. In such cases they may appear more like a fuzzy coating on the cell surface than well-defined markers. Larger markers in the size range of 30–100 nm such as hemocyanin (Brown and Revel, 1976), copolymer microspheres (Molday et al., 1975) and virus particles (Nemanic et al., 1975), are more readily recognized on cell surfaces (Figure 1a) and therefore have been used most extensively in SEM studies. Markers greater than 100 nm, such as polystyrene latex spheres (Linthicum and Sell, 1975) and T–4 bacteriophage (Kumon, 1976), are particularly well suited for the identification of specifically labeled cells in complex cell mixtures where large areas of the specimen can be viewed at low magnification. Morphological features on the cell surface, however, are often obscured by these large markers.

In addition to their morphological features, SEM markers have the following properties required for successful cell labeling:

(1) they show little, if any, tendency to non-specifically bind to most cells which have been studied;
(2) they maintain their distinctive size and shape, i.e. show no degradation or aggregation, during either cell labeling procedures or specimen preparation for SEM; and
(3) they are capable of interacting with various ligands, in particular protein ligands such as antibodies and lectins, through covalent bonding, strong non-specific adsorption or high affinity specific binding, i.e. antibody–antigen binding

A number of these markers can be used to detect surface labeling by TEM and light microscopy as well as SEM. Electron-dense markers such as ferritin and gold particles are particularly useful for labeling studies requiring correlation of surface characteristics of cells as seen by SEM with intracellular ultrastructure as viewed by TEM (Horisberger et al., 1978). In the case of markers containing a sufficient content of a heavy metal, X-ray microanalysis of samples under the SEM may be carried out to confirm the presence of these markers on cell surfaces (Molday, 1980). Visual markers such as copolymer microspheres which have been tagged with fluorescein or tetraethyl rhodamine dyes have been used to study cell surface labeling and cellular endocytosis by correlative SEM and fluorescent microscopy (Maher and Molday, 1979).

METHODOLOGY OF LABELING

Labeling methods for SEM are similar to those originally developed for light and transmission electron microscopy. These are broadly classified as direct and indirect methods based on the manner in which the cell surface specific ligand is attached to the visual marker and the number of steps required to label cells.

Direct labeling method

In the direct method (Figure 2), cells are treated with

previously prepared ligand–marker conjugates in a single step under defined experimental conditions, i.e. time, temperature, concentration, etc. The cells are subsequently washed in buffer to remove unbound conjugate, fixed in glutaraldehyde and prepared for SEM by standard procedures of dehydration, critical-point drying, and heavy-metal coating. The specificity of binding of the conjugates to cells is determined in control experiments run in parallel. Typically, control experiments are carried out by treating the cells with the conjugates in the presence of either excess free ligand or an inhibitor of ligand binding, e.g. simple sugars in the case of lectins. Under these conditions a substantial reduction or elimination of ligand–marker conjugate binding to cells should be observed to support the view that specific cell labeling has been achieved in the test sample.

The direct labeling method is generally used with ligands which are available in purified form, since this enables one to prepare highly active ligand–marker conjugates. The receptor or antigen must also be sterically accessible to the conjugate. Lectin conjugates which bind to specific carbohydrates on cell surfaces have been used most often with the direct method in SEM studies (Molday, 1981). Figures 1b–d illustrate the direct labeling of lectin receptors on Dictyostelium discoideum cells with concanavalin A–microsphere conjugates and lectin receptors on mouse fibroblasts with wheat germ agglutinin–microsphere conjugates.

Indirect labeling methods

In the indirect labeling methods, the cells are treated with the cell surface specific ligand in the first step. In one or more subsequent steps visual markers are attached to the ligands on the cells through high-affinity, specific binding interactions. Indirect techniques have been most widely used with immunological reagents to label cell surface antigens. In the standard indirect 'sandwich' technique (Figure 2), cells are initially treated with an antiserum containing the cell surface specific immunoglobulin (Ig). After the cells are washed, they are treated in a second step with an anti-Ig–marker conjugate which is capable of binding to the cell-bound Ig. Typically, a rabbit antiserum is used in the first step and a goat antirabbit Ig–marker conjugate is used in the second step. In some studies conjugates consisting of the marker coupled to Staphylococcus aureus Protein A which binds to the F_c region of certain subclasses of IgG immunoglobulins

Figure 3 (opposite) SEM of lymphoid cells labeled for surface immunoglobulins (Ig)
a: Lymphocytes isolated from mouse spleen tissue were fixed with glutaraldehyde and subsequently labeled with rabbit anti-mouse Ig antiserum followed by goat anti-rabbit Ig–microsphere conjugates. B-type lymphocyte (left) is densely labeled with the microsphere markers (average diameter 100 nm) whereas the T-type lymphocyte (right) is not labeled
b: Spleen tissue section was fixed in glutaraldehyde and labeled as in (a). Only some lymphocytes are heavily labeled (arrows)
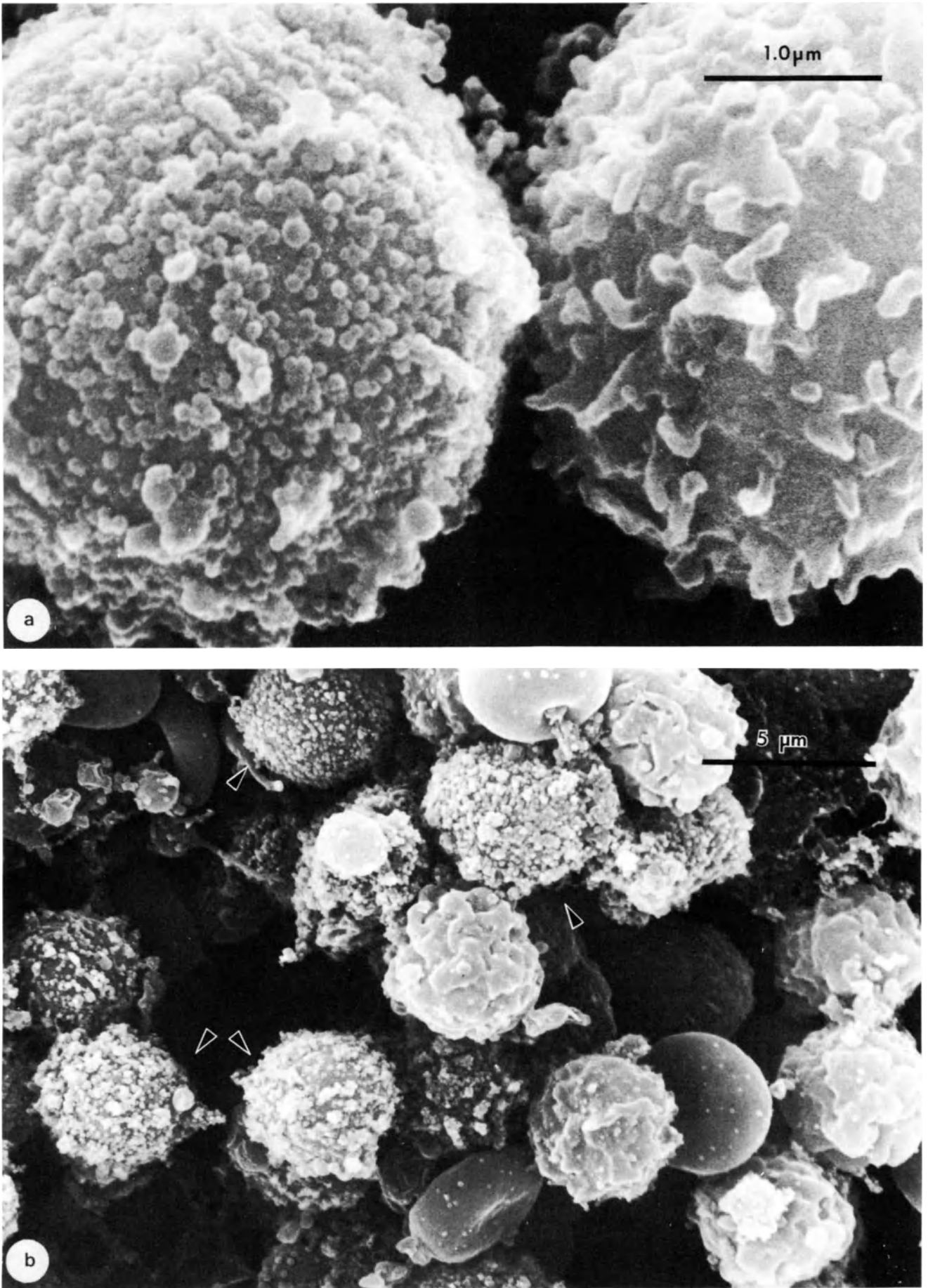
Figure 3

have been used instead of anti-Ig antibody conjugates in the second labeling step (Miller et al., 1980). Application of the indirect technique for labeling human red blood cells with heterologous antibodies produced by conventional immunological techniques is illustrated in Figure 1e and for the labeling of the Thy antigen on rat thymocytes with monoclonal antibodies produced from mouse hybridoma cells (Mason and Williams, 1980) in Figure 1a. A number of more complex indirect immunological methods also have been applied in labeling studies for SEM. These include the unlabeled antibody method (Gonda et al., 1979), the hybrid antibody method (Hämmerling et al., 1975) and the hapten sandwich method (Nemanic et al., 1975).

Ligand–marker conjugates

Ligand–marker conjugates used in the direct method and indirect sandwich method are generally prepared by chemical coupling reactions carried out under mild conditions. Glutaraldehyde has been used most routinely as a bifunctional agent for coupling markers to antibodies or lectins via their amino groups. Reaction conditions have been developed to maintain the specific binding characteristics of the ligands and to minimize aggregation of the conjugates (Otto et al., 1973). The two-step glutaraldehyde reaction has proven most satisfactory. This involves the activation of amino groups on markers with glutaraldehyde in the first step. Excess glutaraldehyde is then removed and the protein ligands are then coupled to the glutaraldehyde-activated markers in the second step. For several SEM markers such as gold particles (Horisberger and Rosset, 1977) and polystyrene latex spheres (Linthicum and Sell, 1975), which do not contain amino groups or other reactive groups, conjugates have been prepared by adsorbing antibodies or lectins to the surface of the markers through electrostatic and/or hydrophobic non-covalent forces.

SELECTED APPLICATIONS

Cell surface labeling techniques have been used by a number of laboratories to detect and localize antigens and lectin receptors on a variety of different cells by SEM. With the use of cell-specific antibodies, cells displaying specific antigens have also been identified in complex mixtures and intact tissues using immunological labeling techniques (Molday et al., 1975; DeHarven et al., 1979; Miller and Teplitz, 1978). This is illustrated in Figures 3a–b for the specific labeling of B-type lymphocytes displaying immunoglobulin receptors in mixed cell populations and in spleen tissue samples.

The distribution and rearrangement of antigens and receptors has also been studied on both culture cells and cells isolated from tissues (Brown and Revel, 1976; Molday et al., 1975; Hämmerling et al., 1975). Figure 1f illustrates the phenomenon of patching of immunoglobulin receptors on B-lymphocytes as viewed under the SEM. This phenomenon has also been observed by immunological labeling techniques for fluorescent microscopy and TEM (Taylor, et al., 1971).

The preferential distribution of Con-A receptors on the head region of rat spermatoza has also been reported using labeling techniques for SEM (Baccetti and Burrini, 1977).

CONCLUDING REMARKS

Several cell surface markers and labeling methods are available for use with SEM. These techniques are useful in the identification of cells displaying specific antigens or receptors, and in mapping the distribution of these components on cell surfaces under varying conditions. With the recent development of cell specific monoclonal antibodies, immunological labeling techniques for SEM should contribute significantly to the analysis of cell structure and function in the normal and pathological states. Labeling studies for SEM should prove particularly valuable in cellular and molecular studies of complex integrated cell systems such as the reproductive system, immune system, neural system and endocrine system.

References

Baccetti, B. and Burrini, A. (1977). Detection of concanavalin A receptors by affinity to peroxidase and iron dextran by scanning and transmission electron micro-scopy and X-ray microanalysis. J. Microsc., 109, 203

Brown, S. S. and Revel, J. P. (1976). Reversibility of cell surface label rearrangement. J. Cell Biol., 68, 629

De Harven, E., Pla, D. and Lampen, N. (1979). Labeling of lymphocyte surface immunoglobulins with T4 as marker for scanning electron microscopy. SEM Symposium, III, 611

Gonda, M. A., Gilden, R. V. and Hsu, K. C. (1979). Immunologic techniques for the identification of virion and cell surface antigens by correlative fluorescence, trans-mission electron and scanning electron microscopy. SEM Symposium, III, 583

Hämmerling, U., Polliack, A., Lampen, N., Sabety, M. and deHarven, E. (1975). Scanning electron microscopy of tobacco mosaic virus-labelled lymphocyte surface antigen. J. Exp. Med., 141, 518

Horisberger, M. and Rosset, J. (1977). Gold granules: A useful marker for SEM. SEM/IITRI, II, 75

Horisberger, M., Rosset, J. and Vonlanthen, M. (1978). Location of glycoproteins on milk fat globule membranes by scanning and transmission electron microscopy using lectin-labeled gold granules. Exp. Cell Res., 109, 361

Kumon, H. (1976). Morphologically recognizable markers for scanning immunoelectron microscopy. Virology, 74, 93

Linthicum, D. S. and Sell, S. (1975). Topography of lymphocyte surface immunoglobulin using scanning immuno-electron microscopy. J. Ultrastruct. Res., 51, 55

Maher, P. and Molday, R. S. (1979). Differences in the redistribution of Concanavalin A and wheatgerm agglutinin binding sites on mouse neuroblastoma cells. J. Supramol. Struct. 10, 61

Mason, D. W. and Williams, A. F. (1980). The kinetics of antibody binding to membrane antigens in solution and at the cell surface. Biochem. J., 187, 1

Miller, M. M. and Teplitz, R. L. (1978). Detection of embryonic surface antigens using SEM. SEM Symposium, II, 893

Miller, M. M., Strader, C. D. and Revel, J. P. (1980). Hemocyanin-protein A: an immunochemical reagent for scanning and transmission electron microscopy. SEM Symposium, II, 125

Molday, R. S. (1980). Labeling techniques for the analysis of cell surface glycoproteins. *Ann. Proc. Electron Microsc. Soc. Am.*, **38**, 716

Molday, R. S., Dreyer, W. J., Rembaum, A. and Yen, S. P. S. (1975). New Immunolatex spheres: Visual markers of antigens on lymphocytes for scanning electron microscopy. *J. Cell Biol.*, **64**, 75

Molday, R. S., Jaffe, R. and McMahon, D. (1976). Concanavalin A and wheat germ agglutinin receptors on Dictyostelium discoideum. Their visualization by scanning electron microscopy with microspheres. *J. Cell. Biol.*, **71**, 314

Molday, R. S. (1981). Labeling of cell surface lectin receptors for scanning electron microscopy. *Biomed. Res.*, **2**, Suppl., 23

Nemanic, M. K., Carter, P. P., Pitelka, D. R. and Wofsy, L. (1975). Immunospecific attachment of cell surface markers suitable for scanning electron microscopy. *J. Cell Biol.*, **64**, 311

Otto, N., Takamiya, N. and Vogt, A. (1973). A two stage method for crosslinking antibody globulin to ferritin by glutaraldehyde. Comparison between the one-stage and two-stage method. *J. Immunol. Methods*, **3**, 137

Peters, K. R., Gschwender, N. H., Haller, W. and Rutter, G. (1976). Utilization of a high resolution spherical marker for labelling of virus antigens at the cell membrane in conventional scanning electron microscopy. *SEM/IITRI*, **II**, 75

Taylor, R., Duffus, W., Raff, M. and De Petris, S. (1971). Redistribution and pinocytosis of lymphocyte surface immunoglobulin molecules induced by anti-immunoglobulin antibody. *Nature New Biol.*, **233**, 225

Tokunaga, J., Fujita, T., Hattori, A. and Muller, J. (1976). Scanning electron microscopic observation of immunoreactions on the cell surface: analysis of *Candida albicans* cell wall antigens by the immunoferritin method. *SEM/IITRI*, **I**, 301

Recommended Reviews

Brown, S. S. and Revel, J. P. (1978). Cell surface labelling for the scanning electron microscope. In Koehler, K. J. (ed.), *Advanced Techniques in Biological Electron Microscopy.* Vol. II, pp. 65-88. (New York: Springer)

De Petris, S. (1978). Immunoelectron microscopy and immunofluorescence in membrane biology. In Korn, E. (ed.), *Methods in Membrane Biology*, Vol. 9, pp. 1-201. (New York: Plenum)

Molday, R. S. (1977). Cell surface labelling techniques for SEM. *SEM/IITRI*, **II**, 59

Molday, R. S. and Maher, P. (1980). A review of cell surface markers and labelling techniques for scanning electron microscopy. *Histochem. J.*, **12**, 273

32

Animal models for SEM studies on cervical carcinogenesis

C. A. RUBIO and I. MAY

Department of Pathology, Karolinska Sjukhuset, S-10401 Stockholm, Sweden

SEM PATTERN IN THE CERVIX OF NORMAL RODENTS

Under the influence of endogenic sexual hormones the cervical epithelium of rodents undergoes morphological variations, which may be registered at the light microscopical level by studying exfoliated cells or histological preparations. The hormonal cycle of rodents is divided, for practical purposes, into four main phases: proestrus, estrus, metaestrus, and diestrus. By detecting the phase of the cycle in exfoliated cells before sacrificing the animal, or in post-scanning histological preparations of the epithelium, it is possible to investigate the SEM changes occurring during a particular phase of the estrous cycle (Figure 1a). Normal animals at proestrus (Figure 1b) display regular cobblestone-like structures, separated by deep furrows. At the surface of the cobblestones, closely packed microvilli of regular size are observed. At estrus (Figure 1c), the epithelium presents a different SEM architecture. The surface demonstrates large, flat mosaics with well-defined borders. These mosaics are covered by a network of continuous, parallel, sometimes branched, microrughae. Animals at metaestrus (Figure 1d) display structures between cobblestones and mosaics (i.e. of intermediate size). The surface of these intermediate structures is furnished with fragmented ridges, broader than microvilli, arranged in rows. These structures are believed to be fragmented microrughae. Animals at diestrus (Figure 2a) show mosaics or intermediate structures covered by short, closely packed, irregular microvilli.

Some individual variations, however, may occur in the four groups. This is not surprising, considering that the classification of the estrous cycle into four main phases is a practical way to separate a dynamic process, being a part of a continuum where transitional steps may be observed.

The administration of estrogens to intact, or to oophorectomized rodents, gives a characteristic picture at the SEM level; flat, polygonal mosaics covered by a mesh-like network of microrughae. Many of the superficial cells are loosely attached to the underlying cells and usually present rolled-up borders.

THE HISTOLOGICAL CLASSIFICATION OF CARCINOGEN-INDUCED CERVICAL ATYPIAS

After repeated application of a potent carcinogen to the cervical epithelium, namely 1,2-benzopyrene, various degrees of epithelial atypia may occur. Based on the degree of severity, they are classified into atypias grade I (Figure 2), II, and III. Atypias grade I–II demonstrate, in addition, cell differentiation towards the epithelial surface, and are therefore considered equivalent to cervical dysplasia in human subjects. Atypias grade III show replacement of the epithelium by malignant cells and no signs of cell maturation towards the surface. They are the counterpart of carcinoma *in situ* in human subjects.

SEM IN ATYPICAL CERVICAL EPITHELIUM

Low-power examination of the epithelial atypias grades I, II, and III, demonstrate polygonal mosaics, cobblestone structures and/or intermediate structures (Figure 3a), differing from their normal counterparts because of the irregularity in size, moderate anisovillosis, sometimes with bizarre anisovillosis (i.e. having long, finger-like protrusions) (Figure 3b), irregular, fragmented microrughae and deep intercellular furrows. Grade III atypias may be difficult to differentiate at the SEM level from invasive carcinoma.

SEM IN INVASIVE CARCINOMA OF THE CERVIX

Invasive carcinomas are characterized by marked irregularity in size and shape of the cells with cell overlapping (Figure 3c). The cells usually demonstrate bizarre anisovillosis (Figure 3d).
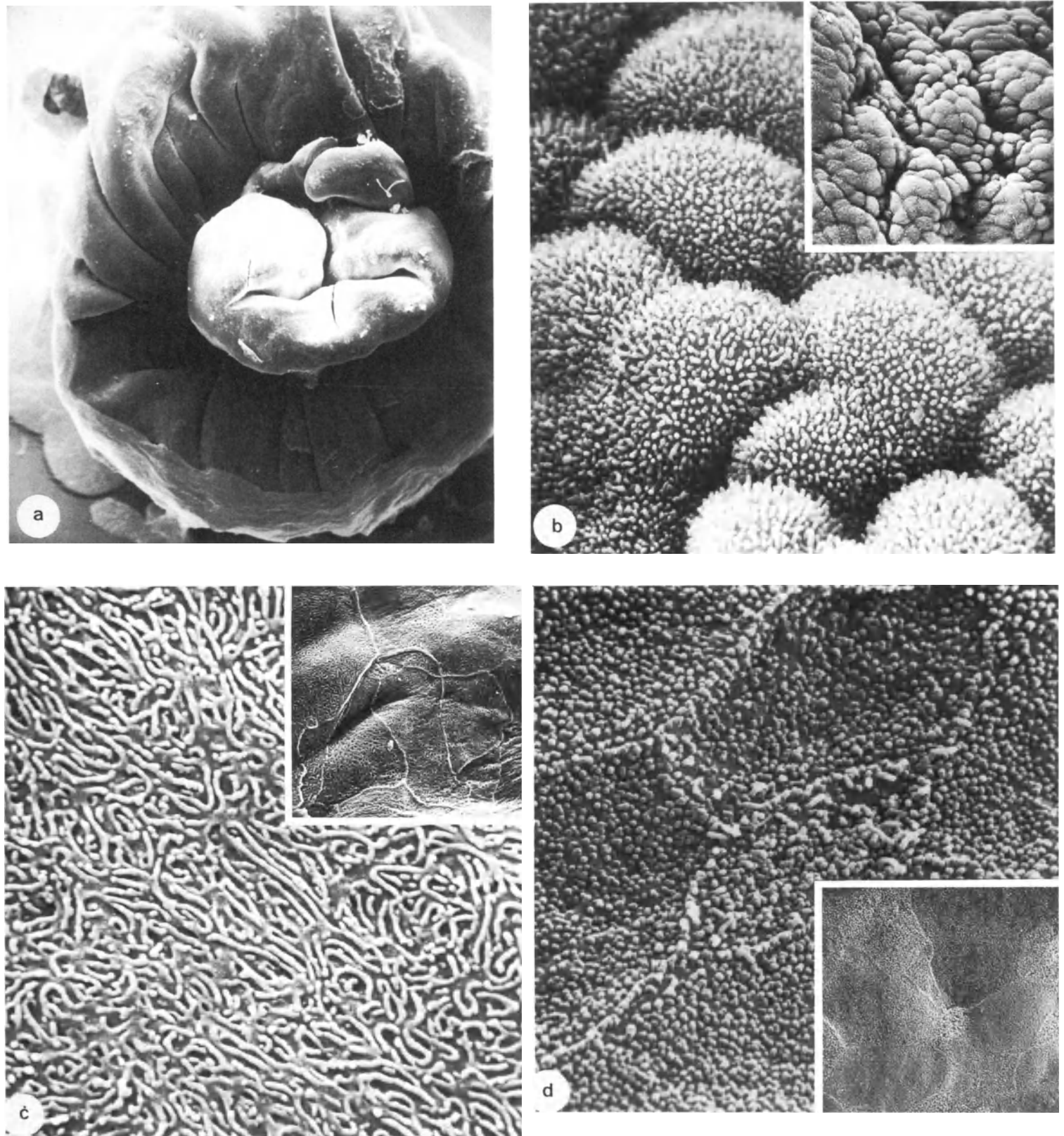
Figure 1

a: Uterine cervix surrounded by folded vaginal cuff (×200)

b: Uterine cervix at proestrus. Note cobblestone structures furnished with regular microvilli (×6200). *Insert:* low magnification in the same animal demonstrating regular cobblestone formation

c: Uterine cervix at estrus with parallel and convoluted

microrughae (×6300). *Insert:* low-power view in the same animal showing large flat mosaics

d: Uterine cervix at metaestrus with fragmented microrughae arranged in rows (×6200). *Insert:* low-power view in the same animal showing intermediate structures between cobblestones and mosaics
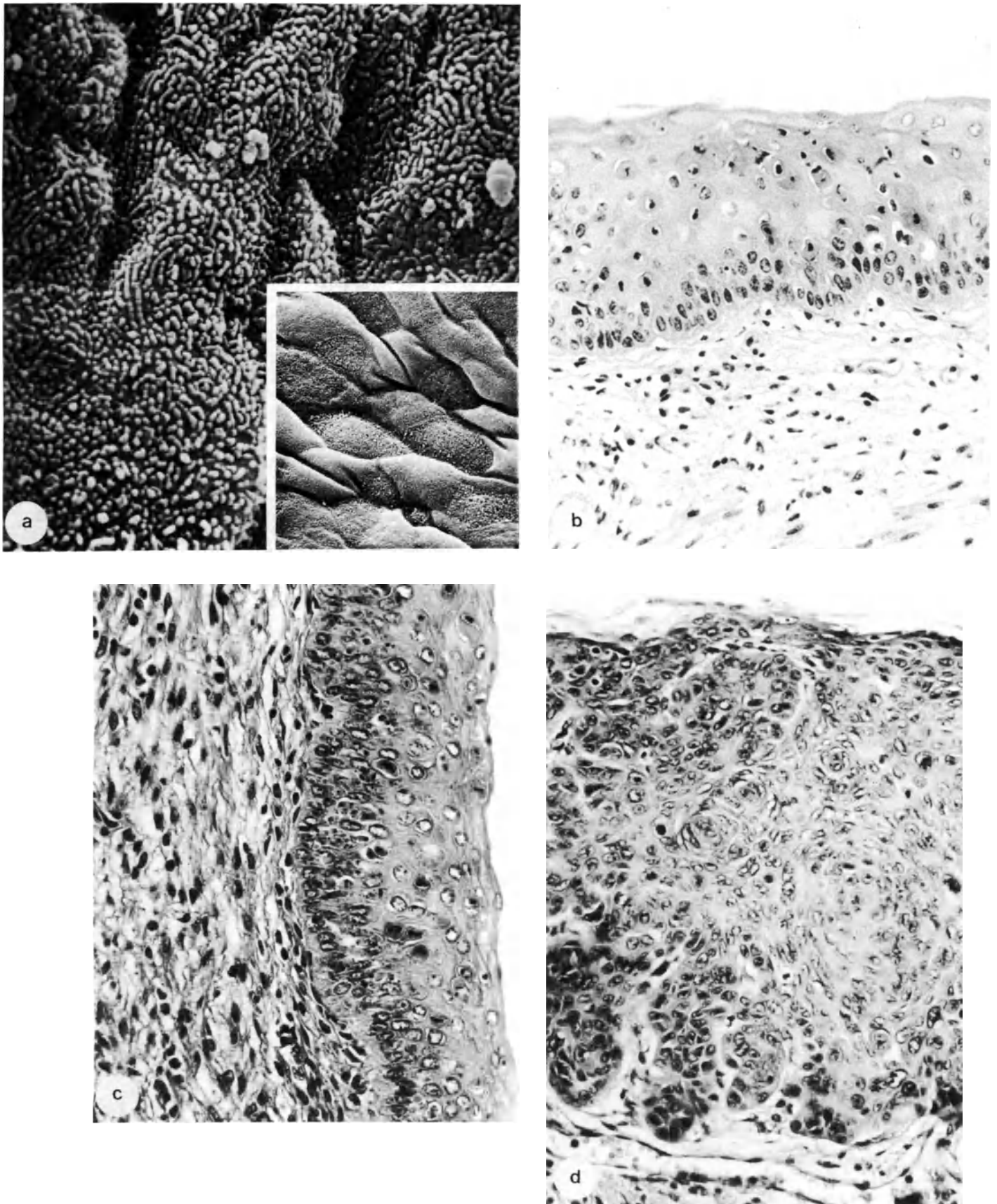
Figure 2

a: Uterine cervix at diestrus showing short microvilli (×6700). *Insert:* low-power view in the same animal showing polygonal or oval mosaics with sharp borders

b-d: Uterine cervix after protracted treatment with 3,4-benzopyrene

b: Atypia grade I (slight dysplasia). Conventional histology (H&E, ×250)

c: Atypia grade II (moderate dysplasia). Conventional histology (H&E, ×250)

d: Atypia grade III (carcinoma *in situ*). Conventional histology (H&E, ×250)
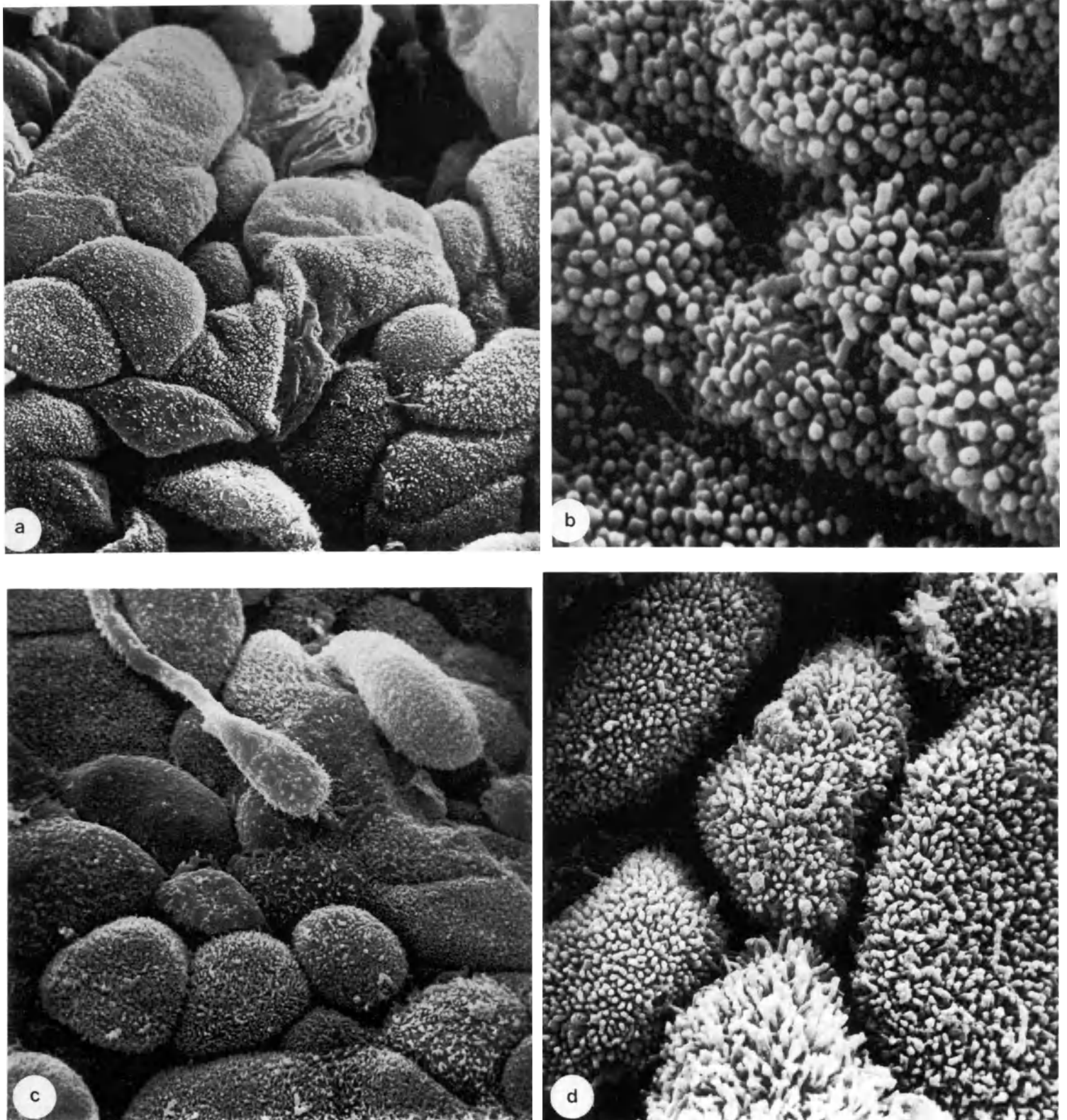
Figure 3 Uterine cervix after protracted treatment with 3,4-benzopyrene
a: SEM in grade II atypia showing irregular cobblestones (×2070)
b: High magnification of Figure 3a. Note irregularity of microvilli (×11 700)

c: Invasive squamous carcinoma. Note irregular cobblestones and overlapping abnormally shaped cells (×2070)
d: Invasive squamous carcinoma. Bizarre irregularity of microvilli is observed (×6120)
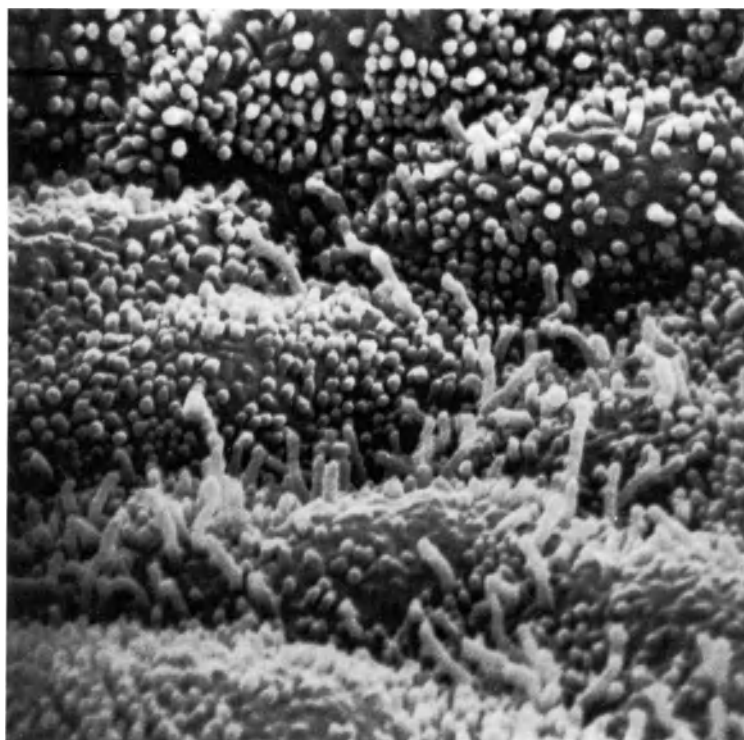
Figure 4 SEM in histologically normal squamous cervical epithelium after protracted treatment with 3,4-benzopyrene. Note bizarre microvilli (×10 980)

SEM IN THE NORMAL EPITHELIUM OF CARCINOGEN-TREATED ANIMALS

Not all animals develop epithelial atypias after iterated application of cervical carcinogens. More than one-third of the animals usually show normal-looking epithelium at the light microscopical level. The SEM examinations reveal in those animals, however, a surface topography which differs from the normal counterpart. Changes such as irregular, fragmented microrughae, moderate anisovillosis and even bizarre anisovillosis (Figure 4) may be present in the histologically normal-looking epithelium.

These changes, which sometimes may resemble genuine atypical epithelium, suggest that alterations at the cell membrane level may precede the nucleocyto-plasmic changes required for the recognition of atypical epithelium in conventional histological preparations.

CONCLUSIONS

Various alterations of the cell surface topography are present during the process of cervical carcinogenesis in rodents. Since similar changes are observed in preinvasive and invasive carcinomas of the human cervix, the animal model allows us to monitor in detail, during a relatively short period of time and under controlled conditions, the ultrastructure of the surface epithelium during the process of cancer development in that organ.

NOTE

All figures correspond to the squamous epithelium of the uterine cervix in C57Bl mice.

Bibliography

Jordan, J. A. and Williams, A. E. (1971). Scanning electron microscopy in the study of cervical neoplasia. *J. Obstet. Gynaecol.*, 78, 940

Kenemans, P., Davina, J. H. M., de Haan, R. W., van der Zanden, P., Stolk, J. G. and Stadhouders, A. M. (1981). Cell surface morphology in epithelial malignancy and its precursor lesions. *Scanning Electron Microsc.*, 3, 23

Rubio, C. A. and Lagerlöf, B. (1974). Autoradiographic studies of dysplasia and carcinoma in situ in cervical cones. *Acta Pathol. Microbiol. Scand., A*, 82, 411

Rubio, C. A. and Lagerlöf, B. (1974). Studies on the histogenesis of experimentally induced cervical carcinoma. *Acta Pathol. Microbiol. Scand. A*, 82, 153

Rubio, C. A. and Kranz, I. (1976). The exfoliating cervical epithelial surface in dysplasia, carcinoma in situ and invasive squamous carcinoma. I. Scanning electron microscopic study. *Acta Cytologica*, 20, 144

Rubio, C. A. (1976). The cervical epithelial surface. III. Scanning electron microscopic study in atypias and invasive carcinoma in mice. *Acta Cytologica*, 20, 375

Rubio, C. A. (1976). The exfoliating cervico-vaginal surface. II. Scanning electron microscopical studies during the estrous cycle in mice. *Anat. Rec.*, 185, 359

Rubio, C. A. and Einhorn, N. (1977). The exfoliating epithelial surface of the uterine cervix. IV. Scanning electron microscopical study in invasive squamous carcinoma of human subjects. *Beitr. Pathol.*, 161, 72

Rubio, C. A. (1977). Animal model: carcinogenesis in the uterine cervix in mice. *Am. J. Pathol.*, 88, 799

Sherman, A. I. (1977). Comparison of cancer cell surfaces of the lower reproductive tract by scanning electron microscopy. *Am. J. Obstet. Gynecol.*, 129, 893

Williams, A. E., Jordan, J. A., Murphy, J. F. and Allen, J. M. (1973). The surface ultrastructure of normal and abnormal cervical epithelia. *Scanning Electron Microsc.*, 3, 597

EPILOGUE

33

Clinical application of SEM to human reproduction

T. K. A. B. ESKES*, E. S. E. HAFEZ† and P. KENEMANS*

* Department of Gynecology/Obstetrics, University of Nijmegen, Nijmegen, The Netherlands
† Department of Gynecology/Obstetrics, Wayne State University School of Medicine, Detroit, Michigan, USA

The surface of cells that line the reproductive tract yields information that is valuable to both the morphologist and the pathologist. Extensive investigations have been conducted on the surface ultrastructure of the epithelium of the female and male genital tract in health and disease (Tables 1 and 2). Both transmission (TEM) and scanning (SEM) electron microscopy have provided new details and dimensions to the already existing scientific knowledge (Hafez et al., 1975; Ferenczy, 1980). In many instances the pathological diagnosis can be unequivocally established by light microscopy (LM), but in some instances it is more advantageous to combine LM with TEM and/or SEM.

TEM has proved to be a complementary technique to LM, shedding new light on problems such as 'benign or malignant?' or 'carcinoma or sarcoma?' The importance of SEM lies in its great sampling capacity and its potential for relating local characteristics to the overall structure. Especially in the field of reproduction, many initial attempts have been made by using SEM in a clinical application. For example, the following organs have been viewed by SEM, and applications have been utilized:

(1) amniotic fluid cells provide important information about the fetus. Studies of the surface ultrastructure of such cells identified four cell populations in mid-gestational fluids (Tyden et al., 1981);
(2) the placenta – description of maturation and various classes of pathological conditions (van Geyn et al., 1975);
(3) the oviduct – description of two types of hydro-salpinges with different prognostic significance (Vasquez et al., 1982). It is possible to use SEM to evaluate the ratio of ciliated to non-ciliated epithelial cells, which may have a prognostic significance in infertile patients (Figure 1);
(4) cervical cytology – SEM's capacity for early discrimination of premalignant cells (Allen et al.,

1976; Kenemans et al., 1981);
(5) spermatozoa – description of pathological spermatozoa with prognostic significance, and classification with the use of X-ray microanalysis (Gould, 1977).

A difference in surface morphology has been observed in cancer cells compared with normal cells, as viewed by SEM. Human epithelial cells from various gynecological malignancies exhibit an abundance of long, pleomorphic microvilli, especially those present in effusions. In squamous epithelium of the vagina and cervix, microridge systems, which are present on normal superficial cells, are progressively replaced by microvilli. During experimental and clinical oncogenesis, these microvilli increase in number and degree of pleomorphism. Cell lines derived from a human cervical tumor (Hela) also show abundant long microvilli.

The question of whether or not the appearance of long, pleomorphic microvilli reflects an irreversible alteration of the epithelium, thus providing an early indicator of irreversible neoplastic transformation, is intriguing yet still remains unanswered. Although SEM has contributed significantly to the description of oncogenesis, it has not, as yet, had any early diagnostic, prognostic or therapeutic significance in the field of gynecological oncology (Kenemans et al., 1980, 1981).

THREE-DIMENSIONALITY WITH SEM

Extensive literature has been reported on numerous ultrastructural changes found in cellular and tissue organizations in relation to physiological changes, pharmacological influences, instrumentation procedures, and pathological processes (Tables 1 and 2). No reports have been made, to date, which treat this dynamic morphology systematically, based on quantitative data.

Scanning electron micrographs create a three-

313

Table 1   Some surface ultrastructural characteristics of human female reproductive organs as viewed by SEM, and their possible application to diagnostic pathology

Organ	Type of syndrome	SEM characteristics	Reference
Ovary	Normal	Superficial epithelium does not completely cover ovarian surface; patchy areas of cells with and without dense microvilli; in preovulatory follicles, most granulosa cells are polyhedral in shape with smooth surface, whereas those facing the follicular cavity are elongated and flattened, and covered with material having a filamentous reticular texture; follicular cells are uniform in size and shape with microvilli and evaginations	
	Polycystic	Superficial epithelium surrounds whole surface and possesses dense microvilli, solitary cilia, and blebs, resembling fetal ovary; follicular cells have irregular size and shape with few microvilli	Hafez and Makabe (1979)
	Benign and low-grade variants of mixed mesodermal tumor	Neoplasms are distinct; stroma is more cellular than that of adenofibroma; epithelium is not malignant, as in carcinosarcoma and mixed mesodermal tumors; remarkable variability in cellularity and atypism of stromal cells	Kao and Norris (1978)
	Endometroid carcinoma	Apical surfaces of cells covered with short and irregular microvilli similar to that of proliferative endometrium	Fenoglio et al. (1978)
	Cyclical changes	Cilia are prominent in early follicular phase, luteal phase, postmenopausally, in late pregnancy and in puerperium	Jansen (1980)
Oviduct	Organ culture challenged with N. gonnorrhoeae and endotoxins	Ciliostatic effects on microciliary activity followed by morphological changes in ciliated cells	Mardh et al. (1979)
Endometrium	Cyclical changes	The epithelium changes characteristically during the menstrual cycle, in the follicular phase the luminal surface of the secretory cells possesses rather long and regular microvilli. In the luteal phase the cells acquire apical protrusions and possess shorter and fewer microvilli – this latter is the appearance when implantation occurs	Fadel (1976) Ferenczy et al. (1972) Ferenczy and Richart(1973) Nilsson and Nygren (1972)
		After administration of estrogen alone the epithelial cells showed a uniform surface area; cell surfaces were bulging and possessed numerous fairly long microvilli which often formed tuft-like structures; length of microvilli seemed to depend upon potency of estrogen After sequential administration of estrogen followed by a gestagen the surface was characterized by microvilli and apical protrusions; microvilli were long and numerous when priming estrogen was estradiol + estriol, while they were shorter when estradiol valerate was given; apical protrusions were large and more numerous after administration of progesterone than after treatment with norgestrel or noretisterone; type of estrogen used also influenced development of protrusions; they were largest and more numerous after treatment with estradiol and estriol followed by progesterone	Nathan et al. (1978)
	Treatment with estriol with and without pro-gesterone (post-menopause)	Treatment with estriol produces an estrogen response in the non-ciliated cells, developing many long microvilli, sometimes in tufts. Sequential treatment with initial estriol priming followed by estriol and progesterone combined caused a slight secretory transformation; e.g. increase in size and number of apical protrusions of cells	Nilsson et al. (1980)

Organ	Type of syndrome	SEM characteristics	Reference

	Cells adherent to non-medicated and medicated IUDs	Surface of inert IUDs contained macrophages with some polymorphonuclear leukocytes, erythrocytes, a few platelets and fibrin fibres.
		    Polymorphonuclear leukocytes were the principal cells on copper IUDs
		    Larger numbers of cells on inert arms than on active part of progestasert IUD
			Sheppard and Bonnar (1980b)

	Response of endometrial blood vessels to copper	Stromal capillaries below the devices show extensive microthrombosis with platelet and fibrin aggregations filling gaps in endothelial linings of vessel.
		    Stromal hemorrhage and erosion of surface epithelium associated with vascular pathology.
		    In stromal vessels of endometrium not in contact with IUD, surface epithelium is intact and underlying stromal capillaries show breaks in endothelial lining but without a hemostatic plug
			Sheppard and Bonnar (1980a)

	Finite cell lines from tissue culture	Epithelial cell lines had numerous microvilli and highly specialized 'junctional complexes' typical of glandular epithelium	Trent et al. (1980)
	Atypical hyperplasia, cystic glandular hyperplasia	Irregular shape and size of glands on the cut surface; thickly ciliated endometrium, with clumping of cilia	Ferenczy and Richart(1973) Ferenczy (1977) Carr et al. (1980)

Cervix uteri	Fine angio-architecture using cast formation to evaluate vascular patterns of cervical lesions	In the squamous epithelial region of normal cervix, vessels of almost the same size communicate with each other forming a well-regulated capillary network right below the epithelium; vessels are running vertically and regularly to the superficial capillary network in lateral view.
		    In vascular cast of columnar epithelial region in the cervical canal the net is more undulating than that of squamous epithelium and has many avascular cavities at the sites of cervical glands. The net layer is thick because of piles of capillary meshworks, a very different pattern from that of squamous epithelium. In the typical ectopic lesions with many grape-like villi the vascular structure is different from that of columnar epithelium or squamous epithelium, with many chain-like vessels corresponding to central blood vessels of grape-like villus. Two types of vascular structure are associated with a pathologic diagnosis of cervical dysplasia. The so-called 'basket structure' corresponding to colposcopic mosaic is easily seen and the network is more dense than the normal. In colposcopic punctation individual tips of hairpin-like vessels are slightly irregular compared to the inflammatory hair pin like vessels.
		    Vascular structure accompanying the so-called irregular mosaic pattern, histologically carcinoma *in situ*, is formed by many baskets of various size. The rim of each basket is thickened and firmly established.
		    In early invasive carcinoma with a more irregular punctation pattern, the tip of each protruding vessel is more irregular and resembles a cauliflower. With frank invasive cancer the fundamental angioarchitecture is completely destroyed; advancing grade of pathologic change is related to striking irregularities in size, shape, course and arrangement of the vascular patterns of hairpin-like and basket-like structures. These changes are predominant in the distal parts of the terminal vessels.
			Sekiba et al. (1979)

Organ	Type of syndrome	SEM characteristics	Reference
	Cellular thorn-like projections	Thorn-like projections in the cilio-secretory epithelium of the ventral surface of endocervix seem to be characteristic of a new cell type noted at different stages of the menstrual cycle (days 8, 14 and 21) in healthy fertile women	Chretien and Guillon(1979)
	Long-term organ culture of ex-plants (24 weeks)	Epithelium was viable for 24 weeks of culture, as demonstrated by ultrastructural morphology and mitotic activity. Epithelium of explants retained a near normal morphology for 2–4 weeks; decreased mucus secretion in columnar cells, focal epidermoid metaplasia and increase in autophagic vacuoles; a slowly progressive transformation of the columnar epithelium into a metaplastic epithelium with loss of mucus-secreting columnar cells and ciliated cells, and appearance of cuboidal and flattened epidermoid cells, forming two or three layers. Metaplasia began at the top of papillae and ridges and extended progressively downwards into clefts. In a few areas deep in the clefts, columnar cells retained evidence of mucus secretion during the entire duration of culture. Epidermoid metaplasia developed in explants by transformation of columnar mucous cells into cuboidal and flattened cells with epidermoid characteristics	Schurch et al. (1978)
	Ectocervical and endocervical cells in tissue culture	Ectocervical cell colonies exhibit a stratified appearance, whereas endocervical epithelial cells grow in a single layer with smooth overlapping of adjacent cells. Cultures should permit observation of effects of steroids, viral and chemical carcinogens, on ultrastructural integrity of cells	Vesterinen et al. (1980)
	Neoplasia	Cytodynamics of neoplastic cells Interesting details of cytomorphology with no absolute criteria to be used for cytodiagnosis	Ferenczy and Gelfand (1979) Murphy (1977)
	Dysplasia and metaplasia	Cells exfoliated from an invasive malignancy are distinct from those derived from carcinoma in situ on the basis of number of microvilli and presence of anisomicrovillosis; no significant SEM characteristics	Rubio and Einhorn (1977) Hafez et al. (1975) Allen et al. (1976) Kenemans et al. (1980)
Cervical mucus	Fertile women with biphasic BBT, with no hormonal medi-cation	The meshes of CM gradually increased toward time of ovulation and reached maximal dimensions (10–25 μm in diameter) at ovulation which then decreased rapidly to 1–2 μm 2 days after ovulation	Takano et al. (1979)
	During menstrual cycle	There were two types of fibrous structures in midcycle CM: (1) long, thick fibers that vary in diameter from 0.5 to 5 μm and run parallel to each other and (2) microfibrils that range from 500 to 1500 Å in diameter, the fibers represent the micelles that give spermatozoa their directional approach through the cervix	Zaneveld et al. (1975)
	During pregnancy and menopause	A striking tightening of the ultrastructural glycoprotein framework: this occurred very rapidly at beginning of pregnancy but was variable near the menopause	Chretien (1978)
	Effect of sodium bicarbonate douching in post-coital test	pH changes, and alteration in cervical mucus electrolyte components detected by SEM and energy-dispersive X-ray analysis	Ansari et al. (1980)

Organ	Type of syndrome	SEM characteristics	Reference
Cervical smears and buccal mucosa cells	Phase contrast visualization	Microridges were identified on mature cells of buccal mucosa and in cervical smears, either alcohol or spray fixed, and even in smears up to 5 years old. Identification of microridges may be of diagnostic interest in the evaluation of cervical smears (can be also observed by phase contrast)	Miles (1978)
Vagina	Tampon-associated vaginal ulceration	Colposcopically visible alterations of vaginal mucosa associated with use of tampons; mucosal drying, epithelial layering and microulcerations. Transient changes involve fluid transfer with subsequent impairment of intercellular bridges and loss of cell coherence. Tampon products containing super-absorbents are more likely to produce microulcerations than are conventional tampons when worn at times other than during active menstruation. These alterations could lead to clinically obvious lesions of the vagina.	Friedrich and Siegesmund (1980)
Neisseria gonorrhoeae on genital epithelium	Attachment of different gonococcal colony phenotypes to explants of human genital tract epithelium was studied by SEM and radioisotope-labeled gonococci	Heavily piliated organisms attached in greater numbers than non-piliated organisms. Gonococci from transparent colony phenotypes attached in higher numbers than gonococci from opaque phenotypes to all tissues. Transitional cells from cervical tissues showing a gradual squamocolumnar transition demonstrated more gonococci attached per surface area than either endocervical or fallopian tube epithelium. Squamous epithelium showed the smallest number of attached gonococci; in all tissues the attachment of the gonococcus was to the tips and surfaces of microvilli	Draper et al. (1980)
Mammary gland	Cancer	Clumping of microvilli	Spring-Mills and Elias (1975)
	Dysplasia vs cancer	SEM differences	Spring-Mills and Elias (1976)
		No differences	Halter et al. (1979) and Domagala and Koss (1980)
	Cells of metastatic mammary carcinoma in fluids	Shaggy surfaces covered with numerous microvilli of variable length, cell borders are well demarcated	Koss and Domagala (1980)

dimensional impression due to the unusually large depth of field perception obtained with this microscopic method. However, these pictures are only quasi-three-dimensional and do not contain adequate information concerning qualitative or quantitative spatial relationships. Therefore, techniques for *stereopsis* (stereovisualization of specimens) and *stereometry* (quantitative stereometric analysis), are of great significance in the field of biological SEM (Boyde, 1974).

In addition to the perception of three-dimensionality, the measurement of depth, height and other distances – which are present in the microstructure – can provide important information when viewed by SEM. Quantitative photogrammetric analysis of stereopairs is possible with either simple or highly sophisticated instruments. The possibility of making sound biological and scientific statistical statements relies on the ability to quantify the qualitative pictures that are available.

FURTHER APPLICATION OF SEM

SEM and conventional TEM seem to be very promising to describe the normal, reactive, and neoplastic cells, as well as tumor histogenesis – particularly from the urogenital epithelia. The extent of use has been broadened by utilizing paraffin block material which has already been available for LM. In retrospect, all materials can therefore be studied (Carr et al., 1980).

It is essential for normal variations in reproductive

Table 2   Some surface ultrastructural characteristics of human gestation as viewed by SEM, and their possible application to diagnostic pathology

Organ	Type of syndrome	SEM characteristics	Reference
Endometrium	Implantation	Apical protrusions at implantation site give the impression that they are flexible and mobile. Perhaps they are adhesive and capable of easily forming a contact with a blastocyst; apical protrusions of the human uterus mucosa might assist at the attachment of the blastocysts	Nilsson *et al.* (1978)
Amniotic membrane	Normal	Surface covered with microvilli and 'blebs'; intercellular junction is formed by desmosomes and a labyrinthine channel system and at the base pedicels extend into the basement membrane. Cell shedding uncovers the basement membrane which seems to preserve the intact amniotic cavity	van Herendael *et al.* (1978)
	Polyhydramnios	Normal incidence of all four patterns found in normal amnion at term without abnormal features	Pollard *et al.* (1979)
	Oligohydramnios	Two of four normal patterns predominated and intercellular canals were sparse	
Amniotic fluid	Cell exfoliation during early pregnancy	No exfoliation from amniotic epithelium; heavy detachment of cells and cell fragments from fetal skin (detachment phenomena are easily produced artifactually by tissue scrapings and improper tissue preparation)	Bergstrom (1979)
	F and AF cell types in culture	F-type cultures have abundant extracellular type I collagen fibers, identical with cultured human dermal fibroblasts. No type I collagen fibers in cultures of AF cells. Instead, fine filamentous material is admixed with amorphous material adjacent to cell membranes where epithelial basement membrane glycoprotein is localized. Parallel arrays of cells are present at confluency of F cultures, typical of cultured dermal fibroblasts. AF cultures show a much looser growth pattern at confluency.	Priest *et al.* (1978)
	Amniotic fluid cells (mid-trimester pregnancy)	Four cell populations; a parallel study of tissue surfaces in contact with or communicating with the amniotic fluid showed that some tissues made no contribution to the cell populations, while others contributed extensively. Two principal cell shedding mechanisms were identified, *viz.* exfoliation of whole cells and detachment of cellular fragments. The latter mechanism was observed from skin and umbilical cords during a limited period in mid-pregnancy. Majority of cells were derived from exfoliation of squamous epithelia	Tyden *et al.* (1981)
	Viable cell populations of AF cells 14–16 weeks of gestation; cell viability judged by Trypan blue stainability	Large squames appeared flattened but in cells with nuclei a small bulge was evident on the surface. Cell surfaces showed numerous regular microvilli or short microridges; surface appearance of AF squames varied; some cells possessed prominent microvilli and in others a delicate network of microridges predominated. These surface variations of AF squames represented differences in tissues of origin from which these cells were desquamated (e.g. skin, bladder, vagina, buccal mucosa); fetal tongue and buccal mucosa revealed that surfaces of epithelial cells from these tissues were strikingly similar to AF squames.	Cutz and Cohen (1978)

Organ	Type of syndrome	SEM characteristics	Reference
		Appearance of amniotic cells was distinctly different from that of squamous epithelial cells. Single amniotic cells usually presented a prominent nuclear bulge and cell surface was evenly covered by delicate, short microvilli	Cutz and Cohen (1978)
Placenta (chorionic villi)	Differentiated regions associated with attachment of chorionic villi, phagocytosis of maternal erythrocytes and syncytiotrophoblast repair	(a) differentiated zones of trophoblast covered by fewer microvilli than adjacent syncytial cell surface and which extend as a narrow, usually distal protrusion of the chorionic villus; (b) during apparent phagocytic uptake of maternal erythrocytes by syncytiotrophoblast, cell surface lining forming vacuole with an irregular microvillous surface; (c) damaged placenta undergoing repair exhibits masses of cells with conspicuous microvillar cell surfaces	Clint *et al.* (1979)
	Young and mature placenta	In young placentas the ramifications of chorionic villi start in form of buds which are transformed into tendrils with swollen extremities; swellings resemble buds ready to bloom; villi intertwine in different positions; both the villi and their tendrils are covered with dense layers of microvilli. In mature placentas the surfaces of the chorionic villi and their ramifications are covered with microvilli which are less numerous and shorter. Invaginations on surfaces of villi, younger and newly budding microvilli, similar to those observed in young placentas, were seen in invaginated regions	Demir (1979)
	After hypertonic saline solution	Serious damage, especially to syncytium, in subchorial zone and transitional and decidual zones; a very short exposure *(in vitro)* to hypertonic solution produces impressive histological changes in placental tissue	Stegeman and Treffers (1980)
	Normal	Syncytial surface has a finely granular appearance due to microvilli, while terminal main stem villi surface has rows of 'tall' microvilli, giving it a wavy appearance. The waves have a parallel arrangement, are spaced with periodic regularity, or may fuse to give a honeycomb appearance. Chorion from the central part of cotyledon has irregular coral-like appearance. Minor stem villi are coarse, rounded with varying calibers. Terminal chorionic villi branch off irregularly. Chorion from the intermediate or dense part of cotyledon has longer terminal villi, which have more regular appearance and uniform caliber than terminal villi from central part of cotyledon	Sandstedt (1979)
	Circumvallate	Abnormal vascular pattern 'seaweed'	
	Histological classification	Peripheral villous tree is roughly divided into stem (ramuli), intermediate and terminal villi; intermediate villi are further subdivided as mature and immature types, which are found between the stem and terminal villi; some of the terminal villi possess a local specialization described as the neck region	Kaufmann *et al.* (1979)
	Functional and pathological	Functional diagnosis of placenta is very difficult with LM and TEM because of complicated surface structure; SEM may be helpful but results are preliminary and sporadic	Bergstrom (1971) Ludwig and Metzger (1976)

Organ	Type of syndrome	SEM characteristics	Reference
Umbilical arteries and veins	Smoking and non-smoking mothers	Severe vascular changes in the smoking group; similar changes may be present in the vessels of the newborn child	Asmussen (1978)
Embryonic tail	Cell death during disappearance	The tail, a prominent feature of human embryo during stage 14, is composed of paired somites, mesenchyme and extensions of neural tube, notochord and gut; the tail grows with the embryo through early stage 17 when it extends more than a millimeter from the trunk; overgrowth by the trunk at the base of the tail may account for the loss of part of its length during late stage 17 and stage 18. During stage 17 cells begin to die in all structures throughout the tail; cell death continues in succeeding stages reaching massive numbers by stages 18 and 19 and the tail becomes progressively less prominent. Most of the dead cells are phagocytosed, debris-laden macrophages migrate from the tail to the body; late stage 21 or early stage 22 there is no free tail.	Fallon and Simandl (1978)
Fetal hair canal	Initial hair eruption in 15–21-week fetuses	At 15–17 weeks of age the epidermal surface of the entire body was still covered with periderm. By 21 weeks fetal age, various stages in development of hair in all areas of the body. Epidermal surface of the entire body was still covered with periderm. By 21 weeks fetal age, various stages in development of hair in all areas of the body. On lower extremities and buttocks, regularly spaced elongate ridges marked position of intraepidermal hair canals which had been excavated within hair tract. Over certain of these ridges the periderm was interrupted, and keratinized cells that lined the canal were exposed. Hair canals were even longer on the trunk and upper extremities and the epidermal surface at these sites had thinned to the extent that hairs contained within the canals were visible within cellular sheaths or were partially released	Holbrook and Odland (1978)

tissues to be investigated further, since the significance of the abnormal findings can only be recognized against the background of the normal. Thus, a much broader range of control material should be examined to define the limits of healthy morphology more clearly. The data obtained by SEM should be more informative than those obtained by LM or TEM, and should be meaningful for the diagnoses needed by the clinician for therapeutic purposes. Also, the results should be reliable enough for such drastic therapeutic consequences as organ resection or treatment with cytostatics.

A simple and quick preparation method is needed to allow the routine subsequent LM examination of cross-sections. This preparative technique should cause minimal alterations in the surface of the tissues in order for the SEM data to be credible and interpretable. Immune and other surface labeling techniques in combination with SEM can be successfully applied for several problems of basic cell research. The improved resolution of SEM enables the application of very small markers such as gold or ferritin, which can eventually be combined with X-ray microanalysis.

Various techniques have to be developed to help quantify results obtained by SEM. SEM has been most widely used in the secondary electron imaging mode. Back-scattered electron imaging should be applied to localize subsurface structures with the help of element contrast. As several biological cellular structures have similar surface ultrastructures, complementary techniques, such as TEM, can be beneficial when used in conjunction with SEM. The combination of such techniques enables a more discriminative evaluation, while quantification may also become easier and better. Several other complementary techniques can be used in conjunction with SEM, such as energy loss spectrometry, laser microprobe mass analysis, secondary ion mass spectrometry, proton microprobe, and X-ray microanalysis. These promising techniques have introduced new functional elements into SEM
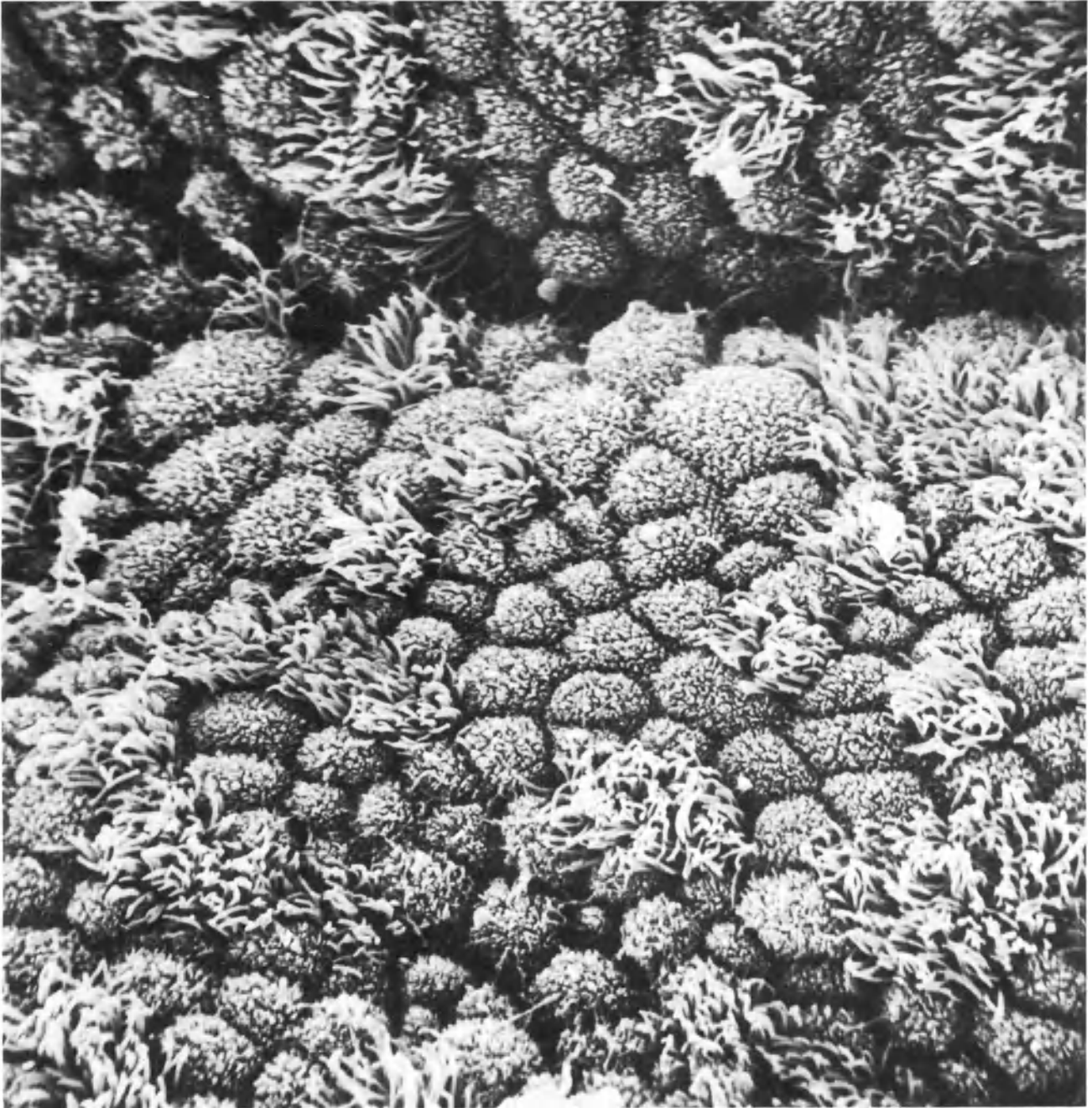
Figure 1 SEM of human fallopian tube. It is possible to use SEM to evaluate the ratio of ciliated to non-ciliated epithelial cells, which may have a prognostic significance in infertile patients

investigation, the significance of which still awaits elucidation.

CONCLUDING REMARKS

At present, the surface ultrastructural characteristics of the human reproductive organs during health and disease have not been fully established. The results of SEM do not totally justify their application to a diagnostic gynecology/andrology. The same results, for instance, can be obtained by routine LM and TEM with their respective adjuvant techniques such as histochemistry or immune histology. Although SEM does have potentially large diagnostic and prognostic significance, further research is essential, especially in the field of fertilty and oncology where clinical applications seem eminent.

References

Allen, J. M., Murphy, J. F. and Jordan, J. A. (1976). The use of scanning electron microscopy in cervical cytology: results from the examination of 218 patients. *SEM IITRI*, 9 (II), 315

Ansari, A. H., Gould, K. G. and Ansari, V. M. (1980). Sodium bicarbonate douching for improvement of the postcoital test. *Fertil. Steril.*, 33, 608

Asmussen, I. (1978). Arterial changes in infants of smoking mothers. *Postgrad. Med. J.*, 54, 200

Bergstrom, S. (1971). Surface ultrastructure of human amnion and chorion in early pregnancy. A scanning electron microscopy study. *Obstet. Gynecol.*, 38, 513

Bergstrom, S. (1979). Amniotic fluid cell exfoliation in early human pregnancy. *Acta Obstet. Gynecol. Scand.*, 58, 353

Boyde, A. (1974). Three-dimensional aspects of SEM images. In Wells, O. C. (ed) *Scanning Electron Microscopy*, Ch. 11, pp. 277–307. (New York: McGraw-Hill)

Carr, K. E., McLay, A. L. C., Toner, P. G., Chung, P. and Wong, A. (1980). SEM in service pathology: a review of its potential role. *SEM Symposium*, 13 (III), 121

Chretien, F. C. (1978). Ultrastructure and variations of human cervical mucus during pregnancy and the menopause. *Acta Obstet. Gynecol. Scand.*, 57, 337

Chretien, F. C. and Guillon, G. (1979). Cellular thorn-like projections in human endocervical epithelium. *Acta Anat. (Basel)*, 104, 323

Clint, J. M., Wakely, J. and Ockleford, C. D. (1979). Differentiated regions of human placental cell surface associated with attachment of chorionic villi, phagocytosis of maternal erythrocytes and syncytiotrophoblast of maternal erythrocytes and syncytiotrophoblast repair. *Proc. R. Soc. Lond. (Biol.)*, 204, 345

Cutz, E. and Cohen, P. E. (1978). Macrophages and epithelial cells in human amniotic fluid: transmission and scanning electron microscopic study. *Am. J. Anat.*, 151, 87

Demir, R. (1979). Scanning electron microscopic observations on the surfaces of chorionic villi of young and mature placentas. *Acta Anat. (Basel)*, 195, 226

Domagala, W. and Koss, L. G. (1980). Surface configuration of human tumor cells. *SEM Symposium*, 13 (III), 101

Draper, D. L., Donegan, E. A., James, J. F., Sweet, R. L. and Brooks, G. F. (1980). Scanning electron microscopy of attachment of Neisseria gonorrhoeae colony phenotypes to surfaces of human genital epithelia. *Am. J. Obstet. Gynecol.*, 138, 818

Fadel, H. E. (1976). The human uterotubal junction: a scanning electron microscope study during different phases of the menstrual cycle. *Fertil. Steril.*, 27, 27

Fallon, J. F. and Simandl, B. K. (1978). Evidence of a role for cell death in the disappearance of the embryonic human tail. *Am. J. Anat.*, 152, 111

Fenoglio, C. M., Puri, S. and Richart, R. M. (1978). The ultrastructure of endometrioid carcinomas of the ovary. *Gynecol. Oncol.*, 6, 152

Ferenczy, A. (1977). Surface ultrastructural response of the human uterine lining epithelium to hormonal environment. A scanning electron microscopy study. *Acta Cytol. Baltimore*, 21, 566

Ferenczy, A. (1980). The female reproductive system. In Hodges, G. M. and Hallowes, R. C. (eds). *Biomedical Research Applications of Scanning Electron Microscopy*, Vol 2, pp. 127–65

Ferenczy, A. and Gelfand, M. M. (1979). The cytodynamics of normal and neoplastic cervical epithelium. *Obstet. Gynecol. Surv.*, 34, 808

Ferenczy, A., Richart, R. M., Agate, Jr. F. J., Purkerson, M. L. and Dempsey, E. W. (1972). Scanning electron microscopy of the human endometrial surface epithelium. *Fertil. Steril.*, 23, 515

Ferenczy, A. and Richart, R. M. (1973). Scanning electron microscopy of hyperplastic and neoplastic endometria. *SEM./IITRI*, 6, 613

Ferenczy, A. and Richart, R. M. (1973). Scanning and transmission electron microscopy of the human endometrial surface epithelium. *J. Clin. Endocrinol. Metab.*, 36, 999

Friedrich, E. G. Jr. and Siegesmund, K. A. (1980). Tampon associated vaginal ulceration. *Obstet. Gynecol.*, 55, 149

Gould, K. G. (1977). Fertility of primate spermatozoa: application of scanning electron microscopy and energy dispersive X-ray analysis. *SEM/IITRI*, 10 (II), 333

Hafez, E. S. E., Barnhart, M. I., Ludwig, H. Jr., Joelson, I., Dancel, J. L., Sherman, A. I., Jordan, J. A., Wolf, H., Stewart, W. C. and Chretien, F. C. (1975). Scanning electron microscopy of human reproductive physiology. *Acta Obstet. Gynecol. Scand.*, Suppl. 40

Hafez, E. S. E. and Makabe, S. (1979). Surface ultrastructure of polycystic ovaries as viewed by electron microscopy. *Acta Eur. Fertil.*, 10, 119

Halter, S. A., Bradbury, E. and Mitchel, W. W. (1979). Diseases of the human breast: Selective isolation and exposure of epithelia and their correlative surface features and histopathology. *SEM Symposium*, 12 (III), 139

Holbrook, K. A. and Odland, G. F. (1978). Structure of the human fetal hair canal and initial hair eruption. *J. Invest. Dermatol.*, 71, 385

Jansen, R. P. (1980). Cyclic changes in the human fallopian tube isthmus and their functional importance. *Am. J. Obstet. Gynecol.*, 136, 292

Kao, G. F. and Norris, H. J. (1978). Benign and low grade variants of mixed mesodermal tumor (adenosarcoma) of the ovary and adnexal region. *Cancer*, 42, 1314

Kaufman, P., Sen, D. K. and Schweikhart, G. (1979). Classification of human placental villi. I. Histology, *Cell Tissue Res.*, 1, 409

Kenemans, P., van der Zanden, P. H. T., Stolk, J. G., Vooys G. P. and Stadhouders, A. M. (1980). Cell surface ultrastructure in neoplasia of the uterine cervix. In Letnansky, K. (ed.), *Biology of the Cancer Cell*, pp. 307–15. (Amsterdam: Kugler)

Kenemans, P., Davina, J. H. M., de Haan, R. W., van der Zanden, P., Stolk, J. G. and Stadhouders, A. M. (1981). Cell surface morphology in epithelial malignancy and its precursor lesions. *SEM Symposium*, 14 (III), 23

Koss, L. G. and Domagala, W. (1980). Configuration of surfaces of human cancer cells in effusions. A review. *SEM Symposium*, 13 (III), 89

Ludwig, H. and Metzger, H. (1976). Zellulare Bestandteile in der Basalplatte der menschlichen Plazenta. *Beitr. Elektronenmikroskop. Direktabb. Oberfl.*, 9, 533

Mardh, P. A., Baldetorp, B., Hakansson, C. H., Fritz, H. and Westrom, L. (1979). Studies of ciliated epithelia of the human genital tract. 3: Mucociliary wave activity in organ cultures of human Fallopian tubes challenged with Neisseria gonorrhoeae and gonococcal endotoxin. *Br. J. Vener. Dis.*, 55, 256

Miles, C. P. (1978). Phase contrast visualization of squamous cell microridges. *Acta Cytol. (Baltimore)*, 22, 500

Murphy, J. F. (1977). The origins of cervical cancer: a scanning electron microscopy study. *Ir. J. Med., Sci.*, 146, 315

Nathan, E., Knoth, M. and Nilsson, B. O. (1978). Scanning electron microscopy of the effect of short-term hormonal therapy on postmenopausal endometrium. *Uppsala J. Med. Sci.*, 83, 175

Nilsson, B. O., Bergstrom, S., Hakansson, S., Lindqvist, I., Ljungkvist, I., Lundkvist, O. and Naeslund, G. (1978). Ultrastructure of implantation. *Uppsala J. Med. Sci. (Suppl)*, 22, 27

Nilsson, B. O., Knoth, M. and Nathan, E. (1980). Scanning

electron microscopy of the responses of postmenopausal endometrium to treatment with estriol and estriol-progesterone. *Uppsala J. Med. Sci.*, **85**, 1

Nilsson, O. and Nygren, K. G. (1972). Scanning electron microscopy of human endometrium. *Uppsala J. Med. Sci.*, **77**, 3

Pollard, S. M., Symonds, E. M. and Aye, N. N. (1979). Scanning electron microscopic appearances in the amnion in polyhydramnios and oligohydramnios. *Br. J. Obstet. Gynaecol.*, **86**, 228

Priest, R. E., Marimuthu, K. M. and Priest, J. H. (1978). Origin of cells in human amniotic fluid cultures: ultrastructural features. *Lab. Invest.*, **39**, 106

Rubio, C. A. and Einhorn, N. (1977). The exfoliating epithelial surface of the uterine cervix. IV: Scanning electron microscopical study in invasive squamous carcinoma of human subjects. *Bietr. Pathol.*, **161**, 72

Sandstedt, B. (1979). The placenta and low birth weight. *Curr. Top. Pathol.*, **66**, 1

Schurch, W., McDowell, E. M. and Trump, B. F. (1978). Long-term organ culture of human uterine endocervix. *Cancer Res.*, **38**, 3723

Sekiba, K., Okuda, H., Fukui, H., Ishkii, Y., Kawaoka, K. and Fujimori, T. (1979). A scanning electron microscopy study of the fine angioarchitecture of the uterine cervix using a newly established cast formation technique. *Obstet. Gynecol. Surv.*, **34**, 823

Sheppard, B. L. and Bonnar, J. (1980a). The response of endometrial blood vessels to intrauterine contraceptive devices: an electron microscopic study. *Br. J. Obstet. Gynecol.*, **87**, 143

Sheppard, B. L. and Bonnar, J. (1980b). Scanning and transmission electron microscopy of material adherent to intrauterine contraceptive devices. *Br. J. Obstet. Gynaecol.*, **87**, 155

Spring-Mills, E. and Elias, J. J. (1975). Cell surface differences in ducts from cancerous and non-cancerous human breasts. *Science*, **188**, 947

Spring-Mills, E. and Elias, J. J. (1976). Cell surface changes associated with human breast cancer. *SEM IITRI*, **9** (II), 1

Stegeman, J. H. and Treffers, P. E. (1980). Histological appearance of the human placenta observed by electron microscopy after hypertonic saline abortion. *Acta Obstet. Gynecol. Scand.*, **59**, 45

Takano, N., Maekawa, I. and Takamizawa, H. (1979). Ultrastructure of human cervical mucus observed by cryo-scanning electron microscopy. *Fertil. Steril.*, **32**, 604

Trent, J. M., Davis, J. R. and Payne, C. M. (1980). The establishment and morphologic characterization of finite cell lines from normal human endometrium. *Am. J. Obstet. Gynecol.*, **136**, 352

Tyden, O., Bergstrom, S. and Nilsson, B. A. (1981). Origin of amniotic fluid cells in mid trimester pregnancy. *Br. J. Obstet. Gynecol.*, **88**, 278

van Geyjn, H. P., Kenemans, P., Hodde, K. C. and Eskes, T. K. A. B. (1975). The human placenta: surface structure of chorionic villi in pathological conditions. *J. Microsc. Biol. Cell.*, **24**, 183

van Herendael, B. J., Oberti, C. and Brosens, I. (1978). Microanatomy of the human amniotic membranes. A light microscopic, transmission and scanning electron microscopic study. *Am. J. Obstet. Gynecol.*, **131**, 872

Vasquez, G., Winston, R. M. L., Boeckx, W. and Brosens, I. A. (1982). The epithelium of human hydrosalpinges: a light optical and scanning electron microscopic study. (In press)

Vesterinen, E. H., Carson, J., Walton, L. A., Collier, A. M., Keski--Oja, J., Nedrud, J. G. and Pagano, J. S. (1980). Human ectocervical and endocervical epithelial cells in culture: a comparative ultrastructural study. *Am. J. Obstet. Gynecol.*, **15**, 681

Zaneveld, D. V. M., Tauber, R. F., Port, C., Propping, D. and Schumacher, G. F. B. (1975). Structural aspects of human cervical mucus. *Am. J. Obstet. Gynecol.*, **122**, 650

34

Diagnostic applications to oncology

G. M. HODGES* and P. KENEMANS†

* Imperial Cancer Research Fund, London, UK
† Institute of Obstetrics and Gynecology, Catholic University Nijmegen, Nijmegen, The Netherlands

INTRODUCTION

The discrimination between normal and neoplastic tissues relies essentially on histopathological criteria. Such criteria are major contributors both to the classification of neoplastic lesions and to the establishment of diagnostic and prognostic evaluations of the neoplastic disease. More recently, other complementary approaches have been sought which may provide a finer assessment of the behavioral potential of the neoplastic lesion and have included the application of scanning electron microscopy (SEM). There is particular need for marker systems which can lead to the recognition and characterization of early lesions preceding the development of overt tumors and which, in epithelial tissues, can reliably distinguish between histologically similar, though biologically different, lesions that may be forerunners of carcinoma in situ (Symposium, 1976). A further need is to predict with certainty the future behavior of residual epithelium following removal of the overt lesion.

That progressive changes may occur over periods of time in the biologic attributes of the cells of a neoplasm is inherent in the currently favored multiphasic concept of carcinogenesis, with transition from initiated to biologically overt neoplastic cell (Foulds, 1969; Prehn, 1976; Farber and Cameron, 1980; Colburn, 1980). From a practical viewpoint marker systems are required which might yield definitive information on such progression. Neoplastic progression in epithelial tissues, it is suggested, involves multiple stepwise changes in cell status from normal to (a) hyperplastic (defined in quantitative terms as a reversible epithelial proliferative change resulting in an increased number of epithelial cells); (b) dysplastic (where hyperplasia is associated with qualitative epithelial cellular abnormality; (c) preneoplastic (defined in terms of an irreversible but not necessarily progressive epithelial proliferative change); (d) neoplastic (where such change is not only irreversible but also progressive, or (e) malignant (associated with cellular anaplasia,

invasion and metastasis). The preneoplastic condition may be able to stabilize, or regress and disappear and not to progress to invasive neoplasms.

As a consequence, studies directed toward evaluating phenotypic markers that define crucial stages of development for various neoplastic diseases assume great interest. Such studies are of obvious significance also, in association with developments aimed at determining prognostic and therapeutic factors which could assist in the establishment of more appropriate clinical intervention therapies as a result of a concise spatial and temporal determination of the neoplastic process. At present, both the various systems of tumor classification and the definitions of the stages of neoplastic development are based almost exclusively on morphological features detected by light microscopy; though identity of cellular atypia based on ultrastructural, antigenic, chromosomal, biochemical or growth differences have been sought. Furthermore, definition of the early lesion in terms of reversible hyperplasia or irreversible preneoplasia, and separation of truly benign papillomas from potentially malignant ones remains still essentially based on a distinction done in biologic rather than in morphologic terms.

As indicated, morphology at the level of the light microscope remains one of the most used criteria upon which the recognition of abnormal structural features associated with neoplasia are based. More recently, morphology at the level of the electron microscope, both by TEM and SEM, has provided the possibility of establishing legitimate structural markers of potential oncological significance. Although TEM has provided much structural information on the cell, this technique alone is inadequate for studies of changes in large areas of the tissue; whereas SEM has provided unique and extensive views of both tissue organization and associated epithelial surface contours and has allowed the ready correlation between local ultrastructure and the overall organization of the cells or tissues of interest. Findings from such studies in relation to

pathogenetic events have supported the concept that cellular dysfunctions marking various stages of a disease process could be recognized on the basis of morphological information comparing and contrasting distinctive surface features (Carr and Toner, 1981; Buss and Hollweg, 1980). Nevertheless, such use of SEM in diagnosis with proven advantage over existing methods remains still at an experimental stage, though its strength for the recognition of minor degrees of pathological change has been underlined.

A criticism of morphological interpretation as a criterion of neoplastic progression has been that it may not totally reflect the biologic potential of the lesion under study. Consequently, a better understanding of the development and pathobiology of the neoplastic lesion together with more significant diagnostic and prognostic assistance may be expected to come from the application of immunologic and other cell-labeling techniques whereby a functional facet is introduced to morphologic analysis. Acquisition of such insight may be accomplished in part by the combined applications of SEM and cell surface markers like colloidal gold, which are now being increasingly demonstrated as potentially significant aids in the study both of clinical and experimental biomedical problems (Becker and Sogard, 1979; Goodman *et al.*, 1980; Molday and Maher, 1980; Horisberger, 1981; Trejdosiewicz *et al.*, 1981). SEM has been most widely used with the secondary electron imaging mode (SEI), attention being focused in particular on cell surface ultra-structural characteristics and on the detection of cell surface markers. More recently, additional modalities of the SEM, including back-scattered imaging (BEI) and X-ray microanalysis (XES), have been tried both to localize subsurface structures and to evaluate elemental composition (for example, of mineralized lesions in tissues), thereby enhancing the potential contribution of the SEM to diagnostic problems (for further discussion see Buss and Hollweg, 1980; Carr *et al.*, 1980; Carter, 1980).

GENERAL CONSIDERATIONS

It is well established that the cell surface may reflect modifications of cell properties which directly relate to neoplastic transformation and other characteristics that indicate states of tumor progression. A considerable convenience would be if these properties could be defined by unique cell surface characteristics which were readily identifiable, could lead to more precise methods of determining tumor grade, and could be also effective in predicting behavior of the early lesion or of the overt tumor. From this arises the question as to whether any specific con-formational cell or tissue change can be detected by SEM which would reflect behaviour predictive of neoplastic transformation or of alterations in biological malignancy, and which could thereby have some diagnostic application in oncology.

Pathological diagnoses of neoplastic disease are based on various criteria, in particular the pattern of tissue growth and of tissue histoarchitecture; the size, arrangement and degree of anaplasia (ie grade) of the component cells; and depth of tumor infiltration and

mode and location of tumor spread (ie clinical and pathological stage). Within this context, the ready accessibility of the natural biological faces of organs to SEM analysis has led, not surprisingly, to a multiplicity of oncological studies. In general these have been aimed at establishing, by analysis of the surface, morphological criteria that could reflect specific and diagnostically significant abnormalities of the epithelium (based on altered cellular and/or tissue patterns) and which could reliably denote specific characteristics with practical value in the differen-tiation between reactive hyperplasia, dysplasia and neoplasia. Additionally, techniques for SEM examination of epithelial anatomic structures not normally exposed to view in intact specimens have allowed insights into various aspects of tissue and cellular organization (Carr and Toner, 1981). But for the present, the limits of the morphological role of SEM in experimental and pathogenetic studies need to be more clearly defined. For this purpose, a broader range of histological and ultrastructural (TEM) controls are required to correlate SEM data to specific disease processes. This has been facilitated by the development of procedures whereby SEM-processed tissue can be reprocessed for further study both by LM and TEM allowing several morphological aspects of the same specimen to be obtained. Conversely, histological blocks have been deparaffinized and processed for SEM (Carr and Toner, 1981).

Induction of neoplasia by various agents, particularly by chemical carcinogens, has been used widely as a means to study the processus of neoplastic development. Information derived from such studies has suggested a sequence of carcinogenic effects in epithelium presenting themselves as hyperplastic–dysplastic–neoplastic changes. There is evidence that this sequence of epithelial events is approximately the same regardless of the experimental animal model used. The epithelial abnormalities may be recognized histologically or cytologically as areas of cell crowding, disrupted tissue organization, abnormal differentiation and cellular atypia. The introduction of SEM has dramatically emphasized the dynamic and complex nature of such epithelial tissue changes. Among different tissue and cell surface features implicated as marking various stages of the neoplastic

---

Figure 1 (opposite)

a,b: Uniform luminal aspects of contracted rat bladder marked by irregular broad folds or rugae (a ×125) patterned by microplicae (↓) (b ×300) and presenting a regular, pavement-like arrangement of polygonal superficial cells

c,d: Superficial cells of human urothelium (c ×2250) and of rat urothelium (d ×4500) showing irregular infoldings of the luminal asymmetric unit membrane (AUM) and tight cell junctions marked by closely set microvilli (↓)

e,f: Scalloped surface topography of superficial cell demonstrating the plaque (P)–interplaque (IP) con-figuration of the AUM by SEM (e ×9000) and by TEM (f ×6260)
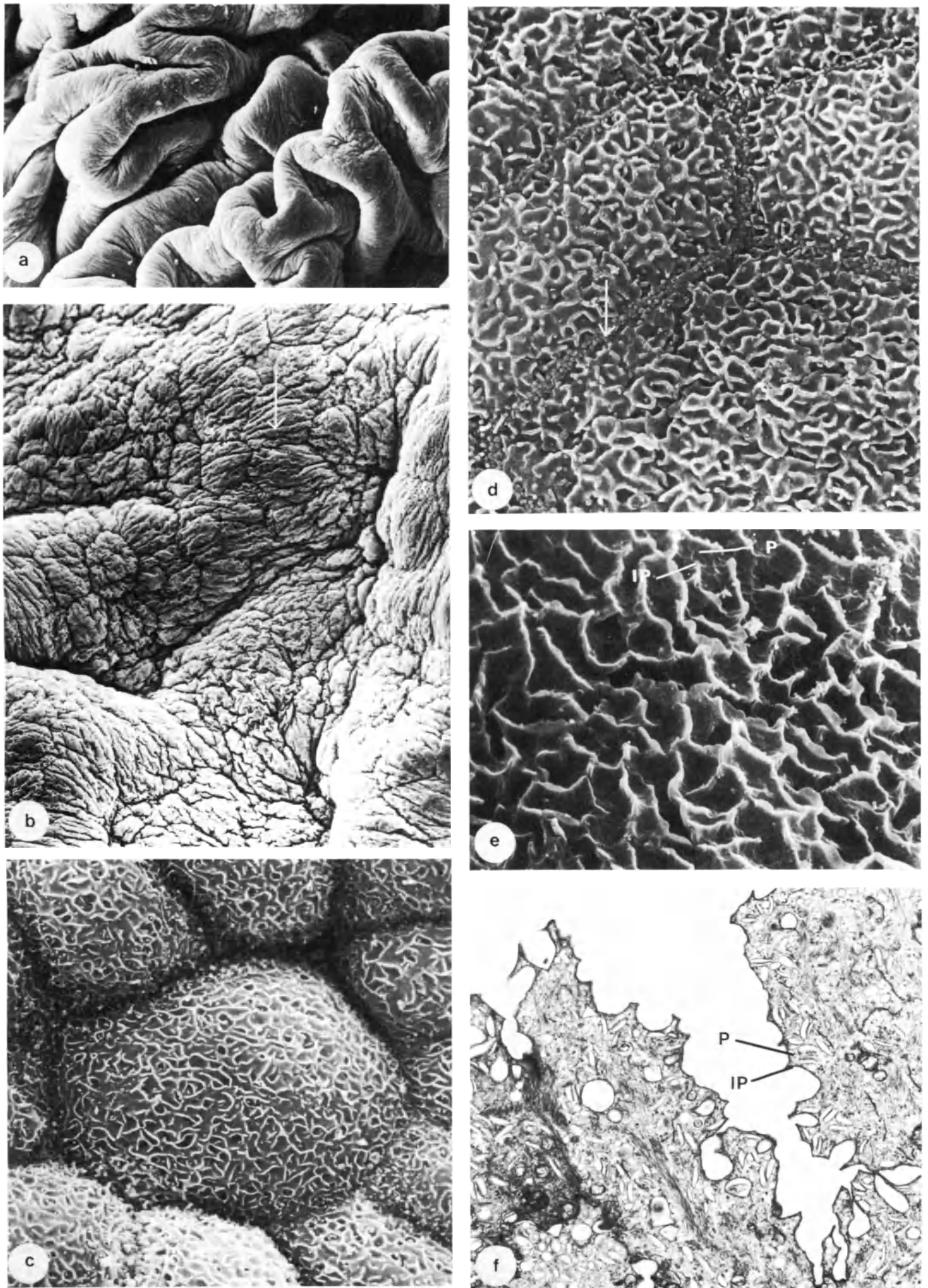
Figure 1

disease process attention has focused on the expression of specialized cell surface protrusions, in particular, that of microvilli. The formation of microvilli of variable size and configuration, as reported on cells during experimental carcinogenesis, has been considered as possibly pathogenomic of the neoplastic process. Some concern has been recently voiced, however, on the emphasis placed on this 'microvillous pathology' where expression of pleomorphic microvilli has been suggested as representing an indicator of malignant transformation in experimental animal models or regarded as being of diagnostic significance in human tumors. The validity of pleomorphic microvilli as a specific diagnostic morphological criterion remains to be established but possibly, as suggested in the literature, it may be appropriate to say that pleomorphic microvilli at least in experimental animal models may represent a morphologic indicator of irreversible but not necessarily progressive epithelial proliferative change. For further views on this question the reader is referred to Buss and Hollweg (1980); Friedell et al. (1977); Hodges (1979); Trump et al. (1980); Kenemans et al. (1981); Newman and Hicks (1981).

In the area of oncological human disease SEM is still in a cataloguing phase with attention focused essentially on the recognition of morphological differences between normal, preneoplastic and neoplastic lesions. The relevance of surface structural change as an early marker of irreversible neoplastic transformation remains to be established and as a consequence a more specific assessment of detectable changes in cell surface properties by SEM is emphasized. A promising approach to the problem may be suggested from the application of correlative SEI, BEI and XES studies as indicated in the previous section and which could offer the facility to identify structural, functional or immunological properties both at the surface and within tissues and cells in a manner not previously possible. For various current views, applications and bibliographies of SEM in both experimental and diagnostic oncology reference can be usefully made to the Proceedings of the Annual Scanning Electron Microscope Symposium volumes (published initially by the Illinois Institute of Technology and, since 1978, by SEM Inc.).

A major aim in this chapter is to provide a representation of the routine component of morphological enquiry aimed at assessing structural characteristics of epithelial lesions in the course of neoplasia both in experimental systems and human patients, and of the progressive approaches offered by some other modalities of analysis in the SEM. For this purpose, illustrations of bladder epithelium have been selected on the basis that this tissue occupies a prominent position in the SEM study of human carcinogenesis and of experimental neoplasia in animal models, next to that of the cervix. (For bladder see Jacobs et al., 1977; Hicks and Chowaniec, 1978; Hodges et al., 1978, 1977; Hodges, 1978, 1979; Tannenbaum et al., 1978; Croft et al., 1979; Nelson et al., 1979a,b; Trump et al., 1980; Newman and Hicks, 1981: for cervix see Ferenczy and Gelfand, 1979; Davina et al., 1981; Kenemans et al., 1981).

Figures 1–3 Urinary bladder surface changes associated with cytodifferentiation of normal epithelium

The urothelial specimens illustrated were derived from (1) normal bladders of young female Wistar rats (120–140 g weight), or from bladders of animals given a single, non-tumorigenic intravesicular dose of 1.5 mg N-methyl-N-nitrosurea (MNU) in order to elicit a regenerative process of normal urothelial differentiation (Hodges et al., 1976; Hicks and Chowaniec, 1978); (2) biopsy samples of normal human bladder obtained from patients undergoing prostatectomy, or from post-mortem cases 6 to 12 h after death. Specimens were fixed (at ambient temperature) and stored (24 h to several months) in 2.5% glutaraldehyde in either 0.1 mol/l sodium cacodylate buffer pH 7.1 or in 0.1 mol/l Sorensen's buffer pH 7.2 until required for further processing involving a modified thiocarbo-hydrazide–osmium procedure; then examined following routine dehydration, critical-point drying and sputter coating procedures (for methodological details see Hodges, 1979). It should be noted that methodologies for the collection and the preparation of specimens are sources of possible artifacts that may influence the quality and interpretation of both SEM and TEM results (for further discussion see Tannenbaum et al., 1978; Bell and Revel, 1980; Brunk et al., 1981).

In the contracted bladder the urinary mucosa is marked by broad, irregularly distributed folds or rugae patterned by microplicae which extend across groups of cells in wave-like arrangements (Figures 1a,b). The structure and dimensions of the rugae, microplicae and intervening clefts change during bladder distension with an attenuation of the mucosal folds and microplicae as distension proceeds. In the moderately to well-distended bladder the normal urothelium presents a uniform luminal aspect with a regular, pavement-like arrangement of clearly outlined large, flattened surface cells mainly hexagonal or, more occasionally, pentagonal or rhombic in shape (Figures 1b–d). Tight contact margins are visible between these cells as well-defined ridges with a central groove, these tight cell junctions appearing as a fusion of lateral microvilli (Figure 1d). The superficial urothelial cell

Figure 2 (opposite)
a,b: Rat urothelium (from animal 2 weeks after receiving a single, non-tumorigenic intravesicular dose of MNU) showing superficial cells (S) and a desquamated focal area with exposure of smaller intermediate cells (I) (a ×1987); and a second focal area demonstrating normal cytodifferentiation with expression of a reticulate pattern of ridges, characteristic of late maturing intermediate cells (b ×3000)
c: Human urothelium showing superficial (S), early differentiating intermediate (D) and immature intermediate (A) cells (×4500)
d–f: Rat urothelium showing sequence of surface topographies associated with intermediate cells at immature (A), early differentiating (D) (d ×12 500), late differentiating (e ×15 000), and early maturing (f ×15 000) stages
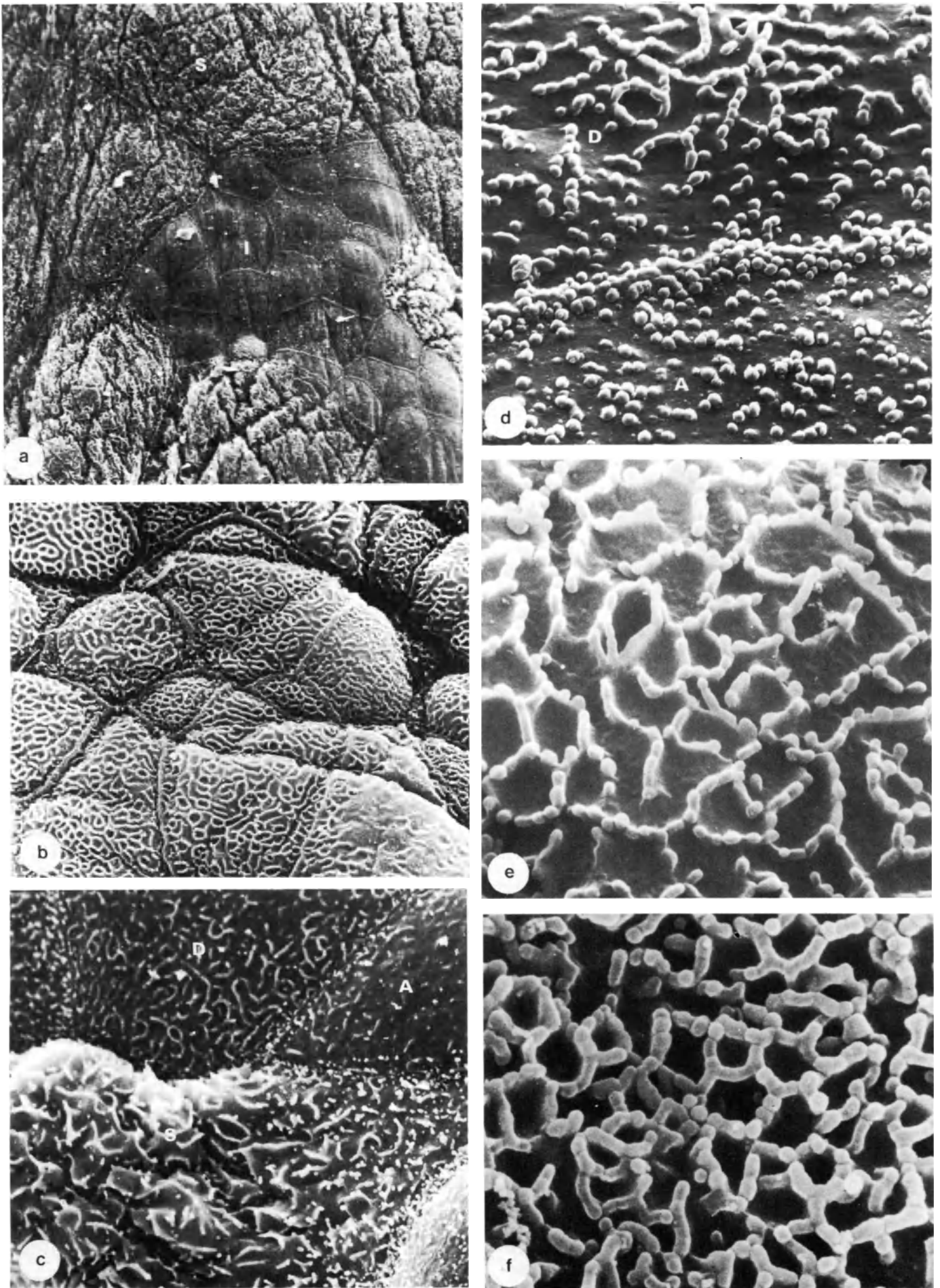
Figure 2
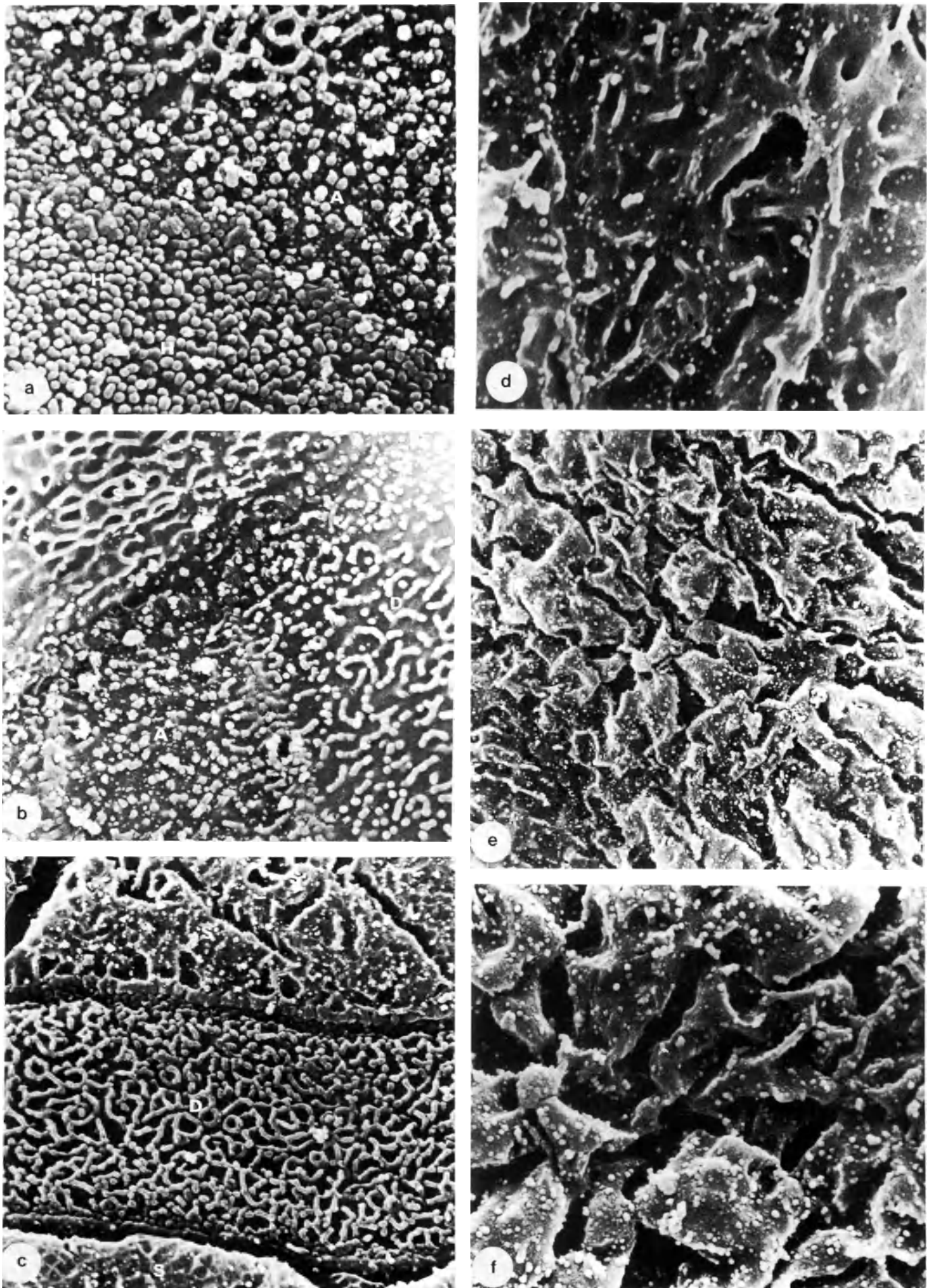
Figure 3

surface demonstrates irregular infoldings of its specialized luminal asymmetric unit membrane resulting in a characteristic scalloped surface topography (Figures 1c–e) clearly related to the unique semi-rigid luminal membrane structure seen by TEM (Figure 2a). From studies of a variety of species it would appear that this pattern of tissue architecture, cellular organization and surface morphology forms a basic design of the terminally differentiated urothelium.

Desquamation of superficial cells exposes smaller cells of the intermediate layer, each superficial cell extending over varying numbers of intermediate cells depending on bladder distension (Figures 2c,d); the intermediate cells in turn extend over the still smaller cells of the basal layer. Structural features associated with urothelial cytodifferentiation have been summarized as a sequence of surface alterations ranging from basal and immature intermediate cells characterized by a generally smooth surface but showing occasional irregular patternings of cytoplasmic blebs, microridges (basal cells) or small, globular microvilli (immature intermediate cells) (Figures 2c,d); differentiating intermediate cells with a surface patterning of globular microvilli arranged in chain-like rows of variable length and contours (Figures 2c,d) which fuse to form ridges in the late differentiating intermediate cells (Figure 2e); maturing intermediate cells showing progressive development of a reticular patterning of ridges (Figures 2b,f); to superficial cells showing characteristic mature reticulated surface patternings and demonstrating plaque–interplaque profiles associated with terminal urothelial differentiation (Figures 1c–e).

Such morphological patterns of differentiative change can be usefully investigated using, as another modality of SEM analysis, cell surface marker procedures. Coupled ligand–colloidal gold complexes have provided a convenient approach for localization of antigen and lectin-binding sites on the surface of urothelial cell membranes and for immunocyto-chemical identification of urothelial cell populations at different stages of differentiation (Hodges et al., 1982). A complex luminal surface distribution pattern is demonstrated by a membrane-associated urothelial differentiation antigen (UMA) which is detected on the immature and early differentiating intermediate cells (Figures 3a,b), absent at the late differentiating inter-mediate stage (Figure 3c), re-expressed as the cells mature and found in greatest abundance on the

terminally differentiated superficial cells (Figures 3b–d). Cellular and regional differences in lectin binding to the urothelial cell surface are suggested with Con-A receptors localized uniformly over the superficial cells (Figures 3e,f), and PNA receptors confined to linear arrays or occasional clusters over the apical surface but evenly dispersed over the lateral surface of these cells.

Figures 4–7 Urinary bladder changes associated with urothelial hyperplasia and neoplasia

The SEM illustrations selected represent a continuum of changes from normal (see Figure 1) to varying grades of atypia expressed by urothelium from (1) bladders of young female Wistar rats given either a single non-tumorigenic or multiple (×4) tumor-inducing intravesicular doses of 1.5 mg N-methyl-N-nitrosurea (MNU) thereby eliciting benign reversible hyperplasia or preneoplastic irreversible hyperplasia and overt neoplasia respectively; (2) human bladder tumor tissue obtained from surgical cases undergoing cystectomy or local tumor excision (with tumor classification based on the histopathology of separate samples of the same tissue).

During experimental bladder carcinogenesis in the rodent model MNU produces a cytotoxic as well as a carcinogenic effect. An early response following acute toxic damage to the urothelium is necrosis and desquamation of the urothelium, the extent of which varies with MNU dose and is accompanied by a reparatory hyperplasia. The areas of urothelial hyperplasia are usually focal, though the expanse of tissue affected can vary considerably (Figure 4a; see also Figures 2a,b).

In benign reversible hyperplasia a common feature is the arrangement of the surface cells into a generally regular cobblestone pattern (Figures 4b,c). Typically, these cells lack the specialized AUM and instead the luminal surface is characterized by symmetric plasma membrane with small stubby or globular microvilli (Figure 4c). Regression of hyperplasia is marked by establishment of a normal pattern of morphogenesis and cytodifferentiation (see Figures 1–3) and production of the normal specialized AUM.

During early preneoplastic (or irreversible) hyperplasia some or all of the morphological features associated with benign reversible hyperplasia may be observed. Progression of the epithelial lesion is associated with changes in tissue architecture (Figures 4d,e); in cellular organization, marked by a less-ordered cobblestone pattern of cell arrangement and by some cellular pleomorphism (Figure 5a); and, with atypical surface patternings of generally more prominent and less uniform microvilli (Figure 5d) which in some instances (unlike that in benign hyperplasia) may be covered by a prominent beaded glycocalyx. These early indications of epithelial disorder are followed by the development of papillary and nodular aggregates of cells projecting from the mucosal surface into the bladder lumen (Figures 4d and 5b). In the overt tumor the urothelium shows progression to a marked polymorphism both in cell arrangement and in cell size and shape (Figure 5c). This

---

Figure 3 (opposite)

a–d: Rat urothelium showing cell surface distribution pattern of a membrane-associated urothelial dif-ferentiation antigen (UMA) marked by indirect labeling with colloidal gold particles on immature intermediate (A) (a ×10 750; b ×7500) and superficial (S) cells (c ×7500; d ×9750); UMA is not expressed on the surfaces of benign hyperplastic (H) (Figure 3a) and mid-late differentiating intermediate (D) (Figures 3b,c) cells

e,f: Rat urothelium showing Con-A receptor sites marked by indirect labeling with colloidal gold (e ×5000; f ×10 750)
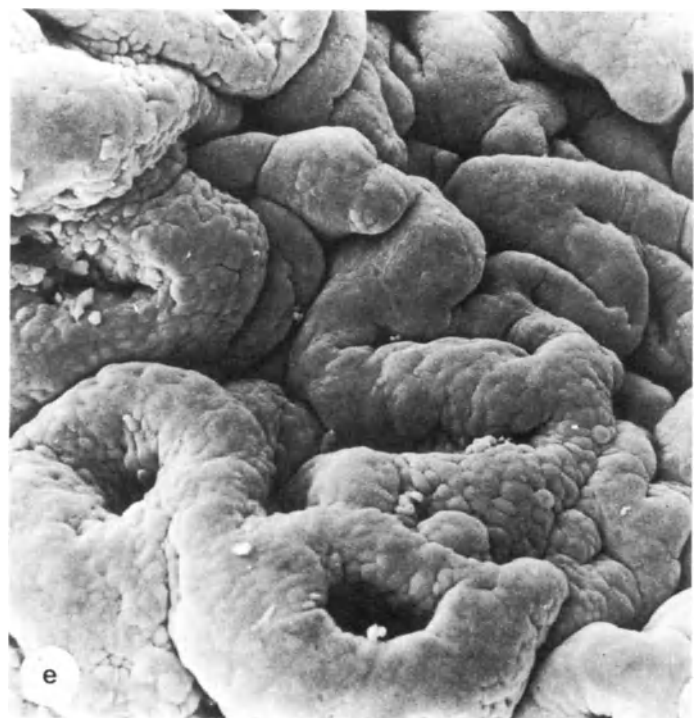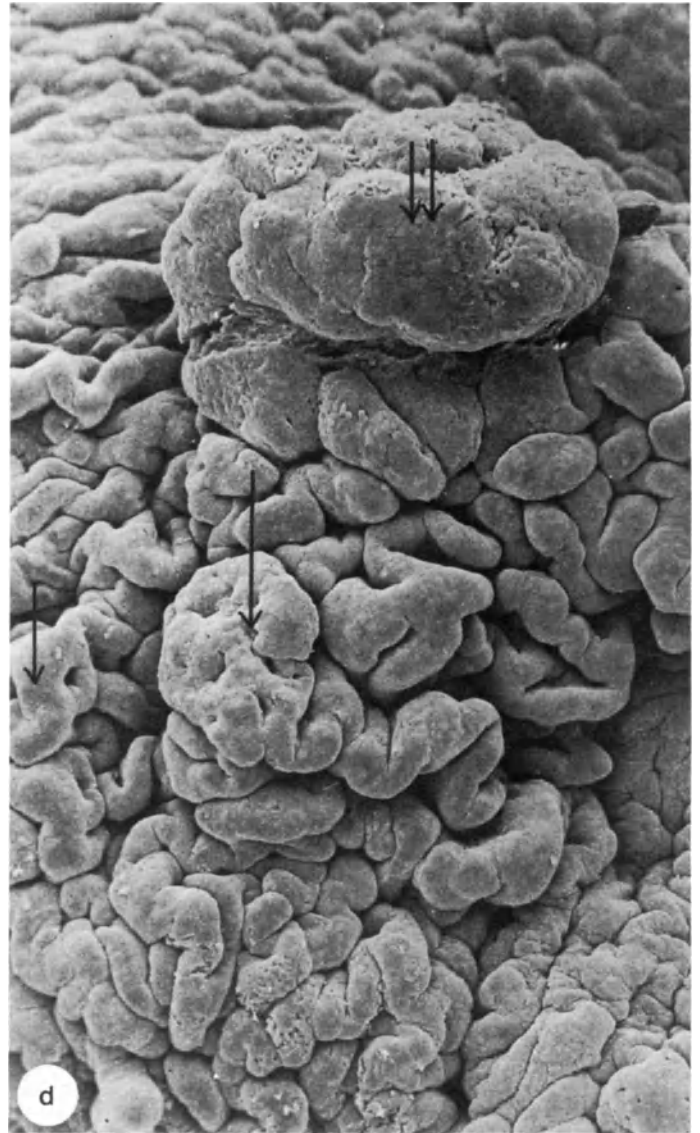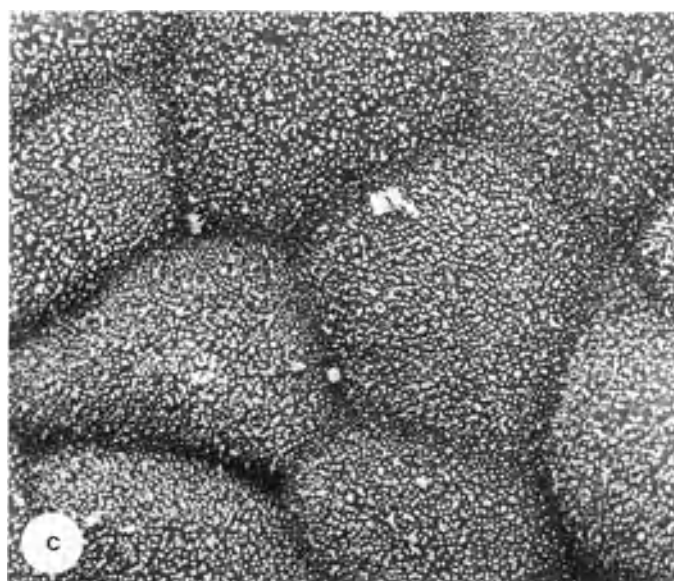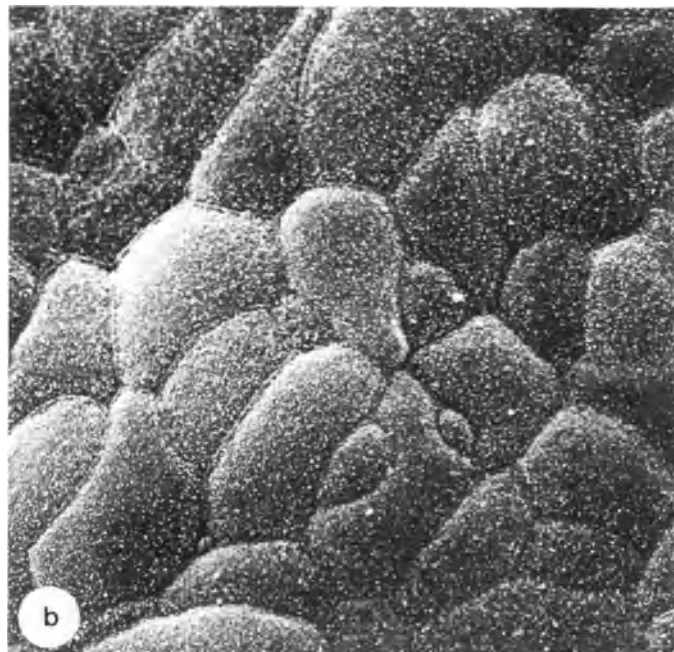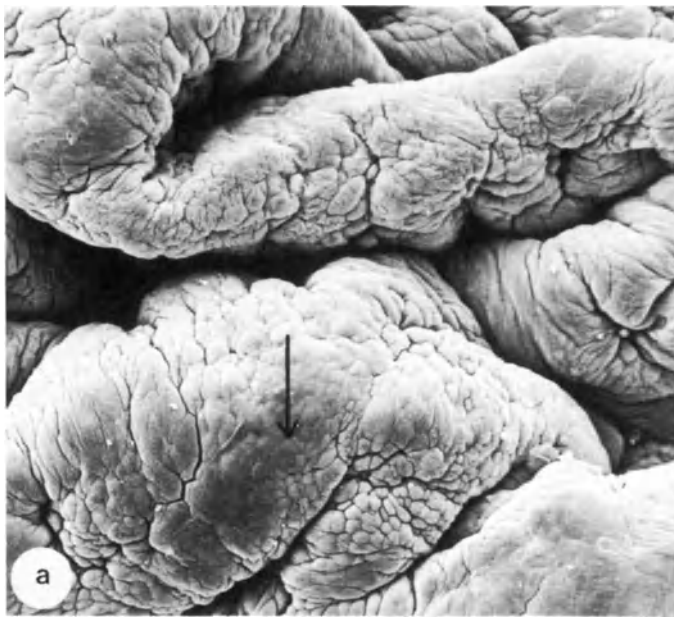
Figure 4

is associated with the appearance of bizarre microvilli of various sizes and configurations (Figures 5d–f) which by TEM have been shown to be covered by a profuse filamentous glycocalyx.

Unique views of both bladder tumors and associated mucosal change can be provided when specimens from human bladder cases are studied by SEM (Fulker *et al.*, 1971); Kjaergaard *et al.*, 1977); Newman and Hicks, 1977; Hodges, 1978; Tannenbaum *et al.*, 1978); Croft *et al.*, 1979; Nelson *et al.*, 1979; Price *et al.*, 1980). These changes appear analogous to those defined in various animal models following treatment with chemical carcinogens, as above (see reviews by Hodges, 1979; Heatfield *et al.*, 1980; Trump *et al.*, 1980). There is evidence that morphologic manifestations of preneoplastic epithelial change may be regularly identified by SEM in mucosal areas of the bladder peripheral to or distant from the overt tumor and which may otherwise not be recognizable as being preneoplastic by light microscopy (Newman and Hicks, 1977). As a consequence, it has been surmised that, in order to ascertain the status of the bladder epithelium outside the area of visible tumor, SEM examination of human biopsies could be used to disclose additional biologic parameters reflecting the biologic potential of putative precancerous lesions of the urothelium.

Tumors of the urinary bladder show three main patterns of histologic differentiation (i.e. urothelial papillary and non-papillary; squamous; or glandular). Of all primary bladder neoplasms approximately 90% have a luminal surface configuration that is papillary (Figure 6a) and these have been the subject of most SEM studies. From such studies have emerged findings supporting the histopathological concept that there may be distinction among the grades of papillary carcinomas based on characteristics of the epithelium. That is, urothelial cells forming the papillae can represent degrees of departure from the morphological appearance of normal urothelial cells that may be marked by SEM. From such SEM data, some attempt has been made to analyze the degree of surface morphological alteration expressed by the constituent urothelial cells of a bladder tumor in terms of its histologic grade, though the relationship of epithelial

abnormality or grade to pathologic stage on the basis of such parameters remains little explored.

Histologic features of the well-differentiated or grade I urothelial tumor generally include a significant increase in the number of epithelial cell layers; these overlie a fibrovascular core with the epithelial cells showing only a very slight loss of polarity and minor degrees of nuclear abnormalities. In the moderately well-differentiated, intermediate or grade II tumors the epithelium is, as a rule, markedly hyperplastic and is associated with a more pronounced loss of polarity and more noticeable nuclear abnormalities as compared with the grade I tumor; there may be also some irregularity on the luminal aspect of the epithelium. In the less- to poorly-differentiated or grade III tumor the epithelium shows both a marked disturbance in its histoarchitecture and a disorderly growth pattern in addition to striking nuclear abnormalities. The degree of epithelial atypia can be subject to variation from one tumor area to another such that the tumor may not be of a uniform grade all over.

Examination of bladder tumors by SEM reveals similar degrees of departure from morphological normalcy marked by increasing variability in the pattern of urothelial tissue histoarchitecture and growth (Figures 6a,c,d and 7d); of urothelial cell size and arrangement (Figures 6b,f and 7a,d); and in degree of urothelial cellular atypia and abnormal differentiation (Figures 6b,e,f and 7a–c,e,f). In the well-differentiated or grade I bladder tumor the urothelial cells may present regular cohesive to slightly irregular cobblestone arrangements (Figures 6a–f). Topographies expressed by the luminal cells range from close similitude to the terminally differentiated normal superficial cells (Figures 6a,b), albeit the luminal cells of the bladder tumor are smaller and are covered to varying extents by fine microvilli; relatively featureless surfaces or surfaces modestly patterned by small globular microvilli (Figures 6e,f); to more striking cellular atypia with marked irregular leaf-like ridges and varying forms of microvilli (Figures 7a–c).

In the moderately differentiated or grade II tumors cellular atypia is generally more marked with a range of surface topographies from grossly modified reticular pattern of microridges (Figure 7e) to cells profusely covered by microvilli of greatly varying size and shape (Figure 7f).

Figure 4 (opposite)
a: Non-uniform luminal aspect of rat bladder, from animal 2 weeks after receiving a single non-tumorigenic intravesicular dose of MNU, marked by irregular gross thickening of rugae and focal areas of reparatory urothelial cytodifferentiation (↓) (×125)
b,c: Urothelium of non-malignant inflammatory human bladder marked by generally regular cobblestone arrangement of the surface cells and a luminal surface topography of small globular mirovilli (b ×1175; c ×2500)
d,e: Luminal aspect of rat bladder 4 weeks after intravesicular treatment with tumorigenic dose (4 × 1.5 ng biweekly) of MNU, showing focal areas of modified tissue architecture (↓) (d ×84; e ×125); and development of papillary tumour aggregates (↓ ↓) (Figure 4d)

References

Becker, R. P. and Sogard, M. (1979). Visualization of subsurface structures in cells and tissues by backscattered electron imaging. *SEM Symposium*. Vol. II, pp. 835–870

Bell, P. B. and Revel, J.-P. (1980). Scanning electron microscope application to cells and tissues in culture. In Hodges, G. M. and Hallowes, R. C. (eds). *Biomedical Research Applications of Scanning Electron Microscopy*, pp. 1–63. (London: Academic Press)

Brunk, U., Collins, V. P. and Arro, E. (1981). The fixation, dehydration, drying and coating of cultured cells for SEM. *J. Microsc.*, 123, 121

Buss, H. and Hollweg, H. G. (1980). Application of scanning electron microscopy to diagnostic pathology. A critical review. *SEM Symposium*. Vol. III, pp. 139–152

Carr, K. E., McLay, A. L. C., Toner, P. G., Chung, P. and Wong, A. (1980). SEM in service pathology: A review of its potential role. *SEM Symposium*. Vol. III, pp. 121–138

Carr, K. E. and Toner, P. G. (1981). Scanning electron microscopy in biomedical research and routine pathology. *J. Microsc.* 123, 147

Carter, H. W. (1980). Clinical applications of scanning electron microscopy (SEM) in North America with emphasis on SEM's role in comparative microscopy. *SEM Symposium*. Vol. III, pp. 115–120

Colburn, N. H. (1980). Tumor promotion and carcinogenesis. In Slaga, T. J. (ed.). *Carcinogenesis – Modifiers of Chemical Carcinogenesis*. Vol. 5, pp. 33–56. (New York: Raven Press)

Croft, W. A., Nelson, C.-E. and Nilsson, T. (1979). Scanning electron microscopy of exfoliated malignant and non-malignant human urothelial cells. *Scand. J. Urol. Nephrol.*, 13, 49

Davina, J. H. M., Stadhouders, A. M., Lamers, G. E. M., van Haelst, M. J. and Kenemans, P. (1981). Surface pattern differentiation of the epithelial cells of the human uterine ectocervix. *SEM Symposium*. Vol. III, pp. 37–48

Farber, E. and Cameron, R. (1980). The sequential analysis of cancer development. *Adv. Cancer Res.*, 31, 125

Ferenczy, A. and Gelfand, M. M. (1979). The cytodynamics of normal and neoplastic cervical epithelium. *Obstet. Gynecol. Surv.*, 34, 808

Foulds, L. (1969). *Neoplastic Development*. Vol. 1. (London: Academic Press)

Friedell, G. H., Jacobs, J. B., Nagy, G. K. and Cohen, S. M. (1977). The pathogenesis of bladder cancer. *Am. J. Pathol.*, 89, 431

Fulker, M. J., Cooper, E. H. and Tanaka, T. (1971). Proliferation and ultrastructure of papillary transitional cell carcinoma of the human bladder. *Cancer*, 27, 71

Goodman, S. L., Hodges, G. M. and Livingston, D. C. (1980). A review of the colloidal gold marker system. *SEM Symposium*. Vol. II, pp. 133–146

Hicks, R. M. and Chowaniec, J. (1978). Experimental induction, histology, and ultrastructure of hyperplasia and neoplasia of the urinary bladder epithelium. *Int. Rev. Exptl. Pathol.*, 18, 199

Hodges, G. M. (1978). Normal and neoplastic urothelium of human bladder *in vivo* and *in vitro* – an assessment of SEM studies. *SEM Symposium*. Vol. II, pp. 983–990

Hodges, G. M. (1979). The urinary system – bladder. In Hodges, G. M. and Hallowes, R. C. (eds). *Biomedical Research Applications of Scanning Electron Microscopy*. Vol. 1, pp. 307–53. (London: Academic Press)

Hodges, G. M., Hicks, R. M. and Spacey, G. D. (1976). Scanning electron microscopy of cell surface changes in methylnitrosurea (MNU)-treated rat bladders *in vivo* and *in vitro*. *Differentiation*, 6, 143

Hodges, G. M., Hicks, R. M. and Spacey, G. D. (1977). Epithelial–stromal interactions in normal and chemical carcinogen-treated adult bladder. *Cancer Res.*, 37, 3720

Hodges, G. M., Smolira, M. A. and Trejdosiewicz, L. K. (1982). Urothelium-specific antibody and lectin surface mapping of bladder urothelium. *Histochem. J.*, 4, 755

Horisberger, M. (1981). Colloidal gold: a cytochemical marker for light and fluorescent microscopy and for transmission and scanning electron microscopy. *SEM Symposium*. Vol. III, pp. 9–31

Jacobs, J. B., Arai, M., Cohen, S. M. and Friedell, G. H. (1977). A long-term study of reversible and progressive urinary bladder cancer lesions in rats fed N-(5-nitro-2-furyl)-2-thiazolyl) formamide. *Cancer Res.*, 37, 2817

Kenemans, P., Davina, J. H. M., de Haan, R. W., van der Zanden, P., Vooys, G. P., Stolk, J. G. and Stadhouders, A. M. (1981). Cell surface morphology in epithelial

malignancy and its precursor lesions. *SEM Symposium*. Vol. III, pp. 23–36

Kjaergaard, J., Starklint, H., Bierring, F. and Thybo, E. (1977). Surface topography of the healthy and diseased transitional cell epithelium of the human urinary bladder *Urol. Int.*, 32, 34.

Molday, R. S. and Maher, P. (1980). A review of cell surface markers and labelling techniques for scanning electron microscopy. *Histochem. J.*, 12, 273

Nelson, C.-E., Croft, W. A. and Nilsson, T. (1979a). Characterization of different regions of the normal human urinary bladder by means of scanning electron microscopy. *Scand. J. Urol. Nephrol.*, 13, 23

Nelson, C.-E., Croft, W. A. and Nilsson, T. (1979b). Surface characteristics of malignant human urinary bladder epithelium studied with scanning electron microscopy. *Scand. J. Urol. Nephrol.*, 13, 31

Newman, J. and Hicks, R. M. (1977). Detection of neoplastic and preneoplastic urothelia by combined scanning and transmission electron microscopy of urinary surface of human and rat bladders. *Histopathology*, 1, 125

Newman, J. and Hicks, R. M. (1981). Surface ultrastructure of the epithelia lining the normal human lower urinary tract. *Br. J. Exp. Pathol.*, 62, 232

Prehn, R. T. (1976). Tumor progression and homeostasis. *Adv. Canc. Res.*, 23, 203

Price, D. A., Morley, A. R. and Hall, R. R. (1980). Scanning electron microscopy in the study of normal, inflamed and neoplastic human urothelium. *Br. J. Urol.*, 52, 370

Symposium (1976). Early lesions and the development of epithelial cancer. *Cancer Res.*, 36, 2475

Tannenbaum, M., Tannenbaum, S. and Carter, H. W. (1978). SEM, BEI and TEM ultrastructural characteristics of normal, preneoplastic and neoplastic human transitional epithelia. *SEM Symposium*. Vol. II, pp. 949–58

Trejdosiewicz, L. K., Smolira, M. A., Hodges, G. M., Goodman, S. L. and Livingston, D. C. (1981). Cell surface distribution of fibronectin in cultures of fibroblasts and bladder derived epithelium: SEM–immunogold localization compared to immunoperoxidase and immunofluorescence. *J. Microsc.*, 123, 227

Trump, B. F., Heatfield, B. M., Phelps, P. C., Sanefuji, H. and Shamsuddin, A. K. (1980). Cell surface changes in preneoplastic and neoplastic epithelium. *SEM Symposum*. Vol. III, pp. 43–60

Figure 5 (opposite)

a,d: Luminal aspects of rat bladder 1 week after intravescular treatment with tumorigenic dose (4 × 1.5 mg biweekly) of MNU, showing focal area of modified tissue architecture, with less-ordered cobblestone pattern of cell arrangement and some cellular pleomorphism (a ×450); and atypical surface patternings of more prominent and less uniform microvilli (d ×6750)

b,c,e,f: Papillary bladder tumor, from rat 10 weeks after receiving a tumorigenic dose of MNU, showing nodular aggregates of cells (b ×109); marked cellular polymorphism (c ×1175); and presence of pleomorphic microvilli (e ×5500); f ×10 500)
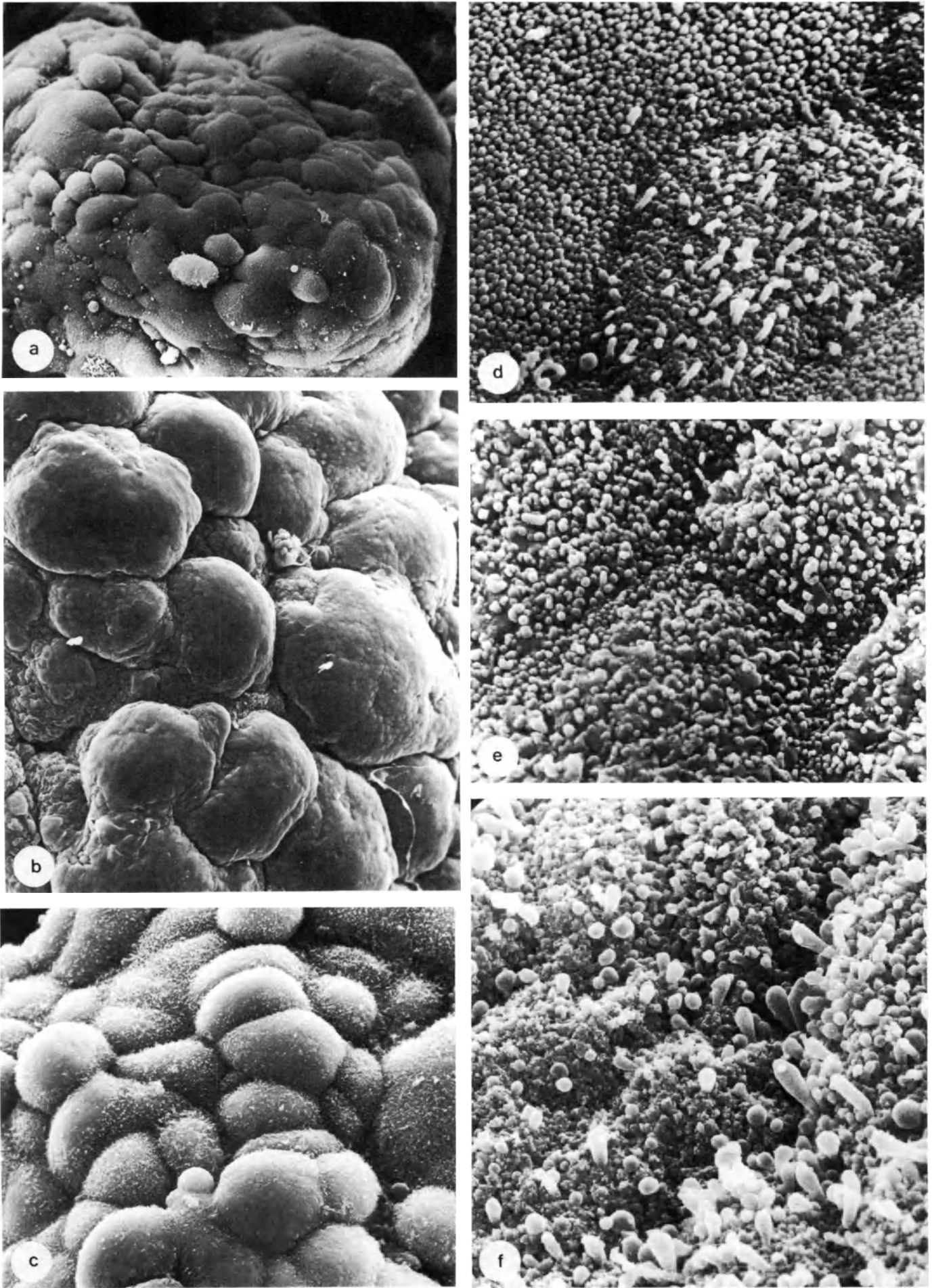
Figure 5
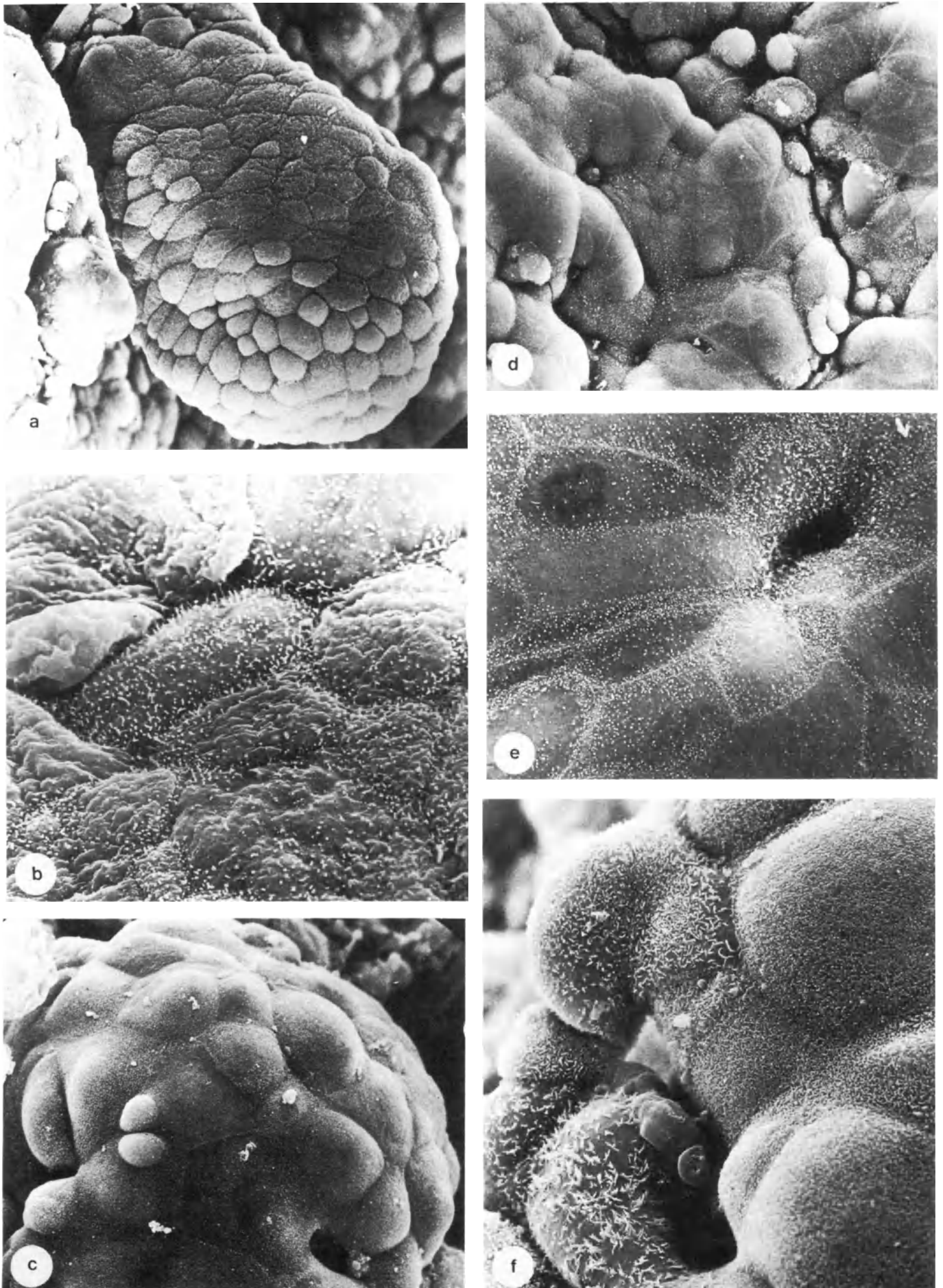
Figures 6 and 7

6a–7c: Luminal aspects of grade I carcinomas showing variability in pattern of tissue histoarchitecture (**6a** ×450; **6c** ×675; **6d** ×675); in cell size and arrangement (**6b** ×2500; **6c–e** ×2000; **6f** ×7750); in surface topography (**6b,e** and **7a** ×9750; **7b** ×13 750; **7c** ×13 750); and showing
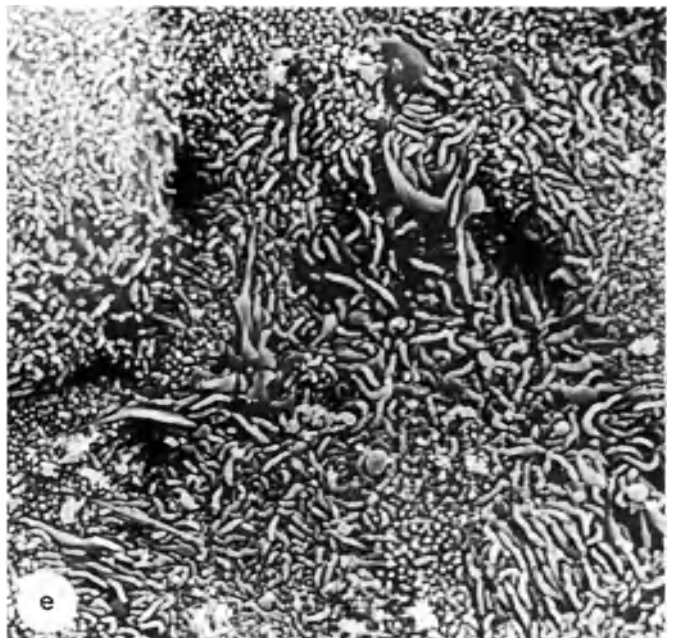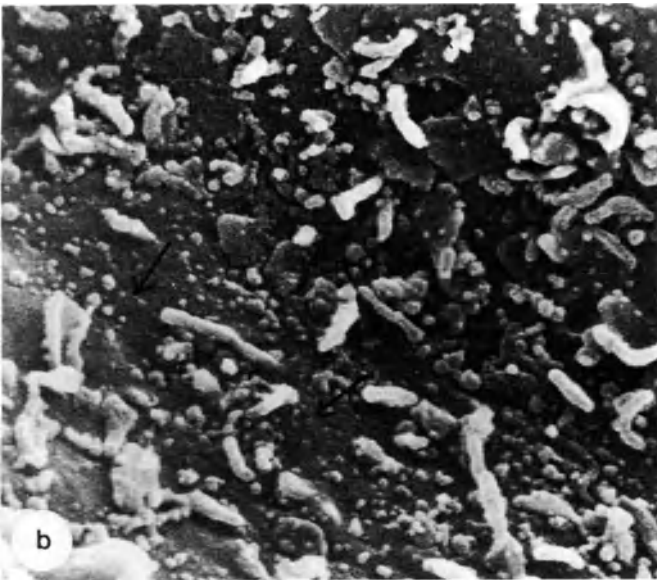
expression of an epithelial membrane antigen (EMA) marked by indirect colloidal gold labeling (↓)

7d–f: Luminal aspects of grade II carcinomas showing thickened urothelium and fibrovascular core in transverse section of a papillar frond (7d ×275); and cellular atypia (7e ×3750; 7f ×6750).

35

SEM technology, parameters and interpretations

E. S. E. HAFEZ* and P. KENEMANS†

* Department of Gynecology/Obstetrics, Wayne State University School of Medicine, Michigan 48201, USA
† Department of Gynecology/Obstetrics, University Hospital, Nijmegen, The Netherlands

SEM TECHNOLOGY

A wide variety of methods have been utilized in the handling, cleaning, fixation, freezing, drying, surface exposure, coating and scanning of samples and biopsy (Table 1). Various buffers have been utilized in the preparation of specific tissues and cells for SEM. A variety of exposures, sprays and tapes is available for the most appropriate adhesive for each type of mounting medium (Witcomb, 1981).

Several complementary techniques have been used in conjunction with SEM, such as backscattered electron imaging, X-ray microanalysis and surface labeling, and also less common techniques such as laser microprobe mass analysis, secondary ion mass spectrometry, and proton microprobe (Table 2). These techniques have introduced new functional elements into SEM investigations. Since several chemical particulates or biological cellular structures have similar surface ultrastructure, complementary techniques of SEM are highly recommended (DeNee, 1976; Buss and Hollweg, 1980).

Autoradiographic techniques have been developed for the localization of isotopes in the scanning electron microscope; all manipulations being carried out on samples that are maintained in a liquid state (Weiss, 1980).

Energy dispersive X-ray microanalysis (EDX), the most widely used complementary SEM technique, can be effectively applied by the pathologist to identify unknown particulates (Abraham, 1977, 1979; DeNee, 1976; Guidotti et al., 1978), calcification stones (Buss et al., 1973; Pritzker and Luk, 1976; Wosievitz, 1978), histochemical reaction products (Coleman and Young, 1979; Okagaki and Clark, 1977), electrolytes (Thurua et al., 1979; Trump et al., 1979) or other artificially

Table 1   Source of variation in SEM preparative techniques

Preparative techniques	Sources of variation
Specimen handling	Specimen size; dissection; identification of the surface of tissue; specimen carriers; fluid exchange; specimen mounting
Fixation	Application of fixative: vascular perfusion, microinjection; drip fixation; immersion fixation. Vehicle osmolarity of fixative; osmium postfixation; washing and storage
Freezing method	Ice crystals; quenching media; quenching procedure
Dehydration and drying	Dehydration; critical point drying by several media; specimen transfer; CO_2 exchange, freeze-drying; air-drying
Rendering specimen conductive	Evaporative coating; sputter coating; OTO method
Surface exposure	Cleaning integument; removal of mucus and luminal fluid; dry fracture; cryofracture; micro-incineration; sectioning or SEM micromanipulation
Scanning	Accelerating voltage; tilt angles; astigmatism; stereo pairs; film; camera focusing
Evaluation	Descriptive; quantitative or morphometry

Table 2 Some supplementary techniques associated with scanning electron microscopy

Technique	Brief methodology
Cell denudation	Specimens are microdissected and placed in phosphate buffered collagenase; reaction terminated according to type of tissue; collagen and related structures are eliminated. Visualization of cellular surfaces covered by connective tissue or basement membrane
Cell maceration 'Os-DMSO-OS' method	Soft part of cytoplasm or cytoplasmic matrix of fractured cells is removed by the macerating effect of OsO_4. The tissue is successively dipped in 25% and 50% DMSO aqueous solutions; freeze-fractured and critical-point dried. Membranous and solid portions of cell organelles are exposed
Ion-etching	Soft materials and contamination covering the specimen are eliminated to reveal intrinsic structures by ion etching, avoiding undirectional cone formation either by tilting the specimen or by using ions of various energies and directions. Alternating current discharge (50 Hz) is made between two aluminum plates under very low vacuum. Rate of atom ejection depends on (a) mass of ejected atoms; (b) mass and velocity of ions, and (c) energy combining the atoms to the material surface
Vascular casts	Preparation of casts, e.g. methyl methacrylate (ester monomer) replicas, of canalicular structures and blood vessels; half polymerized resin is rapidly cooled to a temperature lower than 30 °C; tissue is then macerated with 20% NaOH and the resin cast is washed thoroughly. Methacrylate casts may be coated with metals, but after being placed in osmium gas for a few hours they obtain excellent conductivity and give images even without any coating
Treatment of free cells	Cells (spermatozoa, ova, granulosa cells) are washed and fixed, supernatant is diffused extensively and eliminated by centrifugation. Cell attachment can be ensured by coating the glass surface with a positively charged substance (poly-L-lysine) as cell surfaces are negatively charged. Cell suspensions are passed through millipore filters and polycarbonate membranes with pores of a given diameter

Data from Evan *et al.*, 1976a,b; Fujita *et al.*, 1970, 1974, 1981; Fulker *et al.*, 1973; Leweis *et al.*, 1968; Murakami, 1971, 1973; Nowell *et al.*, 1970; Tanaka and Naguro, 1981; Tokunaga *et al.*, 1969, 1974)

administered elements such as heavy-metal-containing drugs (Buss and Hollweg, 1980).

The inner structure of bulk specimens can be observed with X-ray imaging techniques (Horn and Waltinger, 1978). This technique could enhance the utility of microradiography, with the option of making stereophotographs and obtaining secondary electron images of the same area (Buss and Hollweg, 1980).

Immune and other surface labeling techniques using SEM have been successfully applied to several problems of basic cell research (Molday, 1977; Nemanic, 1979; Lotan, 1979). The high resolution of SEM enables the application of very small markers such as gold or ferritin (Hoyer *et al.*, 1979).

Freeze-fracture techniques have been utilized to demonstrate the formation of specialized intercellular junctions in the developing ovary and testis. Similar findings relate to the formation of the blood–testis barrier, and the co-ordination of cellular activity involved in steroidogenesis (Gondos, 1981).

The backscattered electron imaging (BEI) technique has been used to localize subsurface structures with the help of element contrast, sometimes in combination with EDX (Becker and DeBruyn, 1976; Brody *et al.*, 1977; Matricardi, 1979; Becker and Sogard, 1979). However, structures without a heavy metal content yield a relatively poor BEI (Becker and Sogard, 1979), and may demand a special (silver) staining in order to obtain a good signal. However, common LM and TEM tissue staining techniques can be adapted for selectively presenting structures, e.g. secretory granules, nerve sheaths and enzymes (Becker and DeBruyn, 1976; Buss and Hollweg, 1980). BEI of specifically prepared

samples permits immediate comparison of surface topography and internal structures. There are several theoretical considerations of the feasibility of BEI and staining procedures (Becker and Sogard, 1979). BEI will be a very valuable source of information about clinical specimens and will play an important role in establishing SEM as a diagnostic tool (Carter, 1980).

Tissue culture techniques offer evident advantages, but also pose problems. Cells from tissue culture exhibit several morphological forms under different circumstances, often including diverse behavior of individuals within the population. SEM can be applied to evaluate the cell's condition, as shown by its surface ultrastructure, only if one is aware of the fact that the morphological variations are influenced by both intrinsic and environmental factors. In certain instances it is desirable to study cells in culture from various tissues without using dissociating enzymes such as trypsin or EDTA. Most mammalian cells, when placed in culture, are capable of autonomous motility. SEM can be effective when applied to study the motility pattern and topography of cells or modified substrates (Shay and Walker, 1980).

Microcast replicas of vascular or other hollow tubular systems can be obtained after corrosion of the surrounding biological material. Additional attempts should be made with microvasculature. The recent reports dealing with microcorrosion casts are excellent examples of the usefulness of SEM to evaluate testicular microvasculature and related problems (Figure 1).

It may be desirable to use high-voltage electron microscopy (HVEM) with a range of 1000 kV in combination with SEM. The HVEM has several
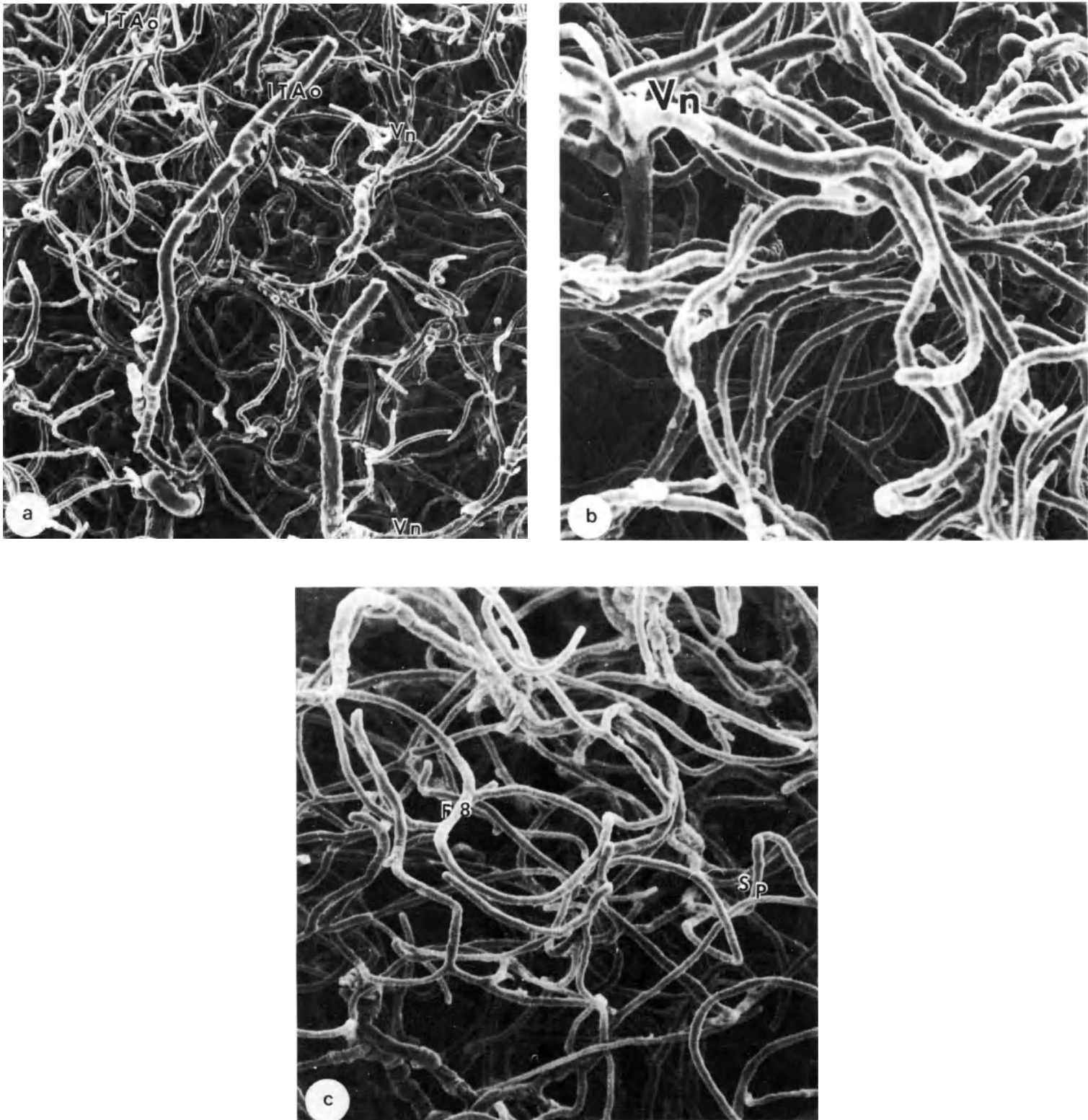
Figure 1 SEM of vascular casts of human testis

a: Intertubular arterioles (ITAo) meander between the intertubular columns. Collecting venules (Vn) connect with many capillaries running from various directions (×70)

b: Higher magnification from a part of Figure 1c. The peritubular capillaries surround the seminiferous tubules and show a branching and a fusion in the intertubular columns.

The intertubular capillaries are not easily distinguished from the peritubular capillaries by their morphologic patterns. Note a venule (Vn) collecting many capillaries from various directions (×90)

c: Capillary network of various forms. F8: Figure-eight-shaped capillary. Sp: Spiral capillary (×140)

(SEM photos courtesy of Dr H. Takayama, Shiga University, Japan.)
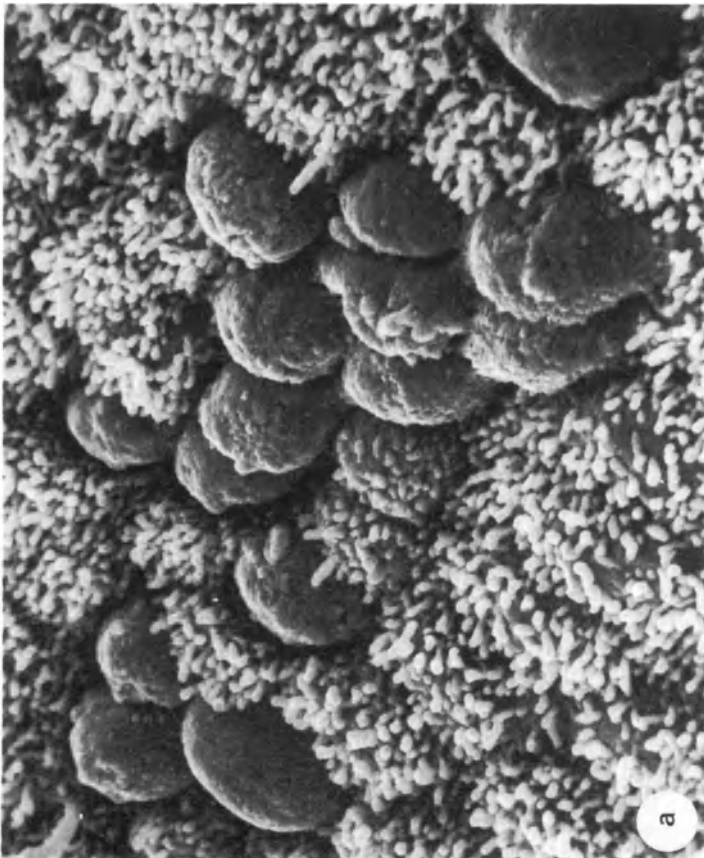
Figure 2 SEM showing patterns of apical microvilli, on superficial epithelium of human ovaries from fertile, anovulatory and polycystic ovary patients
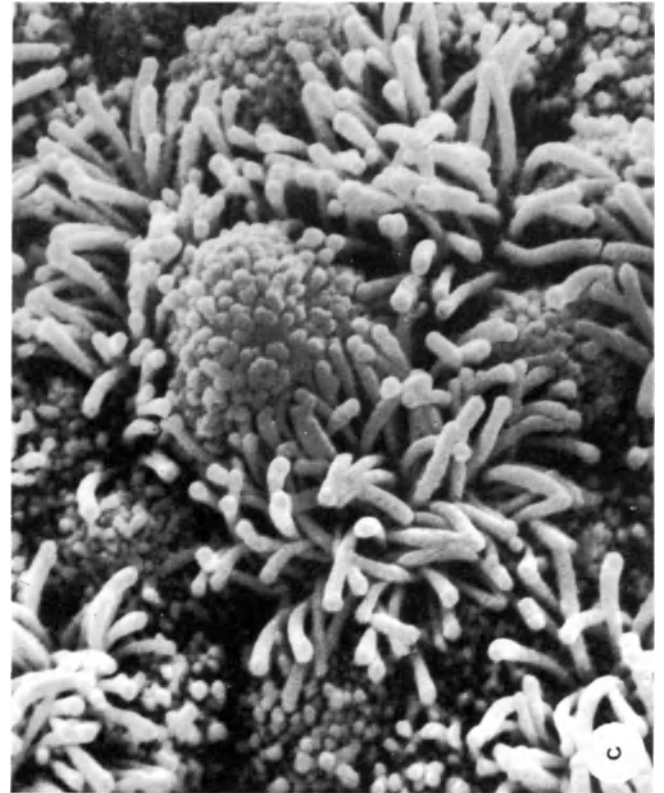
Figure 3 SEM of endometrium from fertile and IUD-wearing patients showing different patterns of ciliated cells

Table 3 Scanning electron microscopic characteristics of microporcesses of cells

Types of cell projections	Ultrastructural characteristics and possible functional significance
Blebs (globular micro-processes, Zeiotic blebs)	Globular microprojections 200–500 nm in diameter often densely grouped. Macrophages are often covered by zeiotic blebs (zeiosis-cell-bubbling) to serve as reservoirs of cell membranes
Filopodia	Slender, smooth filamentous microprojections either straight or curled in course, occasionally surpassing 5 μm in length. They may be branched and may end in a knob-like or a palm-like structure. In cultured cells filopodia occur mainly at the cell margin, extending to touch adjacent cells and substrate (glass) surface. Filopodia may serve as tentacles for detecting objects around the cell. When cells migrate or extend their processes, filopodia may be moved in front and detect the way by a rapid 'scanning' movement. Filopodia increase in number when cells are rounded up for mitosis, suggesting that they serve as cell anchors. Filopodia may perform a role to recognize and capture foreign bodies in macrophages *in situ* or *in vitro*
Kinocilia	Slender, gently waving columns with a smooth surface. Minute secretory granules from adjacent secretory cells, or particulate contaminants may be noted. Curved shape of cilia suggests beating movement and its direction toward the outside of the female and male reproductive tract, ciliary coordination facilitates ciliary beat
Lamellipodia	Web-like thin flabs extending from cell margin in the form of ruffles, showing a waving movement, involving pinocytotic activity of cells. Lamellipodia, very variable in size, are uniform in thickness, 100 nm. Commonly observed in cultured cells. Lamellar micro-projections of smaller but more uniform size may densely cover the cell surface
Microfolia	Tongue-like microprojections serving as a device for deep and fast interdigitation of cells against mechanical abuse
Microlamella	Bulbous projections of shapes like twisted plates
Microridges (Microplicae)	Winding-ridge-like folds, measuring 100–200 nm in width and 200–800 nm in height, occur on the surface of some stratified squamous epithelia (e.g. cervix, vagina). Grooves formed by the ridges may hold a layer of lubricating and cushioning mucin designed to protect the epithelium from abrasive abuse. Microplicae are formed as intercellularly gearing ridges
Microvilli	Columnar projections of the cell with uniform or variable dimension, arrangement and function. Measure 1–1.5 μm in length and 80 nm in thickness. Microvilli tend to increase the cell surface area, thus elevating the efficiency of material transport through the cell membrane; many types of microvilli are motile. Chorionic villi of the placenta glandular cells and free-floating cancer cells are densely covered by complex microvilli. Microvilli may play a role in agglutination of cells or may serve as the reservoir of cell membrane
Stereocilia	Very long, microprojecting, over 10 μm, irregular in length and direction. Their basal portions form brush-like tufts, each of which originates from a cytoplasmic stem projecting at the apex of epithelial cell. Stereocilia do not beat as cilia, but they may be involved in a slow movement. Their mechanical or chemical action is unknown
Solitary cilia	Single or paired thinner column tapered, uneven in thickness or irregularly curved, may serve as the receptor site of the cell, or considered as an 'evolutionary remnant'

Data from Albrechts-Buehler, 1976; Andrews and Porter, 1973; Fujita *et al.*, 1981; Horridge and Tamm, 1969; Mooseker and Tilney, 1975; Muto and Fujita, 1977; Muto *et al.*, 1977; Prakkal *et al.*, 1974; Polliack *et al.*, 1973; Porter *et al.*, 1945; Rajarman *et al.*, 1974; Yamadori, 1978)

advantages: (a) increased specimen penetration which facilitates photography of relatively thick sections; (b) reduced specimen damage under beam exposure; (c) improved resolution due to decrease in the dark-field operation and more versatility, in that with a larger column there is more space for special attachments (Shay and Walker, 1980). HVEM can be easily applied to various biological systems, e.g. thick sections, short exposure times for autoradiography, isolated cell components, selective staining of thick sections, unprepared or wet specimens and whole cells.

SEM PARAMETERS

There are several types of apical cell microprojections (microprocesses) which are extremely variable in both structure and function; e.g. microvilli, kinocilia,

stereocilia, solitary cilia, microridges, filopodia and lamellipodia (Table 3; Figures 2–5).

Microvilli

Apical microvilli are noted on several types of normal cells where a maximization of the cell surface appears beneficial, as in mesothelial cells, glandular cells of the genital tract, intestinal cells (Andrews and Porter, 1973; Fawcett, 1965, 1966), embryonal cells (Overton and Shoup, 1964), on some metaplastic cells (Wong and Buck, 1971), and on carcinoma cells (Kenemans *et al.*, 1980, 1981, 1982). Microvilli on non-malignant cells are usually of constant length and thickness (Overton and Shoup, 1964; Wong and Buck, 1971; Grenwood and Holland, 1972). The diameter of microvilli varies from 0.1 to 0.2 μm and their length from 0.1 to 0.5 μm,
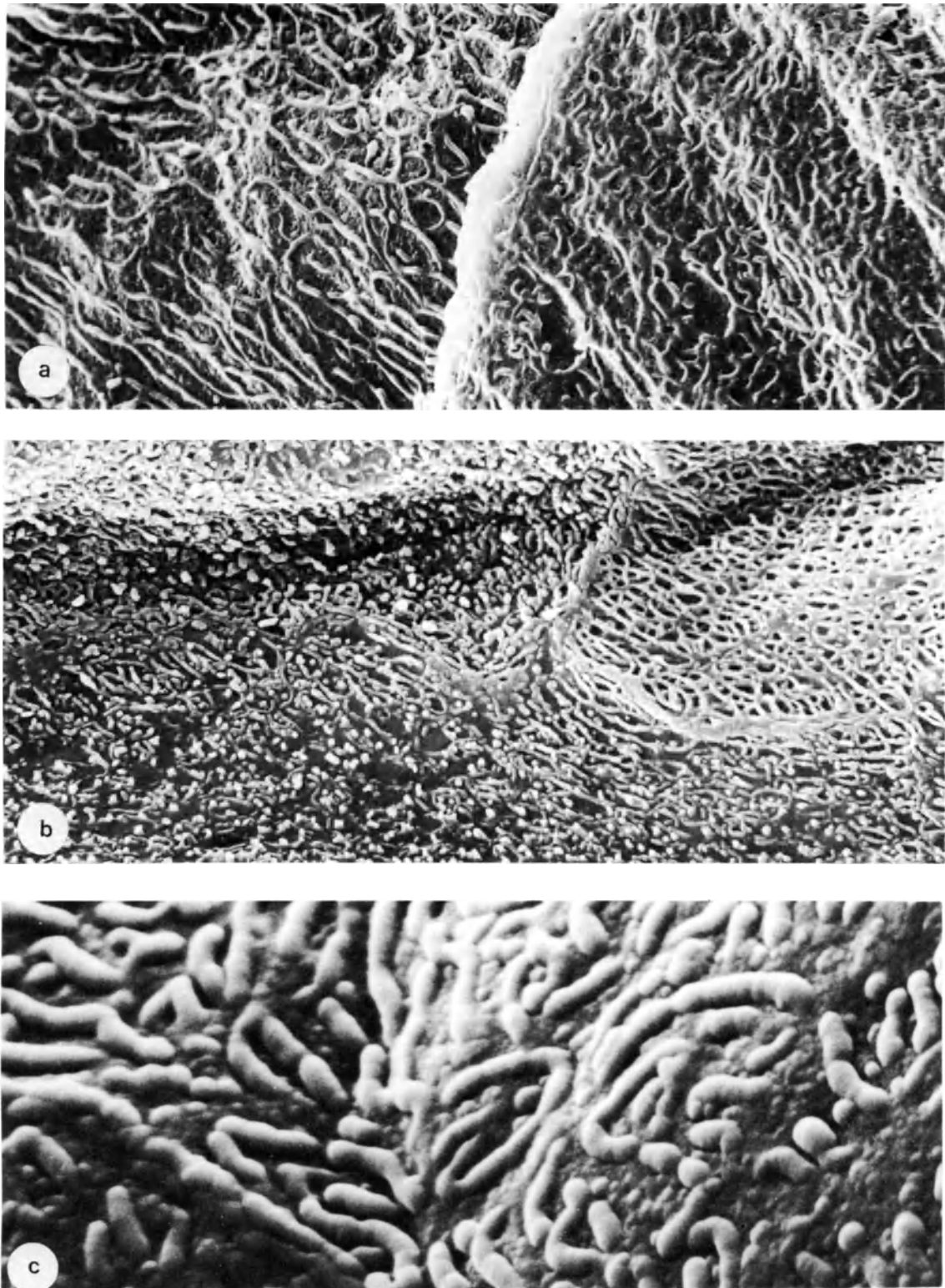
Figure 4 SEM of human vaginal epithelium from different stages of the reproductive cycle. Note variability in pattern of microridges

Figure 5 SEM of cell interconnections in the cleaving fertilized embryo
a: blastomeres;
b: outside surface of the zona pellucida;
c: the inside surface of the zona pellucida (right) as it is removed from the trophoblast (left)
d: human early fetus
(Photos by E. S. E. Hafez and J. E. Flechon.)
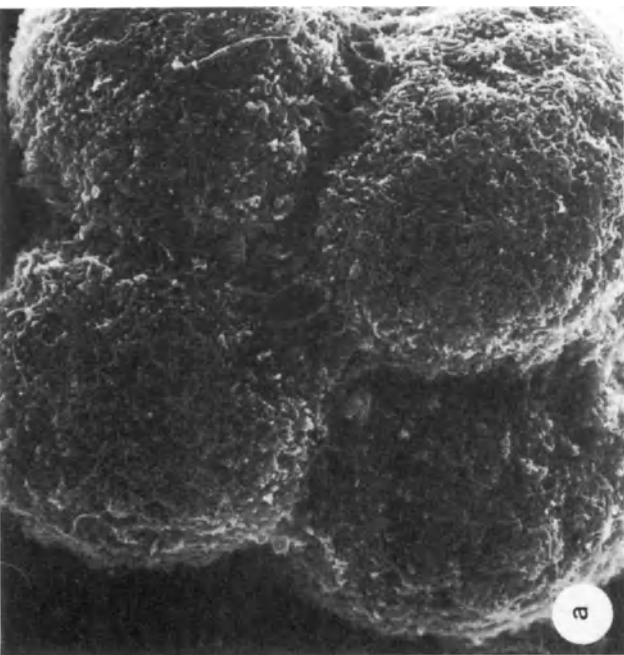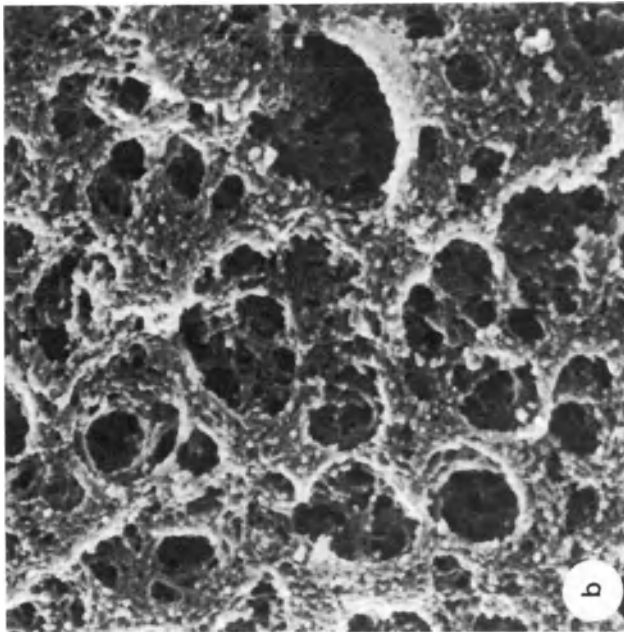
but occasionally there are tufts of much longer microvilli. Microvilli exhibit different shapes, such as regular, rod-like configurations, broader base than the tip, broader tip than the base, branching and fusion. There are also some variations in the morphology of the microvilli among different cells and on the surface of a single cell. Pleomorphic microvilli are noted on cancer cells and in experimental systems of epithelial carcinogenesis (Jacobs et al., 1976; Koss, 1977; Rubio, 1976). Irregular microvilli occur on free-floating malignant cells in effusions, regardless of anatomic origin of the primary tumor, e.g. mammary, ovarian, gastric or bronchogenic (Krivilnkova et al., 1976; Domagala and Koss, 1977; Kaneshima et al., 1978; Berliner et al., 1978). Little is known about the physiological significance of these microvilli (Kenemans et al., 1981, Domagala and Koss, 1977; Vergara et al., 1977; Dick et al., 1970; Enlander et al., 1974; Evans et al., 1974; Fisher and Copper, 1967; Hodges, 1970; Lesseps, 1963).

SEM INTERPRETATIONS

As in LM and TEM preparations, the preparative and instrumental artifacts in SEM are consistent and are interpretable. The preparative SEM technique should cause minimal alterations in the topography and the surface of the tissues. Minimal alterations in the topography of the tissue can be determined by comparing the SEM results, using several alternative methods of preparation. A standardized preparative technique should be used throughout the investigation. However, one should be aware of the fact that a given tissue surface may respond quite differently to the preparation technique than any other surface or tissue.

Several techniques have been utilized for the preparation of gynecological tissues for SEM. However, there is remarkable lack of standardization, so interpretation of the results is difficult, and inter-investigation comparisons are usually impossible.

For practical diagnostic microanalysis, SEM with backscattered electron (BSE) imaging and X-ray microanalysis of cytological material or 5 μm thick tissue sections can be an efficient procedure to study several problems: e.g. identification of particulate materials in tissues; problems of contamination of specimens; and use of high vs low magnification analysis (Abraham, 1981).

References

The references for this chapter will be found under Chapters 1–6.

Subject Index

349